Dynamic Analysis and Control System Design for an Advanced Nuclear Gas Turbine Power Plant

by

Xinglong Yan

B.S.M.E. Tsinghua University, 1984
M.S.M.E. Tsinghua University, 1986

Submitted to the Department of
Mechanical Engineering in Partial Fulfillment of
the Requirements for the Degree of

DOCTOR OF PHILOSOPHY
IN MECHANICAL ENGINEERING

at the

Massachusetts Institute of Technology

June 1990

Signature of Author_____
Department of Mechanical Engineering
May, 1990

Certified by_____
Lawrence M. Lidsky, Thesis Supervisor
Professor of Nuclear Engineering

Accepted by_____
Ain A. Sonin, Chairman
Departmental Graduate Committee
Department of Mechanical Engineering

Dynamic Analysis and Control System Design for an Advanced Nuclear Gas Turbine Power Plant

by

Xinglong Yan

Submitted to the Department of Mechanical Engineering
on May 15, 1990 in partial fulfillment of the requirements for the
Degree of Doctor of Philosophy in Mechanical Engineering

Abstract

A control system design for the Modular High-Temperature Gas-cooled Reactor Gas Turbine power plant (MGR-GT) is presented. The control system is designed to regulate reactor power, control electric load and turbomachinery speed, control the temperature of the helium to the turbine, prevent thermal overstresses in plant components during transients, and support scheduled control maneuvers for plant startup and shutdown. In addition, the control system provides emergency protection to prevent damage to plant components and to mitigate the likelihood of bounding safety events in case of severe accidents. A full-scale transient simulation program, GTSim, was developed as the primary tool in developing the control system and performing transient analysis to investigate the plant dynamic characteristics during normal as well as extreme conditions. Solution algorithms were developed to enable the simultaneous solution of the large, stiff system of nonlinear equations representing the dynamic behavior of the overall power plant. The high structural modularity and flexibility of the code permit independent maintenance and upgrade for the code subsystem modules and require no major changes in the code when the physical design of the plant evolves.

The control system was developed through the integration of advanced control methods, and is based on unique control approaches regarding the requirements of the regulatory and protective control for nuclear power plants. Utilization of inventory control for power regulation yields high system efficiency over extended power ranges, while providing rapid load following capabilities with the assistance of limited bypass control. The reactor power is controlled with reactivity control rods, based on the strategy of maintaining constant temperature for the coolant at the core outlet. This approach minimizes the occurrence of thermal transients and temperature re-distribution in the core during reactor power changes and reduces control efforts in compensating for the temperature feedback of reactivity. The control functions are automated by numerous controllers developed based on the state-space feedback control methodology. The design demonstrates that the MGR-GT is a robust controllable power plant.

This study resulted not only in the design of an effective and high efficiency control system, but also produced a sophisticated transient simulation program capable of simulating a broad range of transient events including off-normal behaviors, which is expected to play a significant role in the future design study of the MGR-GT.

Doctoral Thesis Committee:
Professor Lawrence M. Lidsky, Thesis Supervisor
Professor David Gordon Wilson, Committee Chairman
Professor David D. Lanning

Acknowledgements

The author would like to acknowledge those individuals and institutions who in some ways have contributed to this work.

First and foremost I wish to thank my thesis supervisor, Professor Lawrence M. Lidsky, for his constant assistance to me in the course of this research project. His support is unique in that it has not only reflected his profound professionalism, but has also made the project research increasingly enjoyable. Many thanks are also extended for his help to my family during this period. I would also like to express my appreciation to the other members of my thesis committee, Professor David Gordon Wilson, and Professor David. D. Lanning for their helpful guidance in the research progress, and their time and patience in reviewing many project technical papers and reports including this dissertation.

I cannot possibly give my gratitude to all of the individuals and institutions in the United States, Japan, France, and Germany, who have provided assistance on the project. However, I would like to mention those who gave a particular large part of their effort and resources. First, I wish to give my thanks to the United States Department of Energy, Tokyo Electric Power Co., Inc., and Gas-Cooled Reactor Associates for providing financial support to this project. Many thanks are owed to Mr. D. J. Teare, of the MIT Energy Lab., for both his technical advice and administrative management to the project. I would also like to thank Dr. M. Mori for providing connection between TEPCO and this project, and Dr. C. F. McDonald of General Atomics, Dr. W. H. Day of United Technologies, and Dr. J. C. Cleveland of Oak Ridge National Laboratory for providing technical information on reactor systems and turbomachinery. To my friends at MIT, especially those in our research group, I would like to thank them for the support, experience and encouragement that I have gained from them.

I would like to express my gratitude to Ms. Milena M. Levak, MIT Dean of Student

Affairs, Professor Ain. A. Sonin, Chairman, and Ms. Leslie Regan, staff member of the Graduate Committee of MIT Department of Mechanical Engineering for their diverse help and understanding that made the success of my career at MIT possible.

Finally, I would like to thank my wife, Chih Wang, whose tremendous moral support, understanding, and love contributed in large part to the success of this work, and to whom this work is dedicated. I would also like to thank our parents for their support to me and my family during this period. I want to give my regrets to my little daughter in China, born three years ago, who has lived away from her father for 91.67% of her life, and to give my promise to make it up in the rest of my life.

For My Wife

Table of Contents

List of Figures

List of Tables

Chapter One

Introduction

1.1 Introduction

The high temperature capability of the High-Temperature Gas-Cooled Reactor (HTGR) makes it ideally suited for direct extraction of mechanical power from reactor primary helium coolant by a gas turbine. This potential led to major conceptual design studies of nuclear gas turbine systems, mostly in the United States and in the Federal Republic of Germany during the 70's. However, these studies concluded that this combination did not have sufficient advantages over conventional steam generating systems, a technology that had been well-developed and widely-used in industry, to justify the anticipated development costs. Major HTGR gas turbine programs were terminated by the early 80's.

However, several relevant technological developments in recent years have revived the development of gas turbine power plants. It is now possible to build a direct Brayton-cycle power plant using a Modular High-Temperature Gas-cooled Reactor (MGR), relying on current technology, within existing design code and materials, that will result in a net efficiency in excess of 45% at a substantially lower cost than that of steam generating plants. This claim is the conclusion of several major studies carried out at MIT since 1983[S1][S2][L1][K1], and was demonstrated in a conceptual design of an advanced MGR gas turbine power plant - MGR-GT[S1].

The conceptual design of the MGR-GT was accomplished in 1987. The baseline configuration of the power plant is shown in Figure 1.1, and its salient design parameters are listed in Table 1.1. The following important factors have contributed to the design of the MGR-GT:

A modular, inherently-safe, graphite-moderated, helium-cooled reactor. Recently, emphasis on the safety of reactors has shifted the development of high temperature gas-cooled reactor technology from the large, monolithic HTGR to smaller modular systems. By limiting the thermal power of the core to approximately 200 MW and power density to about 3 W/cm^3, an inherent limitation of the fuel temperature to below its failure temperature can be guaranteed even in the worst postulated accident. Thus, there is no physically achievable way for fuel to exceed its failure temperature, and no radioactivity release from the reactor can ever occur. Development of the MGR technology is based on forty years of successful research and operational experience of the gas-cooled reactors, mainly in Germany. It is expected that the inherent safety of the MGR plus its suitability for high-temperature, high-efficiecy gas turbines will allow the MGR to be a promising near-term energy option for electric power generation in the U.S. market.

A highly-regenerated compact recuperator. Utilization of a high-effectiveness recuperator with low pressure drop and reasonable volume is crucial to the optimal performance of any direct-cycle thermal operations. Recent advances in compact heat exchanger technology in the field of space technology have made it possible to build a recuperator with very high effectiveness for the modular gas turbine power plant.

High-speed, high-efficiency, single-shaft turbo-generator machinery. The evolutionary development of reliable solid state power electronics for frequency conversion eliminates the restriction to synchronous operation

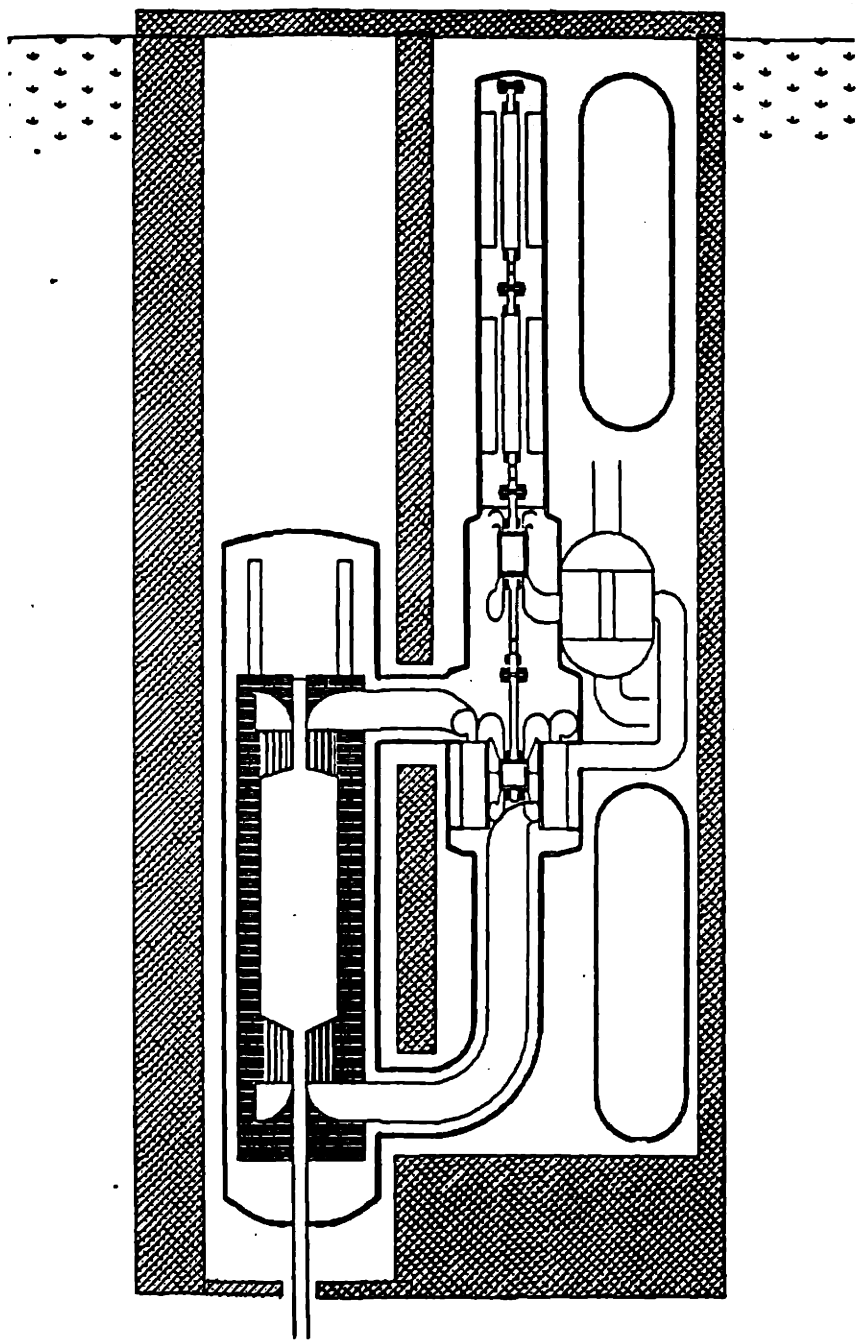

Figure 1.1 The MGR-GT in a below-grade silo[S1].

Table 1.1: MGR-GT Design Specification

Reactor System

Thermal Power	200 MW
Core Diameter	3.0 m
Mean Core Height	9.43 m
Average Power Density	3.0 W/cm3
Coolant Temperature	592/850 C
Coolant Pressure	8.0 MPa
Helium Flow Rate	146.2 kg/s
Pressure Drop	2.56%
Fuel-Cycle	U-Pu
Number of Fuel Pebbles	358,000
Enrichment	7.50%
Heavy Metal per Pebble	7 g
Core K-eff	1.0057
Number of Control Rods	6
Worth of Control Rods	2.60%
Number of Absorber Sphere System	18
Worth of Absorber Sphere System	12.30%

Turbo-Generator

	Turbine	Compressor
Power Rating	200 MW	100 MW
Speed	10,000 rpm	10,000 rpm
Pressure Ratio	2.00	2.00
Efficiency	93.00%	93.00%
Stages	6	15
Max Tip Diameter	0.862 m	0.733 m
Bladed Length	0.63 m	1.30 m

	Generator
Power Rating	2x50 MW
Speed	10,000 rpm
Efficiency	93%
Frequency Coversion	LCI
Weight of Rotors	2x5,000 kg
Inertia of Rotors	650 kg-m2

Heat Exchangers

	Recuperator	Precooler
Thermal Rating	100 MW	100 MW
Type	Helium-to-Helium Counterflow	Helium-to-Water Crossflow
Surface	Strip-fin Plate 1/9-24.12	Tube-to-Shell S1.5-1.0
Effectiveness	95%	0.93%
Helium Flow Rate	146.2 Kg/s	146.2 Kg/s
Pressure	8.0/4.0 MPa	4.0 MPa
Total Pressure Drop	1.20%	0.10%
Total Volume	15.84 m3	5.3 m3
Module Dimension	3.25x1.0x1.22 m	3.6x2.5x0.57 m
Total Heat Transfer Area	17,933 m2	1,168 m2

Plant Performance

Total System Efficiency	> 46%
Electric Power Output	92.5 MW

speed for turbines. This makes it possible, in the design of the MGR-GT turbomachinery, to optimize the performance of both the turbine and the compressor on a common shaft driving a generator at a very high rotational speed. High speed not only reduces the difficulty of designing turbomachinery, particularly the axial compressor, but also allows the size of the machine to be reduced. The operation of the high speed turbomachinery is further supported by the recent development of magnetic bearings. Magnetic bearings enable the control of rotor dynamic performance, such as critical speed or vibration, at high speeds. The use of magnetic bearings ultimately eliminates the problem of lubricant oil ingress into the coolant, as encountered when using conventional bearings. Additionally, the MGR-GT generator can be used directly as a super-motor driving the turbomachinery during startup and shutdown, and spinning the machine to circulate the helium for afterheat removal from the reactor core. This feature significantly simplifies the control procedures required for these operations and eliminates the need of an additional starting motor.

A modular, low cost, stand-alone system. The MGR-GT replaces the large, site-constructed, steam Rankine-cycle power system with a compact, factory-assembled, gas turbine system. Modularity helps reduce the cost of the system significantly. In addition, the MGR-GT is the only modular-reactor concept that offers stand-alone operation, permitting utilities to expand capacity without committing to large steam Rankine-cycle.

The MGR-GT is aimed at near-term deployment. Baseline and conceptual design

studies have been completed. The intent of this study is twofold: to develop a full-scale dynamic simulation program, GTSim, in order to provide a system design and analysis tool to support future MGR-GT development, and to pursue the control system design and dynamic analysis for the MGR-GT.

1.2 An Overview of this Study

Dynamic simulation for nuclear power plants is required to deal with a system having a number of subsystems, the working principles of which depend on entirely different types of physical laws. With regard to the MGR-GT, for instance, it comprises a nuclear reactor, the dynamics of which is subject to neutron kinetic theory, heat exchangers which are governed by thermodynamic principles, turbomachinery with characteristics that depend on the computational fluid and mechanical system dynamics, and a generator which transfers mechanical power into electricity based on the principles of electrical engineering, and yet other assorted components such as pipes, plenums, and valves whose behaviors are determined by laws of conservation.

Because of the complexity and diversity inherent with nuclear systems, development of simulation codes for nuclear gas turbine plants has been acknowledged as a major undertaking in terms of costs and manpower, depending on the sophistication of the program to be developed. The programs available to date are mostly limited to a partial-scale level in order to reduce the task of modeling entire nuclear power plants. Consequently, these programs are inadequate for transient analysis of nuclear powers plants under full-range operating conditions. To support extended control and dynamic simulation of the MGR-GT, a full-scale program must be developed.

There has been limited experience in control of modular nuclear gas turbine power plants, especially in study of interactive control of both reactor and power conversion

systems. Most of the previous control studies have particularly focused on large gas turbine systems since the U.S. nuclear gas turbine programs had been devoted to the development of large HTGR-GT plants. The primary objective of HTGR-GT control is to design complex engineering safeguard systems to assure safety operation of the plants. Because safety considerations dominate the control of the HTGR-GT, operational efficiency has been sacrificed in the control system design[C1].

The MGR-GT has a completely different design concept, characterized by inherent safety and modularity. As a result, emphasis of the control system design can now be placed on accomplishing optimum control maneuvers and high efficient performance of the plant. In addition, the MGR-GT presents many unique control requirements, among them are high speed operation of the turbomachinery, compact flow configuration, high-effectiveness heat exchanger, and a pebble bed reactor with a strong temperature coefficient. Controlling the MGR-GT requires dealing with these unusual conditions in order to produce an effective and high efficiency control system for the plant.

1.2.1 Objectives

This study has three major objectives, to develop a computer code (GTSIM) capable of full-scale simulation of the MGR-GT, to develop a control system design, and finally to carry out transient analysis for a set of selected events ranging from normal operational events to severe accidents. Detailed descriptions of these objectives are given separately in the following sections.

1.2.1a Development of Simulation Program - GTSim

Partially because the technology of nuclear gas turbine power plants is relatively new, at least in comparison with nuclear steam power plants, and partially due to the complexity of nuclear systems, few computer programs have been made available for the simulation of

full-scale gas turbine power plants in the past. Existing simulation programs have mostly been on a partial scale basis, thus limiting their applications in studying simultaneous control of reactor and power conversion systems.

For instance, in the development of simulation programs used for nuclear gas turbine control studies, an assumption commonly made is constant flow temperature at reactor core outlet, based on the theory that the relatively large thermal inertia of the massive graphite core would prevent rapid temperature change in the coolant flow[H1]. This approach completely excludes the modeling of reactor core neutron kinetics and heat conductance processes, and only considers the flow hydraulics in the core. However, the temperature of flow at the reactor core outlet can significantky change during critical pressure transients, such as large flow bypass, due to flow compression and expansion. Therefore, engineering accuracy of the simulation based on this assumption could hardly be achieved.

The second assumption, an improvement from the constant flow temperature assumption, is constant fuel temperature. This method takes into account thermal conduction and convection within the core but exclusive of the model predicting the core power transient behavior. Therefore, given the requirement of engineering accuracy, the simulation would only be regarded valid up to a few minutes. The time beyond this period would exceed the core thermal characteristic time and consequently the assumption of the constant fuel temperature would no longer be adequate. Thus, programs based on the previous two assumptions could not be used to carry out the study of interactive control, which demands long-term simulation under full plant conditions.

Limited experience exists in full-scale simulation for nuclear direct-cycle gas turbine power plants. Such full-scale modeling is necessary if the transients to be simulated last extended period, and if simultaneous control for reactor and power conversion systems is desired. One typical event is the control procedure for plant startup or shutdown. Because

of the complex nature of nuclear gas turbine plants, the development of programs of this kind ordinarily requires the cooperation of specialists with different backgrounds. Example of such cooperation could be found in the development of REALY2 program[G1].

REALY2 is a program developed by General Atomic Company during its HTGR-GT development in the late 70's. The goal of the program was to be capable of simulating a majority of normal and abnormal transients for the company's 2000 MW HTGR-GT Gas turbine power plant. A schematic diagram of the HTGR-GT is shown in Figure 1.2[M1]. It works in a direct-cycle consisting a graphite-moderated prismatic core, single-shaft turbomachinery driving a generator, a recuperator and a precooler. Figure 1.3 shows the plant layout[M1].

The HTGR-GT system model used by REALY2, as shown in Figure 1.4, follows closely the physical layout of the plant, so does the structure of the code. Figure 1.5 shows the structure of the REALY2 program. As can be seen, the model of each component is enclosed in individual subroutine and is handled as being independent from the others during execution. The only conditions that link these components together are the boundary conditions, which are updated with a quasi-static calculation at the end of each integration step. It apparently neglects transport effects inherent in the plant whose behavior is inevitably influenced by simultaneous thermal-hydraulic interactions. With boundary conditions separating component integrations from each other, certain transport phenomena, such as the propagation of critical flow reversal and velocity shock wave across the components in case of rapid system depressurization, could not correctly be predicted. The development of these flow phenomena is largely determined by the simultaneous transient conditions in adjunct components, which undertake the various physical processes with marginally different time scales and interact with each other through simultaneous transport effects at each time step.

Furthermore, REALY2 employs an explicit integration scheme in which the values in

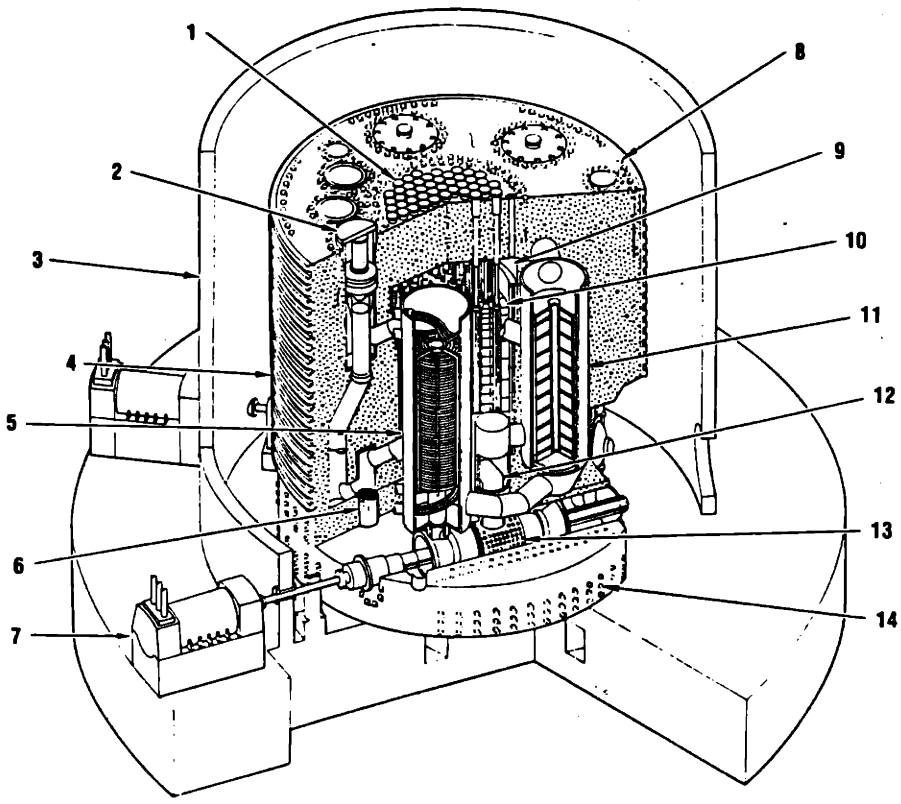

KEY

1 REFUELING PENETRATIONS
2 CORE AUXILIARY COOLING CIRCULATOR
3 SECONDARY CONTAINMENT
4 PCRV
5 PRECOOLER
6 CORE AUXILIARY COOLING HEAT EXCHANGER
7 GENERATOR
8 VERTICAL PRESTRESS TENDONS
9 REFUELING PLENUM
10 CORE
11 RECUPERATOR
12 CORE OUTLET DUCT
13 TURBOMACHINERY
14 HORIZONTAL PRESTRESSED TENDONS

Figure 1.2 HTGR-GT integrated plant[M1]

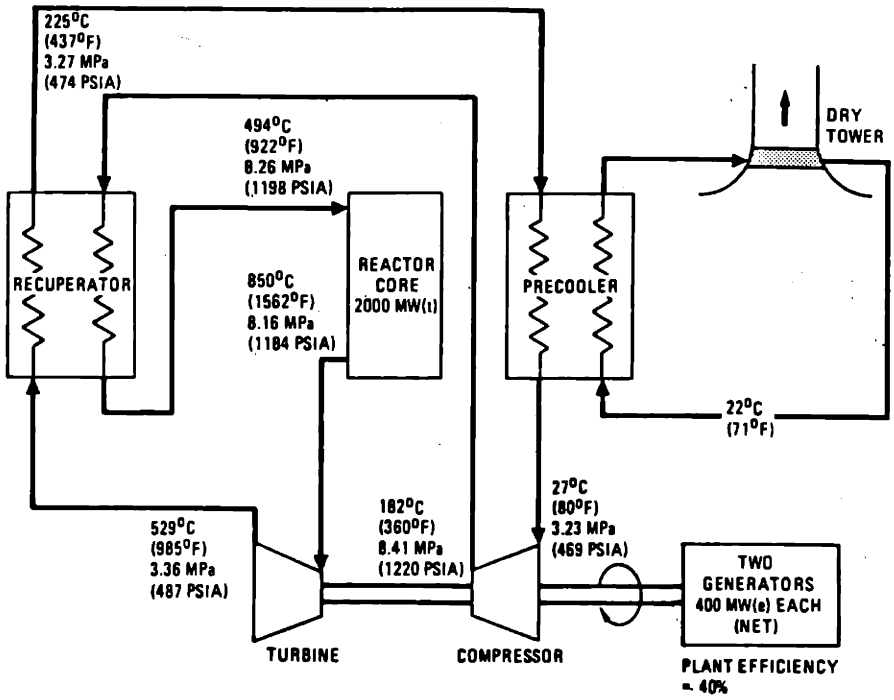

Figure 1.3 Loop cycle diagram for 800-MW(e) HTGR-GT power plant[M1]

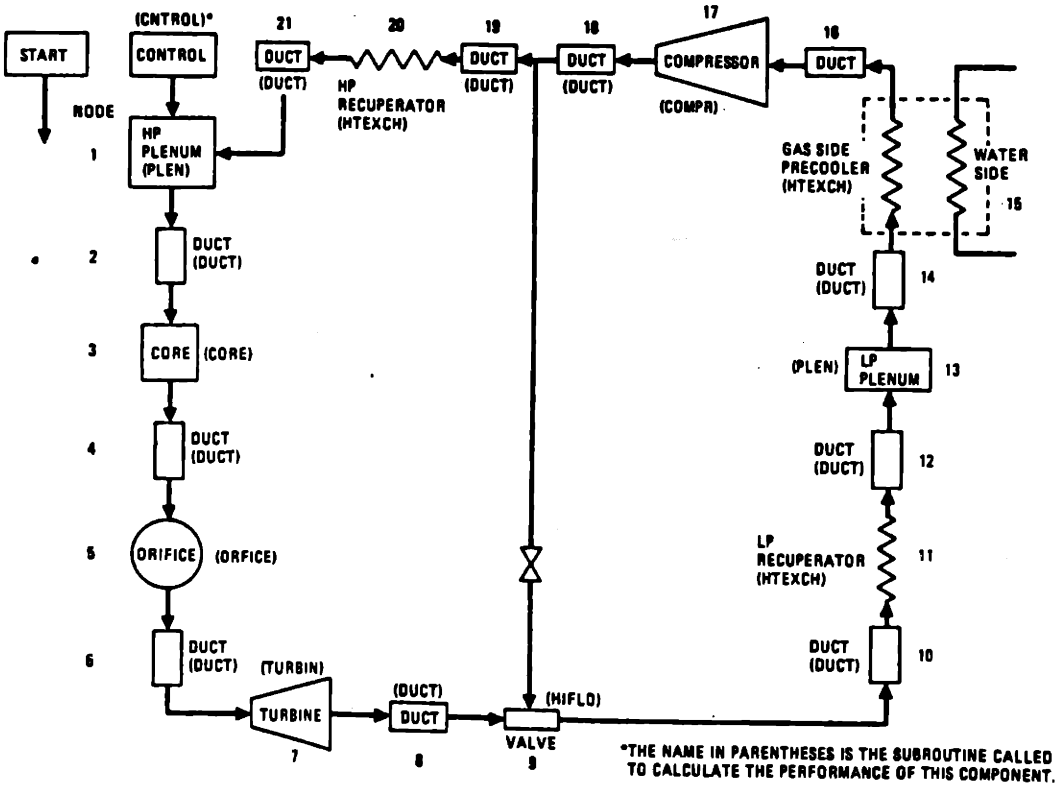

Figure 1.4 REALY2 plant model[G1]

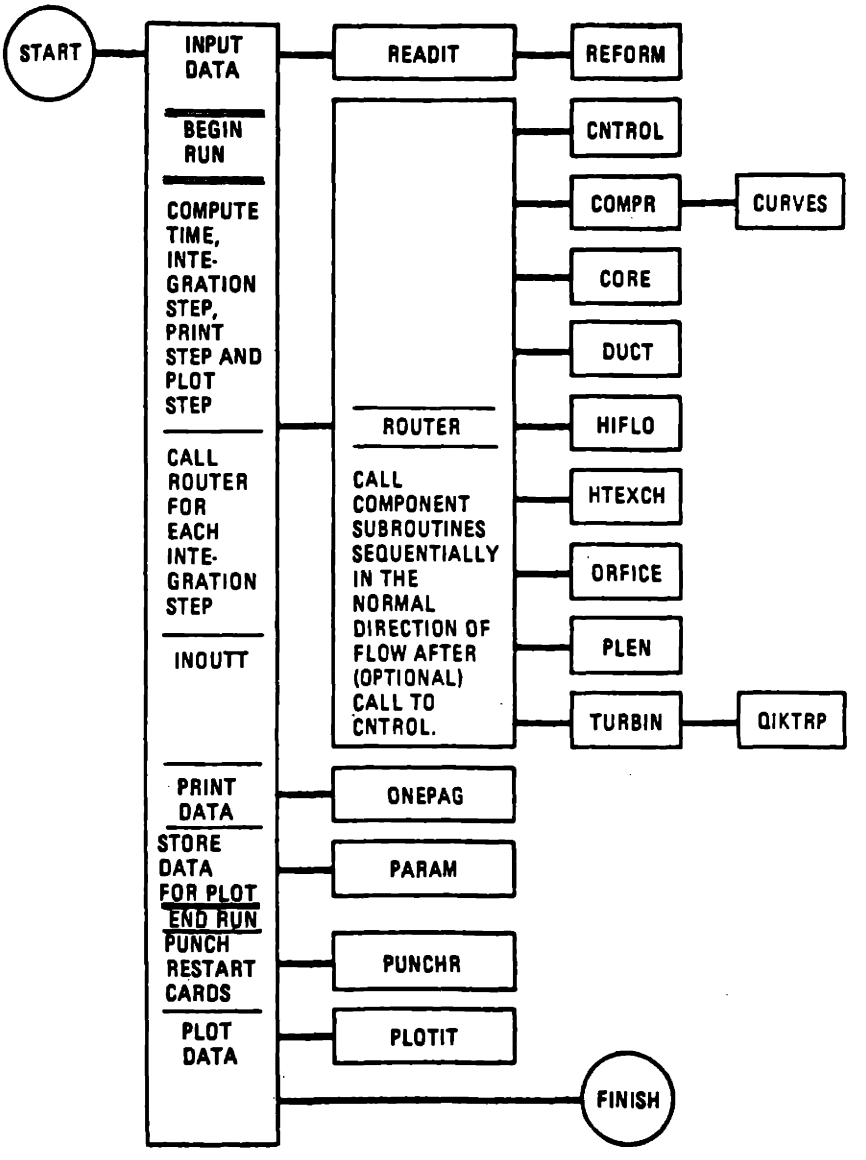

Figure 1.5 Program REALY2 for HTGR-GT transient simulation[G1]

advanced time are evaluated individually for each component. Besides not considering transport and feedback effects among the components, this integration method is subjected to a stringent stability criterion when simulating a nuclear system, the characteristic times of which are widely-distributed, ranging from a few deciseconds to several minutes. In REALY2, very small time steps must be chosen to achieve the stability.

Based on the analysis above, it is apparent that the REALY2 program would be limited in its ability to predict both fast and slow transients with inherent stability and adequate accuracy. In fact, the developers of the program declared that REALY2 was only valid for simulations within five minutes due to the lack of modeling of long term feedback effects in the code[H1]. However, it is by no means obvious that the program is able ever to cover a majority of the normal and abnormal transients for which it was planned. The upper limit of 5 minutes seems not only to result from the lack of feedback modeling but might be imposed by concerns of computational efficiency, stability, and accuracy of the algorithm employed.

GTSim requires a different approach. The requirement of the GTSim is sufficient ability to model a list of selected events that cover both normal and far off-normal behaviors, lasting from a few seconds to several hours. To reach this goal, several difficulties must be overcome.

The prediction of transport effects in closed-cycle nuclear power plants requires simultaneous handling of all major components presented in the system. It is especially crucial to the simulation of the MGR-GT having an extremely high-effectiveness recuperator which closely couples the flows at its two sides. The time constant of heat transfer across the wall of the recuperator is an order of magnitude smaller than energy transport at each side. Other numerous simultaneous thermal and hydraulic interactions also exist between the reactor system and power conversion system, and within each individual system as well.

Simultaneous solution of all component models requires dealing with a set of first-

order differential equations that can be arranged in the following space-state form:

$$\frac{d\bar{y}}{dt} = F[\bar{y}, \bar{U}, t] \tag{1.1}$$

where $\bar{y}$ is the vector of state variables, $\bar{U}$ the vector of control inputs to the system, and t the time. This system of equations is a nonlinear system and can be very large, depending on the degree of transient to be analyzed. In addition, differential equations representing a nuclear system comprise a stiff system with widely-distributed time constants. Transients of some components change rapidly while other components evolve on a much longer time scale. Stability in solving such a stiff system is a difficult goal.

Usual integration methods, such as Runge-Kutta, Bulirsch-Stoer, and predictor-corrector, all fail in dealing with the system of this kind, because the stability of these explicit integration schemes is controlled by the most rapidly varying component: to follow the long-term behavior, time steps must be on the short time scale, and this remains true even after the fast transients have disappeared[P1]. When the time scales vary by many orders of magnitude, such as the situation in nuclear systems, the large number of steps for long-term simulation leads to prohibitively laborious integrations, not to mention large accumulated roundoff errors.

An implicit integration approach is essential to obtaining the stability of the stiff system above. Use of high-order implicit methods has the potential to allow a large time step to be used. To further assure the accuracy of the solution, a sophisticated error control scheme must be implemented[G1]. In sum, the goal of the GTSim development is the full-scale, simultaneous modeling of the MGR-GT with a sophisticated solution approach capable of simulating a broad range of transients. Its capabilities should enable future applications in control system design and transient analysis, in future MGR-GT design development, and eventually in the license process. With the GTSim available, the next contribution of this

study is the control system design and transient analysis for the MGR-GT, which are described separately in the following.

1.2.1b Control of the MGR-GT

The direct-cycle MGR-GT presents several unique control requirements. Unlike nuclear steam turbine systems, the inseparable and near-instantaneous coupling of the reactor cooling and the turbomachine operation demands direct interactive control of the reactor and electrical output. This control requirement is further constrained by the fact that the high thermal inertia of the core prevents rapid temperature changes of the helium delivered to the turbine. These conditions, along with the high speed operation of the turbomachinery, relatively high flow velocity, compact design, and the unique flowpath are expected to bring distinctive dynamic behavior which must be treated in the control of the MGR-GT.

The control system is designed to regulate reactor power, control electric load and turbomachinery speed, control the temperature of the helium to the turbine, prevent thermal shocks on the plant components during critical transients, and provide automatic control maneuvers for plant startup and shutdown. In addition, the control system provides emergency protection to prevent the components from damage and to mitigate the likelihood of bounding safety events in case of severe accidents. Design criteria for the control system will be based on U.S. utilities' requirements to nuclear gas turbine power plants[Y1]. The ultimate goal is a design of a simple, effective, and efficient control scheme integrated from advanced control methods, most of which were outlined in the previous design study[S1].

In general, control of gas turbines may rely on the inventory or pressure control for power regulation, especially in small plants. While power control could be accomplished through inventory control to meet most of load control requirements, it also enables gas

turbine plants to have high efficiency of operation at partial power levels. However, the study shows that this control would have a limited capability to meet load increase demand for direct-cycle gas turbine plants if the typical inventory increase scheme of LP-pressure helium feeding were used. Under the conditions of the MGR-GT, it has been shown that the load increase rate larger than 1%/min could not be met by using the inventory control alone[1]. Therefore, other control modalities need to be employed to meet the requirement of faster load increase demand.

Bypass control is one of the possible solutions to accomplishing rapid control actions. This method, however, degrades the plant performance at partial power levels. For instance, under MGR-GT conditions with bypass control, an electrical output of 50% would require a reactor output of 90%. More to the point, about 60% of the 200 MW reactor thermal power would still be required for maintaining the system at its idle state[2]. Efforts have to be made to develop a solution that is capable of satisfying the requirements of both efficiency of operation and effective power control of the MGR-GT.

In reactor control, the reactor power is regulated by moving control rods. It is desirable to maintain the minimum changes in the fuel temperature during normal power manipulation, in order to avoid excess thermal transient and temperature re-distribution in the core. This approach is particularly favorable for a core with a strong temperature coefficient, like the one in the MGR-GT, because large excursion of fuel temperature from its design value would result in large changes in fuel resonance absorption that could make the manipulation of the reactor power very difficult.

In addition to plant power regulation, it is intended to establish optimum procedures

---

[1]Conclusion is drawn by this study.

[2]Results are based on the calculations by this author, and details can be found in the transient analysis included later in this report.

for plant startup and shutdown. An intrinsic property of gas turbine power plants is that for startup it must be powered by an external source to attain a rotational speed at which the compressor is able to develop a sufficient pressure ratio to allow the turbine to produce the power needed to achieve a self-sustaining running status and further accelerate toward design speed. In the MGR-GT, it is intended to use the generator with external electrical power source to drive the turbomachinery up to 3,600 rpm of synchronous speed. At this speed, it requires raising the reactor power to increase the turbine inlet temperature and to establish the thermal conditioning for the reactor core. The development of the low-speed control and the least external powering method for the startup of the MGR-GT is intended. For shutdown, it is desirable to have the capability to operate the turbomachinery with the control system to continue the circulation of the helium through the core in order to help the removal of decay heat.

Finally, a plant protection system will also be designed based on the protection logic defined for a set of selected accidents. However, only the consideration of investment risks, not the safety concern, is required for such a system. The design of the protection system is intended to define a suitable functioning sequence to handle each of the accidents selected, in order to prevent the major components from damage and to mitigate the possibility of developing into bounding safety events.

1.2.1c Dynamic Analysis

For further design development of the MGR-GT, investigations of the MGR-GT transient pressure, temperature, mass flow, output, and machinery speed during various conditions must be carried out for several reasons. First, the maximum pressure gradients are of major interest in respect to the stresses imposed on the thermal insulations and other delicate components during dramatic pressure transients such as emergency shutdown or

rapid system depressurization. In the MGR-GT, the thermal insulations are applied on the walls of inner pipes of two concentric crossducts connecting the reactor and power conversion units. The insulations isolate the hot helium flow from reaching the steel pipes, which are maintained at the temperature of cold helium leg. For design consideration, the highest possible pressure-induced stresses must be known for these thermal liners.

Furthermore, excessive thermal shock during critical pressure transients must be prevented for the metallic components, especially for the LP-recuperator inlet receiving exhaust flow of the turbine. Information regarding thermal conditions on these components is required for establishing design criteria. For instance, a quick loop shutdown causing sudden reduction of the turbine pressure ratio could result about 150°C temperature increase in a few seconds[3]. This large thermal gradient is normally suppressed by introducing the cold helium from the downstream of the compressor to mix with the hot helium flow before it contacts the LP-recuperator inlet. Still, the recuperator is subjected to a very complicated and critical thermal transient not only at the LP-recuperator inlet, but also along the entire length of the recuperator. The uncovering and mitigation of dramatic thermal transient conditions is crucial to the design of the recuperator.

Other areas of interest in transient analysis include the study of the turbomachinery rotor dynamic behavior after a shaft break, the slow and rapid system depressurization resulting from pressure boundary rupture, and the effectiveness of afterheat removal by driving the turbomachinery to circulate the helium through the reactor core. There are, of course, other issues. However, the GTSim was given sufficient flexibility in its development that the simulation of other interesting events with the GTSim is allowed without any major modification to the code.

---

[3]Calculated for the MGR-GT in this study.

1.3 The Organization of this Report

In chapter two, a preliminary analysis of MGR-GT dynamic characteristics is given to study those design features that have appreciable impacts on the MGR-GT transient behavior and therefore must be considered in the modeling and control of the MGR-GT later in this study.

Chapter three is intended to select candidate control methods for the MGR-GT. The chapter starts with a theoretical analysis for power control principles of nuclear gas turbine plants. Based on the principles described, potential control methods for nuclear gas turbine power plants will be introduced and analyzed. Both the benefits and disadvantages of individual control methods for use in the MGR-GT will be examined, so that appropriate control methods can be identified. The control methods selected were incorporated into the MGR-GT system model as described in the following chapter, and evaluated before being integrated into an overall control system for the MGR-GT.

Chapter four presents the process followed during the development of the GTSim. The chapter demonstrates a methodology that consistently governs each evolutionary step of the code development to ensure that the requirements of the code development are met. The requirements of the code are defined by a list of transients which the GTSim will simulate. Having defined the code requirement, the MGR-GT power plant were modeled at the system level. The construction of the system model had substantial effects on the design of the code structure and algorithms which were designed once the system model was fixed. And then the modeling of major components which also includes numerical and symbolic modeling of the control system was pursued. Finally, implementation and validation of the full-scale GTSim code were carried out.

Chapter five describes various simulations for evaluating the MGR-GT dynamic and control characteristics. The evaluation covers a set of operational events as required by U.S.

utilities for nuclear gas turbine power plants, and a number of selected design and beyond design basis accidents. The simulation of these events is intended to demonstrate some of prominent design features of the plant design, and to address a few accident conditions unique to the concept of the MGR-GT.

Chapter six summarizes the important conclusions of this study. In addition, further development in the simulation of the MGR-GT is recommended. The application of GTSim to future MGR-GT design development is suggested.

References

[C1] Covert, R.E., J.M. Krase, D.C. Morse,"Effect of Various Control Modes on the Steady-State Full and Part Load Performance of a Direct-Cycle Nuclear Gas Turbine Power Plant," ASME 74-WA/GT-7.

[G1] General Atomic "REALY2: the GT-HTGR Transient Performance Analysis Program," GA-A13880, G.A. Backus, L.C. Cheng, M.Z. Croft, E.A.Estrine, F.L. Openshow, T.W. Schoene, March, 1976.

[G2] Greg, P., Gas-Cooled Reactor Associates, Personal Correspondence, 1988.

[H1] Hewing, G.,"Studies on the Operational and Control Behavior of HTR-Helium Turbine Plants," (in German), Ph.D. Thesis, TH Aachin, February 1975, and JUL-1206, 1975.

[K1] Kaburaki,H., L. M. Lidsky:"The effect of Regeneration on the Cycle Thermal Efficiency of Nuclear Direct Cycle Power Plants", MIT Department of Nuclear Engineering, 1985.

[L1] Lidsky, Lawrence M., D.D. Lanning, J.E. Staudt, X.L. Yan, H. Kaburaki, M. Mori,"A Direct-Cycle Gas Turbine Power Plant for Near-Term Application: MGR-GT", presented at the 10th International HTGR Conference, San Diego, Calif., September 19-20, 1988.

[M1] Melese, G., R. Katz,"Thermal and Flow Design of Helium-Cooled Reactors," American Nuclear Society, 1984.

[P1] Press, H.W., S.A. Teukolsky,"Integrating Stiff Ordinary Differential Equations," Computers in Physics, May/Jun 1989.

[S1] Staudt, James E., L. M. Lidsky "Design Study of an MGR Direct Brayton-Cycle Power Plant" MITNPI-TR-018, May 1987.

[S2] Staudt, James E., L. M. Lidsky "An MGR Brayton-Cycle Power Plant Design", presented at 22nd Intersociety Energy Conversion Engineering Conference, Philadelphia, Pennsylvania, August 10-14, 1987.

[Y1] Yan, X.L., L.M. Lidsky,"Control System Design and Dynamic Study of the MGR-GT Power Plant: progress report II on Development of the GTSim Simulation Program," MIT, September 1988.

Chapter Two

Dynamics of the MGR-GT

2.1 Introduction

The MGR-GT is a power plant based on a highly-heat-regenerated Brayton-cycle, consisting of a passively-safe 200 MW pebble bed reactor[1] cooled with high-pressure helium, a single-unit compression and expansion turbomachine directly driving a generator at a rotational speed of 10,000 rpm, a compact, heavily-finned, counterflow recuperator, and a tube-and-shell, helium-to-water, crossflow precooler. All rotating machinery is on a common shaft, possibly supported by active magnetic bearings. Frequency conversion is accomplished by solid-state electronics which converts the plant power output from 167 Hz to 60 Hz.

The dynamic behavior of nuclear direct-cycle gas turbines is mainly determined by the helium volumes in the plant circuit, the thermal inertia of the reactor core, the heat transfer transient behavior of the heat exchangers, and by the characteristics of the turbomachine and the inertial moment on the rotating shaft. The design of the MGR-GT presents many unique conditions that distinguish its dynamic and control behavior from other nuclear direct-cycle gas turbine plants, such as large HTGR-GT. For example, helium inventory control is rarely utilized for the control of large gas turbines. However, since the MGR-GT is a compact system, it is possible to primarily rely on the helium inventory to achieve effective and efficient power control for the MGR-GT. This chapter will present a brief examination of the MGR-GT dynamic and control characteristics to identify the potential problems that must be dealt with

[1]Prismatic core systems could also be used for the MGR-GT, whose thermal cycle is not sensitive to the core configuration.

during subsequent system modeling.

2.2 Basic Process

Figure 2.1 indicates the flow and thermal-hydraulic couplings in the MGR-GT. Starting at the top of the core, the helium enters at about 593°C, flows down through the pebble bed core, and exits at 850°C. At the bottom of the core, the helium passes through a thermal mixing channel to enable the helium to develop uniform temperature streamlines so as to avoid thermal stresses on the adjunct inner pipe of the lower concentric crossduct. Leaving the bottom plenum of the core and flowing into the pipe, the high pressure helium enters the turbine inlet plenum. After being expanded inside the turbine, the helium is exhausted at 610°C and 4.0 MPa into the upper manifolds and ducts of the LP-recuperator inlet, where it is separated and directed into four recuperator modules around the turbine casing. After transferring the heat to the HP-recuperator helium flow, the helium exits the recuperator at 162°C into a large annular cavity containing the recuperator modules, as shown in Figure 2.2. The helium leaves the cavity and travels through the pipe toward the inlet of the precooler. After passing through the tubes in the precooler core and rejecting its residual heat to the water flowing upward inside the tubes, the helium is cooled down to 30°C and induced into the suction of the compressor. The compressor compresses the helium to 8.0 Mpa at a temperature of 137°C and discards it into the large volume housing the compressor casing and the recuperator manifolds and ducts.

At the bottom of this volume, the helium flows through the outer passage of the upper concentric crossduct connecting the reactor system with the power conversion system, and travels downward the annular channel formed by the reactor pressure vessel and core barrel. By sweeping the inner wall of the pressure vessel, the helium maintains the average temperature of the vessel at 142°C during normal operating conditions. At the bottom of the

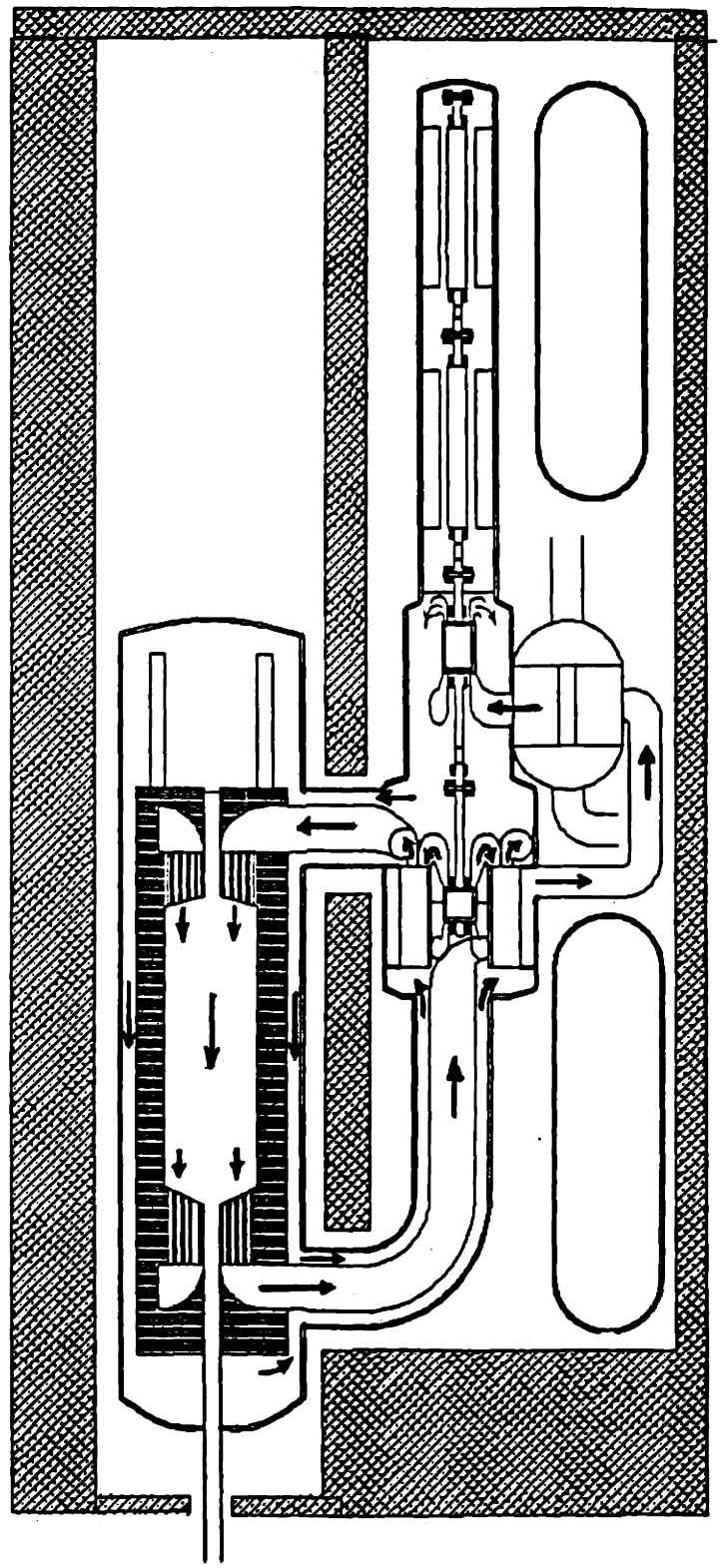

Figure 2.1 The MGR-GT design configuration and flowpaths

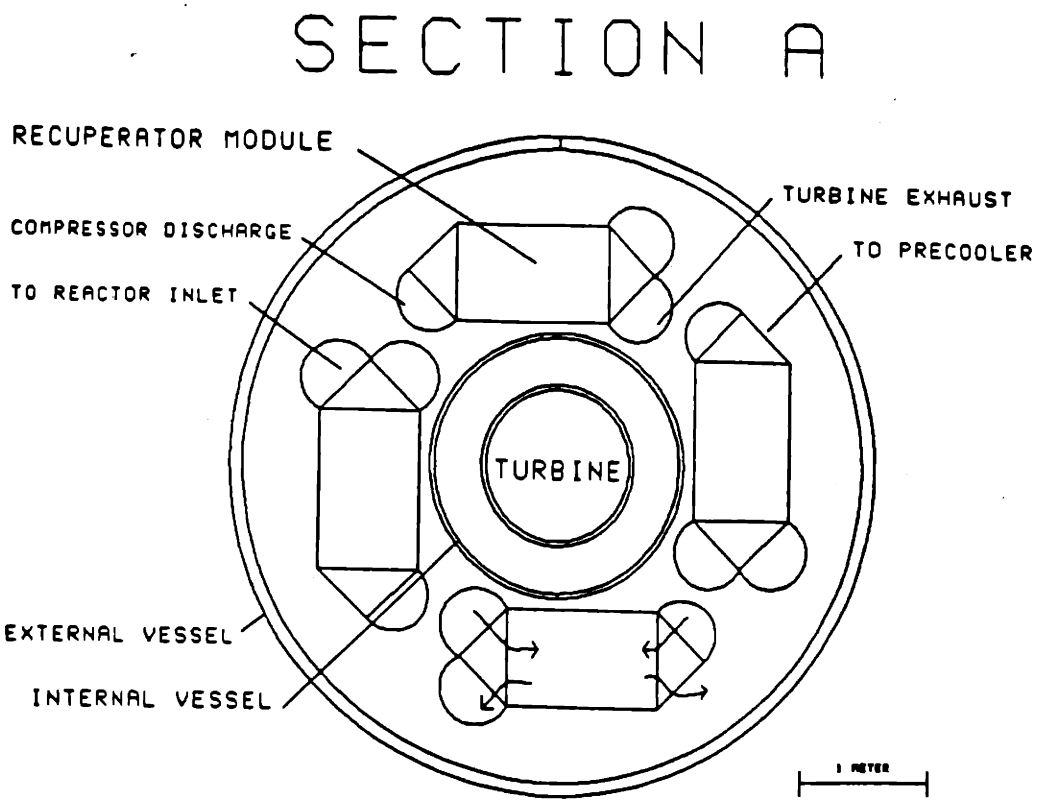

Figure 2.2 Cross-section of the MGR-GT machinery module [S1]

channel, the flow is turned into the outer passage of the lower concentric crossduct and guided up toward the HP-recuperator inlet. The helium flows through the LP-recuperator, recovering the heat from LP-recuperator flow, and exits the recuperator into the upper manifold and ducts. It flows through the inner pipe of the upper concentric crossduct and enters the top plenum of the core, where it will again flow downward the core to begin a new journey.

The primary system flow path is configured such that the pressure boundaries are maintained at cold helium temperature during normal operations. The temperature of the reactor vessel swept by the compressor discharged helium is kept at 142°C, which may be lower than the temperature desirable for the current vessel material, i.e., SA-533. Efforts are being made to resolve this issue. As the helium passes through the annular channel between the pressure and core vessels, it is heated up, resulting in an increase of helium temperature at the HP-recuperator inlet. This increase in temperature is about 10 degrees centigrade, which has little effect on the efficient performance of the overall cycle. This can be explained in the following: First, the temperature of the helium toward the reactor core inlet is effectively maintained by the turbine exhaust helium entering the LP-recuperator inlet. As a result, the core thermal and power conditions will not be altered. Furthermore, the HP-recuperator inelt temperature increase due to the helium heatup in the reactor annular channel causes the corresponding minor increase at the LP-recuperator outlet. However, the extra heat loss to the precooler water, resulting from the temperature increase of the helium at the LP-recuperator outlet, is the heat recovered in cooling the reactor vessel. This means that if the temperature of the vessel were higher, in absence of the reactor vessel cooling, this amount of heat would be lost anyway, as a result of increased radiation for the surface of the reactor

vessel to the air cooling panel on the wall of the reactor silo[2].

The high operating temperature requires thermal liners to be placed on the inner pipes of two concentric crossducts whose outer pipes are maintained at cold helium temperature during normal operations. Complex thermal stresses imposed on the insulation, along with potential natural heat circulation inside the thermal liners due to large temperature differences across the thermal liners, make this a difficult design problem.

System pressurization could be anticipated in the lifetime of the MGR-GT. It could be caused in different ways, for instance, loss of forced circulation followed by the reactor core heatup. Over-pressurization is prevented by pressure-relief valves, which are designed to open passively when the system pressure exceeds the preset value. Another potential problem is the development of thermal-induced reverse flow from the reactor core. Studies in other systems have shown that this reverse flow could be significant such that it might reach the reactor pressure vessel, raising the vessel temperature beyond its design limit. For instance, calculations for a 250 MW pebble-bed steam-plant MGR developed by General Electric Company showed that the reverse flow in a pressurization system could increase the vessel temperature to a peak of 380°C after 60 hours[W1]. Such temperature reached by the vessel would violate (by a small margin) the maximum permitted temperature allowed for SA-533 low-alloy steel of the vessel material by the current design code, 371°C.

However, the MGR-GT flowpath is very different from that of the steam-plant MGR. The MGR-GT sinuous flowpath creates additional flow resistance. It can be expected that any reverse flow during system pressurization would be much less than that in the steam-plant MGR. In addition, 2-1/4 Cr-1Mo steel, which is better in sustaining high temperature and neutron damage, may be used to replace SA-533 as vessel material.

---

[2]The water cooling system receives radiation heat from the surface of the reactor vessel and removes it out of the reactor silo to the environment through natural convection. No active system is required.

On the other hand, in the event of a break on the system pressure boundaries such as the rupture of two concentric crossducts, the system would experience a slow or rapid system depressurization, depending on the size of the break. The flow configuration in the MGR-GT presents three postulated scenarios of depressurization, *i.e.,* two on the upper and lower crossducts, respectively, with the third simultaneously on both crossducts.

2.3 Reactor system

Major components of the MGR-GT reactor system include a pebble bed core, contained by graphite reflector structure, a control rod system, a small absorber sphere shutdown (KLAK) system, and the fuel element supply and discharge lines. The fuel bed and reflector are enclosed by a core vessel which is located inside the reactor pressure vessel. The MGR-GT reactor evolved from the baseline design of the German INTERATOM/KWU MHTGR for a steam plant[8]. A schematic diagram of the German plant is shown in Figure 2.3. Except for the difference in their flowpaths, major design parameters of two reactor systems are nearly identical. These parameters have been listed together in Table 2.1 for comparison. It should be pointed out that the MGR-GT fuel enrichment has been slightly increased to compensate for increased resonance absorption at the higher core temperature, *i.e.,* 593-850°C in contrast to 250-700°C in the German core[11].

2.3.1 Reactor Core

Traditionally, reactors are designed for a specified power output. Engineered safeguards and other measures are then provided to prevent malfunction and to limit the consequences of severe accidents to ensure that no unacceptable levels of radioactivity is released to the environment. The approach results in a redundant, active, safety-class control and protective system that is formidably complex, in terms of its design, construction, and

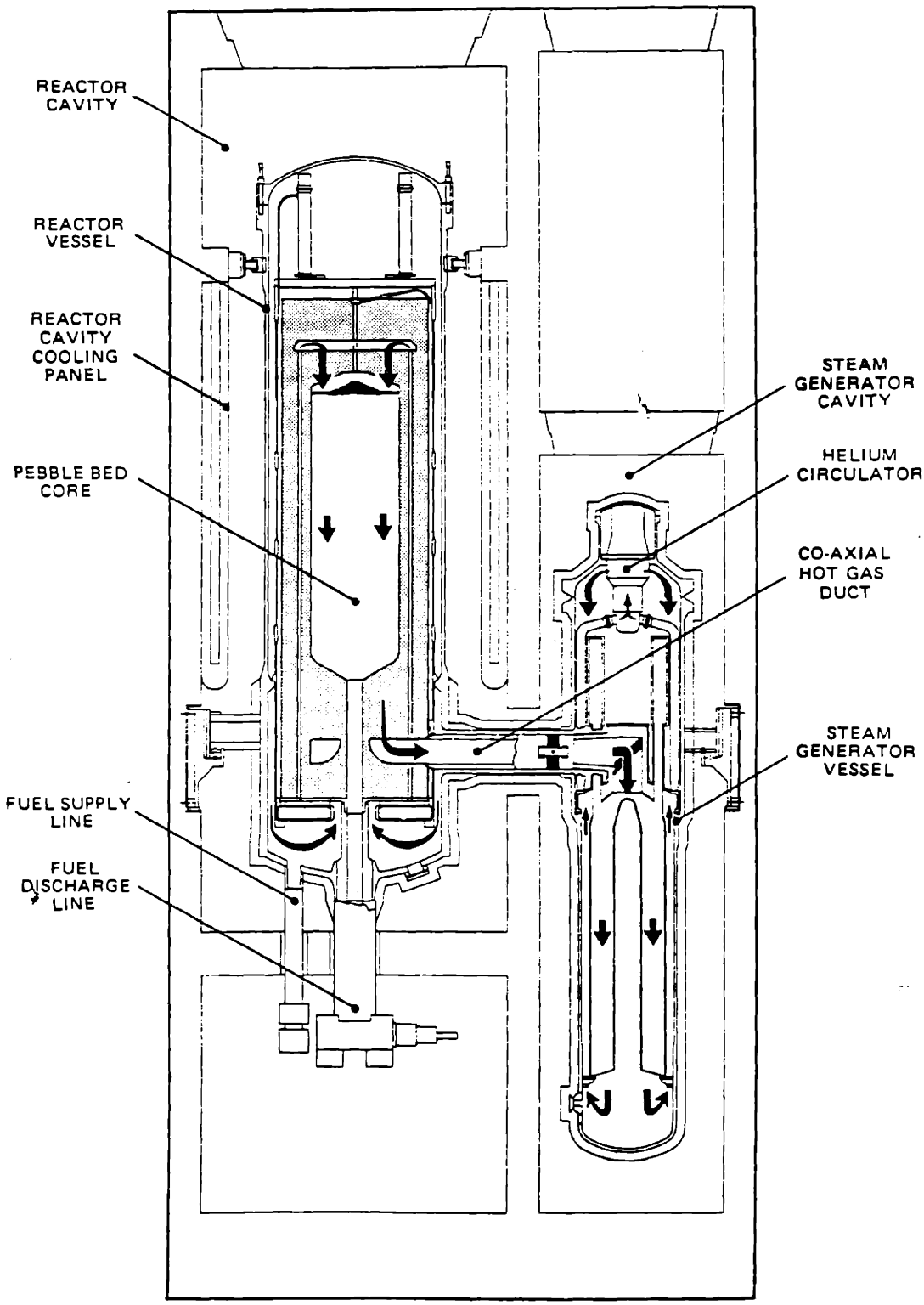

Figure 2.3 INTERATOM/KWU reactor module[A1]

Table 2.1

MGR-GT and Interatom/ KWU Reactor Design Parameters

MGR-GT Reactor		Inter/KWU Reactor	
Thermal Power	200 MW	Thermal Power	200 MW
Core Diameter	3.0 m	Core Diameter	3.0 m
Mean Core Height	9.43 m	Mean Core Height	9.43 m
Average Power Density	3.0 W/cm3	Average Power Density	3.0 W/cm3
Coolant Temperature	593/850 C	Coolant Temperature	250/700 C
Coolant Pressure	8.0 MPa	Coolant Pressure	6.0 MPa
Helium Flow Rate	46.2 kg/s	Helium Flow Rate	85.4 kg/s
Pressure Drop	2.56%	Pressure Drop	2.50%
Fuel-Cycle	U-Pu	Fuel-Cycle	U-Pu
Number of Fuel Pebbles	358,000	Number of Fuel Pebbles	360,000
Enrichment	7.50%	Enrichment	7.30%
Heavy Metal per Pebble	7 g	Heavy Metal per Pebble	7 g
Core K-eff	1.0057	Core K-eff	1.009
Number of Control Rods	6	Number of Control Rods	6
Number of Absorber Sphere System	18	Number of Absorber Sphere System	18

operation.

A different approach has been adopted for the design of the MGR. The core diameter and power density are consciously chosen to ensure that neither an afterheat removal system nor an active shutdown system is needed, and that the maximum fuel element temperature does not exceed 1600°C under the worst possible accident conditions[3]. Afterheat removal is achieved solely by natural heat conduction and radiation from the inner core to the reflector and thereupon through the pressure vessel wall to the surface water cooling coils. Reactivity excursions are limited by the negative temperature coefficient, and reactor control is executed by neutron-absorbing devices acting exclusively within the side reflector region to avoid absorber rods penetrating the pebble bed.

To meet these requirements, the core diameter is limited to 3 m and the permissible average power density to about 3 W/cm^3. The core height is based on control rod dimensions, in-core residence time of fuel elements, burnup, and power distribution, resulting the active core height being 9.34 m and thus the total power 200 MW[R1].

Several studies have shown that the MGR core is able to survive the worst case of accident, *i.e.*, loss of coolant with no scram, without the fuel temperature exceeding the 1600°C limit. For example, Figure 2.4 is the result of the calculation performed for the temperature transients in the MGR-GT core during such an accident[I1].

2.3.2 Reactor Control

In the baseline design, the reactor power is controlled by six gravity-driven absorber rods of 5 m each in length, which move loosely in channels in the side reflector. The reactivity worth of the control rods is sufficient for operational maneuvers and for the hot

[3]Fission product release through the silicon carbide (SiC) layer of the coated particles inside the fuel pebble only occurs at temperatures > 1600 °C [3]

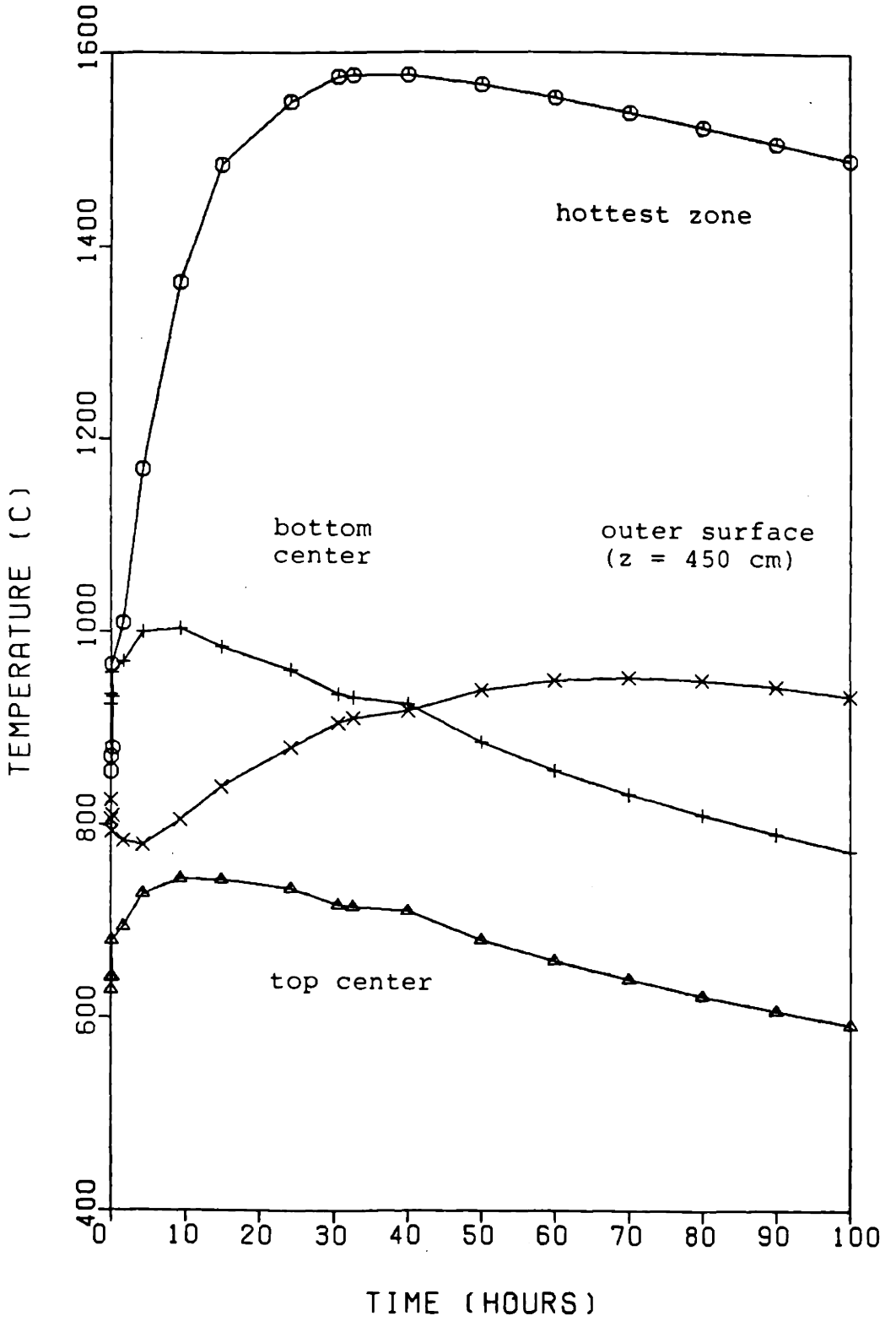

Figure 2.4 Temperature behavior of the MGR-GT reactor core following a postulated depressurization accident [I1]

shutdown of the reactor. A further absorber system is needed and is provided to keep the reactor subcritical at ambient temperature. It consists of small borated balls that are stored in 18 containers above the reflector. On demand, the small absorber balls are gravity-fed into channels of the reflector that are located near the inner reflector surface. The small absorber balls are also used to compensate for the fuel temperature change during reactor startup and to compensate for lack of Xenon buildup in the initial core or during extended periods of operation at reduced power levels. Details of the two separate reactor control systems are shown in Figure 2.5[A1].

The control rod system is effectively six independent subsystems. Each subsystem consists of a drive mechanism with a pipe passageway for the rod to be lowered into or raised out of the side reflector. For power regulation, the drive mechanism can move the control rods at a maximum speed of about 1 cm/s. It takes about 10 minutes to move a rod through its full passageway in the lateral reflector.

Eighteen separate subsystems comprise the small absorber sphere shutdown system. Each subsystem consists of a canister with an electro-magnetic release mechanism. Upon release it takes about 1 minute for the spheres to drop from the canister to fill the channels, and approximately 3 minute to clear one channel over the length of the core. The small sphere shutdown system is designed to be able to clear only one channel at a time, avoiding excess reactivity excursion due to possible malfunction.

Both control systems are designed to be fail-safe. If power to ether system is lost, that system will inherently scram. It takes about 13 seconds for the control rods to drop, under gravity , to full insertion, and 1 minute for the spheres to fill up the channels.

2.4 Power Conversion System

The power conversion system includes all components exclusive of the reactor

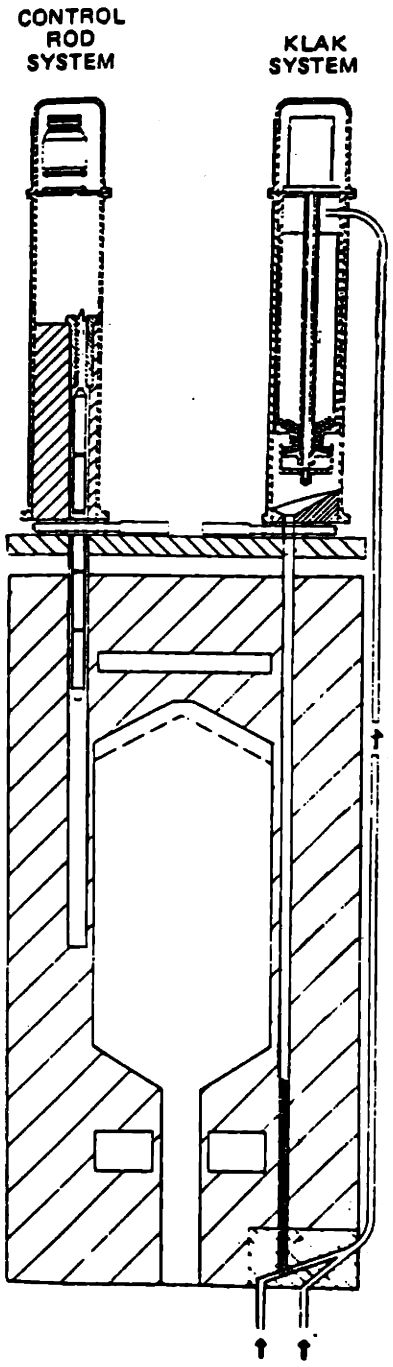

Figure 2.5 Reactor reactivity control and shutdown systems [A1]

system. Figure 2.6 shows the MGR-GT power conversion system with components labelled and flowpath indicated. It consists of a high speed turbomachine (power turbine and compressor) on a single shaft driving a submerged high-pressure-helium cooled generator at a speed of 10,000 rpm, a compact 4-module plate-fin recuperator surrounding the turbine casing, and a simple tube-and-shell precooler. All machinery and heat exchangers are contained in the power conversion system vessel with a largest diameter of 3 meters at the location of the turbine casing.

The dynamic behavior of the MGR-GT is mainly determined by the helium volumes in the plant circuit, the heat capacity of the reactor core, the heat transfer transient behavior of the heat exchangers, and by the characteristics of the turbomachine and the moment of inertia of the rotational shaft. The most important consideration dominating dynamics and control are that the core cooling flow and turbine flow are directly related so that changes in flow affect core cooling as well as turbine power and that the high thermal inertia of the core prevents rapid changes in the turbine inlet temperature. For example, a 20 MW change in the core power would cause the change of the temperature at reactor outlet less than 2°C/min, which virtually limits the rate of the temperature change of the helium delivered to the turbine[S1]. Thus, it is common in nuclear gas turbines to largely rely on flow bypass and mass inventory for regulating the turbine power to match the output demand. The dynamic characteristics of major components in the power conversion system are described below.

2.4.1 Turbomachinery

In the MGR-GT, all its rotating machinery is on the same shaft, with solid couplings between each of the machines. Supported vertically by a group of radial and thrust magnetic bearings, the turbomachinery is oriented to minimize the thrust load on the thrust bearings by opposing the machinery weight with the net aerodynamic thrust of the turbomachinery.

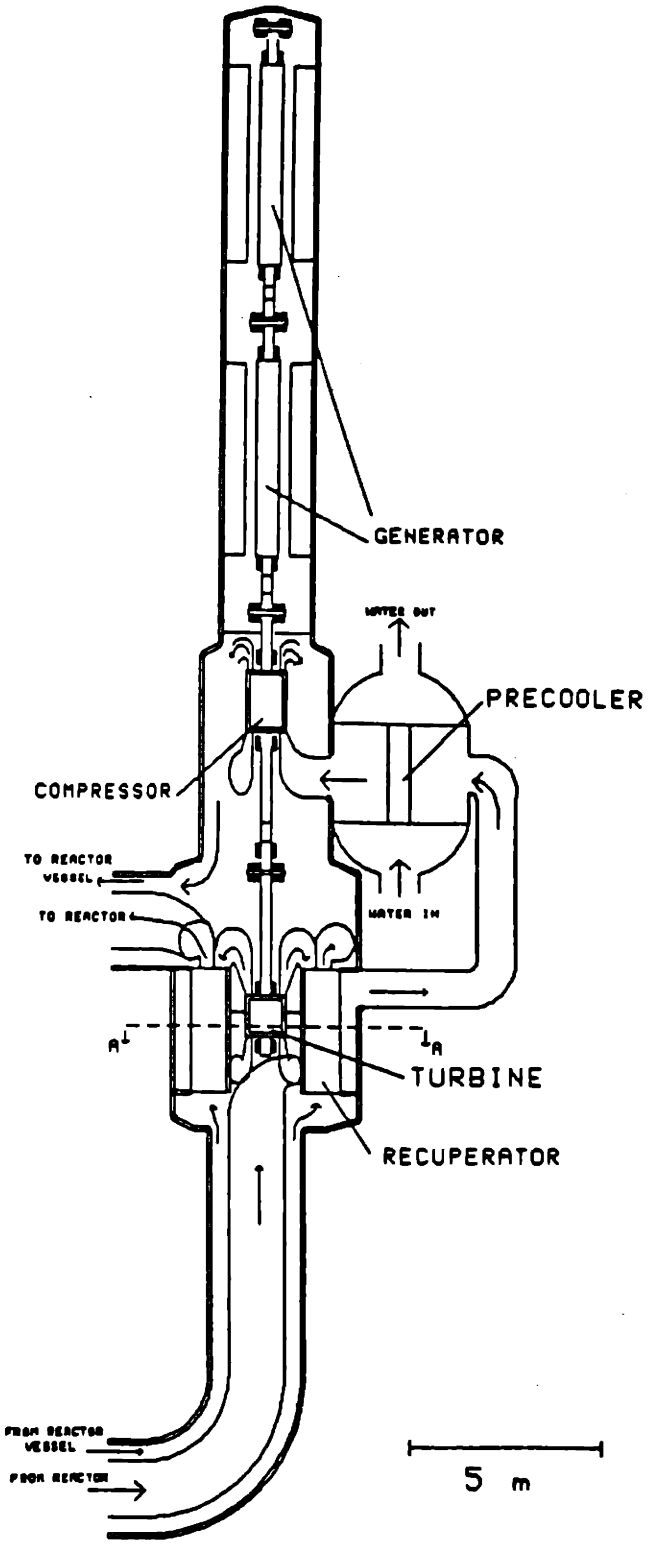

Figure 2.6 The MGR-GT machinery module [S1]

The operation of high-speed rotating machinery in the vicinity of the reactor raises concern over the consequences of a turbomachine rotor failure that could throw missiles and potentially damage the reactor. A catastrophic failure of a rotating machine can be caused in several ways. For instance, possible dynamic imbalance caused by loss of rotor sectional mass such as blading, as a result of excessive overspeed, could induce severe rotor vibration that would damage the rotor. In the MGR-GT, however, the rotor is supported by the active magnetic bearings that would consistently monitor the rotor dynamic performance, with signals fed into the bearing servo control systems. The control systems could effectively negate the bearing stiffness, allowing the rotor freedom to spin about its dynamic, rather than geometric, inertial axis at all times. Critical speeds of the rotor would also be actively controlled. These are major contributions of the magnetic bearing technology to the high speed machinery. If the magnetic bearings fail to function, the dynamic braking capability of the MGR-GT generator could be used as a backup means to quickly stop the machinery, in addition to other normal plant protective actions provided by the plant protection system such as loop shutdown.

It is of great interest in the considerations of investment risk (not a safety concern) to study the consequences of a shaft break. Shaft break is a common postulated accident for gas turbines, especially for single shaft turbo-generator units like the one in the MGR-GT. In the event of generator failure, tremendous forces would quickly be imposed upon the shaft and thus could cause a shaft break, most likely at the location between the turbine and the compressor where the torque is largest. In this case, the overspeed of the turbine, being at full power and speed but virtually zero load is expected to be tremendous. In case of such shaft break, overspeed protection by the magnetic bearings and the generator braking is impossible. Thus, other effective protection must be provided to prevent the turbine overspeed beyond its destructive limit. There are other possible arrangements which would

obtain a more uniform distribution of the torque along the shaft, thus reduce the likelihood of a shaft break. For example, placing the turbine in between the compressor and generator would not only satisfy this purpose but also increase the turbine rotor inertia to reduce overspeed, since, after shaft failure, one of the machines, either the compressor or the generator, would always connect with the turbine, depending on the location of the break. If the compressor is connected with the turbine, an inherent prevention of destructive overspeed might be developed, from aerodynamic point of view, by properly designing the characteristics of the machines such that the compressor would consume more power than that the turbine could produce before reaching the level of destructive overspeed. But any change in the current machinery arrangement would demand re-configuration of the flowpath. In any event, for the consideration of investment risk, the shaft breaks under various rotor configurations will be investigated in this study.

2.4.2 Generator and Electrical System

The MGR-GT generator design was performed by Toshiba Corporation[T1], based on the company's industrial supermotor technology. As shown in Figure 2.7, it consists of two 50 MW generators coupled in tandem to produce the output of 100 MW. The generator is supported by 2 set of radial magnetic bearings and 1 set of thrust magnetic bearings. The size selected for the current design of radial bearings is approximately 300 mm in diameter and the size of thrust disc of thrust bearings is 500 mm. The problem of rotor critical speed can be solved by the use of active magnetic bearings. The generator is cooled in stagnant helium with a pressure at 8.0 Mpa. The windage loss of the rotor in such high pressure environment is very high, and, in fact, contributes 60% of the total loss of the generator system.

The generator operates at 10,000 rpm. To convert the generated high frequency to

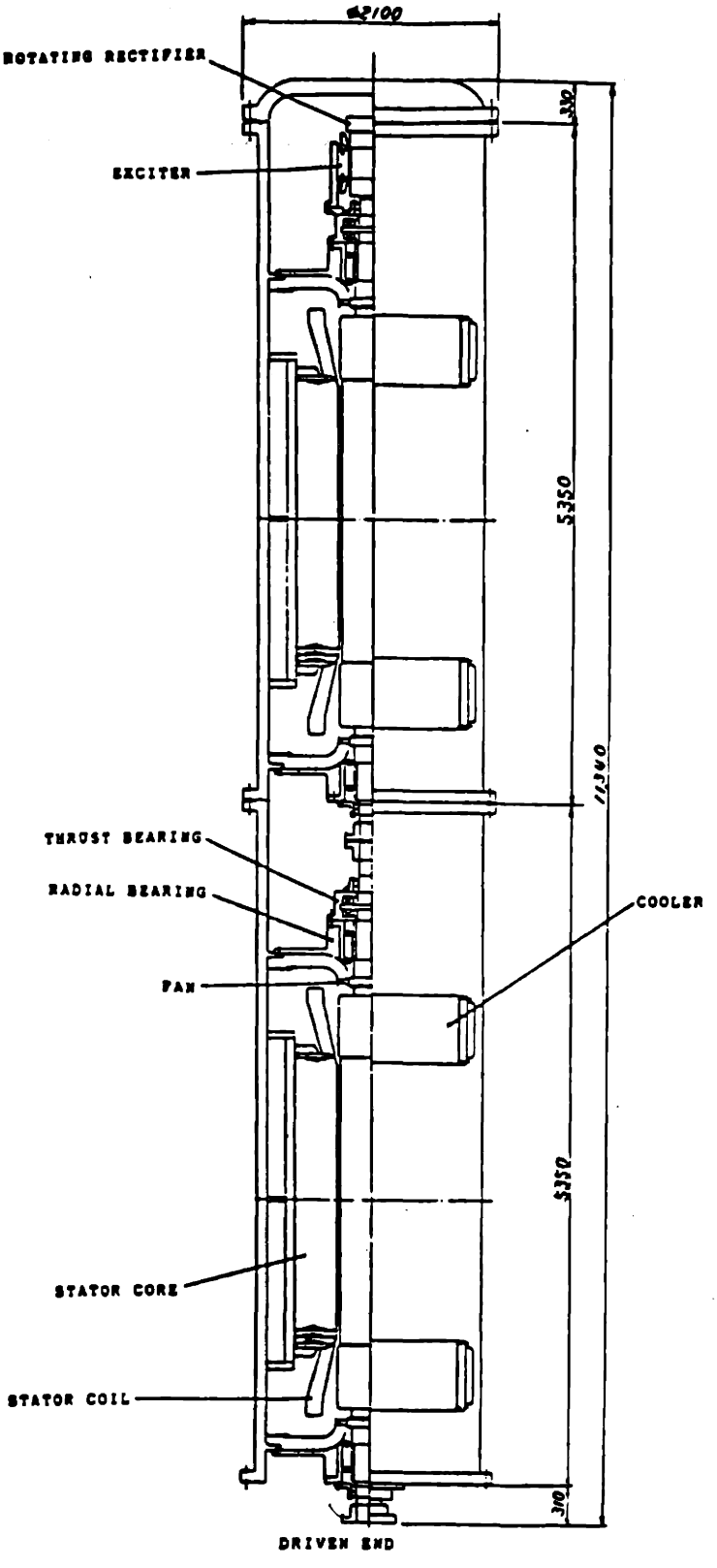

Figure 2.7 The MGR-GT generator [T1]

60 Hz, a Line Commutated Converter-Inverter (LCI) is used. A simplified diagram for this device is shown in Figure 2.8, which consists of a rectifier panel, a DC bridge, an inverter panel, and three winding transformer. The DC bridge of the LCI has access to a dummy DC load, which, if connected, could rapidly load the generator to offset a sudden loss of AC load and to prevent the turbine from overspeed.

In addition, the generator may be operated as a motor to drive the turbomachinery up to 3,600 rpm during plant startup, and may also be used to spin the machine to circulate the helium for decay-heat removal from the core to the precooler. The maximum power consumed by the generator during these operations will be calculated in this study.

2.4.3 Recuperator

The recuperator used in the MGR-GT is a compact, plate-fin, 4-module heat exchanger placed around the turbine casing. One recuperator module is shown in Figure 2.9[W1]. The baseline recuperator is manufactured from 304 stainless steel which can sustain the high temperature operating condition. The wall of the recuperator experiences a pressure differential of 4.0 MPa during normal operation. The recuperator recovers heat from the turbine exhaust helium with an effectiveness of 95%, raising the temperature of the HP helium to 593°C before the helium enters the reactor core. The magnitude of this internal heat regeneration is on the same order as the reactor thermal input. Because of very strong thermal coupling of the flows at both sides, this compact heat exchanger presents mathematical difficulty in modeling.

2.4.4 Precooler

The MGR-GT precooler shown in Figure 2.10 is a crossflow helium-to-water tube-and-shell heat exchanger cooling the helium flow prior to compression. The flow heat capacity

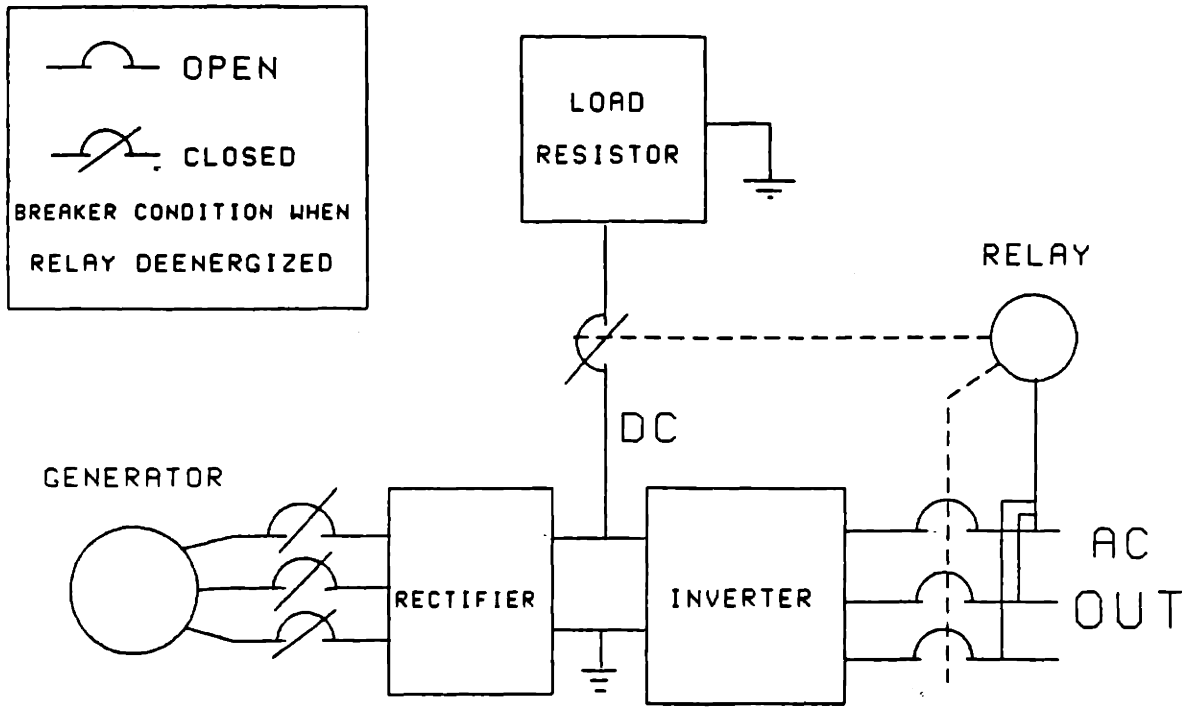

Figure 2.8 The schematic description of the MGR-GT LCI electronics [S1]

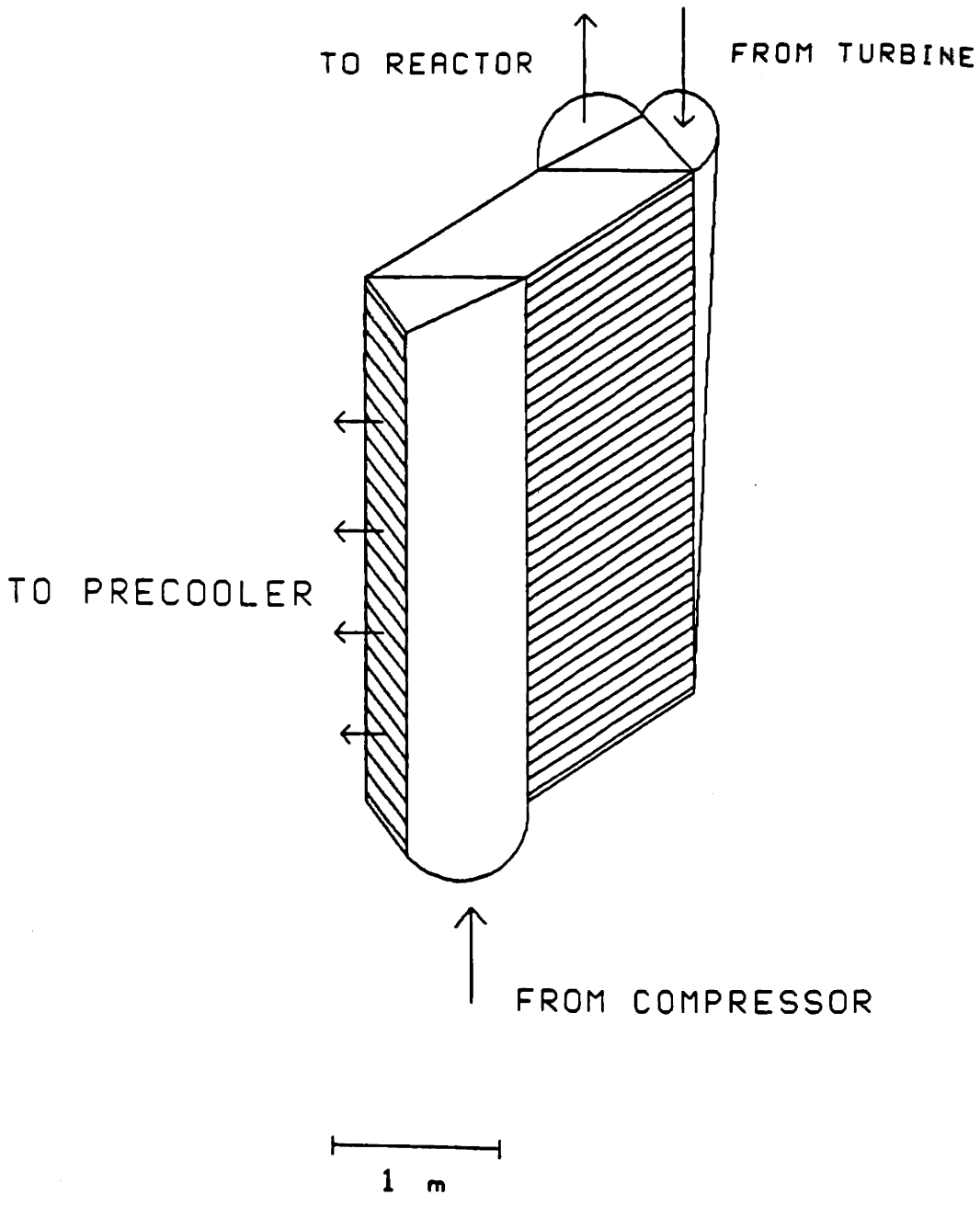

Figure 2.9 An MGR-GT recuperator module[S1]

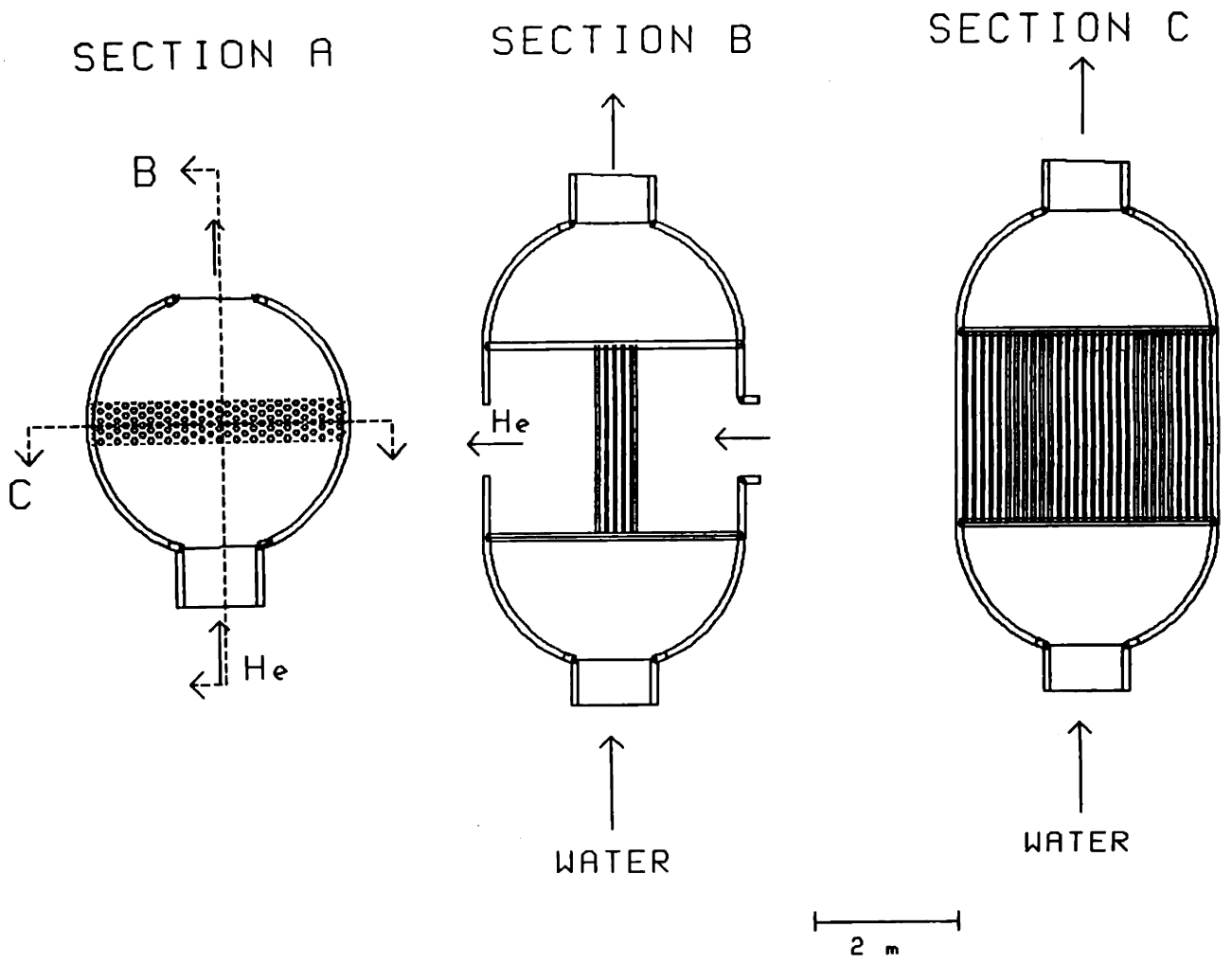

Figure 2.10 The MGR-GT Precooler [S1]

ratio of the helium to the water is about 1/23, resulting a 2,450 kg/s water flow in the tube to cool the helium from 162°C to 30°C.

In the event of a loss of forced cooling water flow, it will be impossible for the MGR-GT to reject its residual heat effectively. However, the precooler of the MGR-GT is configured to allow temperature-induced natural circulation of the water in the tubes. By continuing to circulate the helium with the rotating turbomachinery driven by the generator, it is still possible to move decay-heat from the core to the water in the precooler after the reactor is tripped by the plant protection system (such decay-heat removal is not necessary with regard to the safety of the reactor). The effectiveness of this decay-heat removal will be demonstrated in this study. If the water is completely lost to the precooler, the precooler is not expected to reach a temperature where failure would occur.

Water ingress into the helium flow circuit is considered extremely remote, because the water pressure inside the tubes is maintained well below that of the helium flow in the core of the precooler, and the precooler may use duplex tubes for water flow.

2.4.5 Potential Control Methods

The major control difference between this power plant and other conventional nuclear gas turbines is that active *safety* control is not required in the MGR-GT because it is inherently safe. This greatly reduces the licensing-based requirements of the plant controls. Several advanced control methods have been recommended during the plant conceptual design[S1]. These and other potential control methods will be evaluated in this study.

References

[A1] "An Assessment of the Interatom/KWU Modular HTGR Concept", Gas-Cooled Reactor Associates, Southern California Edison Co., General Electric Co., Combustion Engineering, Inc., Bechtel Group, Inc., September 1985.

[F1] Frewer,H., W. Keller,"The Modular High-Temperature Reactor", Nuclear Science and Engineering, 90 (1985) 411-426.

[I1] Izenson, Michael,"Effects of Fuel Particle and Reactor Core Design on Modular HTGR Source Terms", MITNPI-TR-012, October, 1986

[R1] Reutler, H., G.H.Lohnert,"Advantages of Going Modular in HTRs", Nuclear Engineering and Design 78(1984) 129-136.

[S1] Staudt, James E., L. M. Lidsky "Design Study of an MGR Direct Brayton-Cycle Power Plant" MITNPI-TR-018, May 1987.

[T1] Toshiba Co.,"Feasibility Study of 8,000 rpm - 100 MW Generator For MGR", March, 1987. Original Design was for 8,000 rpm. 10,000 rpm design is currently being evaluated.

[W1] Wu, T.,Cowan, C.L., "Core Heatup Analysis of a small Pebble-Bed HTGR", ANS Trans., vol. 50, November 1985.

Chapter Three

Control System Design for the MGR-GT

3.1 Introduction

It is the intent of this chapter to present a description of the control system design for the MGR-GT power plant. The goal of the control system is the automatic operation of the MGR-GT in accordance with the utility practice for nuclear generation systems[G2], and the protection of the plant components from damage in the event of accident conditions. In addition, it is a basic requirement to develop a control system that is of a simple design with a highly efficient operation over a broad range of power levels.

In this chapter, theoretical background of closed-cycle gas turbine power plant control will be discussed, which then leads to the development of several major control methods. This is followed by a review of the previous application of these methods in control of existing gas turbine power plants. These discussions are intended to develop a suitable approach to the design of the MGR-GT control system, which is the ultimate objective of this chapter.

3.2 Principles of Power Control

MGR-GT operates in a closed-cycle as shown in Figure 3.1, where the helium, as working media, is compressed from P_1 to P_2, heated from T_2 to T_4 when passing through the recuperator and reactor core. Subsequently, it is expanded from P_4 to P_5 in the turbine, giving up a portion of its heat to the HP-flow in the recuperator with a temperature drop from T_5 to T_6, and then is cooled by the water flow in the precooler down to T_1 at the precooler outlet, whereby the cycle is completed.

Based on the perfect gas model and neglecting minor pressure losses in the cycle,

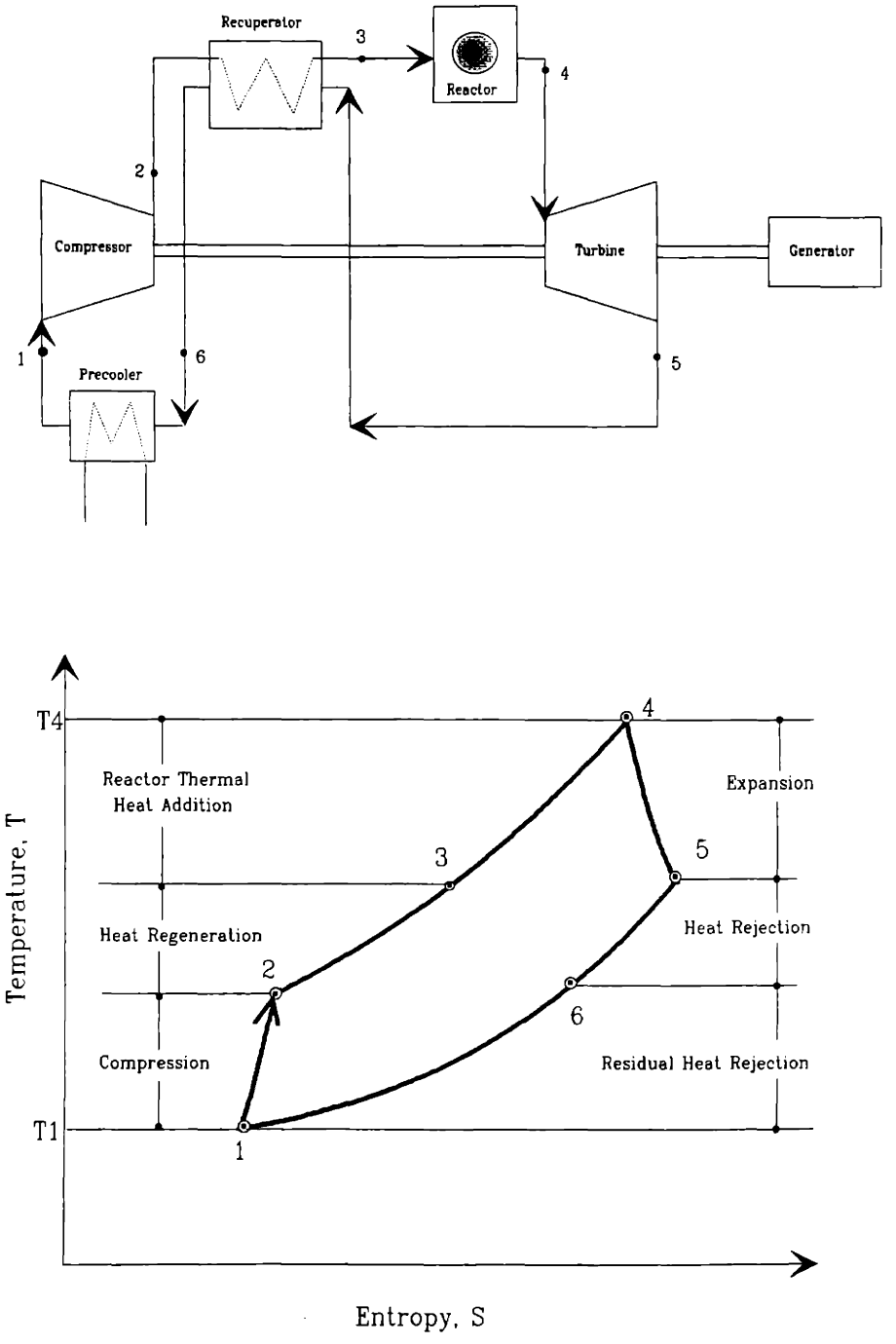

Figure 3.1 Closed Brayton-cycle and T - S diagram

it can be derived that the powers of the turbine and compressor can be given, respectively, by[1]

$$W_T = (\dot{M} C_P T_4)\left(1 - \frac{1}{r_P^{\frac{(\gamma-1)}{\gamma}}}\right)\eta_T \qquad (3.1)$$

$$W_C = \frac{1}{\eta_C}\left[(\dot{M} C_P T_1)\, r_P^{\frac{(\gamma-1)}{\gamma}}\left(1 - \frac{1}{r_P^{\frac{(\gamma-1)}{\gamma}}}\right)\right] \qquad (3.2)$$

where W_T= turbine power,

W_C= compressor power,

$\dot{M}$ = helium mass flow rate,

Cp= helium specific heat at constant pressure,

r_p= cycle pressure ratio,

η_T= turbine efficiency,

η_C= compressor efficiency,

γ = helium gas constant.

The power of the turbine in excess of that required for driving the compressor is the net output of the cycle, which is utilized to drive the generator and equals (W_T - W_C), we have, after simplification,

$$W_{Output} = \dot{M} C_P T_1\left[\left(\eta_T \frac{T_4}{T_1} - \frac{r_P^{\frac{(\gamma-1)}{\gamma}}}{\eta_C}\right)\left(1 - \frac{1}{r_P^{\frac{(\gamma-1)}{\gamma}}}\right)\right] \qquad (3.3)$$

The thermal input of the reactor to the cycle is

---

[1]Many text books on general thermodynamics have detailed analyses for closed-cycle gas turbine power systems. One example, for instance, is [W2].

$$\dot{Q}_{th} = \dot{M} C_P (T_4 - T_3) \tag{3.4}$$

If the use of a recuperator with an 100% effectiveness is assumed in the cycle, which could raise the compressor outlet temperature T_3 to the turbine exhaust flow temperature T_5, the thermal supply to the cycle would be

$$\dot{Q}_{th} = \dot{M} C_P T_4 \left(1 - \frac{1}{r_P^{\frac{(\gamma-1)}{\gamma}}} \right) \eta_T \tag{3.5}$$

The cycle thermal efficiency can thus be determined by the standard definition of

$$\eta_{th} = \frac{W_{Output}}{\dot{Q}_{th}} \tag{3.6}$$

From these equations, it is now possible to identify those key parameters having potential influences on the cycle power output and efficiency. It can be seen from Eqn. (3.3) that the output of the plant power is determined by the mass flow rate of the helium, M, the inlet temperatures of the compressor and turbine, T_1 and T_4, respectively, the machinery efficiencies, η_C and η_T, and the cycle pressure ratio r_p, while the plant efficiency depends on all but the helium mass flow rate.

First, and foremost, it is recognized from Eqn. (3.3) that the power output of the plant is directly proportional to the mass flow rate of the helium. Since the thermal cycle efficiency is not affected by mass flow rate according to Eqn. (3.6), varying the mass flow rate in the circuit, while maintaining other parameters unchanged, will change the plant power but maintain a virtually constant cycle efficiency. This means that the plant can have about the same efficiency performance at partial power levels as that at the full power condition, under which the plant is normally designed to operate with an optimal cycle efficiency.

Next, in general, the compressor inlet temperature, T_1, is stabilized by the large flow

heat capacity of the water in the precooler. As a result, it is known from Eqn. (3.3) that, with all other parameters being kept constant, increasing the turbine inlet temperature, T_4, will raise the plant output power available to the generator. By differentiating Eqn. (3.6) with respect to T_4, it can be shown that higher turbine inlet temperature will also result in a greater thermal efficiency. However, turbine blade materials limit the maximum value of T_4.

Furthermore, effects of pressure ratio r_p on the plant performance can also be discovered by using the same differentiating technique. Wilson has made a detailed analysis on the effects of the pressure ratio on cycle performance[w1]. He demonstrates that for every combination of cycle temperature ratio and machinery efficiencies, there exists an optimum pressure ratio for maximum power output and another optimum pressure ratio for the best thermal efficiency. For a heat-recuperated Brayton-cycle, such as the one used in the MGR-GT, the maximum pressure ratio for the best thermal efficiency is lower than the pressure ratio for the maximum output[w1]. This relation is qualitatively illustrated in Figure 3.2. From design point of view, the plant performance is configured near the pressure ratio of the best plant efficiency. Therefore, for direct cycle power plants, according to Figure 3.2, shifting the system pressure ratio slightly away from the design value tends to reduce the plant thermal efficiency, while the plant power output will be larger with an increased pressure ratio and smaller with a reduced pressure ratio.

As the pressure ratio varies, changes also occur in the machinery efficiencies η_T and η_C. In turbomachinery design, the turbine and compressor are designed such that they deliver the best efficient performance at approximately the same cycle pressure ratio for the best thermal cycle efficiency. When the pressure ratio changes, the heads of the turbomachinery will be altered, causing the velocity of flow through the machines to vary. Consequently, if operating at a constant rotor speed, the velocity triangles of the turbine and compressor will be shifted away from their optimal design shapes. As a result, the overall

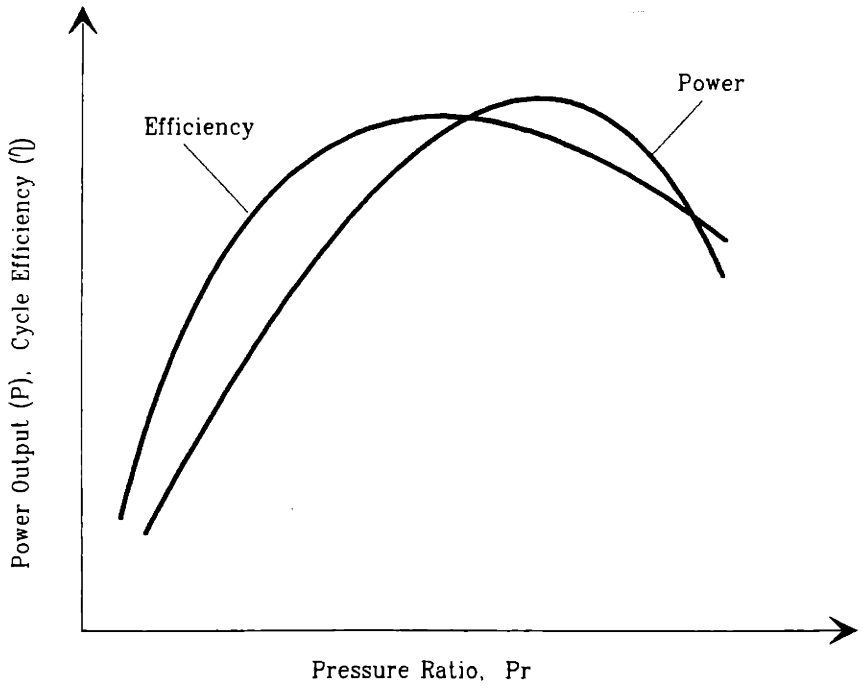

Figure 3.2 **Closed-cycle performance with respect to the cycle pressure ratio**

cycle efficiency will decline.

The foregoing discussion has outlined the influences of the key cycle parameters on the operating condition of closed-cycle gas turbine power plants. In fact, all control methods for gas turbine power plants are developed based on these principles. By maneuvering these key parameters, plant power output may be regulated to match changes in electric load demand, or plants can quickly be brought to an idle or shutdown state in case of accidents. The following sections present a description of several control methods based on these principles.

3.2.1 Inventory Control

In closed-cycle gas turbine power plants, the power output will change with the helium mass flow rate, as indicated above. This is the fundamental behind the pressure level control, or so-called the inventory control for gas turbine power plants. When the electric load on the plant drops, the helium is withdrawn from the cycle circuit, while with an increased load demand, the helium is returned to the circuit. Hereby, the turbomachinery efficiencies remain practically unchanged, since the pressures at every point of the cycle vary in the same ratio to one another whereas the flow velocities and temperatures remain unaltered if the machine speed and the reactor outlet temperature are kept constant. The overall cycle efficiency is thus nearly constant at its design value. What changes during the inventory control is only the density of the helium flow.

Therefore, the inventory control is known to be the most efficient control method available to gas turbine power plants. A typical installation of the inventory control system is illustrated in Figure 3.3. As it is shown that two possible inventory control schemes may be used and they differ in the way in which they connect with the plant circuit.

The first control scheme consists of vessel 1, valves V_{a1} and V_{b1} with the solid-lines

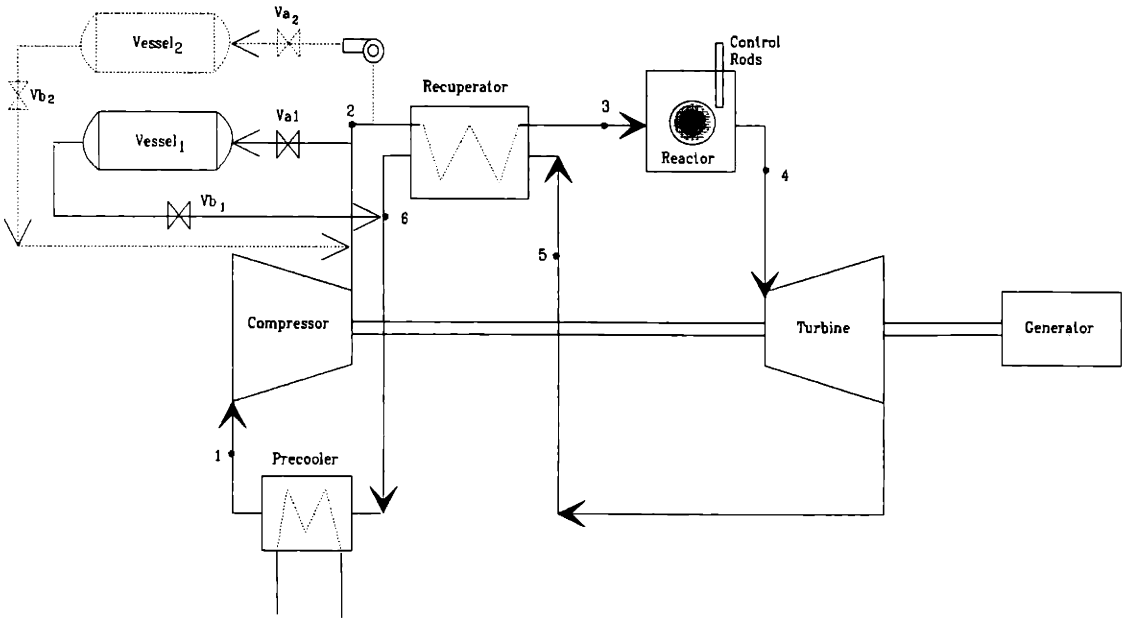

Figure 3.3 Potential inventory control schemes

of control helium flowpath. On request of power output decreases, it opens valve V_{a1} to withdraw the helium from the downstream of the compressor at the cycle point 2 where the pressure is the highest in the cycle. It subsequently returns the helium to the cycle LP-side at the upstream of the precooler if the power output is to be raised again. In general, this control is capable of reducing power output sufficiently fast to meet load reductions. However, it has a limited capability to match rapid load increase demands. This could be explained with the aid of Figure 3.4, which shows a calculated inventory control process for a closed-cycle gas turbine power plant[S1]. As shown, the plant initially operates at 50% of nominal power before a load increase request represented by the linear dashed line is issued. Notice that the time in the plot is normalized by Tg which is the time within which the deviations from the steady state condition return to the fraction 1/e. The smaller Tg, the quicker the system reaches its steady state. Tg is of the magnitude of a few seconds for typical closed-cycle gas turbine systems. As can be seen from Figure 3.4, in spite of increasing the gas inventory in the circuit, the output drops as a consequence of the reduced pressure ratio. The power output recovers only after a certain time has elapsed. Thus when speedy adaptation to load increases is required, the supply of the gas into the circuit has, at first, an opposite effect and would thus lead to quite unstable condition. If the machine loses its speed rapidly, it would be possible that the plant never be able to pick up the power at all.

The second inventory scheme is comprised of vessel 2, valves V_{a2} and V_{b2}, a transfer compressor, and the control flowpath indicated by the doted-lines. Unlike the first scheme, it connects with the circuit at the same location for both inventory reduction and increase. The pressure inside the inventory vessel must always be kept higher than the highest cycle pressure at point 2, so that the helium could be fed into the circuit from the vessel through valve V_{b2} under pressure gradient. As a result, a compressor has to be utilized to pump the

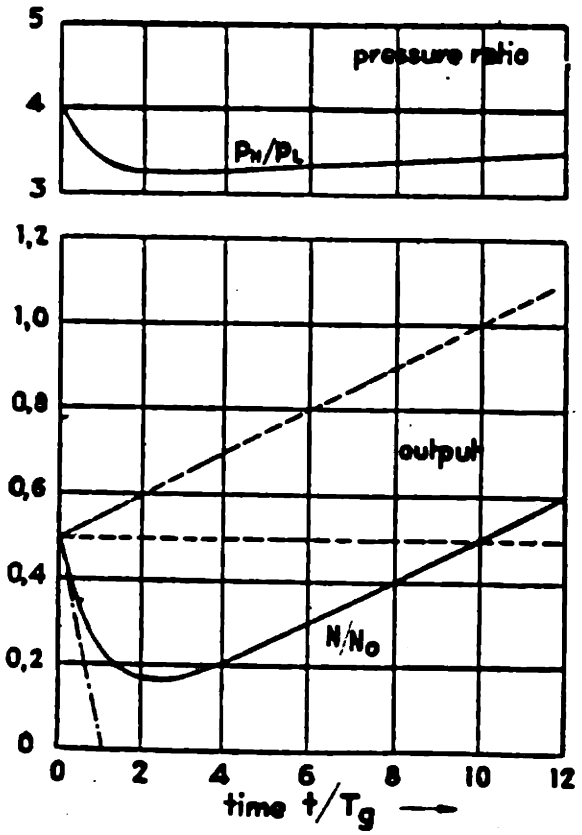

Figure 3.4 Course of pressure ratio and useful output when feeding gas into LP-side of the cycle [S1]

helium from the plant system into the vessel through V_{a2} during inventory reduction. It is evident that the design and operation of the second inventory scheme is more complex than the previous one. However, the capability of this control to meet load increases is far superior to the first inventory scheme. It is demonstrated in the Figure 3.5, in which the plant experiences the same load increase demand as in the previous case. As can be seen, when the gas is fed into the HP side of the cycle on demand of the power increase, the output power has an instant increase as a result of immediate increase in the pressure ratio. In fact, the rate of the output increase is even faster than it is demanded.

Because of the simplicity in design and operation, inventory control scheme 1 is more favored for use in control of gas turbine power plants, even though its capability of meeting load increase demand is limited. For those load changes that this control is unable to handle, other control means could be provided. Therefore the further discussion will focus on inventory scheme 1, only.

There are several problems regarding to the use of the inventory control. First, it requires a control vessel to store the helium withdrawn from the plant. The size of the vessel could be very large, depending on the scale of the plant and the power range to be controlled. Secondly, the permissible rate of power change is mostly limited by the size of the control valves. Large valves are difficult to operate and demand large power input to drive them. Large power plants must rely on large valves in order to alter the massive helium inventory in the circuit rapidly enough to match quick load changes. Therefore, the inventory control is not economically feasible for control of large gas turbine systems.

The power control range that a particular plant could accomplish with an inventory control is determined by the size of the vessel to be used. The inventory control is disabled once the pressure in the vessel reaches an equilibrium level with the circuit point to which it is associated. Bitsch and Chaboseau have analyzed the relationship between inventory-

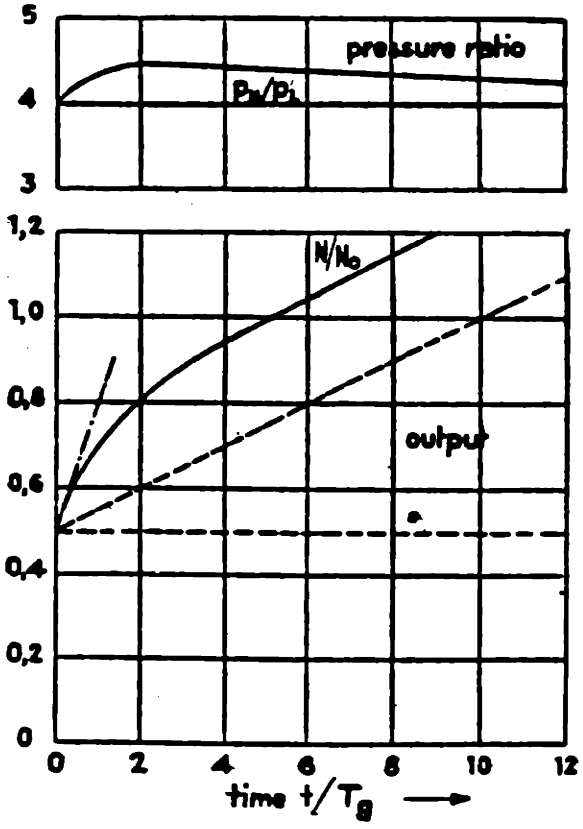

Figure 3.5 Course of pressure ratio and useful output when feeding gas into HP-side of the cycle[S1]

control power range, inventory-control volume, and total helium inventory in the cycle circuit[B1]. To simplify the analysis, the temperature of the helium in the vessel is assumed constant. They show that the lower limit of the equilibrium inventory-control power range is given by

$$P_L = \frac{1 + \frac{M_v}{M_p}}{1 + y\frac{M_v}{M_p}} \tag{3.7}$$

here M_v is the helium mass in the vessel, M_p the helium inventory in the plant circuit, and y is ratio of the cycle HP-pressure to initial vessel pressure. The upper limit of the equilibrium inventory-power range is

$$P_u = \frac{1 + \frac{M_v}{M_p}}{1 + \frac{y}{r_p}\frac{M_v}{M_p}} \tag{3.8}$$

where r_p is the cycle pressure ratio. Figure 3.6 shows the results of calculations for a particular plant, beginning from the initial conditions as indicated. As can be seen, if inventory-control-vessel pressure is set to be equal the initial LP-pressure of the cycle at full power, better control range is available at the higher load ranges. On the other hand, however, if inventory-control vessel pressure is initially below this value, the control band between the lower and upper limits is much narrower and lower, and a compressor is required for returning to 100% load.

The inventory system employing a single vessel demands large vessel volume for extended power control range. However, if more than one vessel can be used, their study shows, use of vessel storage volume is more efficient and thus less volume is needed to accomplish the same control range. The relation between the number of the equal-sized

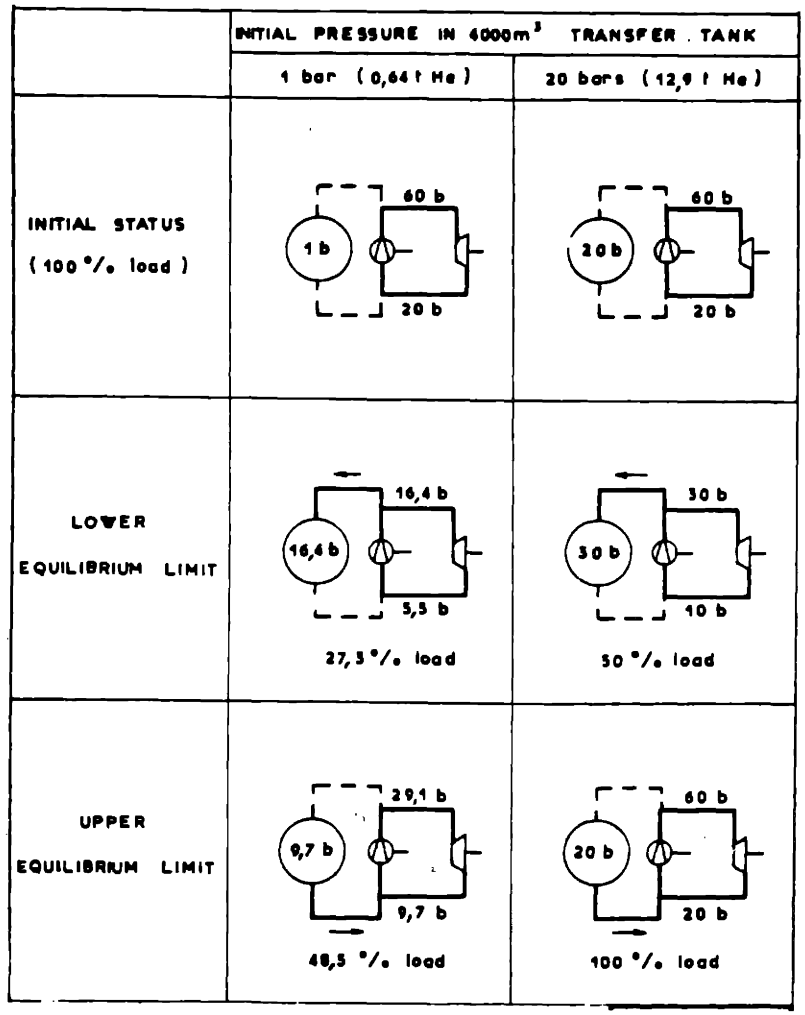

Figure 3.6 Typical examples of closed-cycle gas turbine load control with one inventory-control vessel [B1]

vessels, n, lower power limits, P_L and P_{TL} with individual vessel and total volume of the combined n vessels is

$$P_L = P_{TL}^{\frac{1}{n}} \tag{3.9}$$

Figure 3.7 shows the improvement of multi-vessel system over the previous single vessel control in efficiency of use of the total volume. A typical installation of multi-vessel inventory control systems in gas turbine power plants is shown in Figure 3.8. It should be pointed out that the multi-vessel systems demand a more complicated operating procedure to perform control functions.

3.2.2 Bypass Control

Bypass control utilizes the approach of maneuvering the cycle pressure ratio to control power output. In general, the cycle pressure ratio is selected such that systems could operate near the best thermal efficiency at full power condition. Subsequent changes in the cycle pressure ratio will alter the overall thermal efficiency, and the power output as well. Figure 3.9 shows a typical bypass installation in closed-cycle gas turbine power plants. It consists of a bypass valve V_c which, once opened, vents the cycle HP-side at the downstream of the HP-recuperator outlet to the LP-side of the cycle immediately after the turbine outlet.

On demand of power output decreases, part of the high pressure helium is conducted by valve V_c to the LP-side. As a result, the mass flow to the turbine and, according to the cycle pressure ratio, the head of the turbine, too, drop, so that the turbine output decreases. Because of the reduced cycle pressure ratio, the mass flow through the compressor increases while that in the turbine decreases. If the machine speed is kept

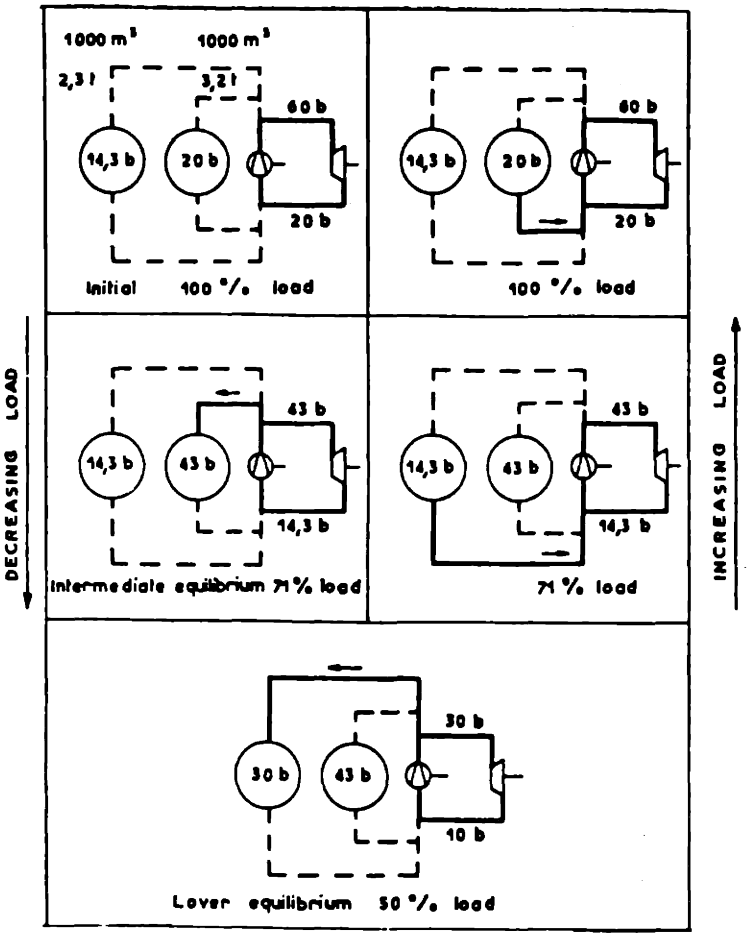

Figure 3.7 Closed-cycle inventory control with two inventory-control vessels[B1]

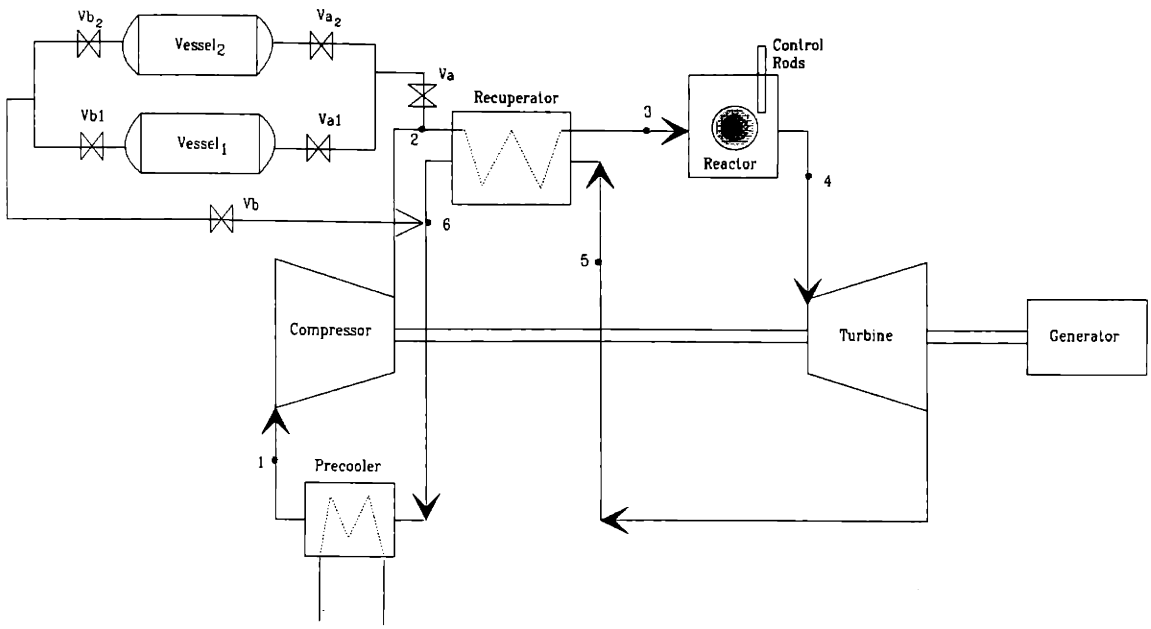

Figure 3.8 Multi-vessel inventory system

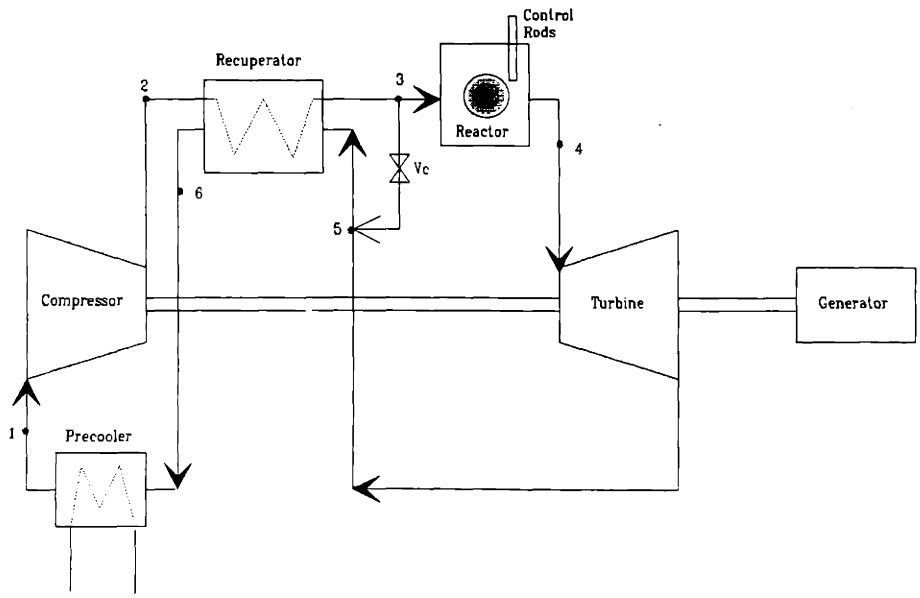

Figure 3.9 Bypass control scheme

constant, both the turbine and compressor would no longer operate on their design velocity triangles and thus be incapable of delivering the optimum efficiencies. Therefore, the overall cycle efficiency would be reduced. For instance, in large HTGR-GT which has a design cycle efficiency of 37%, the plant efficiency at 25% power level under the bypass control is only 9.8%[C1].

However, the advantage of the bypass control, particularly over the inventory control, is its capability of changing the power output rapidly to meet fast changes in load demand. It is especially important to large gas turbine systems in which the inventory control could not be used effectively for power control. In most large closed-cycle gas-turbine power plants, bypass control is commonly used as a primary control method, in spite of its inefficient performance at partial-power operation. In addition, in both large and small gas turbine systems, the fast control action of the bypass control is utilized as an emergency means to provide system shutdown in case of severe accidents, such as a sudden loss of AC load.

3.2.3 Turbine Inlet Temperature Control

The analysis in section 3.2 indicates that the turbine power can be altered by changing the temperature of the helium at the turbine inlet. The higher the turbine inlet temperature, the larger the turbine power and the greater the cycle efficiency. The turbine inlet temperature control utilizes this principle for power control.

In HTGR gas turbine power plants, the turbine inlet temperature is controlled by altering the reactor power and, thus the heat transferred to the helium. However, because of the large thermal inertia of the HTGR core, the turbine inlet temperature can not be changed rapidly. The characteristic time of the HTGR core temperature is on the order of minutes[O1]. Therefore the fast power control is not achievable with this control approach.

3.2.4 Reactor Control

Reactor thermal power is the sole power input to gas turbine plants using high-temperature gas-cooled reactors as heat sources. As the mechanical power output of the turbomachinery is regulated to match various load demands, the reactor power must be simultaneously controlled to provide required thermal power input to the power conversion system.

In fact, the reactor control is needed more than just for power control. It is also required to be capable of shutting the reactor down and keeping it subcritical under any credible operating conditions. Also, the control system must be capable of compensating for the core temperature feedback effect during startup and between different power levels, and to allow for Xenon override and burn-up compensation[M1].

To accomplish these control tasks, it is necessary to introduce changes in the reactivity of the core which one can adjust or control at will. This control reactivity can be used both to compensate the excess reactivity necessary for long-term core operations and also to adjust the power level of the reactor in order to bring the core to power, follow load demands, and shut the reactor down. The control reactivity is present in the form of strong neutron absorbers that can be inserted into or withdrawn from the core. This leads to the presence of two independent control systems in MGR, the control rods and small absorber spheres, as shown in Figure 3.10[G1].

The two reactivity control systems share the tasks of the reactor control. The control rod system, which lowers or raises the absorber rods inside the reflector, provides control functions to control the operating power level of the reactor, to compensate the effects of minor temperature variations in the core between different power levels, and to provide shutdown from operating power to subcriticality at hot temperature condition. The small absorber sphere system, which fills the absorber spheres into the channels located in the

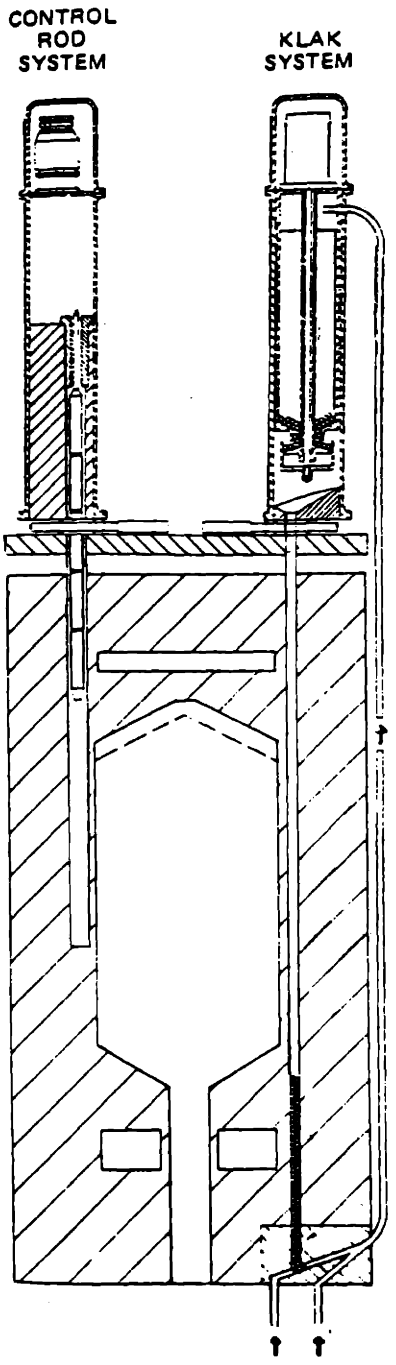

Figure 3.10 Reactivity control and shutdown systems [G1]

reflector, is used for long-term operation control. It is used to compensate for fuel temperature change during reactor startup and to compensate for lack of Xenon buildup in the initial core or during extended periods of operation at reduced power levels. The small absorber sphere system is also used to provide long-term shutdown of the reactor at ambient temperature. Both of the reactor control systems are designed to provide the worth of the reactivity necessary to perform their control functions.

3.2.5 Simultaneous Control

Four control methods for control of nuclear closed-cycle gas turbine power plants have been presented above, they include the helium inventory control, the flow bypass control, the turbine inlet temperature control, and finally the reactor control. For a particular power plant, either all or part of these control methods must simultaneously be utilized to meet diverse control requirements of operation. Therefore, an overall control system is normally integrated with several subsystems to allow the interactive control actions as required for power plant operation. For instance, a control system of a small gas turbine power plant is most likely designed as the one shown in Figure 3.11, which consists of an inventory control system to allow moderate power regulation, a bypass control to provide fast control action and loop shutdown capability, and a reactor control system to alter the reactor power, to shutdown the reactor, and to provide the reactivity manipulation necessary for long-term operation.

3.3 Control of Gas Turbine Power Plants

Having discussed the theoretical background of potential control methods, it is intended in this section to review the previous application of these methods in the control for several existing gas turbine power plants. Emphasis is placed on understanding both the

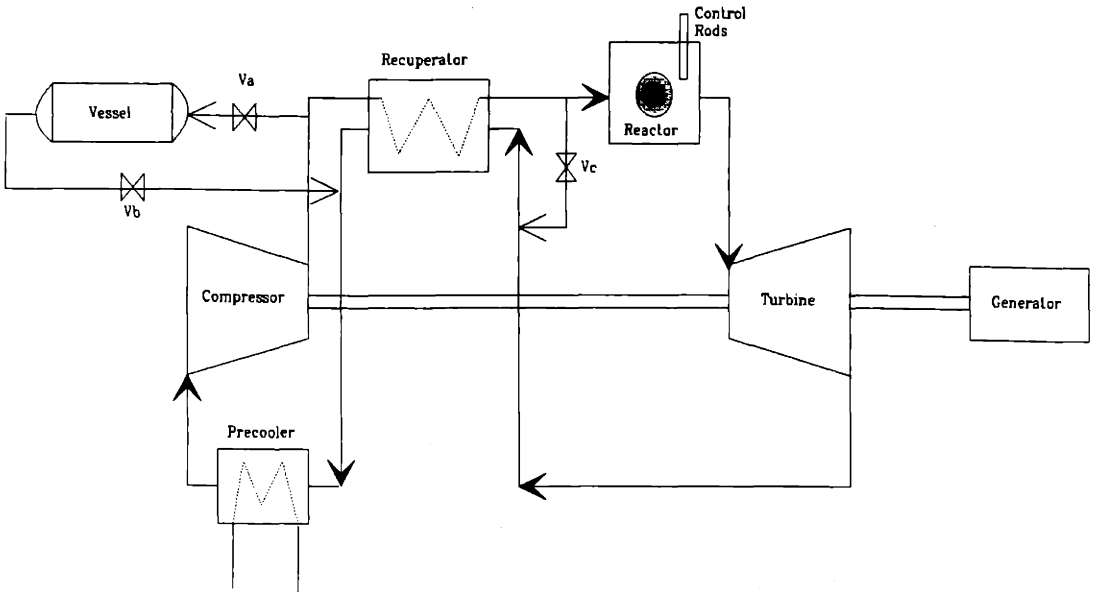

Figure 3.11 Integrated control scheme for closed-cycle gas turbine

benefits and disadvantage of individual control method so that appropriate control methods could be selected and integrated for the control of the MGR-GT.

3.3.1 KSH Gas Turbine

In the European High Temperature Reactor (HTR) program, the 25-MW Schleswig-Holstein nuclear power plant (KSH) was designed and planned to be built to demonstrate the commercial feasibility of nuclear closed-cycle gas turbine power plant technology. The KSH cycle and control scheme are shown in Figure 3.12[B2] and cycle parameters are listed in Table 3.1[B3]. The plant cycle consists of three compression units and a single expansion unit and utilizes a single-shaft configuration for the helium turbomachinery running at 8,000 rpm. Synchronous speed is accomplished through a reduction gear (h) to 3,000 rpm for the generator. A HTGR is used to provide the power input to the plant.

The plant integrated control system includes three subsystems: inventory control, bypass control, and reactor control. The inventory control system consists of a single vessel I, valves V_3 to V_6, and a transfer compressor m connected with a cooler at its upstream to cool the control helium flow prior to compression. The inventory control system is operated by controller R_1 to which the load demand is the regulatory input. The bypass control is comprised of valves V_1 and V_2 which are located in between the HP-side and LP-side of the cycle. The bypass valve V_1 is actuated by controller R_1, while valve V_2 is controlled by the temperature controller R_2 in such a way that when using the bypass control the reactor inlet temperature is kept nearly constant. The reactor outlet temperature is controlled by the temperature controller R3, the output signal of which is conducted to the power controller R4, which determines the reactor power required. The difference between the actual power and that desired is fed into the rod controller R_5 which varies the position of the control rods in the reactor core, accordingly.

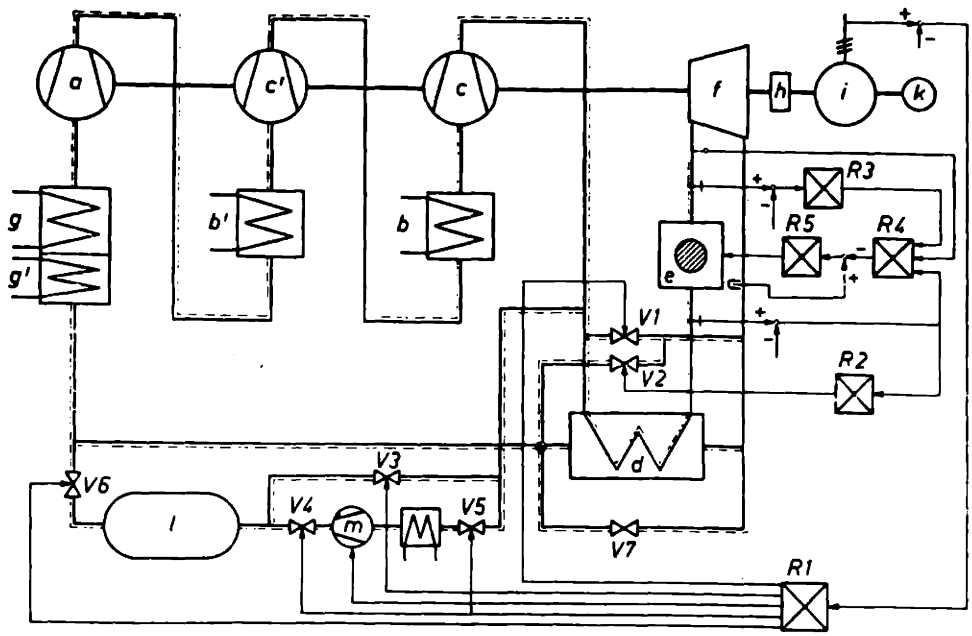

a = LP-compressor
b' = 1st intercooler
c' = MP-compressor
b = 2nd intercooler
c = HP-compressor
d = heat exchanger
e = reactor
f = turbine
g = cooling part of the precooler
g' = heating part of the precooler
h = gear
i = alternator
k = starter motor
l = control vessel
m = charging compressor
V1 ... V7 = valves
R1 ... R5 = controllers

Figure 3.12 KSH plant circuit and control [B2]

Table 3.1

KSH Plant Cycle Parameters[B3]

Location	T (°C)	P (MPa)	m (kg/s)
Turbine Inlet	730	2.500	40.58
Rec. Inlet (LP)	450	0.980	40.77
Precooler Inlet	101	0.965	41.26
LP Comp. Inlet	15	0.953	41.35
Intercooler Inlet	64	1.338	41.22
MP Comp. Inlet	15	1.328	41.10
Intercooler Inlet	60	1.810	41.10
HP Comp. Inlet	15	1.801	40.88
Rec. Inlet (HP)	71	2.630	40.71
Reactor Inlet	421	2.568	40.58

The inventory control is used for most power level changes from 100% to 50%. When the power output is to be reduced, valve V_3 is opened so that the helium flows from the HP-side of the circuit into the inventory control vessel I, in which at full load the pressure is set to be slightly in excess of the pressure at the precooler inlet. After the pressure equilibrium has been reached, a further quantity of helium is fed into the inventory vessel by means of compressor m. For this control purpose, valves V_4 and V_5 are opened and valve V_3 is closed. Use of the compressor in the KSH is intended to minimize the size of the inventory vessel employed and to enable extended power control range. If the power output is to be raised, the helium stored in the vessel can be fed into the circuit at the upstream of the precooler by opening valve V_6.

The dynamic responses of changing inventory have been calculated for the KSH[B2]. The calculations assume a constant reactor outlet temperature. The results of calculating the change in the inventory are shown in Figure 3.13, in which the inventory F, the power output N, and the isentropic heads h_s of the compressors, related to the inlet temperatures T_E, are plotted against the time. During the time from t=0 s until t=20 s the inventory is linearly reduced from 100% to 40% in the cycle which corresponds to an inventory changing rate of 3%/sec. Within the time of t=50 s up to 70 sec the inventory is raised again with equal rate up to full inventory. The basic conclusions are the following ones: On withdrawing the helium from the HP-side of the circuit in the first moment the power output rapidly decreases, then runs down with a gradient equal to that of the inventory, and finally increases to a steady state value after shutting the inventory valve. Thereby the LP-compressor approaches its surge limit and would reach it in the case of an inventory changing rate greater than 3%/sec. Increasing Inventory at first results in an output decrease which is based on the fact that during feeding the LP-pressure rises causing the turbine head and thus the useful turbine output to fall. The additional power required by the compressors to compress the increased

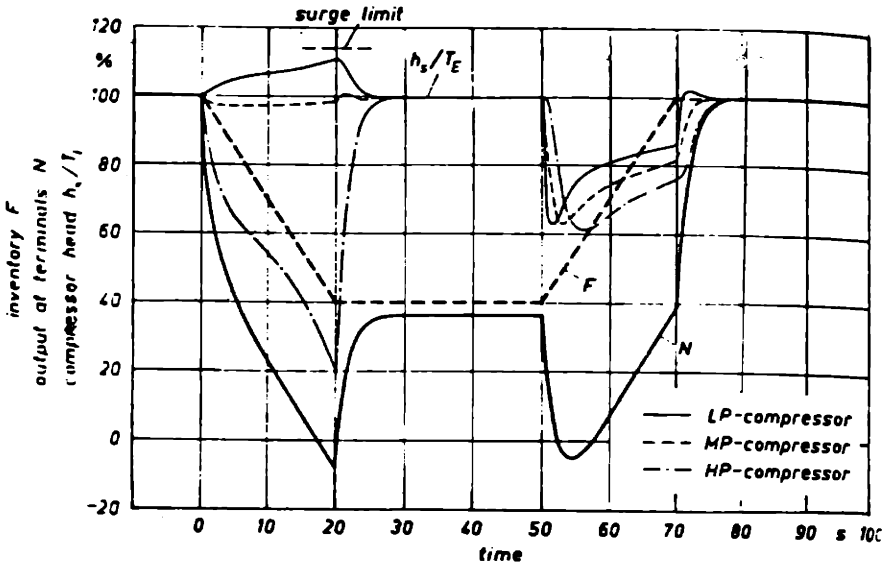

Figure 3.13 Change of inventory [B2]

amount of the helium from the LP-side to the HP-side also contributes to the initial drop of the power output N. As it is clearly shown that the power output at one time becomes negative, which implies an unstable condition associated with rapid inventory increases. There is, however, no compressor surge concern during the inventory increase because all compressors are removed from their surge limits. Because of the unstable condition encountered during the inventory increase, the inventory control is only used for slow power changes.

For rapid changes in power and for loads less than 50%, bypass control is used. In the case of bypass control, the helium discharged from the HP-compressor is conducted by V1 to the LP-side of the cycle. As a result the mass flow and the heat of turbine decrease so that the turbine output drops. By the aid of the bypass the head of the turbine can rapidly be reduced, which means the bypass control is characterized by its high control rate. Figure 3.14 shows the results of calculations[B2] for a bypass control process, during which the bypass valves V_1 and V_2 are opened at t=0 sec, and shut again at t= 30 sec. The power output and the high and low pressures are plotted against the time. During the time t=0 sec up to t=30 sec the bypass mass flow is kept constant and chosen such that the output could come to zero. The power output can be raised again by closing the valves after t= 30 sec. It is seen that the output follows the bypass operation with delay. As the total cycle pressure ratio decreases when opening the valves, the operational points of all compressors remove from the surge limits.

3.3.2 50-MW Power Plant Oberhausen

Oberhausen is a closed-cycle gas turbine power plant designed as a test facility to acquire operating experience with nuclear gas turbine during the High-Temperature Helium Turbine (HHT) program in Germany and Switzerland[B2,B4,B5,B6,B7]. The cycle circuit and

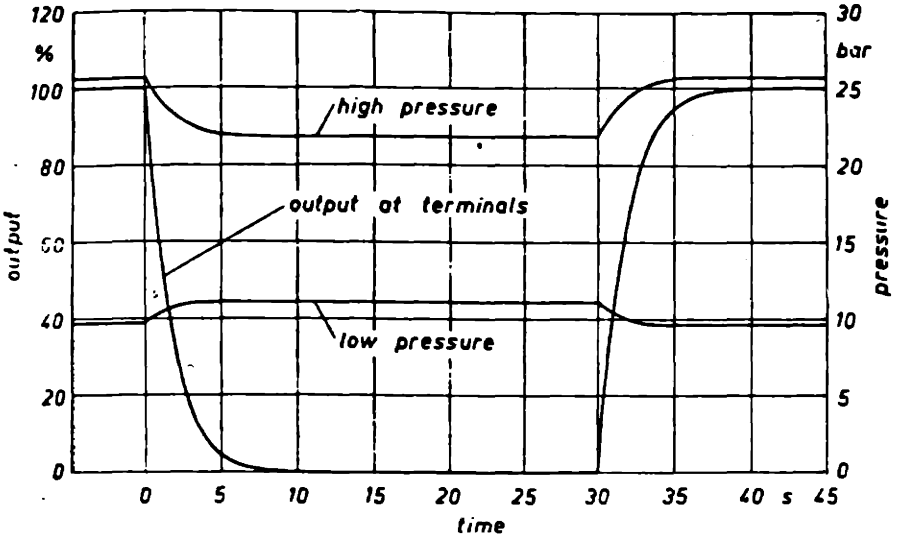

Figure 3.14 Bypass control [B2]

control scheme are shown in Figure 3.15 with the plant design specification and performance parameters listed in Tables 3.2 and 3.3. The plant uses a two-stage compression and expansion cycle scheme with intercoolering between the two compressors. Two-shaft configuration is chosen for the turbomachinery. The compressors and the HP-turbine on a shaft rotate at 5,500 rpm, which allows the performance of the compressors to be optimized at high speed, and the LP-turbine runs at synchronous speed driving an 50 MW generator. Two sets of the rotating machines are connected by a gear k to establish single-shaft dynamic characteristics.

Oberhausen is provided with an inventory control system for power-level control which allows part loads to be adjusted with optimum efficiency of operation. Unlike the inventory control system used in the KSH, Oberhausen employs a multi-vessel inventory system to make efficient use of vessel volume and to allow extended power range control without using transfer compressors. The inventory control system consists of the regulating vessels, I_1 to I_3, with a volume of 120 m^3 each. If the circuit inventory is to be reduced for less load demand , a certain quantity of helium is conducted from the downstream of the HP-compressor into the inventory vessels, which are filled one after the other until the particular equilibrium pressure is attained. If the inventory is to be increased to raise the power output, the stored helium is allowed to leave the vessels in reverse order and re-enter the circuit at the upstream of the precooler. The power control rate allowed by the inventory system is about 1%/min[B6].

Vessels, m_1 to m_2, are for long-term storage of the helium when the plant is scheduled to operate at part load for a long period of time. For filling these vessels, which also have a volume of 120 m3 each, the transfer compressors, n1 and n2, are required.

For rapid load change and for controlling the speed after a load release, the bypass control is used. Two bypasses branch off the downstream of the HP-compressor. The

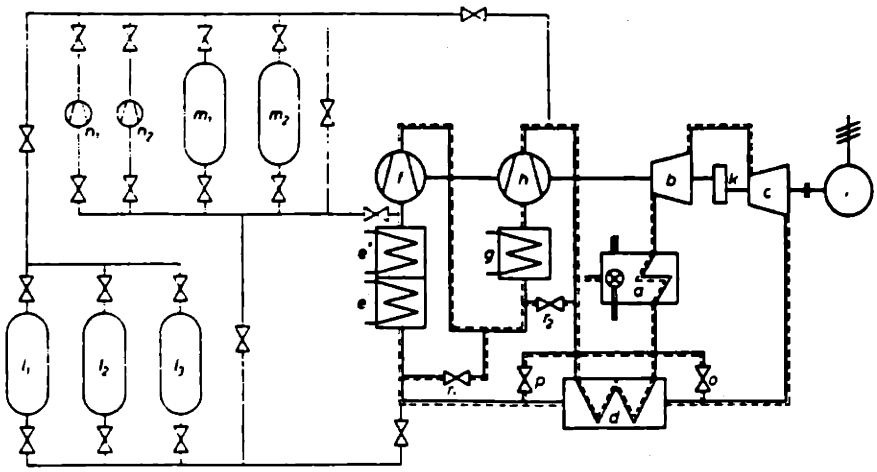

a - heater
b - HP turbine
c - LP turbine
d - heat exchanger
e' - heating part of precooler
e" - cooling part of precooler
f - LP compressor
g - intercooler
h - HP compressor
i - alternator (starter motor)
k - gear
$l_1 \ldots l_3$ - regulating reservoirs
m_1, m_2 - storage reservoirs
n_1, n_2 - transfer compressors
o - control valve
p - shutdown valve
r_1, r_2 - recirculating valves

Figure 3.15 Oberhausen plant circuit and control [B6]

Net electric output	50.0 MW
Heating output	53.5 MW
Rejected heat of cooler	37.5 MW
Fuel heat input	159.6 MW
Net electrical efficiency	31.3 %
Overall efficiency (electricity + district heating)	65.0 %
Heater efficiency	92.2 %
Helium mass flow rate at HP turbine inlet	84.4 kg/s
Heat exchanger temperature difference	40.0 K
Total pressure losses	10.4 %

Table 3.2 The Oberhausen plant design parameters [B7]

No.	Component	Temperature °C	Pressure bar
1	Low-pressure compressor	25	10.5
2	Intercooler	83	15.5
3	High-pressure compressor	25	15.4
4	Heat exchanger, HP side	125	28.7
5	Heater	417	28.2
6	High-pressure turbine	750	27.0
7	Low-pressure turbine	580	16.5
8	Heat exchanger, LP side	460	10.8
9	Precooler	169	10.6

Table 3.3 The Oberhausen cycle parameters [B7]

bypass valve o with a diameter of 27.5 cm leading to the inlet of the LP-recuperator is used as a primary control valve by which the plant can be kept on speed in case of a sudden loss of load, and is controlled during isolated operation. When the bypass valve is opened, the turbine head drops causing the turbine outlet temperature to rise. However, by adding the cold helium from the downstream of the HP-compressor to the turbine exhaust helium, thermal overstressing on the recuperator can be avoided. Since the bypass primarily acts to control the speed, the thermal condition by means of the same bypass valve can only be controlled indirectly, and thus large thermal gradients experienced by the recuperator may still be caused during critical bypass transients. Figure 3.16 shows a calculated process of bypass control. At time t=0 sec, a full-load release is assumed, and subsequently 50% of the nominal load is re-connected after steady state conditions are reached again at t=17.5 sec. After load release the overspeed reaches a maximum of less than 7% of the design value and approaches zero quickly and aperiodically, which shows highly damped transient characteristics. On connection of the load the speed drops below the nominal value to a lowest level of 4.2% underspeed and, after a period of minor overshoot, quickly climbs back to the design speed. The somewhat less favorable transient behavior on load connection has its reason in the valve lift, b, which, after connection of the load, temporarily drops to zero and thus causes unsteadiness in the control operation.

Figure 3.17 shows the power output to the generator and the gear power input as functions of the mass flow through the bypass valve, which is obtained from calculations of steady-state operations. As can be seen, the power output decreases linearly with respect to increased bypass flow rate and reaches to zero, which represents an isolated state, at a bypass flow of approximate 37.2% of nominal flow rate. At the same time, the gear input, b, rises from 2% at the full operation to about 50% when running idle.

The second bypass valve p is used for emergency shutdown. This valve is rated to

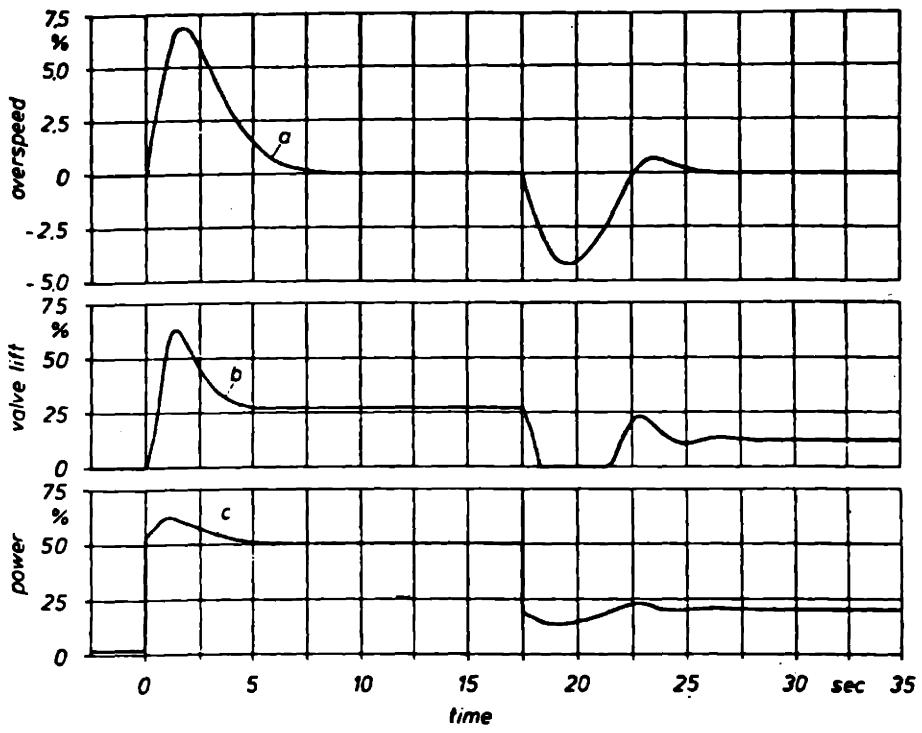

a - overspeed
b - control-valve lift
c - power input at gear shaft

Figure 3.16 Calculated process of control [B6]

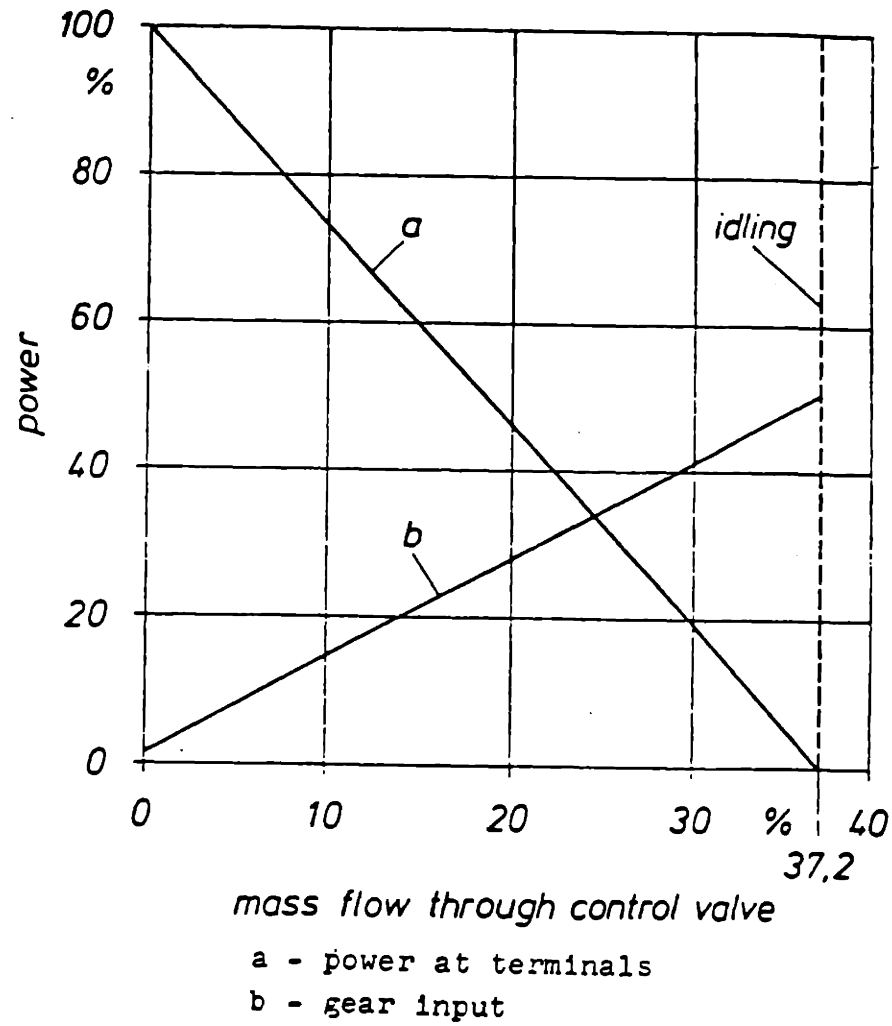

Figure 3.17 The effect of control valve bypass massflow on plant steady-state electrical power and shaft power [B6]

a size of 25 cm such that it could cause the cycle pressure ratio to be dropped to 1 within a few seconds and the machine set to be stopped after a short period. In order to protect the LP-recuperator inlet from thermal shocks, cold gas is led to the inlet of the LP-recuperator simultaneously, by slightly opening the bypass control valve o. Figure 3.18 demonstrates the effects of bypasses for the emergency shutdown. At t=0 sec, the electric load is disconnected, the heater is turned off and the emergency shutdown valve p is fully opened. The speed,a, drops within 30 sec to approximate 27%, and the pressures upstream and downstream of the two turbines, c and d, quickly approach an equilibrium value of 14.6 bar. Since the expansion ratio of the turbine decreases, the turbine outlet temperature rises considerably. To avoid thermal overstressing of the LP-recuperator inlet, a small bypass stream is convened to the LP turbine outlet so that the temperature of the LP-recuperator inlet does not rise to an intolerable extent.

The requirements of conditions for startup and run-down of Oberhausen helium turbine plant were established[B6]. For the plant startup, the generator (alternator i in Figure 3.15) is used as a motor driving the machine up to certain speed, after which, depending on the turbine inlet temperature and the helium inventory in the circuit, the turbomachinery may run up without the aid of the generator and is then controlled via the control bypass to the synchronous speed of 3,000 rpm. Figure 3.19 shows the results of calculations for the requirements of the plant startup. Therein the power at coupling is plotted over the speed at an 20% of nominal circuit inventory and at several HP-turbine inlet temperatures. As can be seen, the coupling power is negative at the beginning, owing to the assorted mechanical losses and the low machine efficiencies. With speed increased, the negative power is reduced. When the power at coupling becomes zero, the self-sustaining speed is obtained. At this point, the turbine power is just enough to provide the power for the compressors and to compensate for the mechanical losses. The self-sustaining speed depends on the HP-

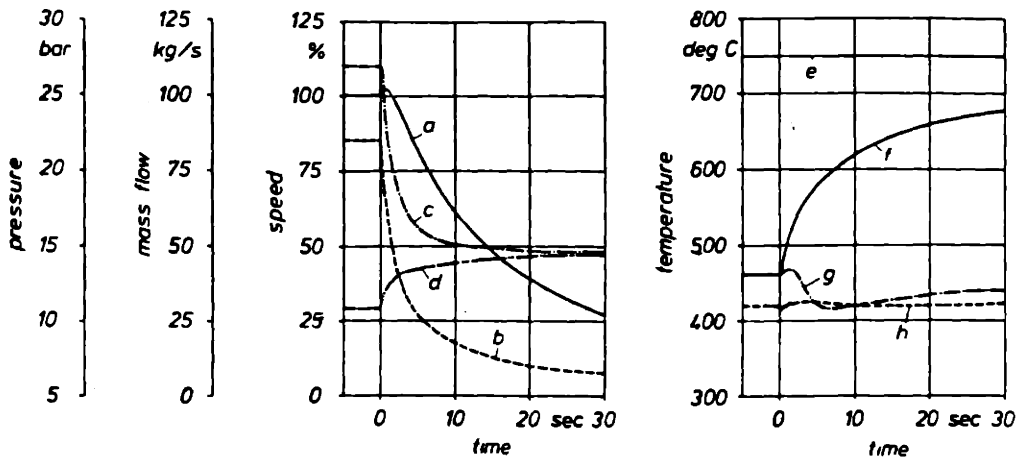

a - speed
b - mass flow at heater outlet
c - HP-turbine inlet pressure
d - LP-turbine outlet pressure
e - heater outlet temperature
f - LP-turbine outlet temperature
g - heat exchanger inlet temperature, LP part
h - heater inlet temperature

Figure 3.18 Emergency shutdown [B6]

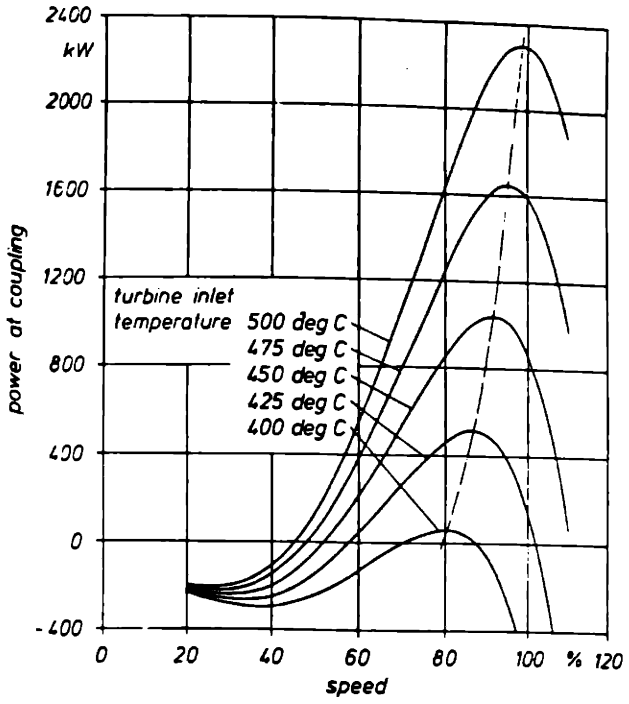

Figure 3.19 Startup of the turbine[B6]

turbine inlet temperature, as shown. The higher the HP-turbine inlet temperature, the earlier can a self-sustaining speed be reached. The second significant result is that the power curves show distinct peaks, due to the effect of the turbine efficiencies, which move in the direction of higher speeds with rising turbine inlet temperature.

For the plant run-down, the first step is to lessen the turbine inlet temperature and, at the same time, to reduce the circuit inventory. When the power output is at zero, the generator is disconnected from the mains. Then, further reducing the turbine inlet temperature will reduce the speed. In addition, the machine set can be electrically braked with the generator. During cooling down the plant, the turbomachinery is driven by the generator at low speed to circulate the helium.

3.3.3 HTGR-GT

The HTGR-GT is a large closed-cycle power plant design developed by General Atomics[B8,C2,O1,O2]. The plant layout is shown in Figure 3.20 with design parameters labeled at key cycle locations. It utilizes an 2000 MW HTGR providing the power input to two identical power conversion loops, each rated at 400 MW electric power output. Each loop consists of turbomachinery on a common shaft driving a generator at synchronous speed of 3,600 rpm, a recuperator and a precooler. The reactor and power conversion systems are integrated into a prestressed concrete reactor vessel (PCRV). The turbines, compressors, heat exchangers, and the reactor core are interconnected by large internal ducts.

Unlike in small gas turbine power plants, inventory control is not used for the HTGR-GT power control. Because of large helium inventory in the HTGR-GT circuit, helium transfer from and to the operating inventory would be expected to be very slow so that inventory control for fast load changes are not economically attainable. Instead, bypass control and turbine inlet temperature control are adopted for regulating the plant power output and for

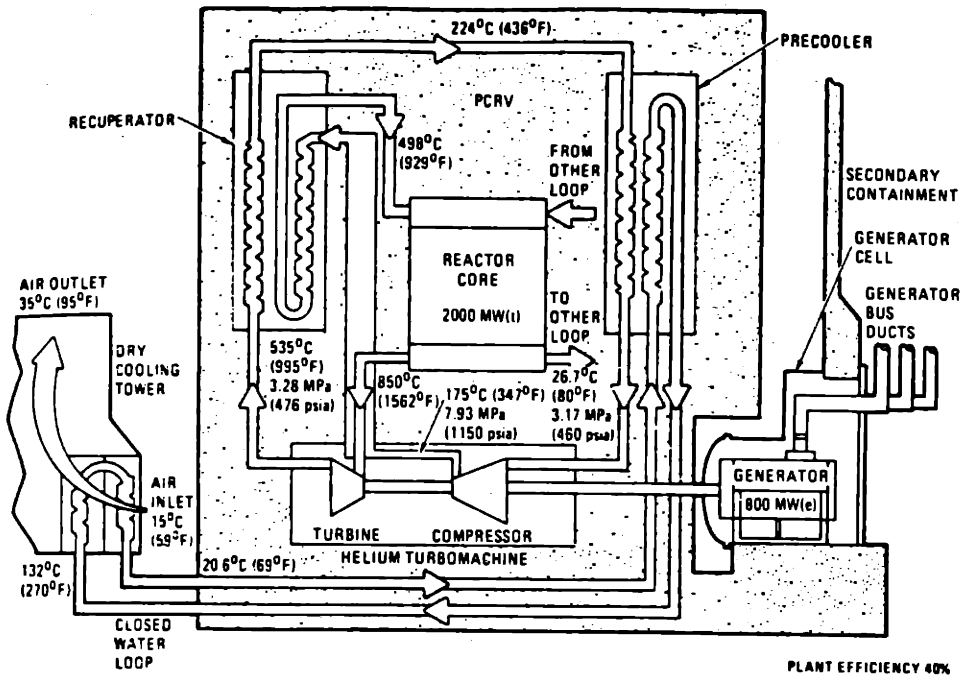

Figure 3.20 loop cycle diagram for 800-MW(e) HTGR-GT power plant [C2]

controlling the machine speed. The control scheme is depicted schematically in Figure 3.21, and a block diagram of the HTGR-GT integrated control system is shown in Figure 3.22.

The control system is designed to automatically operate the plant at any electric load from 100% down to 25% of rated load, with the performance of the following three functions:

1. control load and speed;

2. control turbine inlet temperature; and

3. control thermal conditions during transients.

To perform these control functions, several plant variables are manipulated by the controllers of the control system. As shown in Figure 3.21, they are:

1. electric power output E,

2. turbomachinery shaft speed N,

3. turbine inlet temperature T_{ti},

4. core neutron flux F, and

5. HP-recuperator exit and LP-recuperator inlet temperatures THPR and TLPR.

Load and speed control is accomplished by the primary bypass valve (valve 1) which, once opened, leads the helium from the HP-recuperator outlet to the downstream of the turbine. The load/speed controller adjusts the primary bypass valve as required to keep the machine on speed and to regulate the power equal to the demanded electrical power throughout the normal load control range. Proportional-plus-integral control approach is used by the load/speed controller, in which a term proportional to speed error is designated to ensure promote control action as required to prevent excessive overspeed and to provide damping necessary to achieve a favored speed transient behavior, while the integral action regulates the ultimate valve position for accurate matching of load and speed.

The turbine inlet temperatures are pre-determined for operations at various power levels and the interpolation of these temperatures are stored inside the block of the turbine

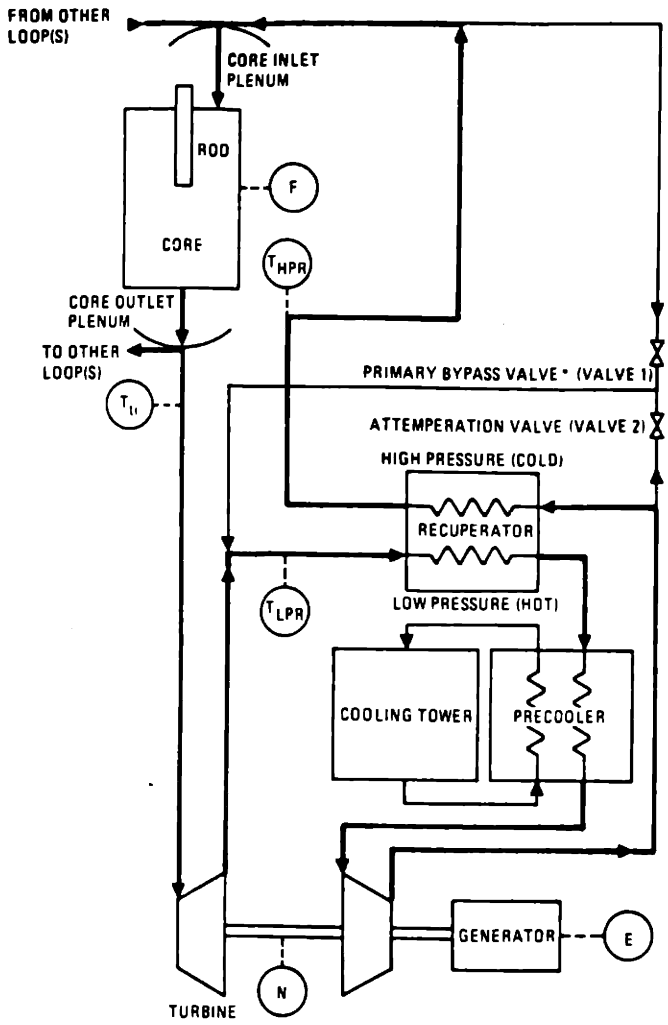

SYMBOLS

N – SPEED

E – ELECTRICAL POWER

T_{HPR} – TEMPERATURE-HIGH PRESSURE RECUPERATOR OUTLET

T_{LPR} – TEMPERATURE-LOW PRESSURE RECUPERATOR INLET

T_{ti} – TEMPERATURE-TURBINE INLET

F– NEUTRON FLUX

*THE SAFETY VALVE AND THE TRIM VALVE ARE AT THIS SCHEMATIC POSITION ALSO.

Figure 3.21 HTGR-GT flow schematic [O2]

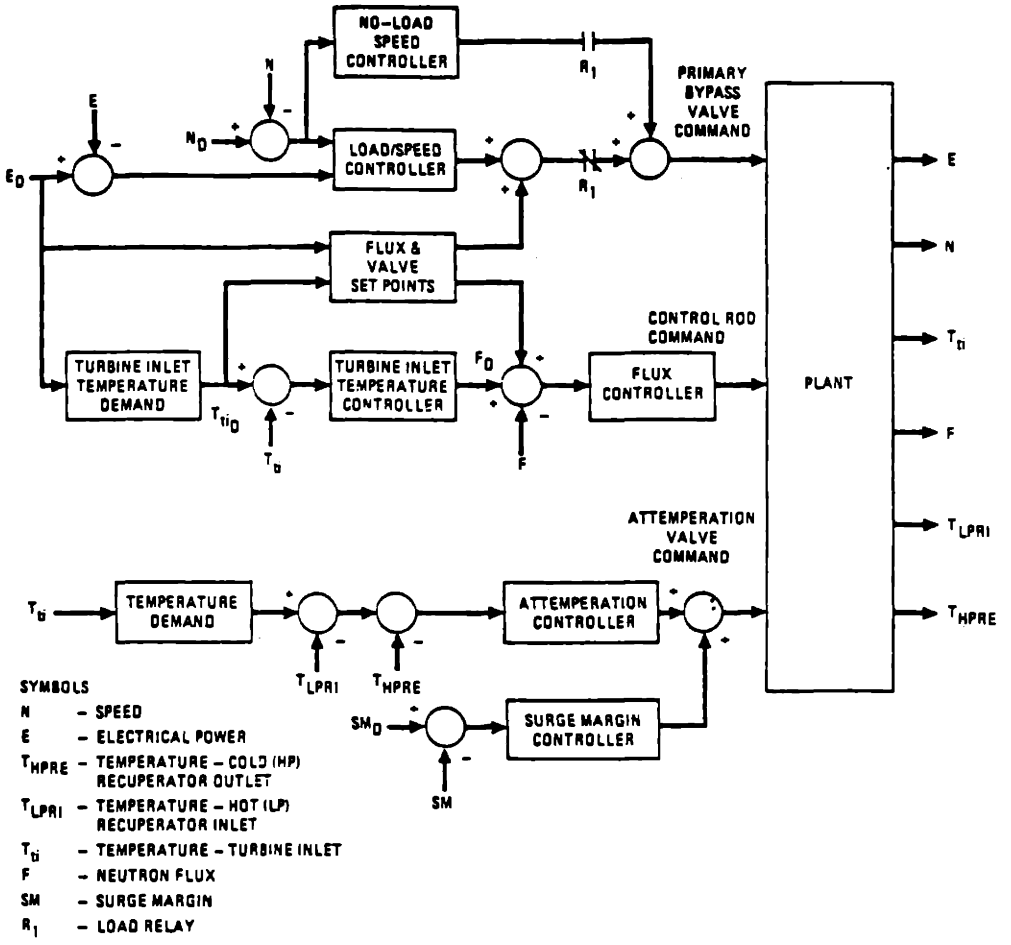

Figure 3.22 Block diagram of the HTGR-GT plant control system[O2]

inlet temperature demand (shown in Figure 3.22). If load is to be varied, the required turbine temperature is calculated against the new load demand and then used by the turbine inlet controller, which provides commanding signals to the reactor neutron flux controller. The neutron flux controller adjusts the position of the control rods to regulate the reactor power and thus, the heat available to the helium. However, the response of the turbine inlet temperature to such control is on the order of minutes due to the large thermal inertia of the HTGR core. The turbine inlet temperature control is insufficient for the rapid power regulation, which is mostly accomplished by the previous bypass control.

The thermal transients experienced by the plant components are controlled by the attemperation controller. The controller adjusts the HP-recuperator exit temperature THPR and LP- recuperator inlet temperature TLPR to a demanded value that is a programmed function of the turbine inlet temperature at different power levels. Control is accomplished by actuation of the attemperation valve (valve 2) which introduces the cold helium from the compressor exit to the turbine outlet.

In addition, supplementary control functions are also provided by the control system for plant startup and shutdown, and for protection of compressor surge. For plant startup and shutdown, programmed commands are issued to the turbine speed, turbine inlet temperature, and attemperation controllers to perform the startup and shutdown control functions. The compressor surge is controlled by the compressor surge margin controller which ensures the sufficient surge margin for the compressor. Control is accomplished with the same attemperation valve as used for the thermal control. Opening of this valve reduces the compressor pressure ratio, causing an increase in the compressor surge margin.

The control performance of the HTGR-GT control system is demonstrated in Figure 3.23(a)-(c), which show the automatic load-following control capabilities in the 100% to 25% power range[C2]. Plant transient response to a 5%/min ramp load demand decrease begins

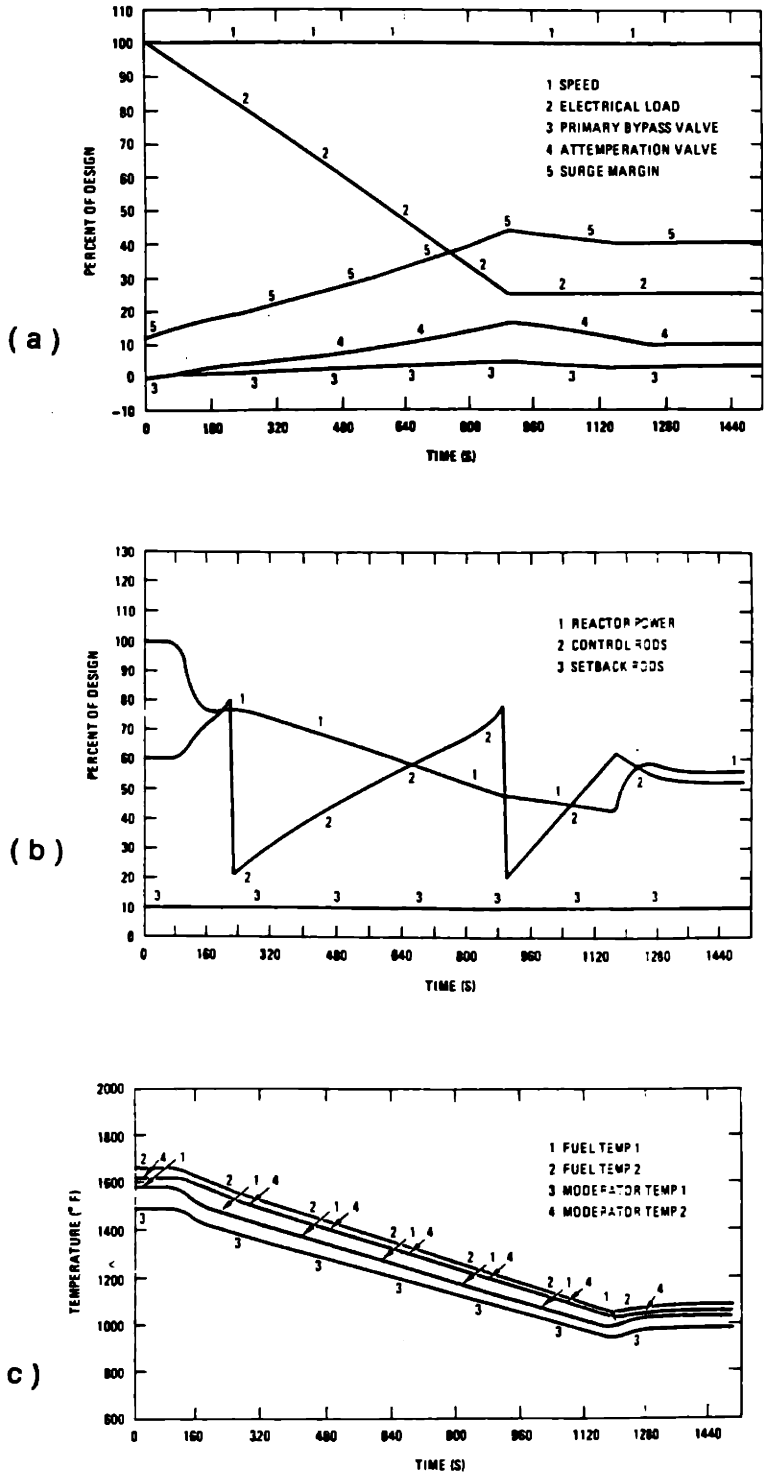

Figure 3.23 Rapid load decrease at 5%/min (100% to 25% range)[C2]

with the opening of the primary bypass valve (curve 3 in Figure 3.23a) commanded by the load/speed controller. As the valve opens, reactor power is almost constant (Figure 3.23b) until about 90 sec, when the load has been reduced by -7.5%. At this point the turbine inlet temperature controller reduces the turbine inlet temperature setpoint, which is programmed as a function of load demand. Accordingly, the flux demand is computed and is fed into the neutron flux controller which actuates the control rod drive mechanism to insert the control rod bank. The reactor reactivity decreases rapidly as the bank is inserted, as a result, the core power begins to drop. As shown in Figure 3.23b, manual shimming of the control rod bank occurs twice in this transient to permit 75% of normal load reduction. The reactor power gradually reaches its steady state as the plant moves toward the equilibrium at the 25% load level. The power output matches load demand (Figure 3.23a), while core temperatures follow the turbine inlet temperature setpoint (Figure 3.23c). The core outlet temperature reaches setpoint at 1450 sec as both the attemperation and the primary bypass valves show fixed positions (Figure 3.23a) and the plant reaches equilibrium.

The shutdown effects of the bypasses are clearly demonstrated in Figures 3.24a-d, which show the plant response to a sudden loss of the electric load in a single loop. Initially, turbomachine speed rises rapidly. The primary bypass valve (valve 1) opens fully in 1 sec in a safety manner. Turbine speed turns down and rapidly falls. Turbine pressure-ratio drops and turbine exhaust temperature increases dramatically causing the Attemperation Controller to open valve 2. As a result of the control action by the attemperation valve, LP-recuperator inlet temperature, which initially rises, is quickly turned down. As loop pressure approaches equilibrium, the primary bypass valve closes as a result of low pressure gradient across the loop, and the attemperation valve begins to close due to the reduced cooling required to attemperate the significantly reduced turbine flow to the inlet of LP-recuperator.

Figure 3.24 HTGR-GT response and plant transient resulting from sudden loss of electric load in one PCL [O2]

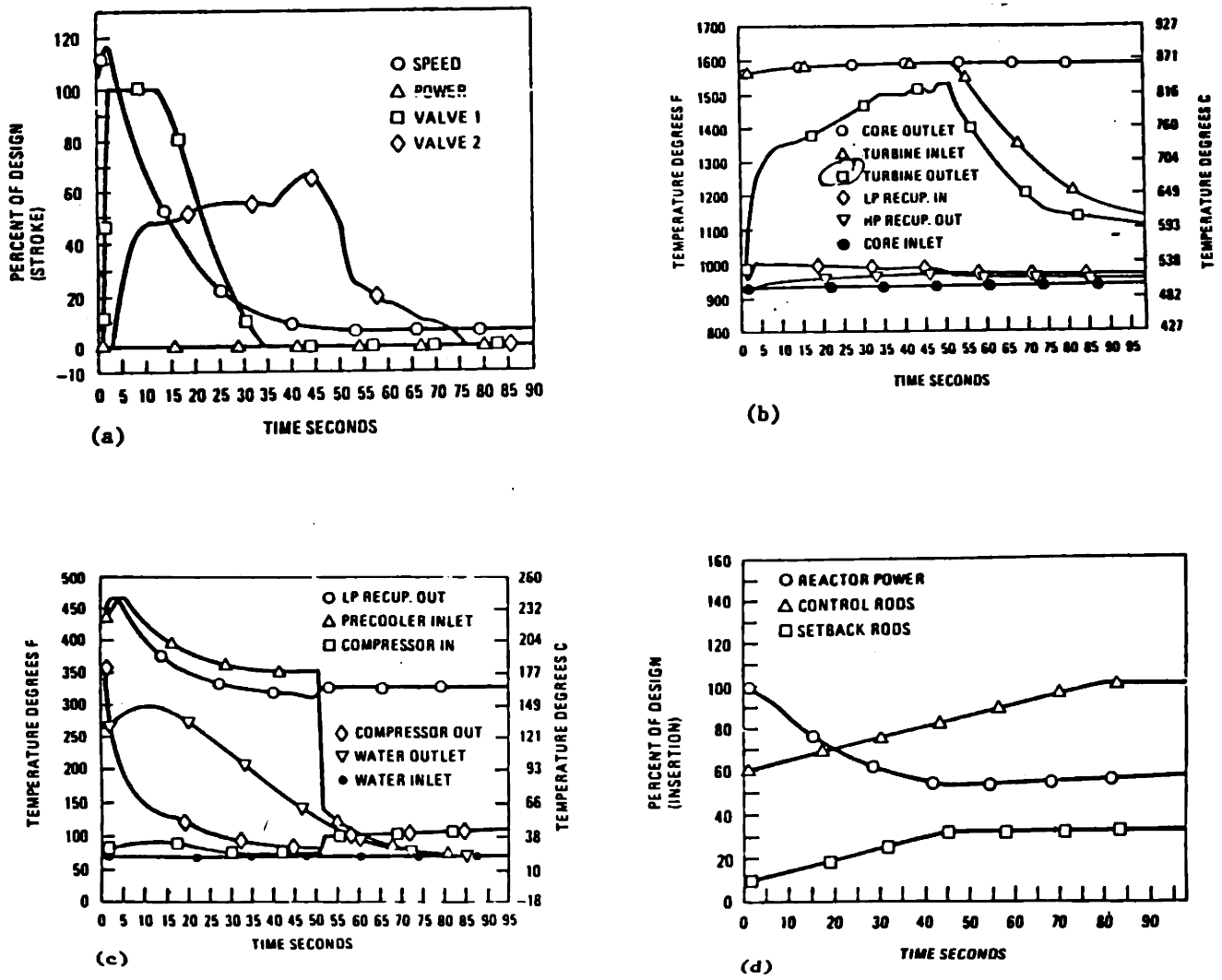

3.3.4 Summary of Conclusions

In the forgoing sections of this chapter, the theory of nuclear closed-cycle gas turbine power plant control has been discussed, followed by a review of previous experience in the control of several power plants. In summary, control of nuclear gas turbine power plants is primarily achieved through the interactive control actions of all or a few of the following means: (a) helium inventory which varies the pressure levels in the circuit to regulate the power output, (b) bypass control which changes the system pressure ratio and the helium flow path to control the power as well as to keep the plant on speed, (c) turbine inlet temperature control to alter the turbine power, and (d) reactor reactivity control to regulate the reactor power and to shut down the reactor.

The most efficient control method is the inventory control. Ideally, the inventory control reduces the system pressure level, but causes limited variation of the system pressure ratio across the circuit. If the turbine and compressor inlet temperatures are kept constant, the velocities of flow remain unchanged so that the turbomachinery works near its design points, the efficiency of the plant being an optimum. The inventory control is effective for power control of small gas turbine systems. However, it has not been shown to be economically attainable for large gas turbine systems.

Bypass control maneuvers the system pressure ratio to perform control functions. On demand of power output decreases, part of the helium flow from the cycle HP-side is bypassed through bypass valves to the LP-side of circuit. As a result, the mass flow to the turbine and, according to the cycle pressure ratio and the efficiency, the head of the turbine, too, drop, so that the turbine output decreases. Bypass control reduces the cycle thermal efficiency at partial power operation. However, it enables rapid power control to match fast load changes and to keep the plant on speed. Therefore, its application can commonly be found in gas turbine power plants, particularly in large systems where inventory control is not

feasible.

Utilizing the principle that turbine power is proportional to its inlet temperature results in turbine inlet temperature control for power regulation. The response of turbine inlet temperature control, however, is on the order of minutes because of the large thermal inertia of the HTGR core. It is only used for slow power regulation, and most likely for use in combination with bypass control in order to improve the plant performance at long-term reduced power operation.

Reactor reactivity control is required to regulate the reactor power to follow load changes. It is also required to shut down the reactor and keep it under controlled condition under any credible operating conditions, to compensate for the effects of the core temperature during startup and between various power levels, to allow for Xenon override and burn-up compensation. Control of reactor reactivity is accomplished by introducing an amount of negative reactivity into the core as required for specific control purpose. The control reactivity is presented in the form of neutron absorber materials, *i.e.*, control rods and small absorber spheres in the MGR, which can be insert into or withdrawn from the core.

Different control methods have diverse impacts on the overall plant performance at reduced power levels. Covert has given a quantitative evaluation of the effects of these control methods in case of the HTGR-GT control[C1]. Figure 3.25 shows the result of the evaluation. As can be seen, the helium inventory control is able to offer high efficiency performance over a broad range of power levels. The bypass control almost linearly deteriorates the performance of the plant as the load being reduced, while the temperature control has some improvement over bypass control. The combination of the bypass control and turbine inlet temperature control offers a better performance than the use of the bypass control alone, which is the precise reason that the HTGR-GT adopts the turbine inlet temperature control for power control purpose.

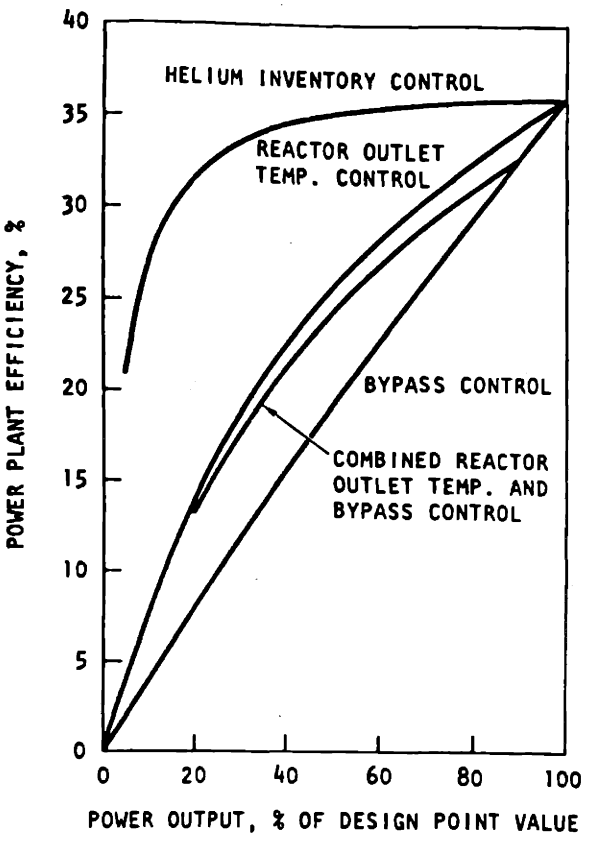

Figure 3.25 Part-load efficiency for the various control modes [C1]

3.4 Design of the Control System for MGR-GT[2]

The foregoing discussion of the fundamentals and experience in gas turbine power plant control has formed a sufficient basis for the development of a candidate control system for the MGR-GT, which is the intent of this section. The control system to be developed consists of a Plant Regulation System (PRS) and a Plant Protection System (PPS). The PRS is to be designed to regulate reactor power and to control turbomachinery output to match electric load demand from grid, control the machine speed, maintain the temperature of the helium delivered to the turbine, control thermal conditions experienced by the system components. The PRS is also required to control the procedures for plant startup and shutdown. The PPS is designed to handle transients during emergency conditions, such as a load rejection or system depressurization, to protect the plant components from damage.

It is essential to develop such control system in consistence with the MGR-GT design approach, *i.e.*, being of simplicity in design, high efficiency and reliability in performance, and effective in operation. The inherent safety of the MGR-GT eliminates the need of redundant engineering safeguard components from the control system as they normally exist in conventional nuclear power plants. By an appropriate selection and optimal integration of potential control methods, an effective control system can be realized with a relatively simple design. The control system to be developed must offer high efficiency performance over a broad power range. The ability for the MGR-GT to operate at high efficiency is one of its major advantages over other nuclear power systems.

3.4.1 Plant Regulation System

The PRS is designed to operate the plant using automatic control at any electric load within the operating range between the 100% and 25% of nominal load. Specifically, the PRS

[2]For the MGR-GT design information, see [S2].

provides automatic load-following capabilities at various rates of electric load changes in accordance with the U.S. utility requirements[G2], which are as follows:

1. Normal-rate load change: up to ±3% of rated load per minute.
2. Maximum-rate load change: ±5% of rated load per minute.
3. Maximum step load change: ±10 % of rated load.

And the major control functions of the PRS include:

1. Control reactor power and maintain the reactor outlet temperature.
2. Control the power and speed of the turbomachinery to match load changes.
3. Provide automatic control for plant startup and shutdown.
4. Control thermal conditions imposed on the components during transients.

3.4.1a Reactor Power and Temperature Control

The MGR-GT reactor core has a strong negative temperature coefficient ensuring its inherent shutdown capability. From the control point of view, however, noticeable temperature changes in the core demand extended control rod movements to compensate for the reactivity generated by such strong temeprature coefficient. Furthermore, the core temperatures are very difficult to be changed at will due to the large thermal capacity of the core. Therefore, it is not practical that the core temperature manipulation be used as an active control means in the MGR-GT.

Instead, the reactor power regulation uses the strategy of the constant reactor outlet temperature control, *i.e.*, at all operating power levels, the average helium temperature at the reactor outlet will be maintained constant at its design value 850°C. The reactor power is so adjusted as required to keep the core outlet temperature unchanged. The effectiveness of this control approach will be evaluated later in this study.

3.4.1b Load and Speed Control

Inventory control is a control method suitable to the control of small power plants. It offers the potential for high efficiency over a broad power range. It allows power control of small systems to match most of the load changes. Operation of an inventory control may be quite simple if designed properly. Considering these advantages, the inventory control has been selected as a primary method for load and speed control in the MGR-GT.

A few questions must be answered to culminate the design of the inventory control system. First, it is required to determine the size of inventory valves sufficient to permit maximum rate of load change since permissible rate of load change is determined by the size of the valves. The larger the size of valves, the more the helium is allowed to pass through per unit time and the faster the power can be altered. However, large valves are difficult to operate. Because the MGR-GT is a very compact system, it is anticipated that valves with a reasonable size will be able to satisfy most of the control requirements. The actual size of the inventory valves will be determined during the evaluation of the control system design later in this study.

Secondly, there are two possible schemes of installing the inventory control system in the MGR-GT, one is the HP-feeding of helium for inventory increase, and the other the LP-feeding. The former scheme is more effective to allow power control to meet load increases. However, the HP-feeding requires a transfer compressor to compress the helium into the inventory vessel the pressure of which must be kept higher than that of the HP-side of the cycle. In addition, rapid inventory feeding to the HP-side of the circuit may cause compressor surge which is hazard to the compressor. The LP-scheme eliminates the need of a transfer compressor and does not cause the problem of compressor surge, and thus is chosen to be used in the MGR-GT inventory system. Since the inventory control with the LP-feeding has a limited capability to raise the power quickly to meet fast load increase demands, other

control means must be provided to assist the inventory control.

In addition, the inventory vessel volume must be determined for the load control range. Preliminary calculation in this study indicates that an inventory vessel with a volume of 500 m3 enables 24.7% load reduction from full load, without use of a transfer compressor[Y1]. Further load reduction requires either larger inventory vessel volume or the use of a transfer compressor. The use of the transfer compressor is not an attractive alternative for the MGR-GT, because design and operation of such inventory system are too complex. Therefore, larger vessel volume must be used in order to permit a wider load control range. A multi-vessel inventory control system can make more efficient use of the storage volume, and thus is proposed to be adopted in the MGR-GT inventory control system. The load control range as a function of the number of vessels used in a multi-vessel inventory control system has been calculated for the MGR-GT and the result is shown in Figure 3.26.

Finally, inventory control has a limited ability to stabilize the turbomachinery speed because of its inherent large dynamic characteristic time due to the large vessel volume. Theoretically, to stabilize a system by means of control requires that the time constants or system poles of the control system be less than those of the system to be controlled. This leads to a conclusion that the responsibility of the turbomachinery stability must be taken by other faster control methods. The inventory control is only capable of providing rough power regulation. In addition, fast control is also required to help the inventory control to meet quick load increases as indicated before.

Bypass control enables quick control responses to rapid load increases and is also capable of stabilizing the turbomachinery speed, for the time constant of the bypass control is much smaller (on the order of deciseconds) than the characteristic time of the rotor (on the order of seconds)[B2]. However, it is unfortunate that the bypass control is incapable of efficient operation at reduced power, which prevents it from being used as a primary control

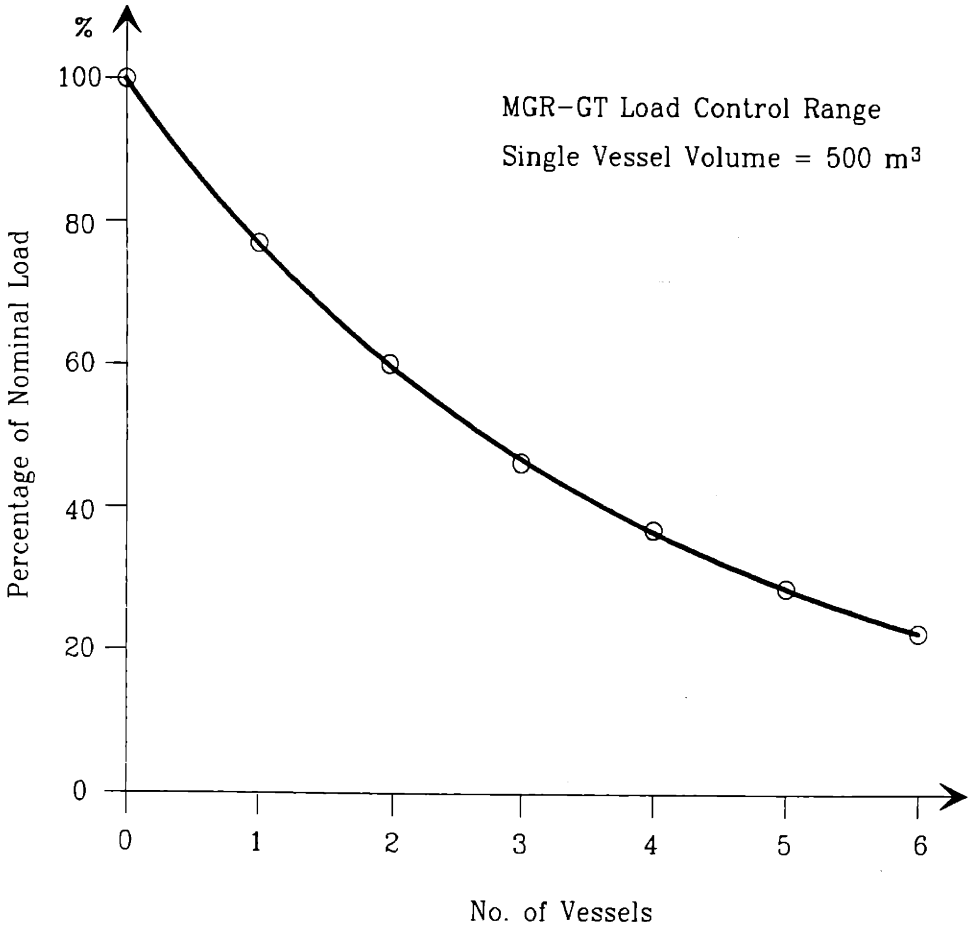

Figure 3.26 MGR–GT load control range with inventory control system

method in the MGR-GT. Instead, it will be chosen to assist the inventory control to perform those control functions that the inventory control alone is incapable of. Based on this approach, a bypass valve rated with a 10% load control capacity should satisfy all the requirements of load and speed control for the MGR-GT.

The MGR-GT load and speed control approach is summarized in Figure 3.27. As can be seen, the control for the first 10% load reduction is provided by the bypass system alone. As a result, potential power to meet quick load increase is reserved in the form of bypass flow, which could be used in the inventory control range followed. The load control between 90% and 68% of nominal load is accomplished by the inventory system which fills the helium into the first inventory vessel, while the load between 68% to 50% is controlled by filling the helium into the second vessel after the pressure in the first vessel has reached equilibrium with the system pressure. Because of the use of the inventory control, high efficient operation is realized for the MGR-GT in the above load control range. The bypass control is again used for the load control range from 50% to 25%. Since long-term operations within this low-load range are not expected, the less efficient performance of the bypass control is not a serious concern in this low load range. The effects of the load and speed control will be evaluated in this study.

3.4.1c Plant Shutdown and Startup

For plant shutdown with full inventory, a procedure is proposed as follows:

(1) reduce AC load at a rate of -10%/min. After the load is completely disconnected, the system is allowed to operate at an idle state for 5 mins until most transients being over. The reactor outlet temperature will be maintained at 850°C through the reactor power control.

(2) reduce the turbomachinery speed. Commands of the speed reduction is issued to the PRS. The PRS opens the bypass valve to follow the speed reduction commands which

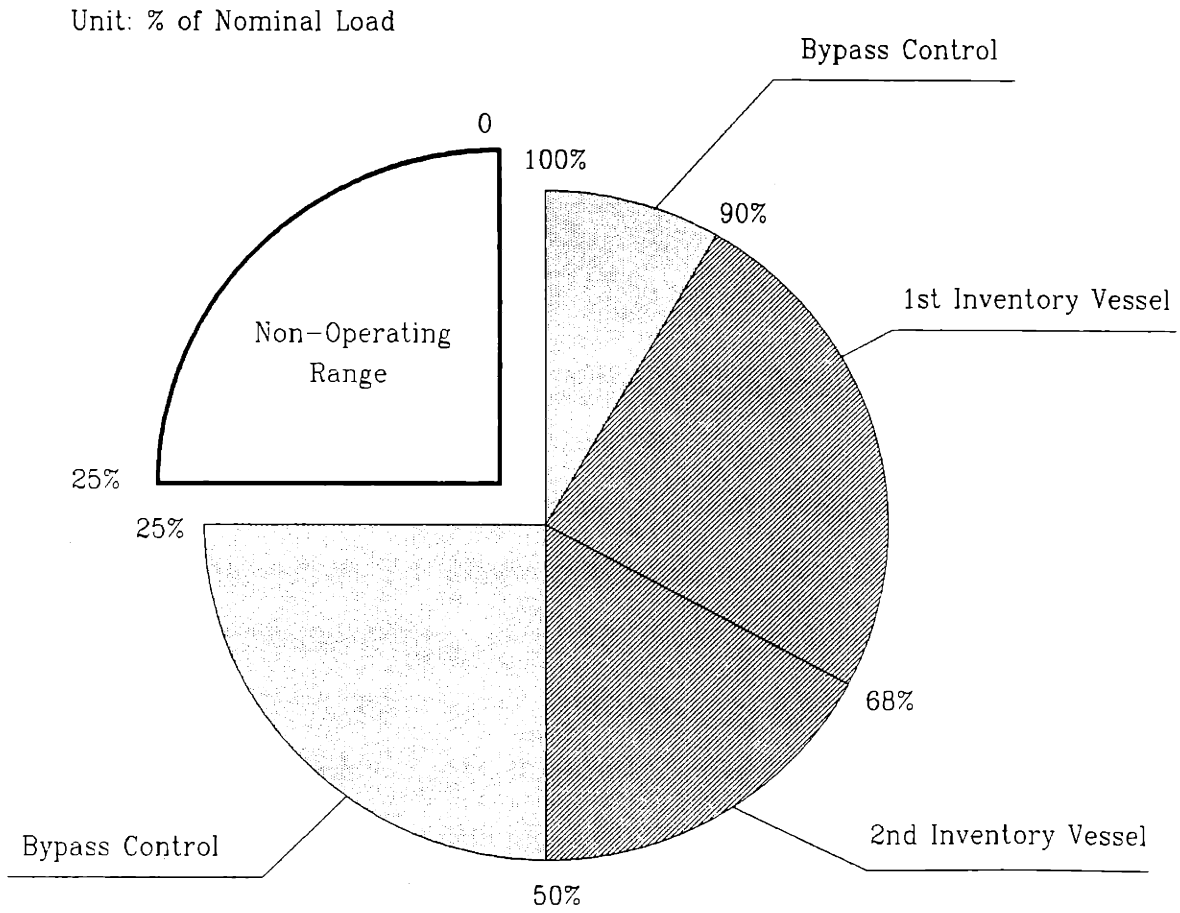

Figure 3.27 MGR-GT load control approach: combined bypass and inventory control

are programmed at -1,000 rpm/min for the rotor speed beyond 8,000 rpm and -250 rpm/min for the speed thereafter. The stability of the turbomachinery at low speed is far worse than running near its design speed. The slower speed reduction rate at the low speed region is necessary to avoid transient-induced instability of the turbomachinery. Final state of this step is the operation of the plant at zero load, running at 3,600 rpm on the bypass control, with the reactor outlet temperature remaining at 850°C. After this point, the plant could operate indefinitely at such a self-sustaining state. A regular, full power operation can easily be resumed by starting up the plant in a reverse order from this state.

(3) if a complete plant shutdown is instead desired at this point, the control rods will be inserted into the side reflector. As the reactor power drops, the core outlet temperature decreases, resulting in the reduction of the turbine inlet temperature. As a result, the turbine will gradually lose its power and come to a stop. For a permanent plant shutdown, the absorber spheres are released into the reflector to secure the cold shutdown condition. To keep the core temperature low, the helium can be circulated by rotating the turbomachinery with external power source to help decay heat removal from the core.

3.4.1d Thermal control

Thermal control is mainly required for the recuperator during large bypass control. The thermal control may not be necessary for the normal power control since the large bypass control is not used in the MGR-GT. However, during plant startup and shutdown with full helium inventory, substantial bypass control is used. As the head of the turbine is reduced by the bypass control, the turbine outlet temperature will rise considerably. Consequently, thermal control must be provided to prevent excessive thermal stresses upon the LP-recuperator inlet. A separate bypass valve will be installed to introduce cold helium from the downstream of the compressor to the LP-recuperator inlet so that the thermal

condition at the LP-recuperator inlet would be controlled.

3.4.1e Integration of the Plant Regulation System

Combining the control methods selected above results in an integrated plant regulation system which automatically controls the plant operation at any load within the operating range. Figure 3.28 shows the PRS control components in the plant circuit, while the controllers maneuvering the PRS are shown in Figure 3.29. The PRS controllers manipulate several plant variables to perform the control functions. Theses are:

1. turbomachinery speed N,
2. helium mass inventory in the inventory vessels M_v,
3. reactor outlet helium temperature T_r, and
4. LP-recuperator inlet temperature T_h.

The location of each manipulated variable is designated in Figure 3.28. The PRS consists of five controllers which issue commanding signals to five major control subsystems to perform integrated control functions.

The load demand is the primary input to the PRS; from this demand, means of control is determined, and appropriate control subsystems are initiated to carry out the control functions. For load larger than 90% of nominal level, the bypass control acts alone to regulate the power output and to maintain the turbomachinery running at 10,000 rpm of design speed. The control bypass conducts the helium from the HP-recuperator exit to the turbine outlet. If the load drops to the level between 90% and 50% of nominal load, the inventory control is activated to control the power output. The helium is withdrawn from the circuit at the downstream of the compressor and filled into two inventory vessels (vessel-1 and vessel-2 in Figure 3.28) one after another until the vessel pressure reaches equilibrium with that of the circuit. The required amount of inventory change is pre-determined for the

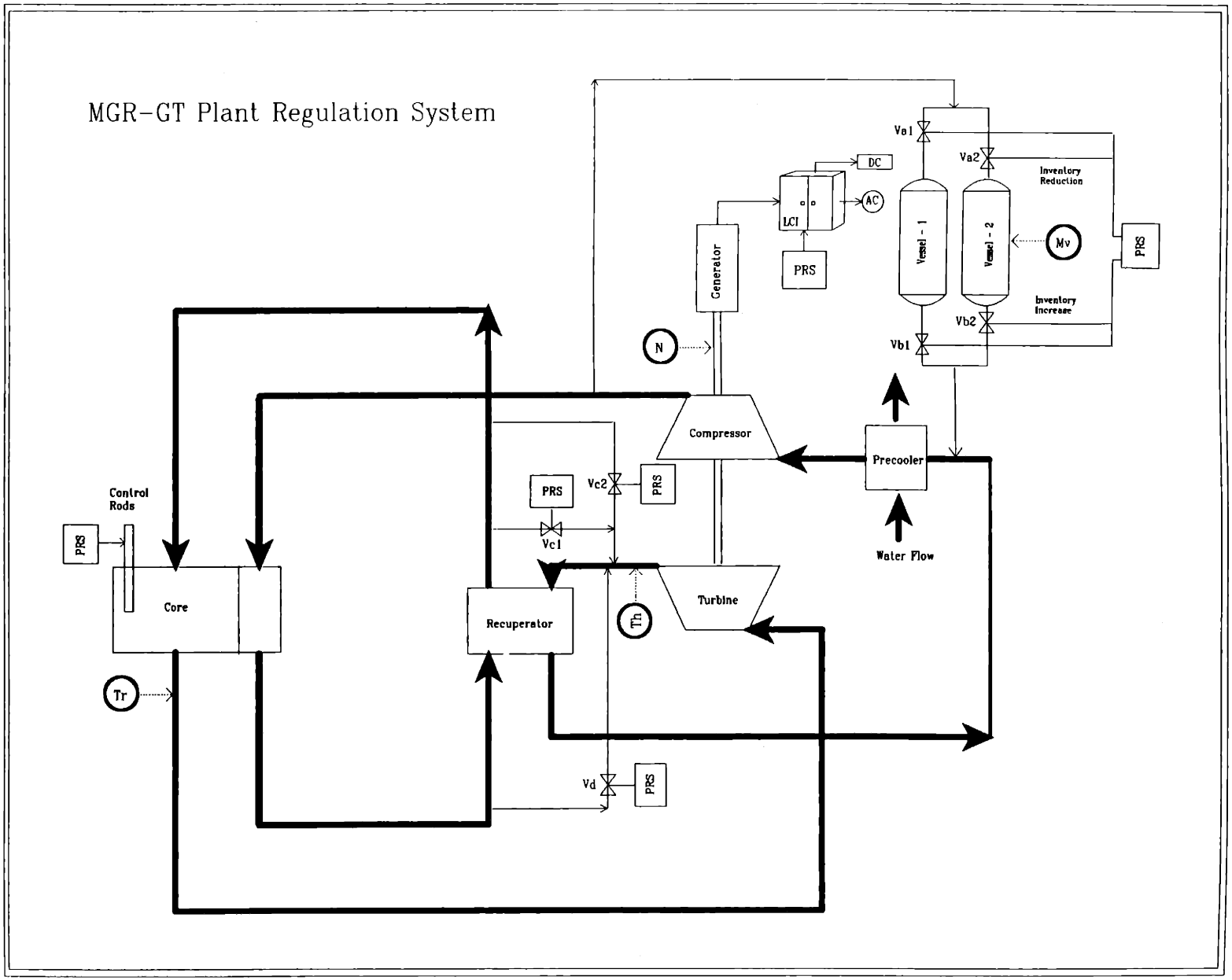

Figure 3.28 MGR-GT Plant Regulation System (PRS)

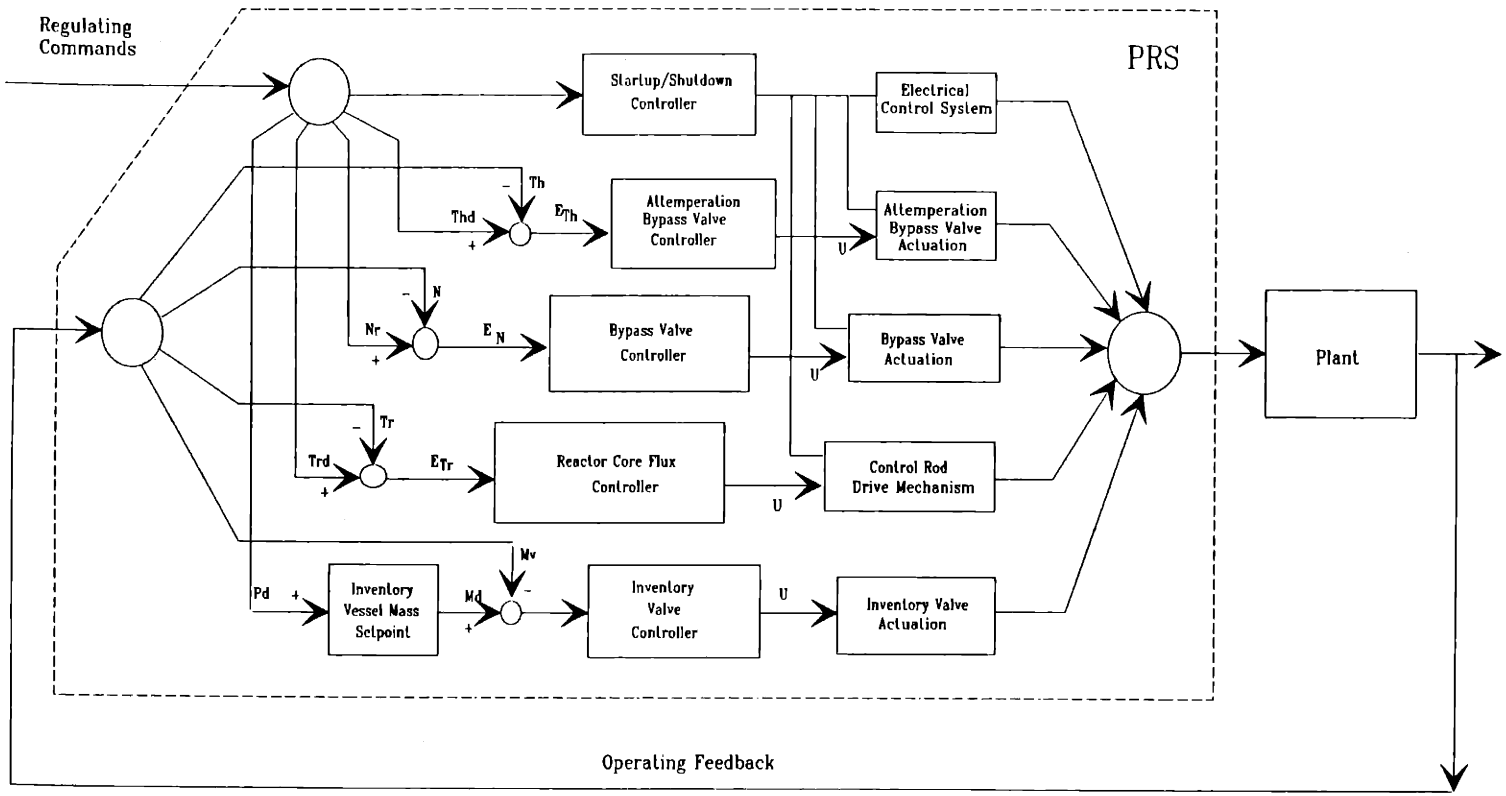

Figure 3.29 MGR–GT PRS controllers

steady-state operations against load demands. The error between desired helium inventory and actual inventory in the vessels, which is calculated using the vessel pressures and temperatures, is fed into the inventory controller which then maneuvers the opening or closing of the inventory reduction valves V_{a1} and V_{a2}. If the load is to be raised again, the required amount of helium inventory is determined with the new load demand. The inventory controller then opens the inventory valves V_{b1} and V_{b2} to allow the helium to leave the vessels in a reverse order into the circuit.

The inventory control is expected to be sufficient to match rapid load reductions. For load increases, it will be assisted by the bypass control to ensure rapid promote power output increases. The combination of inventory control and bypass control should be capable of maintaining the turbomachinery speed during all anticipated normal load changes. For the operation of the plant on the load between 50% to 25%, the bypass control is again utilized to control the power output and speed. Throughout the entire operational control, the reactor outlet temperature controller will regulate the reactor power by moving the control rods to maintain the core outlet temperature constant at 850°C.

The PRS provides automatic control based on a programmed procedure to carry out normal plant startup and shutdown. The programmed procedure, which will be fully evaluated later in this study, is located in the Startup/Shutdown Controller which issues the control commands to the PRS control components to alter the turbomachinery speed and reactor outlet temperature. The attemperation controller controls thermal conditions to ensure no thermal overstressing being imposed on the LP-recuperator inlet. In addition, commands are issued to the electric control system to motor the turbomachinery with the generator during plant startup from stationary state up to 3,600 rpm of synchronous speed.

So far, the PRS is only a preliminary design. The dimension of the control components, such as the size of the control valves, and the control rules that each controller

follows will be determined after the system models have been developed in the next chapter.

3.4.2 Plant Protection System

Although the safety protection of the MGR-GT is not required, a protection system is necessary to mitigate possible severe accidents and to prevent the plant components from damage during upset conditions. The PPS is currently designed to deal with the following anticipated accidents:

1. Total load rejection from full power,
2. turbomachinery overspeed,
3. turbomachinery failure,
4. inner pressure surface leaks,
5 system depressurization, and
6. inadvertent withdrawal of control rods or clearup of absorber spheres.

The protective actions of the PPS include loop and reactor shutdown in different modes which are:

1. Loop shutdown to an idle state for decay heat removal, or for rapid load recovery.
2. Emergency loop shutdown to a complete stop if a permanent shutdown is required.
3. Reactor scram to shut the reactor in hot temperature condition.
4. Reactor trip to keep the reactor subcriticality at ambient temperature condition.

3.4.2a Loop shutdown

The loop shutdown is accomplished by a shutdown bypass valve which, once opened, allows the helium to flow from the HP-recuperator outlet to the turbine outlet and thus quickly reduce the heat of the turbine. This bypass is designed to provide two shutdown modes with one to shutdown the system to an idle state as in case of a load rejection, and

the other to shutdown the loop completely to a stop as in case of the turbomachinery failure. The loop shutdown is accompanied by the thermal control which prevents thermal overstressing of the recuperator during critical shutdown processes. In addition, the generator circuit breaker is automatically invoked by any of these two shutdown actions in order to protect the electrical system.

3.4.2b Reactor shutdown

The hot reactor shutdown is accomplished by ordering the control rods to drop on gravity into the reflector which takes about 13 seconds[G1]. The reactor trip can be used to provide the cold shutdown of the reactor for an infinite period of time and is initiated either by operators or by the PPS when the PPS detects a need for a permanent shutdown condition. For a reactor trip, the absorber spheres fall by gravity into the channels located in the side reflector and fill up the channels in about 60 seconds[G1]. The use of the absorber sphere shutdown system is for emergency or complete long-term shutdown, because subsequent clearup of the spheres from the channels in the reflector involves a complicated procedure that would make a quick recovery of the reactor operation nearly impossible. Since an active reactor shutdown is not required for the safety operation of the reactor, the absorber sphere shutdown system is normally not used unless it is initiated by an on-line operator or a permanent shutdown condition has been met.

3.4.2c The Overall Plant Protection System

The overall PPS is the integration of the loop and reactor shutdown systems, the components of which are depicted schematically in Figure 3.30. To perform the PPS functions, several plant operational parameters require to be monitored by the PPS controllers. These are,

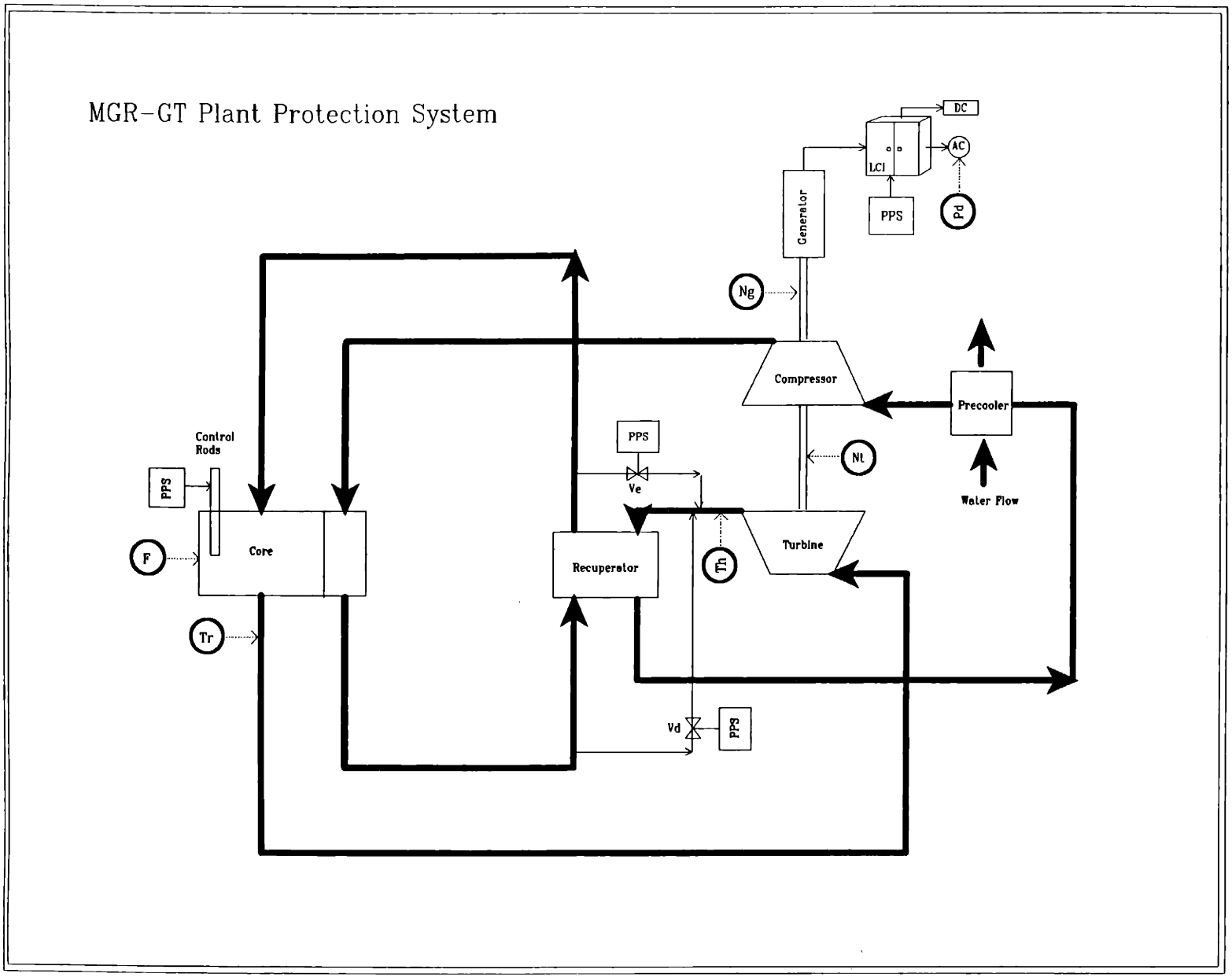

Figure 3.30 MGR-GT Plant Protection System (PPS)

(1) neutron flux in the core F,

(2) reactor outlet temperature T_r,

(3) turbine and generator speed N_t and N_g, respectively,

(4) electric load P_d, and

(5) LP-recuperator inlet temperature T_h.

The location of each parameter above is shown in Figure 3.30. The PPS controllers shown in Figure 3.31 issue protective commanding signals to the PPS components. The protective logic on which the PPS actions are based has been developed for each of the anticipated accidents, and is shown in Figure 3.32. The first column from the left in Figure 3.37 is a list of the accidents to be dealt with, while the second column lists a set of rules defining whether or not the status of each protective parameter has exceeded its setpoint of initiating protective actions. The arrowed lines from each of the events in the first column indicate the possible consequences of the accidents and resultant changes in the PPS parameters. The dotted-matrix area shows the possible protective actions which may be taken by the PPS in case that a setpoint has been exceeded.

As an example of the use of the protection logic, consider the case of a turbomachinery shaft-break which is the third event from the top in the first column. The consequences of a shaft break may be a speed discrepancy between the rotating machines, *i.e.*, the turbine, compressor, and generator, or an excessive overspeed of the turbine. If either of these two parameters monitored by the PPS sensors exceeds its setpoint as defined in the second column, the subsequent protective actions would be (1) to initiate emergency loop shutdown using the shutdown bypass valve, (2) to initiate the reactor scram to setback the reactor power, and (3) to invoke the generator circuit breaker to protect the electrical system.

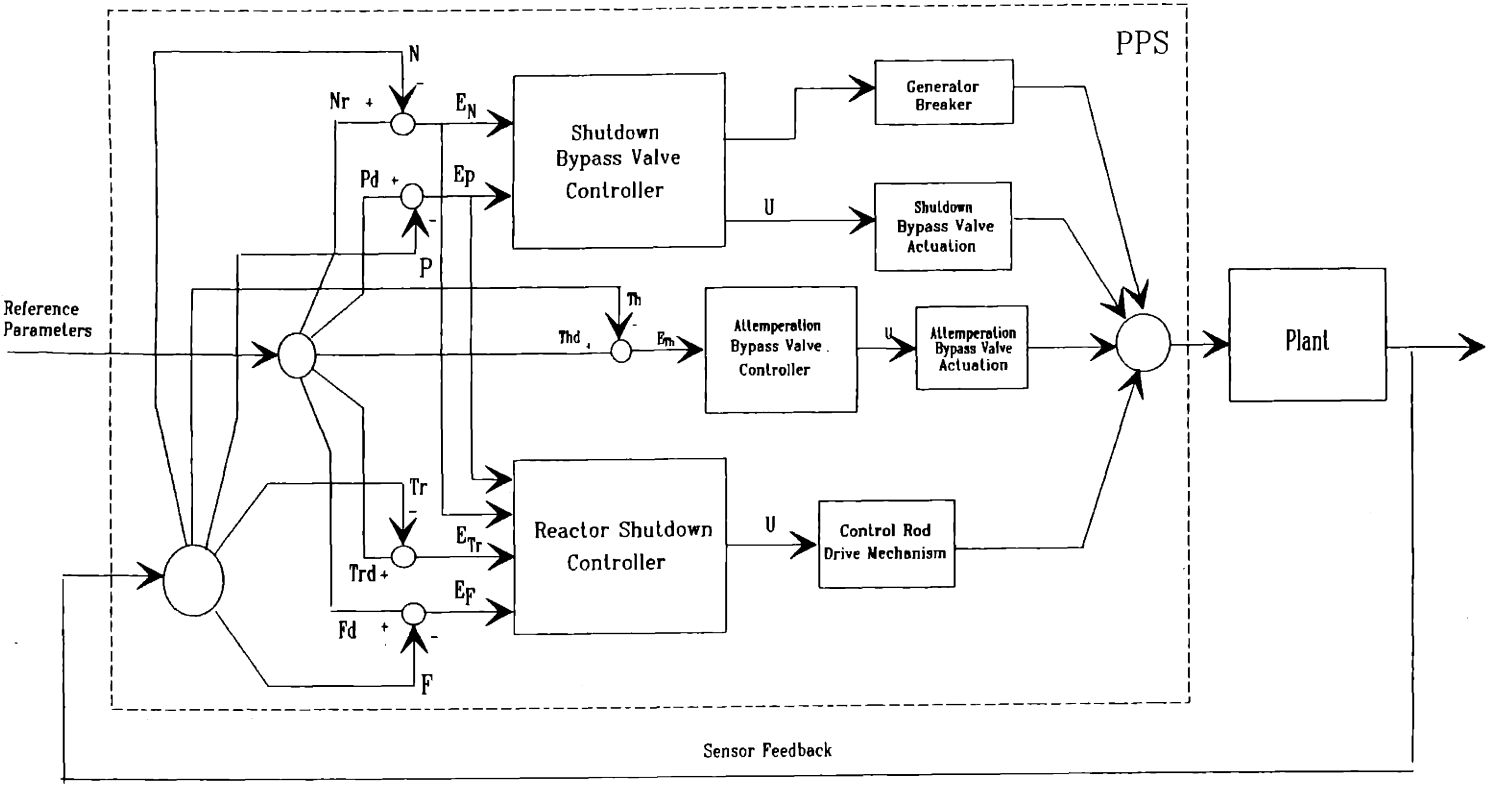

Figure 3.31 MGR-GT PPS controllers

Figure 3.32 MGR-GT PPS control logic

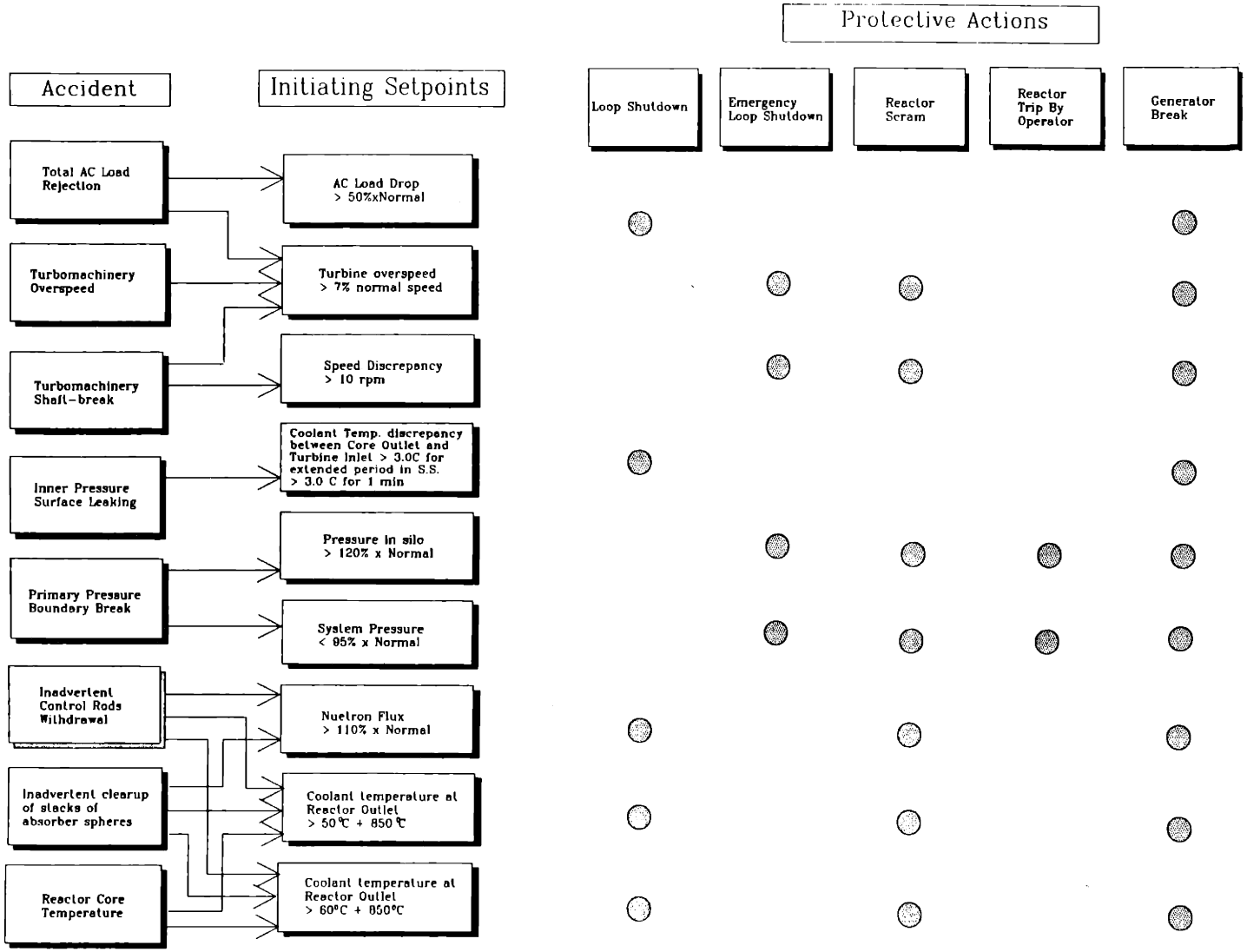

3.4.3 Design Conclusions

So far, the baseline design of the MGR-GT control system has been accomplished, which is developed to offer the automatic control functions required for the plant normal operation and to provide numerous protective actions to handle a list of anticipated accidents in the MGR-GT. The detailed evaluation of this control system will be pursued after the MGR-GT system model has become available in the next chapter.

References

[B1] Bitsch, D., Chaboseu, J.,"Power Level Control of a Closed Loop Gas Turbine, By Natural Transfer of Gas Between the Loop and Auxiliary Tanks," International Conference of the British Nuclear Energy Society, London, April 8-9, 1970.

[B2] Bammert, K., G. Krey, "Dynamic Behavior and Control of Single-Shaft Closed-Cycle Gas Turbines," Journal of Engineering for Power, P447-453, October 1971.

[B3] Bammert, K., J. Rehbach,"Gas Turbine for a Nuclear Power Plant," Atomkernenergie, Bd. 18 (1971), Lfg. 2.

[B4] Bammert, K.,"Design of a Fossil-Fired Helium Turbine Plant for Combined Power and Heat Production," Atomkernenergie, Bd.18, 1971, Lfg.3.

[B5] Bammert, K.,"Layout and Present Status of the Closed-Cycle Helium Turbine Plant Oberhausen," ASME paper 74-GT-132.

[B6] Bammert, K.,"Operation and Control of the 50-MW Closed-Cycle Helium Turbine Oberhausen," ASME paper 74-GT-13.

[B7] Bammert, K., G. Duester,"Experience with Fossil Fired CCGT Power Plants and its Transfer to Nuclear, Solar and Space Applications," Keynote Address 31st Annual International Gas Turbine Conference of the American Society of Mechanical Engineers, Dusseldorf, W. Germany, June 8-12, 1986.

[B8] Bardia, A.,"Dynamics and Control Modeling of the Closed-Cycle Gas Turbine (GT-HTGR) Power Plant," Fourth Power Plant Dynamics, Control, and Testing Symposium, Gatlinburg, Tennessee, March 17-19, 1980.

[C1] Covert, R.E., J.M. Krase, D.C. Morse, "Effect of Various Control Modes on the Steady-State Full and Part Load Performance of a Direct-Cycle Nuclear Gas Turbine Power Plant," ASME paper 74-WA/GT-7.

[C2] Chan, T., F. Openshaw, and D. Pfremmer,"HTGR-GT and Electrical Load Integrated Control," ASME paper, 80-WA/DSC-25.

[D1] Duderstadt, J.J., L.J. Hamilton,"Nuclear Reactor Analysis," John Wiley & Sons, New York, 1976

[G1] "An Assessment of the Interatom/KWU Modular HTGR Concept," Gas-Cooled Reactor Associates, SCE Co., GE Co., CE Inc., BG Inc., September 1985.

[G2] Greg, P., Gas-Cooled Reactor Associates, Personal Correspondance, 1988.

[M1] Massimo L., "Physics of High-Temperature Reactors,"Pergamon Press, Oxford/New York, 1976.

[O1] Openshaw, F., E. Estrine and M. Croft, "Control of a Gas Turbine HTGR," ASME paper 76-GT-97.

[O2] Openshaw, F., T.W. Chan,"Operational, Control and Protective System Transient Analyses of the Closed-Cycle GT-HTGR Power Plant," ASME paper 80-WA/GT-1.

[S1] Salzmann, F.,"Regulation Theory for Thermal Power Plants Employing a Closed Gas Cycle," ASME Trans.,69 (1947) 329-335

[S2] Staudt, J.E., L.M. Lidsky,"Design Study of an MGR Direct Brayton-Cycle Power Plant," MITNPI-TR-018, M.I.T., May 1987.

[W1] Wilson, D. G.,"The Design of High-Efficiency Turbomachinery and Gas Turbines," The MIT Press, Cambridge, 1984.

[W2] Weisman, J., L.E. Eckart,"Modern Power Plant Engineering," Prentic-Hall, Inc./Englewood Cliffs, 1985.

[Y1] Yan, X.L., L.M. Lidsky,"Control System Design and Dynamic Study of the MGR-GT Power Plant: *Progress Report IV*," MIT Department of Nuclear Engineering, December 1989.

Chapter Four

GTSim Code Development

4.1 Introduction

GTSim is a transient simulation program developed for use in dynamic analysis and control system design for the MGR-GT. The goal of the code is a full-scale plant system model capable of simulating a broad range of events including both normal and far-off normal transient behaviors. Such capability is ensured by a development approach that gives explicit consideration to the requirements of full-scale simulation for a nuclear power system. The development of GTSim includes the following steps:

1. A clear definition of objectives in order to specify the range of the code applicability. The objectives will be defined by a list of transient events to be simulated with the code. The time scales of the transients and their variations associated with the numerous transport processes will be examined. This information is valuable as it provides a guidance to what physical phenomenon is most important for modeling purposes. At the same time, the information offers the basis for identifying those components which are expected to have significant impacts on the transients to be studied and which, therefore, should be included in the system model.

2. Development of the system model. The system model to be developed is an actual representation of the MGR-GT physical design. The model is made as detailed as required by the objectives of the simulation, containing a layout of all those components having appreciable influences on the plant dynamic behavior. The components of the control system whose design was

presented in the foregoing chapter will be fully incorporated into the system model for evaluation. The construction of the system model takes into account the coupling relations among thermal hydraulic and energy transport processes as well as mechanical interactions in the actual plant system. The structure of the system model has significant implication on design of the code structure and solution approach.

3. Solution methods and code structure. The code structure is to be formed to specify the organization and interfaces of the code computational platforms and the system model. The executing unit of the code consisting of several computational modules will be built independently from the plant system model. This allows the system model to be changed, as the plant design evolves, without major modification to the code. Such potential flexibility is to be realized by a particularly designed interface that is capable of interpreting the system model to the code computational unit. Since the plant components behave on significantly different time scales during transients and transport effects between them play a major role in determining the characteristics of the plant behavior, it is essential that a simultaneous solution of all component models be used. Combining all the component models results in a stiff system, *i.e.*, a system with widely-distributed time constants. The stability of solutions to such system is a difficult goal. In addition, accuracy of the solution must be obtained for both short and long term simulations.

4. Modeling of the plant components. In order that the simulation enables accurate prediction to the MGR-GT performance, close representation of the physical components will be made in the development of component models.

The detail of the component models as well as the underlining assumptions will be consistent with the objectives of simulation. Efforts are to be made in validating each component model developed

5. Implementation and validation of the full-scale code. The implementation of the full-scale simulation program will be approached in two steps: first, to combine the individual components into major partial-scale systems which will then be tested and verified, and secondly, to integrate the partial systems into the final full-scale program.

4.2 Objectives of the Code Development

GTSim was developed to simulate the spectrum of transient events listed in Table 4.1. The events that specify the range of the code applicability are categorized into four groups. The first two groups are for use in the evaluation of the control system, whereas the last two groups are provided for the investigation of the plant performance under severe accident conditions.

4.2.1 Operational Events

Listed in the first group in Table 4.1 are the operational events selected based on the utility requirements for nuclear generation systems[G5]. These events are to be simulated to evaluate the MGR-GT control system design.

The load control range covers from 100% to 25% of nominal load. The load control is accomplished by the combined actions by the inventory control system and bypass control system. The plant power output as well as speed will be controlled to match load changes at various rates up to 5%/min. In addition, control for ±10% step changes in load is required at various power levels, which is considered as the most stringent load control requirement

GTSim Simulation Events

1. Operational Events

- Startup with full/partial helium inventory
- Normal shutdown with full helium inventory
- −3%/min normal load decrease (100% − 25%)
- −5%/min rapid load decrease (100% − 25%)
- +3%/min normal load increase (25% − 100%)
- +5%/min rapid load increase (25% − 100%)
- −10% step load reduction
- +10% step load increase

2. Operational Accidents

- Total electric load rejection from full power
- Turbomachinery/generator shaft break
- Control rod withdrawal at full power

3. Design Basis Accidents

- Inadvertent withdrawal of all control rods followed by normal protective control actions.
- Inadvertent withdrawal of all control rods and failure of control rod re−insertion.
- Simultaneous system depressurization and withdrawal of control rods followed by reactor shutdown.
- Simultaneous system depressurization and withdrawal of control rods without reactor shutdown.
- Inner pressure surface leakage on the lower crossduct.

4. Beyond Design Basis Accidents

- Loss of water flow in the precooler without loop shutdown.
- Double breaks of pressure boundary at upper and lower crossducts.

Table 4.1 GTSim Simulation Events.

for normal operation. The simulations of load control last from a few minutes to approximately an hour, and involve simultaneous control of the reactor and power conversion systems.

The simulation of plant startup and shutdown is intended to establish control requirements and to evaluate the proposed procedures for these operations. The normal shutdown from full power is accomplished by a few sequential steps; disconnection of electric load, run-down of the turbomachinery speed, and shutdown of the reactor. Plant startup is accomplished in a reverse order with either full or partial helium inventory in the plant circuit. The control conditions to be established include the rates at which load and speed are changed in order to ensure the system stability, the size of control bypass valves required for the full range of power and speed manipulation, cycle thermal conditions, and the level of external power required for motoring the turbomachine from stationary state to a self-sustaining speed during initial period of plant startup.

4.2.2 Operational Accidents

Three operational accidents to be simulated are listed in the second group in Table 4.1. Numerous protective means have been proposed to handle them in order to prevent plant components from damage and to mitigate them from developing into severe accidents.

In case of a total load rejection from full power, substantial excess power will be quickly imposed upon the turbomachine shaft, resulting in potential turbomachine overspeed. Several control methods have been proposed to prevent rotor overspeed from exceeding prohibited limits. First, the simplest and fastest control action is to quickly connect a dummy DC load to the electrical system to offset the loss of AC load. It is also possible to utilize the dynamic braking capability of magnetic bearings to minimize the overspeed of the rotor. In addition to these control means, a shutdown bypass valve in the Plant Protection System is installed, which enables rapid reduction of the loop pressure ratio to provide system

shutdown control. For the total load rejection, it is intended to shutdown the loop to an idle state on bypass so that a quick recovery of normal operation is possible. Simultaneously, the reactor power will be controlled by positioning the control rods so as to maintain the core outlet temperature unchanged during loop shutdown.

In the event of a turbomachinery shaft break, however, overspeed protection by the electrical system and magnetic bearings would fail. Loop shutdown thus becomes sole means for overspeed protection. Most likely, shaft break would be caused by generator failure. For example, if coils of the generator became lodged in the gap between the generator rotor and stator, the mechanical forces would be large enough to break the shaft. Based on the current rotor configuration, the shaft would most likely fail at the location in between the turbine and compressor. After shaft failure, the rotor of the turbine is left running without load connected. In addition, only small inertia is available to the turbine rotor after shaft break. It is required that the shutdown bypass valve size and actuating speed be designed to prevent the turbine from reaching a destructive overspeed limit.

It is possible to mitigate the consequence of shaft failure by choosing an alternative rotor configuration. For instance, situating the turbine between the compressor and generator in replacing the current turbomachinery arrangement would allow the turbine to be associated with either the compressor or the generator. As a result, additional inertia would become available to the turbine rotor in accident mode. This could extend the time window for the response of the shutdown bypass control before the rotor reaches the overspeed limits. The effect of bypass shutdown overspeed protection with different rotor configurations will be evaluated.

Control rod withdrawal from full power would cause positive reactivity excursion. In the MGR-GT reactor, the maximum positive reactivity insertion is 0.35% which is the amount of reactivity reserved for reactor power regulation near the full power operation. The core

temperature responds to power changes with some time delay due to the large thermal inertia of the core. A reactor scram is normally initiated by the reactor shutdown system receiving the signal indicating the neutron flux in the core greater than 110% of nominal value. If the scram signal triggered by the neutron flux fails, the reactor scram would be alternately initiated via a reactor outlet temperature signal (*i.e.*, $T > T_{normal} + 50°C$). Following the reactor scram, generator circuit breakers will be triggered to isolate the electrical system for protection, and the loop will be shutdown with bypass valve to the idle state. As the turbomachine continues to rotate, the helium will be circulated through the core to help the removal of decay heat. To prevent core from criticality after hours of reactor shutdown, the KLAK shutdown system could be used to secure cold shutdown condition.

4.2.3 Design Basis Accidents

A number of severe accidents are considered as the Design Basis accidents for the MGR-GT concept. Four design basis accidents as listed in the third group of Table 4.1 will be investigated, including the worst accident related to the plant design as far as the safety of the reactor is concerned. In contrary to the simulations of the operational events and accidents, the simulations for the design basis accidents last substantial periods, up to a few days.

Inadvertent withdrawal of all control rods causes positive reactivity disturbance of steady state in the core. Normally, such reactivity disturbance will be followed by reactor scram with control rod re-insertion on the signal of neutron flux in exceeding 10% of nominal flux level or reactor outlet temperature being 50°C higher than normal value. Upon the initiation of the reactor scram, loop will be shutdown to the idle state to continue the circulation of the helium for the removal of the decay heat from the core. Long-term shutdown of the reactor can be offered by use of the KLAK reactivity shutdown system. The simulation

is intended to evaluate the reactor shutdown operation and the effects of the helium circulation for decay heat removal.

In contrast to the normal reactor shutdown operation above, the control rod withdrawal with subsequent failure of control rod re-insertion would result in the absence of active reactor reactivity shutdown action. Consequently, the negative temperature coefficient would be relied on to setback the reactor power, and to control the core temperature below fuel failure temperature. In addition, a loop shutdown to run the turbomachine at idle will be initiated by the PPS to continue the helium circulation through the core for afterheat removal and fuel temperature control. This simulation is performed to study the reactivity transient behavior, and to acquire the core temperature transient profile as well as the maximum fuel temperature to be reached. The significance of this simulation is the evaluation of the effects of the helium circulation on the decay heat removal even though the reactor shutdown is not available. The temperature transient profiles as well as the maximum fuel temperature reached can be compared with those obtained in the previous simulation in which the active reactor shutdown is assured.

In case of simultaneous withdrawal of control rods and system depressurization, decay heat removal by helium circulation would not be available. The system depressurization event is assumed to follow pressure boundary breaks at the crossducts. The rate of depressurization varies depending on the size of breaks. Following the breaks, the reactor shutdown is initiated once there is an indication of abnormal low system pressure or high pressure in the reactor confinement building. The rate of system depressurization, the flow development in the circuit, and the maximum fuel temperature reached during core heatup are of the primary concern in this simulation.

The combination of the system depressurization and control rod withdrawal with failure of control rod re-insertion is considered to be the worst possible accident related to the MGR-

GT design concept. However, the reactor shutdown will nevertheless be provided within a short time because of the negative temperature coefficient of reactivity. The heat conduction and radiation will be the only heat transfer mechanism for decay heat removal from the inner core to the reflector and thereupon through the pressure vessel wall to the surface water cooling coils. The maximum fuel temperature to be reached is the most important parameter to be obtained in this simulation.

Inner pressure surface leakage on the inner pipe of the lower crossduct will be simulated to investigate the disturbance of steady-state operation condition. Because the pressure difference across the inner pipe is small, being the sum of the pressure drops in the core and the HP-recuperator, significant disturbance of steady-state condition following small leaks is not expected. Conditions must be established for the control system to correctly detect such "steady-state" failure.

4.2.4 Beyond Design Basis Accidents

Beyond Design Basis accidents are those extremely improbable accidents with potential severe consequences. Three beyond design basis accidents will be simulated, which are listed in the last group of the events in Table 4.1.

The simulation of loss of precooler water accident without loop shutdown is intended to study the temperature response of the precooler steel tubes which are manufactured of 304 stainless steel. It is expected that the temperature of the precooler core will increase substantially after loss of the water coolant since the helium is assumed to continuously flow through the core of the precooler. As a consequence of the precooler heatup, the inlet temperature of the compressor would increase. An inherent protection of the precooler could become possible as follows: the increase of the compressor inlet due to initial precooler heatup would increase the compressor power consumption. As the net power of the

turbomachine becomes negative, the rotor would be decelerated and might eventually be stopped. This inherent loop shutdown would prevent the helium from circulating in the precooler so that the precooler overheat could be avoided. It is unknown whether or not the maximum temperature of the precooler would exceed the failure temperature of the precooler material before a complete loop shutdown is possible. This is the primary interest of the simulation for this event.

The utilization of double crossduct configuration in the MGR-GT flowpath produces a unique accident of simultaneous ruptures of the two crossducts. It is important to know the development of the pressure and flow in the circuit, in particular, the transient stresses imposed on the components in the recuperator and reactor are of concerns.

4.3 Development of the MGR-GT System Model

The system model to be developed is an actual representation of the MGR-GT physical design. This representation is made as detailed as required by the objectives of simulation, containing all those components that are anticipated to have appreciable impacts on the system behavior. The system model will be required to reflect the significant coupling relations and transport effects among the components to be included. Substantial efforts must be made in the construction of the system model, since the structure of the system model will virtually determine the mathematical modeling and implementation of the system model and place important constraints on the design of the code solution algorithms.

4.3.1 Examination of the plant system

The MGR-GT is a closed cycle power plant consisting of a number of subsystems or major components, the working principles of which depend on entirely different types of physical laws. In spite of the complexity of the plant and the diversity of working principles,

the physical procedures the dynamic behavior is based on can be categorized into a few groups according to the most fundamental criterion in system dynamics - the characteristic time, or the time constant. Based on this approach, three groups can be identified.

To the first group of physical phenomena which run with small characteristic times belong to such dynamic processes as the time behavior of the neutronic flux after reactivity disturbance of steady state, and the mass inertia of the helium flow such as the flow compression or shock wave caused by pressure changes. The time period of these procedures amounts to fractions of a second.

The second group of medium time constants is made up by the procedures of heat diffusion through metallic wall of the recuperator and precooler, of mass storage in the volumes of the helium ducting components and storage vessels, of the energy storage of the rotating masses affecting the rotor speed. The time scales of these procedures are normally in the range of a few seconds.

Finally, there is a third group with long characteristic times which include heat storage in components with massive capacity such as the graphite core, buildup of fission products, and the radioactive decay process. Normally, these time constants range from minutes to hours.

With regard to general system modeling, the physical procedures of one or more groups must be considered depending on the purpose of the model. If, for example, the flow compressible phenomena during system depressurization are of interest, the procedures of the first group must be included. On the other hand, the dynamic behaviors of the various components ascribed to the second group must be considered if speed control of turbomachinery is to be investigated. When studying long-term control procedures such as plant startup and shutdown or calculating the processes of decay heat removal after reactor shutdown, the dynamic procedures of the third group must be considered at any case.

Based on the simulation objectives of the code, it is essential that the dynamic procedures in all three groups be considered in the MGR-GT system model. A detailed study of the MGR-GT physical design has therefore been performed to identify those components and physical processes which fall into these three categories and thus must be included in the system model. Such identification study which was briefly presented in chapter two is based on information provided by [1] for the components in the baseline design, [2] and [3] for the components of the pebble bed reactor, and [4] for the generator and electrical system. In summary, the following major components or subsystems have been included in the system model:

Reactor System

- core pebble bed
- graphite reflector, carbon brick, and core barrel
- control elements
- reactor vessel and reactor vessel cooling system
- reactor confinement building cavity.

Power Conversion System

- turbine and compressor
- generator and electrical system
- recuperator and precooler
- control components
- power conversion system silo

4.3.2 The MGR-GT System Model

Based on the foregoing, a layout of the MGR-GT system model was developed, as shown in Figure 4.1. The layout of the system model shows the plant components that have

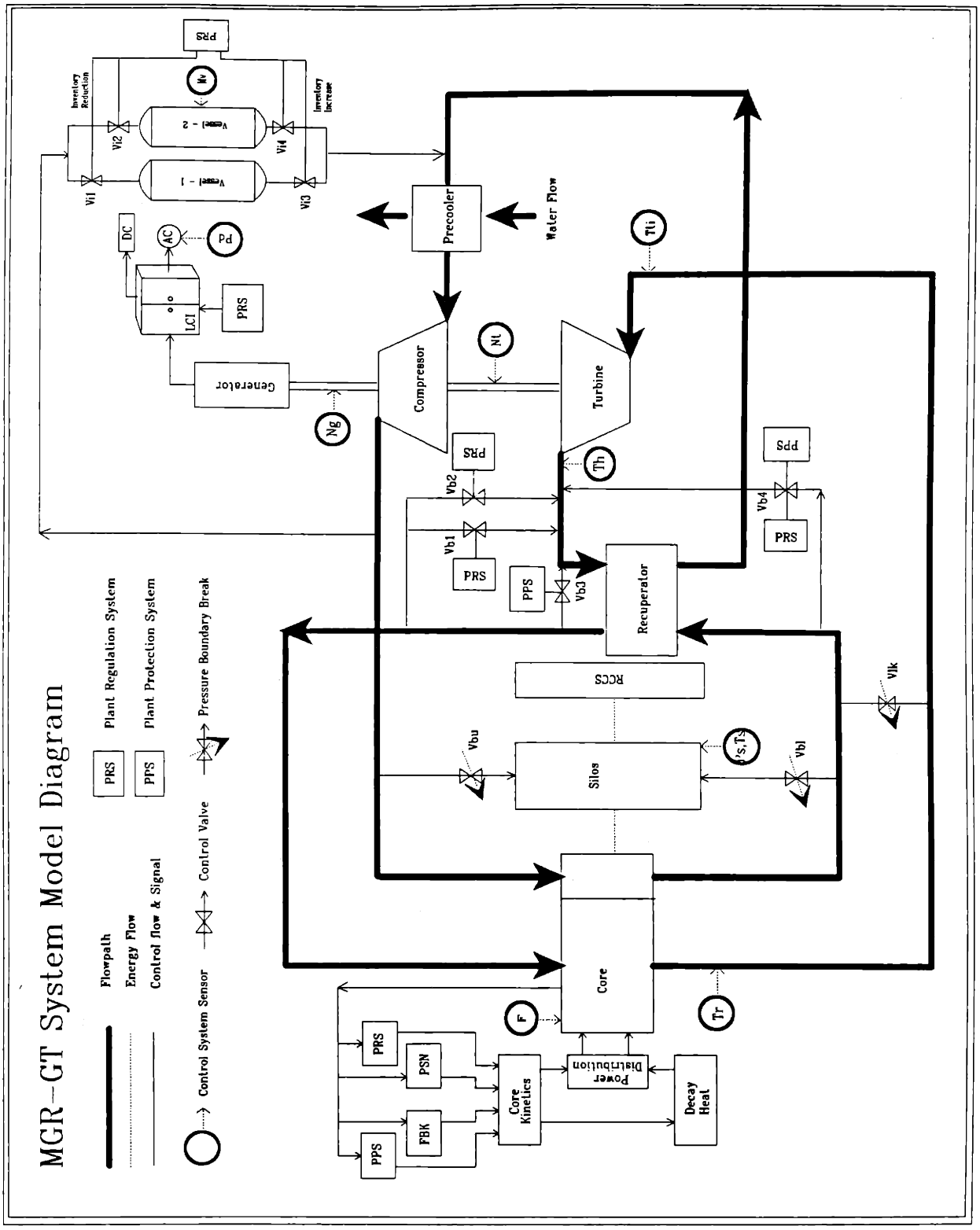

Figure 4.1 The layout of the MGR-GT system model.

been included in the system model, the couplings between the components in the forms of flowpaths, heat transport and mechanical connections, and the control system represented by numerous control components, control flowpaths, and parameters and their measurement locations with signal flow directions.

4.3.2a The Reactor Module

The core model considers such phenomena as neutron kinetics, thermal power and power distribution in the core, decay heat generation, fission product poisoning, and heat conductance including heat convection between fuel and helium, heat conduction and radiation through the fuel pebble bed.

The control components in the reactor model consists of two separate reactivity control and shutdown systems, *i.e.*, the control rod and Klak shutdown system, with a number of controllers for each system. In addition, the temperature reactivity feedback of the core negative temperature coefficient is incorporated as an inherent reactivity shutdown mechanism. The control parameters monitored by the reactor control system are neutron flux, core outlet helium temperature, and the gas temperature and pressure in the reactor confinement building.

The reactor peripheral components considered include the graphite reflector, carbon brick, core vessel, pressure vessel, and reactor vessel silo and cooling system. The thermal power generation and power distribution are considered in the graphite reflector. The heat conductance assumes one-dimensional heat transfer from the center of the core through the core lateral structure to the water cooling coils on the wall of the reactor building.

Two helium flow branches connect the reactor module with the power conversion system, the hot helium flow going through the core and cold helium flowing though the annulus formed by the core and reactor vessels. Two valves are installed between the cold

helium flow branch and the reactor confinement silo in order to emulate pressure boundary breaks for accident initiation. The reactor silo is modeled as an adiabatic volume in which mass and energy conservation are imposed.

4.3.2b The Power Conversion System Module

The power conversion system module consists of the models of all the components that participate in converting reactor thermal power into electricity, and a number of control component models including control valves and flowpaths, automatic controllers, control parameters, electrical control components, and two inventory vessels.

The dynamic performance of the turbomachine is described by the characteristics maps of the turbine and compressor. The inlet and exhaust plenums of the turbine and compressor, which have significant impact on the rotor dynamics, are modeled separately. Although the turbomachine has single-shaft configuration, the rotors of the machinery are individually modeled in order to simulate the dynamic behavior of individual rotors after shaft break. The generator model includes electric load and electrical control system components. In addition, the generator windage loss is considered for the rotor dynamics.

The recuperator model considers heat transfer between the flows at the two sides of the recuperator which couple the high and low pressure sides of the cycle. The transient behavior of the heat transfer with high rate of diffusion through the recuperator metallic wall is modeled. Similarly, the transient heat transfer in the precooler between the helium and water is modeled. Detailed models of the inlet and outlet cavities of the heat exchangers are included.

The control system model for the power conversion system consists of the inventory control system and bypass control system. The inventory control system model includes two inventory vessels, four inventory valves, Vi1 to Vi4, controllers, and control helium flowpaths.

The inventory vessels are modeled as adiabatic volumes. The bypass control model is represented by various bypass valves of the PRS and PPS. Among them are load and speed control valve Vb1, startup and shutdown valve Vb2, PPS loop shutdown valve Vb3, and attemperation valve Vb4. The bypass valves connect the high and low pressure sides of the loop at different locations. The control parameters for the automatic operation of the power conversion system include electric load Pd, helium mass in the inventory vessels Mv, rotational speeds of the turbine and generator rotors Nt and Ng, respectively, and temperature at the inlet of the LP recuperator Th.

4.3.2c The Balance of Plant

The major component models are interconnected by a series of flow passages. Mass, momentum, and energy transport inside the flow passages will be modeled adequately to enable the predication of the dynamics associated with flow compression and expansion, and flow reversal.

4.3.3 Nodalization of the Plant System Model

Based on the layout of the system model, the nodalization of the system model is developed, as shown in Figure 4.2. A brief description of the system model nodalization is given in the following, whereas more detailed information and mathematical modeling will be presented later during the development of individual component models.

4.3.3a Reactor system

The reactor core is subdivided in cylindrical coordinate into five axial segments and five concentric radial sections around core centerline, resulting in a total of 25 nodes in the core, to properly account for power distribution and temperature variation in the core. In

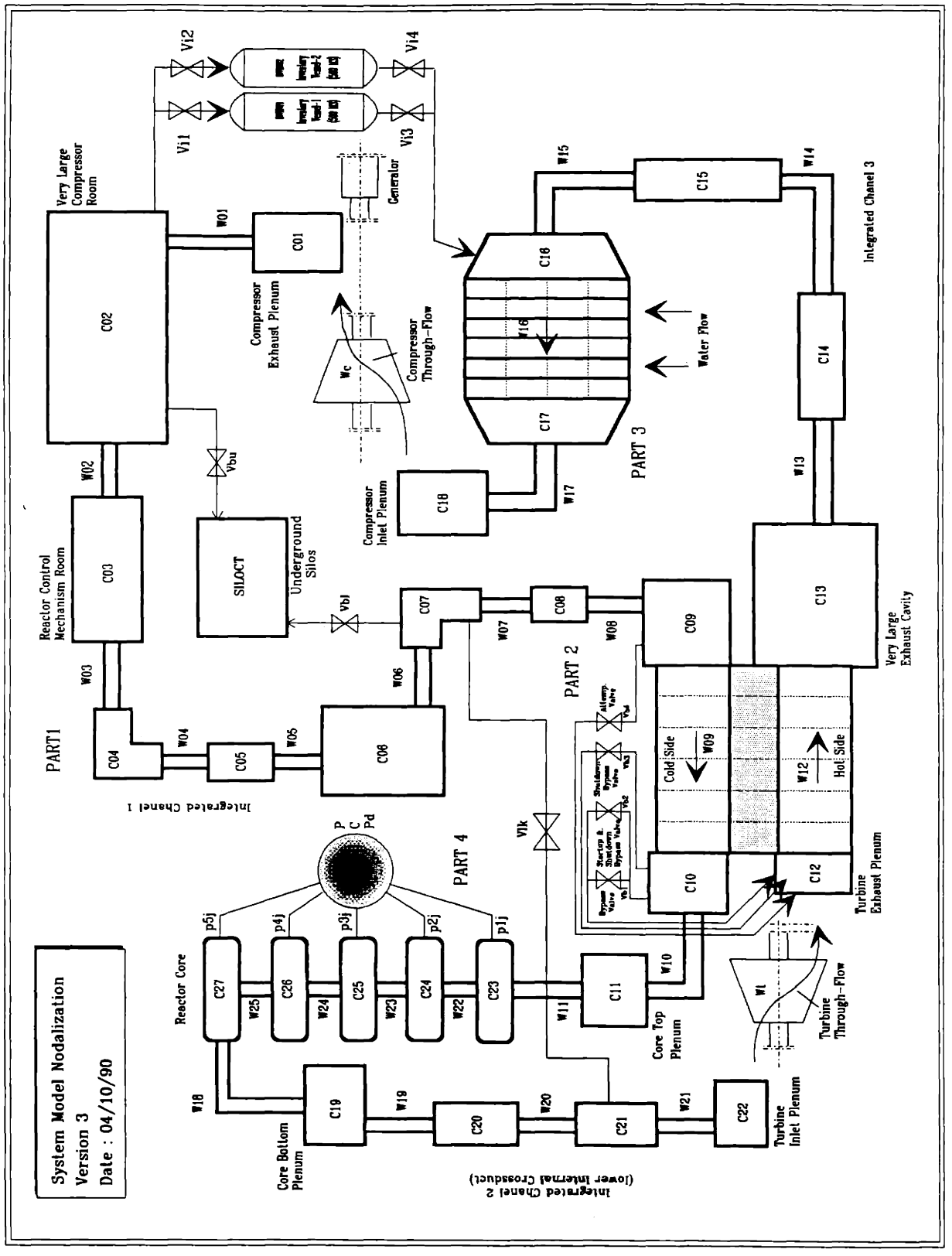

Figure 4.2 The nodalization for the MGR-GT system model.

addition, six equivalent flow segments are used to model the hydraulic processes in the core. Detailed nodalization for the reactor system is shown in Figure 4.3.

The core neutronics is described by the point reactor kinetic equations with one-effective group of delayed neutrons[D1]. The decay heat generation is to be modeled by KFA decay curves[W2]. The dynamic modeling of fission product poisoning is accounted for ^{135}I and ^{135}X. The temperature reactivity feedback due to the core negative temperature coefficient is based on the curves generated by the U.S. MHTGR program[W4]. The reactor reactivity control mechanism of the control rods and Klak absorber spheres is modeled with the specification provided in the INTERATOM/KWU reactor design[A1]. The controllers for the control system design are fully incorporated into the reactor system model.

The core surrounding components are subdivided as shown in Figure 4.3. The top reflector is modeled as a flat block of graphite penetrated by a number of borings (represented by a single equivalent flow passage), and the entrance plenum enclosed by graphite bricks. The exit of the core abuts the bottom reflector with borings and an outlet plenum. The lateral side of the core includes the side reflector, carbon brick, core vessel, helium flow passage, reactor pressure vessel, and reactor vessel cooling coils. These components are each divided into five sections along the main length of the core, to account for longitudinal thermal conditions.

4.3.3b Recuperator and Precooler

The recuperator is a counterflow, helium-to-helium heat exchanger consisting of four identical modules. The core of each module has a physical length along flow direction of 1.22 meters only. The temperature gradient from the inlet to the outlet of the recuperator is about 450°C, and the temperature difference across the two sides of the recuperator is approximately 20°C. In general, such large heat transfer effectiveness would require an

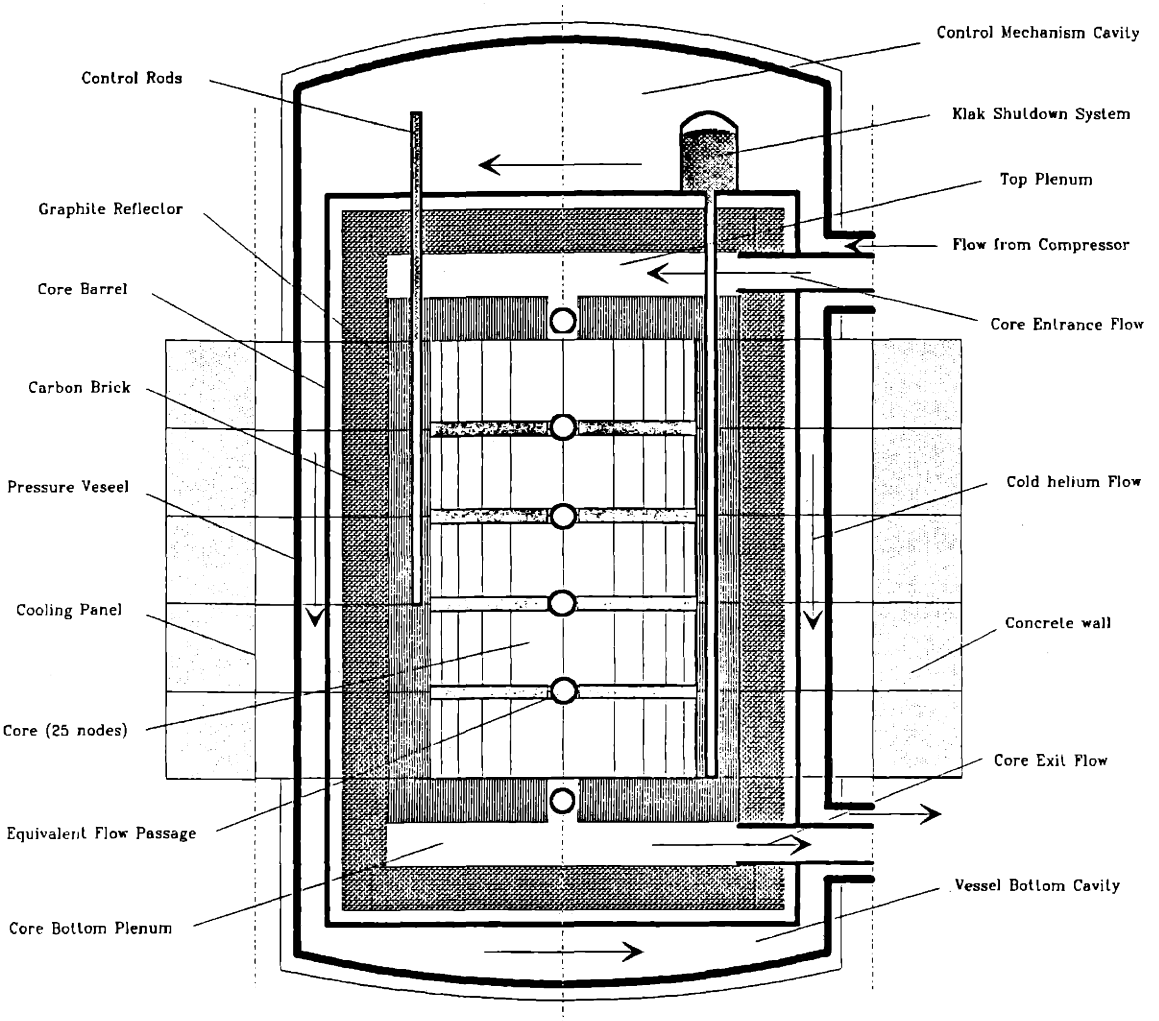

Figure 4.3 The nodalization of the MGR–GT reactor system.

extremely detailed nodalization scheme in order to provide correct prediction of transient heat diffusion between flows at the two sides of the recuperator. Otherwise, non-physical numeric results could be generated in simulation[Y1]. However, a new heat diffusion scheme has been developed to model the recuperator. As a result, only seven nodes are required for the recuperator discretization. In addition, inlet and outlet cavities are included for each side of the recuperator to model the thermal hydraulic processes in these volumes.

The precooler is a crossflow, helium-to-water, and shell-and-tube heat exchanger. The water flows inside the circular tubes while the helium passes around outer surface of the tubes in mixing flow. The helium flow is divided in the longitudinal (flow) direction of the precooler core into six subsections, in addition to an inlet and outlet plenum at each end. The average temperature of the helium in each subsection is used for calculation of heat transfer. To account for the temperature distribution, the water flow is separated into six streamlines, as indicated, each of which is further divided into four nodes. The steel tubes have the same number of nodes as the water flow.

4.3.3c Turbomachinery

The turbomachinery is modeled as a single-shaft machine consisting of the 200 MW turbine, 100 MW compressor and 2x50 MW generator. The dynamic performance of the turbine and compressor is represented by the characteristics maps, which are derived from the performance maps of the similar helium turbomachines provided by General Atomics and United Technologies[M5][D2]. The inlet and outlet plenums of the turbomachine are modeled to establish boundary conditions for use of the characteristic maps. The dynamics of three individual rotors, i.e., the rotors for the turbine, compressor, and generator, is modeled separately in order to simulate the rotor behaviors in the aftermath of shaft breaks.

4.3.3d Control System

It is important to include all the control components in the system model for evaluation. As can be seen in Figure 4.2, the inventory control system contains two inventory vessels, each with a volume of 500 m_3, and two inventory reduction valves Vi1 and Vi2 connecting the vessels with the large cavity housing the compressor casing, and two inventory increase valves Vi3 and Vi4 being located between the vessels and the precooler inlet plenum. The controllers of the inventory control system are also fully included in the system model. Four bypass valves, Vb1 to Vb4, are shown in Figure 4.2. They are load and speed control valve Vb1, shutdown and startup valve Vb2, loop shutdown valve Vb3, and attemperation valve Vb4. Valves Vb1 to Vb3 are installed between the outlet of the HP recuperator and the inlet of the LP recuperator. Attemperation valve Vb4 is located between inlets of the HP and LP sides of the recuperator. The models of the controllers for the bypass valves are contained in the system model. In addition, Vbu, Vul and Vlk shown are the valves installed to emulate the initiation of pressure boundary break and inner pressure surface leak accidents.

4.3.3e Thermal Hydraulic Components

There are numerous flow pipes and ducts in the MGR-GT plant circuit. They are modeled as a series of thermal nodes (represented by rectangular boxes), interconnected by flow segments. The thermal nodes are used to account for the mass and energy storage and transport, while the flow segments are employed to simulate hydraulic processes. A number of thermal nodes and hydraulic segments may be combined to constitute integral thermal hydraulic channels representing relatively long flow pipelines in the physical design of the plant. Based on the geometric configuration of the plant, three integrated channels are formed in the system model nodalization. These thermal hydraulic channels interconnect the

major plant components and subsystems and play an important role in the system dynamic behavior.

4.4 Solution Approach and Code Structure

Mathematical representation is made by combining mathematical models of individual components or subsystems to form a system of ordinary differential equations. Representing a nuclear power plant, such system of equations possess a wide variety of time constants, *i.e.*, is a "stiff" system. The physical phenomena can change and interact on very different time scales. It is essential that simultaneous solution to the system of equations be adopted in order to correctly predict the characteristics of the system behavior. However, assuring stability of simultaneous solutions to a stiff system is a difficult goal.

The code structure is designed to specify the organization and interfaces of the major code subsystems. The simulation procedures are fully embodied in the code structure. In addition, it is required that potential flexibility and modularity be provided in the code structure so that the code subsystems could be modified independently. The idea is to ensure that no major change would have to be made when the physical design of the plant evolves.

4.4.1 Mathematical Representation of the System Model

The diverse physical procedures and interactions on widely disparate time scales in a nuclear power plant make it fallacious to treat the equations of one component or subsystem in isolation. Sufficient consideration of transport interactions between components or subsystems during solution is crucial to the correct predication of system behavior. It is therefore required that the mathematical equations representing the models of individual components be dealt with simultaneously. The result is a system of ordinary differential equations which can be written in the space-state form as follows:

$$\frac{d\bar{y}}{dt} = F[\bar{y}, \bar{U}, t] \tag{4.1}$$

where $\bar{y}$ is the state vector determining the evolution of the system, $\bar{U}$ is control input vector maneuvering the course of the evolution, and t is the time. The full-scale MGR-GT plant requires approximately two hundred individual equations for the current system nodalization.

4.4.2 Development of Solution Algorithms

In this section, development of two algorithms as means to solve the system (4.1) will be described. The problems encountered lead to the selection of specific solution approaches in the design of the algorithms. Two algorithms, with different order formulas, have both been implemented into the GTSim code. The lower-order algorithm with a stronger stable solution scheme can be used for critical, short-term solutions, whereas the higher-order algorithm enables long-term simulations with a higher computational efficiency.

4.4.2a Problem Statements

Systems of ordinary differential equations demonstrate *stiff* behavior when the state variables change on two or more very different scales of the independent variable, i.e., the time in transients. The following example illustrates this phenomenon:

$$\begin{pmatrix} \dot{X}_1 \\ \dot{X}_2 \end{pmatrix} = \begin{bmatrix} -2000 & 999.75 \\ 1 & -1 \end{bmatrix} \begin{pmatrix} X_1 \\ X_2 \end{pmatrix} + \begin{pmatrix} 1000.25 \\ 0 \end{pmatrix} \tag{4.2}$$

The system above is a small, linear but highly-stiff system. The two eigenvalues are λ_1=-2000.5 and λ_2=-0.5, respectively. The large negative eigenvalue represents the very fast transient rate of the system with a time constant τ_1 = 5.0 x 10-4 sec, while the small

eigenvalue represents the relatively slow transient rate which has a time constant τ_2 = 2.0 sec. The analytical solution to system (4.2), with initial conditions $X_1(0) = 0$ and $X_2(0) = -2$, is

$$\begin{aligned} X_1 &= 0.499875e^{-2000.5t} - 1.499875e^{-0.5t} + 1 \\ X_2 &= -0.00025e^{-2000.5t} - 2.99975e^{-0.5t} + 1 \end{aligned} \tag{4.3}$$

Usual integration methods such as Runge-Kutta, Bulirsch-Stoer, predictor-corrector, all fail in integrating this system, because the stability of these explicit integration schemes is controlled by the most rapidly varying component: To follow the long-time behavior, one is forced to choose time steps that are on the smallest time scale. This remains true even when the fast transient has virtually vanished at t > 0.002 sec and the solution starts to be dominated by changes on the larger time scale. When the time scales vary by many orders of magnitude, the large number of steps leads to prohibitively laborious integrations, not to mention large accumulated roundoff errors. For instance, a fourth-order explicit Runge-Kutta method will require 7,692 steps to reach the steady-state solution[S3].

4.4.2b The Second-Order Method

Successful integration for stiff systems requires an implicit solution approach. One such method is the trapezoidal integration scheme. When the initial values of the state vector y in Eqn. (4.1) are known at the time t, it can be approximated for the time t+h as follows:

$$\bar{y}_{t+h} = \bar{y}_t + \frac{h}{2}[F_t + F_{t+h}] \tag{4.4}$$

which is second-order in the step size h. Since the F_{t+h} at the right hand is unknown and F is nonlinear, iteration is required for determining $\bar{y}_{t+h}$, using, for instance, a generalized Newton's method for system iteration, as follows:

$$(I-\frac{h}{2}F^{I(k-1)}_{t+h})\bar{y}^{(k)}_{t+h}=\bar{y}_t+\frac{h}{2}(F_t+F^{(k-1)}_{t+h})-\frac{h}{2}F^{I(k-1)}_{t+h}\bar{y}^{(k-1)}_{t+h} \tag{4.5}$$

where

$$F^I=\frac{\partial F}{\partial y} \tag{4.6}$$

is the matrix of partial derivatives of the right-hand side in Eqn (4.1), called the Jacobian Matrix, and I is the identity matrix. The iteration process thus requires matrix manipulation at each integration step: One selects $\bar{y}_{t+h}{}^{k-1}$ and generates $\bar{y}_{t+h}{}^{k}$ iteratively by an appropriate matrix manipulation method until the following convergence criterion has been met:

$$\left|\frac{y^{(k)}_{t+h}-y^{(k-1)}_{t+h}}{y^{(k)}_{t+h}}\right|<\epsilon \tag{4.7}$$

where ϵ is a small number. Theoretically, this implicit algorithm based on the Trapezoidal scheme is an absolutely stable (A-Stable) method and allows time steps of any sizes to be used. However, to ensure sufficient accuracy, the time step would have to be limited, depending on the requirements of accuracy. The time steps can be automatically adjusted by incorporating error control technique into the integration scheme (4.4).

The algorithm based on the above solution approach has been implemented[Y1]. To demonstrate its capabilities, the algorithm is used to solve the small system (4.2). Figure 4.4 shows results from a stability test in which a constant time step is set to be 0.05 sec, which is quite large comparing to the fast time constant of the system, and error control is temporarily disabled. The numerical integration is plotted against the exact solution from (4.3). As can be seen, one of the numerical solutions oscillates around a central curve being one of the curves from the analytical solutions, and is very stable during the initial fast transient period although accuracy is not obtained. Accuracy of the solution is gradually

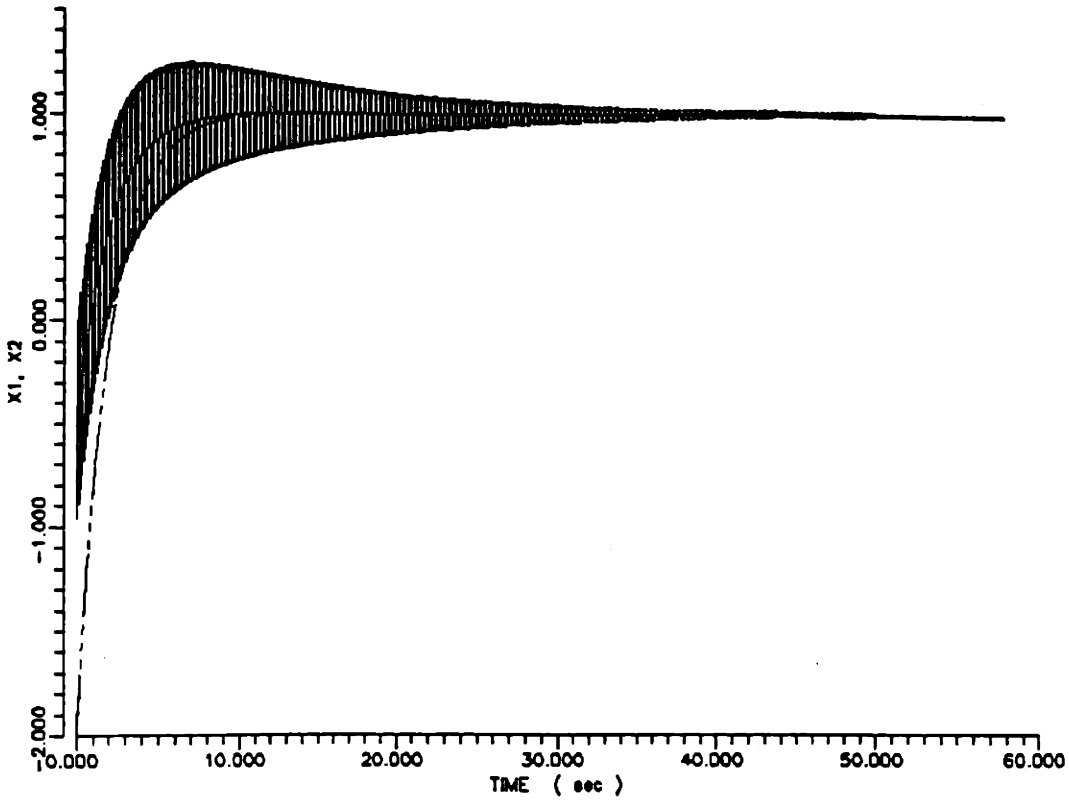

Figure 4.4 GTSim Algorithm Stability Test.

regained as the solution becomes more stable. Having incorporated the error control which evaluates the error for each step of the integration and automatically adjusts the time step accordingly, the algorithm is again used to solve the same system. The result is shown in Figure 4.5. It can be seen that the numerical solution represented by scattered dots has accurately predicted transient behavior of the system plotted by the solid-line curves from analytical solution (4.3) during both initial fast and later slow transient periods. The simulation requires only 32 steps to reach the steady-state conditions[Y1].

4.4.2c The Fourth-Order Method

The objectives of this study include both short and long term simulations. For the long-term simulations, computational efficiency becomes more crucial. To increase the efficiency of computation, larger time steps must be allowed in integration without sacrificing the accuracy of solution. The resolution to this problem is the use of higher order integration schemes. Practical high-order algorithms for stiff systems in use before about 1980 are quite complicated. An example is gear's popular method[G3], which is a variable order, variable step size, predictor-corrector method. It and its descendants are still widely used in many engineering and scientific applications; however, it does not lend itself to concise description or implementation. The more recent algorithm developed by Kaps and Rentrop is more efficient in implementation and generalization for specific problem[K3][P1]. The Kaps-Rentrop method seeks a solution for the system (4.1) of the form

$$\bar{y}_{t+h} = \bar{y}_t + \sum_{i=1}^{s} c_i \bar{K}_i \tag{4.8}$$

where the corrections $\bar{K}i$ are found by solving s linear equations that generalize the structure of Newton's method in (4.5):

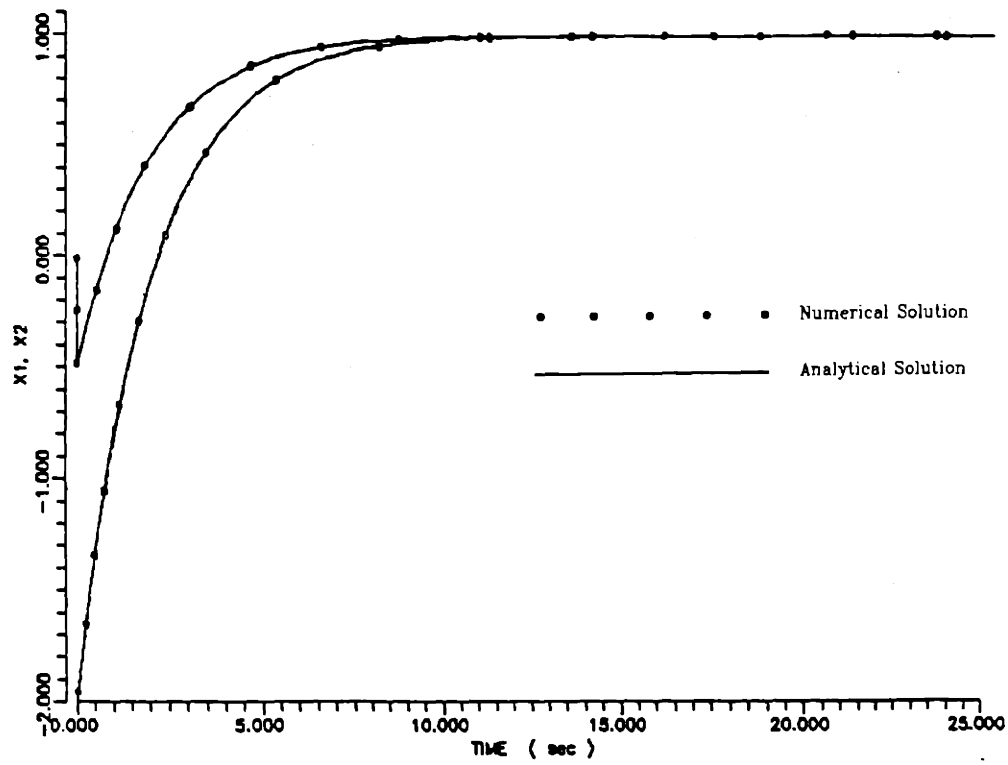

Figure 4.5 GTSim Algorithm Stability and Accuracy Test.

$$(I-\gamma hF')\bar{K}_i = hF_{t+h\sum_{j=1}^{i-1}a_{ij}} + hF'\sum_{j=1}^{i-1}\gamma_{ij}\bar{K}_j, \quad i=1,\ldots,s \tag{4.9}$$

where the coefficients γ, c_i, α_{ij}, and γ_{ij} are fixed constants independent of the system (4.1). Eqn. (4.9) can be solved successively by suitable matrix-vector manipulation for K1, K2,... .

Crucial to the success of this stiff integration scheme is an automatic step size adjustment algorithm. The Kaps-Rentrop scheme uses an embedded technique, similar to Runge-Kutt-Fehlberg method: two estimates of the form (4.8) are calculated, a high-order one, $\bar{y}$, and a lower-order estimate $\hat{\bar{y}}$ with different coefficients, $\hat{c}_i$, $i=1,\ldots,\hat{s}$, where $\hat{s} < s$ but the Ki are the same. The difference between $\bar{y}$ and $\hat{\bar{y}}$ leads to an estimate of the local truncation error, which can then be used for time step size control. Raps and Rentrop show that the smallest value of s for which embedding is possible is $s = 4$, $\hat{s} = 3$, leading to a fourth-order method. The constant coefficients for the fourth-order methods can be found in [K3].

The time step control depends on the fact that

$$\begin{aligned} \bar{y}_{true} &= \bar{y}+h^5\bar{g}+\cdots, \\ \hat{\bar{y}}_{true} &= \hat{\bar{y}}+h^4\hat{\bar{g}}+\cdots, \end{aligned} \tag{4.10}$$

where only the leading terms in powers of h are kept in the error series. Thus

$$|\bar{y}-\hat{\bar{y}}| = h^4\bar{g}+\cdots, \tag{4.11}$$

Suppose an initial integration step is successful, that is,

$$|\bar{y}-\hat{\bar{y}}| \le \varepsilon \tag{4.12}$$

for some error tolerance ε. This implies that

$$|h^4\bar{g}| \le \varepsilon \tag{4.13}$$

For the next step size h_{next} to be successful, it is required that

$$|h_{NEXT}^4\bar{g}_{NEXT}| \le \varepsilon \tag{4.14}$$

However, to leading order in h one has $\bar{\delta}_{Next} = \bar{\delta}$, and thus (4.12) and (4.14) mean

$$h_{NEXT} \le h\left(\frac{\varepsilon}{|\bar{y}-\bar{\hat{y}}|}\right)^{1/4} \tag{4.15}$$

This estimate can also be used to reduce the time step size when repeating a step because (4.12) was not satisfied.

The following small-scale system[1] has been solved with this algorithm:

$$\begin{aligned} \dot{y}_1 &= -0.013y_1 - 1000y_1y_3 \\ \dot{y}_2 &= -2500y_2y_3 \\ \dot{y}_3 &= -0.013y_1 - 1000\dot{y}_1y_3 - 2500y_2y_3 \end{aligned} \tag{4.16}$$

with initial conditions $y_1(0)=1$, $y_2(0)=1$, and $y_3(0)=0$. Even though the ratio of largest to smallest time constants for this system is up to 10^6, the integration for t = 50 sec requires only 29 steps with an error limit ε = 10-4. By contrast, however, the Runge-Kutta method requires 33,596 steps[P1].

4.4.2d System Matrix Manipulation

Both of the GTSim integration schemes require system matrix manipulation for the solution to the nonlinear systems (4.5) and (4.9), respectively. One method has been developed based on Successive Over-Relaxation (SOR) method[B1]. Eqns. (4.5) and (4.9) can both be transformed into the following linearized system when seeking the solution of the state vector $\bar{X}$ which represents $\bar{y}_{t+h}^{k}$ in (4.5) and K_i in (4.9):

$$\hat{F}'_t \, \bar{X}^k_{t+\delta t} = \bar{F}^{k-1}_{t+\delta t} \tag{4.17}$$

where $\hat{F}'$ is the n x n quasi-Jacobian system matrix which is the replacement of the left-hand sides of (4.5) and (4.9), evaluated with the values of the state vector at time t. $\bar{F}$ on the right-hand side of Eqn. (4.17) is a n-dimensional vector consisting of the sum of the right-hand

[1]This problem is chosen from the test case D4 in [E1].

sides of Eqns. (4.5) and (4.9), calculated with the values of the state vector from the previous iteration within the same integration step. To determine the values of the state vector of the current iteration $\bar{X}_{t+dt}^{K}$, the SOR method, as described in the following, is used.

The SOR method seeks the solution to system (4.17) by the following iteration procedure:

$$x_i^{(m)} = (1-\omega)x_i^{(m-1)} + \frac{\omega}{\hat{f}_{ii}}\left[\bar{f}_i - \sum_{j=1}^{i-1}\hat{f}_{ij}x_j^{(m)} - \sum_{j=i+1}^{N}\hat{f}_{ij}x_j^{(m-1)}\right] \qquad i=1,2,\cdots,N \tag{4.18}$$

where x_i is the ith variable in the state vector $\bar{X}_{t+dt}^{K}$, $\hat{f}_{ij}$ the entry at row (i) and column (j) in matrix $\hat{F}'$ of system (4.17), and $\bar{f}_i$ the ith component in the $\bar{F}$. w in (4.18) is a positive constant. Ostrowki-Reich theory states that for a positive definite matrix $\hat{F}_t'$ and $0 < w < 2$ the SOR method converges for any choice of initial approximate condition vector $\bar{X}$ (0)[B1]. For choices of $0 < w < 1$, the procedure can be used to obtain convergence for some ill-conditioned systems. For choices $1 < w$ the procedure can be used to accelerate convergence of well-behaved systems. The convergence criterion for (4.18) can be chosen as:

$$\left|\frac{x_i^{(m)} - x_i^{(m-1)}}{x_i^{(m)}}\right| < \varepsilon, \qquad i=1,2,\cdots n \tag{4.19}$$

where ε is a small number.

The above matrix manipulation method has been implemented to support both of the GTSim integration algorithms. Since the system (4.1) representing the MGR-GT power plant is a sparse system, a special designed interfacing subroutine is built into the code that is capable of translating the structure of the system matrix to the matrix manipulation algorithms so that the actual system manipulation will deal mostly with non-zero elements in the system matrix. This substantially reduces the amount of computational efforts required.

4.4.3 Design of the Code Structure

The code structure is intended to provide great flexibility and modularity for maintenance and upgrade. The flexibility is desired as it facilitates simple changes when the physical design of the MGR-GT evolves. The modularity permits the subsystems of the code to be upgraded independently. Based on this design approach, the code is constructed as shown in Figure 4.6. As can be seen, the code entity consists of three performance platforms, *i.e.*, the computing platform, the system model platform, and the operating platform. The maintenance for these three subsystems such as modification, compiling, and portability is independent of one another. They are linked together by means of interface only during run-time simulation. In addition, each of the platforms contains several modular units which are interrelated based on run-time instruction during simulation, and their non-operational maintenance is also separable.

4.4.3a The Computing Module

The computing platform is the center of the code, consisting of a run-time instruction "chip" named as GTSim Running Router, three algorithm cards, a utility library, and a result storage "disk". The instruction chip contains a simulation flowchart listing the run-time routines for directing the course of simulation for specific tasks. The interior design of the instruction chip is shown in Figure 4.7. As indicated, any simulation starts from the top of the flowchart and enters the second step at which the user will be prompted to instruct the current simulation. For instance, the information required from the user at this step includes the nature of running, *i.e.*, steady-state convergence or transient simulation. If the steady-state convergence is intended by the user, then further information to be asked will be which type of convergence, steady converging or dynamic converging, is to be pursued. On the other hand, if transient simulation is to be performed, the information such as which accident

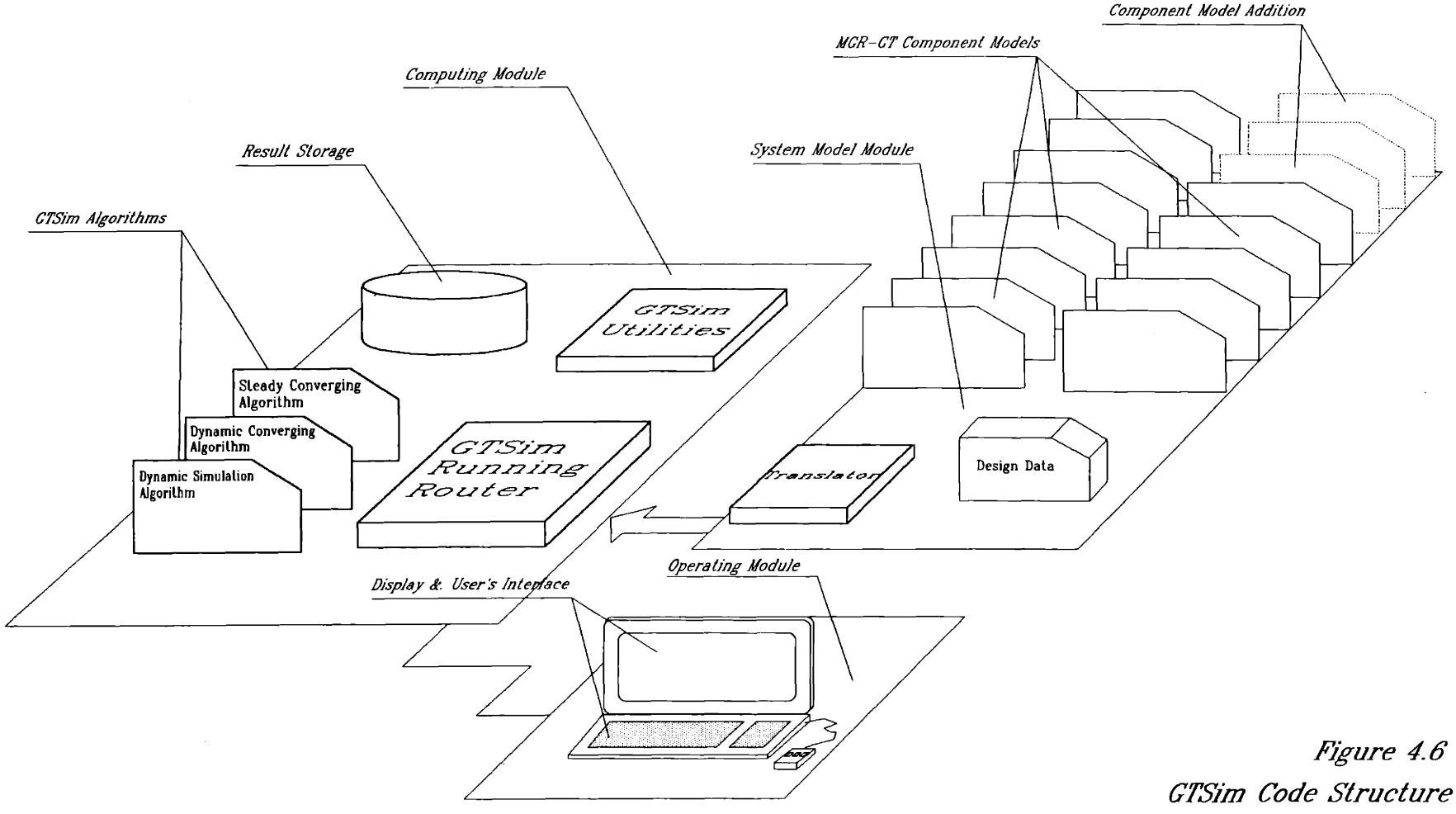

Figure 4.6
GTSim Code Structure

Figure 4.7 GTSim Running Router

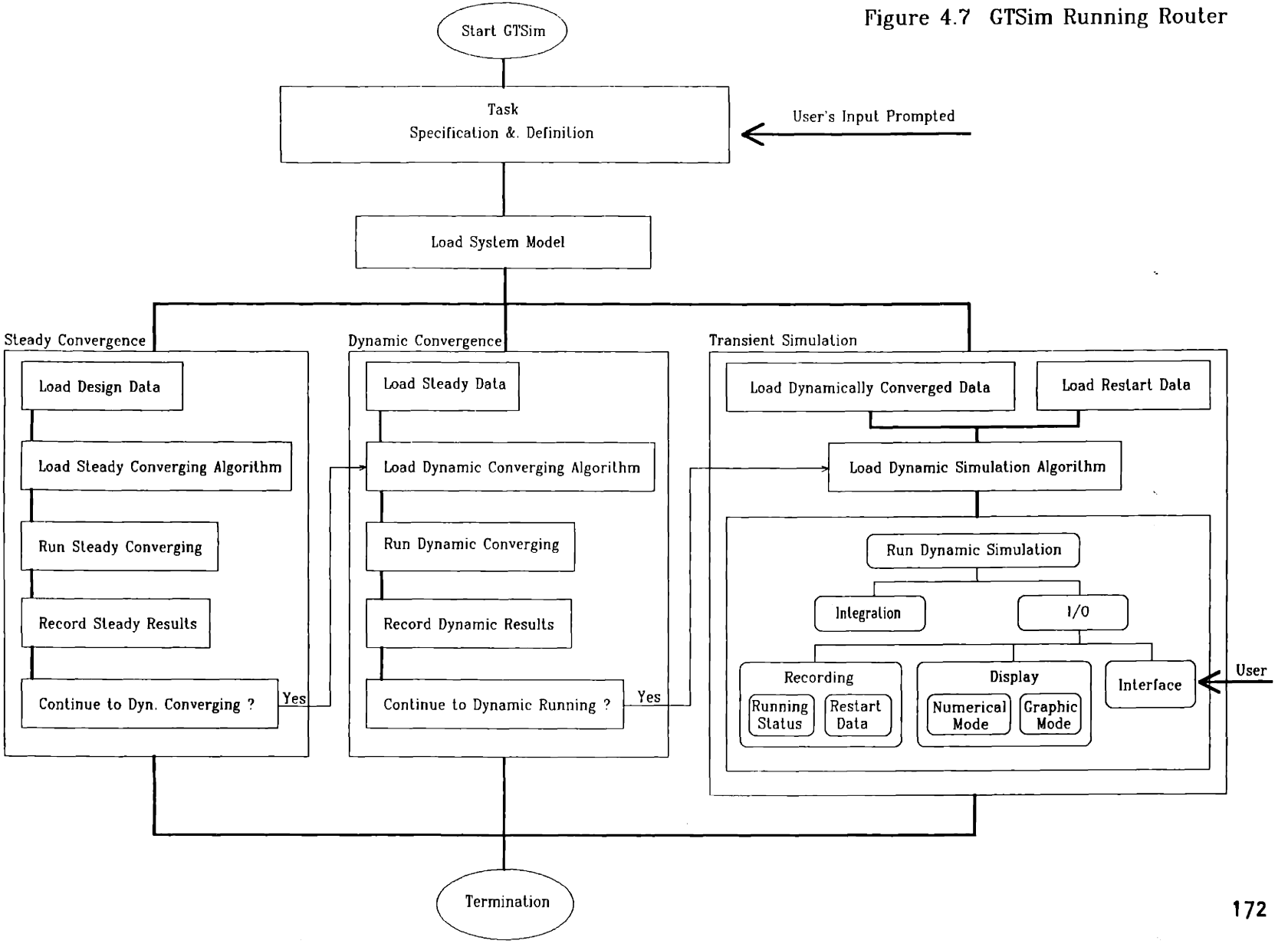

event is to be simulated is required.

Having acquired the above information, GTSim will begin, at the third step, to load the system model from the system model platform and then continue to pursue the task of simulation according to the specification by the user. Based on the nature of running, necessary data and algorithms will be loaded and the simulation will proceed following the listed instruction. Run-time data will be sent to the operating platform for display. The user may interface with the simulation on the operating platform. The simulation ends at the bottom of the flowchart when the desired task has been accomplished.

The utility library on the computing platform contains the utility programs and subroutines to support such operations as compiling, linking, run-time I/O processing, and graphic display, and user interfacing.

4.4.3b The System Model Module

The system model platform contains the mathematical models representing the MGR-GT power plant. The MGR-GT component models are located in array of individual model boards on the system model platform. They may be independently designed, modified, and maintained. In addition, any new component models resulted in the plant design evolution can be added onto the platform, as indicated with the cards in dashed-outlines. The plant design data, including physical design specification and operation parameters, are also located on this platform. The information on the structure of the system model is contained in the Translation Chip which explains the system model structure to the GTSim Running Router when it interfaces with the Translation Chip to load the system model onto the computing platform during run-time.

As the plant physical design changes, only the Translation Chip requires corresponding modification so as to accommodate the new structure. Such modification,

however, is normally very straightforward for any minor design variations, because the transport phenomena among the plant components and dynamic processes in both spatial and temporal dimensions have inherently been considered by means of simultaneous solution to the system equations.

4.4.3c The Operating Module

The operating module consists of hardware including display monitors, keyboard, and pointing mouse. Run-time results are sent from the computing platform to the operating platform for display in numeric and graphic modes. The required utilities for display are supplied from the GTSim utility library on the computing platform. Users may interface and control simulations on a number of developed interfacing windows with either keyboard command input or mouse pointing.

4.5 Modeling of Plant Components

In this section, the mathematical modeling for the major MGR-GT components will be presented. Description for the component models and their nodalization schemes has been given during the design of the system model.

4.5.1 Thermal Hydraulic Modeling

In the MGR-GT system model, there are situations in which the helium flows through long pipelines. Typical of such situations are the three integrated thermal hydraulic channels interconnecting the component models to form the balance of plant. The mathematical representation for such channels will be developed based on conservation laws in the following.

4.5.1a Partial Differential Equations of State

Laws of conservation of mass, momentum, and energy may be used to describe the physical processes inside the thermal hydraulic channels. If one-dimensional flow is assumed, these conservation laws can be written, respectively, as[M2]:

$$\frac{\partial \rho}{\partial t}+\frac{\partial G}{\partial x}=0 \tag{4.20}$$

$$\frac{\partial G}{\partial t}+\frac{\partial (G^2/\rho)}{\partial x}=-\frac{\partial p}{\partial x}-f\frac{|G|G}{2D_e\rho}-\rho g \tag{4.21}$$

$$\rho\frac{\partial h}{\partial t}+G\frac{\partial h}{\partial x}=\frac{\partial q}{\partial x}+\left(\frac{\partial p}{\partial t}+\frac{G}{\rho}\frac{\partial p}{\partial x}\right)+f\frac{|G|G^2}{2\rho^2 D_e} \tag{4.22}$$

where

ρ = helium density, kg/m^3,

G = mass velocity, kg/m^2-s

p = pressure, Pa,

f = flow friction coefficient, including frictions with pipe wall and due to geometric variation effects,

D_e = equivalent hydraulic diameter of pipeline, m,

g = vertical component of gravity constant in the negative direction, m^2/s,

h = enthalpy per unit mass, J/kg, and

q = sum of heat flux, including heat source, heat transfer, mechanical work, and etc, J/m^2-s.

From the above basic conservation laws, the state equations used for the thermal hydraulic model are developed in the following.

In Eqn. (4.3), h is, by definition, the sum of stagnant enthalpy and kinetic energy of

helium flow and can be written as:

$$h=h_s+\frac{1}{2}\left(\frac{G}{\rho}\right)^2 \tag{4.23}$$

Eqns. (4.22) and (4.23) may be combined to yield a time derivative for h_s in replacing that for h:

$$\rho\frac{\partial h_s}{\partial t}-\frac{\partial p}{\partial t}=\frac{\partial q}{\partial x}-G\frac{\partial h}{\partial x}+\frac{G}{\rho}\frac{\partial p}{\partial x}+f\frac{|G|G^2}{2\rho^2 D_e}+\left(\frac{G}{\rho}\right)^2\frac{\partial \rho}{\partial t}-\frac{G}{\rho}\frac{\partial G}{\partial t} \tag{4.24}$$

Furthermore, the stagnant enthalpy h_s may be assumed as a function of state variables - temperature T (in K) and pressure p, and can be expressed as:

$$h_s=h_s(T,p) \tag{4.25}$$

and the differential form of eqn. (4.25) is

$$\frac{\partial h_s}{\partial t}=\frac{\partial h_s}{\partial T}\frac{\partial T}{\partial t}+\frac{\partial h_s}{\partial p}\frac{\partial p}{\partial t}=h_{sT}\frac{\partial T}{\partial t}+h_{sp}\frac{\partial p}{\partial t} \tag{4.26}$$

Using (4.26) in (4.24) to eliminate the time derivative of h_s results in

$$\rho h_{sT}\frac{\partial T}{\partial t}+(\rho h_{sp}-1)\frac{\partial p}{\partial t}=\frac{\partial q}{\partial x}-G\frac{\partial h}{\partial x}+\frac{G}{\rho}\frac{\partial p}{\partial x}+f\frac{|G|G^2}{2\rho^2 D_e}+\left(\frac{G}{\rho}\right)^2\frac{\partial \rho}{\partial t}-\frac{G}{\rho}\frac{\partial G}{\partial t} \tag{4.27}$$

The equation of state of helium can be given by

$$\rho=\rho(T,p) \tag{4.28}$$

The differential form of the state equations is

$$\frac{\partial \rho}{\partial t}=\frac{\partial \rho}{\partial T}\frac{\partial T}{\partial t}+\frac{\partial \rho}{\partial p}\frac{\partial p}{\partial t}=\rho_T\frac{\partial T}{\partial t}+\rho_p\frac{\partial p}{\partial t} \tag{4.29}$$

Eqns. (4.27) and (4.29) may then be combined to yield one equation with only ∂t/∂t and a second with only ∂p/∂t:

$$(\rho h_{sT}\rho_p-\rho h_{sp}\rho_T+\rho_T)\frac{\partial T}{\partial t}=\rho_p\frac{\partial q}{\partial x}-\rho_p G\frac{\partial h}{\partial x}+\rho_p\frac{G}{\rho}\frac{\partial p}{\partial x}+\rho_p f\frac{|G|G^2}{2\rho^2 D_e}$$
$$+[\rho_p(\frac{G}{\rho})^2-(\rho h_{sp}-1)]\frac{\partial \rho}{\partial t}-\rho_p\frac{G}{\rho}\frac{\partial G}{\partial t} \tag{4.30}$$

and

$$(\rho h_{sp}\rho_T-\rho h_{sT}\rho_p-\rho_T)\frac{\partial p}{\partial t}=\rho_T\frac{\partial q}{\partial x}-\rho_T G\frac{\partial h}{\partial x}+\rho_T\frac{G}{\rho}\frac{\partial p}{\partial x}+\rho_T f\frac{|G|G^2}{2\rho^2 D_e}$$
$$+[\rho_T(\frac{G}{\rho})^2-\rho h_{sT}]\frac{\partial \rho}{\partial t}-\rho_T\frac{G}{\rho}\frac{\partial G}{\partial t} \tag{4.31}$$

The time derivatives of the density ρ and flow mass velocity G at the right-hands of Eqns. (4.30) and (4.31) can be substituted with (4.20) and (4.21), resulting in:

$$(\rho h_{sT}\rho_p-\rho h_{sp}\rho_T+\rho_T)\frac{\partial T}{\partial t}=\rho_p\frac{\partial q}{\partial x}-\rho_p G\frac{\partial h}{\partial x}+2\rho_p\frac{G}{\rho}\frac{\partial p}{\partial x}+\rho_p f\frac{|G|G^2}{\rho^2 D_e}$$
$$-[\rho_p(\frac{G}{\rho})^2-(\rho h_{sp}-1)]\frac{\partial G}{\partial x}+\rho_p\frac{G}{\rho}\frac{\partial(G^2/\rho)}{\partial x}+\rho_p G g \tag{4.32}$$

and

$$(\rho h_{sp}\rho_T-\rho h_{sT}\rho_p-\rho_T)\frac{\partial p}{\partial t}=\rho_T\frac{\partial q}{\partial x}-\rho_T G\frac{\partial h}{\partial x}+2\rho_T\frac{G}{\rho}\frac{\partial p}{\partial x}+\rho_T f\frac{|G|G^2}{\rho^2 D_e}$$
$$-[\rho_T(\frac{G}{\rho})^2-\rho h_{sT}]\frac{\partial G}{\partial x}+\rho_T\frac{G}{\rho}\frac{\partial(G^2/\rho)}{\partial x}+\rho_T G g \tag{4.33}$$

Writing Eqns. (4.21), (4.32), and (4.33) together, after some minor algebraic reorganization, produces a set of equations:

$$\frac{\partial G}{\partial t}=-\frac{\partial p}{\partial x}-f\frac{|G|G}{2D_e\rho}-\frac{\partial(G^2/\rho)}{\partial x}-\rho g \tag{4.34}$$

$$\frac{\partial T}{\partial t}=\frac{1}{(\rho h_{sT}\rho_p-\rho h_{sp}\rho_T+\rho_T)}\{\rho_p\frac{\partial q}{\partial x}-\rho_p G\frac{\partial h}{\partial x}+2\rho_p\frac{G}{\rho}\frac{\partial p}{\partial x}+\rho_p f\frac{|G|G^2}{\rho^2 D_e}$$
$$-[\rho_p(\frac{G}{\rho})^2-(\rho h_{sp}-1)]\frac{\partial G}{\partial x}+\rho_p\frac{G}{\rho}\frac{\partial(G^2/\rho)}{\partial x}+\rho_p G g\} \tag{4.35}$$

and

$$\frac{\partial p}{\partial t}=\frac{1}{(\rho h_{sp}\rho_T-\rho h_{sT}\rho_p-\rho_T)}\{\rho_T\frac{\partial q}{\partial x}-\rho_T G\frac{\partial h}{\partial x}+2\rho_T\frac{G}{\rho}\frac{\partial p}{\partial x}+\rho_p f\frac{|G|G^2}{\rho^2 D_e}$$
$$-[\rho_T(\frac{G}{\rho})^2-\rho h_{sT}]\frac{\partial G}{\partial x}+\rho_T\frac{G}{\rho}\frac{\partial(G^2/\rho)}{\partial x}+\rho_T G g\} \tag{4.36}$$

Carefully observing Eqns. (4.34) to (4.36), it can be seen that they only concern three variables T, P, G since other variables and items, including density ρ, and enthalpies h_s and h, are the functions of these three variables. Eqns. (4.34) to (4.36) are the basic state differential equations with the state variables being G, T, and P, which govern the dynamic behavior of thermal hydraulic pipelines.

The state equations of the helium for density and d can be used to obtain coefficients in (4.34) to (4.36). Consider helium as real gas, the density as a function of temperature and pressure is given by[G4]

$$\rho=\frac{p}{RT+B(T)p} \tag{4.37}$$

where R is the gas constant of helium and B(T) is given by

$$B(T)=C_1+\frac{C_2}{1-C_3T}+\frac{C_4}{1+C_5T} \tag{4.38}$$

where C_1 to C_5 are constants which are given in [G4]. Similarly the stagnation enthalpy of helium as a function of temperature and pressure may be expressed as follows:

$$h_s=h_{s0}+C_pT+[B(T)-T\frac{dB(T)}{dT}]p \tag{4.39}$$

where Cp is helium specific heat at constant pressure, and h_{s0} is a reference constant being 5557 J/kg, such that the enthalpy at 315.6 K and 1 atm equals the value determined by Akin[A2]. Since differences in enthalpy are of main interest, the exact value of this constant is not important.

4.5.1b Finite Difference Equations of State

The partial differential equations of state (4.34) to (4.36) must be discretized into the finite element approximation form in order to solve them numerically. The task is approached by dividing a long pipeline into a number of flow and thermal nodes as shown schematically in Figure 4.8, and then converting the state equations into corresponding difference equations on these nodes.

For the flow node (j), the difference equation of (4.34) is

$$\frac{\partial W_j}{\partial t}=-\frac{(p_i-p_{i-1})A_j}{\Delta x_j}-f_j\frac{|W_j|W_j}{2D_e\rho_j A_j}-\frac{1}{\Delta x_j A_j}\left(\frac{W_i^2}{\rho_i}-\frac{W_{i-1}^2}{\rho_{i-1}}\right)-\rho_j g\frac{A_j(H_i-H_{i-1})}{\Delta x_j} \qquad (4.40)$$

where A is the cross-section area of pipeline, in m^2, W is the mass flow rate in kg/s which is the product of the flow mass velocity G and cross-section area A, and H is the elevation head in the gravity field. The properties in equation (4.40) are evaluated at the locations as indicated by their subscripts. The boundary flow rates W_i and W_{i-1} of the flow node (j) are defined as:

$$W_{i-1}=\frac{W_{j-1}+W_j}{2}$$
$$W_i=\frac{W_j+W_{j+1}}{2}$$

For thermal node (i), the finite element forms of two partial differential equations of state (4.35) and (4.36) can be obtained as:

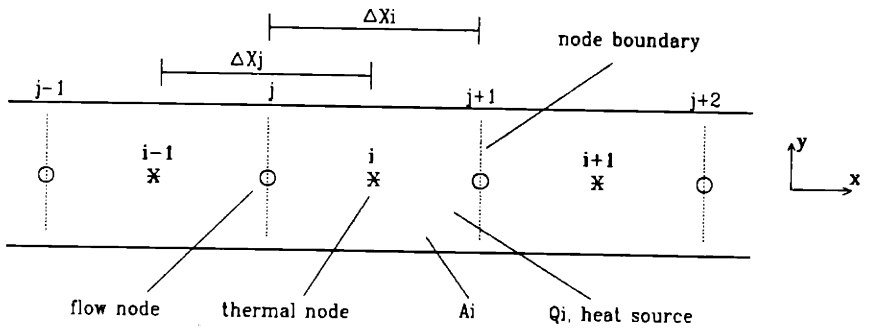

Figure 4.8 Finite element thermal hydraulic pipeline model

$$\frac{\partial T_i}{\partial t}=\frac{1/A_i}{(\rho_f h_{sfl}\rho_{gi}-\rho_f h_{sgi}\rho_{fl}+\rho_{fl})}\{\rho_{gi}\frac{Q_i}{\Delta x_i}-\rho_{gi}\frac{W_{j+1}h_{j+1}-W_j h_j}{\Delta x_i}+\frac{2\rho_{gi}}{\rho_i}\frac{W_{j+1}p_{i+1}-W_j p_{i-1}}{\Delta x_i}$$
$$+\rho_{gi}f_i\frac{|W_i|W_i^2}{\rho_i^2 D_{ei}A_i^2}-[\rho_{gi}(\frac{W_i}{\rho_f A_i})^2-(\rho_f h_{sgi}-1)]\frac{W_{j+1}-W_j}{\Delta x_i} \qquad (4.41)$$
$$+\rho_{gi}\frac{W_i}{\rho_i\Delta x_i A_i^2}(\frac{W_{j+1}^2}{\rho_{j+1}}-\frac{W_j^2}{\rho_j})-\rho_{gi}g\frac{(W_{j+1}H_{j+1}-W_j H_j)}{\Delta x_i}\}$$

and

$$\frac{\partial p_i}{\partial t}=\frac{1/A_i}{(\rho_f h_{sgi}\rho_{fl}-\rho_f h_{sfl}\rho_{gi}-\rho_{fl})}\{\rho_{fl}\frac{Q_i}{\Delta x_i}-\rho_{fl}\frac{W_{j+1}h_{j+1}-W_j h_j}{\Delta x_i}+\frac{2\rho_{fl}}{\rho_i}\frac{W_{j+1}p_{i+1}-W_j p_{i-1}}{\Delta x_i}$$
$$+\rho_{fl}f_i\frac{|W_i|W_i^2}{\rho_i^2 D_{ei}A_i^2}-[\rho_{fl}(\frac{W_i}{\rho_f A_i})^2-\rho_f h_{sfl}]\frac{W_{j+1}-W_j}{\Delta x_i} \qquad (4.42)$$
$$+\rho_{fl}\frac{W_i}{\rho_i\Delta x_i A_i^2}(\frac{W_{j+1}^2}{\rho_{j+1}}-\frac{W_j^2}{\rho_j})-\rho_{fl}g\frac{(W_{j+1}H_{j+1}-W_j H_j)}{\Delta x_i}\}$$

where Q_i is the total heat generating rate, in J/s, within node (i), including possible power sources of, for instance, heat generation, heat transfer into or out of the node, mechanical energy, and *etc*. The flow densities ρ_j and ρ_{j+1} at the nodal boundaries are determined by the following equations:

$$\rho_j=\frac{\rho_{i-1}+\rho_i}{2}$$
$$\rho_{j+1}=\frac{\rho_i+\rho_{i+1}}{2} \qquad (4.43)$$

Depending on the direction of the thermal nodal boundary flows, enthalpies h_j and h_{j+1} at the nodal boundaries are defined as:

$$h_j=\begin{cases}h_{i-1}, & W_j\geq 0\\ h_i, & W_j<0\end{cases}$$
$$h_{j+1}=\begin{cases}h_i, & W_{j+1}\geq 0\\ h_{i+1}, & W_{j+1}<0\end{cases} \qquad (4.44)$$

All the properties and parameters in nodal difference equations (4.41) and (4.42) are

evaluated at the locations indicated by subscripts. It should be noticed that the properties of helium, such as densities, enthalpies, and their partial derivatives with respect to the state variables, should be evaluated with the state variables by means of the relations given early.

Eqns. (4.40) to (4.42) are the basic thermal hydraulic difference equations of state for thermal hydraulic pipelines, and are capable of predicating such complex thermal hydraulic processes inside pipelines as flow compression, shock wave, flow reversal, flow irreversibility due to friction, and simultaneous interior heat generation and heat transfer across the wall of the pipe. Unlike most modeling approaches, the helium in these equations is considered as real gas, although the nonlinear nature of helium state equations for enthalpy and density substantially increases the complexity of the model as well as computational efforts. The real gas model is necessary for transient analysis under high temperature and pressure conditions[Y1].

4.5.1c Verification of the Thermal Hydraulic Model

Applying Eqns. (4.40) to (4.42) to each of the flow nodes results in a set of equations determining the dynamic behavior of the entire pipeline. This integrated model was tested on a small scale for a pipe consisting of four thermal and five flow nodes as shown in Figure 4.9. The physical dimension of the pipe is 1.0 m in diameter and 40 m in length. The test results are shown in Figures 4.9 (a) to (c), in which at t=0, the flow inside the pipe experiences a 5% step flow rate increase at the inlet while the exit flow is kept constant. The temperature and pressure of the helium flowing into the pipe remain unchanged.

As indicated in Figure 4.9 (a), the transient behavior of the helium flow during the initial period of the transient demonstrates the damped oscillatory characteristics which are typical of compressible flow due to flow inertia. As the transient becomes more stable at t > 3 sec, the helium shows a prominent nonlinear compression behavior which only real gas

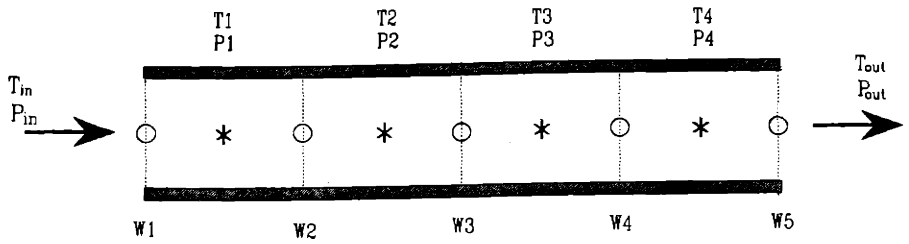

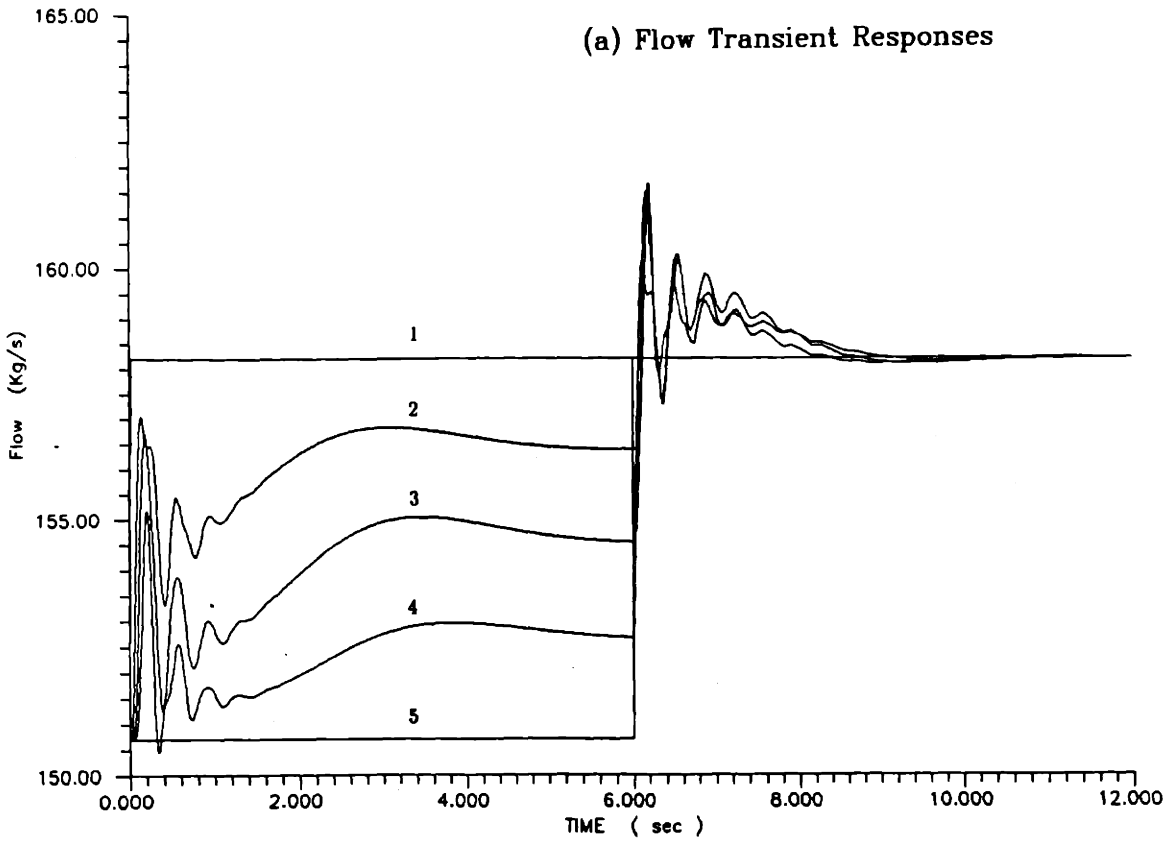

Figure 4.9 Thermal Hydraulic Model Test

(b) Pressure Transient Responses.

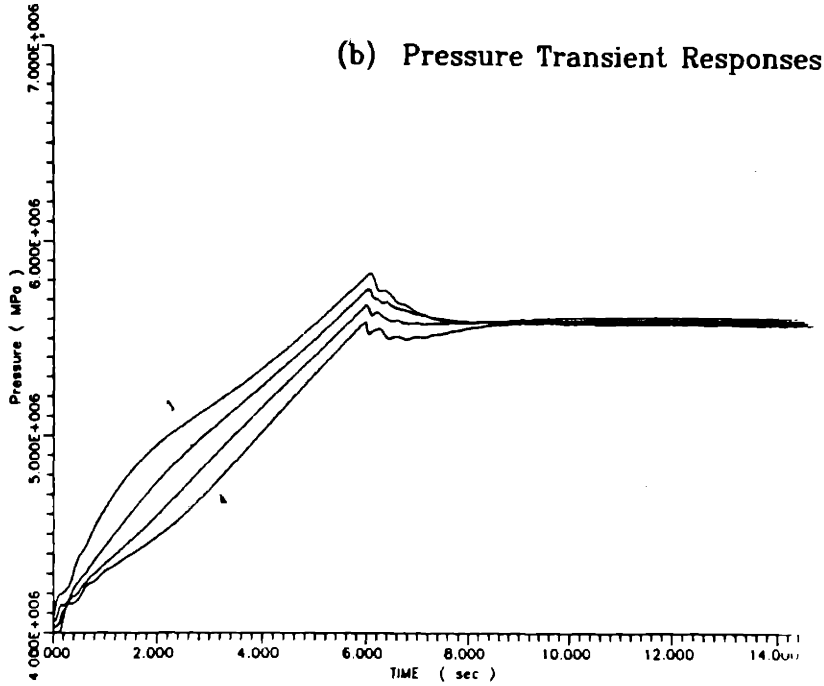

(c) Temperature Transient Responses.

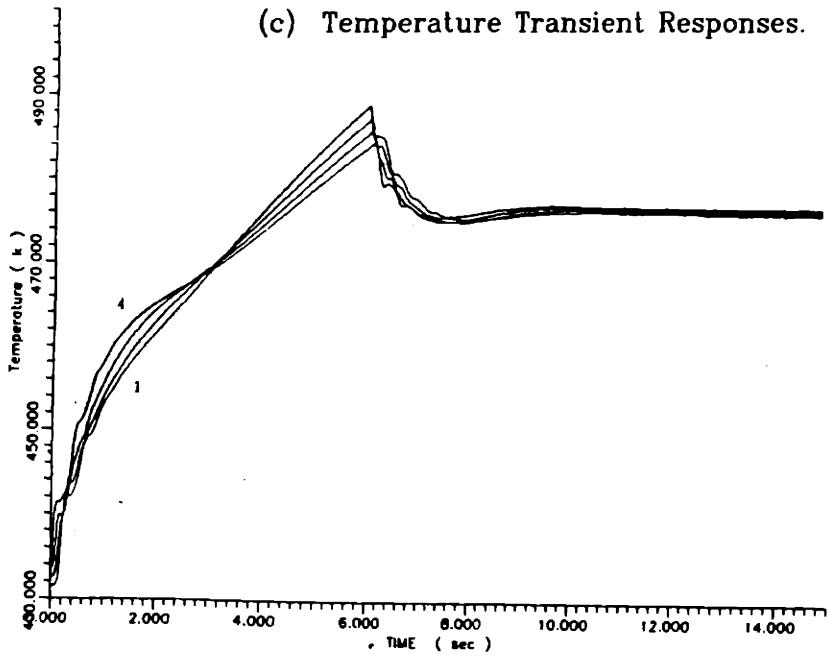

Figure 4.9 Thermal hydraulic model test

model of helium is capable of predicting[2]. At t = 6 sec, a 5% exit flow step increase is initiated, the helium experiences a short expansion process, again, with expected oscillatory behavior, and approaches to a new steady state as the time elapses. It can be seen in Figure 4.9 (c) that there exists small difference in temperatures from the pipe inlet to outlet at steady-state, which is the result of flow irreversibility due to frictional dissipation inside the pipe. The pressure difference in Figure 4.9 (b) between the inlet and outlet is the pressure drop throughout the pipe.

4.5.2 Pebble Bed Reactor Model

The MGR-GT utilizes a 200 MW pebble bed high-temperature helium-cooled reactor whose physical design and operating parameters were outlined in chapter 2, a more detailed design description can be found in[A1]. The discretization scheme for the reactor system was presented during the development of the plant system model and model nodalization. Figure 4.10 shows the detailed reactor model. The mathematical modeling of the MGR-GT reactor system will be presented in the following.

4.5.2a Thermal Conductance

The heat conductance processes in the reactor includes the heat convection between fuel pebbles and helium, heat conduction and radiation within fuel pebbles and through voids, heat conduction from the core through the lateral structure, i.e. the side reflector, carbon bricks, and core barrel. Upon this point, heat transfer becomes twofold: first, heat is transmitted to the reactor vessel by means of radiation through the helium annulus and thereupon from the outer surface of the vessel to the cooling coils mounted on the wall of the

[2]A similar test was performed but with an ideal helium model by [S2] in which the helium was clearly predicted as having linear characteristics.

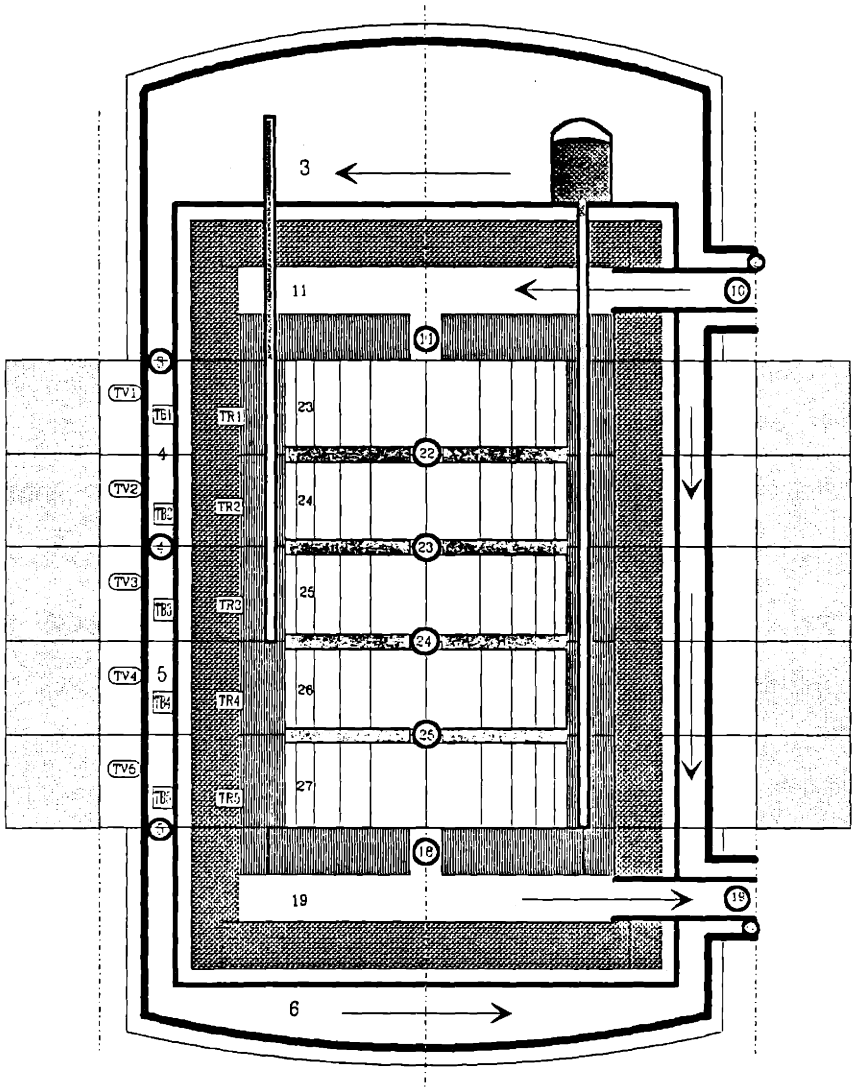

Figure 4.10 The MGR–GT reactor system model.

reactor confinement building, and second, heat convection exists between the helium and the core barrel and reactor vessel as the helium flows down the annulus, sweeping the core barrel and pressure vessel.

In order to model these heat transfer phenomena, the main reactor region is divided into 5 axial zones of equal length to account for the variation of thermal and power conditions in this direction, and 10 radial zones: 5 in the core, and 1 each for the reflector, core barrel, helium flow, reactor vessel and cooling coils. The core is such divided in the radial direction that each radial drop zone has equal cross-section area. As a result, the fuel pebbles have an equal drop probability as uniform radial pebble flow profile and void fraction are assumed. The detailed schematic description of radial discretization for each of axial zones is shown in Figure 4.11, in which the vertical solid lines represent the centers of the radial zones, and dashed lines are the boundaries separating each zone. The helium in five streamlines flows from top into each of the radial zones in the core, as indicated.

The following assumptions are made in modeling the thermal conductance:

1. The heat conductance in the solid is one-dimensional in the radial direction. Considering heat transfer in only one dimension will produce a conservative calculation for the safety analysis.
2. The core is treated as a homogeneous region of graphite - the graphite of fuel pebbles is smeared over the entire core to obtain an equivalent core density.
3. The helium heat conduction is small and thus negligible in contrast to heat conductance in solid.
4. The contribution to reactor vessel heat transfer by air natural convection on the outer surface of the reactor vessel is negligible.

The partial differential equation describing heat conductance in cylindrical coordinates is

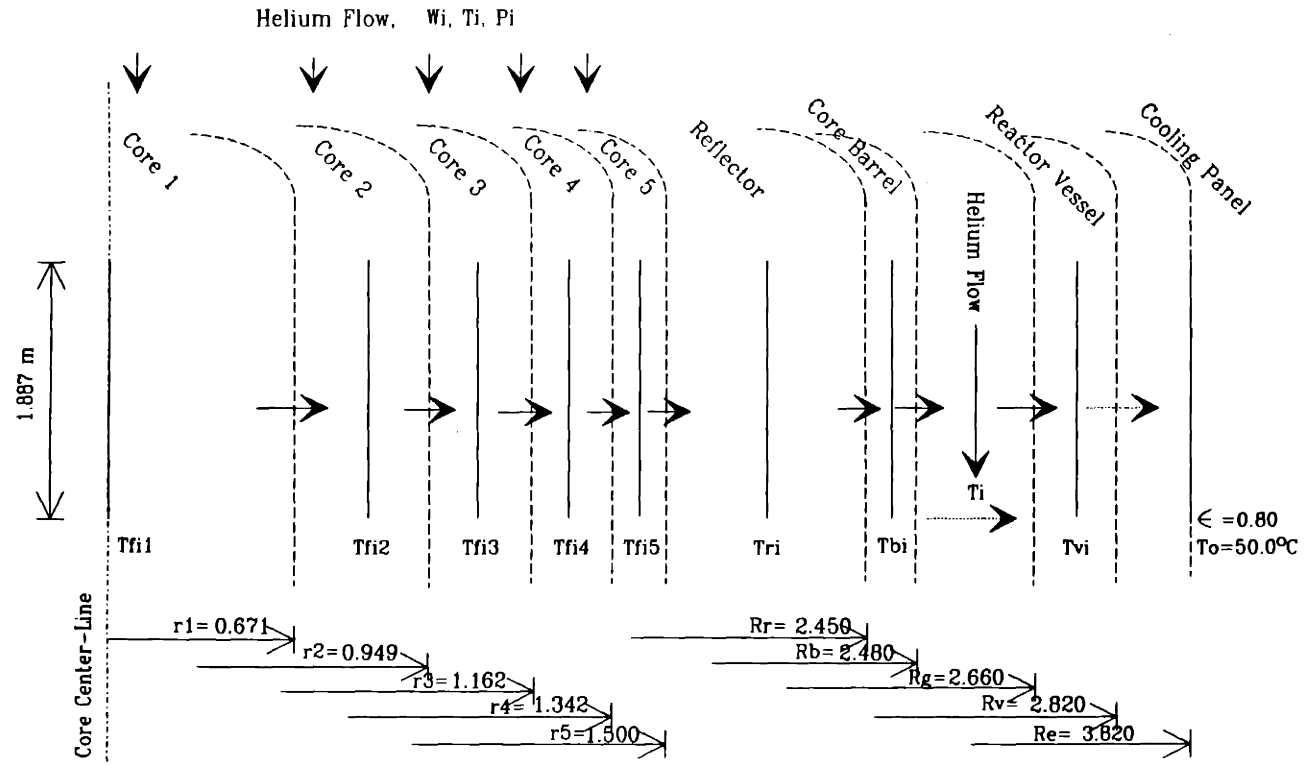

Figure 4.11 Pebble-Bed Reactor Radial Heat Transfer Model

$$\rho(T)C_p(T)\frac{\partial T(r,t)}{\partial t}=\frac{1}{r}\frac{\partial}{\partial r}\left(K(r,t)\,r\frac{\partial T(r,t)}{\partial r}\right)+q_T(r,t)+q_C(r,t)+q_R(r,t) \tag{4.45}$$

where

T = nodal temperature, in K,

ρ = nodal density, kg/m^3,

Cp = material specific heat at constant pressure, J/kg-K,

K = heat conduction coefficient, W/m-K,

Q_t = thermal power density, W/m^3,

q_C = convective heat transfer rate density, W/m^3,

q_R = radiative heat transfer rate density, W/m^3.

The finite difference form of Eqn. (4.45) can be developed with the aid of Figure 4.12 which shows enlarged portion of radial nodes on the axial layer (i). For node (ij), the finite difference equation may be derived by first integrated along radial direction from r_{j-1} to r_j, and the result is written in the following:

$$\begin{aligned}\rho_{ij}C_{pij}\frac{\partial T_{ij}}{\partial t}(r_j^2-r_{j-1}^2)=&2r_jK_{ij,j+1}\frac{T_{i,j+1}-T_{ij}}{\Delta r_{j,j+1}}-2r_{j-1}K_{ij,j-1}\frac{T_{ij}-T_{i,j-1}}{\Delta r_{j,j-1}}\\&+q_T(r_j^2-r_{j-1}^2)+q_C(r_j^2-r_{j-1}^2)+q_R(r_j^2-r_{j-1}^2)\end{aligned} \tag{4.46}$$

where $K_{ij,j-1}$ is the heat conduction coefficient on the nodal boundary between nodes (i,j-1) and (ij), as indicated in Figure 4.12, and similarly, $K_{ij,j+1}$ is the heat conduction coefficient on the boundary between nodes (ij) and (i,j+1). By multiplying both sides of Eqn. 4.46 with π, and then utilizing the following relations for nodal heat transfer areas $A_{ij,j-1}$ and $A_{ij,j+1}$, and volume V_{ij}:

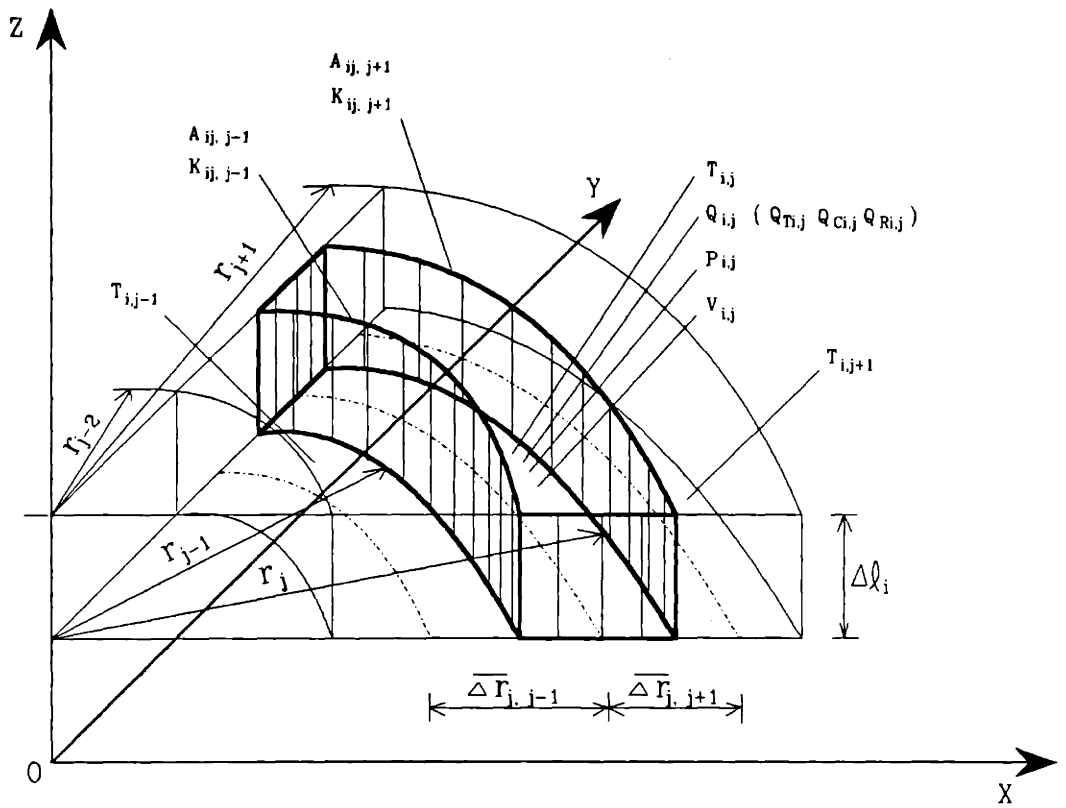

Figure 4.12 Finite Element for Core Heat Transport in Cylindrical Coordinates

$$A_{ij,j-1}=2\pi r_{j-1}\Delta l_i$$
$$A_{ij,j+1}=2\pi r_j\Delta l_i \qquad (4.47)$$
$$V_{ij}=\pi(r_j^2-r_{j-1}^2)\Delta l_i,$$

Eqn. (4.46) may then be transformed into

$$V_{ij}\rho_{ij}C_{pij}\frac{\partial T_{ij}}{\partial t}=A_{ij,j-1}K_{ij,j-1}\frac{T_{i,j-1}-T_{ij}}{\Delta r_{j,j-1}}+A_{ij,j+1}K_{ij,j+1}\frac{T_{ij+1}-T_{ij}}{\Delta r_{j,j+1}}+Q_{Tij}+Q_{Cij}+Q_{Rij} \qquad (4.48)$$

where Q_{Tij} are the total thermal power generated inside node (ij), and Q_{Cij} and Q_{Rij} are the total heat transfer rates by convection and radiation, respectively, of node (ij). Eqn. (4.48) is the finite difference equation describing the heat conductance in radial direction. Applying this equation for each of the radial nodes on each axial layer results in a total of 50 differential equations governing the heat transfer in the reactor system.

Several constitutional relations and material properties must be supplied to support the application of Eqn. (4.48). These include the effective thermal conductivity of the pebble bed, the heat convection correlation between fuel pebbles and helium, heat radiation correlation, and material properties for graphite, core barrel and pressure vessel steels. The development of the relations and properties that are used in the GTSim is described in the following.

Pebble Bed Effective Thermal Conductivity

The use of equation (4.48) for heat transfer in the core requires determining the effective thermal conductivity λ_e to replace K in the equation, since the heat transfer in the core involves both thermal conduction through fuel elements and radiation through the voids between pebbles (heat convection between helium and fuel pebbles will be modeled separately). Zehner and Schlunder used a cell model to determine the effective thermal conductivity taking into account both heat conduction and radiation. Breitbach and Barthels

developed a modified Zehner-Schlunder model which had been validated with experimental date[B2].

The pebble bed is modeled as an arrangement of unit cells, as shown in Figure 4.13. The calculation of the effective thermal conductivity λ_{eff} is made by considering such unit cell. The cell contains two halves of the particles in contact, and the bounding surfaces that contain the sections of the particles are named "base areas." It is assumed that the open portions of the base areas have the same emittance as the pebbles with the other boundaries being considered to be specular reflecting surfaces. The following relation is established for calculating the effective thermal conductivity λ_{eff} for pebble bed:

$$\lambda_{eff}^{zs} = \left\{ \frac{1-(1-\varphi)^{1/2}}{2/\varepsilon - 1}\varphi + \frac{(1-\varphi)^{1/2}}{2/\varepsilon - 1} \frac{(B_z+1)/B_z}{1+1/[\Lambda(2/\varepsilon-1)]} \right\} 4 \cdot \sigma \cdot T^3 \cdot d \qquad (4.49)$$

where

φ = porosity of the pebble bed,

ε = emissivity of pebble,

σ = Stefan-Boltzmann constant,

d = diameter of pebble,

B_z = $1.25\,[(1-\varphi)/\varphi]^{10/9}$,

Λ = $\lambda_f/(4\,\sigma\,T^3\,d)$, and

λ_f = thermal conductivity of pebble graphite.

The first term in the brackets represents the radiation exchange between the base areas, which is the dominating factor at high temperatures.

The modified form of the Zehner-Schlunder relation by Breitbach and barthels assumes that the open portions of the base areas are black surfaces rather than surfaces with the same emittance as the pebbles. As a result, the modified version of Eqn. (4.49) is as follows:

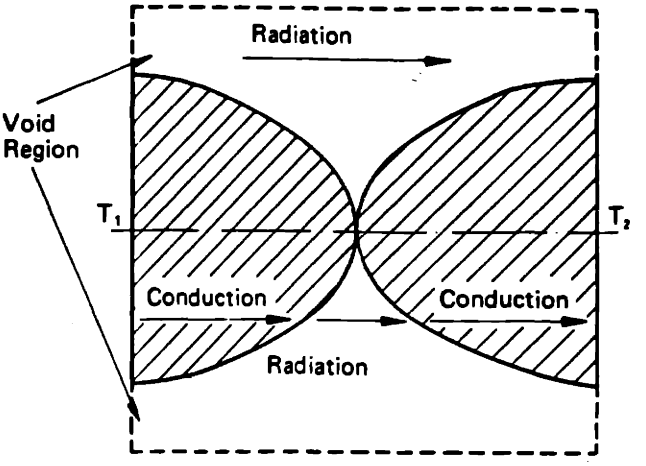

Figure 4.13 The unit cell. In the model, the packed bed is replaced by a regular system of unit cells[B2]

$$\lambda_{eff}^{s}=\left\{[1-(1-\varphi)^{1/2}]\varphi+\frac{(1-\varphi)^{1/2}}{2/\varepsilon-1}\frac{(B_z+1)/B_z}{1+1/[\Lambda_f(2/\varepsilon-1)]}\right\}4\cdot\sigma\cdot T^3\cdot d \qquad (4.50)$$

where B_z and Λ_f are determined by the same means as before. The thermal conductivity of pebble graphite λ_f used in (4.49) and (4.50) depends on the temperature and neutron fluence. This relation is shown in Figure 4.14, which was obtained from experimental data in Germany and the United States[S3].

General Electric developed a correlation for the calculation of the pebble bed thermal conductivity which depends only on core temperature[3] and is given by[S3]

$$K(T)=1.1536\times10^{-4}(T-173.16)^{1.6622} \qquad (4.51)$$

where

K(T) = temperature dependent thermal conductivity of pebble bed, W/m-K,

T = temperature, K.

For comparison, the pebble bed thermal conductivities calculated by Eqns. (4.50) and (4.51) are plotted in Figure 4.15. As can be seen, the GE prediction of the temperature dependent thermal conductivity is slightly lower, throughout the full temperature range, than that obtained with the Zehner-Schlunder relation which is widely accepted as benchmark relation for pebble-bed reactors. The use of the GE correlation requires less computational effort, and produces conservative results for core heatup simulation, with only minor discrepancy from those of Eqn. (4.50). Therefore, the GE correlation (4.51) has been selected for use in the GTSim.

[3]The study performed at KFA of Germany also concluded with a correlation which is also temperature dependent only, as follows: $K(T)=1.9\times10^{-5}(T+150)^{1.29}$[C1]. This was used in the THERMIX-KONVEK code for pebble bed core heatup simulation.

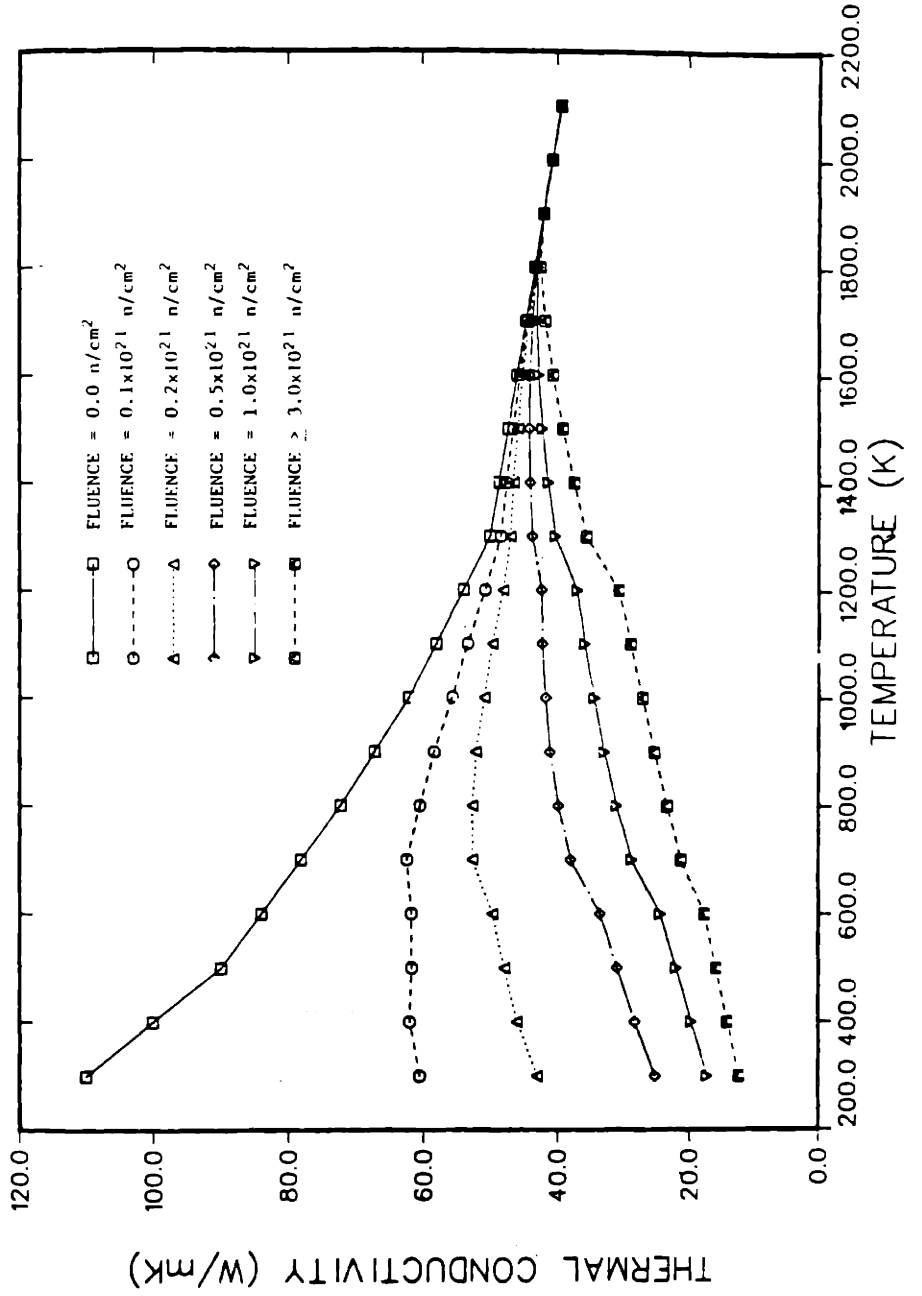

Figure 4.14 Temperature- and Neutron-Fluence-Dependent Graphite Thermal Conductivity[S3]

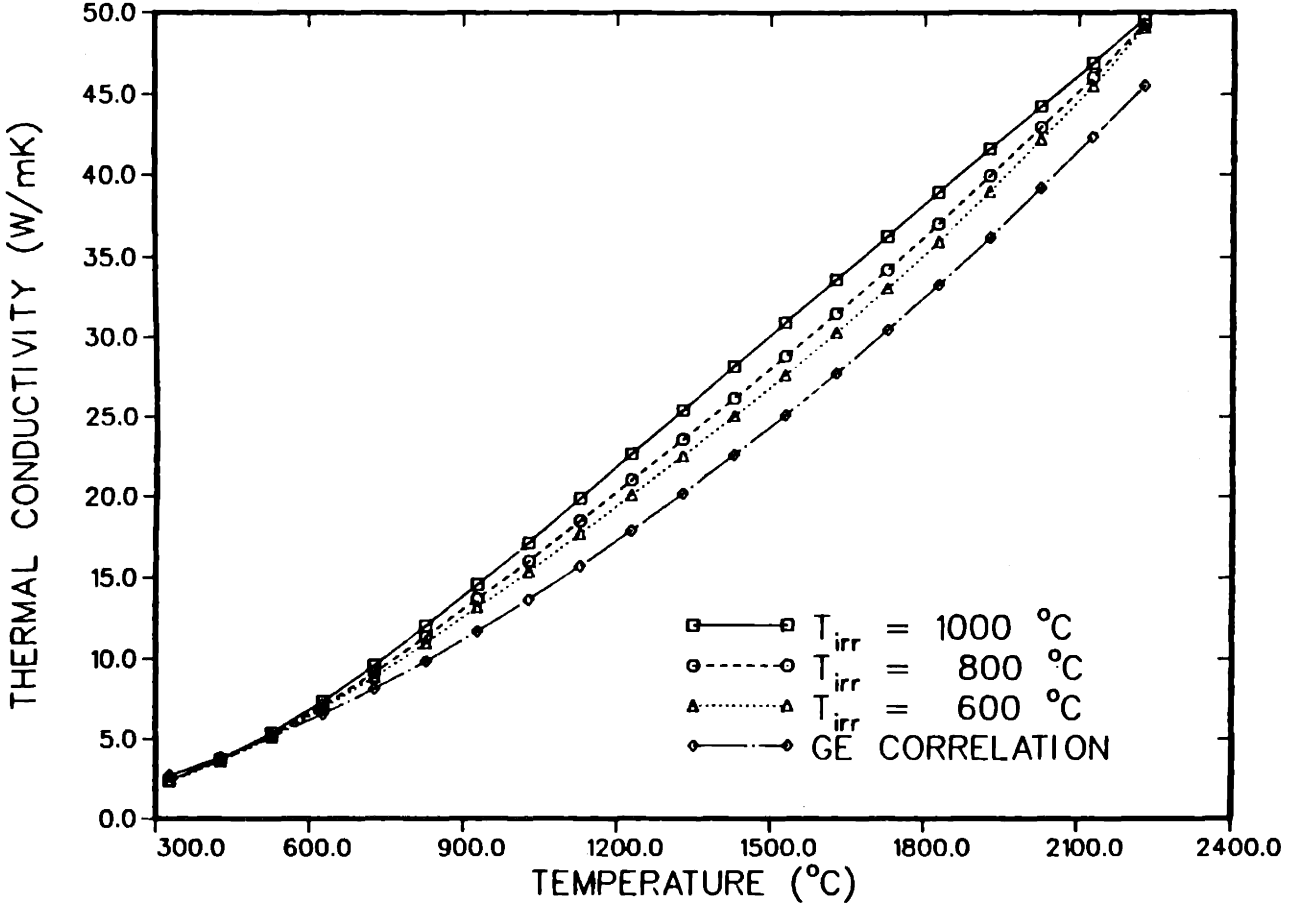

Figure 4.15 Modified Zehner–Schlunder Effective Pebbel–Bed Thermal Conductivity (at 3x10 n/cm and different irradiation temperatures) and GE Pebble–Bed Thermal Conductivity Coorelation**[S3]**

Heat Convection Correlations

In the thermal conductance equation (4.48), Q_{Cij} is used to account for the convective heat transfer between fuel and helium nodes inside the core. For helium in mixing flow in the core, the average temperature is thus chosen for the helium in each of axial layers and is used for heat convective transfer with each of the five radial fuel nodes in the same axial layer. Based on this assumption, Q_{Cij} for the fuel node (ij) can be determined by

$$Q_{Cij}=hA_{Cij}(T_{ij}-T_{gi}) \tag{4.52}$$

where T_{gi} is the average helium temperature of axial layer (i), T_{ij} is the fuel temperature of node (ij), A_{Cij} is the total heat transfer area of node (ij). h is the convective heat transfer coefficient which has been developed by KFA based on the experimental data from several independent studies of heat convection in pebble beds[S5] and is given by

$$h=\frac{\lambda}{d}Nu \tag{4.53}$$

where

λ = helium thermal conductivity, W/m-K,

d = fuel pebble diameter, m,

and Nu, the Nusselt Number, is determined by

$$Nu=1.27\frac{Pr^{0.333}}{\varepsilon^{1.18}}Re^{0.36}+0.033\frac{Pr^{0.5}}{\varepsilon^{1.07}}Re^{0.86} \tag{4.54}$$

where the Reynolds number, Re, is calculated by

$$Re=\frac{W}{A_C\eta d} \tag{4.55}$$

in which

d = pebble diameter, m,

W = helium mass flow rate, kg/s,

A_c = empty-core cross-sectional area, m^2,

η = helium viscosity, N-s/m^2,

Pr = helium Prandtl number, and

ε = void fraction of pebble bed.

For each node the helium viscosity η and thermal conductivity λ are computed at the average of fuel nodal temperature T_{ij} and helium temperature T_{gi}. The range of application for the above convective heat transfer coefficient is

$100 < Re < 10\,5$,

$0.36 < \varepsilon < 0.42$,

$D/d > 20$ (D is core diameter),

$H > 4d$ (H is mean core height).

The MGR-GT reactor core satisfies all these conditions.

Heat Radiation Correlation

Radiation occurs through gaps between the core barrel and reactor vessel, and between the rector vessel and water cooling coils. Q_{Rij} in Eqn (4.48) is used to take such radiative heat transfer into account. For calculation, it is the intent to seek an effective radiative heat transfer coefficient, based on the fundamental radiative heat transfer equation:

$$Q_{Rij}=A_{Rij}\,\sigma\,\varepsilon_{ij,j+1}(T_{ij}^4-T_{i,j+1}^4)=A_{Rij}\,h_{Rij,j+1}(T_{ij}-T_{i,j+1}) \qquad (4.56)$$

where

Q_{Rij} = radiative heat transfer rate between nodes (ij) and (i,j+1), W,

σ = Stefan-Boltzmann constant, σ = 5.669 x 10 -8 W/m^2-K_4,

ε = emittance from node (ij) to (i,j+1),

A_{Rij} = radiative heat transfer area of node (ij), m^2,

T = surface temperature, K, and

h_{Rij} = effective radiative heat transfer coefficient from node (ij) to (i,j+1).

Solve Eqn. (4.56) for effective heat transfer coefficient h_{Rij}:

$$h_{Rij,j+1}=\sigma\varepsilon_{ij,j+1}\frac{T_{ij}^4-T_{i,j+1}^4}{T_{ij}-T_{i,j+1}}=\sigma\varepsilon_{ij,j+1}\frac{(T_{ij}^2+T_{i,j+1}^2)(T_{ij}+T_{i,j+1})(T_{ij}-T_{i,j+1})}{T_{ij}-T_{i,j+1}}=\sigma\varepsilon_{ij,j+1}(T_{ij}^2+T_{i,j+1}^2)(T_{ij}+T_{i,j+1}) \quad (4.57)$$

The emittance $\varepsilon_{ij,j+1}$ for radiation between infinite concentric cylinders is given by:

$$\varepsilon_{ij,j+1}=\frac{1}{\frac{1}{\varepsilon_{ij}}+\frac{A_{Rij}}{A_{Rij,j+1}}\frac{1-\varepsilon_{i,j+1}}{\varepsilon_{i,j+1}}} \quad (4.58)$$

where

ε_{ij} = surface emissivity of node (ij),

$\varepsilon_{i,j+1}$ = surface emissivity of node (i,j+1),

A_{Rij} = radiative transfer area of node (i,j), m^2, and

$A_{Ri,j+1}$ = radiative transfer area of node (i,j+1), m^2.

It should be mentioned that if $A_{Ri,j+1}$ is used to replace A_{Rij} in Eqn. 4.56 for the calculation of radiation between node (i,j+1) and node (ij), the effective coefficient $h_{Ri,j+1,j}$ of radiative heat transfer from node (i,j+1) to node (ij) should be used, which utilized the emittance $\varepsilon_{i,j+1,j}$ of node (i,j+1) as given below:

$$\varepsilon_{ij+1,j}=\frac{1}{\frac{1}{\varepsilon_{i,j+1}}+\frac{A_{Rij,j+1}}{A_{Rij}}\frac{1-\varepsilon_{ij}}{\varepsilon_{ij}}} \quad (4.59)$$

Heat Capacity of Pebble bed

For each node (ij), the heat capacity (ρ_{ij} C_{pij}) in Eqn. (4.48) can be determined by the

correlation given by[S6]:

$$\rho_{ij}C_{pij}(T_{ij})=1.75(1-\varepsilon)\left[0.645+3.14\left(\frac{T_{ij}-T_0}{1000}\right)-2.809\left(\frac{T_{ij}-T_0}{1000}\right)^2+0.959\left(\frac{T_{ij}-T_0}{1000}\right)^3\right] \quad (4.60)$$

where

ε = void fraction of pebble bed,

T_{ij} = nodal temperature, K,

T_0 = 273.16

$\rho_{ij}\, C_{pij}$ = nodal heat capacity density, J/K-CM^3.

Materials Properties

The thermal conductivity of the reflector is determined with the relation as shown in Figure 4.14. The density of the reflector is 1394.8 kg/m^3[S6]. The specific heat C_p of the reflector as a function of temperature [N1][E1] is shown in Figure 4.16.

The core barrel is manufactured of 304 stainless steel whose density is taken as a constant value of 7849.8 kg/m^3[V1]. The temperature-dependent thermal conductivity of the steel is determined by

$$K_{304}(T)=9.01748+0.0162997\cdot T-4.80329\times10^{-6}\cdot T^2+2.18422\times10^{-9}\cdot T^3 \quad (4.61)$$

where T is temperature in (K), and K_{304} is the thermal conductivity in (W/m-k). The specific heat of the steel is given by

$$C_{p304}(T)=380.962+0.535104\cdot T-6.10413\times10^{-4}\cdot T^2+3.02469\times10^{-7}\cdot T^3 \quad (4.62)$$

in which the temperature T is in K. The emissivity of core barrel is assumed to be 0.6 for the calculation of radiative heat transfer.

The density of the 2-1/4 Cr-Mo steel used as the reactor material is assumed to be

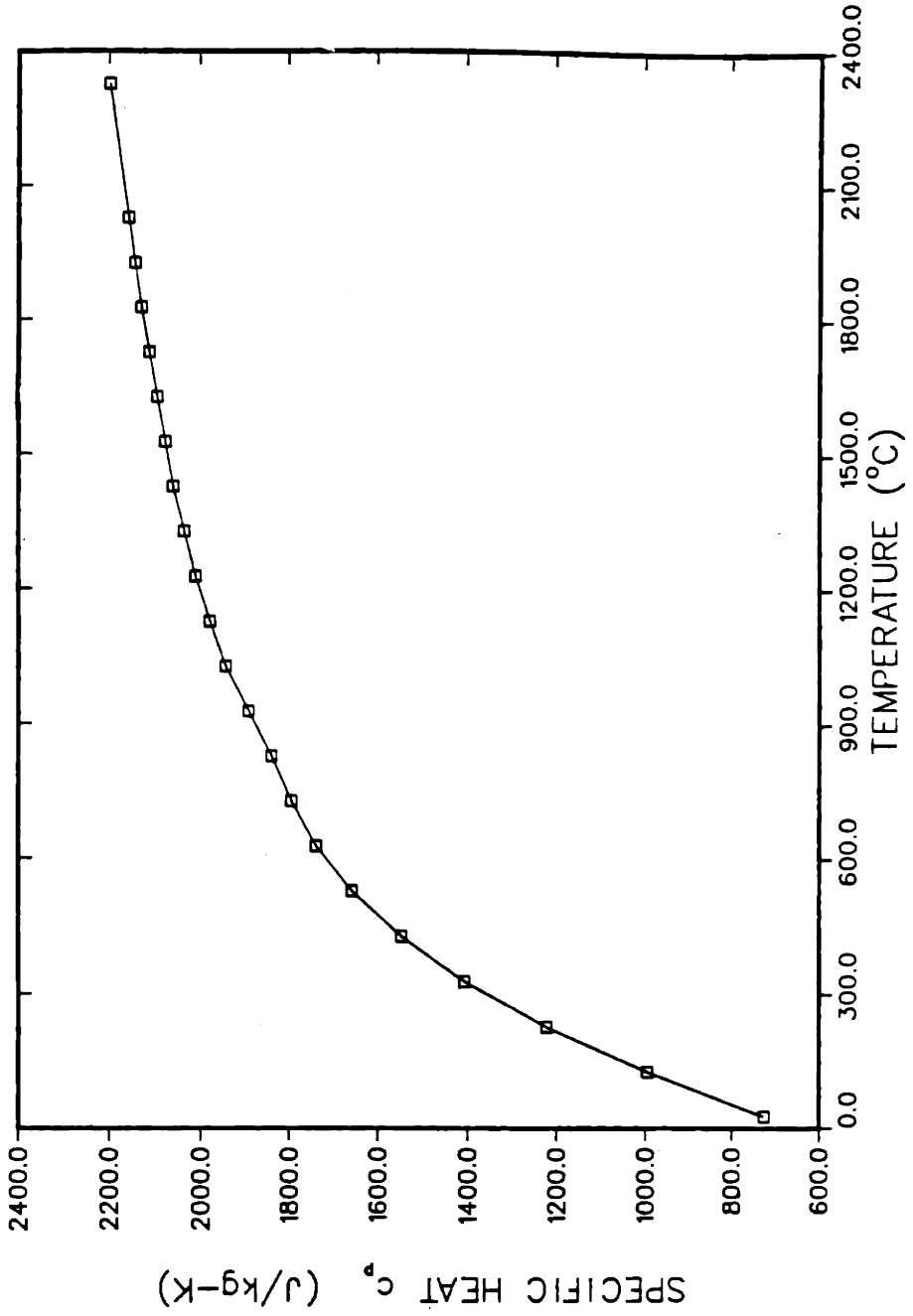

Figure 4.16 Temperature-Dependent Graphite Specific Heat[N1]

constant at 7833.35 kg/m^3[V1]. The thermal conductivity of the vessel as a function of temperature is computed by

$$K_{2\text{-}1/4Cr\text{-}Mo}(T)=49.341695-0.0171228\cdot T \tag{6.63}$$

where T is the vessel temperature in (K), and $K_{2\text{-}1/4\ Cr\text{-}Mo}$ is the thermal conductivity in (W/m-K). And the specific heat of the vessel material may be determined using the same equation (4.62) as for 304 stainless steel. The emissivity of the reactor vessel is assumed to be the same as that for the 304 stainless steel core barrel.

The thermal conductivity and viscosity of helium are required for calculating heat convection in the core. They are listed in Table 4.2 along with other major helium thermal hydraulic and transport properties which will frequently be used throughout the modeling.

4.5.2b. Core Neutronics

The core neutronics is represented by the point reactor kinetics equations describing the time-dependent behavior of neutron flux in the reactor, which can be used to determine the reactor thermal power Q_{Tij} in Eqn. (4.48). Based on the assumptions of one-speed diffusion approximation and time-independent spatial shape of neutron flux, the point reactor kinetics equations with six groups of delayed neutron precursors are given by[D1][M1]

$$\begin{aligned}\frac{d\phi}{dt}&=\frac{\rho-\beta}{\Lambda}\phi+\upsilon\sum_{i=1}^{6}\lambda_i C_i+\upsilon S,\\ \frac{dC_i}{dt}&=\frac{\beta_i}{\Lambda\upsilon}\phi-\lambda_i C_i \quad (i=1,\ldots,6)\end{aligned} \tag{4.64}$$

where

Φ = core spatial and energy averaged neutron flux,

C_i = Concentration of delayed neutron precursors of group i,

λ_i = decay constant for delayed neutron precursors of group i,

Thermodynamic and Transport Properties of Helium

(273 - 1500 K, 0.1 - 10 MPa)

	Uncertainty
1. Gas Constant	
$R = 2077.22$ (J/Kg-K)	< 0.05%
2. Equation of State	
$PV = RT + PB(T)$	
where	
$B(T) = C1 + \frac{C2}{1 - C3\,T} + \frac{C4}{1 - C5\,T}$	
$C1 = 9.489433 \times 10^{-4}$ (m /kg)	
$C2 = 9.528079 \times 10^{-4}$ (m /kg)	
$C3 = 3.420680 \times 10^{-2}$ (K^{-1})	
$C4 = 2.739470 \times 10^{-3}$ (m3/kg)	
$C5 = 9.409120 \times 10^{-4}$ (K^{-1})	
3. Compressibility	
$Z = 1 + \frac{P}{R\,T} B(T)$	< 1.0%
4. Specific Heat	
$Cp = 5193.0$ (J/kg-K)	<0.5%
$C_v = 3116.0$ (J/kg-K)	<0.5%
5. Enthalpy	
$H - Ho = Cp\,T + [\, B(T) - T\frac{d}{dT}B(T)\,]\,P$	<1.0%
6. Entropy	
$S - So = Cp \ln (T/To) - R \ln (P/Po) - P\frac{d}{dT}B(T)$	<1.0%
7. Sonic Velocity	
$c = Z\sqrt{\gamma R T}$	<1.0%
8. Viscosity	
$\eta = 3.953 \times 10^{-7}\, T^{0.687}$ (N-s/m)	σ_η =1.5%
9. Thermal Conductivity	
$k = 2.774 \times 10^{-3} T^{0.701}$ (W/m-K)	σ_k =2.4%
10. Prandtl Number	
$Pr = \frac{\eta Cp}{k} = 0.740\, T^{-0.014}$ where T in (K)	<3.0%

Table 4.2 Thermodynamic and Transport Properties of Helium.

β_i = fraction of the total number of fission neutrons emitted as delayed neutrons of group i,

S = neutron source,

υ = neutron velocity corresponding to energy E,

and the total yield fraction β, reactivity ρ, and mean neutron generation speed Λ are obtained by

$$\begin{aligned} \beta &= \sum_{i=1}^{6} \beta_i, \\ \rho &= \frac{k_{eff}-1}{k_{eff}} = \frac{\Delta k}{k_{eff}}, \\ \Lambda &= \frac{1}{k_{eff}} = \frac{1}{\upsilon \nu \Sigma_f}. \end{aligned} \tag{4.65}$$

where k_{eff} is effective core multiplication, and Δk is the sum of reactivity contributions by the core temperature feedback, reactivity control systems, fission product poison concentrations, and any possible external disturbance of reactivity. Delayed neutron data describing the MGR-GT reactor are given in Table 4.3.

The total reactor thermal power $Q_T(t)$ is related to the averaged neutron flux $\Phi(t)$ by

$$Q_T(t) = \omega_f V \Sigma_f \phi(t) \tag{4.66}$$

where ω_f is usable energy released per fission event, V is the active volume of reactor core, and $\sum_f$ is macroscopic fission cross section, m^{-1}, which is defined as:

$$\Sigma_f = N \sigma_f$$

where N is the number of fissile nuclei/m^3 in the core, and σ_f is the fission cross section per nucleus, m^2/nucleus. Using Equ. (4.66), the point reactor kinetics equations (4.64) may be transformed into ones for $Q_T(t)$ in replacing the averaged neutron flux $\Phi(t)$ as dependent variable. This is arrived, after some algebraic manipulation, as follows:

$$\frac{dQ_T}{dt}=\frac{\rho-\beta}{\Lambda}Q_T+\sum_{i=1}^{6}\lambda_i C_i+S,$$
$$\frac{dC_i}{dt}=\frac{\beta_i}{\Lambda}Q_T-\lambda_i C_i \quad (i=1,\ldots,6) \tag{4.67}$$

Note that the precursor concentration C_i in Eqn. (4.67) has been slightly modified to $C_i = C_{inew} = \omega_f V \sum_f \upsilon C_{iold}$, and neutorn source $S_{new} = \omega_f V \sum_f \upsilon S_{old}$.

Rather than attempting to solve the full set of point reactor kinetics equations, it is intended to represent all delayed neutrons with one effective delayed group, characterized by an average decay constant:

$$\lambda=\left[\frac{1}{\beta}\sum_{i=1}^{6}\frac{\beta_i}{\lambda_i}\right]^{-1} \tag{4.68}$$

The point reactor kinetics equations for one effective group of delayed neutrons becomes[D1]

$$\frac{dQ_T}{dt}=\frac{\rho-\beta}{\Lambda}Q_T+\lambda C+S,$$
$$\frac{dC}{dt}=\frac{\beta}{\Lambda}Q_T-\lambda C \tag{4.69}$$

Hence a set of two coupled ordinary differential equations is obtained to describe both the transient behaviors of the reactor thermal power and the decay of the delayed neutron precursors.

The derivation of the point reactor kinetics equations assumes a time-independent power distribution in the reactor, which means that the power distribution during a transient remains the same as in the steady-state. For the discretization scheme of the MGR-GT reactor model, such power distribution is shown in Figure 4.17, which is derived from the data generated with a more detailed analytical model for the MGR-GT reactor[I1]. This power distribution is used to determine the nodal power Q_{Tij} in Eqn. (4.48), based on the percentage of the total thermal power Q_T that each node contributes.

Table 4.3 MGR-GT Reactor Core Neutronic Data

Mean neutron generation time: 4.0 x 10 sec

Delayed neutron data:

group #	β_i	λ_i
1	2×10^{-4}	0.01
2	1×10^{-3}	0.02
3	1×10^{-3}	0.12
4	2×10^{-3}	0.30
5	6×10^{-4}	1.10
6	2×10^{-4}	2.90

Figure 4.17 MGR-GT Reactor Power Distribution

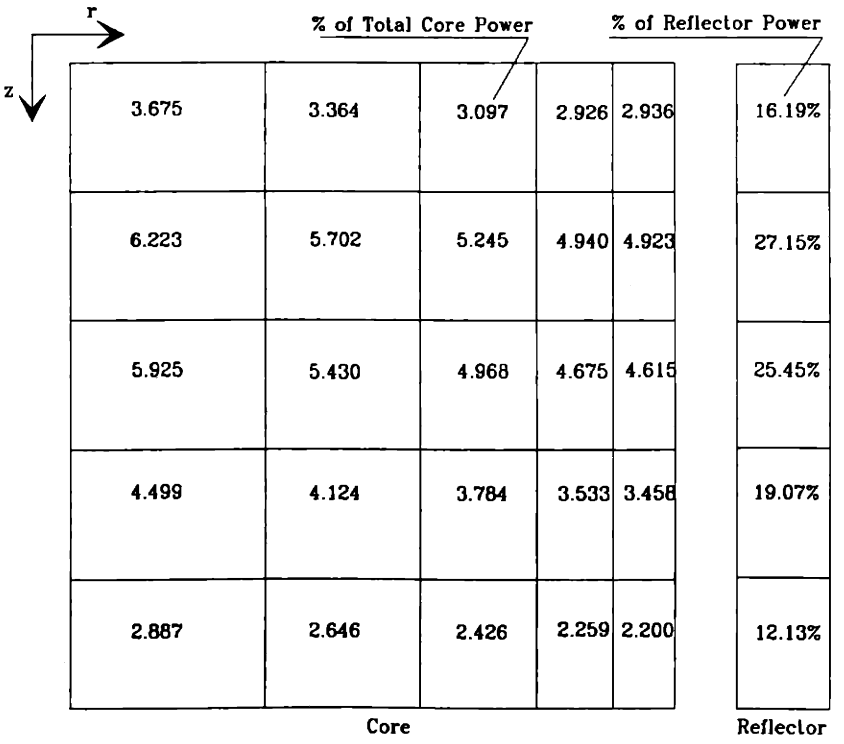

Total Power: 200 MW Core Fraction: 95% Reflector Fraction: 5%

4.5.2c Fission Product Poisoning

The most important fission product poison is ^{135}Xe because of its enormous thermal neutron absorption cross section-about 2.65×10^6 barns-for thermal neutrons and its relatively large fission yield. Such fission product poisoning has an important influence on the reactivity and can significantly affect core multiplication and long-term reactor operations, such as reactor shutdown and startup. The time-dependent behavior of ^{135}X poisoning during reactor transients is modeled in the following.

^{135}Xe can be produced not only directly as a fission product but may also result from the β-decay of ^{135}Te. A portion of the production decay scheme for A=135 chain is illustrated in Figure 4.18. However, this rather complicated decay scheme can be considerably simplified by assuming that the decay of ^{135}Te to ^{135}I is instantaneous, *i.e.*, ^{135}I is produced directly as a fission product[D1]. Furthermore the short-lived isomeric state ^{135m}Xe may be ignored, and it is assumed that all ^{135}I nuclei will decay directly to the ground state ^{135}Xe. These assumptions lead to an effective decay scheme on which the modeling of fission product poisoning will be based, which is shown in Figure 4.19.

The rate equations governing the simplified decay scheme are given by

$$\frac{dI}{dt} = \gamma_I \Sigma_f \phi - \lambda_I I \tag{4.70}$$

$$\frac{dX}{dt} = \gamma_X \Sigma_f \phi + \lambda_I I - (\lambda_X + \sigma_a^X \phi) X \tag{4.71}$$

where

I = ^{135}I concentration,

X = ^{135}Xe concentration,

Φ = neutron flux,

γ_I, γ_X = effective fractions of ^{135}I and ^{135}Xe,

λ_I, λ_X = β-decay constants of ^{135}I and ^{135}Xe,

Σ_f = macroscopic fission cross section, and

σ_a^X = microscopic absorption cross section of ^{135}Xe.

Corresponding to the illustration of the decay scheme in Figure 4.19, the first item at the right-hand side of Eqn. (4.70) is the ^{135}I buildup rate directly from fission, where second item ^{135}I decay rate. At the right hand of Eqn. (4.71), the first item is the ^{135}Xe buildup rate due to fission, the second item the ^{135}Xe production rate due to ^{135}I decay, and the last two items in the parenthesis is the sum of ^{135}Xe decay and absorption rates. The effective fractions and β-decay constants of ^{135}I and ^{135}Xe are given in Table 4.4.

The time-dependent behavior of ^{135}Xe is therefore determined by solving equations (4.70) and (4.71). The reactivity that the ^{135}Xe concentration contributes during reactor operation is determined by:

$$\Delta\rho = -\frac{\Sigma_a^X}{\Sigma_a} = -\frac{\sigma_a^X X}{\Sigma_a} \tag{4.72}$$

This amount of the reactivity enters the point reactor kinetics equation (4.69) through the reactivity given by Eqn. (4.65). The equilibrium reactivity due to the ^{135}Xe concentration under steady-state condition with neutron flux $\Phi(0)$, can be found by setting the left hands of both equations (4.70) and (4.71), and with algebraic manipulation, as follows:

$$\begin{aligned} I(0) &= \frac{\gamma_I \Sigma_f}{\lambda_I}\phi(0) \\ X(0) &= \frac{\gamma_X \Sigma_f \phi(0) + \lambda_I I(0)}{\lambda_X + \sigma_a^X I(0)} = \frac{\gamma_X + \gamma_I}{\lambda_X + \sigma_a^X \phi(0)}\Sigma_f \phi(0) \\ \Delta\rho(0) &= -\frac{\sigma_a^X}{\Sigma_a} X(0) = -\frac{\sigma_a^X(\gamma_X + \gamma_I)\Sigma_f \phi(0)}{\Sigma_a(\lambda_X + \sigma_a^X \phi(0))} \end{aligned} \tag{4.73}$$

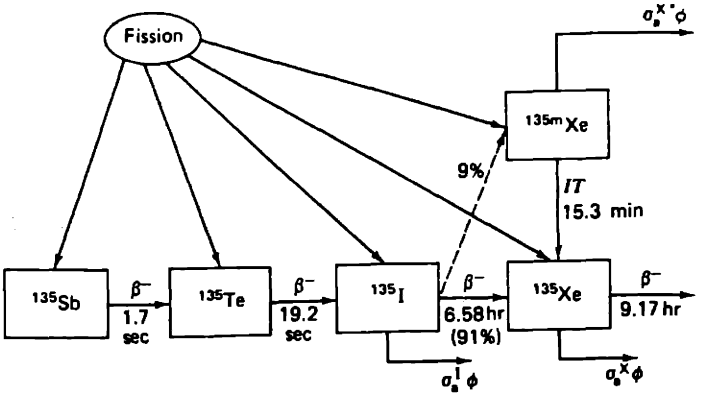

Figure 4.18 A Portion of the Decay Scheme for A = 135[D1]

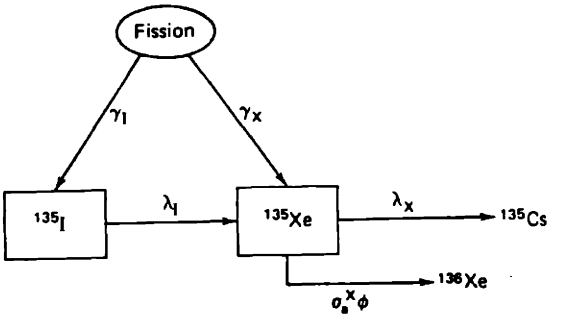

Figure 4.19 The Simplified Decay Scheme ^{135}Xe [D1]

Table 4.4 Fission Product Fractions and Decay Constants

	^{135}I	^{135}Xe
Fission Product Fraction γ (%)	6.386	0.288
β - Decay Constant λ (1/s)	2.87×10^{-5}	2.09×10^{-5}

4.5.2d Temperature Coefficient of Reactivity

The temperature coefficient of reactivity may be defined as the rate of change of reactivity per unit temperature change as follows:

$$\alpha_T = \frac{\partial \rho}{\partial T} = \frac{1}{K_{eff}} \frac{\partial K_{eff}}{\partial T} \tag{4.74}$$

The K_{eff} is core multiplication constant, and α_T is the temperature coefficient of reactivity which is a function of temperature. A negative temperature coefficient leads to a self-stabilizing reactor. In contrast, if the temperature coefficient is positive, the reactor is unstable and any flux disturbance tends to amplify itself.

The MGR-GT reactor temperature coefficient of reactivity is shown in Figure 4.20[M4]. The average temperature of the core is employed to define the isothermal coefficient. Changes in reactivity due to core temperature variations can therefore be calculated by integrating Eqn. (4.74) over the temperature changes.

During core heatup, the temperature profiles in the core may change considerably over long-term period of time. The distortion in the temperature profiles results in uneven distributions of negative reactivity generated by the temperature coefficient of reactivity. The hot spots can have a stronger temperature reactivity feedback than that of the average core temperature. This would facilitate an earlier power shutdown for the hot spots so that temperature increases could be limited. Therefore, the modeling of temperature reactivity feedback based on the average core temperature yields a conservative predication to peak temperatures during core heatup.

4.5.2e Reactor Reactivity Control

Two separate reactivity control and shutdown systems are provided for the MGR-GT reactor. The design specification of the control systems is shown in Figure 4.21.

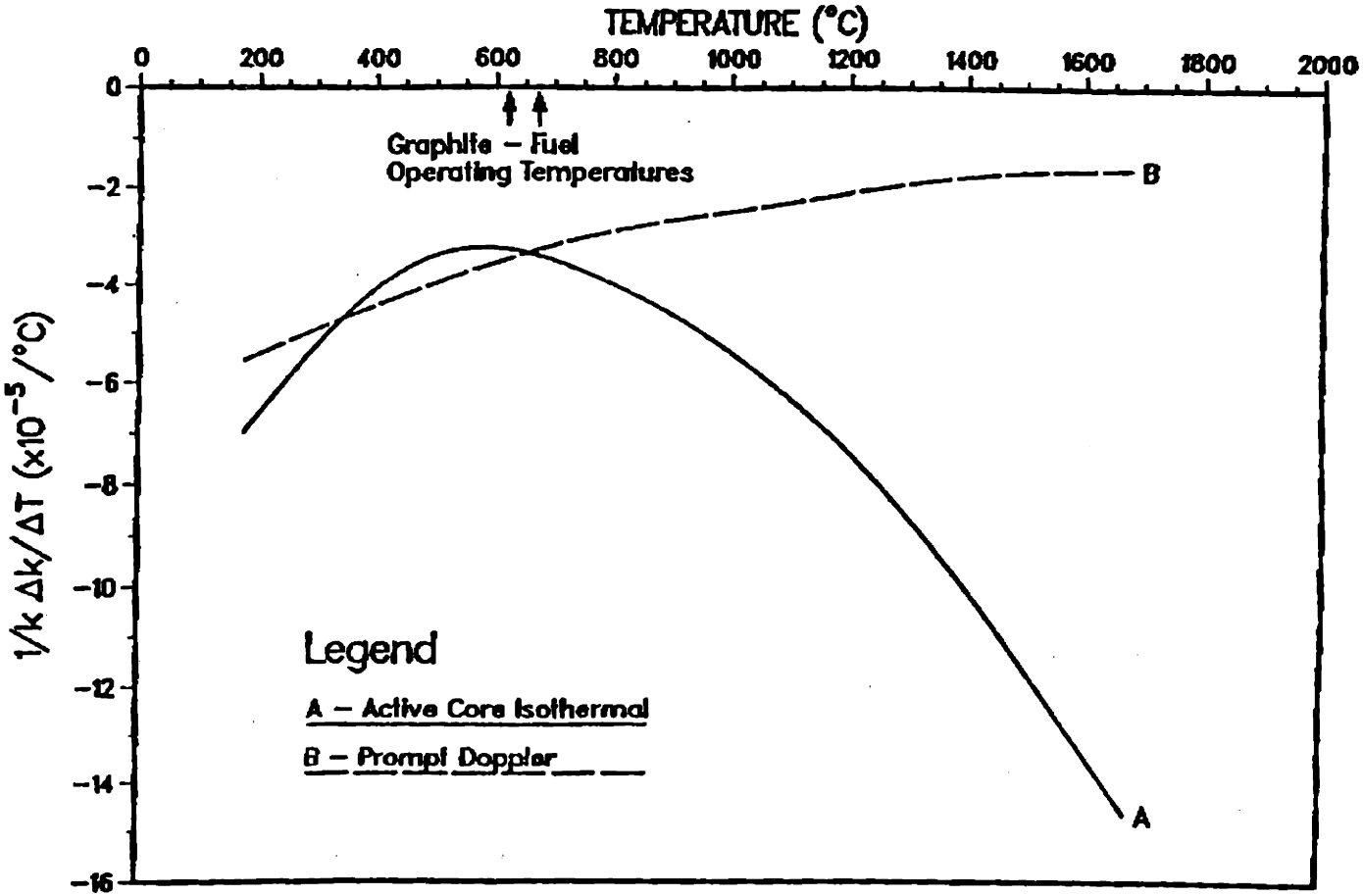

Figure 4.20 MGR–GT Core Temperature Coefficient (end of fuel cycle)[M4]

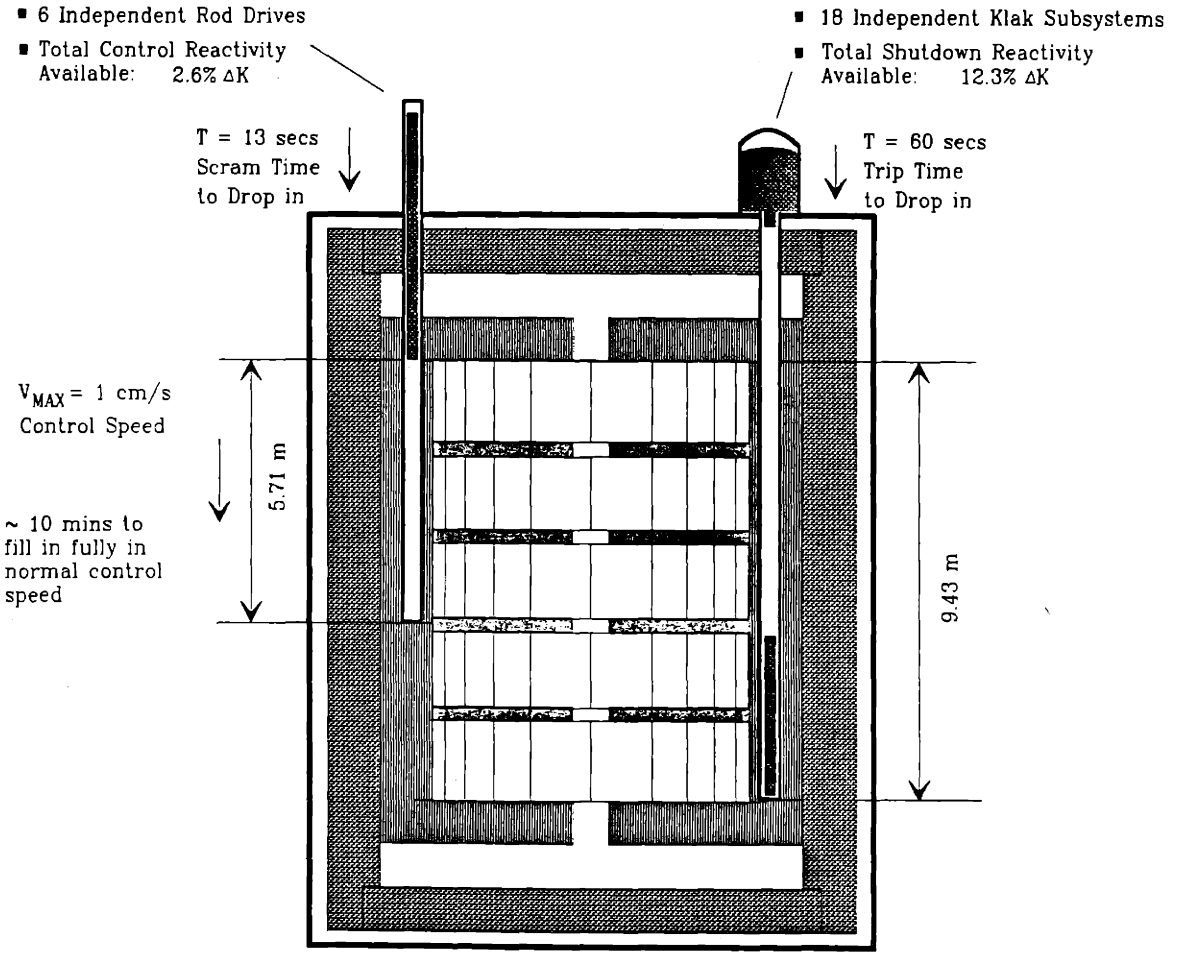

Figure 4.21 MGR–GT Reactor Control System Specification

The control rods are used for reactor power regulation, and for reactor scram at hot temperature condition. The control rods are modeled as moveable rods driven by the control rod drive mechanism with a speed limit of 1cm/sec. The control rods are maneuvered by the reactor controllers. At full power condition, the rods are slightly inserted into the core with approximately 0.3% worth of reactivity for power regulation. At partial power levels, the control rods are partially moved into the core under the automated control of the reactor control system to compensate for the temperature effects. However, if a reactor scram is required, the control rods could be dropped under gravity into the core within 13 sec.

The second reactivity control system is small absorber sphere shutdown system, which is used to provide long-term shutdown. The reactor trip would be actuated primarily by operator. However, if a severe accident condition is met, the PPS is also able to initiate the reactor trip. When the reactor is to be tripped, the small absorber spheres are released into the channels inside the side reflector within 60 sec. In addition, the small absorber spheres are used to compensate for the fuel temperature changes during reactor startup and to compensate for lack of ^{135}Xe buildup in the clean core or during extended periods of operation at reduced power levels. When such compensation of reactivity is required, the small absorber spheres are partially loaded into the core based on the reactivity requirements of specific operation.

4.5.2f Decay Heat Generation

After the reactor shutdown, decay heat is the major contributor to power production in the reactor as the power from the delayed neutrons becomes increasingly small after a short period of time. The decay heat production of the fission products depends on the reactor power level prior to shutdown, the history of the operation, and the shutdown period of time. The following KFA formula, which was generated based on the experimental

results[W2], is used to approximate the decay heat generation:

$$Q_{DH}(t_0,t_s)=Q_T A(t_s^{-a}+(t_0+t_s)^{-a}) \tag{4.75}$$

where Q_T is the reactor power prior to shutdown, t_0 and t_s are reactor operating time and shutdown time, respectively, in sec. A and a in (4.75) are constants given for different time intervals

	A	a
$10^{-1} < t_s \leq 10^1$	0.0603	0.0639
$10^1 < t_s \leq 1.5 \times 10^2$	0.0766	0.181
$1.5 \times 10^2 < t_s \leq 4.0 \times 10^6$	0.130	0.283
$4.0 \times 10^6 < t_s \leq 2.0 \times 10^8$	0.266	0.335

4.5.2g Verification of the Reactor System Model

Several test simulations have been performed to verify the reactor model developed. Two of them are described in the following. The verification is through the comparison between numerical solutions and approximate theoretical solutions.

The first test is a simulation of reactivity disturbance. The simulation is performed for both positive and negative reactivity insertion of amount $|\Delta\rho| = 0.22\%$. The results are shown in Figure 4.22. It is possible to verify this solution against approximate theoretical solution by the point reactor kinetics equations (4.69). It is intended to seek solutions to the point kinetics equation in the exponential forms

$$Q_T(t)=Q_T(0)e^{st}, \qquad C(t)=C(0)e^{st}, \tag{4.76}$$

where s are the eigenvalues of the system to be determined, and $Q_T(0)$ and C(0) are the initial conditions prior to the reactivity disturbance, which, by setting the left sides of Eqn. (4.69) to be zero, can be obtained as:

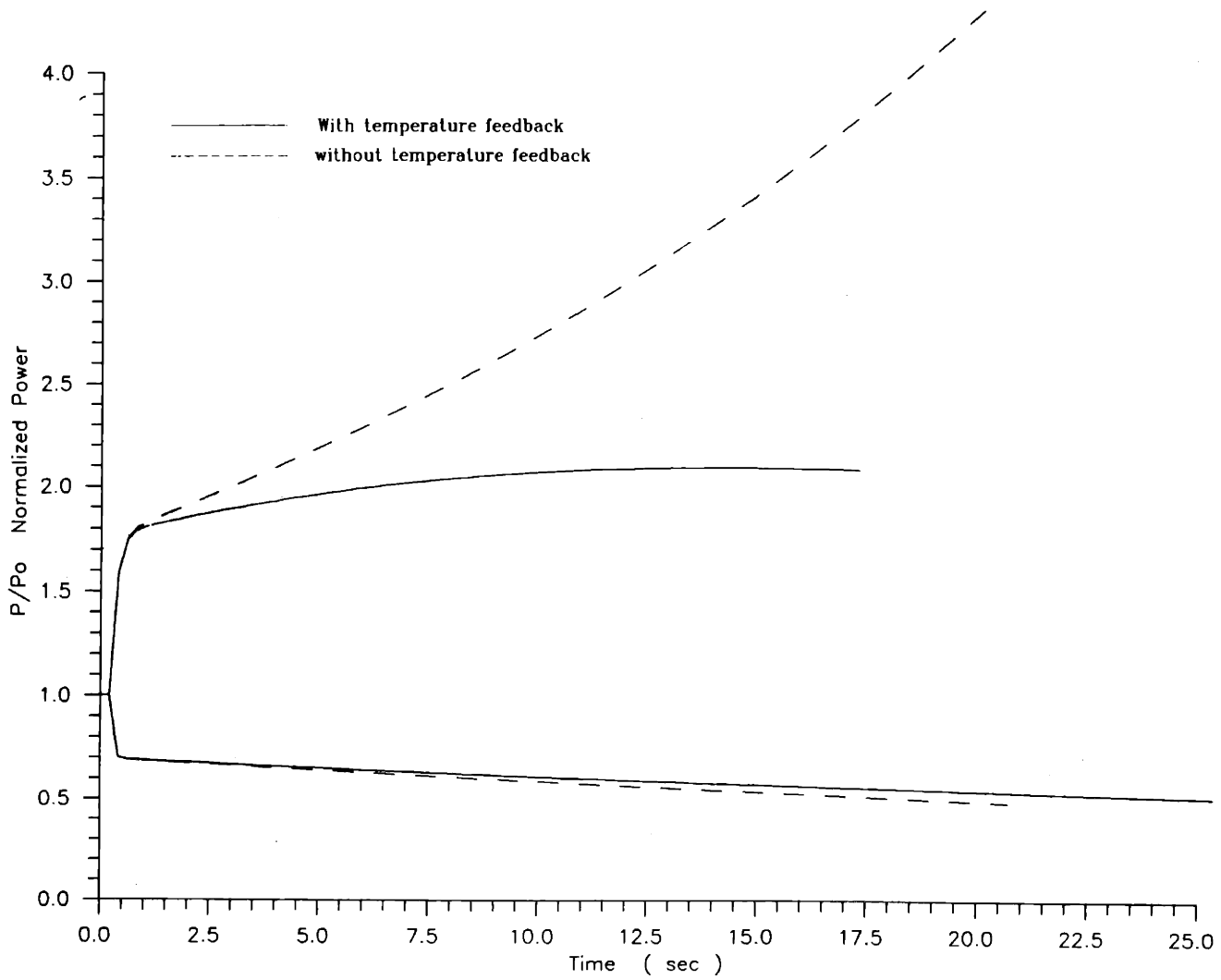

Figure 4.22 MGR-GT Reactor Core Power Transients following Reactivity Disturbances

$$Q_T(0)=Q_{T0} \qquad C(0)=\frac{\beta}{\lambda\Lambda}Q_{T0} \tag{4.77}$$

The MGR-GT reactor is characterized by $\Lambda = 4.0 \times 10^{-4}$ sec, $\beta = 5.0 \times 10^{-3}$, and $\lambda = 5.84 \times 10^{-2}$ sec^{-1}. By substituting (4.76) into Eqn. (4.69) and solving resultant characteristic equations for the eigenvalues, the power $Q_T(t)$ in Eqn. (4.69) may be described as follows[4]:

$$\frac{Q_T(t)}{Q_{T0}}=\left[\left(\frac{\beta}{\beta-\Delta\rho}\right)e^{\frac{\lambda\Delta\rho}{\beta-\Delta\rho}t}-\left(\frac{\Delta\rho}{\beta-\Delta\rho}\right)e^{-\frac{\beta-\Delta\rho}{\Lambda}t}\right] \tag{4.78}$$

The first exponential on the right-hand of Eqn. (4.78) represents slow transient response whose time constant is 21.7 sec for the positive reactivity disturbance, and 56.2 sec for the negative reactivity insertion, whereas the second exponential represents the initial, rapid or jump, behavior after the reactivity insertion, whose characteristic times are 0.14 sec and 0.05 sec for the positive and negative reactivity disturbances, respectively. The coefficient of the fast exponential is the jump magnitude of the reactor power, which cause $Q_T(t)$ to increase approximately 78.5% for $\Delta\rho$ = 0.22% at t > 0.56 sec (= 4 x time constant), and decrease 38.5% for $\Delta\rho$ = -0.22% at t > 0.2 sec after the reactivity insertion. As can be seen in Figure 4.22, the above characteristics during the initial period of the transients are correctly predicted by the numerical reactor model. For extended time period, the negative temperature feedback of reactivity in the core acts to prevent the reactor power from continuous increase asymptotically, which implies an inherent stable characteristics of the reactor power in the event of reactivity disturbances.

Another test is carried out to verify the prediction of Xenon poisoning by the reactor model after reactor shutdown. The accurate simulation of fission product poisoning is crucial

[4]For detailed derivation of analytical solution, see [D1].

to long term control processes since the reactivity generated by fission product buildup has significant impact on the movement of the reactor control rods in the control of reactor startup after temporary shutdown. The results of the test simulation are shown in Figure 4.23. As can be seen, the ^{135}Xe and ^{135}I concentrations prior to shutdown, which may be verified with the values calculated with the Eqn. (4.73), are X(0) = 7.769x 10^{19} and I(0) = 2.070 x 10^{20}, respectively. By solving the eqns (4.70) and (4.71) with the initial condition $\Phi(0)=0$, it can be obtained that the maximum negative reactivity occurs at[D1]

$$t_{max}=\frac{1}{\lambda_I-\lambda_X}\ln\left[\frac{\lambda_I/\lambda_X}{1+\frac{\lambda_X}{\lambda_I}\left(\frac{\lambda_I}{\lambda_X}-1\right)\frac{X(0)}{I(0)}}\right] \tag{4.79}$$

and the ^{135}I and ^{135}Xe concentrations and negative reactivity due to ^{135}Xe buildup at $t = t_{max}$ are

$$\begin{aligned}
&\frac{I(t=t_{max})}{I(0)}=e^{-\lambda_I t_{max}}\\
&\frac{X_{max}}{X(0)}=e^{-\lambda_X t_{max}}+\frac{\lambda_I}{\lambda_I-\lambda_X}\frac{I(0)}{X(0)}\left(e^{-\lambda_X t_{max}}-e^{-\lambda_I t_{max}}\right)\\
&\rho^X_{max}=-\frac{1}{\nu}\left[\frac{(\gamma_X+\gamma_I)\phi_0}{\lambda_X/\sigma_a^X+\phi_0}e^{-\lambda_X t_{max}}+\frac{\gamma_I\sigma_a^X\phi_0}{\lambda_I-\lambda_X}\left(e^{-\lambda_X t_{max}}-e^{-\lambda_I t_{max}}\right)\right]
\end{aligned} \tag{4.80}$$

where Φ_0 = 4.947 x10^{17} m^{-2}, which is the neutron flux in the core prior to shutdown. From the equations, the values for the MGR-GT reactor are

I(t=t_max)/I(0) = 44.5%

X_{max}/X(0) = 162.4%, and

ρ^X_{max} = - 3.80%.

These values are all closely predicted by the numerical solution as shown in Figure 4.23.

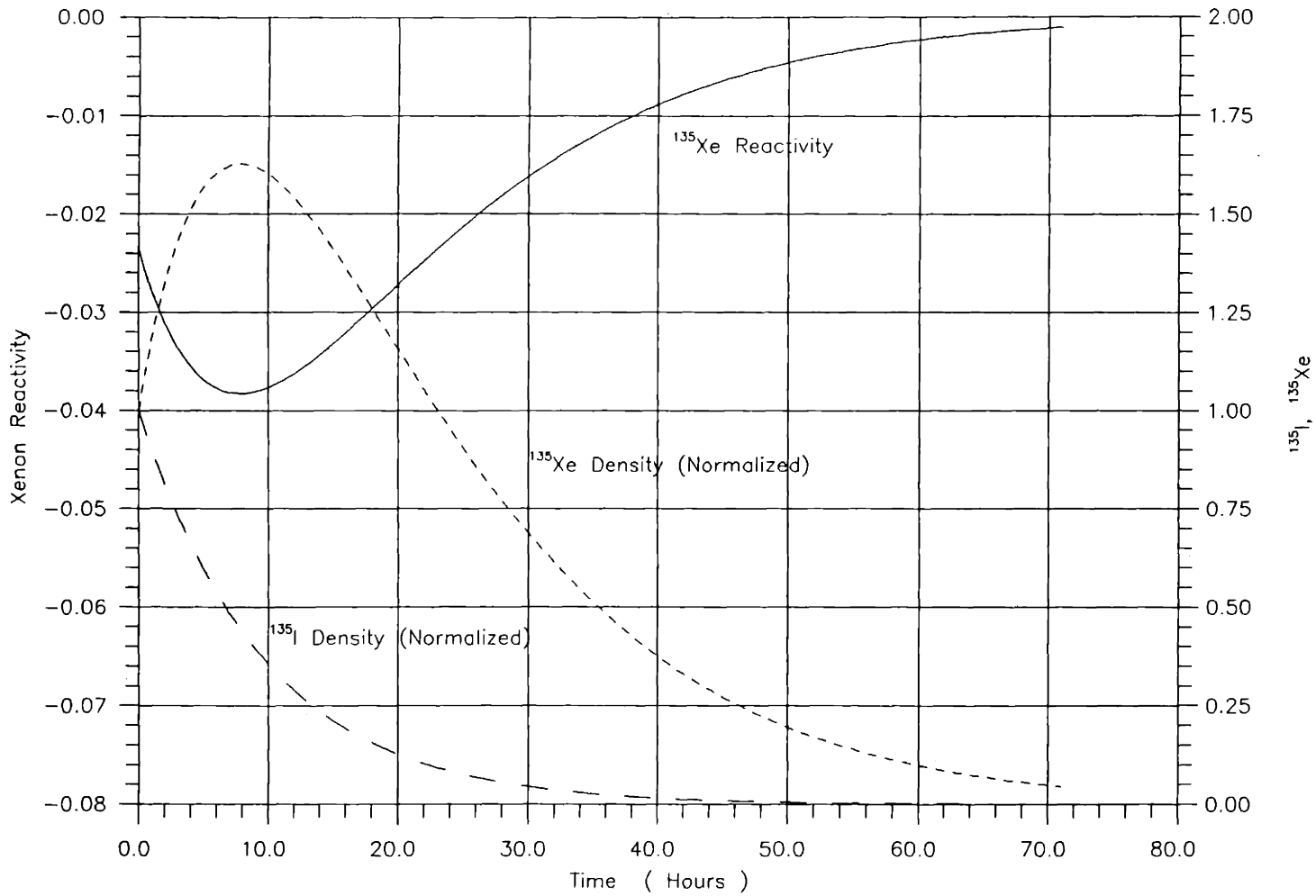

Figure 4.23 Negative reactivity due to ^{135}Xe buildup following shutdown in the MGR–GT core

4.5.3 Recuperator Model

The recuperator used in the MGR-GT is a compact counterflow heat exchanger with strip-fin plate-fin heat transfer surface 1/9-24.12[K1]. The effectiveness of the heat transfer is 95%. Such high heat transfer effectiveness implies a large heat diffusion between the flows at the two sides of the recuperator, which presents mathematical difficulty in modeling.

The recuperator is discretized into three regions in the cross direction, for the hot (LP) and cold (HP) side flows, and the recuperator wall, and a number of longitude nodes for each of the three regions. A schematic description of the model is shown in Figure 4.24.

4.5.3a Modeling Condition for High Effectiveness Heat Exchangers

Based on the nodalization, the differential equations of nodal heat transfer for the flow and wall temperature are given below:

For the hot side

$$\frac{\partial T_i}{\partial t}=\frac{1/A_h}{\rho_i h_{sm}\rho_{pi}-\rho_i h_{spi}\rho_m+\rho_m}\{\rho_{pi}\frac{-Q_{hi}}{\Delta x_i}-\rho_{pi}\frac{W_{j+1}h_{j+1}-W_j h_j}{\Delta x_i}+\frac{2\rho_{pi}}{\rho_i}\frac{W_{j+1}p_{i+1}-W_j p_{i-1}}{\Delta x_i}$$
$$+\rho_{pi}f_i\frac{|W_i|W_i^2}{\rho_i^2 D_{ei}A_i^2}-[\rho_{pi}(\frac{W_i}{\rho_i A_i})^2-(\rho_i h_{spi}-1)]\frac{W_{j+1}-W_j}{\Delta x_i} \qquad (4.81)$$
$$+\rho_{pi}\frac{W_i}{\rho_i \Delta x_i A_i^2}(\frac{W_{j+1}^2}{\rho_{j+1}}-\frac{W_j^2}{\rho_j})\}$$

For the wall

$$\frac{dT_{wi}}{dt}=\frac{1}{C_{pwi}\rho_{wi}V_{wi}}(Q_{hi}-Q_{ci}) \qquad (4.82)$$

For the cold side

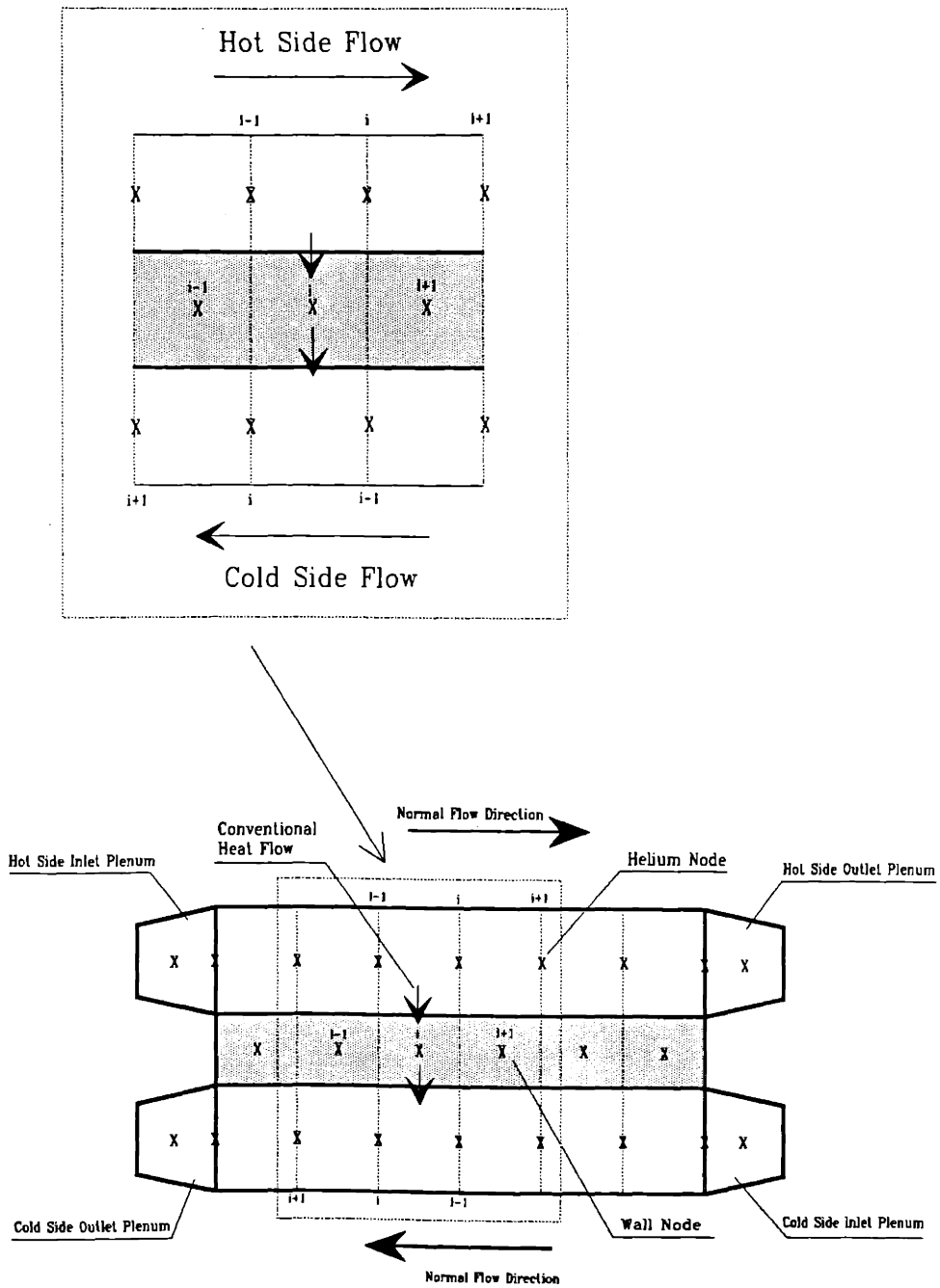

Figure 4.24 Conventional Average-Temperature heat Transfer Scheme

$$\frac{\partial T_i}{\partial t}=\frac{1/A_C}{\rho_f h_{sm}\rho_{wi}-\rho_f h_{wpi}\rho_m+\rho_m}\{\rho_{wi}\frac{Q_{Ci}}{\Delta x_i}-\rho_{wi}\frac{W_{j+1}h_{j+1}-W_j h_j}{\Delta x_i}+\frac{2\rho_{wi}}{\rho_i}\frac{W_{j+1}p_{i+1}-W_j p_{i-1}}{\Delta x_i}$$
$$+\rho_{wi}f_i\frac{|W_i|W_i^2}{\rho_i^2 D_{ei}A_i^2}-[\rho_{wi}(\frac{W_i}{\rho_i A_i})^2-(\rho_f h_{wpi}-1)]\frac{W_{j+1}-W_j}{\Delta x_i} \qquad (4.83)$$
$$+\rho_{wi}\frac{W_i}{\rho_i \Delta x_i A_i^2}(\frac{W_{j+1}^2}{\rho_{j+1}}-\frac{W_j^2}{\rho_j})\}$$

The symbols are those of the thermal hydraulic equation (4.48) with

A_h, A_C = flow cross-section areas of the hot and cold sides, respectively, m^2,

Q_{hi}, Q_{Ci} = nodal heat transfer rates of the two sides, W,

T_{wi} = wall nodal temperature, K,

C_{wpi} = wall specific heat, J/kg-K,

ρ_{wi} = wall density, kg/m^3, and

V_{wi} = wall nodal volume, m^3.

In order to derive the modeling condition, Eqn. (4.81) of the hot side is examined, however, the discussion below is equally applicable to Eqn. (4.83) for the cold side.

The nodal heat transport rate for the helium flow in normal direction is

$$Q_{hm}=W_j h_{i-1}(T_{i-1},p_{i-1})-W_{j+1}h_i(T_i,p_i) \qquad (4.84)$$

Conventionally, the heat diffusion rate from the flow to the wall, Q_{hi} is obtained based on the following average temperature of node[S2][R1]

$$Q_{hi}=U_{hi}(\frac{T_{i-1}+T_i}{2}-T_{wi}) \qquad (4.85)$$

where U_{hi} is the overall heat transfer coefficient of heat convection between the flow and wall, and heat conduction inside the wall. The detailed derivation of the heat transfer coefficient will be given later in section (4.5.3c). The heat transfer coefficient for compact heat exchangers with high heat transfer effectiveness is much larger than that for conventional heat

exchangers. In order that Eqn. (4.84) can be applied to the discretized recuperator model, the following condition is necessary:

$$\frac{\partial Q_{hT}}{\partial T_{i-1}} \geq \frac{\partial Q_{hi}}{\partial T_{i-1}} \tag{4.86}$$

For the MGR-GT recuperator, such condition would require as much as 125 longitudinal flow nodes for each side of the recuperator, leading to prohibitively laborious numerical solution. Models that do not meet the modeling condition (4.86) may generate numerical solution with non-physical meanings. One test was performed to illustrate such difficulty. The result of the test is shown in Figure 4.25, in which the recuperator is subjected to an 100°C step change in the inlet temperature of the hot side at t=2.0 sec. The model used in the test is made up just by 8 longitudinal nodes for each side of the recuperator. As can be seen, as the inlet temperature of the hot side increases, the subsequent nodes respond with "numerical rocking" behaviors: the temperature of the second node has an instance drop due to the improper modeling of the heat diffusion, while the third node has an immediate temperature increase. Such numerical unstable phenomena continue to propagate to the succeeding nodes.

The numerical difficulty for compact heat exchangers can be overcome by modifying the conventional heat flow direction of diffusion so that the constraint of the condition (4.85) on the model nodalization scheme could be relaxed. One approach is to use the modified heat flow direction of diffusion, as shown in Figure 4.26. The equation of heat transfer for the new heat diffusion scheme is

$$Q_{hi}=U_{hi}(T_i-T_{wk}) \tag{4.87}$$

where T_{wk} is the temperature on the boundary of the wall node (i), and is determined by

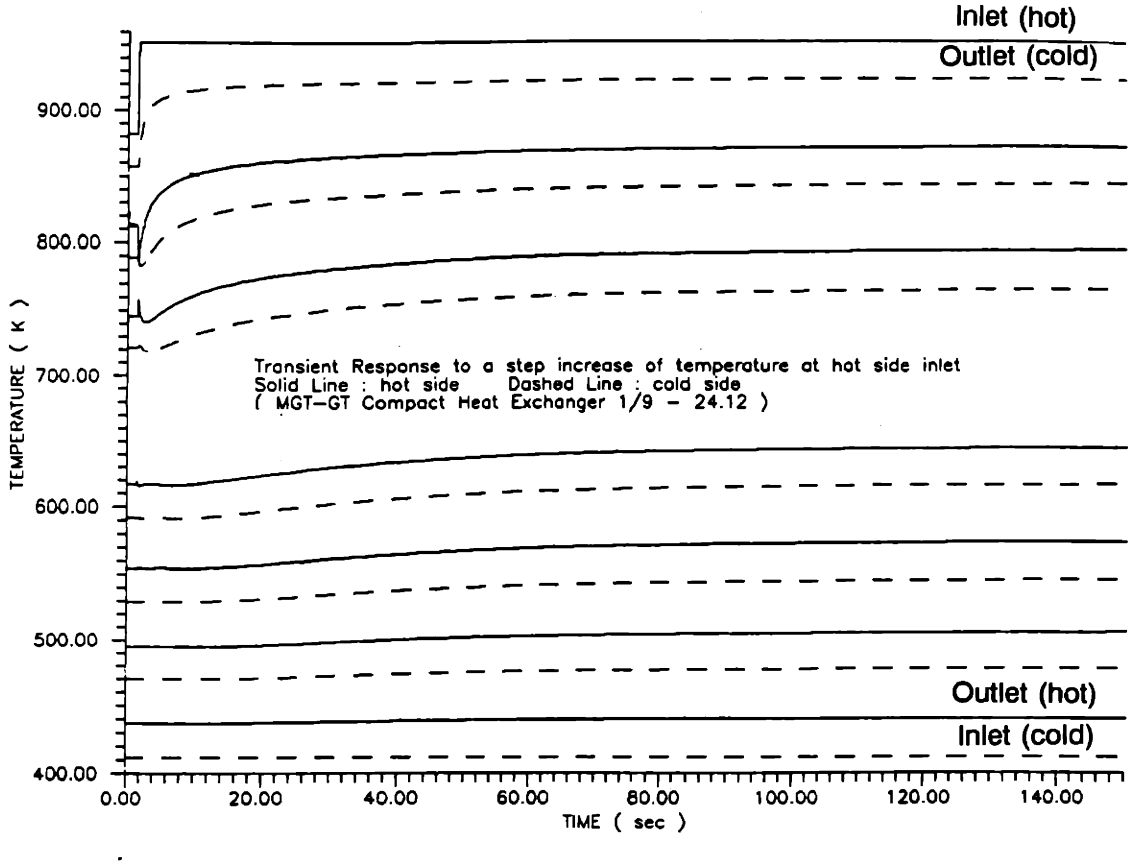

Figure 4.25 Simulation Results using the Conventional Heat Diffusion Scheme.

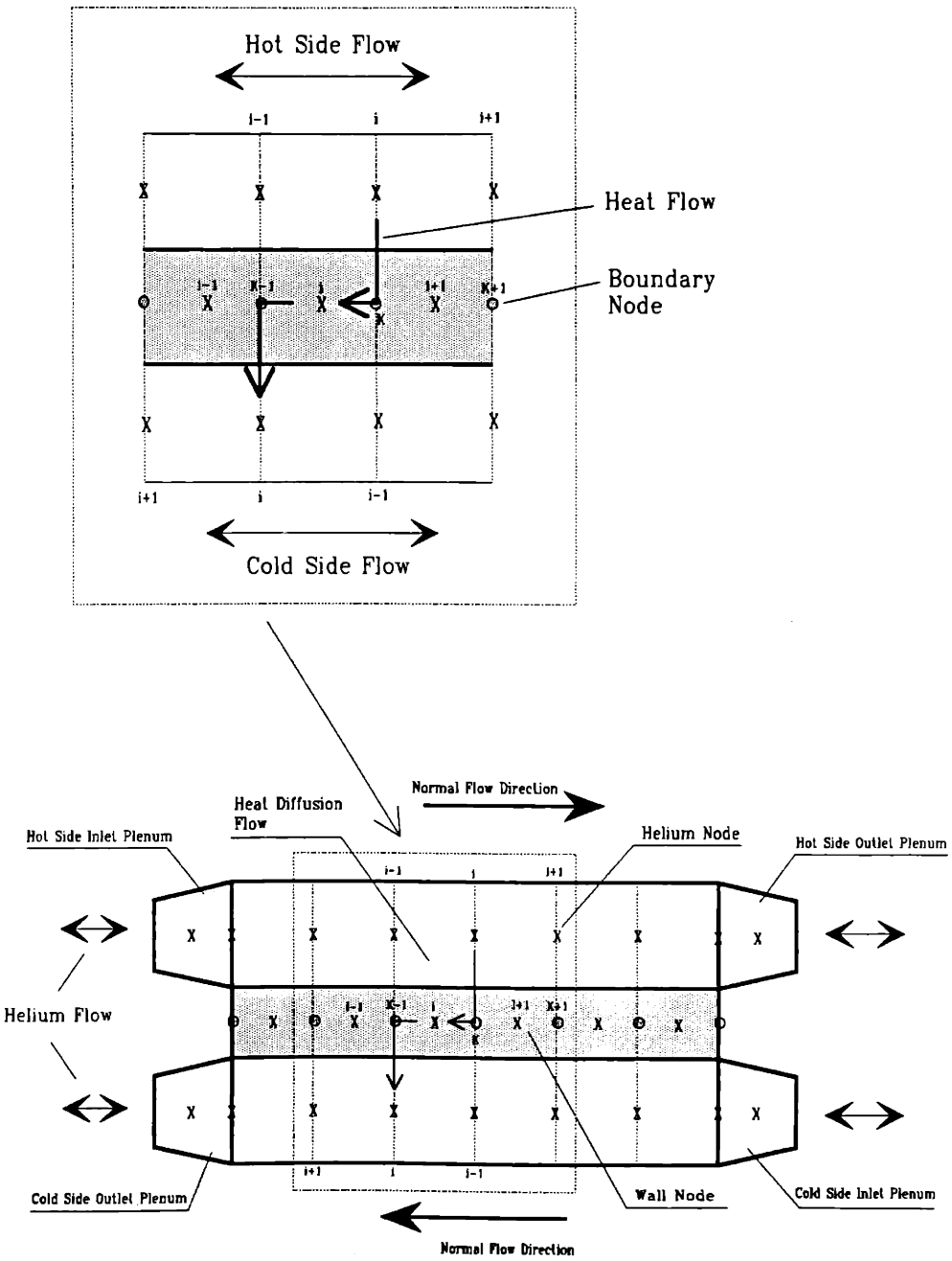

Figure 4.26 MGR-GT Recuperator Model with Modified Heat Diffusion Scheme.

$$T_{wk}=\frac{T_{wi}+T_{wi+1}}{2} \tag{4.88}$$

The modified heat diffusion equation (4.87) does not depend on the temperature of adjunct nodes so that $\partial Q_{hi}/\partial T_{i-1} = 0$. However, since $\partial Q_{hTi}/\partial T_{i-1}$ is always positive, the modeling condition (4.87) for high effectiveness heat exchangers is always assured regardless of the nodalization scheme.

4.5.3b Recuperator Modeling

Based on the newly developed diffusion scheme, the complete set of differential equations governing the dynamic behavior of the recuperator is as follows: For the hot side

$$\frac{\partial T_{hi}}{\partial t}=\frac{1/A_h}{\rho_f h_{sTi}\rho_{pi}-\rho_f h_{spi}\rho_{Ti}+\rho_{Ti}}\{\rho_{pi}\frac{U_{hi}(\frac{T_{wi}+T_{wi+1}}{2}-T_{hi})}{\Delta x_i}-\rho_{pi}\frac{W_{j+1}h_{j+1}-W_j h_j}{\Delta x_i}+\frac{2\rho_{pi}}{\rho_i}\frac{W_{j+1}p_{i+1}-W_j p_{i-1}}{\Delta x_i}$$
$$+\rho_{pi}f_i\frac{|W_i|W_i^2}{\rho_i^2 D_{ei}A_i^2}-[\rho_{pi}(\frac{W_i}{\rho_f A_i})^2-(\rho_f h_{spi}-1)]\frac{W_{j+1}-W_j}{\Delta x_i}$$
$$+\rho_{pi}\frac{W_i}{\rho_i\Delta x_f A_i^2}(\frac{W_{j+1}^2}{\rho_{j+1}}-\frac{W_j^2}{\rho_j})\} \tag{4.89}$$

$$\frac{\partial p_{hi}}{\partial t}=\frac{1/A_h}{\rho_f h_{spi}\rho_{Ti}-\rho_f h_{sTi}\rho_{pi}+\rho_{Ti}}\{\rho_{Ti}\frac{U_{hi}(\frac{T_{wi}+T_{wi+1}}{2}-T_i)}{\Delta x_i}-\rho_{Ti}\frac{W_{j+1}h_{j+1}-W_j h_j}{\Delta x_i}+\frac{2\rho_{Ti}}{\rho_i}\frac{W_{j+1}p_{i+1}-W_j p_{i-1}}{\Delta x_i}$$
$$+\rho_{Ti}f_i\frac{|W_i|W_i^2}{\rho_i^2 D_{ei}A_i^2}-[\rho_{Ti}(\frac{W_i}{\rho_f A_i})^2-\rho_f h_{sTi}]\frac{W_{j+1}-W_j}{\Delta x_i}$$
$$+\rho_{Ti}\frac{W_i}{\rho_i\Delta x_f A_i^2}(\frac{W_{j+1}^2}{\rho_{j+1}}-\frac{W_j^2}{\rho_j})\} \tag{4.90}$$

For the wall

$$\frac{dT_{wi}}{dt}=\frac{1}{C_{pwi}\rho_{wi}V_{wi}}[U_{hi}(T_{hi}-\frac{T_{wi}+T_{wi+1}}{2})+U_{Ci}(T_{Ci}-\frac{T_{wi-1}+T_{wi}}{2})] \tag{4.91}$$

For the cold side

$$\frac{\partial T_{Ci}}{\partial t}=\frac{1/A_C}{\rho_i h_{sTi}\rho_{pi}-\rho_i h_{spi}\rho_{Ti}+\rho_{Ti}}\{\rho_{pi}\frac{U_{Ci}(\frac{T_{wi}+T_{wi+1}}{2}-T_{Ci})}{\Delta x_i}-\rho_{pi}\frac{W_{j+1}h_{j+1}-W_j h_j}{\Delta x_i}+\frac{2\rho_{pi}}{\rho_i}\frac{W_{j+1}p_{i+1}-W_j p_{i-1}}{\Delta x_i}$$
$$+\rho_{pi}f_i\frac{|W_i|W_i^2}{\rho_i^2 D_{ei}A_i^2}-[\rho_{pi}(\frac{W_i}{\rho_i A_i})^2-(\rho_i h_{spi}-1)]\frac{W_{j+1}-W_j}{\Delta x_i}$$
$$+\rho_{pi}\frac{W_i}{\rho_i\Delta x_i A_i^2}(\frac{W_{j+1}^2}{\rho_{j+1}}-\frac{W_j^2}{\rho_j})\} \tag{4.92}$$

$$\frac{\partial p_{Ci}}{\partial t}=\frac{1/A_C}{\rho_i h_{spi}\rho_{Ti}-\rho_i h_{sTi}\rho_{pi}+\rho_{Ti}}\{\rho_{Ti}\frac{U_{Ci}(\frac{T_{wi}+T_{wi+1}}{2}-T_{Ci})}{\Delta x_i}-\rho_{Ti}\frac{W_{j+1}h_{j+1}-W_j h_j}{\Delta x_i}+\frac{2\rho_{Ti}}{\rho_i}\frac{W_{j+1}p_{i+1}-W_j p_{i-1}}{\Delta x_i}$$
$$+\rho_{Ti}f_i\frac{|W_i|W_i^2}{\rho_i^2 D_{ei}A_i^2}-[\rho_{Ti}(\frac{W_i}{\rho_i A_i})^2-\rho_i h_{sTi}]\frac{W_{j+1}-W_j}{\Delta x_i}$$
$$+\rho_{Ti}\frac{W_i}{\rho_i\Delta x_i A_i^2}(\frac{W_{j+1}^2}{\rho_{j+1}}-\frac{W_j^2}{\rho_j})\} \tag{4.93}$$

The momentum differential equations for the flow nodes connecting the thermal nodes are the same as (4.40). Currently, seven longitudinal nodes are used for each side of the MGR-GT recuperator.

4.5.3c Heat Transfer Correlation

The heat transfer surface of the MGR-GT recuperator is characterized by the correlations shown in Figure 4.27[K1], which is used to obtain the flow friction and heat transfer coefficients. The friction and heat transfer coefficients are functions of Reynolds Number Re, which is defined as:

Strip-fin plate-fin surface 1/9–24.12.

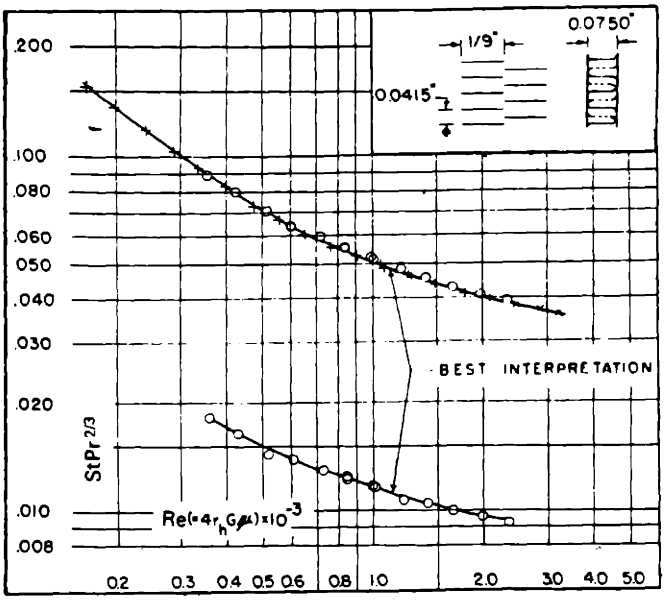

Fin pitch = 24.12 per in = 950 per m
Plate spacing, b = 0.075 in = 1.91 x 10^{-3} m
Fin length = 0.111 in = 2.8 x 10^{-3} m
Flow passage hydraulic diameter, $4r_h$ = 0.003966 ft = 1.209 x 10^{-3} m
Fin metal thickness = 0.004 in = 0.102 x 10^{-3} m
Total heat transfer area/volume between plates, β = 862.7 ft^2/ft^3 = 2,830 m^2/m^3
Fin area/total area = 0.857

Figure 4.27 MGR-GT recuperator heat transfer surface[K1]

$$Re=\frac{D_e G}{\eta}=\frac{4r_h W}{A\eta} \tag{4.94}$$

where $D_e = 4r_h$ is the hydraulic diameter given by the data in Figure 4.30, and A is the flow cross section area. The heat transfer coefficient per unit heat transfer area is determined by

$$h=\frac{yWC_p}{AP_r^{2/3}} \tag{4.95}$$

where Pr is Prandtl Number, Cp is the helium specific heat, and y is

$$y=St\,P_r^{2/3} \tag{4.96}$$

which is given in Figure 4.27.

Since the finned surface is employed, and temperature gradients along the fins extending into the flow reduce the temperature effectiveness of the heat transfer surface, the actual heat transfer coefficient must take the fin effectiveness into consideration. The fin effectiveness is given by

$$\eta_f=\frac{\tanh(ml)}{ml}$$
$$m=\sqrt{\frac{2h}{k\delta}} \tag{4.97}$$

where

δ = fin thickness given in Figure 4.27, m,

l = effective fin length which is half the wall spacing for 1/9-24.12, m, and

k = fin material heat conductivity, W/m-K.

The overall surface effectiveness, η_o is thus determined by a weighted average over the finned and unfinned heat transfer areas, which is given by

$$\eta_o=1-\frac{A_f}{A_T}(1-\eta_f) \tag{4.98}$$

where A_T is the total heat transfer area, finned and unfinned, and A_f/A_T is given in Figure 4.27 as a characteristic of the surface. Finally, the nodal heat transfer coefficient U_i can be calculated by

$$U_i = \frac{A_{Ti}}{\frac{1}{\eta_o h_i} + \frac{a}{k_k}} \tag{4.99}$$

where A_{Ti} is the total nodal heat transfer area, a is the half of the wall thickness, and K_k is the heat conductivity of wall node (K) corresponding to the flow node (i) as defined in Figure 4.26.

4.5.3d Test of the Recuperator Model

Simulations were performed to test the developed recuperator model. Figure 4.28 shows the steady state temperature distribution for the MGR-GT recuperator. The results from one of the transient simulations performed are shown in Figure 4.29 which shows the response of the recuperator temperatures to an inlet temperature step increase by 100°C of the hot side at t = 0 sec, followed by a corresponding inlet temperature reduction back to the initial value at t = 1000 sec. The inlet temperature of the recuperator cold side remains constant throughout the transient. Figure 4.29 shows the transient behavior of the temperatures for the hot side (solid-lines), wall (dotted-lines), and cold side (dashed-lines). The temperatures initially rise in response to the inlet temperature increase and reach a new steady state, with increasing time delays along the longitude direction which is largely due to the heat capacity of the recuperator wall. As the inlet temperature of the recuperator hot side drops to the initial level, the nodal temperatures follow to decrease, again, with time delays and return to the original steady state at t > 2000 sec, as shown in Figure 4.29. The temperatures near the outlet of the cold side have no significant changes during the transient.

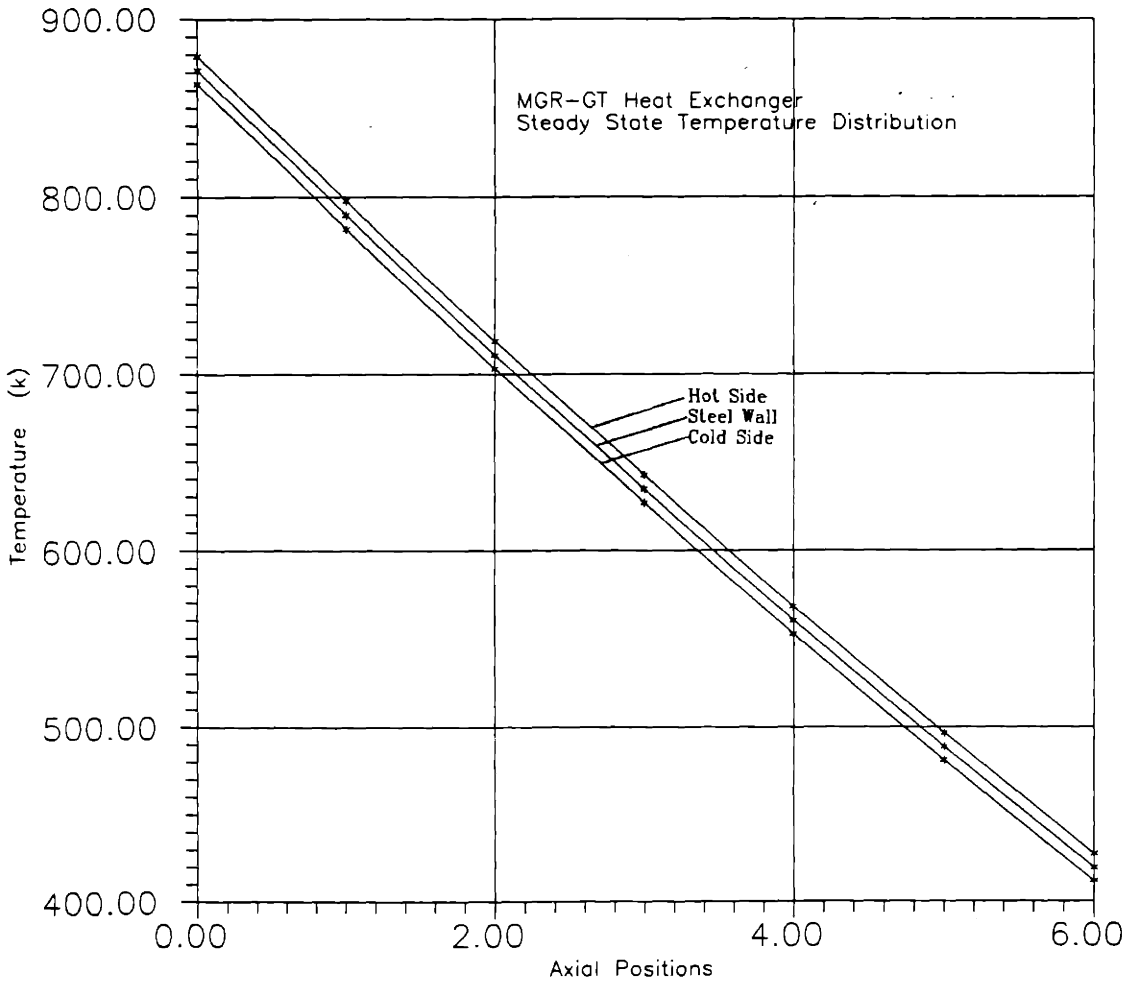

Figure 4.28 MGR-GT recuperator steady-state temperature distribution

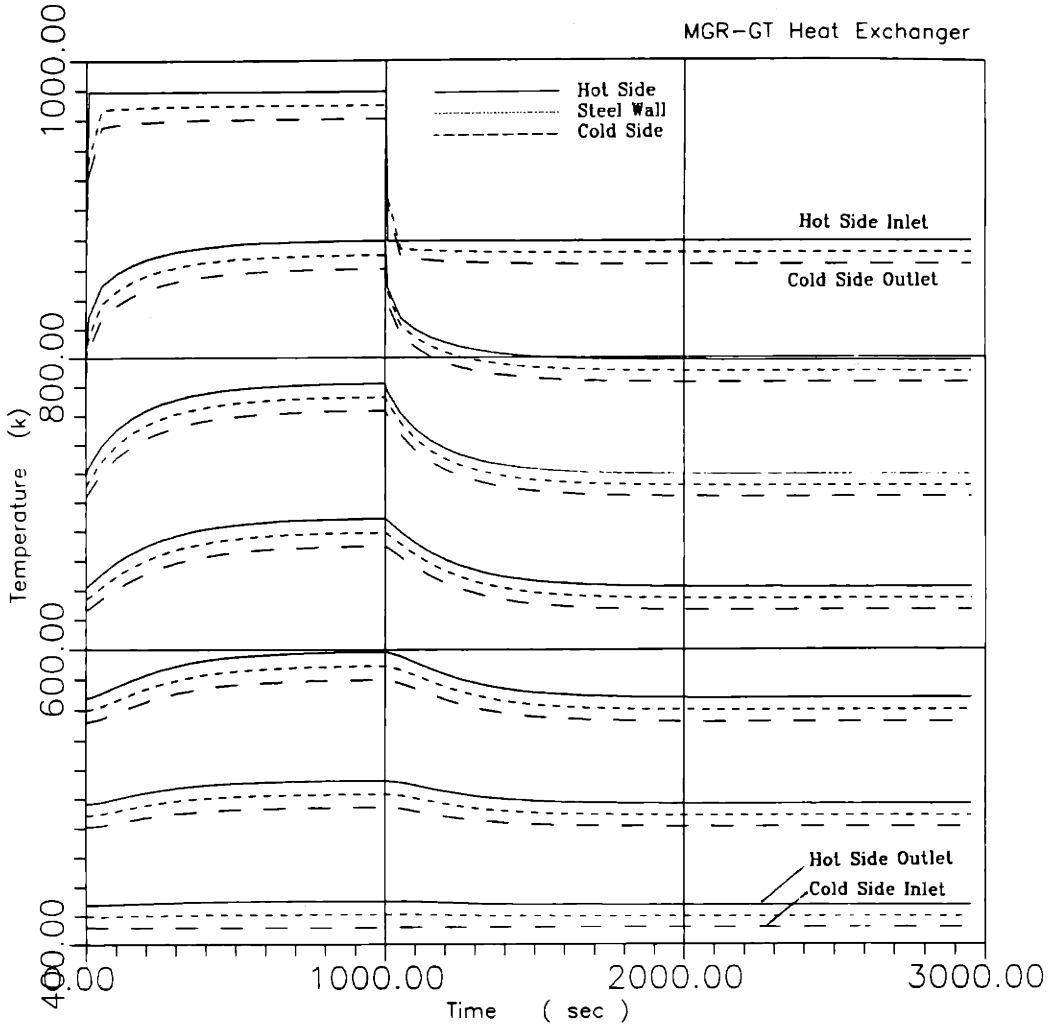

Figure 4.29 **MGR-GT recuperator transient response to a step temperature increase of 100°C at hot side inlet**

This is because that the cold side inlet temperature has been kept constant.

4.5.4 Precooler Model

The MGR-GT precooler is a crossflow tube-and-shell, helium-to-water heat exchanger with an unfinned heat transfer surface S1.50-1.00[K1]. The helium flows around the outside of the tubes, while the water flows inside the tubes. Therefore, the helium in the precooler core is in mixing flow. Because the axial dimension of the core is small, 0.565 meter, and the flow cross-section area is relatively large, about 3 m^2, the flow moment of flow inertia is very small, and flow compression phenomena are not significant inside the precooler core region.

The nodalization scheme of the precooler model is shown in Figure 4.30. As can be seen, the model consists of 7 axial helium nodes in the core and two nodes for the inlet and outlet cavities, and 24 nodes each for the tubes and water flow. Because of the limited flow inertia, the mixing helium flow in the precooler core is represented by a single flow segment. In addition, the helium pressure in the core makes use of the average pressure of the inlet and outlet pressures. The water flow is separated into six streamlines, as shown in Figure 4.30, to account for the thermal distribution of the water along the direction of the helium flow. The mathematical modeling is presented in the following.

4.5.4a Precooler Modeling

The approach to deriving the precooler model is the use of the basic thermal hydraulic conservation laws given by (4.20) to (4.22), which were used in developing the thermal hydraulic mathematical model. However, because of the assumptions that are made above for the modeling of the precooler, the derivation from the conservation laws to the precooler mathematical model is simplified. Based on the discretization scheme of the precooler as shown in Figure 4.30, the nodal energy equation is

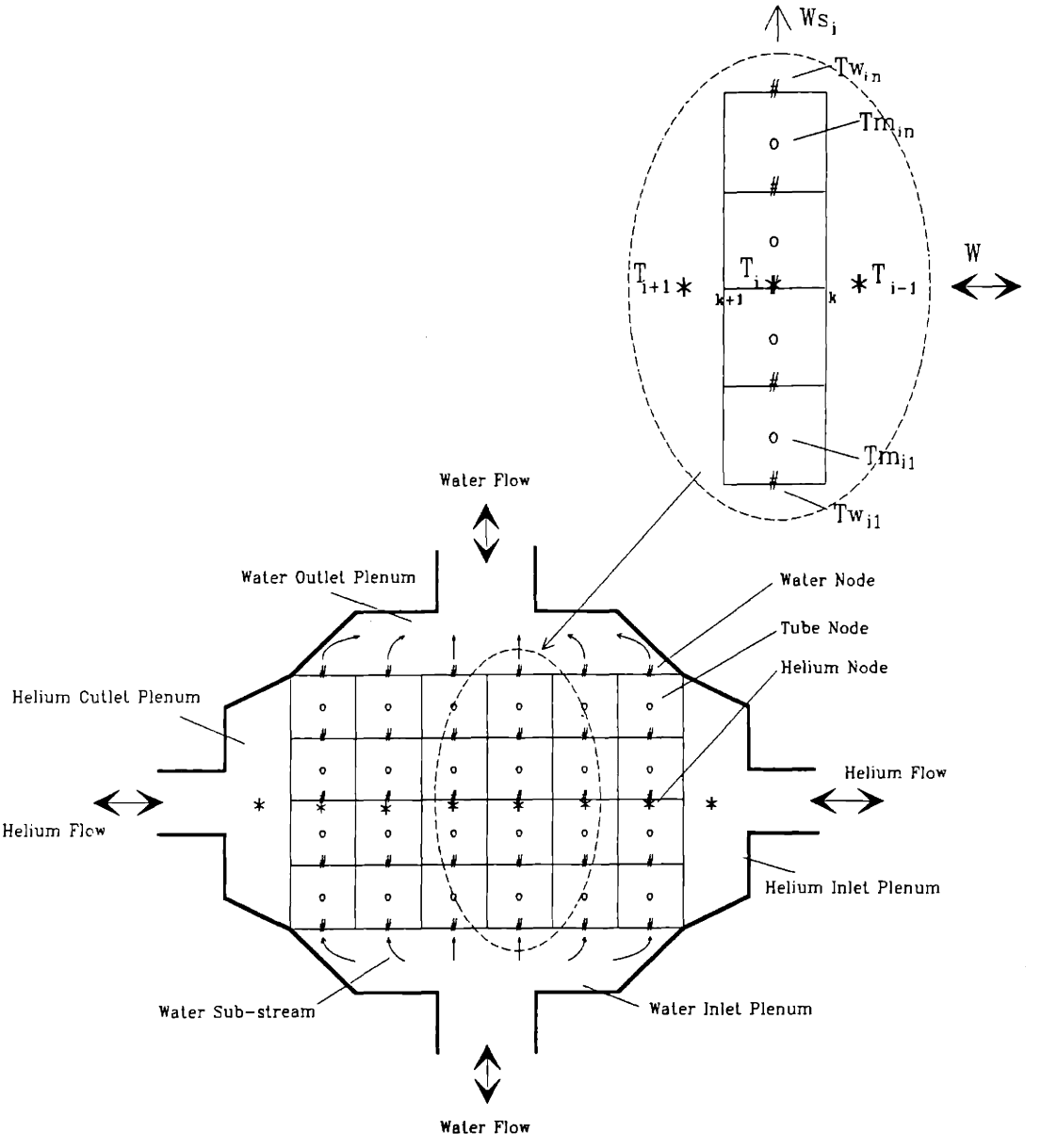

Figure 4.30 MGR-GT crossflow precooler model

$$A_f \rho_i \frac{dh_i}{dt} = \frac{Q_i}{\Delta x_i} - W\frac{h_{k+1} - h_k}{\Delta x_i} + f_i \frac{|W|W^2}{\rho_i^2 D_e A_f^2} + A_f \frac{dP_m}{dt} \tag{4.100}$$

where the symbols are those in Eqn.(4.22) with exceptions that A_f is the precooler flow cross section area, and W is the precooler helium flow. The boundary enthalpies, h_k and h_{k+1}, of the helium node (i) are defined as:

$$h_k = \begin{cases} h_{i-1}, & W \geq 0 \\ h_i, & W < 0 \end{cases}$$

$$h_{k+1} = \begin{cases} h_i, & W \geq 0 \\ h_{i+1}, & W < 0 \end{cases}$$

The nodal enthalpy h_i in Eqn. (4.100) is assumed to be approximated by the nodal stagnant enthalpy which is defined as:

$$h_i = h(T_i, p_m) \tag{4.101}$$

where p_m is the average pressure of the precooler inlet and outlet, as given by

$$p_m = \frac{1}{2}(p_{inlet} + p_{outlet}) \tag{4.102}$$

The inlet and outlet pressures are integrated with the thermal hydraulic models for the inlet and outlet plenums. Differentiating Eqn (4.101) results in

$$\frac{dh_i}{dt} = \frac{\partial h_i}{\partial T_i}\frac{dT_i}{dt} + \frac{\partial h_i}{\partial p_m}\frac{dp_m}{dt} = h_{Ti}\frac{dT_i}{dt} + h_{pi}\frac{dp_m}{dt} \tag{4.103}$$

By substituting (4.103) into (4.100), the nodal energy equation for the temperature of the helium flow becomes

$$A_f h_{Ti} \rho_i \frac{dT_i}{dt} = \frac{Q_i}{\Delta x_i} - W\frac{h_{k+1} - h_k}{\Delta x_i} + f_i \frac{|W|W^2}{\rho_i^2 D_e A_f^2} + A_f(1 - \rho_i h_{pi})\frac{dP_m}{dt} \tag{4.104}$$

The calculation of the nodal heat transfer rate Q_i is made by

$$Q_i=\sum_{j=1}^{4} U_{ij}(T_{wij}-\bar{T}_i) \tag{4.105}$$

where U_{ij} is the total heat transfer coefficient of square node (ij), T_{wij} is the temperature of tube node (ij), and $\bar{T}_i$ is the average temperature of the helium node (i), which is defined by

$$\bar{T}_i=\frac{1}{2}(T_{i-1}+T_i) \tag{4.106}$$

for helium flow in normal direction, and

$$\bar{T}_i=\frac{1}{2}(T_i+T_{i+1}) \tag{4.107}$$

when flow being reversed.

The energy equation for water node (ij) are given below:

$$\frac{dh_{sij}}{dt}=\frac{1}{A_{si}(\rho_{sij}+\rho_{hsij}h_{sij})\Delta x_{ij}}\left\{W_{si}(h_{si,j-1}-h_{sij})+U_{sij}(T_{wij}-\frac{T_{si,j-1}+T_{sij}}{2})\right\} \tag{4.108}$$

where W_{si} is the water flow of the ith streamline, A_{si} is the flow cross-section area of the ith streamline, and h_{sij} is the water nodal enthalpy. The temperature T_{sij} and density ρ_{sij} are functions of the water enthalpy and pressure. Assuming subcooled water, the temperature and density of water may be determined by[V1]

$$T_{sij}=\sum_{m=0}^{1}\sum_{n=0}^{3} CT_{mn}P_{sij}^{m}h_{sij}^{n} \tag{4.109}$$

$$\rho_{sij}=e^{-\sum_{m=0}^{2}\sum_{n=0}^{4} CN_{mn}P_{sij}^{m}h_{sij}^{n}} \tag{4.110}$$

where T_{sij} is water nodal temperature in K, ρ_{sij} is water density in kg/m^3, h_{sij} is water nodal enthalpy in J/kg, and p_{sij} is water pressure in Pa. The coefficients CT_{mn} and CN_{mn} are as given in Tables 4.5 and 4.6.

The heat balance equation for tube node (ij) is

Table 4.5 Coefficients CT_{mn} for Calculation of Water Temperature

m \ n	0	1	2	3
0	273.42	2.332 E −4	1.907097 E −11	−2.067247 E −17
1	2.708826 E −7	−1.9388325 E −12	2.411277 E −18	−7.558857 E −25

Table 4.6 Coefficients CN_{mn} for Calculation of Water Density

m \ n	0	1	2	3	4
0	−6.891704	−1.63856 E −7	7.96312 E −13	−7.279005 E −19	2.739196 E −25
1	−6.98704 E −10	4.83059 E −15	−1.873972 E −20	2.20968 E −26	−8.7246 E −33
2	−3.831966 E −17	1.30374 E −22	−8.100242 E −29	−6.027144 E −35	5.32613 E −41

$$\frac{dT_{wij}}{dt}=\frac{1}{M_{wij}C_{pwij}}\left[U_{ij}(\bar{T}_i-T_{wij})+U_{aij}(\bar{T}_{aij}-T_{wij})\right] \tag{4.111}$$

where M_{wij} is the mass of tube node (ij), Cp_{wij} is the tube nodal specific heat, and T_{sij} is the average temperature of the water node (ij), as given by

$$\bar{T}_{aij}=\frac{1}{2}(T_{aij-1}+T_{aij}) \tag{4.112}$$

4.5.4b Heat Transfer Correlations

For the helium flow, the heat transfer surface of the MGR-GT precooler is characterized by the data shown in Figure 4.31, which can be used to obtain the flow friction and heat transfer coefficients. The friction and heat transfer coefficients are given as functions of the Reynolds Number, Re, which is defined as:

$$Re=\frac{D_eG}{\eta}=\frac{4r_hW}{A\eta} \tag{4.113}$$

where $D_e = 4r_h$ is the hydraulic diameter given in Figure 4.31, and A is the helium flow cross-section area of the precooler core. The specific heat transfer coefficient is determined by

$$h=\frac{yWC_p}{AP_r^{2/3}} \tag{4.114}$$

where Pr is Prandtl Number, and y is

$$y=St\,P_r^{2/3} \tag{4.115}$$

which is given as a function of the Reynolds Number in Figure 4.31.

Since no finned surface is employed in the precooler, the temperature effectiveness of the heat transfer surface is unity. The nodal heat transfer coefficient U_{ij} can be calculated as:

S 1.50 – 1.00.

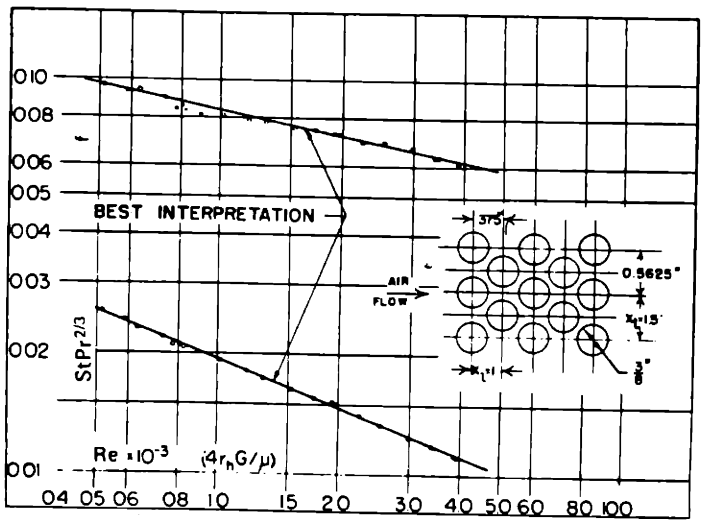

Tube outside diameter = 0.375 in = 9.525×10^{-3} m
Hydraulic diameter, $4r_h$ = 0.0196 ft = 6.071×10^{-3} m
Free-flow area/frontal area, σ = 0.333
Heat transfer area/total volume, α = 67.1 ft^2/ft^3 = 220.144 m^2/m^3
Note: Minimum free-flow area is in spaces transverse to flow.

Figure 4.31 MGR-GT precooler heat transfer surface[K1]

$$U_{ij}=\frac{A_{ij}}{\frac{1}{h_i}+\frac{a}{k_{ij}}} \tag{4.116}$$

where A_{ij} is the nodal heat transfer area, which can be determined by the data given in Figure 4.31, a is the half of the tube wall thickness, and K_{ij} is the heat conductivity of the tube node (ij) corresponding to the flow node (i) as defined in Figure 4.31.

For the water flow inside the tubes, the Dittus and Boelter convective heat transfer coefficient is used[H2]:

$$h=\frac{k}{D}(0.023Re^{0.8}Pr^{0.4}) \tag{4.117}$$

where k is the water thermal conductivity, D is the tube diameter, Re and Pr are the Reynolds Number and Prandtl Number, respectively. For the Reynolds Number, it can be obtained as:

$$R_e=\frac{4\frac{W}{N}}{\pi D\eta} \tag{4.118}$$

where N is the total number of the tubes in the core, and η is the water viscosity. All water properties are evaluated with the correlations provided in [V1].

4.5.4c Evaluation of the Precooler Model

The simulation has been performed to evaluate the precooler model. Figure 4.32 shows the steady-state temperature distribution for the MGR-GT precooler. The temperatures for tube and water are those at the streamline outlets of the water.

Figure 4.33 shows the precooler transient response to an inlet helium flow temperature step increase by 65°C at t = 0. The transient history of the temperature distributions for the helium and water flows is depicted at every time interval of Δt = 0.5 sec from t = 0.0 to 2.5 sec. As can be seen, because of the large heat capacity of the water flow, the water

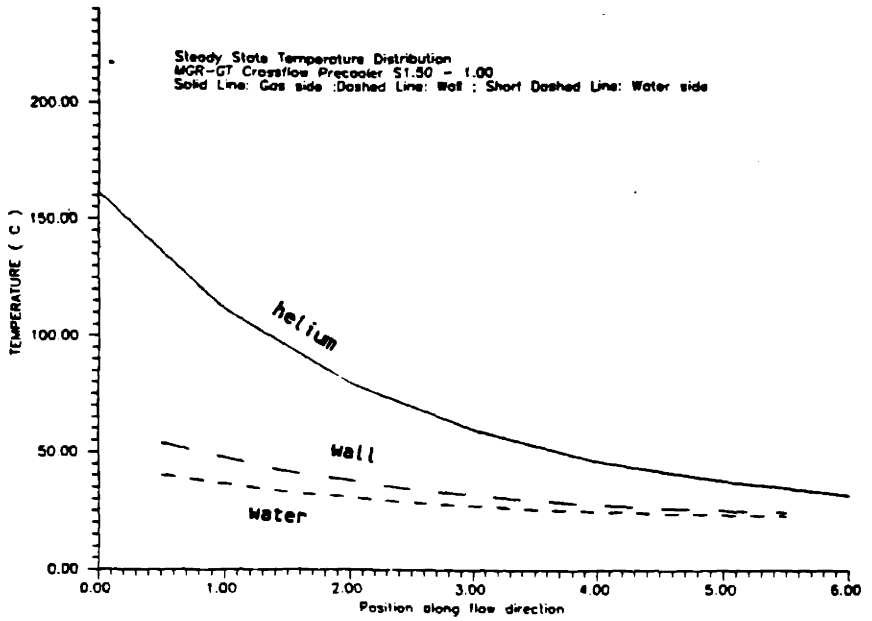

Figure 4.32 Precooler temperature Distribution.

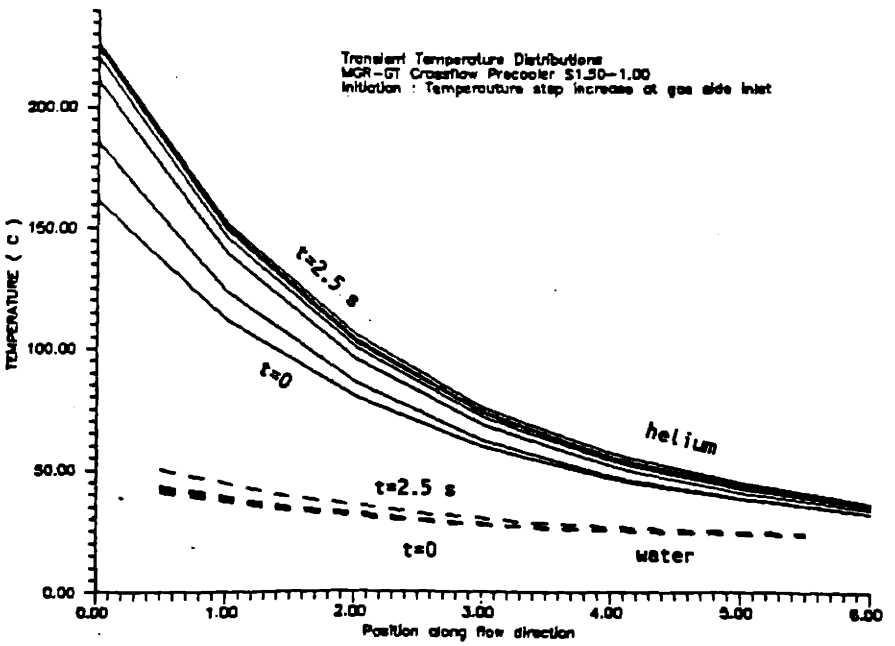

Figure 4.33 Precooler Temperature Transient Response to an inlet temeprature increase by 65°C

temperature has only a limited temperature increase at the outlet, with apparent time delay. The time delay is attributed to the tube mass heat capacity. The precooler exit temperature, rising only by about 10°C, demonstrates is insensitive to the relatively large temperature disturbance at the inlet of the precooler. The temperatures gradually approach to a new steady-state distribution at approximately t = 2.5 sec.

4.5.5 Turbomachinery Model

The conceptual design of the direct cycle turbomachine used in the MGR-GT consists of a 200 MW helium turbine of six stages on a single shaft connecting with a 15 stage, 100 MW compressor. In general, the performance of turbomachines is represented by the characteristics maps. Normally, these maps can be obtained from actual component tests or by the complex multi-dimensional flow analysis. But these methods, requiring detailed design and experimental data, are not feasible for the modeling of turbomachines at the conceptual design stage. Another approach, often used adequately in system control study, estimates the performance from the available characteristics of other, similar machines. Such methodology is utilized in the development of the model for the MGR-GT turbomachine.

4.5.5a Characteristics Maps

The design basis for large helium turbomachines for use in direct-cycle nuclear power plants has been well-established in the U.S. during the early HTGR-GT program[1][2]. Some of the design efforts were made by General Atomics and United Technologies[M3][M5][D2]. Characteristics maps obtained from these two companies include ones for a 400 MW HTGR helium turbomachine consisting of a 8-stage turbine and 16-stage compressor with design speed of 5,058 rpm and cycle pressure ratio of 2.25. These performance maps were generated largely based on the extended industrial experience of the companies in gas

turbine technologies. The far off-design characteristics of the turbomachine are included.

The performance maps obtained are utilized to estimate the characteristics of the MGR-GT turbomachine. Because of the similarity of stage configuration, system pressure ratio, and because of the utilization of the same working media (thus the same specific heat and sonic speed), it is plausible that the characteristics maps assumed could be replicated for the MGR-GT turbomachine. In any event, the actual performance maps would be sufficiently similar that the design considerations based on the assumed maps would be qualitatively correct.

The performance maps are first scaled around the design point to estimate the characteristics of the MGR-GT turbomachine design performance, and then extended to scale the maps for off-design operation. The resulted characteristics maps are converted into 3D surfaces covering both design and off-design performances for a wide range of operational speeds. Figures 4.34 and 4.35 show the generated performance maps for the MGR-GT turbine and compressor, respectively.

4.5.5b Rotor Dynamics

The performance maps can be used to determine the net power available to the turbomachine shaft. This will be combined with the power dissipated in various losses, such as windage loss, and the electrical power to form the net torque on the shaft. The resultant torque is then used to calculate the acceleration of the rotor.

The turbomachine efficiencies, which are obtained from the characteristic maps, and pressure ratios are used to calculate the temperature changes of the helium flow after passing through the turbine and compressor:

Tf-3D

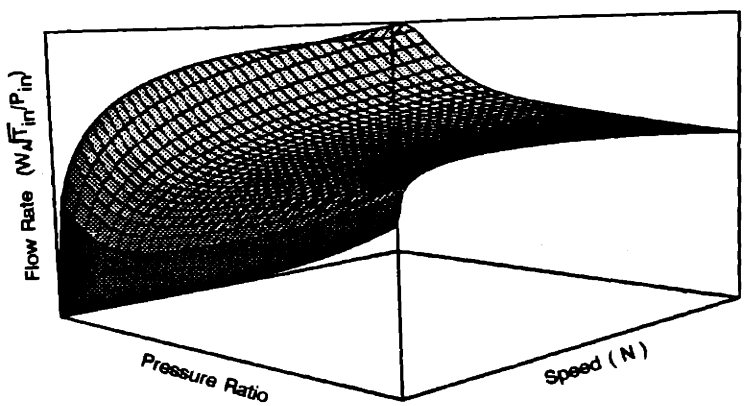

Te-3D

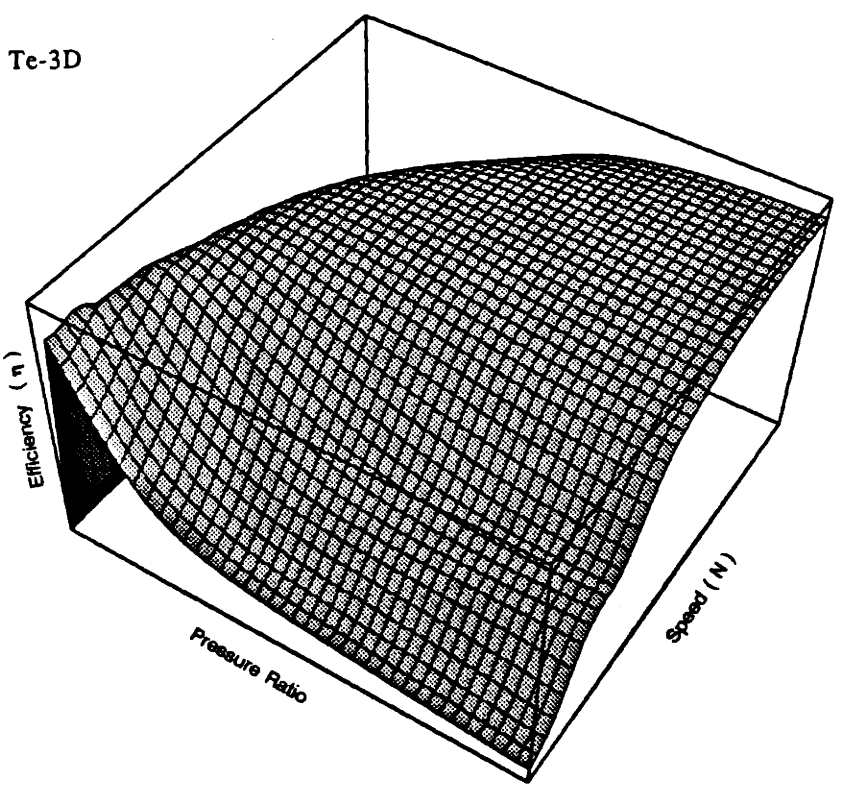

Figure 4.34 MGR–GT Turbine Performance Maps

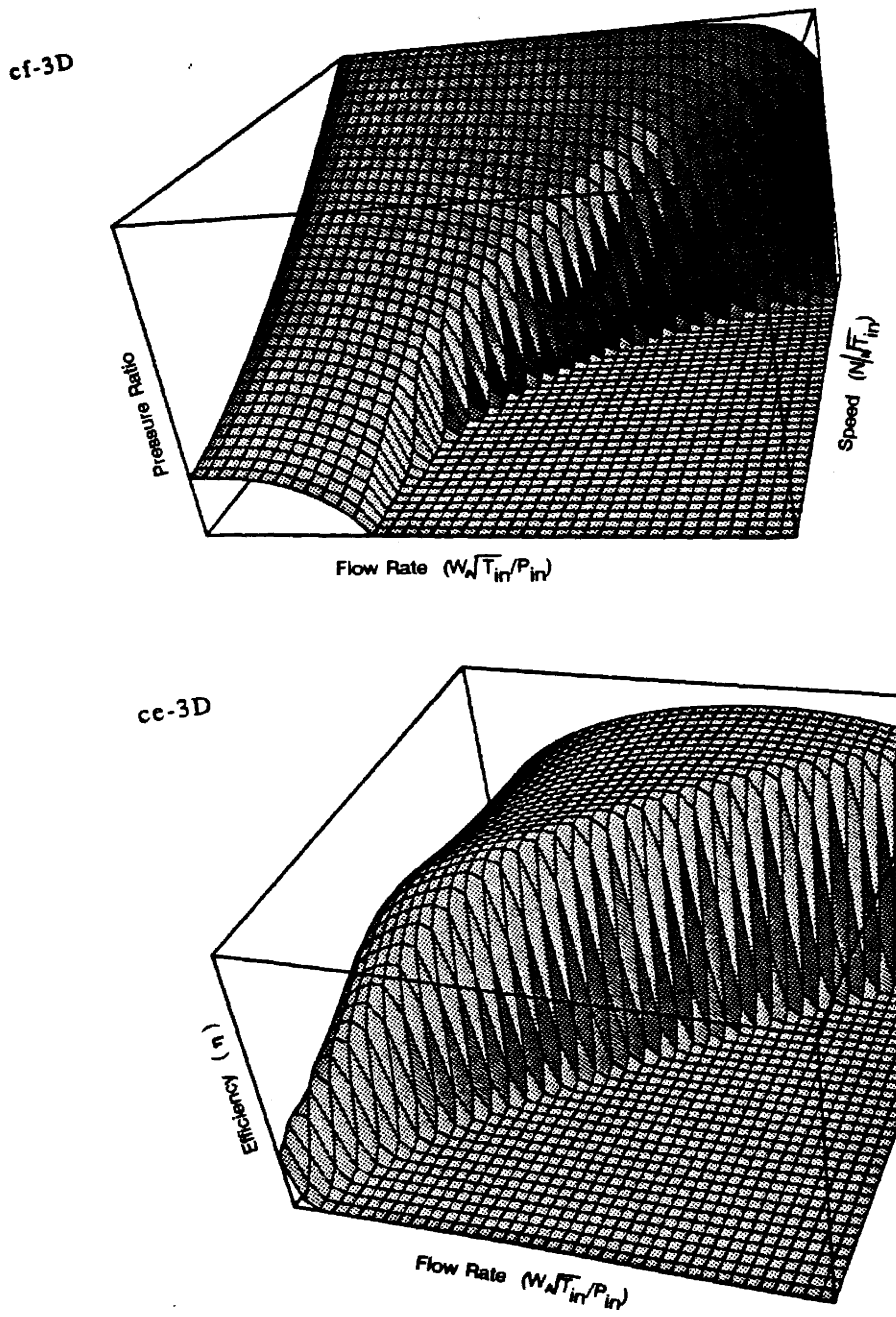

Figure 3.35 MGR-GT Compressor Performance Maps

$$\Delta T_t = \eta_t T_{tin}\left[1 - Pr_t^{-\frac{\gamma-1}{\gamma}}\right]$$
$$\Delta T_c = \frac{1}{\eta_c} T_{cin}\left[Pr_c^{\frac{\gamma-1}{\gamma}} - 1\right] \tag{4.119}$$

where Pr_t and Pr_c are the pressure ratios of the turbine and compressors, respectively, η_t and η_c are the efficiencies of the machines, T_{tin} and T_{cin} are the machinery inlet temperatures, and γ is the helium gas constant. The power that the turbine provides and the power that the compressor consumes can be estimated by:

$$P_t = W_t C_p \Delta T_t, \qquad P_c = W_c C_p \Delta T_c \tag{4.120}$$

where P_t and P_c are the powers of the turbine and compressor, W_t and W_c are the turbine and compressor flows which are determined from the characteristic maps. The net power of the turbomachine is the power generated by the turbine less that of the compressor, and assorted losses, mostly the windage loss of the generator submerged in the high pressure helium. Depending on the operating conditions of the turbomachinery shaft, the rotor runs in one of the following modes:

1. driving the generator on a single shaft in normal operation.
2. driven by the generator as a motor at low speed region during startup.
3. running with speed discrepancy between the machines after shaft failure.

For the normal shaft condition of mode 1, the rotor dynamics is described by

$$\frac{d\omega_s}{dt} = \frac{P_t - P_c - P_g/\eta_g - P_l}{(I_t + I_c + I_g)\omega_s} \tag{4.121}$$

where I_t, I_c, and I_g are rotational inertia of, respectively, the turbine, compressor, and generator, P_g is the electric load connected to the generator mains, P_l is the total loss associated with the rotors, and η_g is the combined efficiency of the generator and electrical

system. The characteristics of the combined efficiency is depicted in Figure 4.36, which is estimated from the supermotor performance[T2].

In the second mode of the rotor operation condition, the dynamic behavior of the rotor is governed by

$$\frac{d\omega_s}{dt}=\frac{P_t-P_c+P_e\eta_g-P_l}{(I_t+I_c+I_g)\omega_s} \tag{4.122}$$

where P_e is the external power delivered to the line-side of the generator electronics.

In the event of shaft failure in mode 3, the rotor dynamics depends on the location of the shaft break. Based on the current rotor configuration, two variations of break are possible: one on the portion of the shaft between the turbine and compressor, and the other in between the compressor and generator. For other potential shaft configurations, however, other scenarios of shaft failure may exist.

As an example, the rotor dynamics for the shaft failure between the turbine and compressor under the current rotor configuration are given below:

For the turbine

$$\frac{d\omega_t}{dt}=\frac{P_t}{I_t\omega_t} \tag{4.123}$$

For the compressor connected with the generator

$$\frac{d\omega_c}{dt}=\frac{-P_c-P_g/\eta_g-P_l}{(I_c+I_g)\omega_c} \tag{4.124}$$

where W_t is the turbine rotational speed, and W_c is the speed of the compressor and generator. It can be predicted from Eqn. (4.123) that the turbine rotor, loaded with full power but zero load, will experience rapid acceleration immediately after the shaft break. Unless the turbine power could be quickly reduced, damaging overspeed would result.

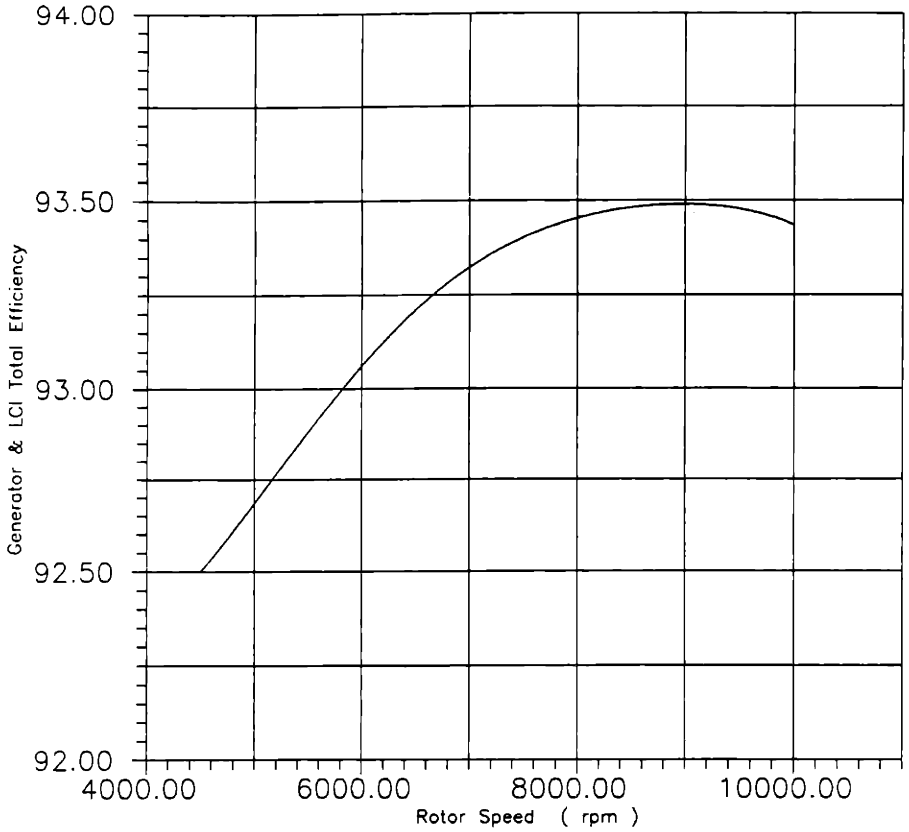

Figure 4.36 Overall Efficiency of the Generator and Electrical System.

4.5.6. Plant Control System Model

The baseline design of the MGR-GT control system was presented in chapter 3. The control system including the PRS and PPS is automatically operated by numerous controllers to accomplish control functions. Based on this baseline design, the mathematical modeling of the controllers will be presented. The method to be used in the modeling is state-space feedback control.

4.5.6a. State-Space Feedback Control Method

State-space representation of dynamic system was first introduced in the early 1960s by a group of talented engineers and mathematicians committed to the development of advanced control theory. The spiritual father of the effort was Professor Solomon Lefschetz who led the systems control research group at the Research Institute of Advanced Studies (RIAS) in Baltimore, MD[F1].

The basic premise of the state-space system dynamics is that the state of a dynamic system is a set of physical quantities, called state variables, the characteristic behavior of which completely determines the evolution of the system. The behavior of the state variables is represented by a system of ordinary differential equations. According to Newtonian dynamics, the future evolution of the state variables is entirely determined by present conditions. When control inputs are incorporated, the system equations takes the following state-space form:

$$\frac{d\bar{y}}{dt}=F[\bar{y},\bar{U},t] \tag{4.125}$$

where $\bar{y}$ is the vector of state variables, $\bar{U}$ is the vector of the control inputs, and t is the time as an independent variable. In practice, Eqn. (4.125) for complex thermal hydraulic systems, such as the MGR-GT, is a coupled, nonlinear system.

The control is accomplished by the control input vector which is designed based on the state-feedback laws[F1][K2]. By means of the state-feedback control, the dynamic behavior of the system can be reshaped and regulated at the cost of amplifier power consumption, provided the system is controllable.

In order to illustrate the principles of state-feedback control, a simplified system is employed. The problem is the following: Given

$$\frac{d\bar{y}}{dt}=A\bar{y}+B\bar{U} \tag{4.126}$$

where A is the n x n system matrix whose dynamic characteristics may be unstable, and B is the n x m input matrix (n is system dimension, while m is the number of feedback control inputs). It is desired to find a state-feedback operation

$$\bar{U}=-K(C\bar{y}-H\bar{R}) \tag{4.127}$$

where K is the m x n control gain matrix, C is the n x n sensor matrix, $\bar{R}$ is the s x 1 regulating vector, and H is the n x s regulating matrix (s is the number of regulating variables), such that the system (4.126) could be transformed into

$$\frac{d\bar{y}}{dt}=(A-BKC)\bar{y}+BKH\bar{R} \tag{4.128}$$

and new characteristic matrix (A-BKC) would become stable and be capable of following the regulation command $\bar{R}$ with the desirable dynamic behavior by the selection of the control gain matrix K. The above control approach is schematically described by the feedback control loop shown in Figure 4.37.

The following example illustrates the application of the state-feedback control:

$$\begin{pmatrix}\dot{y}_1\\ \dot{y}_2\end{pmatrix}=\begin{bmatrix}-1 & 1\\ 9 & -1\end{bmatrix}\begin{pmatrix}y_1\\ y_2\end{pmatrix}+\begin{pmatrix}0\\ 5\end{pmatrix}U \tag{4.129}$$

If y_1 is the state to be controlled, the system transfer function can be obtained by Laplace transform as:

$$\frac{y_1(s)}{U(s)}=\frac{5}{s^2+2s-8} \tag{4.130}$$

The characteristic denominator possesses a positive pole s = 2, implying that such system is unstable to any disturbance. It is intended to form a feedback control and regulation loop

$$U=-K(y_1-R) \tag{4.131}$$

such that the system would become stable and the output y_1 could be regulated according to the regulating command R.

For simple, linear systems such as that given by (4.129), the selection of K can be performed, analytically, by working on the closed-loop system matrix (A-BKC) of (4.128) with the pole replacement technique in order to stabilize the original system. However, this method is not practical for complex, nonlinear dynamic systems. Instead, the approach of trail and error through simulation is often used. To illustrate this approach, it is used to control the unstable system above.

The control feedback loop based on the control establishment (4.131) may be constructed in frequency-domain for the system as shown in Figure 4.38. As can be seen that three individual control parameters, *i.e.*, P, D, and I parameters, representing proportional, derivative, and integral feedback laws, have been chosen to establish the control gain. Numerical integration is performed to demonstrate the procedure for the selection of these control parameters in shaping the system dynamic characteristics.

It is assumed that the regulating command intends to regulate y_1 from initial value

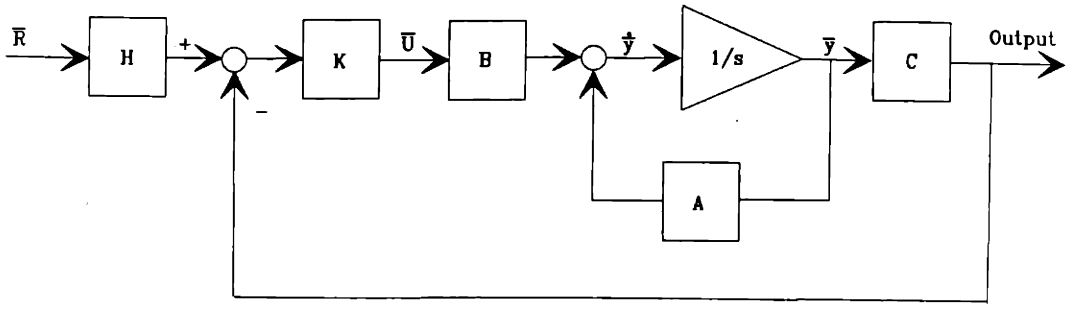

Figure 4.37 State–Space Feedback Control Loop

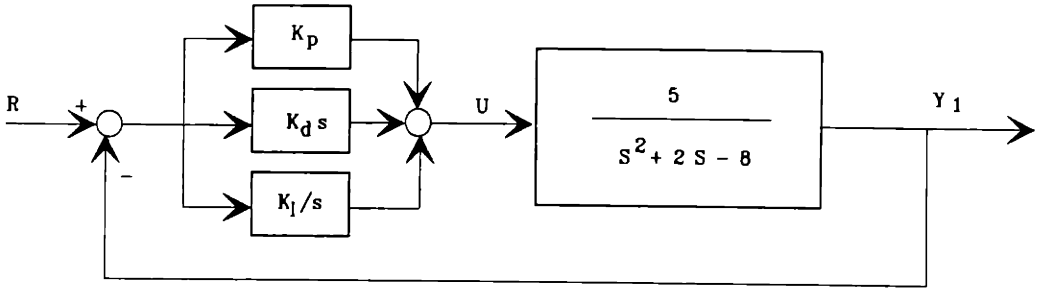

$$H = 1 \qquad C = \begin{vmatrix} 1 & 0 \\ 0 & 0 \end{vmatrix}$$

Figure 4.38 An Example of the State–Feedback Control Design

y_1=0 to a new state y_1 = 50, by issuing a step input R = 50/s. The results of numerical integration are shown in Figure 4.39.

The curve-1 represents the response of the open system, *i.e.*, uncontrolled system. As indicated by the values of the parameters in the first row of the appended table, all control parameters are set to be zero. As the input signal R (= U = 50) is issued at t = 0.5 sec, the system output climbs indefinitely, exhibiting the inherent instability of the system due to the positive pole of the system.

It is possible to eliminate the system instability by forming a preliminary feedback control loop with proportional control gain Kp. As can be seen that setting Kp=2.0 to obtain a feedback signal proportional to the error E = R - y_1 would stabilize the system from indefinite climbing, as indicated by curve-2. However, the proportional control, as shown, is unable to regulate the output of the system to equal state R.

Having stabilized the system, the transient behavior of the system can be shaped through the utilization of other control parameters. The derivative control that is proportional to the rate of change in the regulating error E, is capable of providing early control action following disturbance of steady-state. This effect is clearly demonstrated by the system behavior represented by the curve-3. Theoretically, the D-control alone has no control capability over the long-term stability of the system, and the system regulation. In order to regulate the output y_1, the Integral control, which integrates the error E = R - y_1 over the transient period of time, must be incorporated. Integral control effect is depicted by curve-4. As can be seen, the system output after a short time is regulated to the state as demanded.

In reality, two or all of the three control laws are combined in an actual control system in order to manipulate the system at will. The curve-5 shows the response under combined actions of the three feedback control loops. The curve-5 is replotted for extended period of time in Figure 4.40, represented by the curve-1. As can be seen, not only is the overshoot

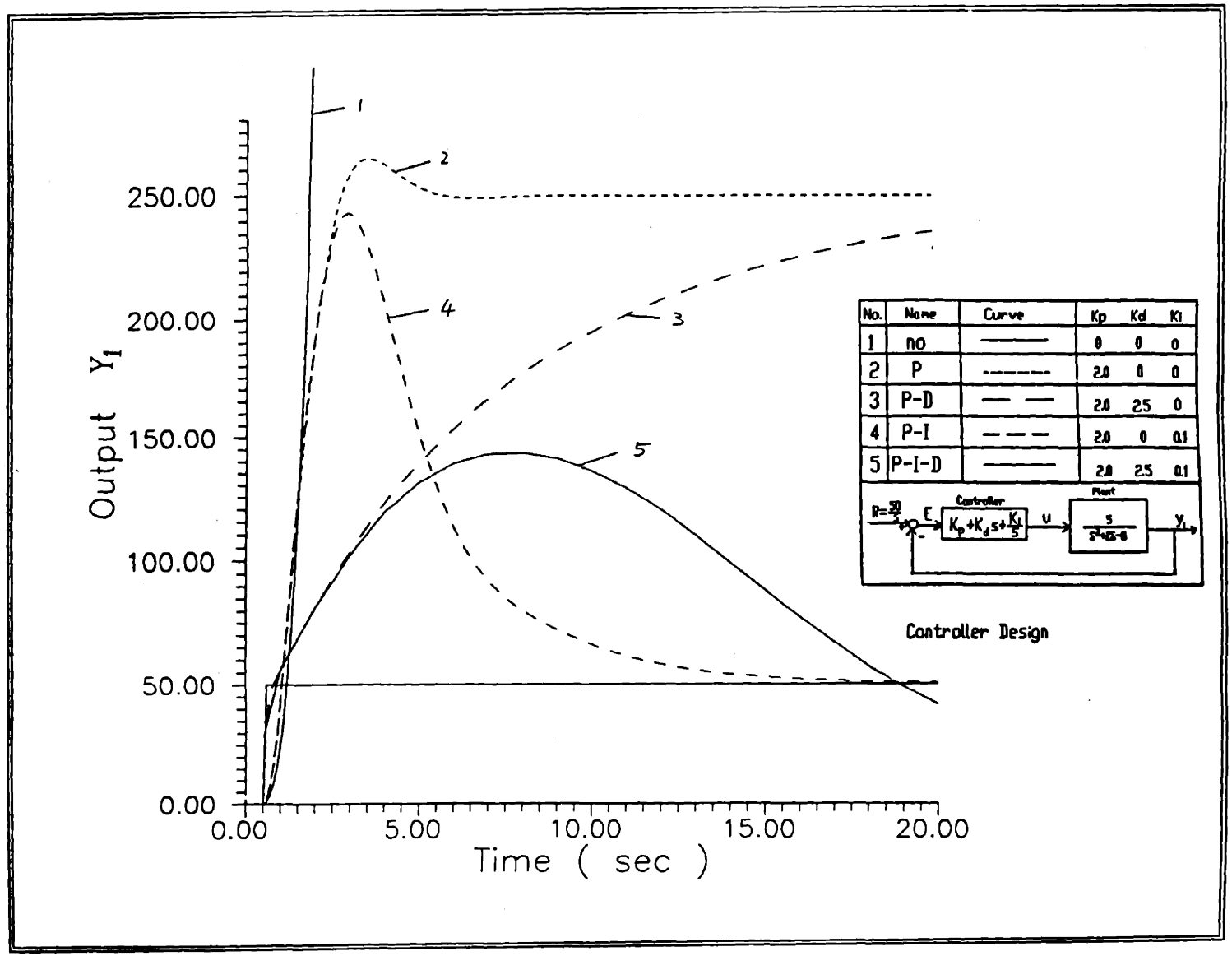

Figure 4.39 Introduction to state-space feedback controller design

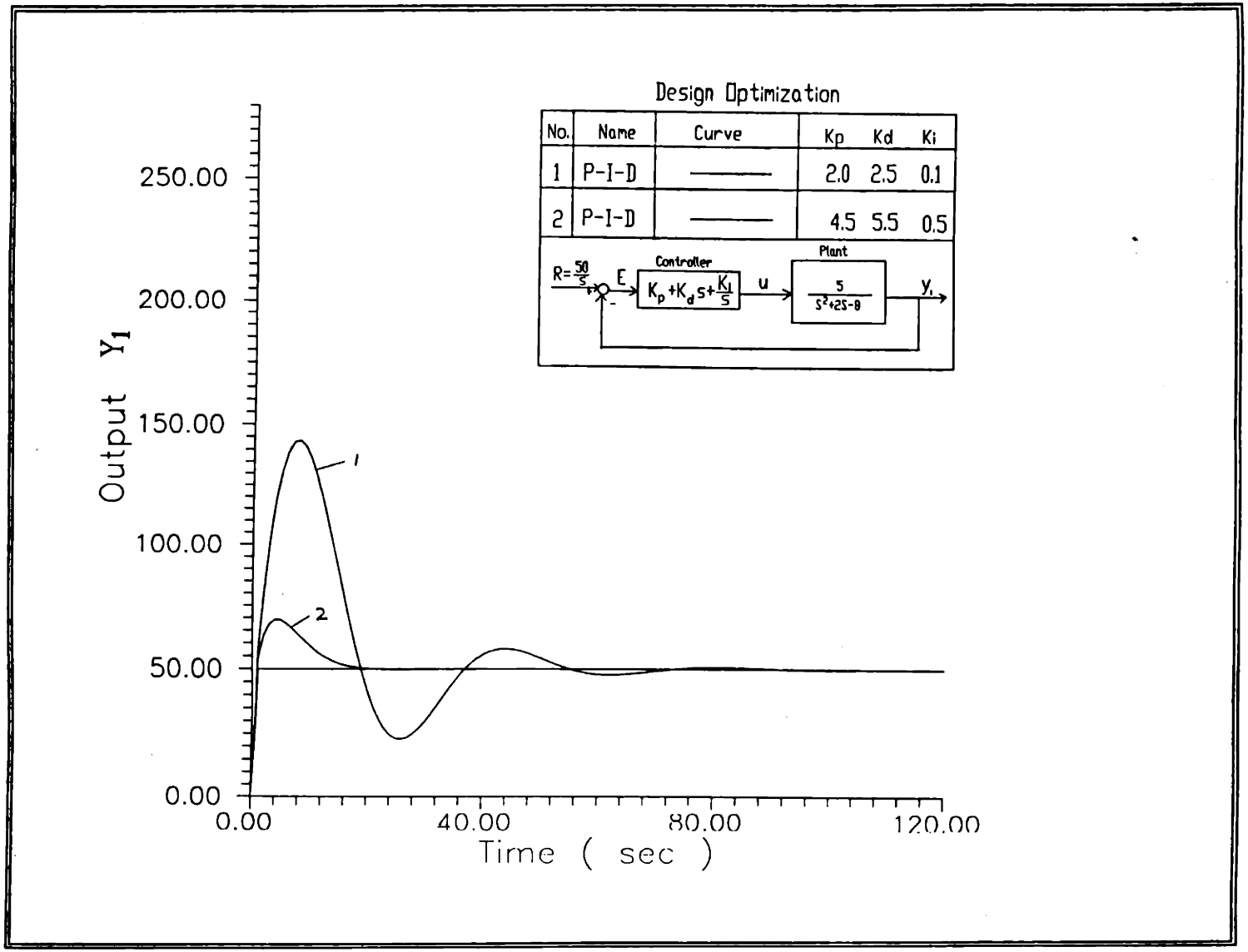

Figure 4.40 Controller design optimization

of the early response reduced, mostly due to the virtue of the derivative control, but also the regulation of the output is achieved with the aid of the integral control. The somewhat oscillatory behavior can be eliminated by the optimization of these control parameters. The optimization effect is demonstrated by the behavior represented by the curve-2, which is controlled by the parameters listed in the second row of the appended table.

The procedure of trial and error selection for control parameters has been successfully used to stabilize and regulate the simple system (4.129). This selection approach will be employed for the development of the controllers for the MGR-GT control system in the following.

4.5.6b Modeling of the Plant Regulation System

The baseline design of the PRS controllers was proposed and illustrated in Figure 3.29. The PRS controllers are required for the automatic operation of the inventory control system, bypass control system, reactor control system, and electrical system. The controllers rely on different state feedback control laws depending on the specific control functions each of the PRS subsystems provides. By analyzing the control functions, the feedback control laws have been established for each of the PRS controllers. The detailed design of the PRS controllers is shown in Figure 4.41. There are total six individual controllers, each of which will be discussed in the following.

The bypass control is used to control the turbomachine speed throughout the load control range by the adjustment of the bypass valve. In the bypass controller, the speed of the turbomachine, N, is the manipulated variable which is regulated based on the speed regulating signal, Nr. The control loop is composed of proportional, derivative, and integral gains with rate and magnitude limits filtering the amplified control signals. The filtering of the control signals is essential to preventing the control actuators from saturation which could

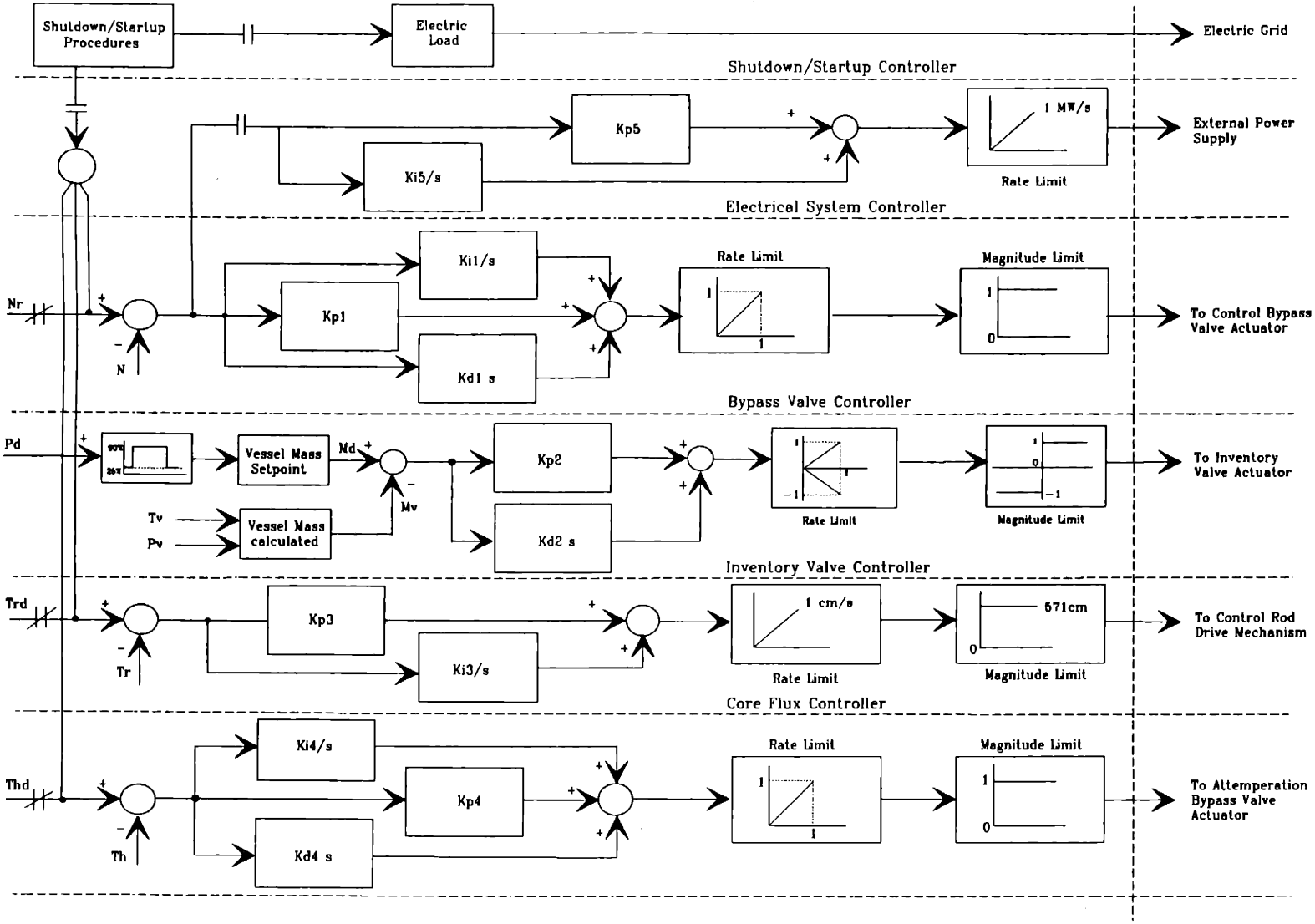

Figure 4.41 MGR-GT PRS Controllers

cause control-induced system instability. The proportional portion of the control loop is intended to stabilize the speed of the turbomachine in the event of load disturbance. The proportional feedback blended with the derivative signal of speed error provides the capability of reshaping the speed behavior with prompt response and desirable damping. The integral control action which integrates the speed error over the transient period of time enables the regulation of the turbomachine speed according to the speed regulating signal.

The inventory control is used to regulate the helium inventory in the plant circuit in order to change the power output to match load changes in the range from 90% to 50% of nominal load. The actual electric load is used to calculate the setpoint of helium mass in the inventory vessels. The setpoint of the helium mass is then compared with the current helium inventory in the vessels which are determined based on the measurement of the temperature and pressure in the vessels. The joint proportional and derivative feedback is used with forward rate and magnitude limits of control signal. The inventory valves are remained open until the helium storage in the inventory vessels reaches the setpoint.

The core flux controller is used to manipulate the core neutron flux through the control of reactivity by adjusting the control rods. The control approach is to maintain the reactor outlet temperature constant at the 850°C design value throughout the load control range. The actual temperatures at the reactor outlet are sensed, and the average temperature is fed into the core flux controller. The error signal between the average temperature and design temperature is forwarded through the control gains which provide both proportional and integral amplification to the signal. The control signal is then filtered with rate and magnitude limits and sent to the control rod mechanism which accordingly manipulates the movement of the control rods to alter the reactivity presented in the core for reactor power control. The integral portion of control action would permit the control rods to reach such position as required for the maintenance of the reactor outlet temperature.

The attemperation bypass is used to control the thermal conditions imposed upon the plant components during large bypass control processes. The attemperation controller manipulates the bypass valve to keep the temperature of the LP-recuperator inlet at the design value. During bypass control processes, the temperature of the LP-recuperator inlet is measured. The difference between the actual and design temperatures is forwarded through the control gains constituted by proportional, derivative, and integral amplification with rate and magnitude limits. The proportional action with the aid of the derivative control offers the rapid response with optimum damping to prevent thermal shock on the recuperator, while the integral control enables the correct opening position of the attemperation valve so as to maintain the temperature at the design value.

The procedures for plant startup and shutdown were proposed during the control system design. These procedures are programmed and installed in the shutdown/startup controller. During plant startup and shutdown operation, the controller issues the control commands programmed at various stages to a number of correlative controllers. The controllers used include bypass valve controller, attemperation controller, core flux controller and electric system controller. When shutdown or startup operation is initiated, normal regulating signals to the controllers are switched off. Instead, they receive the programmed commands from the shutdown/startup controller. The control feedback gains used for shutdown and startup operation in the controllers are the same as those for normal power control. The electrical system controller is only utilized during initial period of startup to control the external power supplied to the generator, which, as a motor drives the turbomachine from stationary state to 3,600 rpm. Integral and proportional control laws are incorporated in the electrical system controller with rate limit of power supply. The control gains are so selected as to accomplish the optimal dynamic characteristics of the rotor during this period of operation.

The PRS controllers presented above have been fully incorporated into the system model in the state-space feedback form (4.60). The control gains for each of the PRS controllers will be selected and optimized to meet the requirements of the plant regulation and to offer improved dynamic behavior for the MGR-GT. This task is pursued through simulation when the full-scale system model becomes available.

4.5.6b Modeling of the Plant Protection System

In chapter 3, the PPS was designed to handle a list of selected accident events for the protection of the plant components. Based on the proposed design, the PPS protection logic is developed, which is shown in Figure 4.42.

The PRS protection logic model consists of four columns including accident events, sensor setpoints, logic and diagnosis circuit, and controllers and mechanisms. In the first column from the left is a list of the accidents to be dealt with. The PPS sensors detect the occurrence of each accident and send signals to the second column for comparison with sensor setpoints. The sensor setpoints provide gateways from sensor measurements to the logic and diagnosis circuit. If any setpoint were exceeded, the corresponding signal would be allowed to pass the gateway and flow into the circuit. The signal will then be analyzed in the logic and diagnosis circuit and eventually guided into the appropriate PPS controllers in the far-right column to initiate protective actions. The controllers included in the PPS are loop shutdown controller, reactor shutdown controller, and attemperation controller. These controllers are functionally independent from those used in the PRS. Details of these controllers are shown in Figure 4.43.

The loop shutdown is accomplished by the shutdown bypass valve. Depending on the nature of accidents, two modes of loop shutdown may be actuated, with one to shutdown the system to an idle state with the turbomachine running at design speed as in case of a

Figure 4.42 The MGR-GT PPS protection logic

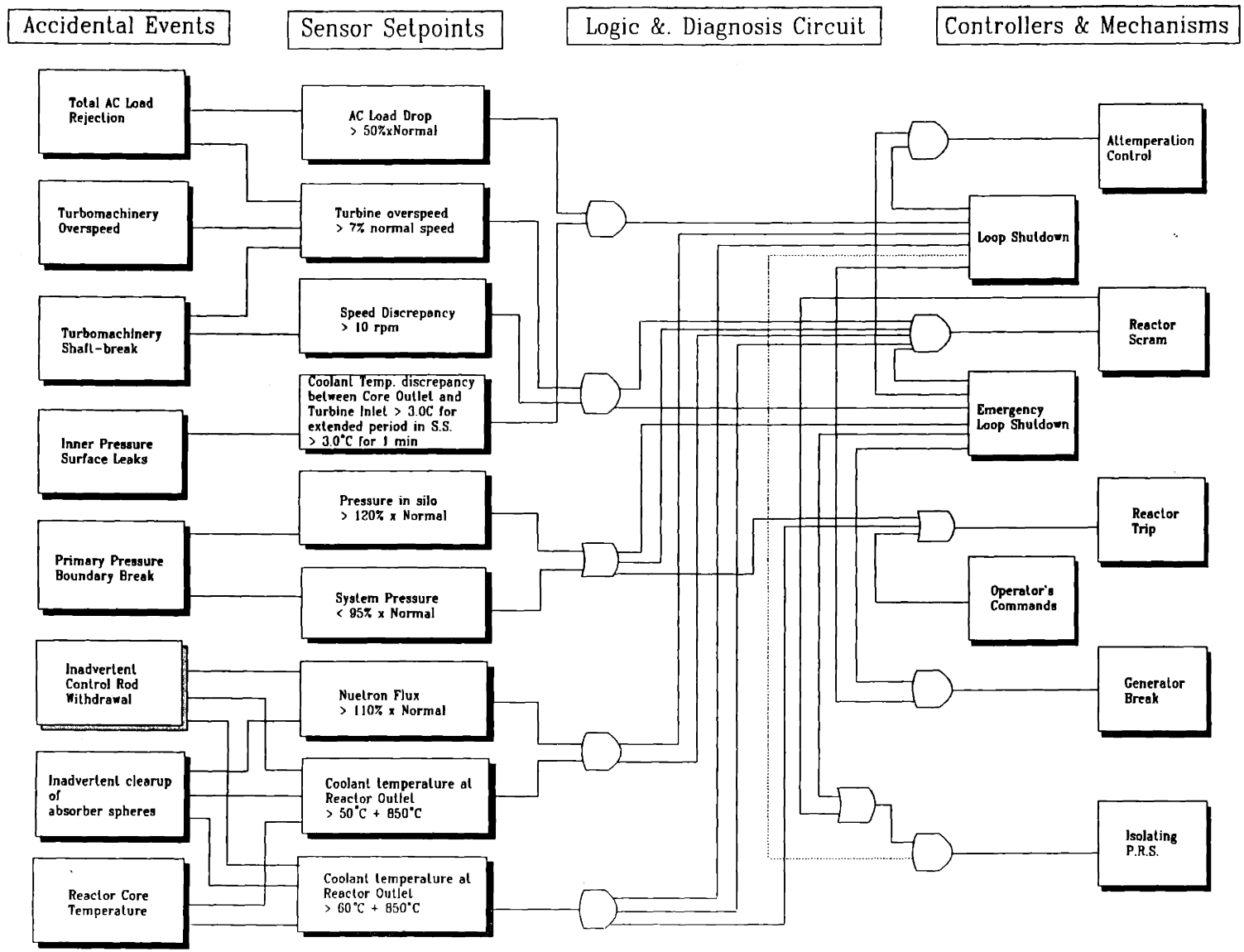

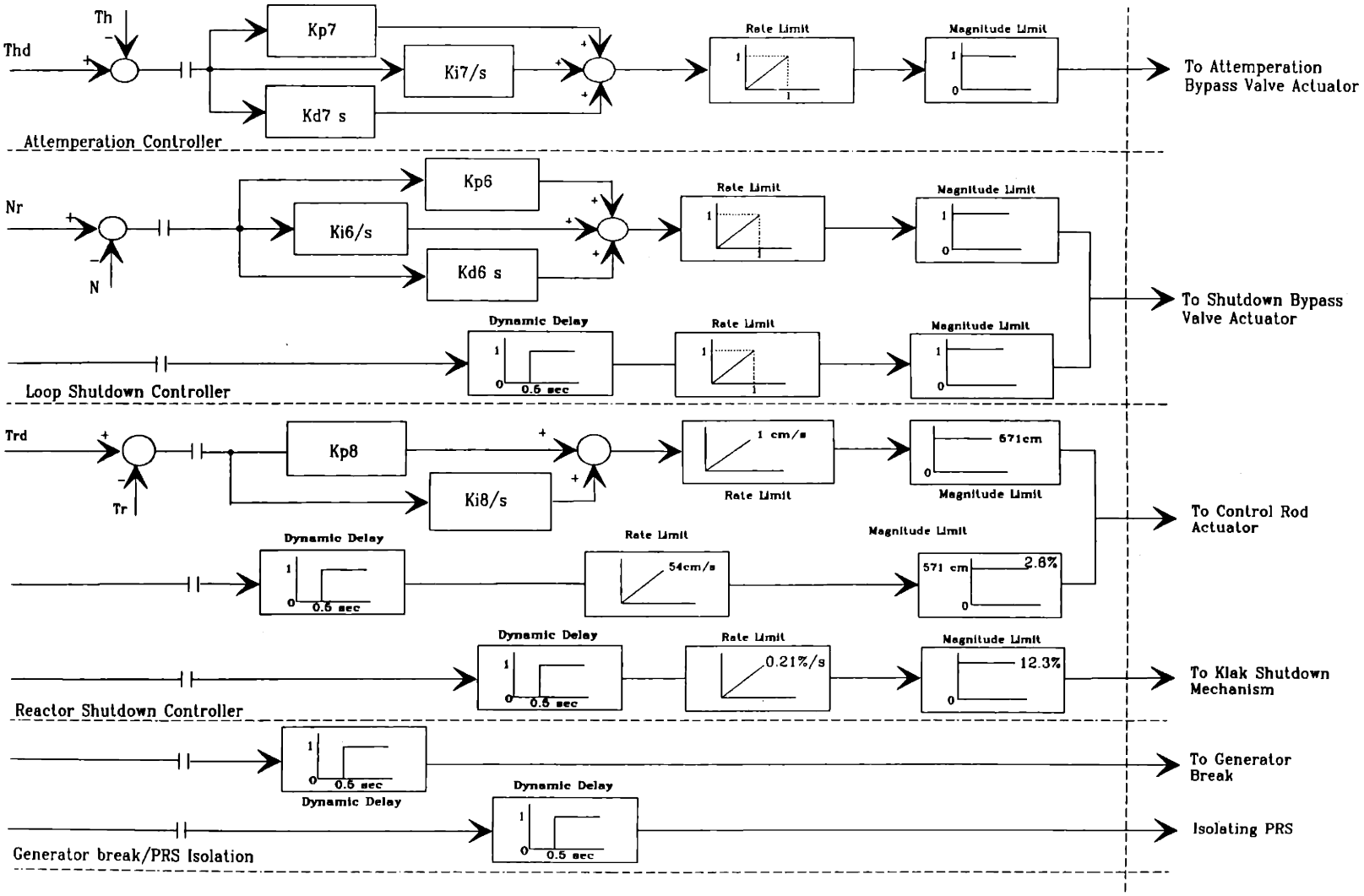

Figure 4.43 MGR-GT PPS Controllers

load rejection, and the other to shutdown the turbomachine completely to a stop as required in the event of turbomachine failure. For loop shutdown, the speed error between turbomachine speed, which is often at overspeed, and design speed is formed and fed into the loop shutdown controller. It will then pass a set of control gains with rate and magnitude limits. Proportional, derivative, and integral actions are used. Among them, the proportional action is essential to preventing the turbomachine from excess overspeed. With the aid of the derivative control effort, the turbomachine overspeed can be substantially minimized. The integral control, on the other hand, is necessary to bring the rotor speed back to the design speed from overspeed. In the second shutdown mode, i.e., emergency shutdown, the bypass valve is assumed to open 0.5 sec after receiving shutdown signals at a maximum rate 100%/sec until it is fully open. The 0.5 sec delay is set to reflect reaction time of control apparatus whereas the rate limit is a realistic model of the bypass valve.

The loop shutdown is always accompanied by the attemperation control to protect the plant components from thermal shock during critical flow bypass. Although the attemperation valve used for the PPS is the same as that used for the PRS, the PPS attemperation controller is functionally independent of that in the PRS. The combination of proportional, derivative, and integral gains with rate and magnitude limits is employed for the feedback loop. The proportional action with the support of derivative action enables the stable and quick suppressing of thermal overstresses while the integral control acts to maintain the temperature at nominal value.

For reactor protection, two control modes are offered by the PPS: active reactor power control and reactor scram. The active reactor power control is designated to accompany the idle loop shutdown. Control is approached by maintaining the reactor outlet temperature at normal value. Joint proportional and integral control feedback is employed. Since the reactor power is still actively controlled and the core outlet temperature is maintained at regular value,

no significant reactivity excursion is induced for this control operation. As a result, it would be possible to recover the full reactor power with the minimum movement of the control rods when the loop is to be run up from idle state. The reactor scram is used to setback reactor power in hot temperature condition. This is accomplished by dropping the six control rods, on gravity, into the channels located in the side reflector. The time delay, and rate and position limits are considered for this operation.

The reactor trip is used to provide long-term reactor shutdown. It is also used as a backup means to the reactor scram if it fails. To accomplish the reactor trip, the small absorber spheres are released and dropped, on gravity, from the scantier on the top of the core into the columns in the side reflector. Similarly, the time delay and limits are incorporated to reflect the reality of control actuation.

In addition, the generator circuit breaker will be initiated to protect the electrical system whenever the loop shutdown action occurs. To avoid the functional conflicts between the PPS and PRS, and to protect the PRS control components, the PRS will be isolated when the PPS is in action. The time delay is assumed to reflect the limited time lag for necessary electronic switching in these operations.

4.6 Implementation of Full Scale Code

The models of individual components and subsystems are combined in forming a full-scale system model. The implementation of the system model is based on the structural requirement of the solution algorithms. However, considerable efforts have been made in the development of the algorithms to simplify the procedure for the implementation of the full-scale system model. This results in a straightforward implementation procedure as described in the following.

4.6.1. Implementation of the system model

The full-scale system model is obtained by combining the equations representing the component models, based on the structure and discretization of the system. This results in a system of coupled, nonlinear ordinary differential equations governing the dynamic behavior of the system state variables. The MGR-GT system model consists of about 200 equations. Organizing the system of equations in the standard state-space form yields:

$$\frac{d\bar{y}}{dt} = F[\bar{y}, \bar{U}, t] \tag{4.132}$$

where $\bar{y}$ is the vector containing all the system state variables, $\bar{U}$ is the vector of state-feedback inputs, and t is the time as an independent variable.

The solution algorithms have been so implemented that only the following Jacobian Matrix of system (4.132) is required to be provided:

$$J[\bar{y}, \bar{U}, t] = \frac{\partial F}{\partial \bar{y}} = \begin{bmatrix} \frac{\partial f_1}{\partial y_1} & \frac{\partial f_1}{\partial y_2} & \cdots & \frac{\partial f_1}{\partial y_n} \\ \frac{\partial f_2}{\partial y_1} & \frac{\partial f_2}{\partial y_2} & \cdots & \frac{\partial f_2}{\partial y_n} \\ \vdots & \vdots & \cdots & \vdots \\ \frac{\partial f_n}{\partial y_1} & \frac{\partial f_n}{\partial y_2} & \cdots & \frac{\partial f_n}{\partial y_n} \end{bmatrix} \tag{4.133}$$

The characteristics of the system matrix (4.133) are asymmetric and sparse. Non-zero elements are mostly banded near the diagonal of the matrix with a few of them scattered outside the band. An optimal scheme of the system discretization could reduce the bandspace to minimize the computational efforts in matrix manipulation. A schematic description of the MGR-GT system matrix is shown in Figure 4.44.

Automatic loading of the system equations, state vector, and system matrix is incorporated in the code algorithms. However, information is required for the interpretation

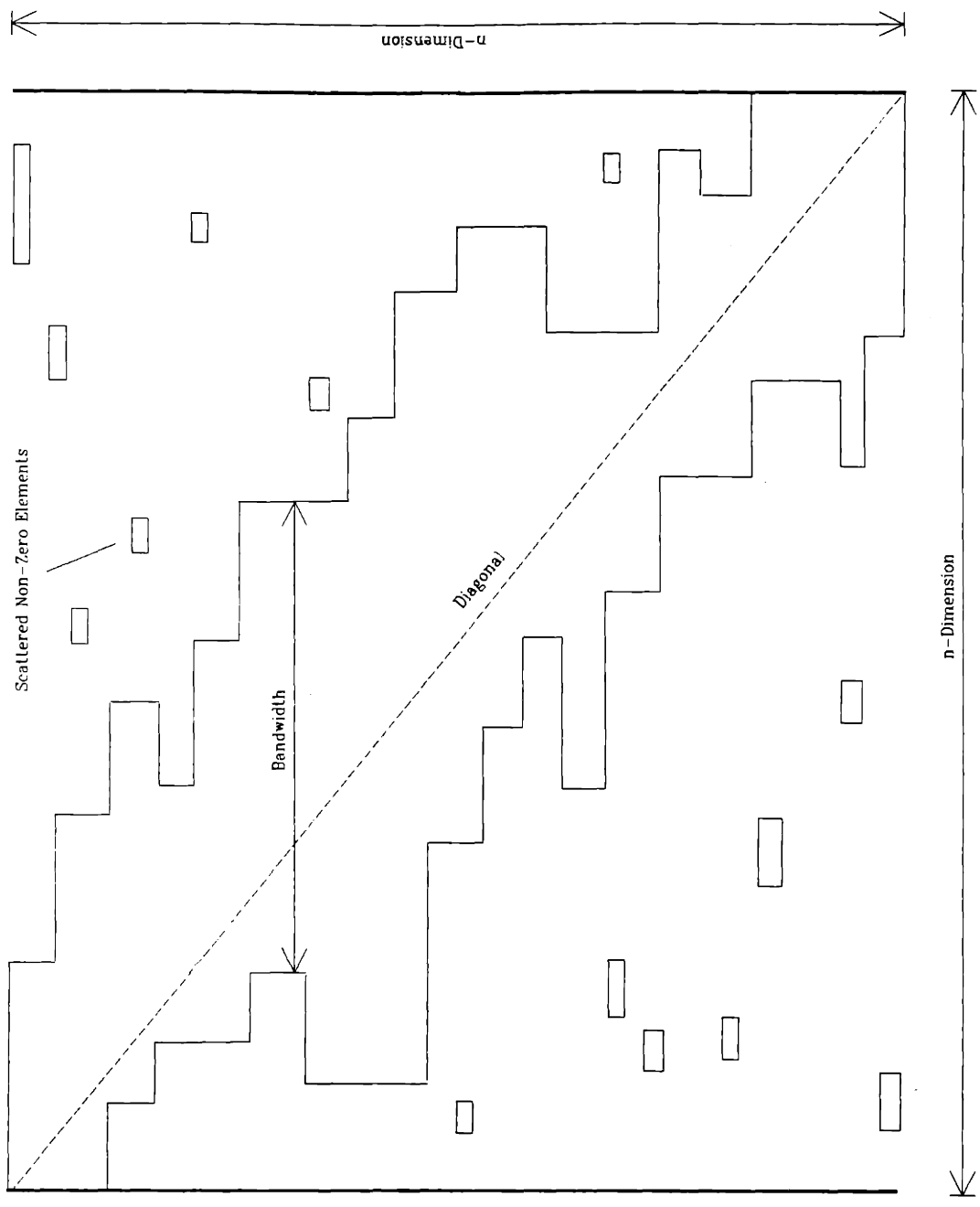

Figure 4.44 Schematic Description of the System Matrix Structure

of the system matrix structure to the algorithms, including the dimension of the system, band width for each row of the matrix, locations of non-zero elements outside the banded area along the matrix diagonal. This information is also used to instruct communications between the algorithms and system model.

The actual implementation of the MGR-GT system model is twofold: first, to construct two partial systems, and secondly, to combine them into the full-scale model. Two partial systems are the reactor and power conversion systems, respectively. The subsystem models are subjected to intensive verification procedures before combining them into the full-scale code. While detailed description of the code implementation and verification tests have been given in a separate report[Y1], the results of one of tests for the power conversion system model are shown in Figure 4.45.

In making the partial model for the power conversion system, a constant reactor outlet fuel temperature is assumed. But temperature changes due to flow compression or expansion in the core are considered with a simplified thermal hydraulic model for the reactor. The transient is initiated by the total load rejection from full power at t = 1 sec. The results in Figure 4.45 show the transient response of the power conversion system as the PPS acts to shutdown the loop to idle state. Four levels (a) - (c) of the plot show, from top to bottom, the turbomachine overspeed, control valve movement, temperature transients at various locations, and turbomachine powers.

As can be seen, the overspeed is controlled less than 5% of nominal speed and becomes zero at about t = 10 sec. In the aftermath, the turbomachine runs idle on bypass control. A shutdown bypass of 30 cm in diameter is installed for loop shutdown. As can be seen that only a maximum opening of 50% is actually used. The rest of shutdown capacity is reserved for speed protection in more dramatic events, such as turbomachine shaft break.

The loop shutdown causes rapid reduction in the turbine pressure ratio. As a

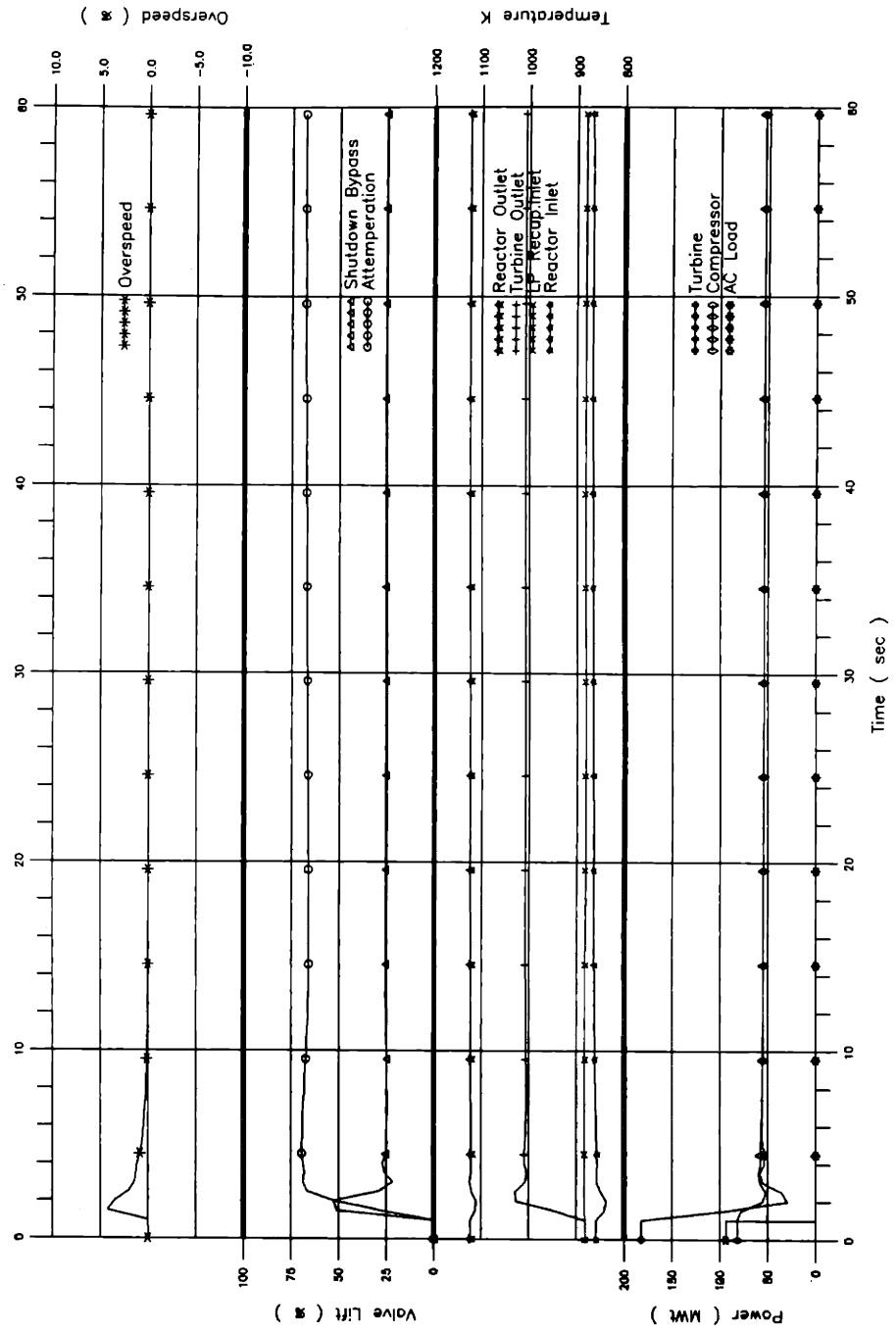

Figure 4.45 Shutdown process from full power to an idle state in case of the total AC load release

consequence, the temperature at the turbine outlet increases quickly. This is indicated on the third level of the plot. However, because of the thermal control action taken by the attemperation bypass valve, which is 14 cm in diameter, the temperature of the LP-recuperator inlet is kept virtually unchanged, even though the turbine outlet temperature has increased by about 100°C. The reactor inlet temperature is also controlled with only minor temperature fluctuations which are largely due to rapid flow expansion at the beginning of the loop shutdown. The control of the reactor inlet temperature is desirable since it would reduce the control effort made by the reactor control rods for the core reactivity control. The turbine and compressor powers as shown in the bottom level of the plot come to an equilibrium after initial transient period.

4.6.2 Convergence and Dynamic Simulation

Prior to any transient simulation, two stages of convergence are required for the establishment of initial conditions: one is steady convergence for generating hydraulic data based on the design specification, and the other is dynamic convergence obtaining initial conditions for specific transients to be simulated.

In general, pressure drops in the pipes and components specified in the design specification are not exactly the same as those predicted by GTSim, due to the different hydraulic models employed to estimate the pressure drops. To meet the design specification, equivalent hydraulic lengths must be obtained. This is performed by GTSim during the steady convergence. The steady convergence works only with the equations representing the system hydraulic models, while remaining the thermal and other conditions as the same as those given in the design specification.

Dynamic convergence is designed to obtain the initial conditions for specific transient events. For instance, if a transient simulation is to be started from a partial power level, the

initial steady-state conditions at that specific power level can be dynamically converged from the design or full power conditions. Hence, the name - dynamic convergence - changing initial conditions can be used as input during the transient simulation. The complete set of the system equations is loaded and used in the dynamic convergence. The convergence parameters are the temperatures at the turbine and compressor outlets, and turbomachine speed. The calculation of the dynamic convergence continues until these parameters have met the user-defined convergence criteria of accuracy.

The results from both stages of convergence are stored for use in the subsequent transient simulation. At the beginning of the transient simulation, the converged data will be automatically loaded into the program as initial conditions. When the MGR-GT design evolves, however, any change in design specification would require re-convergence of the initial conditions.

References

[A1] "An Assessment of the INTERATOM/KWU Modular HTGR Concept," Gas-Cooled Reactor Associates, September 1985.

[A2] Akin, S.W., Trans. ASME Vol 72, 751, 1950.

[B1] Burden, R.L., J.D. Faires, A.C. Reynolds:"Numerical Analysis," Prindle, Weber & Schmidt, Boston, 1981.

[B2] Breitbach, G., H. Barthels:"The Radiant Heat Transfer in the High Temperature Reactor Core After Failure of the Afterheat Removal Systems," Nuclear Technology, Vol. 49, August 1980.

[B3] Bammert, K., G. Krey:"Dynamic Behavior and Control of Single-Shaft Closed-Cycle Gas Turbines," Journal of Engineering for Power, October 1971.

[C1] Cleveland, J.C., S.R. Greene:"Application of THERMIX-KONVEK Code to Accident Analyses of Modular Pebble Bed High Temperature Reactors (HTRs)," NUREG/CR-4694, ORNL/TM-9905, Oak Ridge National Laboratory, August 1986.

[C2] Cohen, H., G.F.C. Rogers, H.I.H. Saravanamuttoo:"Gas Turbine Theory," Longman Scientific & Technical, England, 1987.

[D1] Duderstadt, J.J., L.J. Hamilton:"Nuclear Reactor Analysis," John Wiley & Sons, 1976.

[D2] Day, W.H. of United Technologies: private correspondence with L.M.Lidsky of MIT, April 1989.

[E1] Etherington, H. et. al.:"Nuclear Engineering Handbook," McGraw-Hill, New York, 1968.

[F1] Friedland, B.:"Control System Design - An Introduction to State-Space Methods," McGraw-Hill, New York, 1986.

[G1] "Gas Turbine HTGR - A Technology Assessment," NUS-3041, NUS Corporation, October 1977.

[G2] Glasstone S., A. Sesonske:"Nuclear Reactor Engineering," Van Nostrand Reinhold Company, New York, 1981.

[G3] Gear, W.C.:"Numerical Initial Value Problems in Ordinary Differential Equations," Prentice-Hall, Englewood Cliffs, NJ, 1971.

[G4] "The Thermodynamic and Transport Properties of Helium," GA-A13400, General Atomic Company, October 1975.

[G5] Greg, P., Gas-Cooled Reactor Associates, Private Correspondence, 1988.

[H1] Holman, J.P.:"Heat Transfer," McGraw-Hill, New York, 1981.

[I1] Izenson, M.:"Effects of Fuel Particle and Reactor Core Design on Modular HTGR Source Terms," MITNPI-TR-012, MIT, October 1986.

[K1] Kays, W.M., A.L. London:"Compact Heat Exchangers," McGraw-Hill, New York, 1984.

[K2] Kailath, T.:"Linear Systems," Prentice-Hall, Inc., Englewood Cliffs, N.J., 1980.

[K3] Kaps,P., P. Rentrop, Numer. Math. 33, 55, 1979.

[M1] Massimo, L.:"Physics of High-Temperature Reactors," Pergamon Press, Oxford, 1976.

[M2] Meyer, J.E.:"Hydrodynamic Models for the Treatment of Reactor Thermal Transients," Nuclear Science and Engineering, Vol 10. 1961.

[M3] McDonald, C.F., M.J. Smith:"Turbomachinery Design Considerations for the Nuclear HTGR-GT Power Plant," ASME 80-GT-80

[M4] McDonald, C.F.of General Atomics: private correspondence with L.M. Lidsky of MIT, January 1990.

[M5] McDonald, C.F.of General Atomics: private correspondence with L.M. Lidsky of MIT, April 1989.

[N1] Nightingale, R.E. ed.:"Nuclear Graphite," Academic Press, New York, 1962.

[P1] Press, W.H., S.A. Teukolsky:"Integration Stiff Ordinary Differential Equations," Computers in Physics, May/June 1989.

[R1] "REALY2: The GT-HTGR Transient Performance Analysis Program," GA-A13880, General Atomics, March 1976.

[R2] Reutler, H., G.H. Lohnert:"Advantages of Going Modular in HTRs," Nuclear Engineering and Design, Vol 78, 1984.

[S1] Saphier, D.:"Transient Analysis of the Pebble-Bed HTGR with the DSNP Simulation Language," RASG-107-84, Soreq Nuclear Research Centre, Israel, April 1984.

[S2] Saphier, D.:"DSNP Models Used in the Pebble-Bed HTGR Dynamic Simulation," RASG-108-84, Soreq Nuclear Research Centre, Israel, April 1984.

[S3] Saphier, D.:"HTGR Transient Analysis with the DSNP Simulation Language," RASG-111-84, Soreq Nuclear Research Centre, Israel, December 1984.

[S4] Staudt, J.E., L.M. Lidsky:"Design Study of an MGR Direct Brayton-Cycle Power Plant," MITPI-TR-018, MIT, May 1987.

[S5] "Wärmeübergang im Kugelhaufen," KTA 3102.1 KTA, June 1978.

[S6] Savage, M.G."A One-Dimensional Modeling of Radial Heat Removal Dyring Depressurized Heatup Transients in Modular Pebble-Bed and Prismatic High Temperature Gas-Cooled Reactors," ORNL/TM-9215, Oak Ridge National Laboratory, July 1984.

[T1] Tanaka, H. of Toshiba Corporation: MGR-GT Generator Feasibility Study, private correspondence, March 1987.

[T2] "Super Motor Drive System - Super High Speed Motor and Load Commutated Inverter," Toshiba Corporation, Houston, Texas.

[V1] Van Tuyle, G.J., T.C. Nepsee, J.G. Guppy:"MINET Code Documentation," BNL-NUREG-51742, Brookhaven National Laboratory, New York, February 1984.

[W1] Wilson, David Gordon:"The Design of High-Efficiency Turbomachinery and Gas Turbines," The MIT Press, Cambridge, 1984.

[W2] Way, K., E.P. Wigner: Phys. Rev. 70, 1318, 1948.

[Y1] Yan, X.L., L.M. Lidsky:"Control System Design and Dynamic Study of the MGR-GT Power Plant - *Progress Report I, II, II, and IV*," MIT, December 1989.

Chapter Five

Transient Analysis for the MGR-GT

5.1 Introduction

A number of transients have been simulated with GTSim to analyze the dynamic and control characteristics of the MGR-GT. The transient events simulated are those listed in Table 4.1. These events are categorized into four groups, i.e. operational events, operational accidents, design basis accidents, and beyond design basis accidents. The simulations for the operational events and accidents were carried out to evaluate the control system design based on the operational requirements for nuclear gas turbine power plants, whereas the design and beyond design basis accidents were simulated to demonstrate the inherent plant safety features and protection capability. The results of the simulations are presented in the following.

5.2 Evaluation of the Control System Design

The MGR-GT control system consists of the Plant Regulation System (PRS) and Plant Protection System (PPS). The PRS has been designed to automate the plant operation to match electric load changes and to control the procedures for plant startup and shutdown. The automated operation requires regulating reactor power, controlling turbomachinery power and speed, maintaining the temperature of the helium exiting the reactor outlet at constant temperature, and preventing thermal overstress imposed on the plant components. These control functions are accomplished with the simultaneous and interactive control actions by the reactor control system, bypass control system, and inventory control system.

The PPS has been developed to handle a set of anticipated accidents. It provides

both loop and reactor shutdowns to prevent the turbomachine from overspeed and to setback the reactor power in case of accidents. Depending on the nature of accidents, the PPS provides two plant shutdown modes, *i.e.*, idle and permanent shutdowns. The idle state allows the quick recovery of normal operation. The PPS is integrated with the bypass shutdown system and reactor reactivity shutdown system.

5.2.1 Evaluation of the Plant Regulation System

The PRS enables stand-alone, automated operation for the MGR-GT. Simulations have been performed to evaluate the controllability and responsiveness of a plant using the current PRS design. The transients simulated include ramp load changes at the rates of ±3%/min and ±5%/min in the range of 100% to 70% of nominal load, ±10% step load changes from 100% to 90%, and plant startup and shutdown. The results of these simulations are presented in the following.

5.2.1a Load and Speed Control

The automatic load following characteristics and plant operability are evaluated by simulating the plant transient response to the ramp electric load changes at the rate of ±3%/min. The plant is controlled by the bypass control system, inventory control system, and reactor control system. The inventory valves are each configured to be 14 cm in diameter, while the bypass valve is rated to be 10 cm in diameter. The results of this simulation are shown in Figures 5.1 (a) to (f).

The steady-state, full power operation is disturbed with the electric load reduction starting at t = 0. The electric load is reduced at -3%/min until t = 10 min when it has reached 70% of the nominal level. The recovery of the electric load from 70% to 100% starts at t = 11 min. Figure 5.1 (a) shows the turbomachine power and speed transient responses, along

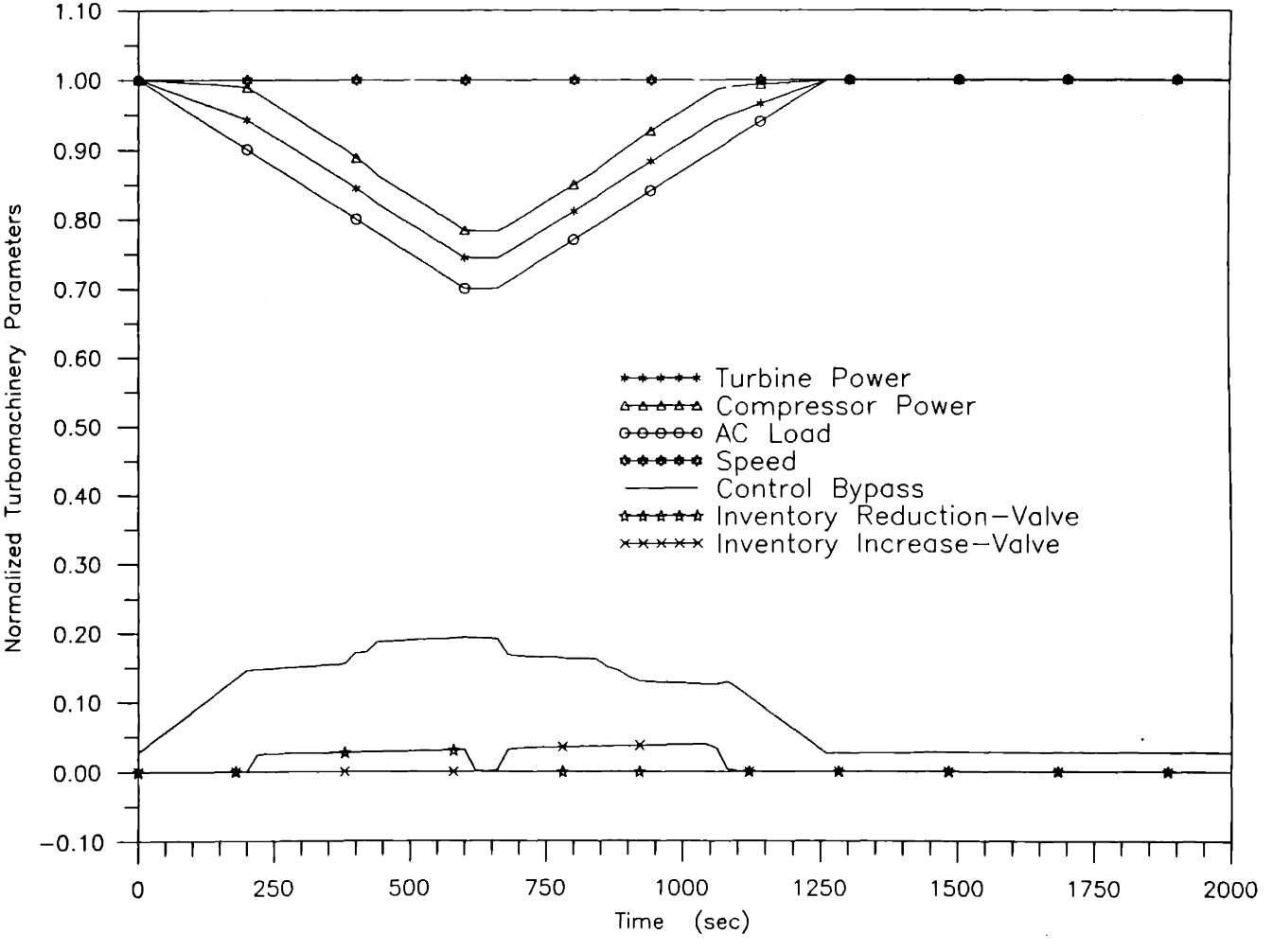

Figure 5.1 (a) Turbomachine parameters in control process for ±3%/min AC load changes

with the control adjustment of the bypass and inventory valves. For the first 10% load reduction, the bypass valve acts alone to control the turbomachinery power to maintain the speed, while the inventory valve remains closed. The flow bypass drops the pressure head of the turbine, resulting in the reduction of the turbine power. The rate of the turbine power decrease is less than that of the load reduction, which implies a decreasing cycle efficiency associated with the bypass control.

As the load drops below 90% of the nominal level, the inventory valve is opened to withdraw the helium from the plant circuit into the inventory vessel. As can be seen, both the turbine and compressor powers decrease at approximately the same rate as that of the load reduction, demonstrating a constant cycle efficiency with the inventory control.

When the load is raised again at t = 11 min, the bypass valve responds rapidly to control the turbomachine speed while the inventory valve opens to allow the helium to flow from the inventory vessel into the plant circuit in order to raise the plant power. The turbomachine powers show symmetric responses to those during the load reduction, with the inventory valve being closed at 90% of the nominal load and the bypass valve returning to the initial position at full load. The bypass valve remains partially open at full power, offering the capability to stabilize the turbomachine operation in case of minor transient disturbance. The bypass flow at full power is about 1.8 kg/s.

The simultaneous control process for the reactor power in the course of the ramp load change is shown in Figure 5.1 (b). The reactor control rods change the core reactivity to control the reactor power, as well as to compensate for the temperature reactivity feedback and the limited reactivity change due to the change of fission product concentrations associated with the power variation. As shown in Figure 5.1 (b), the reactor thermal power decreases at a rate less than that of the load reduction in the power range of 100% to 90% within which the bypass control is used, indicating the reduction of the cycle thermal

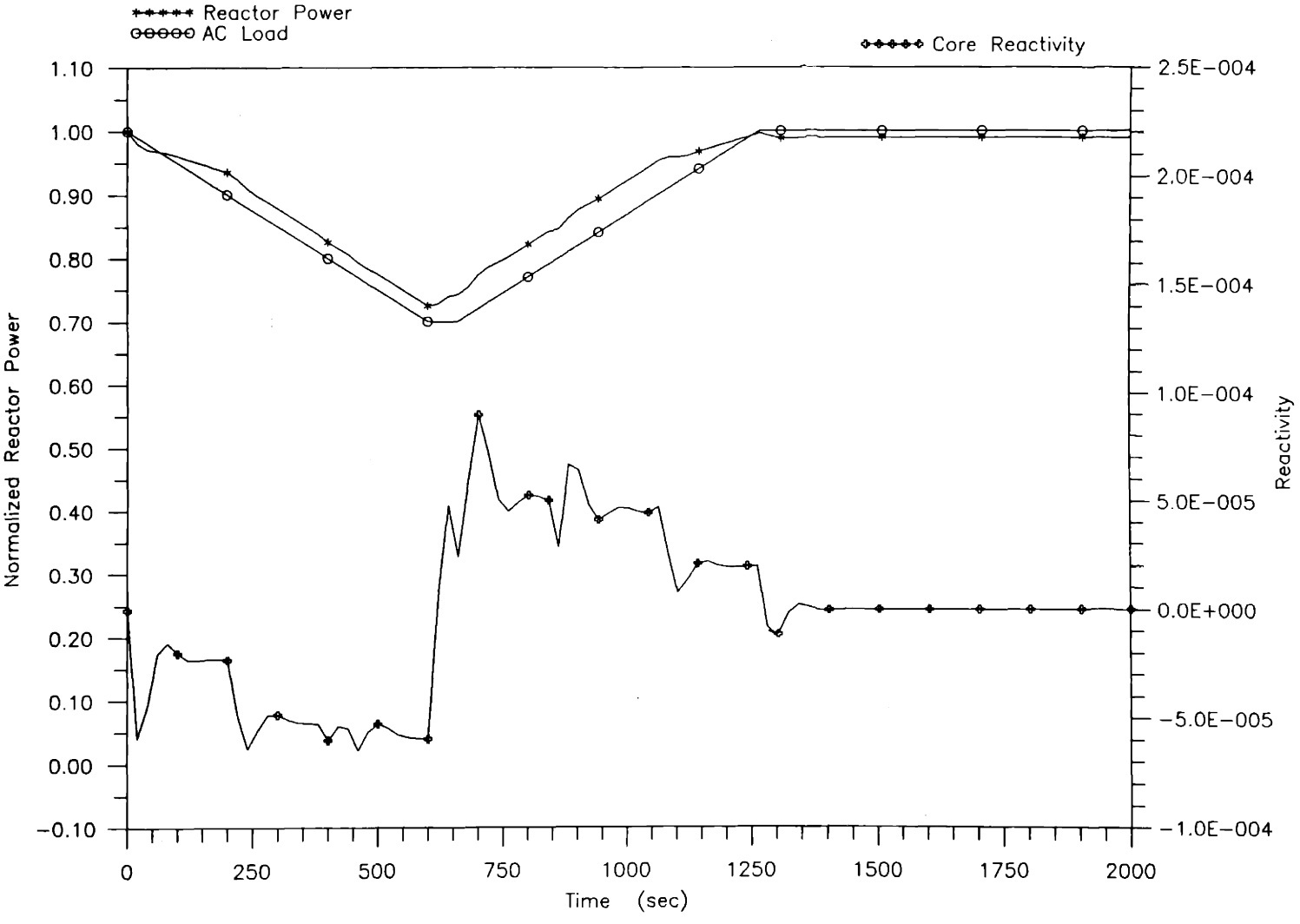

Figure 5.1 (b) Reactor power control during ±3%/min AC load changes

efficiency due to the use of the bypass control. However, the reactor power demonstrates the same rate of changes as that of the load changes in the load range below 90% when the inventory control is used, offering a constant thermal efficiency for the plant operation. As the load is raised to the normal level, the total reactivity in the core becomes zero, maintaining the reactor critical at the full power condition.

The pressure transient responses at the turbomachinery inlets and outlets are shown in Figure 5.1 (c). At the beginning of the load reduction, the heads of the turbine and compressor are reduced because of the bypass control. When the plant power is regulated by the inventory control, the pressures at both the inlets and outlets change in the same direction, so that the cycle pressure ratio is kept constant, allowing the turbomachinery to operate at its optimum conditions.

Figure 5.1 (d) shows the temperature responses during the load changes. As can be seen, the reactor outlet temperature, thus the inlet temperature of the turbine, is controlled at constant temperature throughout the entire transient period. Since the inventory control is the primary control means, the cycle pressure ratio varies little. As a result, temperature changes are relatively minor. The attemperation control is thus not necessary for the load control with the inventory control. Figure 5.1 (f) shows the transient responses of the radial temperatures in the core mid plane. As can be seen, although the reactor power has been changed considerably, the temperatures remain virtually unchanged because of the constant temperature control at the reactor outlet. Such stable thermal condition in the core minimizes the need for reactivity manipulation by the control rods.

Figure 5.1 (e) shows the flow transient responses at various cycle locations. During the initial period of the load reduction during which the bypass control is used, the turbine flow decreases as a result of the reduction of the cycle pressure ratio, while the compressor flow increases. After the inventory control is initiated, both the turbine and compressor mass

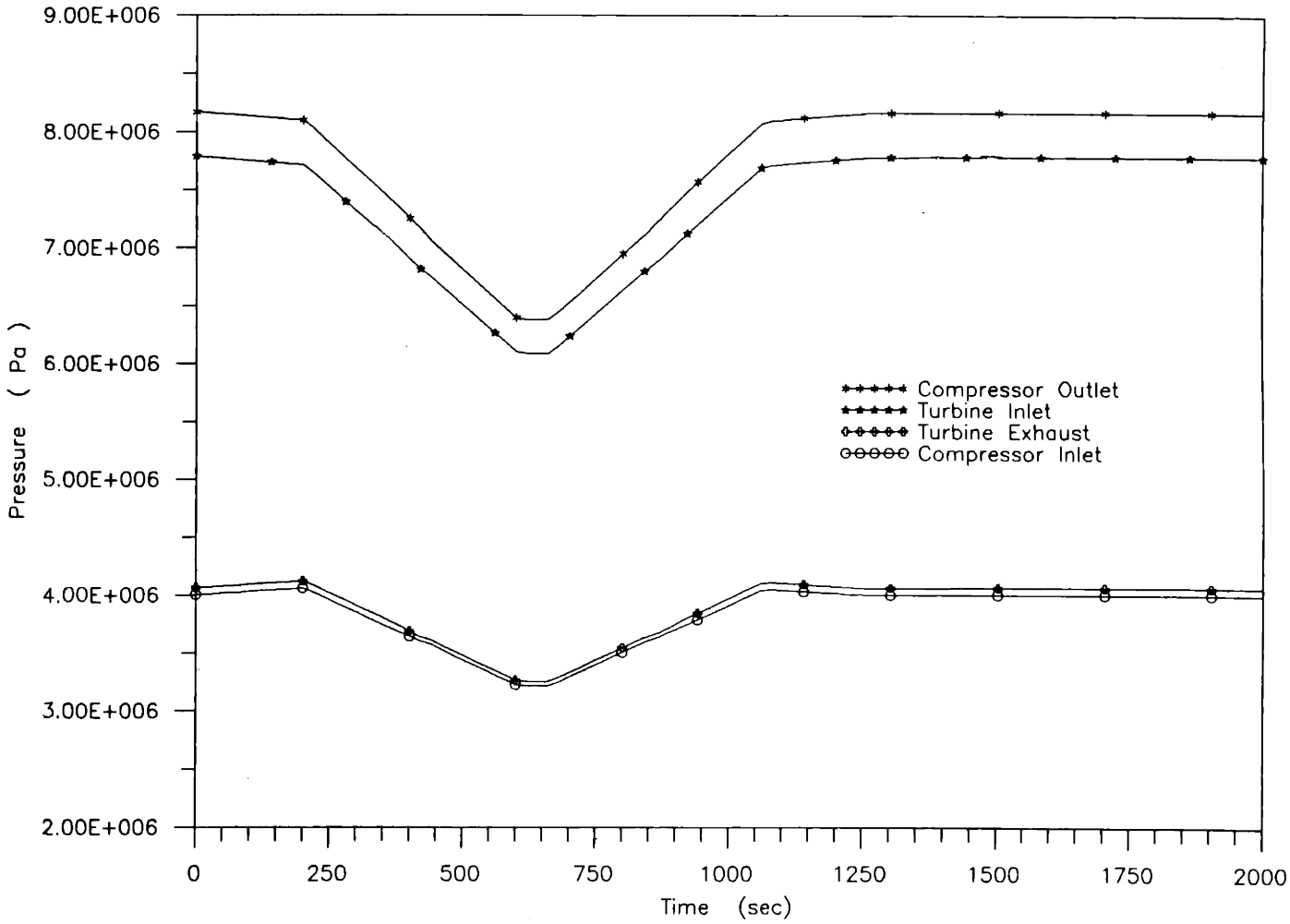

Figure 5.1 (c) Pressure transient responses to ±3/min AC load changes

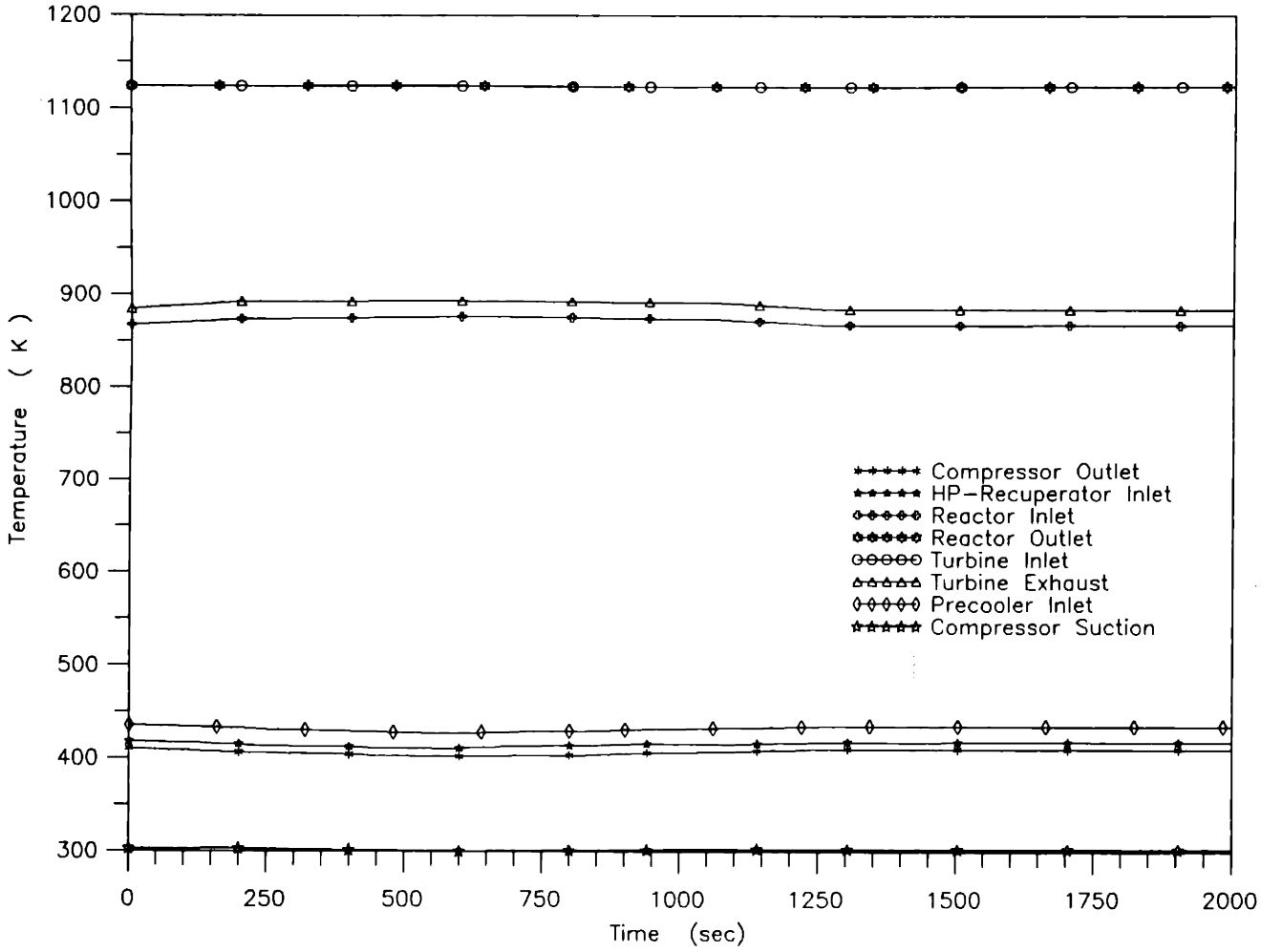

Figure 5.1 (d) Temperature transient responses to ±3/min AC load changes

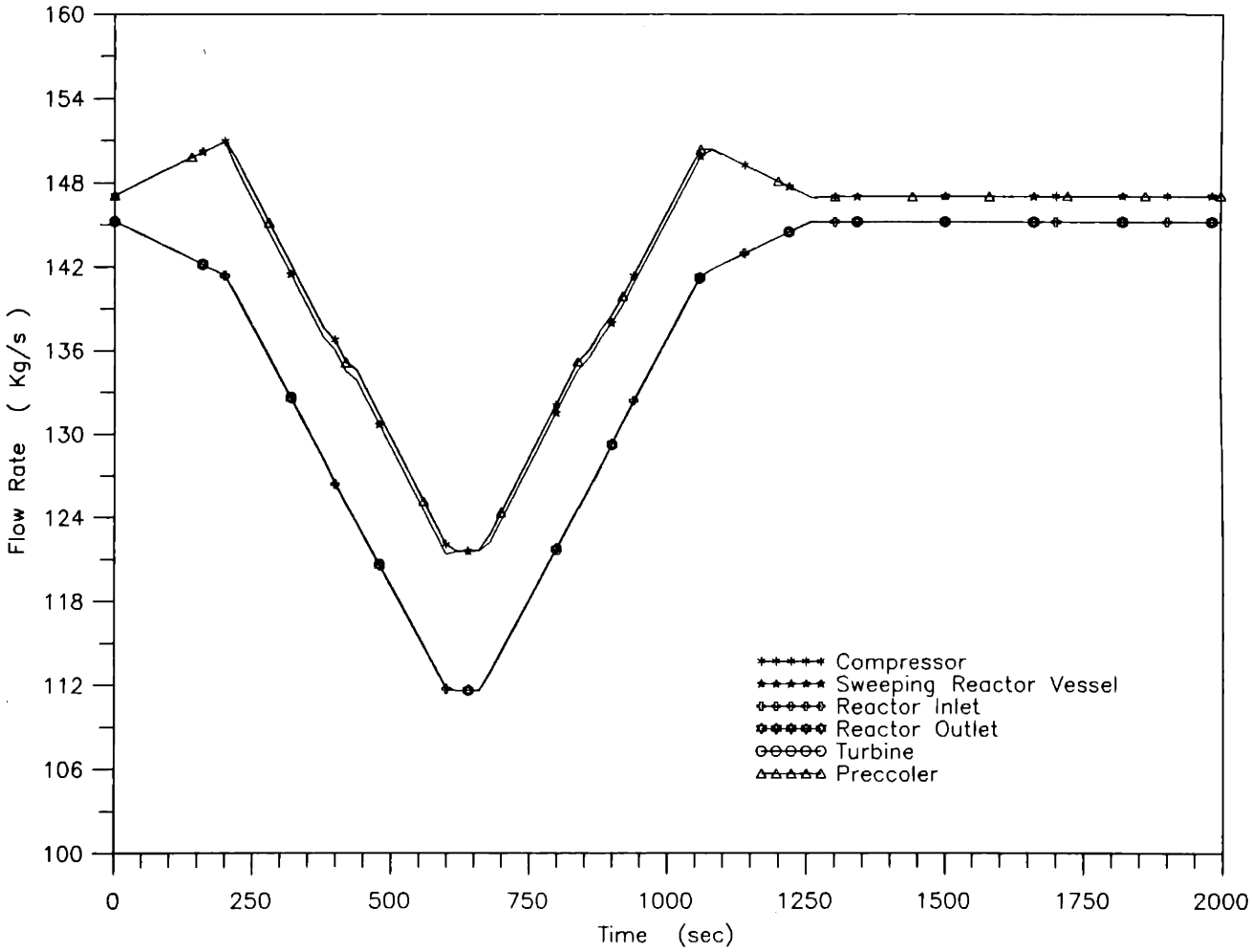

Figure 5.1 (e) Flow transient responses to ±3/min AC load changes

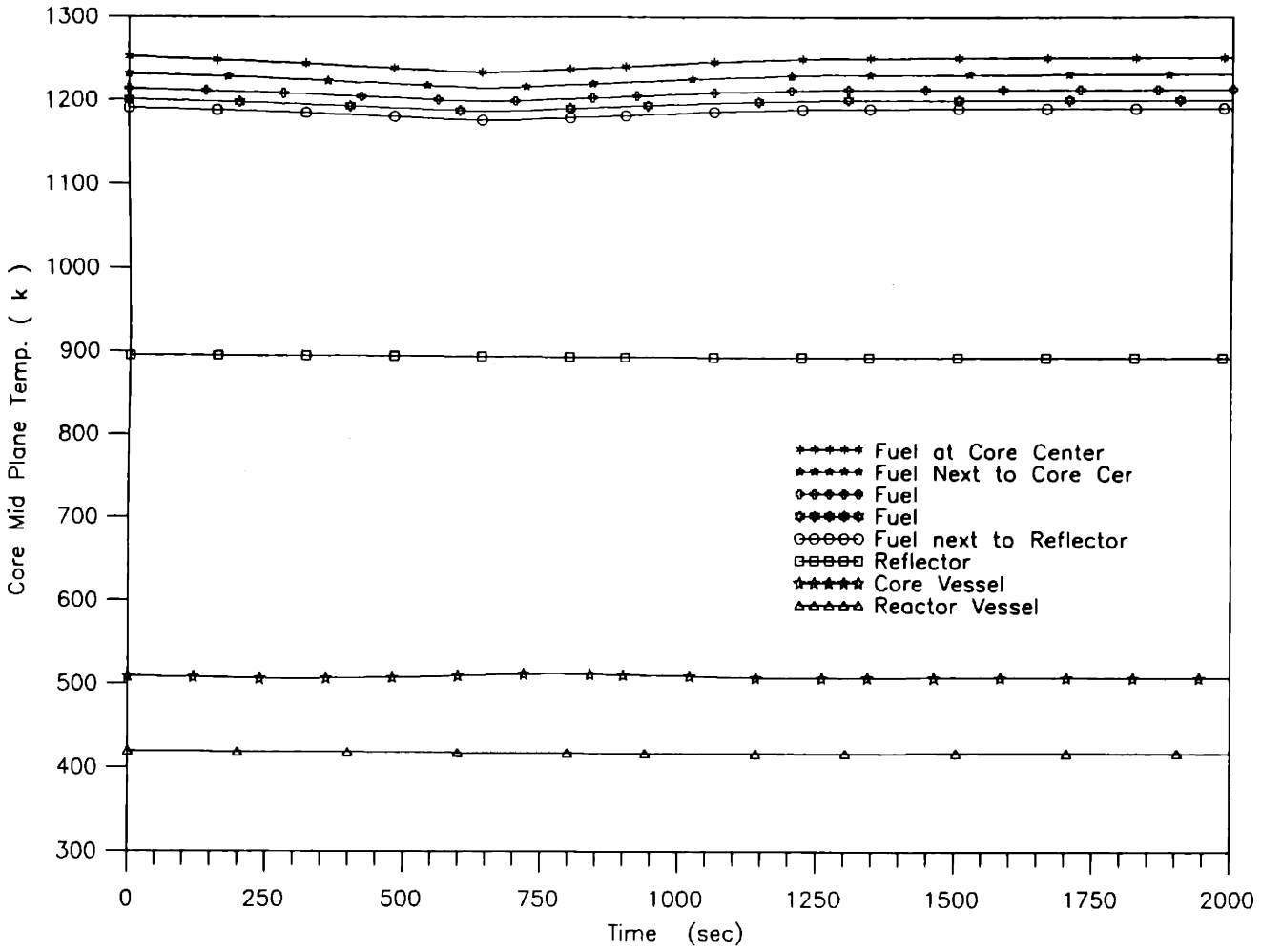

Figure 5.1 (f) Radial temperature transient responses in the core mid plane to ±3/min AC load changes

flow rates are reduced at approximately the same rate due to the helium inventory reduction in the circuit. During the period of the load increase, symmetric flow responses are indicated.

In sum, the plant demonstrates satisfied load following capabilities for the ±3%/min ramp load changes. The plant operation also requires following the ramp load changes up to ±5%/min as well as ±10% step load changes. Figures 5.2 (a) to (f) and Figures 5.3 (a) to (g) outline the results of the simulations for these two control operations.

5.2.1b Shutdown and Startup

This simulation is intended to evaluate the programmed procedures developed for normal plant shutdown and startup. The shutdown proceeds in the following steps:

(1) disconnect the electric load at 10%/min.

(2) operate the plant to achieve steady-state, idle condition.

(3) reduce the turbomachine speed from 10,000 rpm to 3,600 rpm.

(4) operate the plant at 3,600 rpm to establish the low speed operation condition.

The plant startup from the low-speed steady state condition is pursued in a reversed order of the above shutdown steps.

Figures 5.4 (a) to (g) show the control process for the normal shutdown followed by the subsequent startup of the plant. In Figure 5.4 (a), it can be seen that the AC load is gradually disconnected, the bypass valve, which is installed for plant startup and shutdown operation with the size of 28 cm in diameter, opens to reduce the turbine and compressor powers following the AC load reduction. The turbomachine remains running at regular speed. After the electric load is completely disconnected, the plant is further allowed to operate for 5 minutes in order to establish the steady-state, idle condition.

At t = 15 min, the speed reduction command signal is issued. The turbomachine speed is to be reduced at 1000 rpm/min from 10,000 rpm to 8,000 rpm, and 250 rpm/min

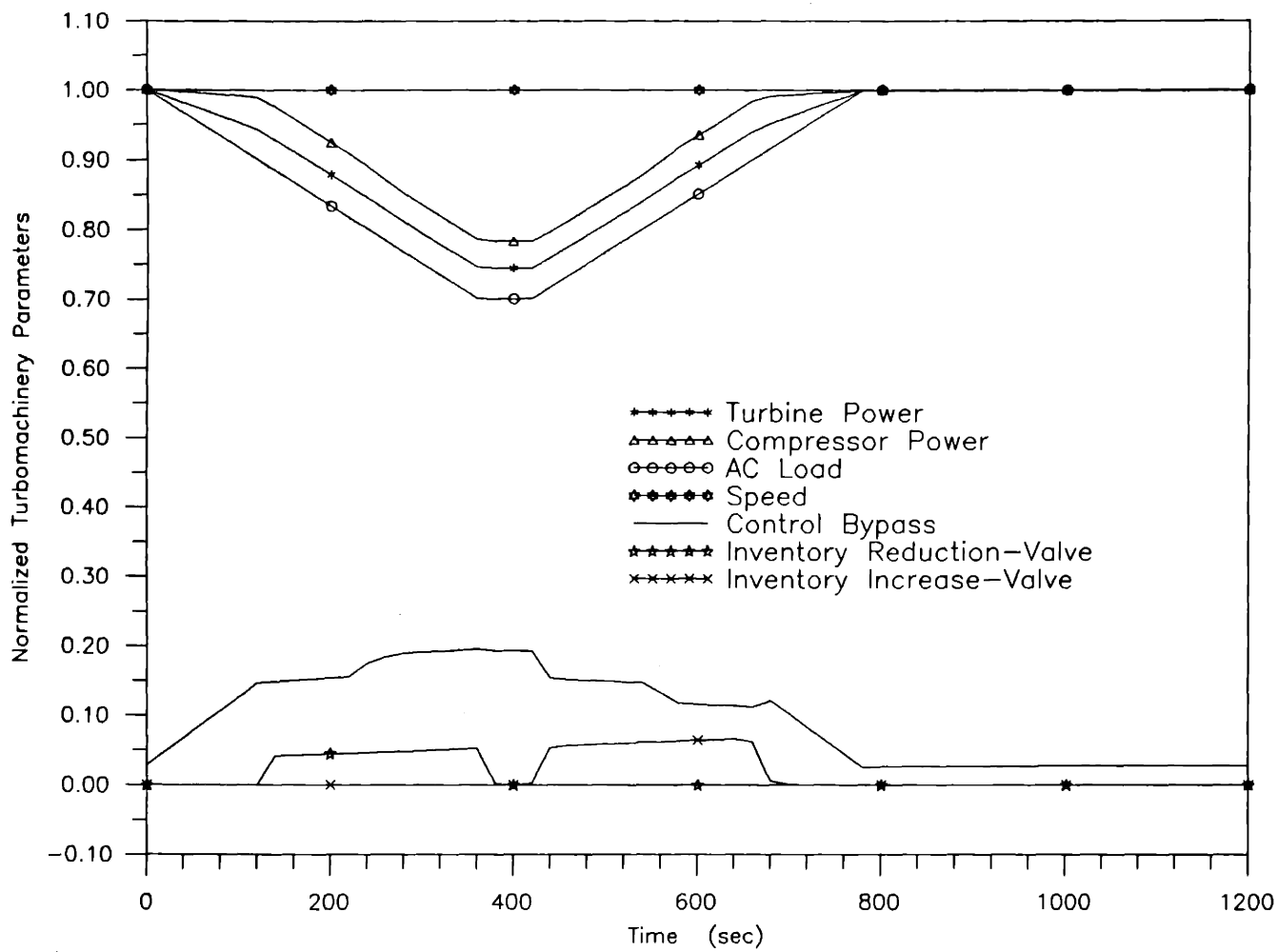

Figure 5.2 (a) Turbomachine parameters in control process for ±5%/min AC load changes

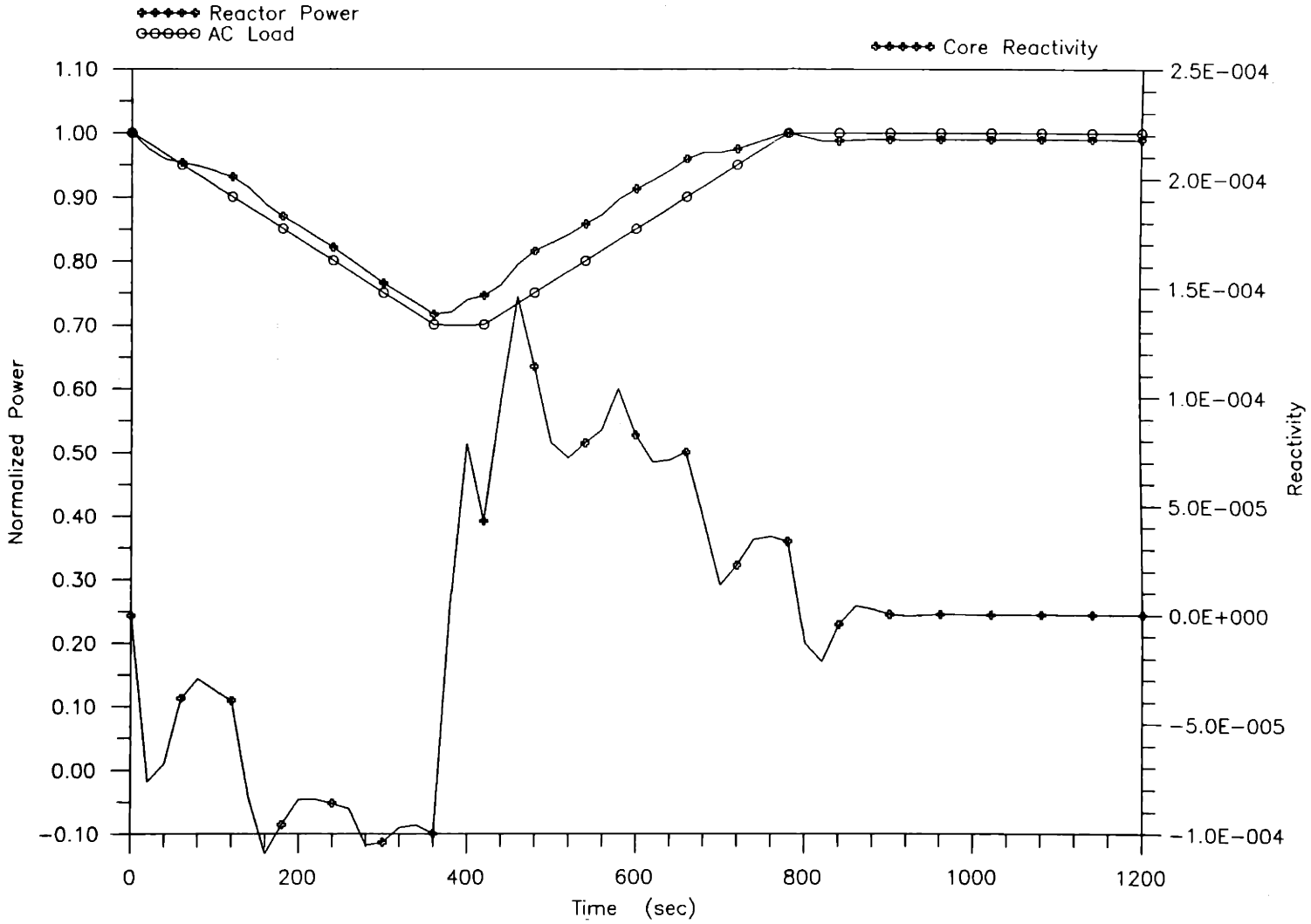

Figure 5.2 (b) Reactor power control during ±5%/min AC load changes

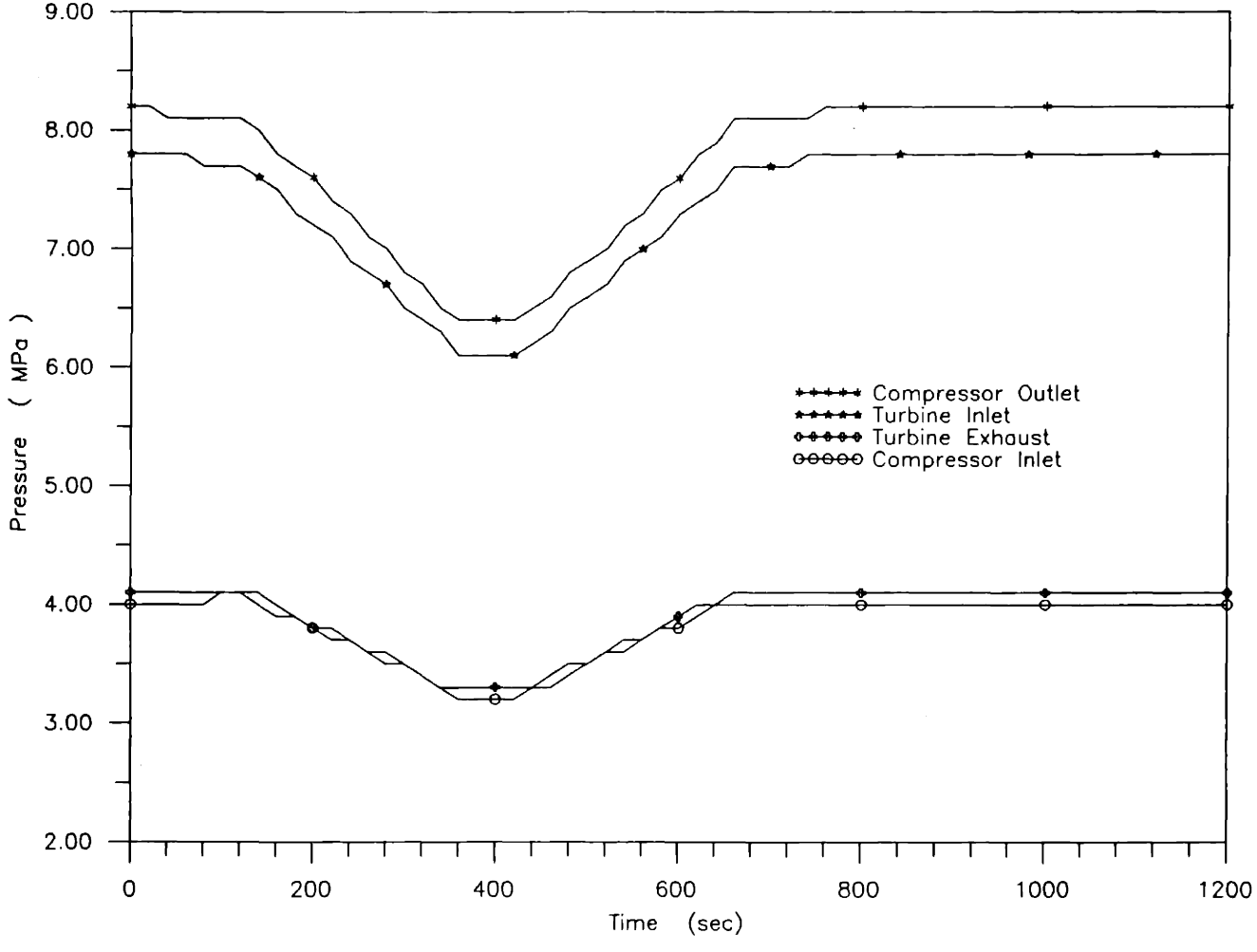

Figure 5.2 (c) Pressure transient responses to ±5/min AC load changes

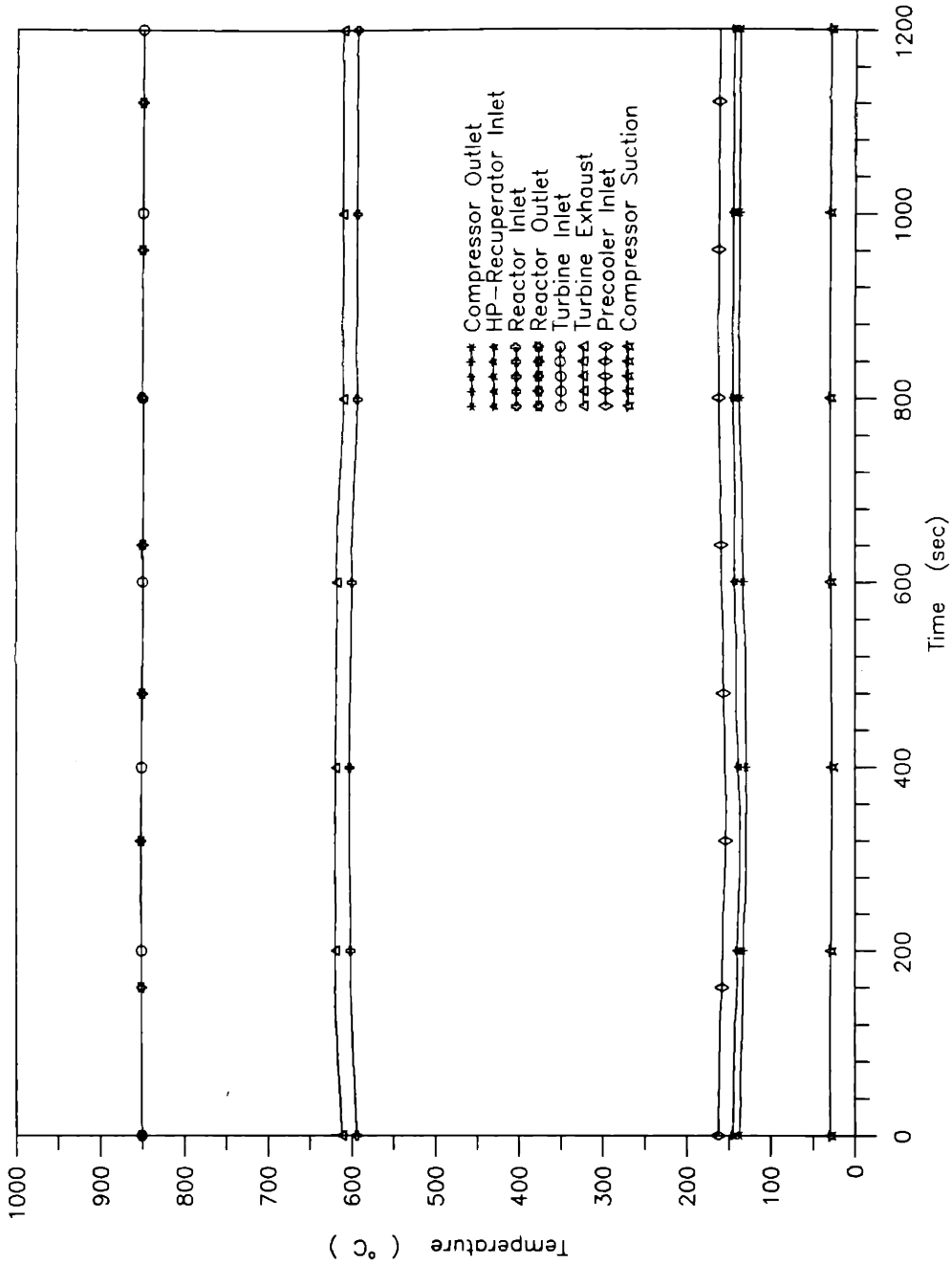

Figure 5.2 (d) Temperature transient responses to ±5/min AC load changes

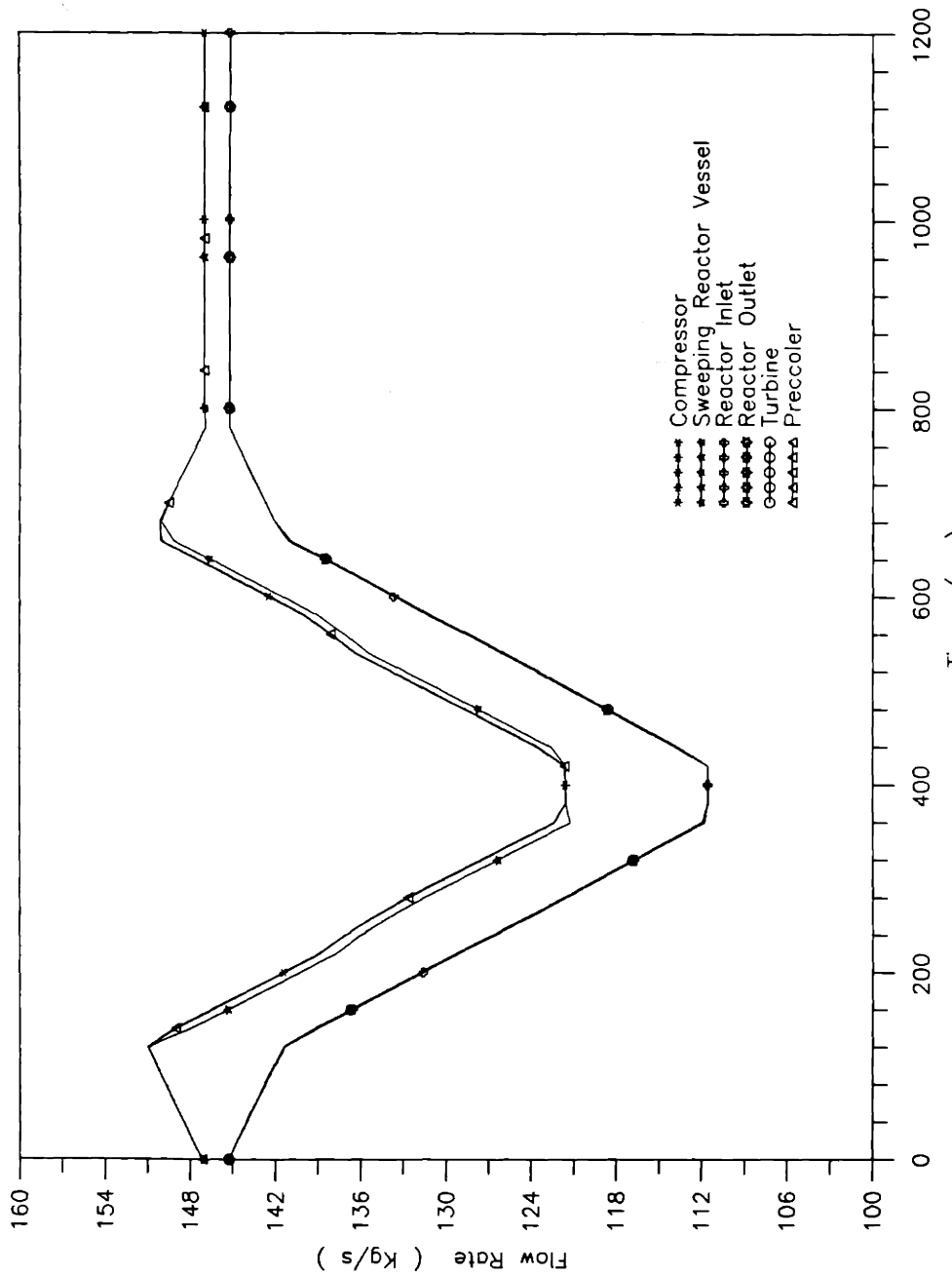

Figure 5.2 (e) Flow transient responses to ±5/min AC load changes

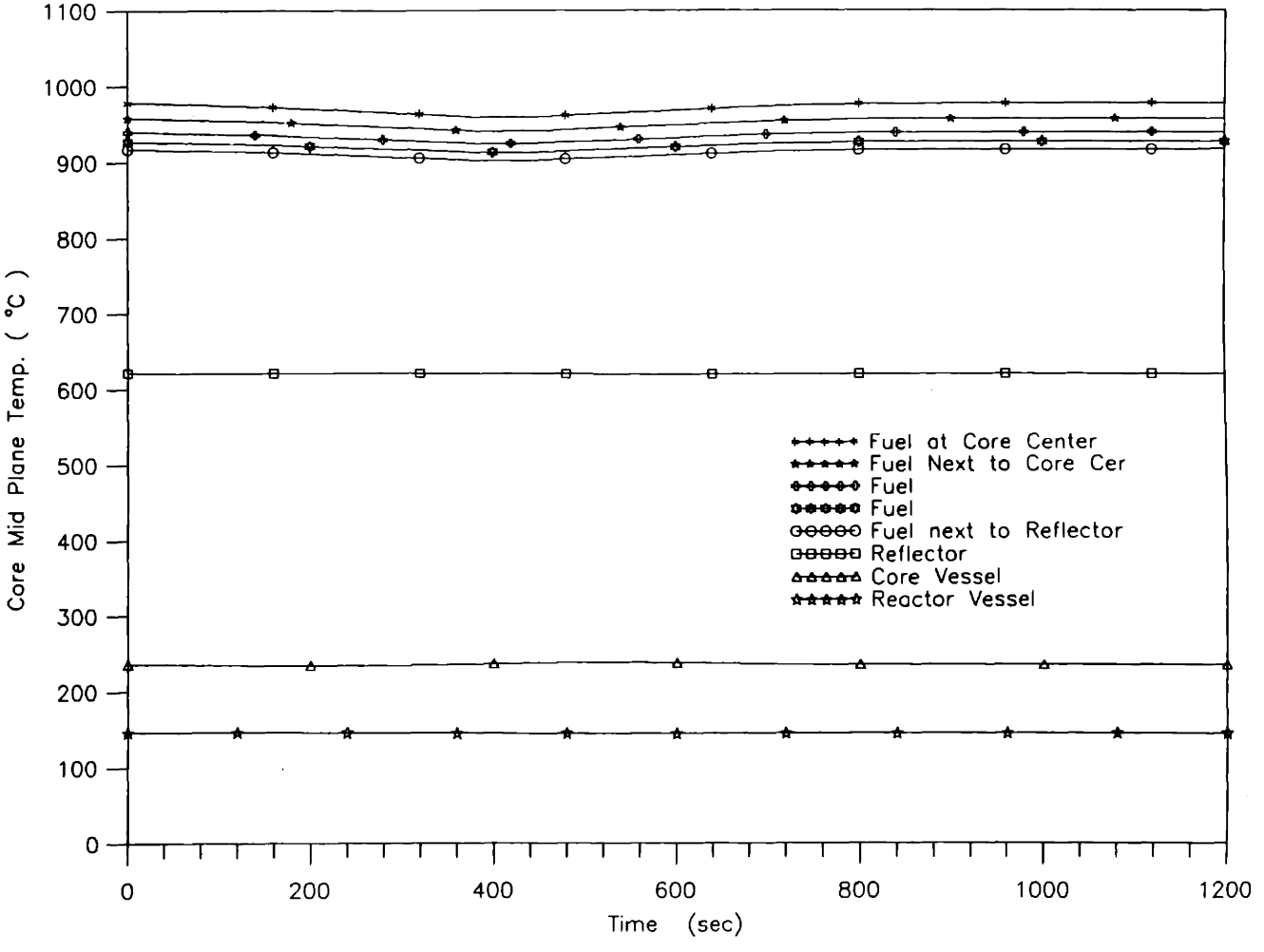

Figure 5.2 (f) Radial temperature transient responses in the core mid plane to ±5/min AC load changes

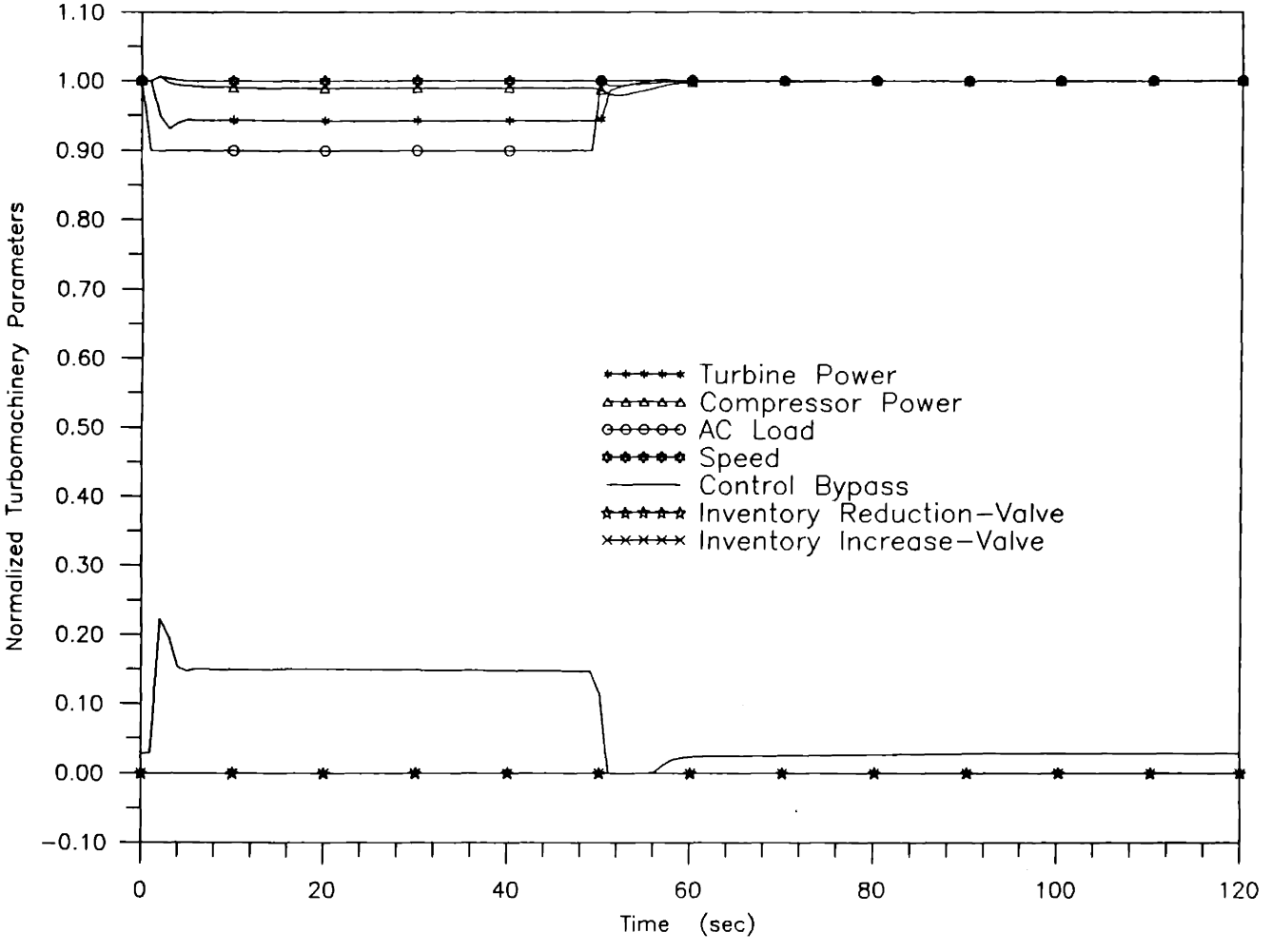

Figure 5.3 (a) Turbomachine parameters in control process for ±10 step AC load changes

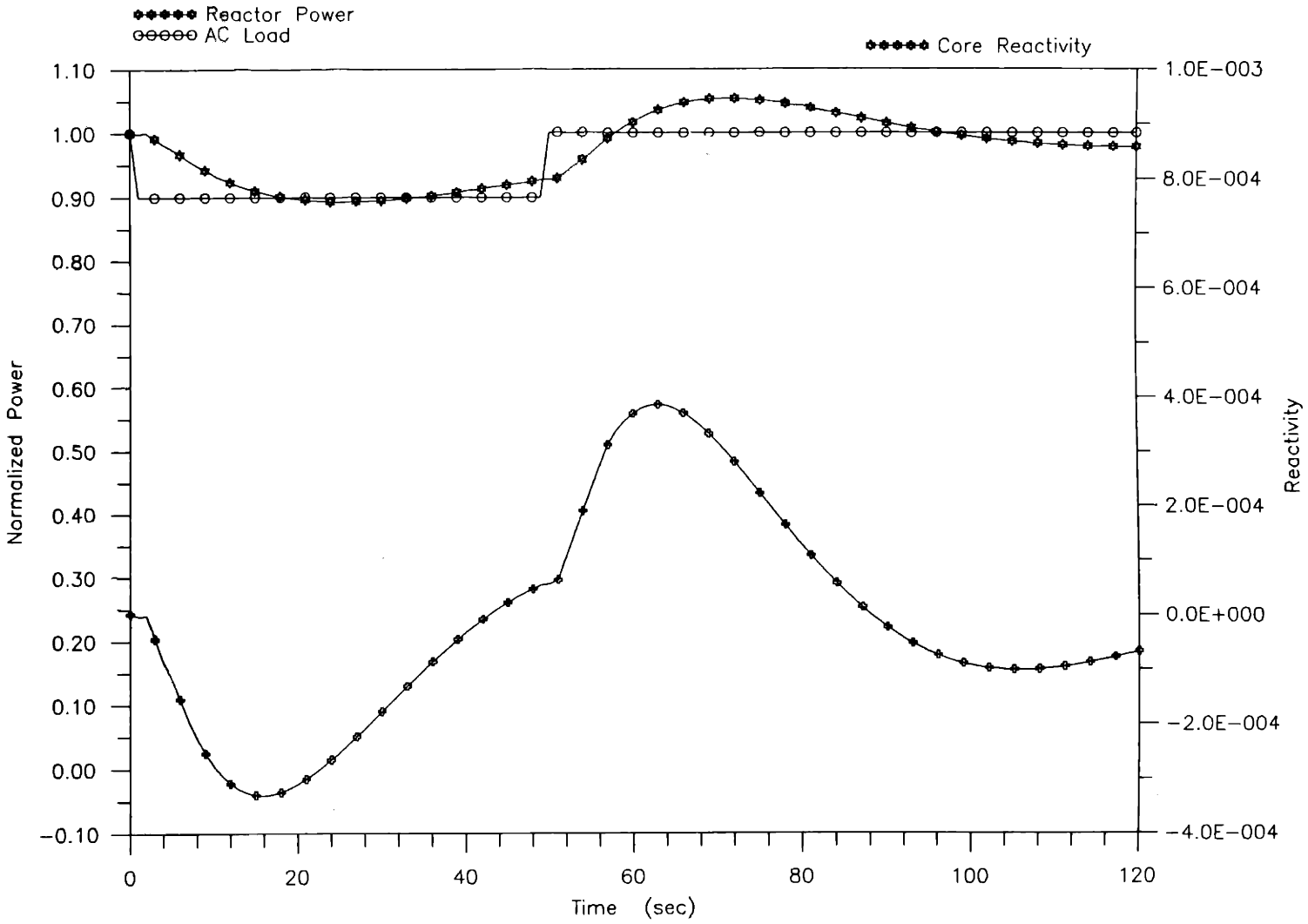

Figure 5.3 (b) Reactor power control during ±10 step AC load changes

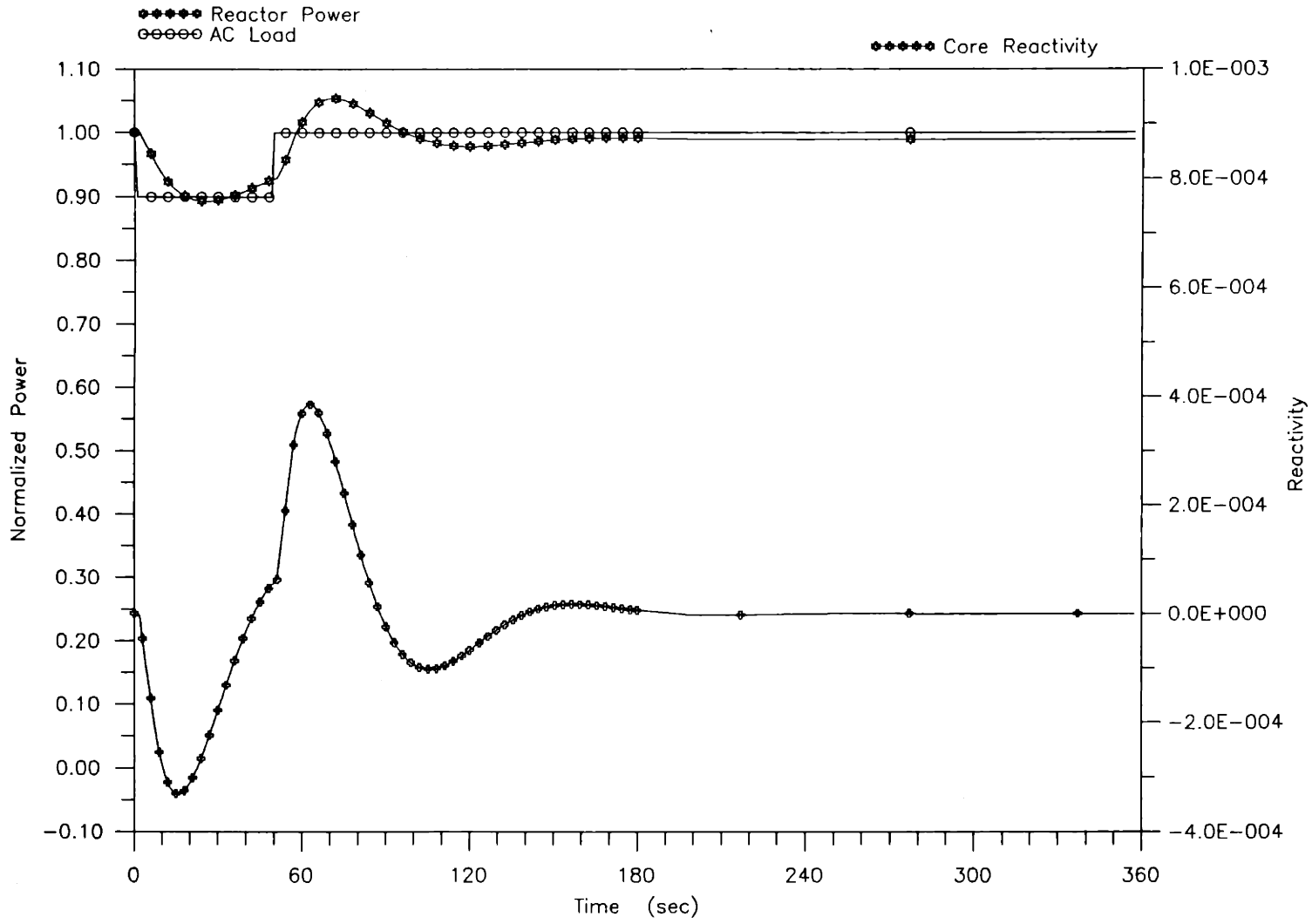

Figure 5.3 (c) Reactor power control in extended time period during ±10 step AC load changes

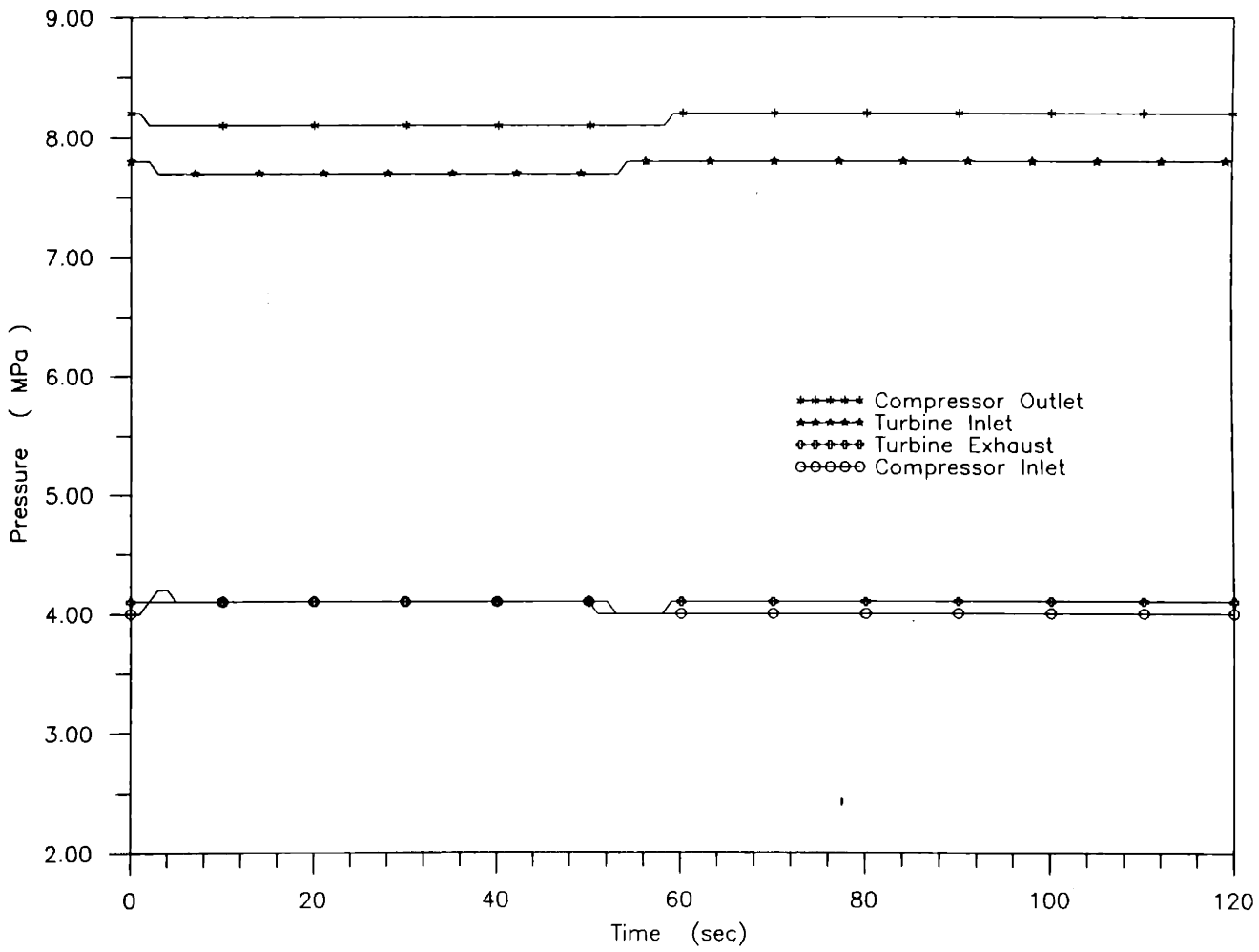

Figure 5.3 (d) Pressure transient responses to ±10 step AC load changes

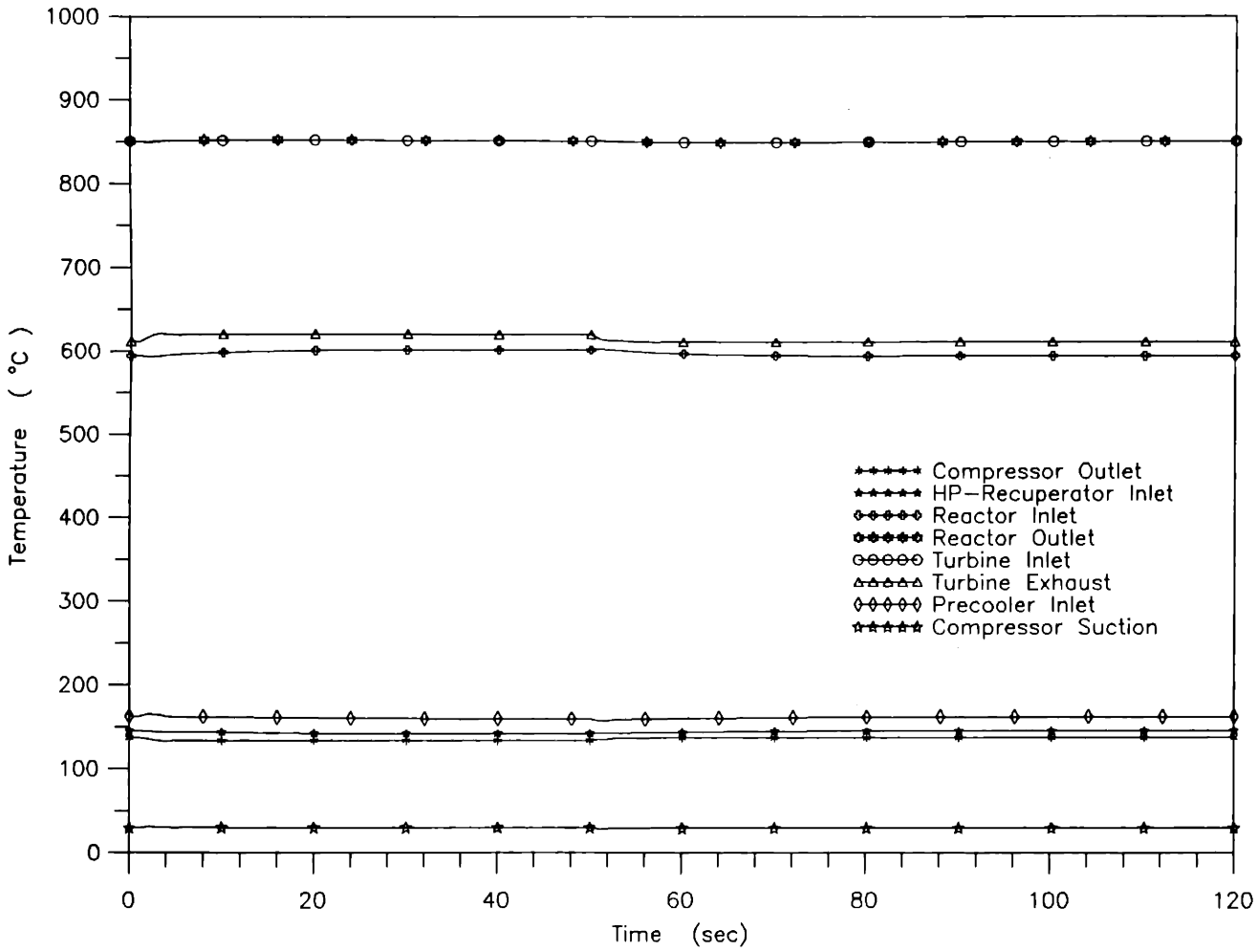

Figure 5.3 (e) Temperature transient responses to ±10 step AC load changes

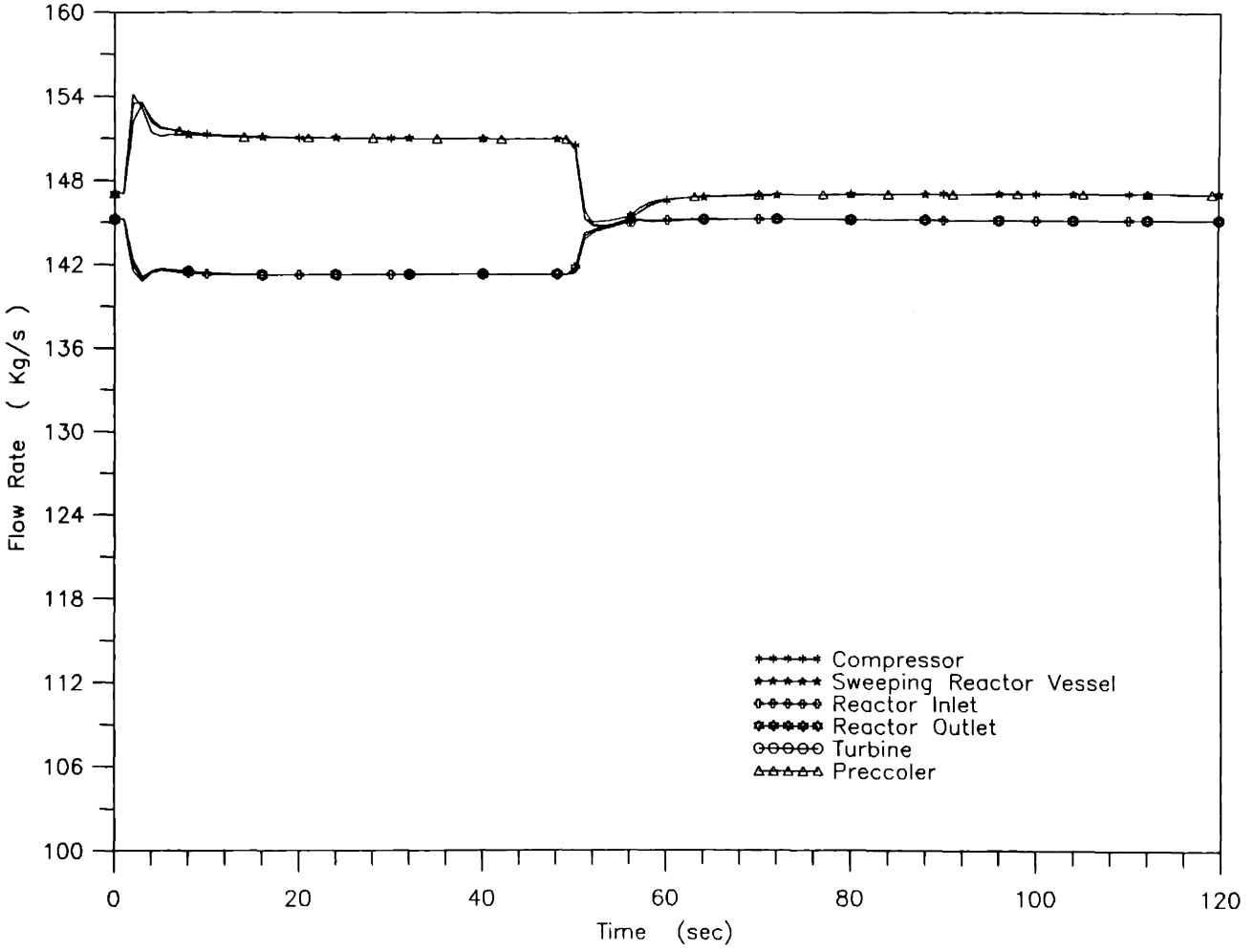

Figure 5.3 (f) Flow transient responses to ±10 step AC load changes

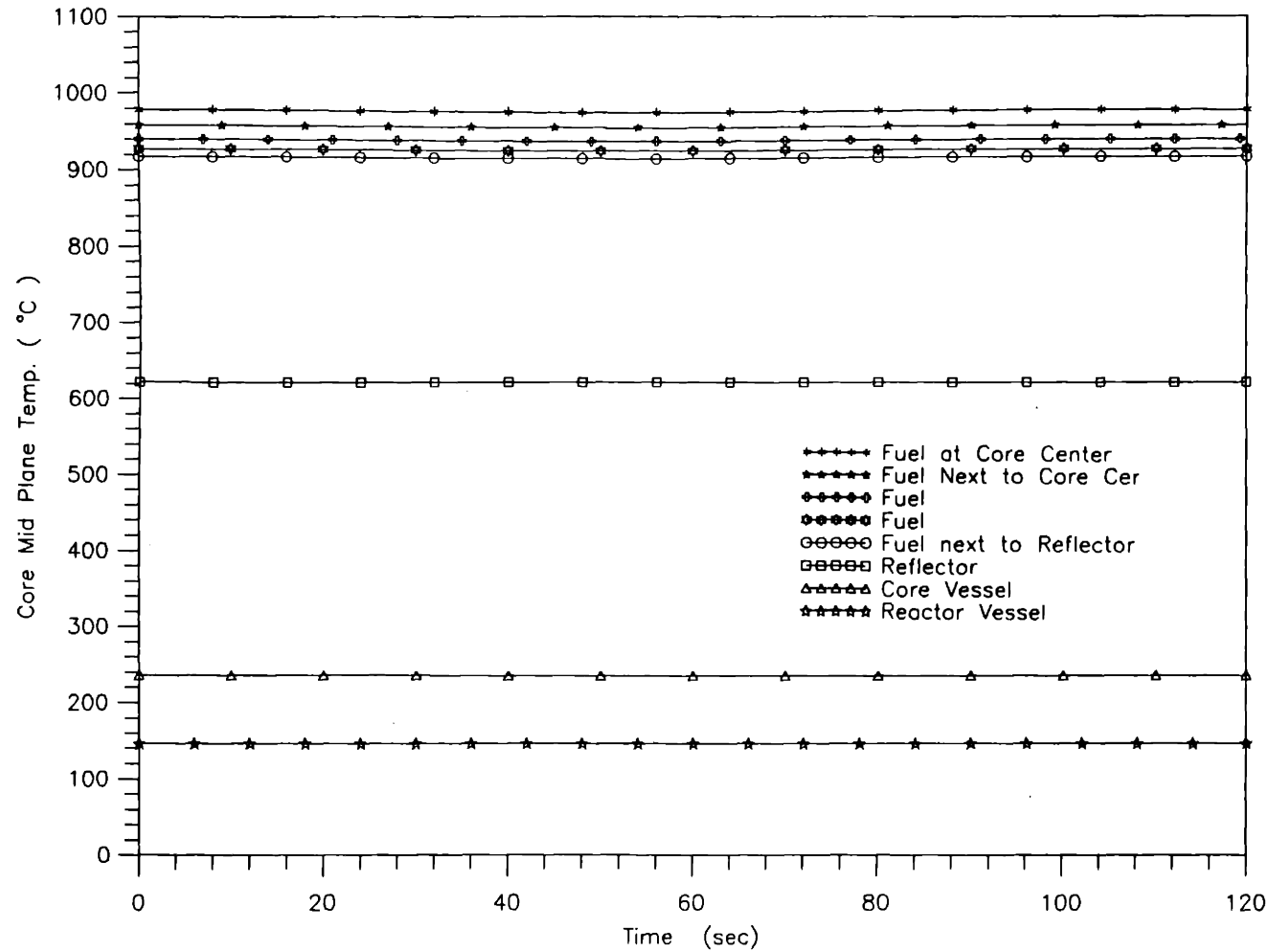

Figure 5.3 (g) Radial temperature transient responses in the core mid plane to ±10 step AC load

thereafter. The slower reduction rate of the speed is necessary in order to avoid instability of the turbomachine at low speed region. As can be seen, the bypass controller follows the speed regulating signal to adjust the bypass valve such that the turbine speed is smoothly reduced.

The speed reduction ends at t = 35 minutes. The plant approaches the steady-state operation at 3,600 rpm. The turbine power is approximately 2.5% of nominal power while the compressor consumes about 5% of nominal power. The power consumption by the compressor, which amounts about 4.5 MW, is the power that must be supplied by an external power source in order to motor the turbomachine from stationary state to such low-speed, self-sustaining condition.

The simultaneous control of the reactor power during the plant shutdown is shown in Figure 5.4 (b). As can be seen, the reactor power is reduced almost linearly by the reactor control system so as to maintain the constant reactor outlet temperature. In fact, the reactor control system manipulates the core reactivity not only to accomplish the reactor power control but also to compensate for the reactivity effect of fission product poisoning and temperature feedback. Details of the reactivity contributions by different sources are shown in Figure 5.4 (c). Because of relatively large temperature discrepancy from the design temperature distribution in the core, as shown in Figures 5.4 (h) and (i), the temperature reactivity feedback is significant as indicated in Figure 5.4(c). Long-term control and considerable power changes in the core result in large changes in fission product concentrations, which generate a great deal of negative reactivity.

Having reached the low-speed, steady-state operation condition, two further control operations, i.e., further shutdown or subsequent startup, may be pursued. The further plant shutdown can be pursued by lowering the control rods into the side reflector to setback reactor power. This control operation in combination with the previous shutdown control is

shown in Figure 5.4 (d). (Notice that the reactivity contributed by the control rods shown is the total control rod reactivity contribution less that of the steady-state reactivity of the control rods at full power). It can be seen that the reactor thermal power is shutdown to zero by the insertion of the control rods. The temperature reactivity coefficient generates positive reactivity as the core temperature decreases after reactor shutdown. For long-term reactor shutdown, the small absorber spheres can be released into the side reflector to compensate for the substantial positive reactivity contributed by both temperature reactivity feedback and the decay of certain fission products.

The startup from the low-speed, self-sustaining operation proceeds in the following steps:

(1) run-up of the turbomachine speed from 3,600 to 10,000 rpm at 500 rpm/min.

(2) operate the plant for a short period to achieve idle operation condition.

(3) connect the electric load at the rate of 5%/min to full load.

(4) operate the plant to accomplish the steady-state full power operation.

It can be seen in Figure 5.4 (a) that the turbomachine speed runs up following the issued speed regulating signal. As the plant operates at idle, the turbine and compressor powers reach the same power levels as those of the idle operation during the previous shutdown process. As the AC load is gradually connected, the turbomachine power is raised by bypass valve closing. The corresponding reactor power and reactivity transients are depicted in Figures 5.4 (b) and (c). It can be seen that the total reactivity is manipulated by the control rods such that the reactor power is increased up to full power. The total reactivity becomes zero as the reactor criticality is obtained for the full power operation.

It is of interest that the control rods as shown in Figure 5.4 (c) do not return to the original position after the reactor power has reached the full power level. The reason for this is that the residual reactivity of the control rods is utilized on a long-term basis to compensate

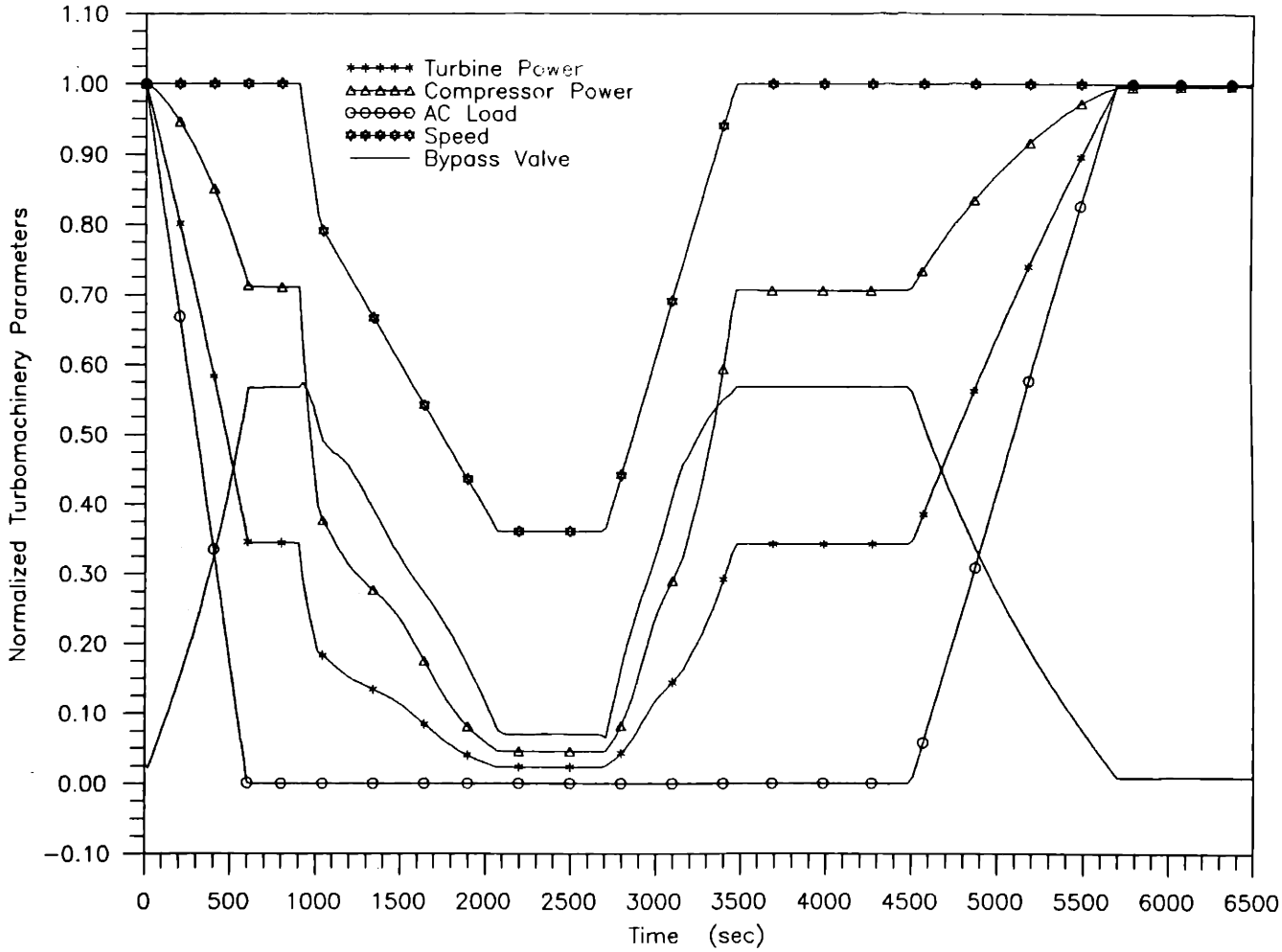

Figure 5.4 (a) Turbomachine parameters in control process for normal shutdown and subsequent startup

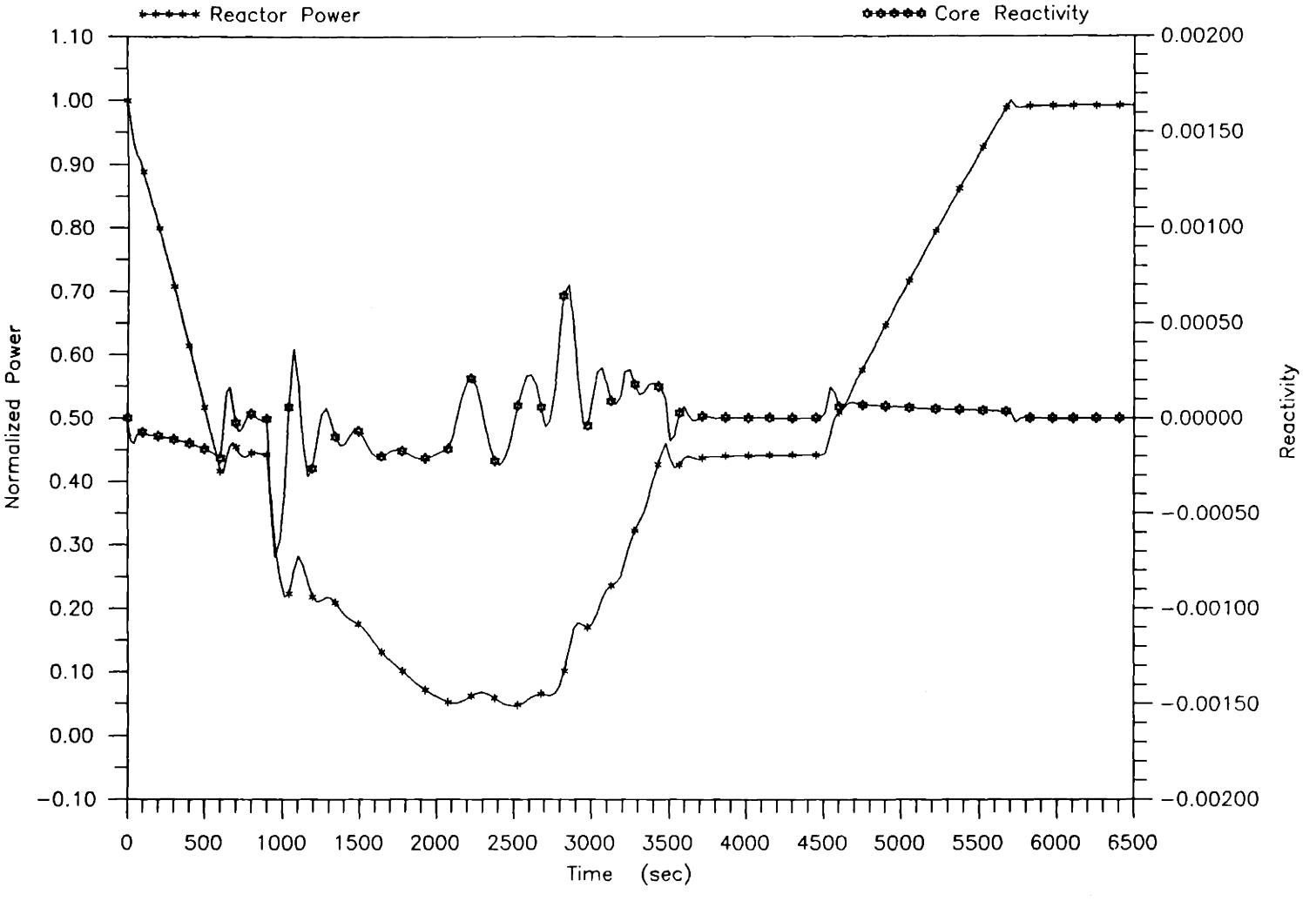

Figure 5.4 (b) Reactor power control during normal shutdown and subsequent startup

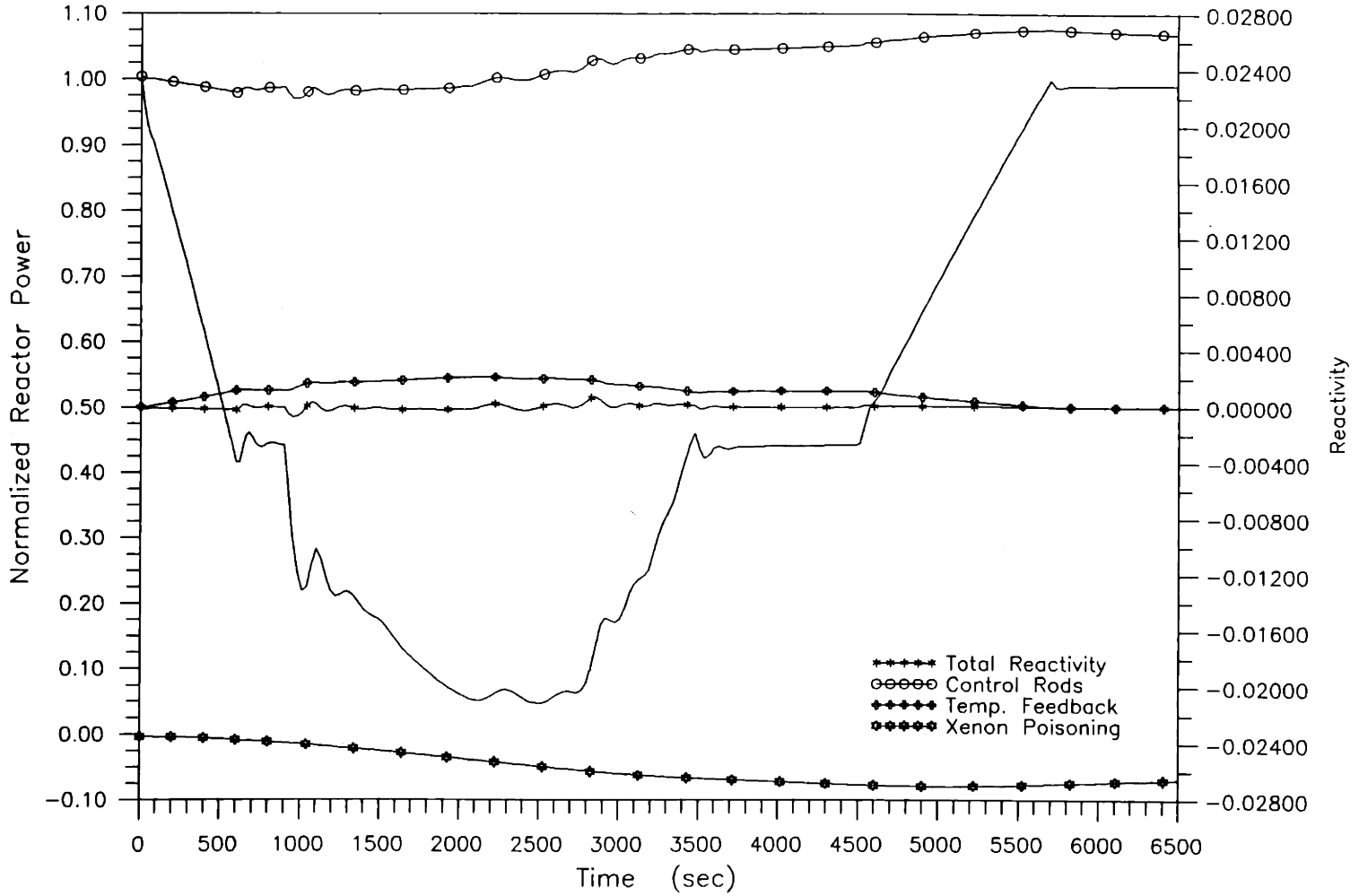

Figure 5.4 (c) Reactor power control and reactivity contributions during normal shutdown and subsequent startup

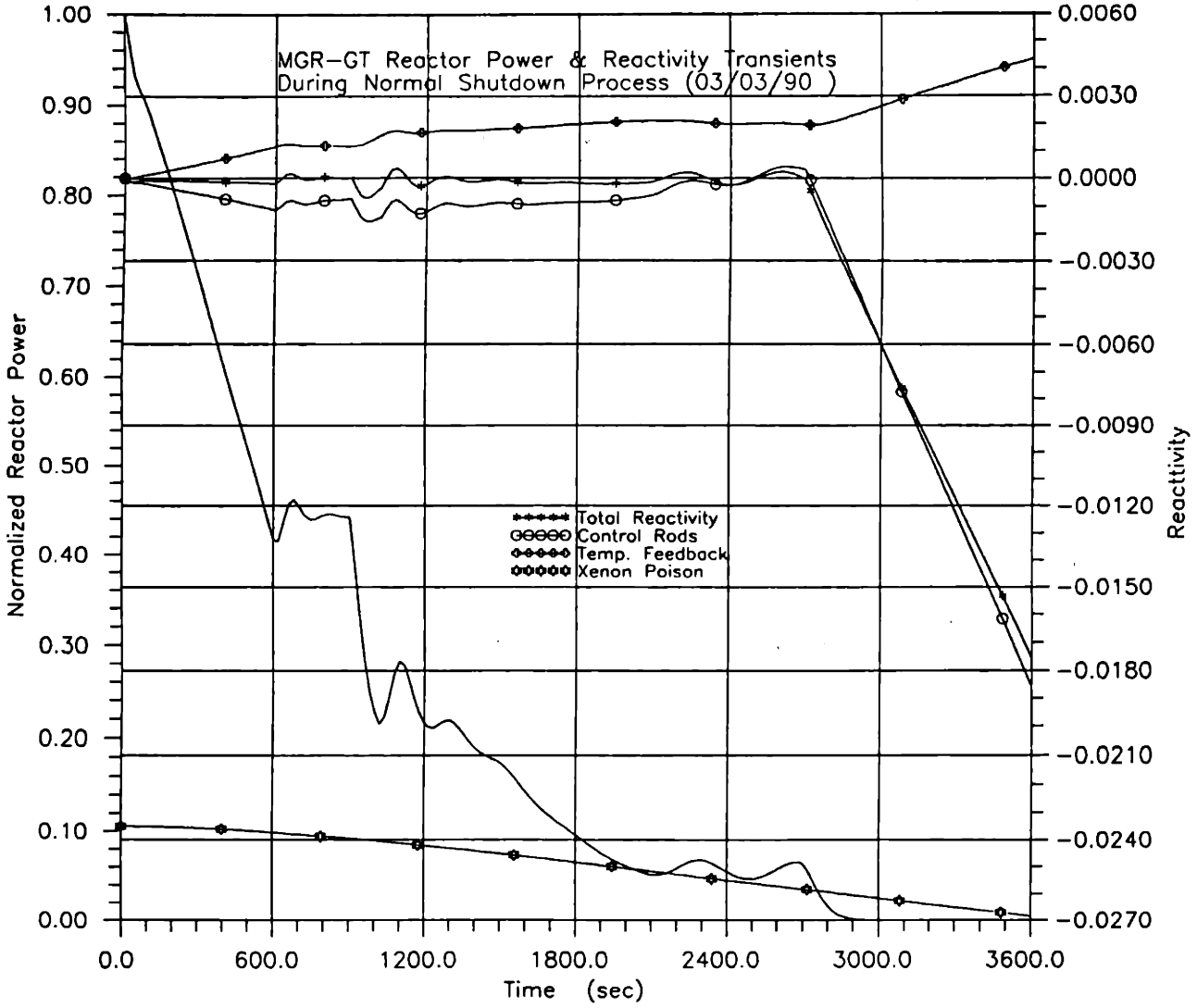

Figure 5.4 (d) Reactor power control and reactivity contributions during normal shutdown

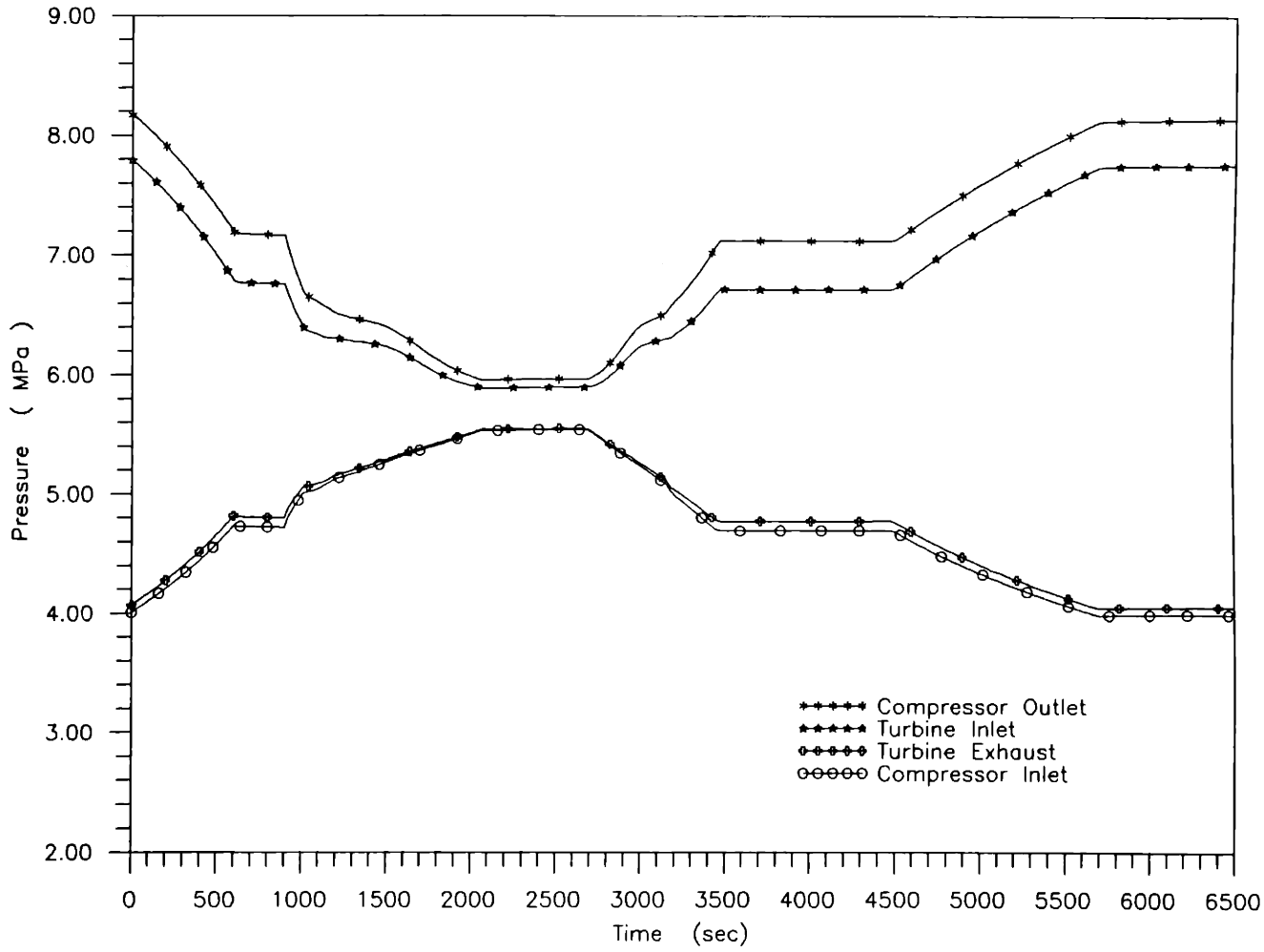

Figure 5.4 (e) Pressure transient responses during normal shutdown and subsequent startup

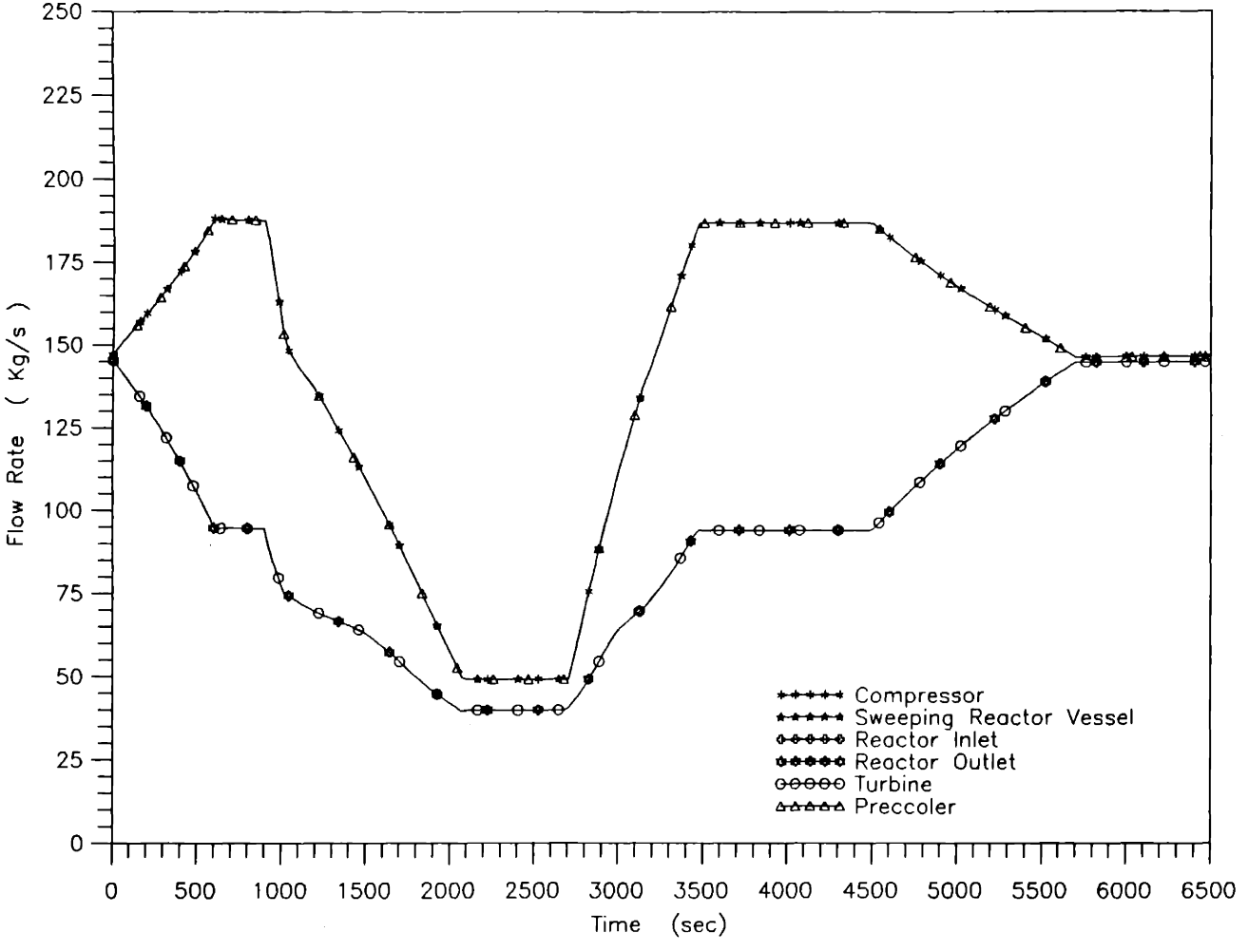

Figure 5.4 (f) Flow transient responses during normal shutdown and subsequent startup

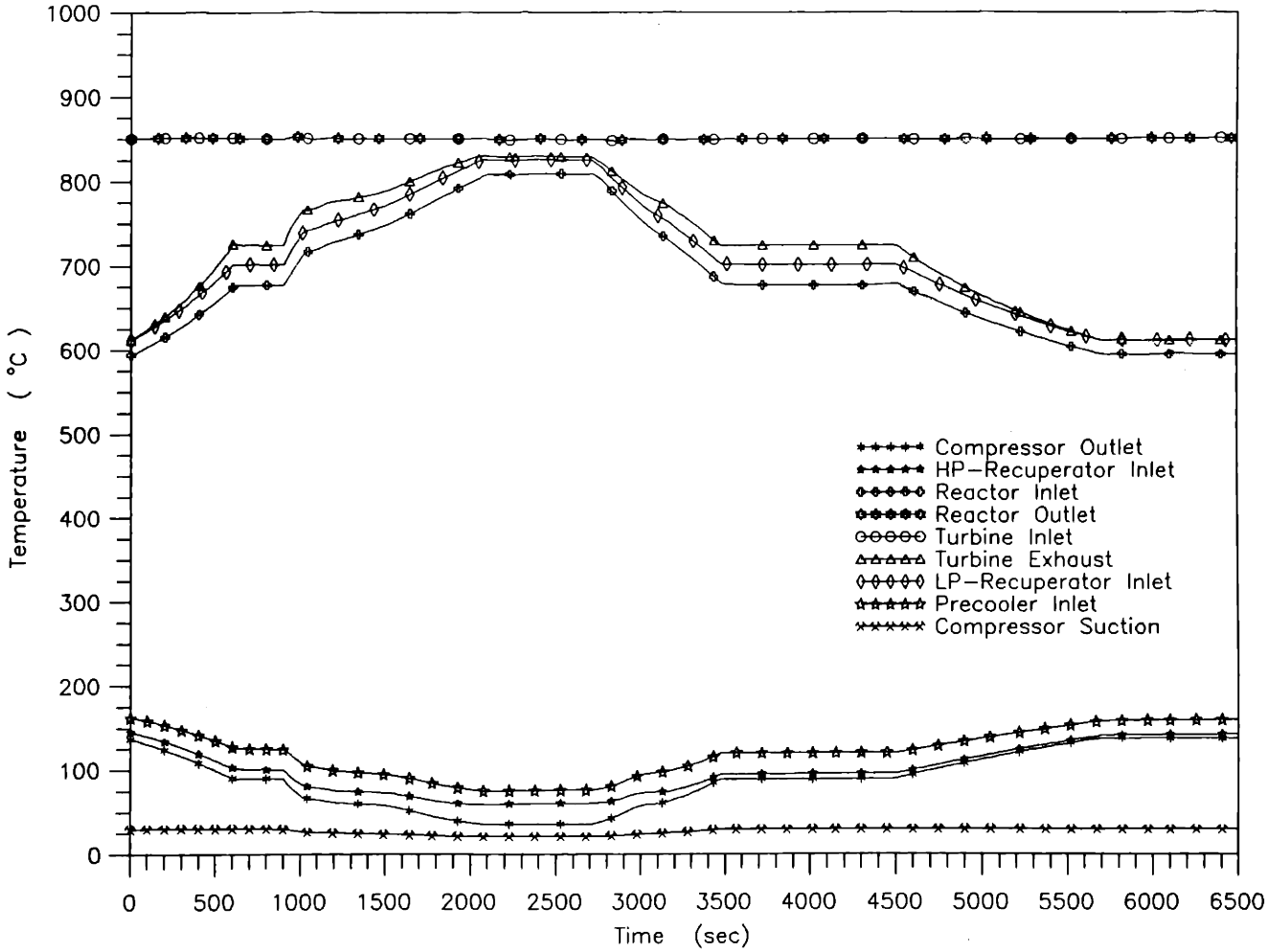

Figure 5.4 (g) Temperature transient responses during normal shutdown and subsequent startup

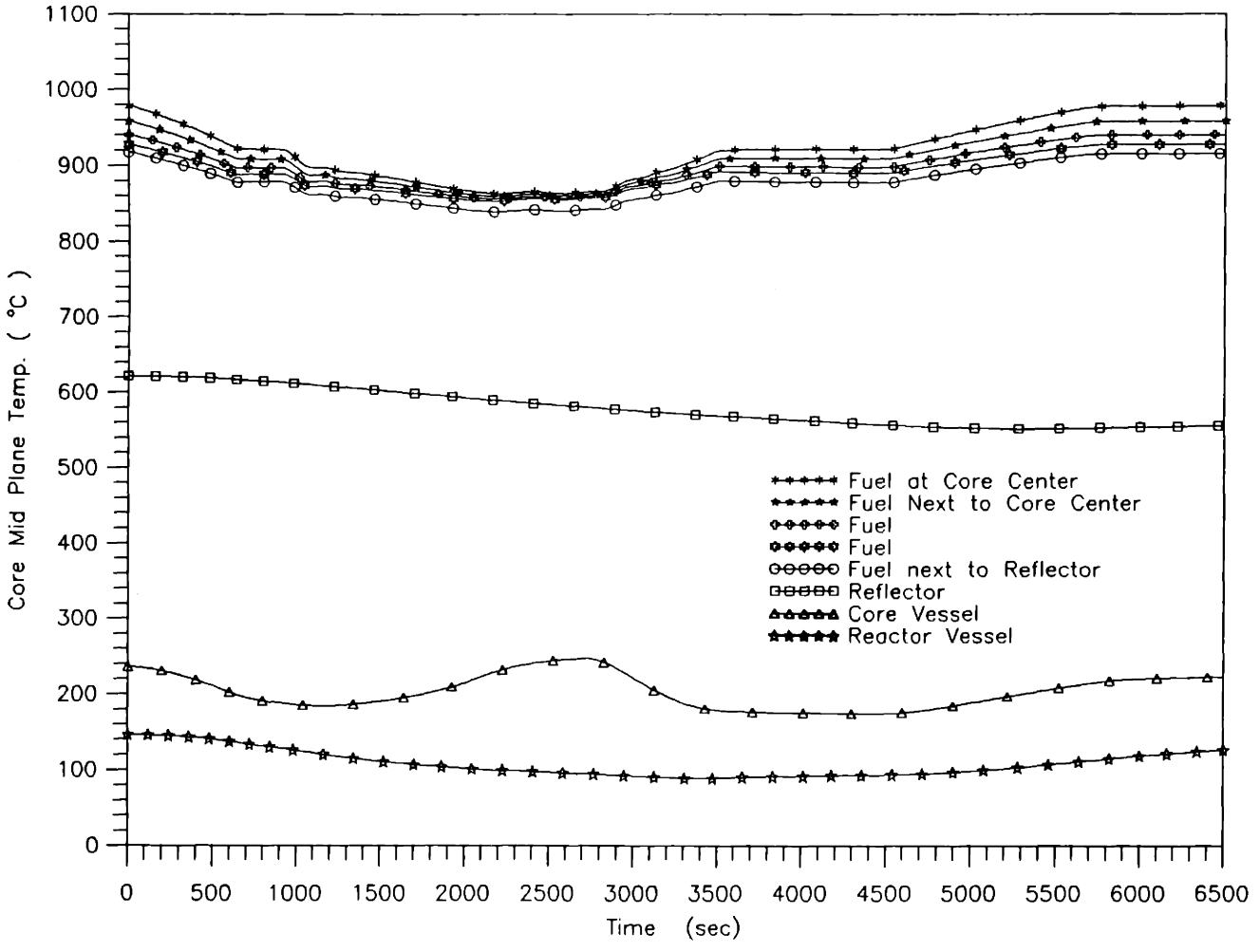

Figure 5.4 (h) Radial temperature transient responses in the core mid plane to ±10 step AC load changes

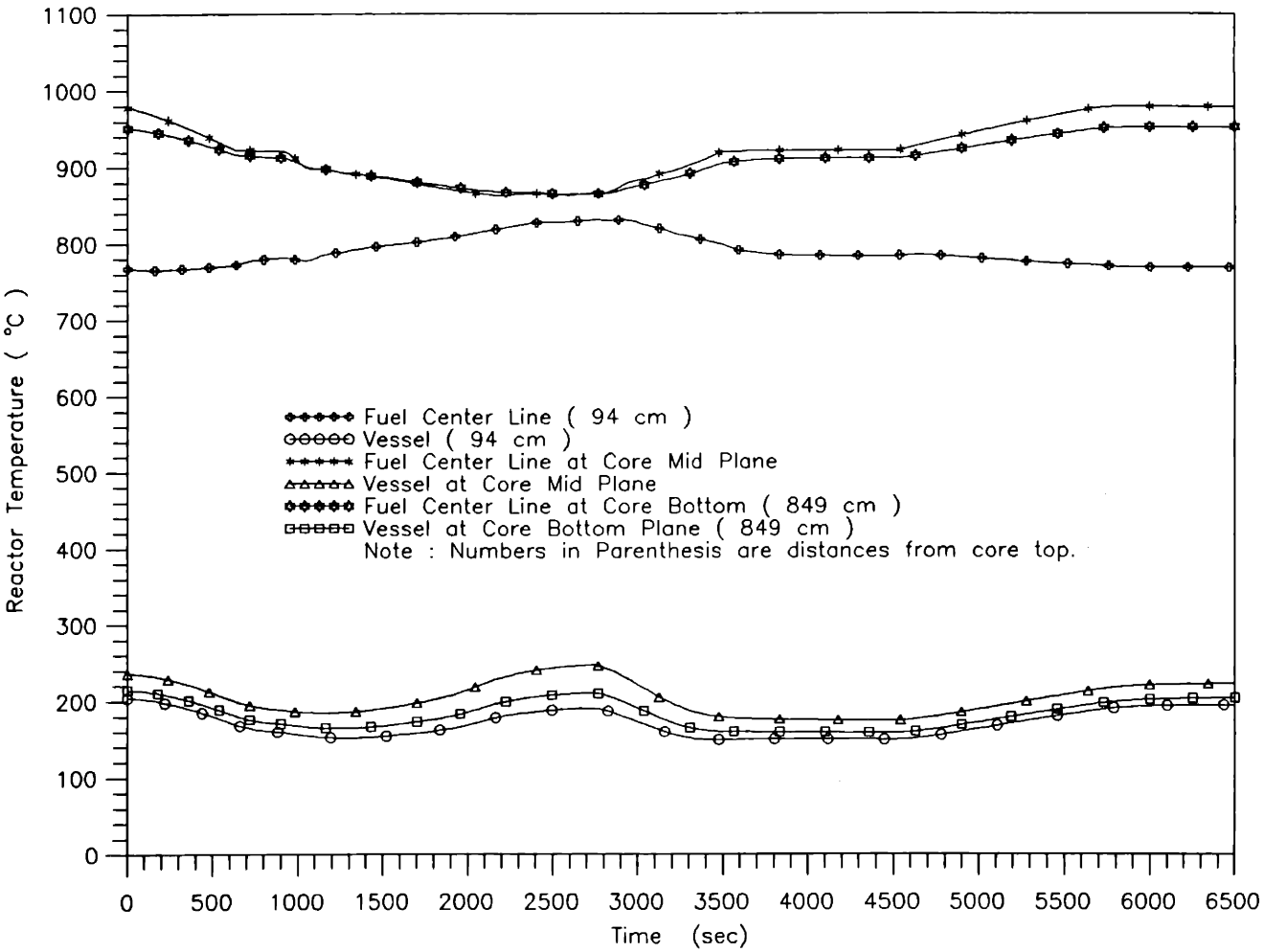

Figure 5.4 (i) Axial core temperature transient responses to ±10 step AC load changes

for the reactivity contributed by the fission product poisoning. Buildup of the fission products lasts over relatively long period of time due to the large characteristic time. As can be seen, the reactivity of the fission product poisoning starts to increase at about t = 5250 sec, approximately 45 minute delay from the time when the reactor power starts to be increased.

The transient responses of pressure, temperature, and flow are shown in Figures 5.4 (e) to (g), respectively, for the entire period of shutdown and startup. The reactor outlet temperature remains constant. The bypass flow at the idle, design speed operation is 94.5 kg/s or approximately 62% of the nominal flow rate, while it is about 15 kg/s at the self-sustaining condition at 3,600 rpm.

5.2.2 Evaluation of the Plant Protection System

Three transients have been simulated in order to evaluate the PPS design. They are total electric load rejection from full power, turbomachinery shaft failure, and positive reactivity disturbance at full power. The simulations for these accidents are described in the following.

5.2.2a Total Load Rejection from Full Power

In case of a sudden electric load release, loop shutdown is triggered by the PPS sensor signal indicating the load drop greater than 50% of the nominal load. The loop shutdown is accomplished by the bypass valve which is 33 cm in diameter. The shutdown control process is shown in Figures 5.5 (a) to (i).

The transient starts at t = 1 sec when the electric load is suddenly dropped to zero, as shown in Figure 5.5 (a). The shutdown bypass valve opens quickly to prevent the turbomachine from overspeed. As can be seen, the maximum overspeed is controlled to less than 5% of the nominal speed. The overspeed is sensitive to the rate of the bypass valve opening. For the PPS bypass valve, the maximum rate of the opening is limited to 100%/sec.

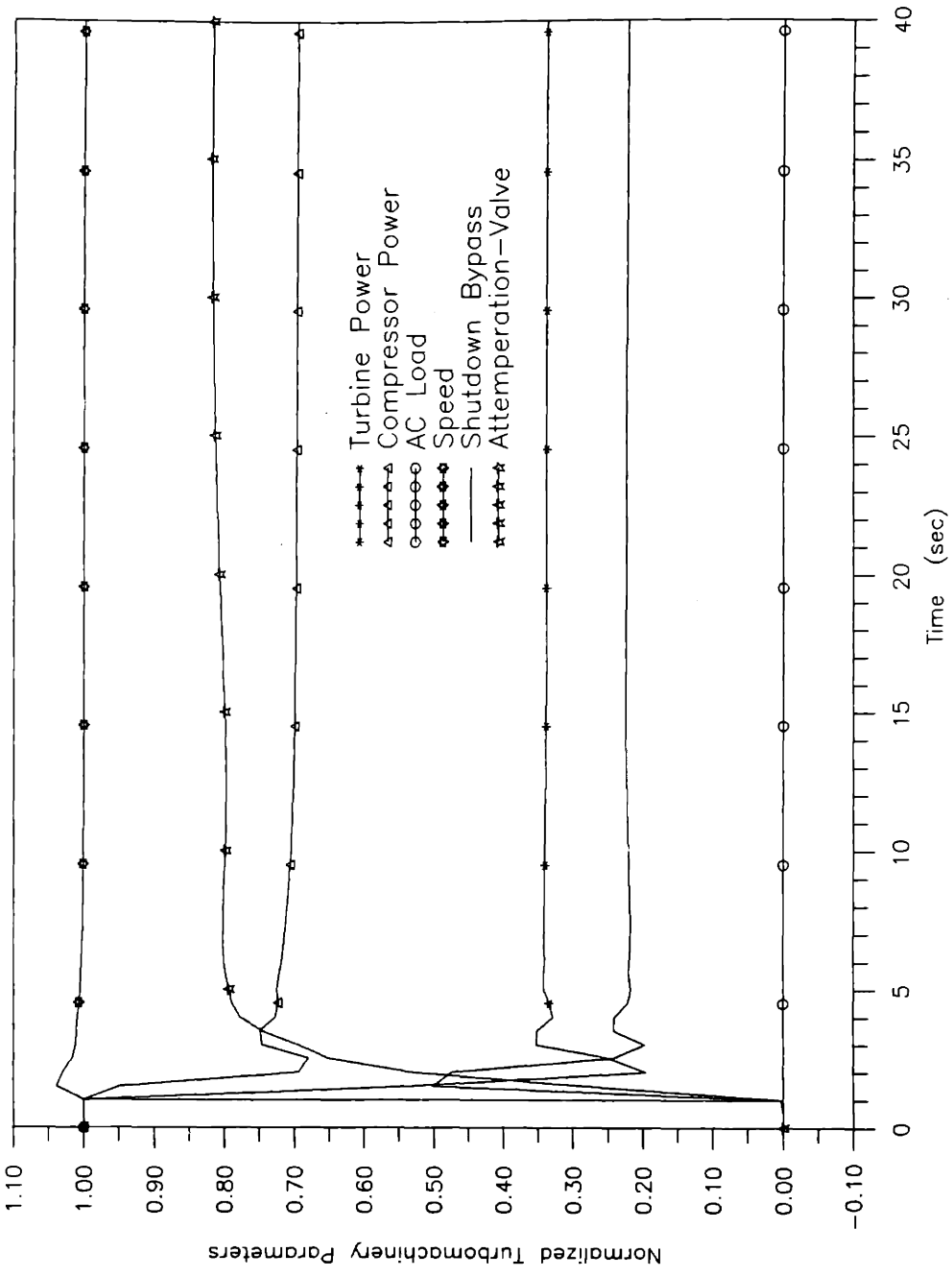

Figure 5.5 (a) Turbomachine parameters in shutdown control in case of AC load rejection

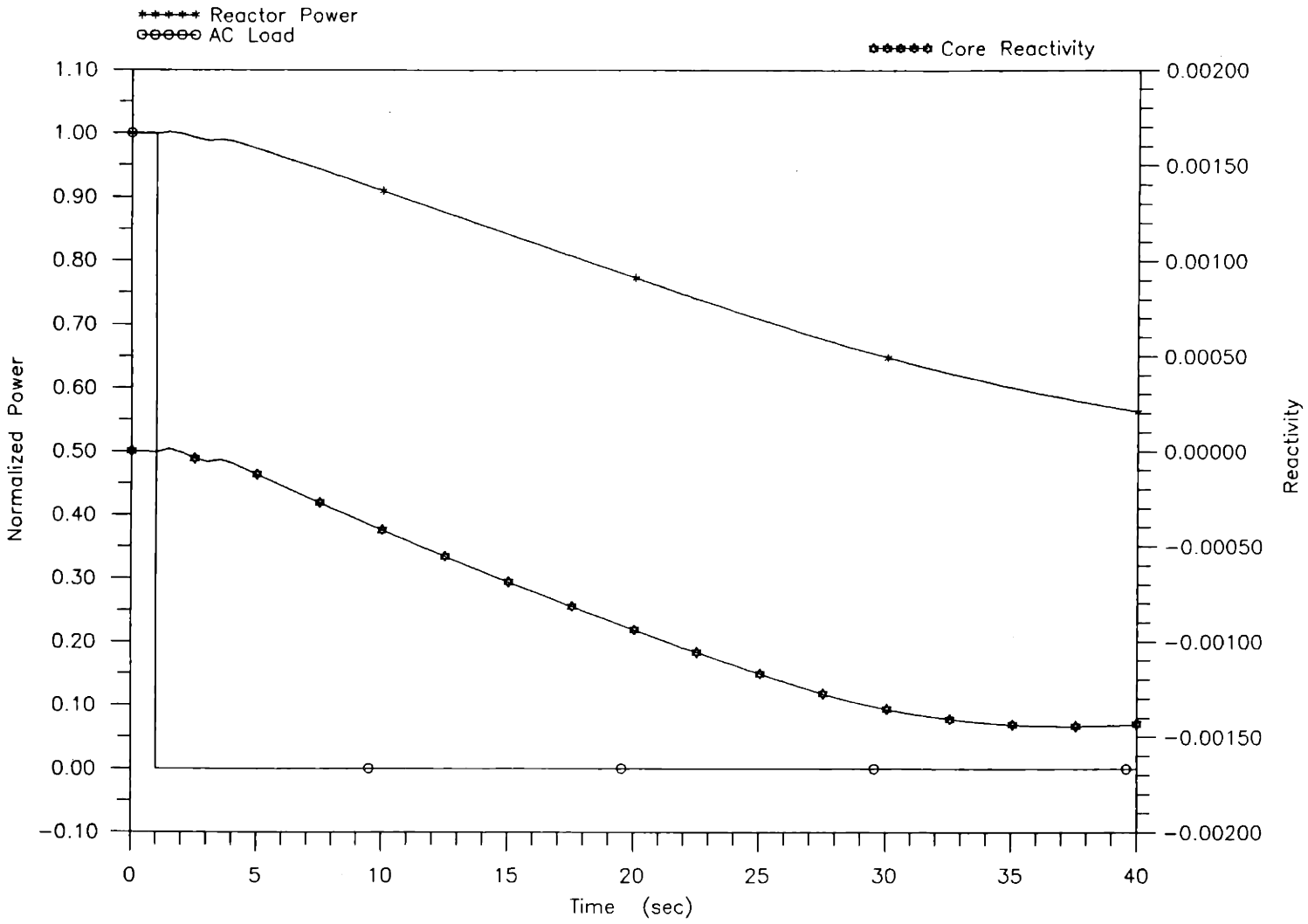

Figure 5.5 (b) Reactor power control in case of AC load rejection

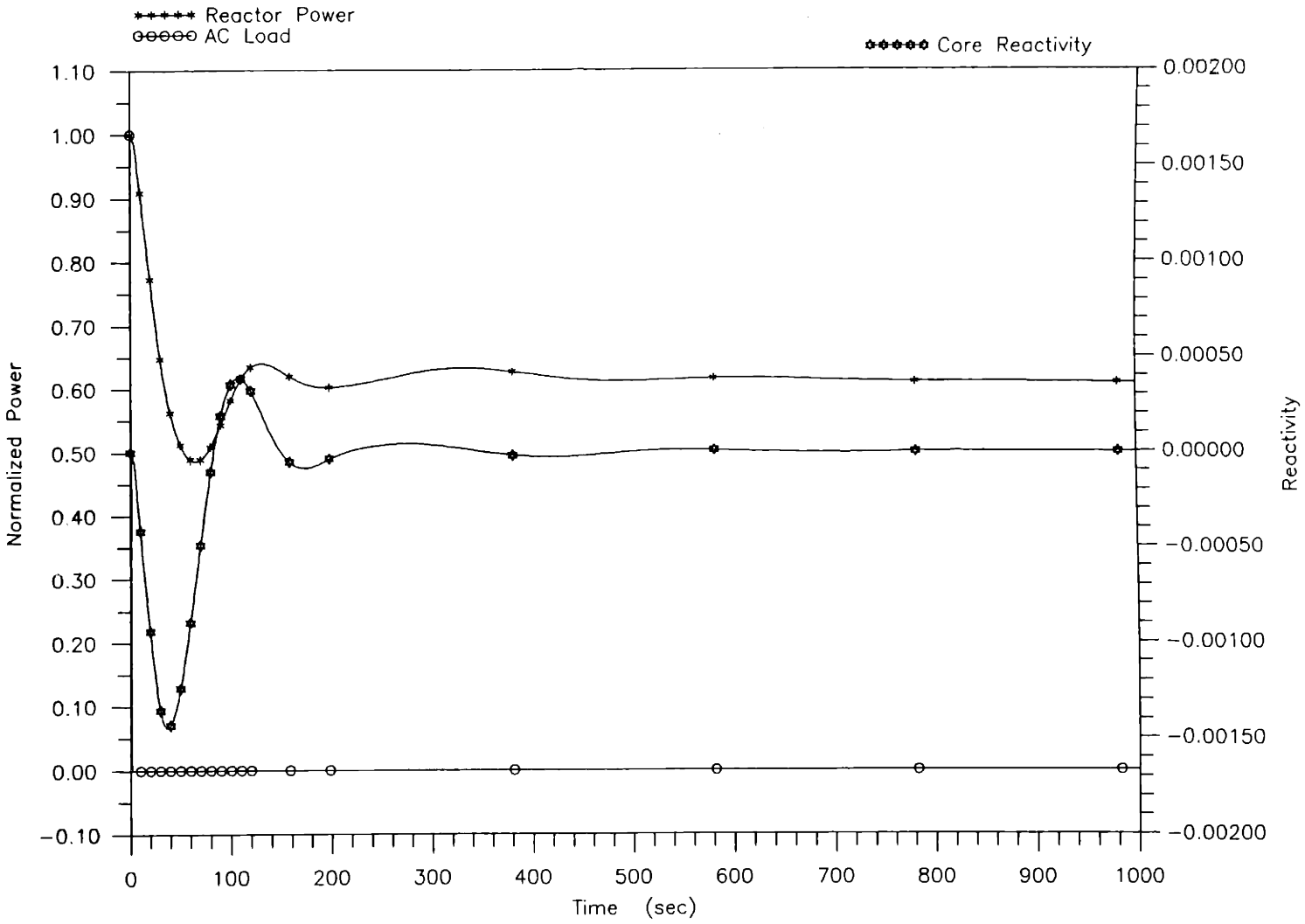

Figure 5.5 (c) Reactor power control over extended period of time in case of AC load rejection

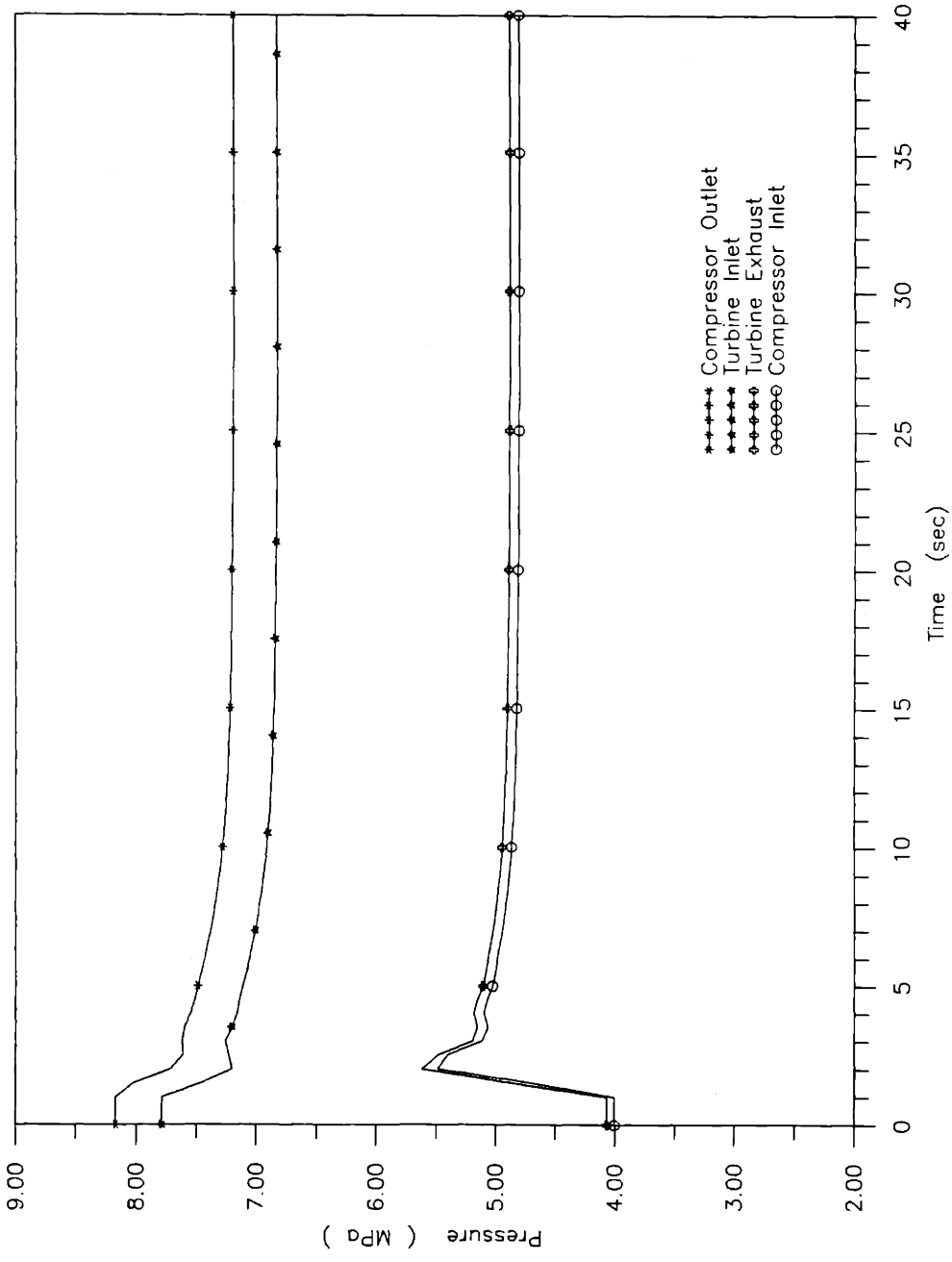

Figure 5.5 (d) Pressure transient responses during shutdown process in case of AC load rejection

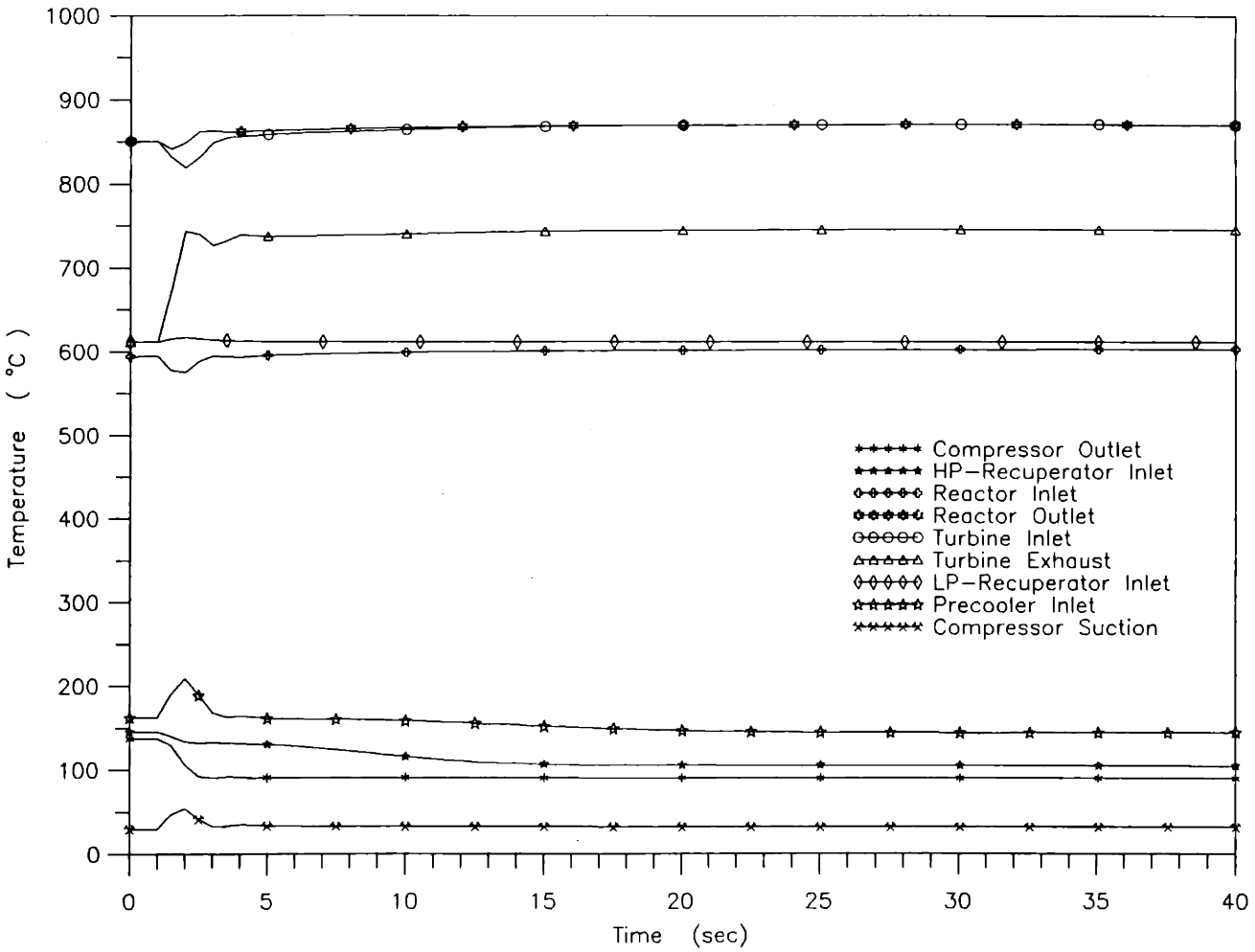

Figure 5.5 (e) Temperature transient responses during shutdown process in case of AC load rejection

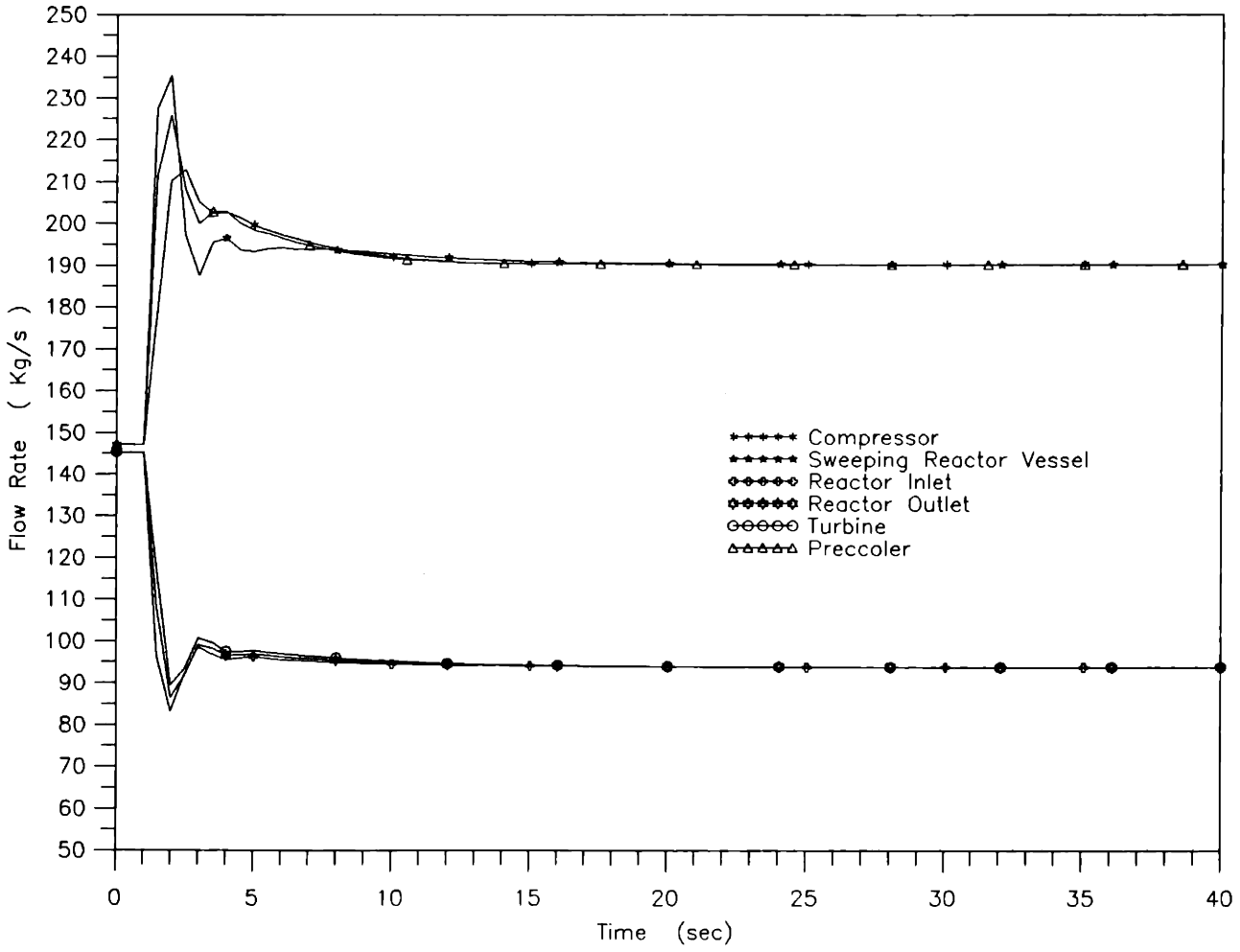

Figure 5.5 (f) Flow transient responses during shutdown process in case of AC load rejection

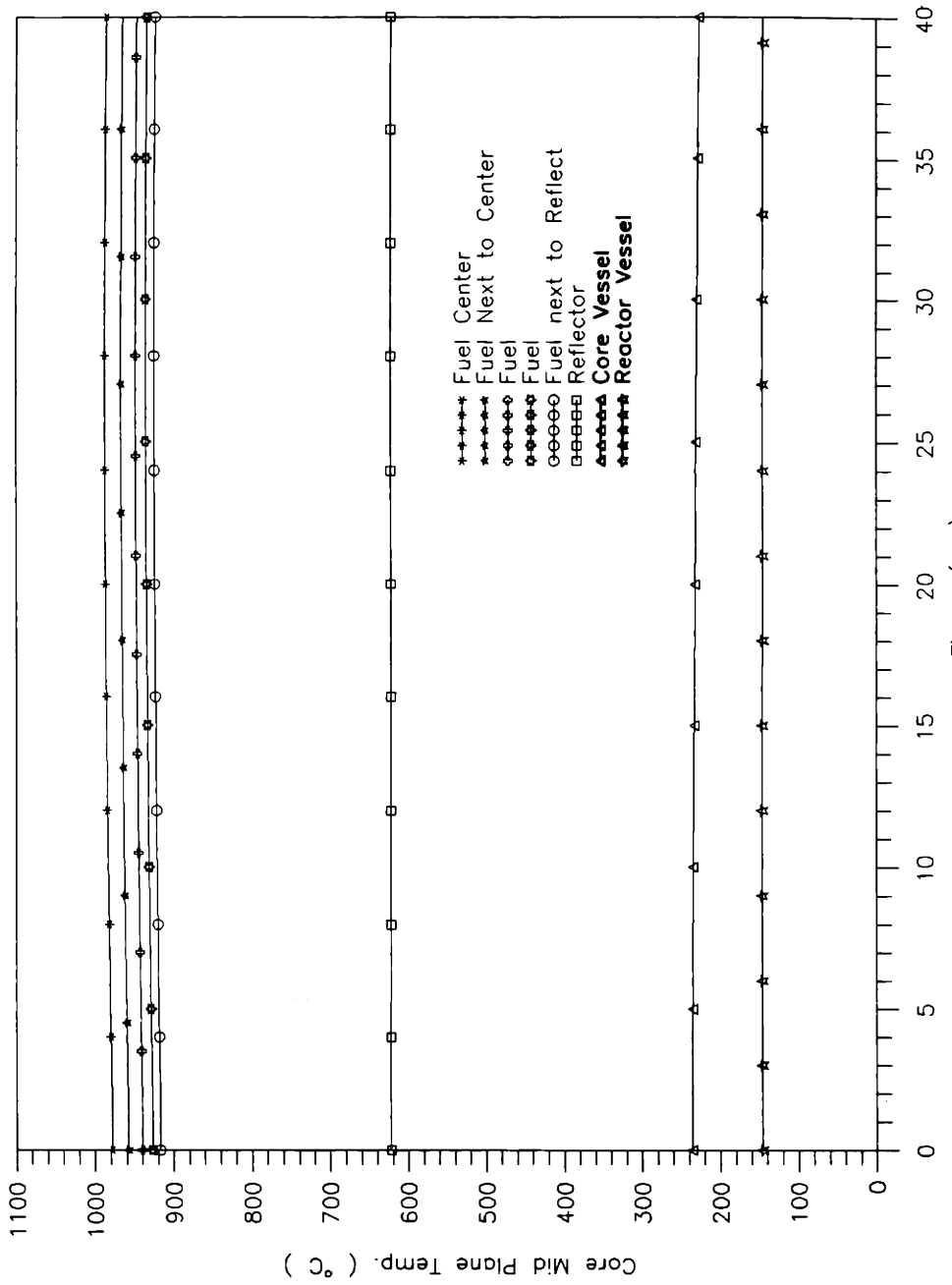

Figure 5.5 (g) Radial temperature transient responses in the core mid plane during shutdown process in case of AC load rejection

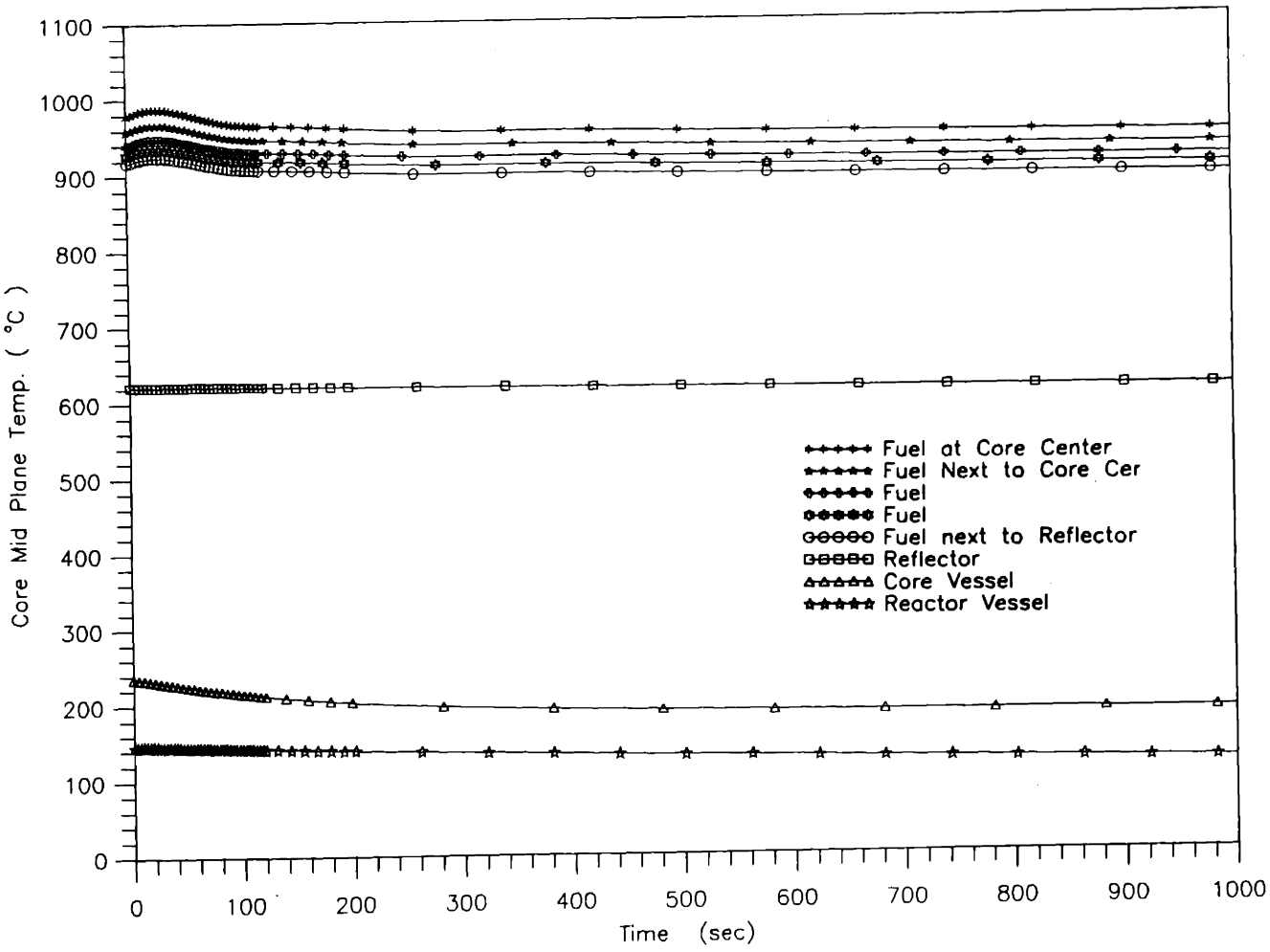

Figure 5.5 (h) Radial temperature transient responses in the core mid plane over extended time period during shutdown process in case of AC load rejection

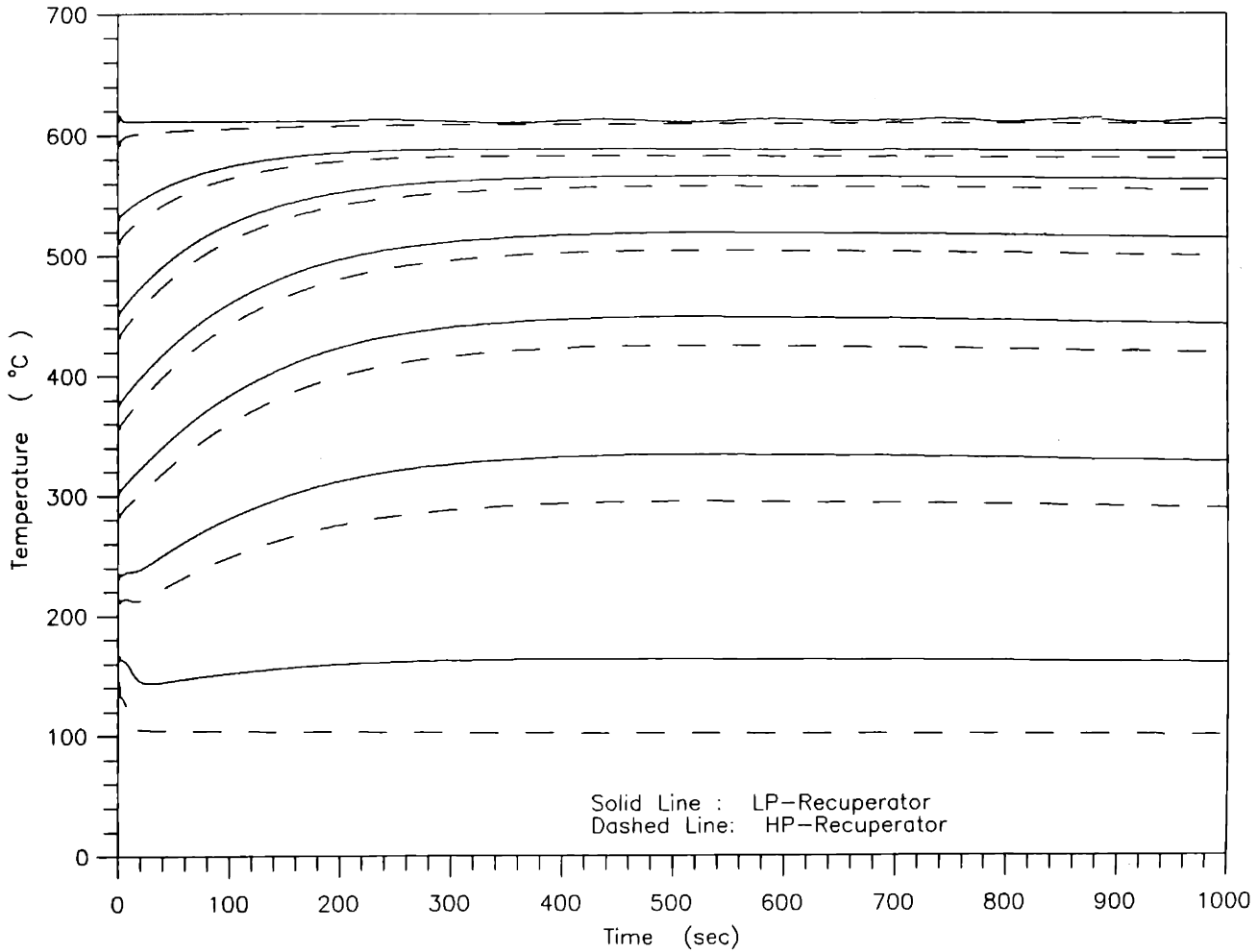

Figure 5.5 (i) Transient responses of nodal temperatures in the recuperator during shutdown process in case of AC load rejection

Although only 50% of the bypass valve opening has been reached for this shutdown control, the large valve control capacity is rated for more critical accidents, such as the turbomachine shaft failure.

After a brief speed overshoot, the turbomachine approaches design speed quickly and aperiodically. The turbine and compressor powers are dropped to about 33% and 70% of the nominal power, respectively. The simultaneous reactor power control is shown in Figures 5.5 (b) and (c) for different time scales. As can be seen, the reactor power is setback by the control rods and approaches 60% of the nominal power for running at idle.

Substantial bypass flow results in large reduction of the turbine pressure head, as shown in Figure 5.5 (d). The reduction of the turbine pressure ratio causes the increase of the turbine outlet temperature, as shown in Figure 5.5 (e). However, because of the thermal control by the attemperation bypass valve as shown in Figure 5.5 (a), the temperature at the inlet of the LP-recuperator is maintained nearly constant even though the turbine outlet temperature has increased by about 120°C. In addition, the reactor outlet temperature is maintained at 850°C with only minor temperature fluctuation during initial period, which is largely the result of the critical flow compression at the beginning of the bypass control. The flow transient responses are shown in Figure 5.5 (f). The temperature transients in the reactor are shown in Figures 5.5 (g) and (h) on different time scales.

5.2.2b Turbomachine Shaft Failure

Turbomachine shaft break could be induced by generator failure. For example, if coils of the generator became lodged in the gap between the generator rotor and stator, the resultant mechanical forces might be large enough to break the shaft. Based on the current rotor configuration, the shaft would most likely fail at the location in between the turbine and compressor where the torque is largest. The schematic description of this shaft failure

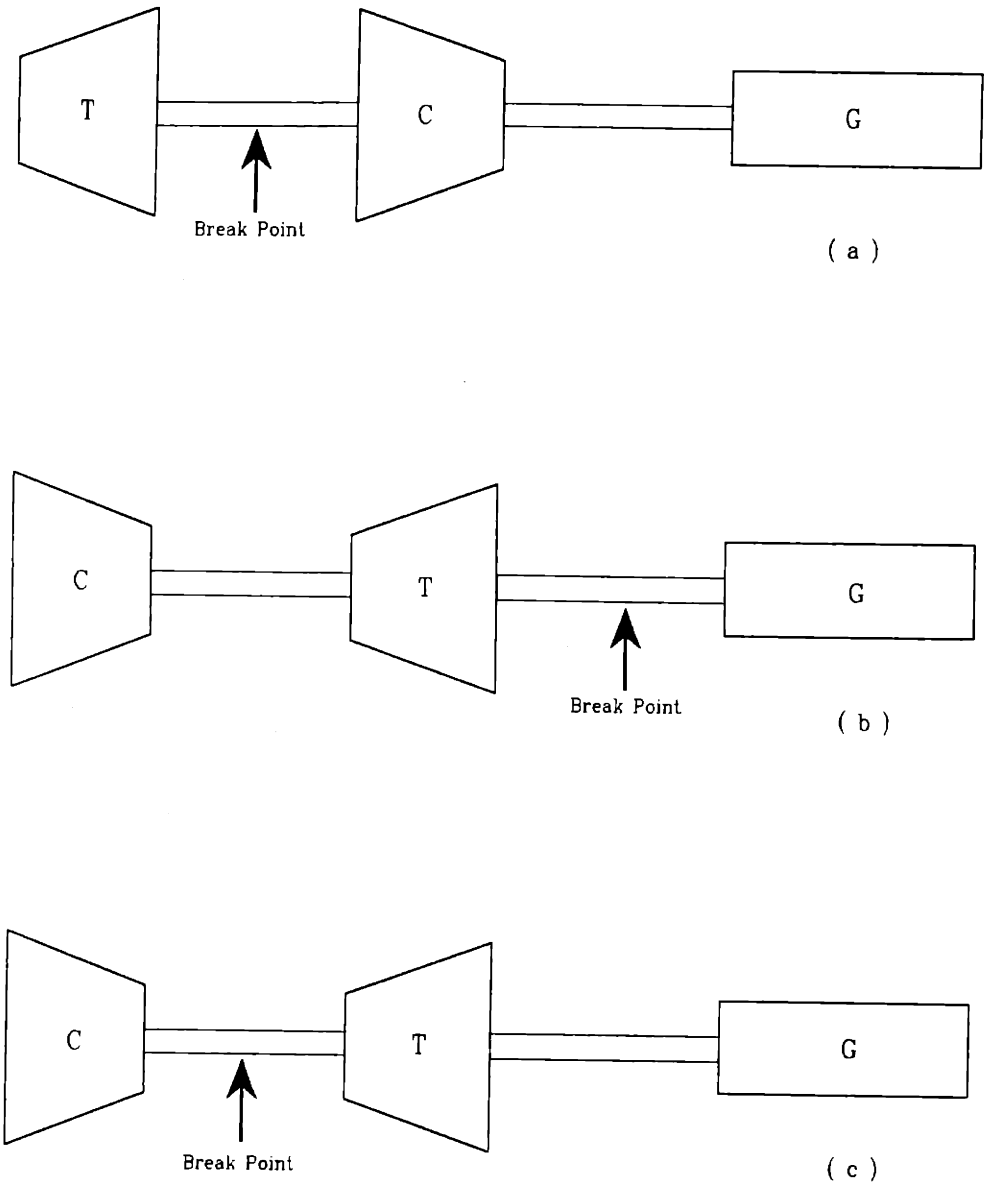

Figure 5.6 Rotor configurations and failure scenarios

scenario is shown in Figure 5.6 (a). It is expected that the overspeed of the turbine rotor would be tremendous in this shaft failure scenario, since little inertia would be associated with the turbine rotor.

Figures 5.7 (a) to (h) show transient responses of the plant to the current shaft failure. The shaft break is assumed to occur at t = 1 sec. The loop shutdown is initiated by the sensor signal indicating a speed discrepancy of 10 rpm between the turbine and compressor rotors. Concurrent protective actions by the PPS include reactor shutdown, thermal overstress protection, and initiation of the generator circuit breaker to protect the electrical system.

Figure 5.7 (a) shows the transient responses of the turbine and compressor parameters. As can be seen, the emergency shutdown bypass valve opens quickly to drop the turbine pressure head, as indicated in Figure 5.7 (b), resulting in rapid reduction of the turbine power. The maximum overspeed of the turbine rotor reached is 25% of the nominal speed 0.75 sec after the accident initiation. The turbine rotor speed will then decrease gradually as the turbine begins to consume power when the speed is high and the helium flow small as shown in Figure 5.7 (f). The transition of the turbine power from supply to absorption is clearly indicated by the efficiency transient behavior as shown in Figure 5.7 (c). It can be seen that the turbine efficiency decreases and passes the transition point from positive to negative at t = 1.75 sec, which is the time when the turbine power becomes negative.

Because of the dramatic reduction of the turbine pressure ratio, the turbine outlet temperature increases rapidly, as shown in Figure 5.7 (e). The attemperation bypass valve, as shown in Figure 5.7 (a), opens to prevent thermal shock at the LP-recuperator inlet at the downstream of the turbine. As a result, the LP-recuperator inlet temperature experiences only minor temperature increase even though the turbine outlet temperature has risen by about 200°C.

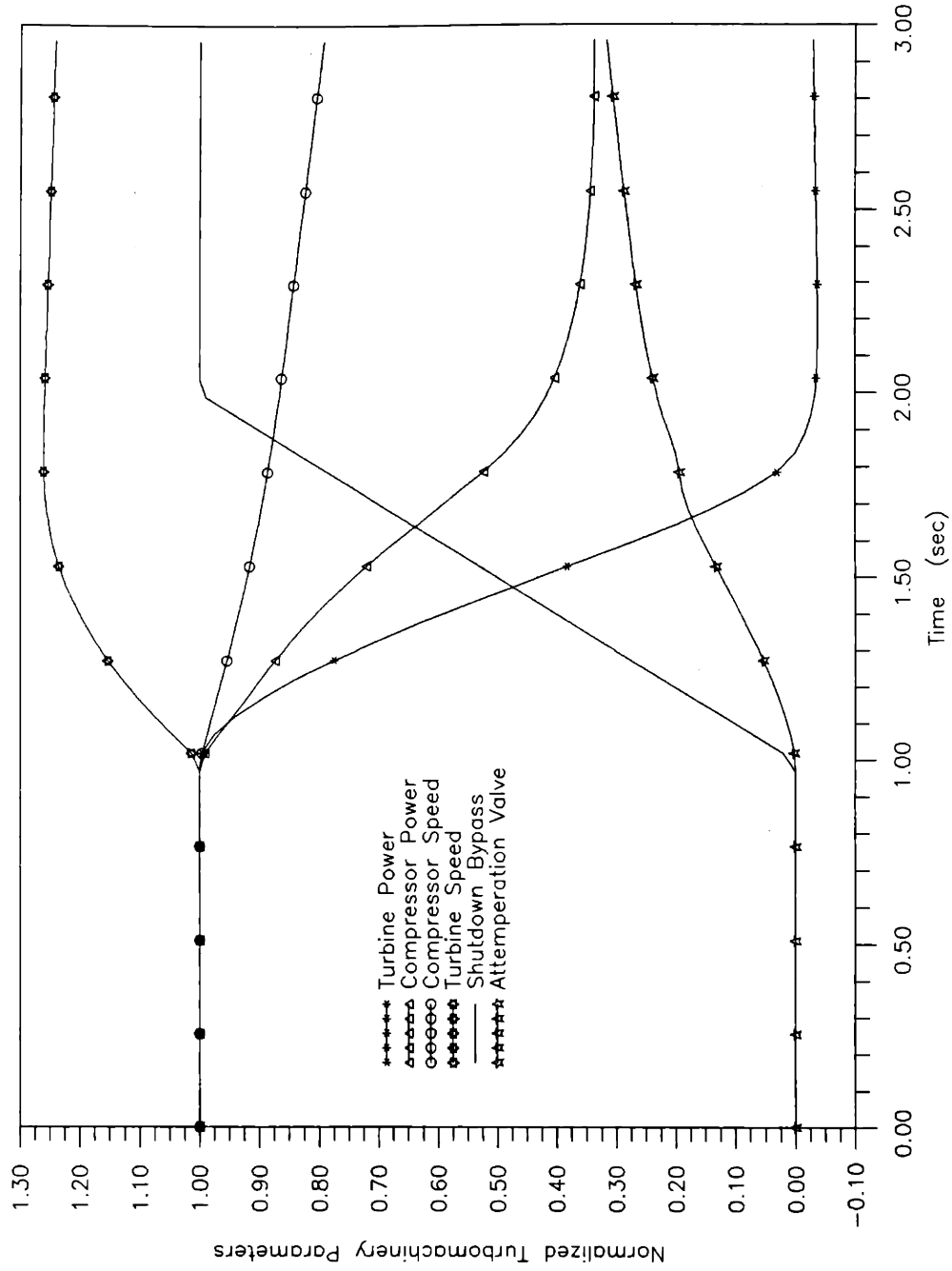

Figure 5.7 (a) Turbomachine parameters in shutdown process in case of a shaft break

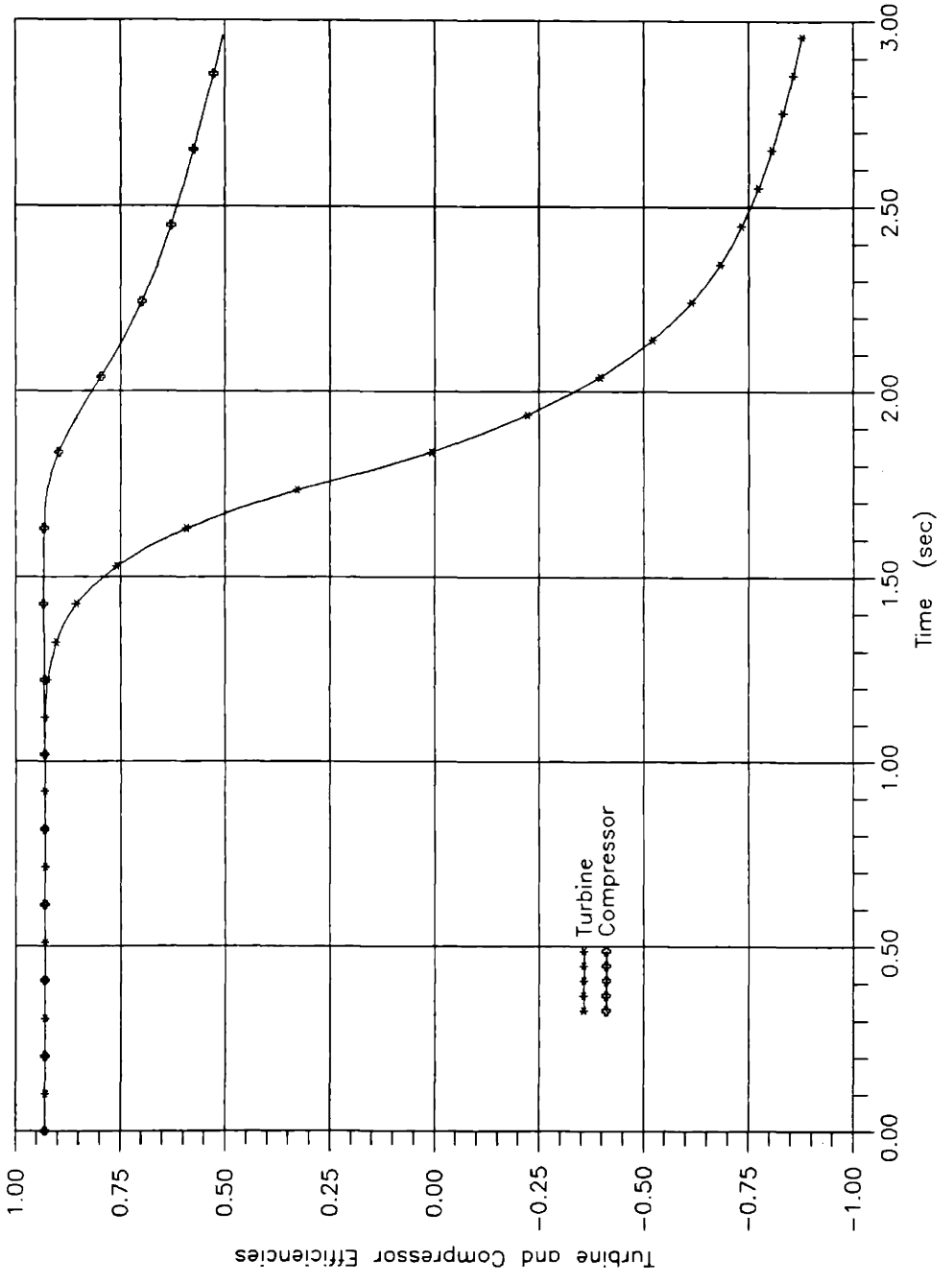

Figure 5.7 (b) Turbine and compressor pressure ratios during shutdown process in case of a shaft break

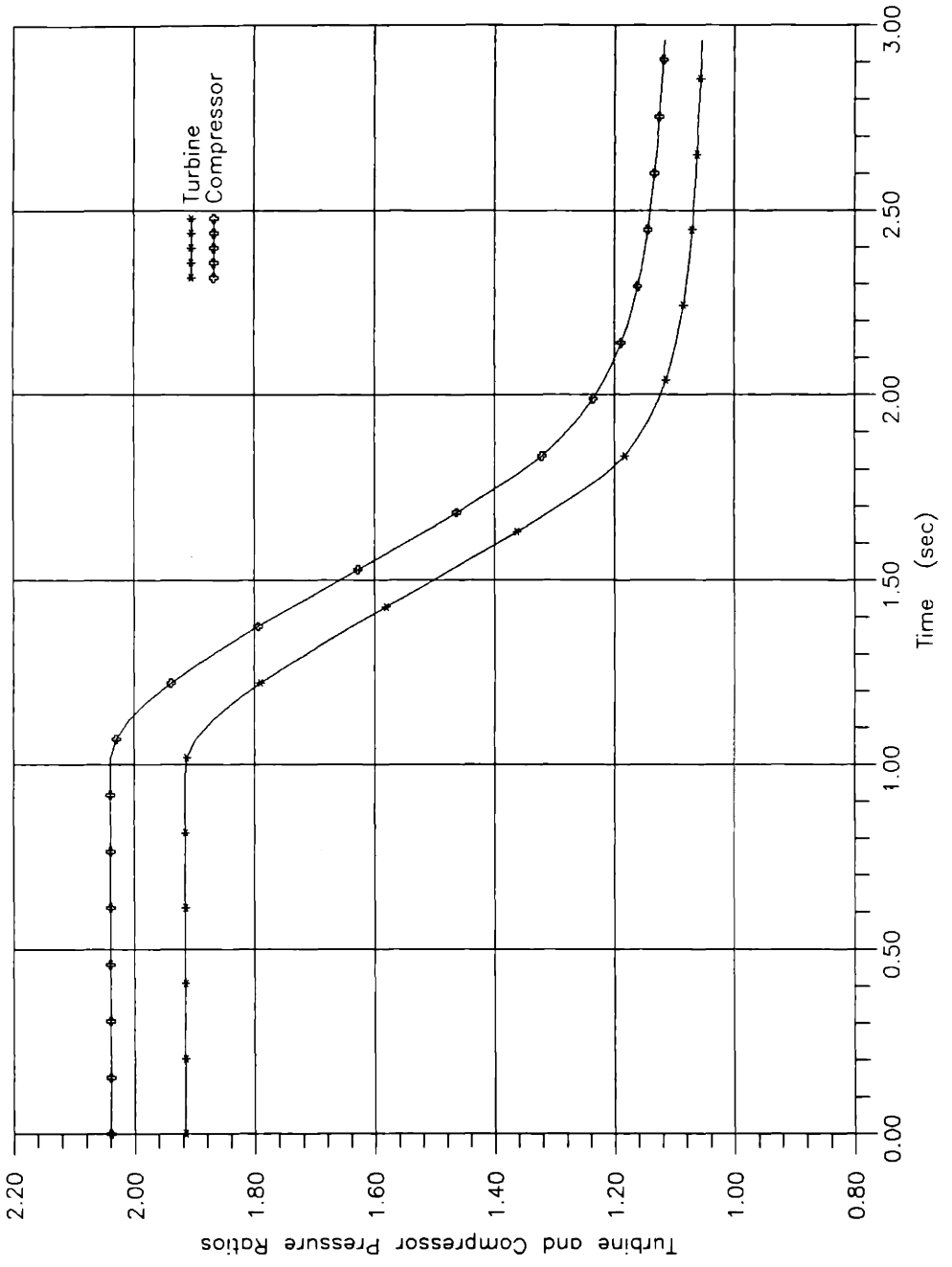

Figure 5.7 (c) Turbine and compressor efficiencies during shutdown process in case of a shaft break

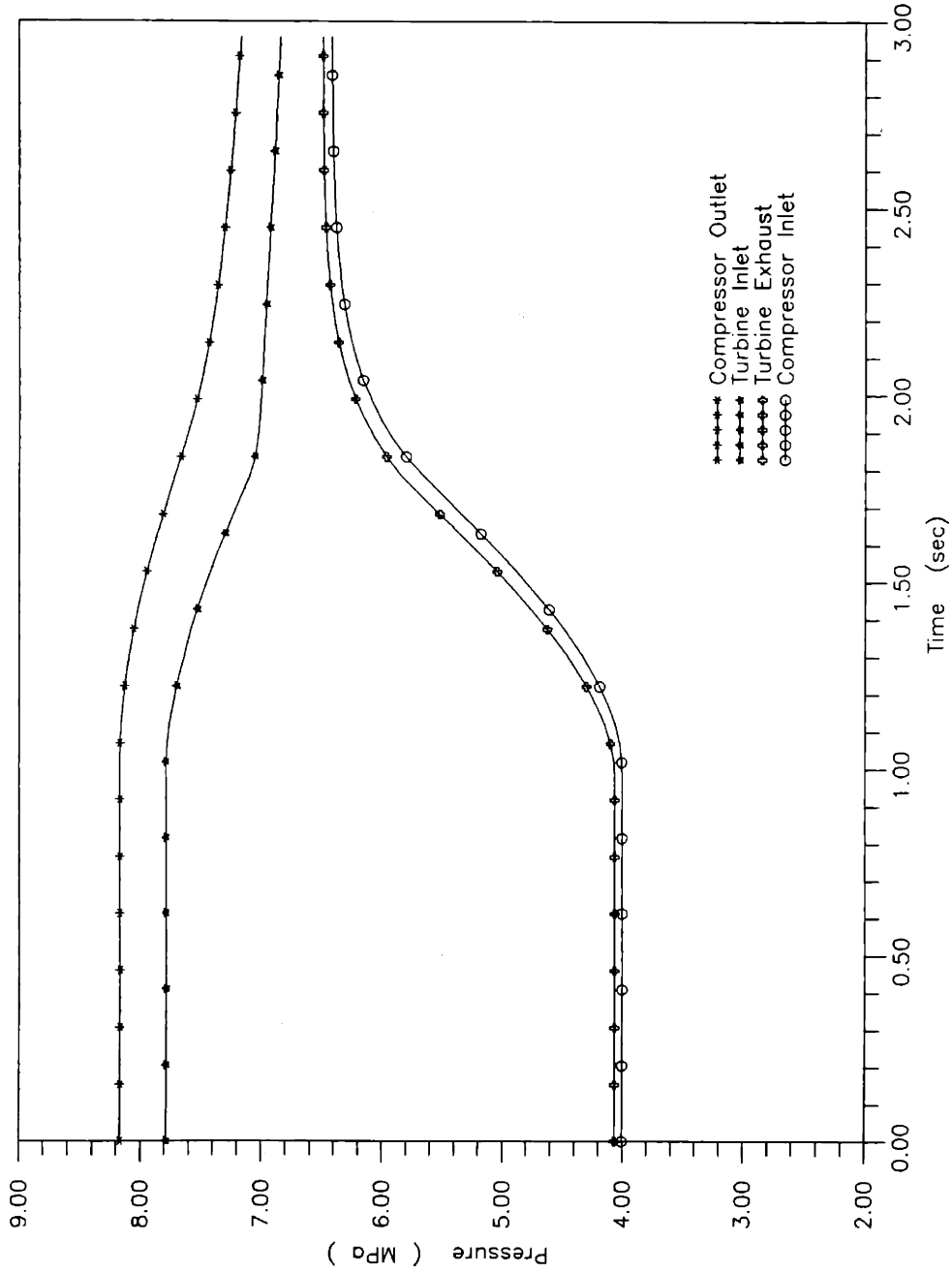

Figure 5.7 (d) Pressure transient responses during shutdown process in case of a shaft break

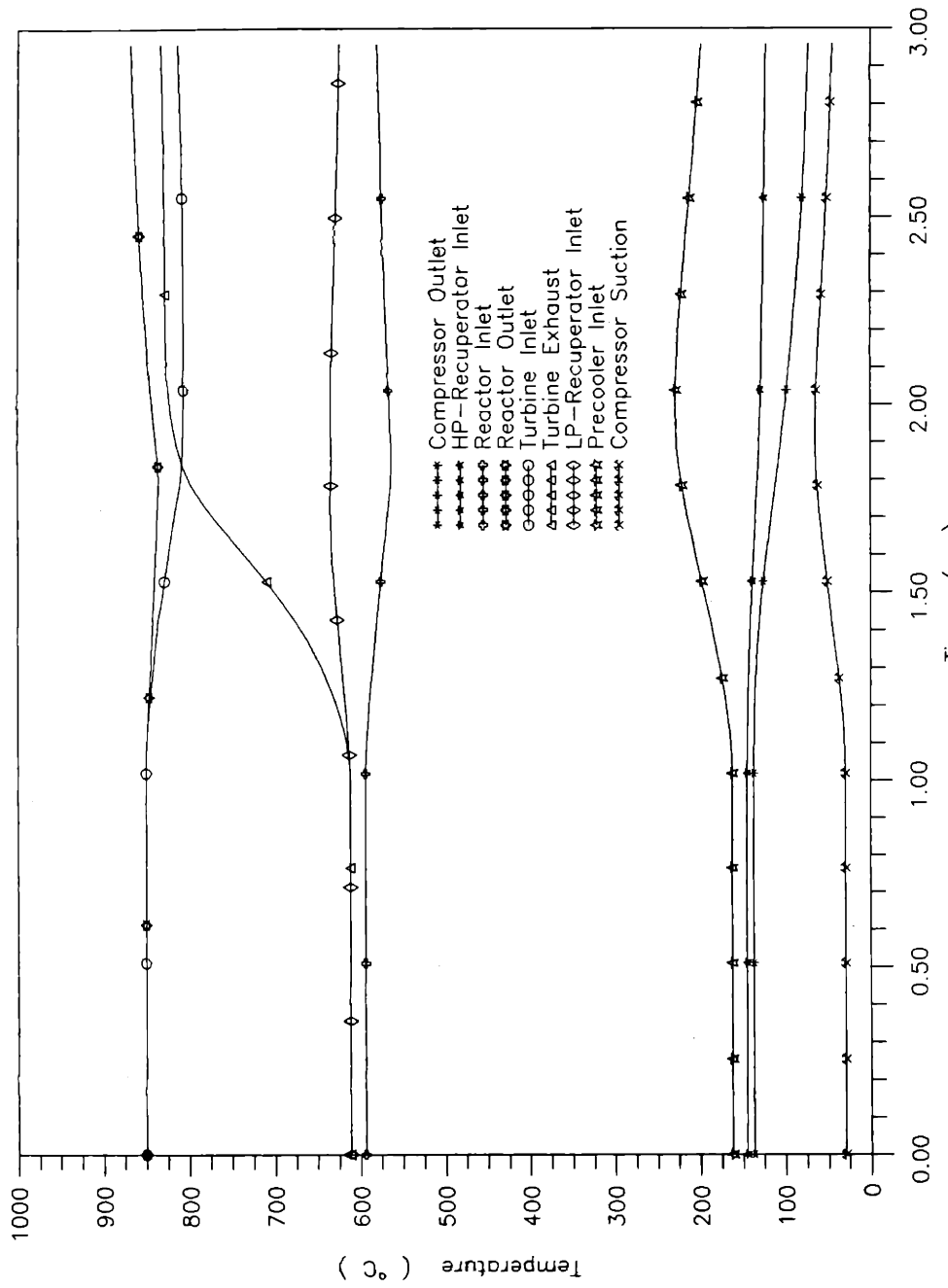

Figure 5.7 (e) Temperature transient responses during shutdown process in case of a shaft break

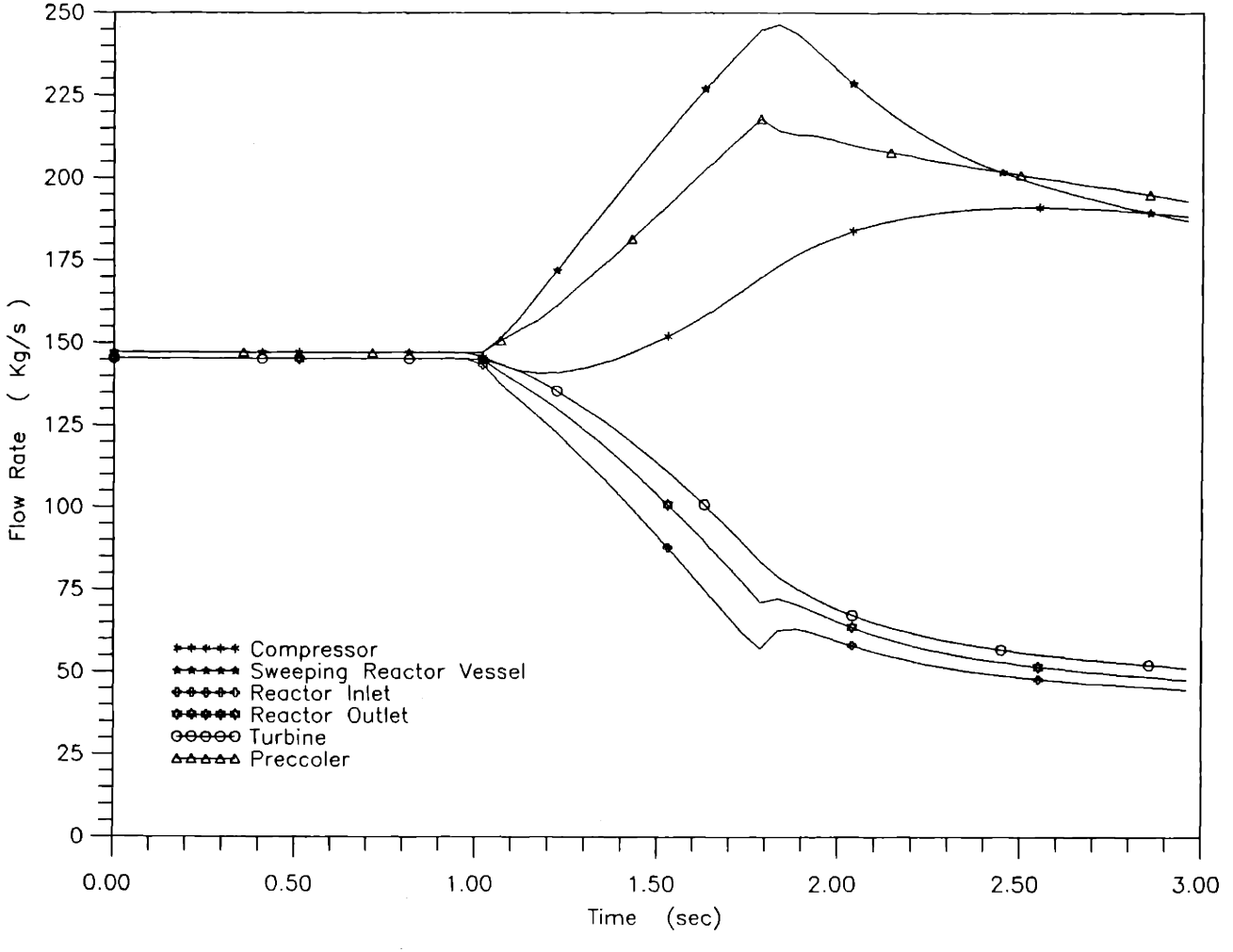

Figure 5.7 (f) Flow transient responses during shutdown process in case of a shaft break

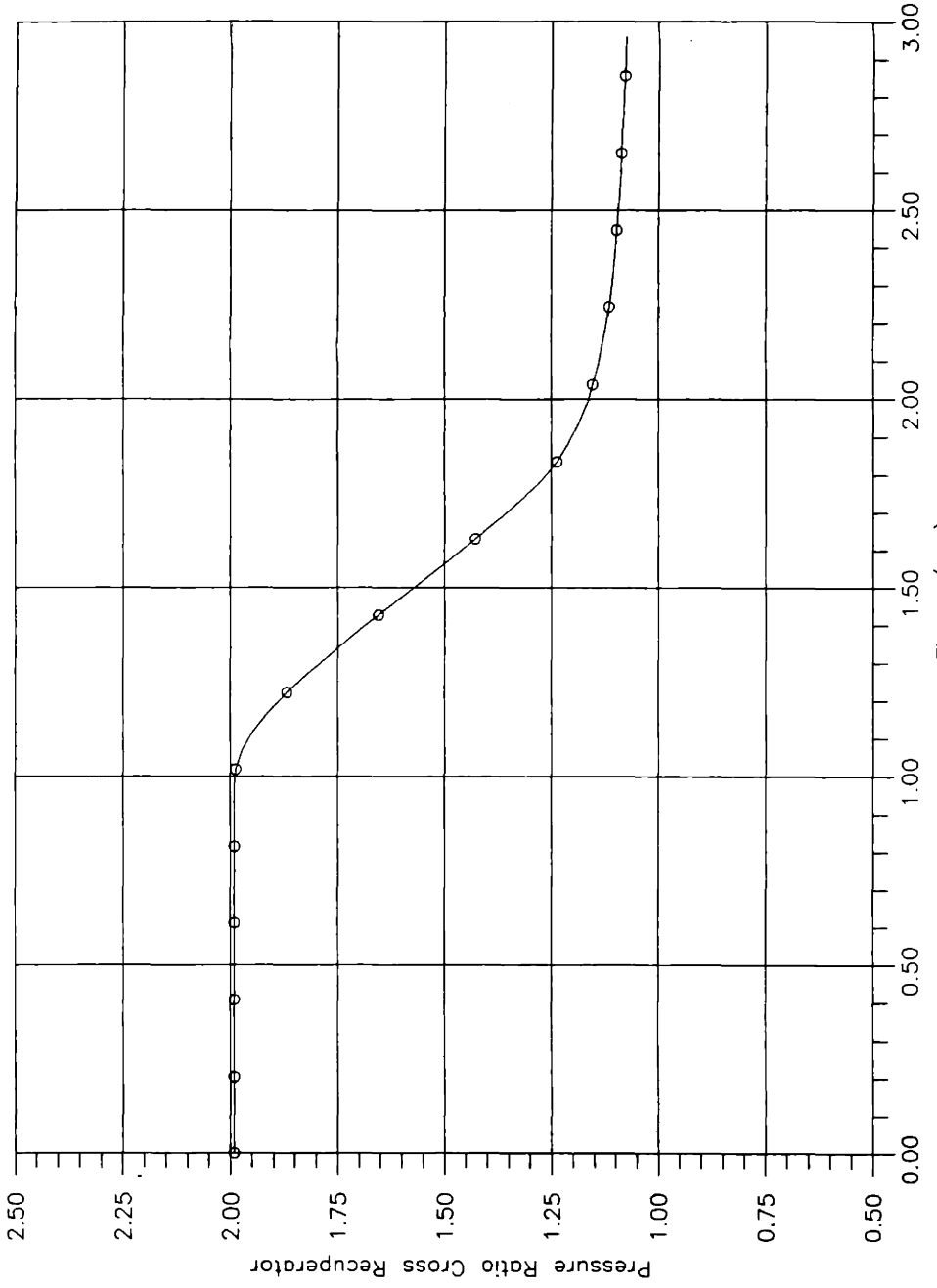

Figure 5.7 (g) Transient pressure difference across the wall of the recuperator during shutdown process in case of a shaft break

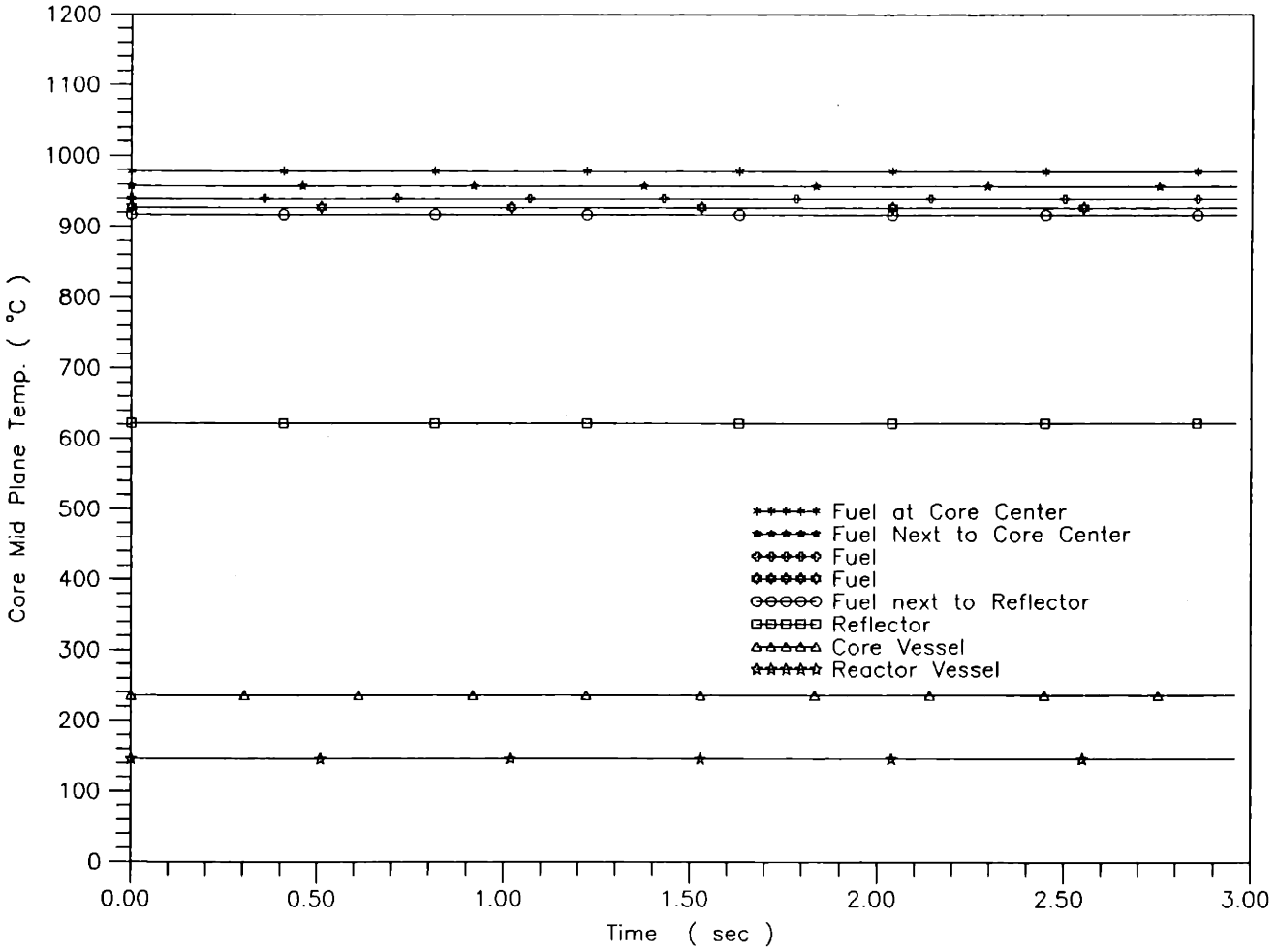

Figure 5.7 (h) Radial temperature transient responses in the core mid plane during shutdown process in case of a shaft break

Figure 5.7 (g) shows the transient behavior of the pressure difference across the wall of the recuperator. As can be seen, the pressure difference is largest prior to the loop shutdown. During the shutdown, the pressure difference experiences a very smooth reduction and gradually approaches equilibrium between the helium flows at the two sides. Therefore, there is no hazardous pressure transient imposed on the recuperator metallic wall.

It is possible to reduce turbine overspeed by choosing the alternative rotor configuration as shown in Figures 5.6 (b) and (c). The new rotor configuration situates the turbine between the compressor and generator. Two potential scenarios of shaft failure associated with the new rotor configuration are illustrated in Figures 5.6 (b) and (c). It can be seen that the turbine rotor will always be connected with either the compressor or generator depending on the location of the shaft break. As a result, additional rotor inertia would become available to the turbine. This could extend the time window for the response of the shutdown bypass control and thus the overspeed of the rotor could be reduced. The complete sets of the simulation results for the two shaft break scenarios associated with the new rotor configuration are shown, respectively, in Figures 5.8 (a) to (h) and Figures 5.9 (a) to (h), which can be compared with the simulation results obtained for the previous rotor configuration.

5.2.2c Positive Reactivity Disturbance at Full Power

In case of inadvertent control rod withdrawal, positive reactivity would be inserted into the core. In the MGR-GT reactor, the worth of the positive reactivity of the control rods at full power is 0.35% which is the amount of reactivity reserved for reactor power regulation near full power operation.

The addition of the positive reactivity into the core causes neutron flux, thus the core power, to increase. The reactor is scrammed by the PPS on the sensor signal indicating that

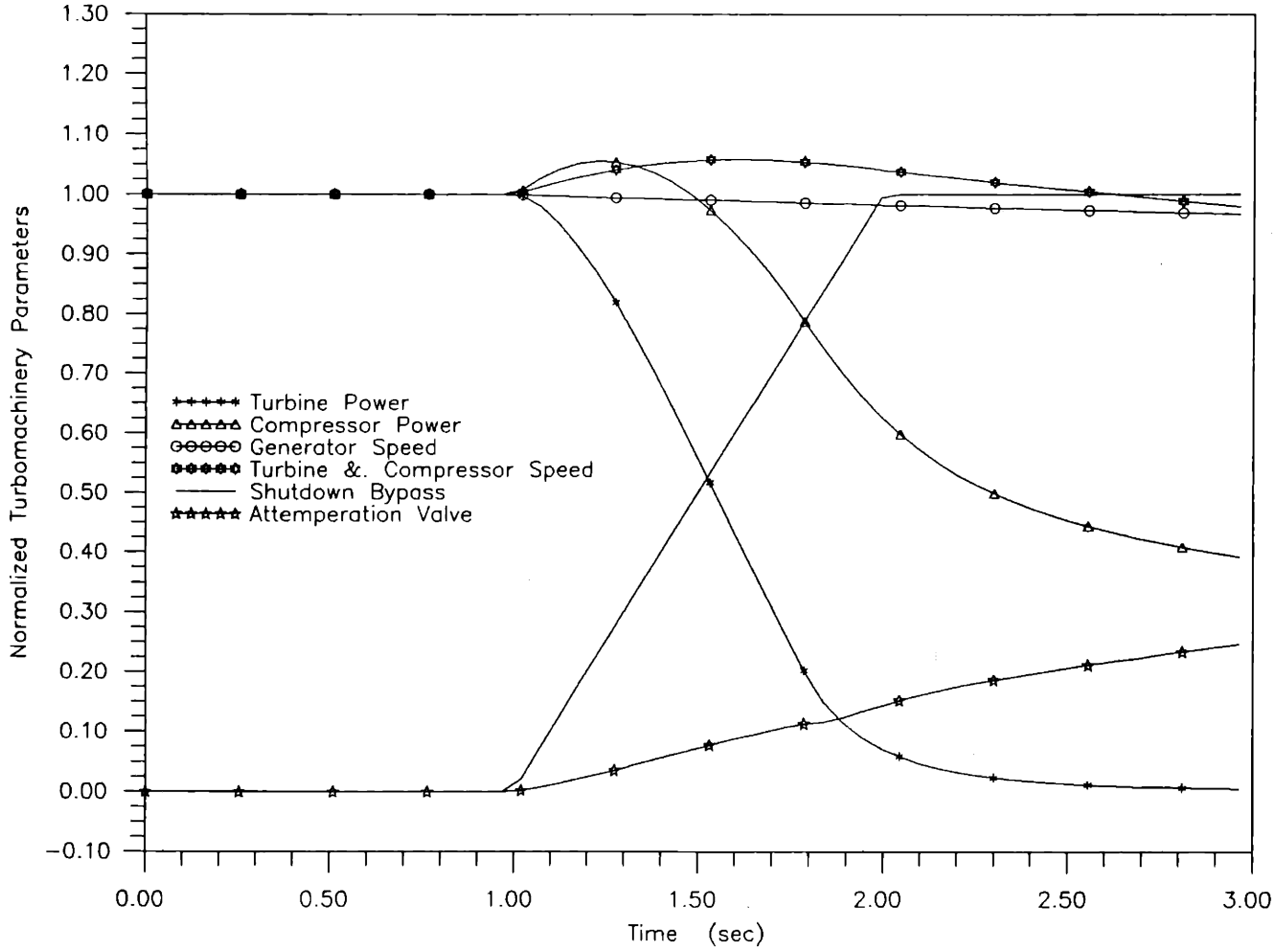

Figure 5.8 (a) Turbomachine parameters in shutdown process in case of the shaft break between turbine and generator in the alternate rotor configuration

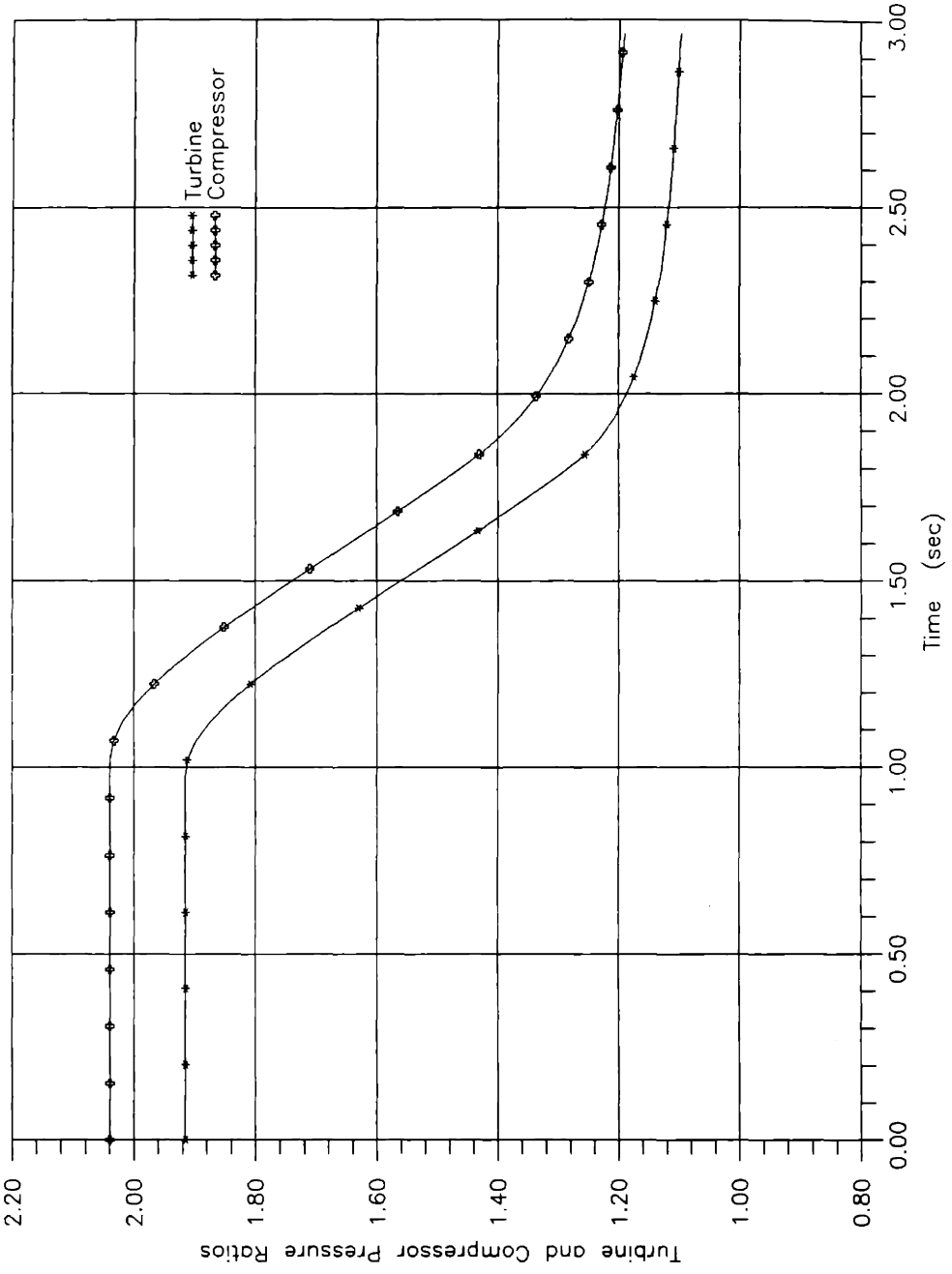

Figure 5.8 (b) Turbine and compressor pressure ratios during shutdown process in case of the shaft break between turbine and generator in the alternate rotor configuration

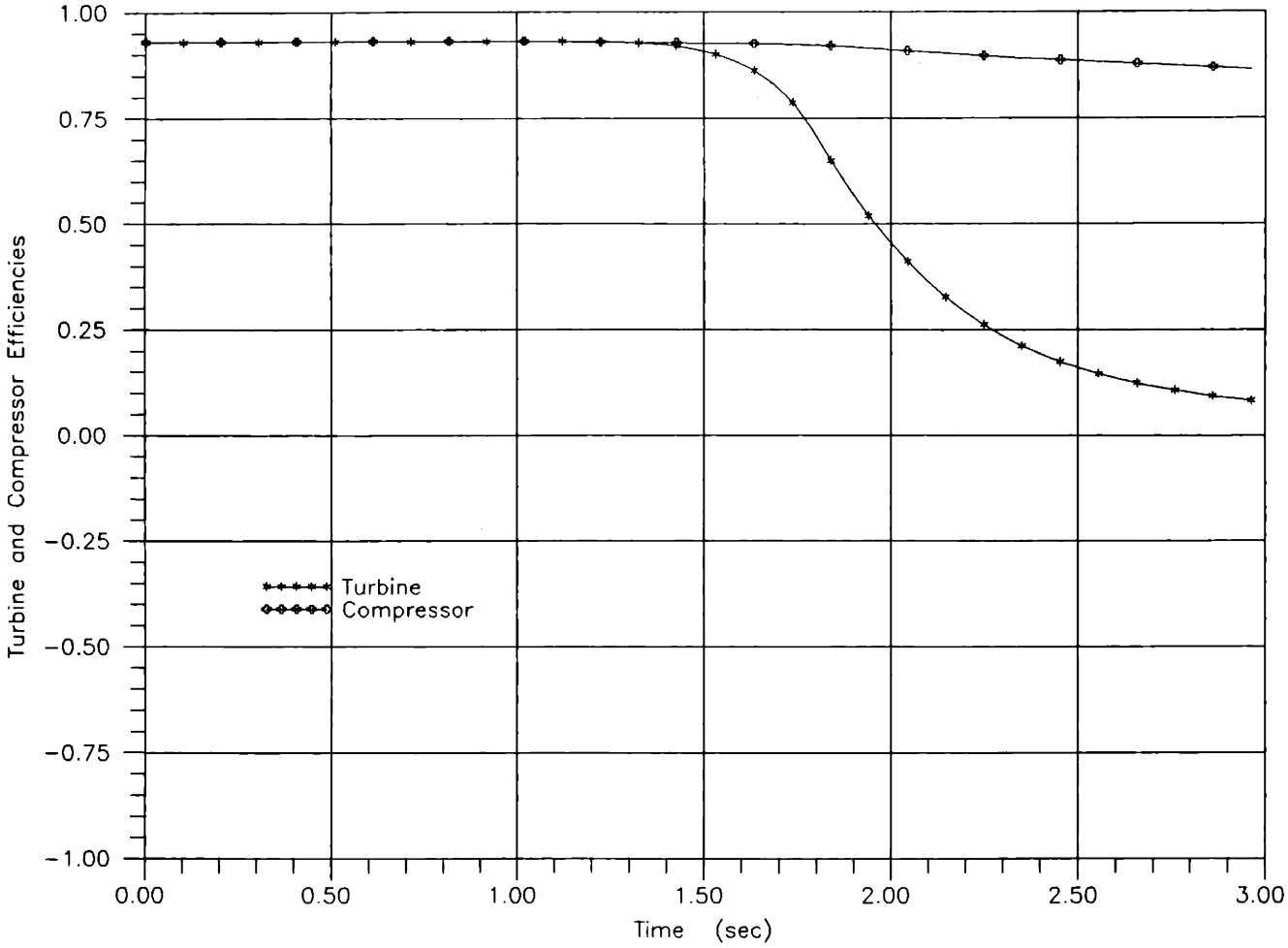

Figure 5.8 (c) Turbine and compressor efficiencies during shutdown process in case of the shaft break between turbine and generator in alternate rotor configuration

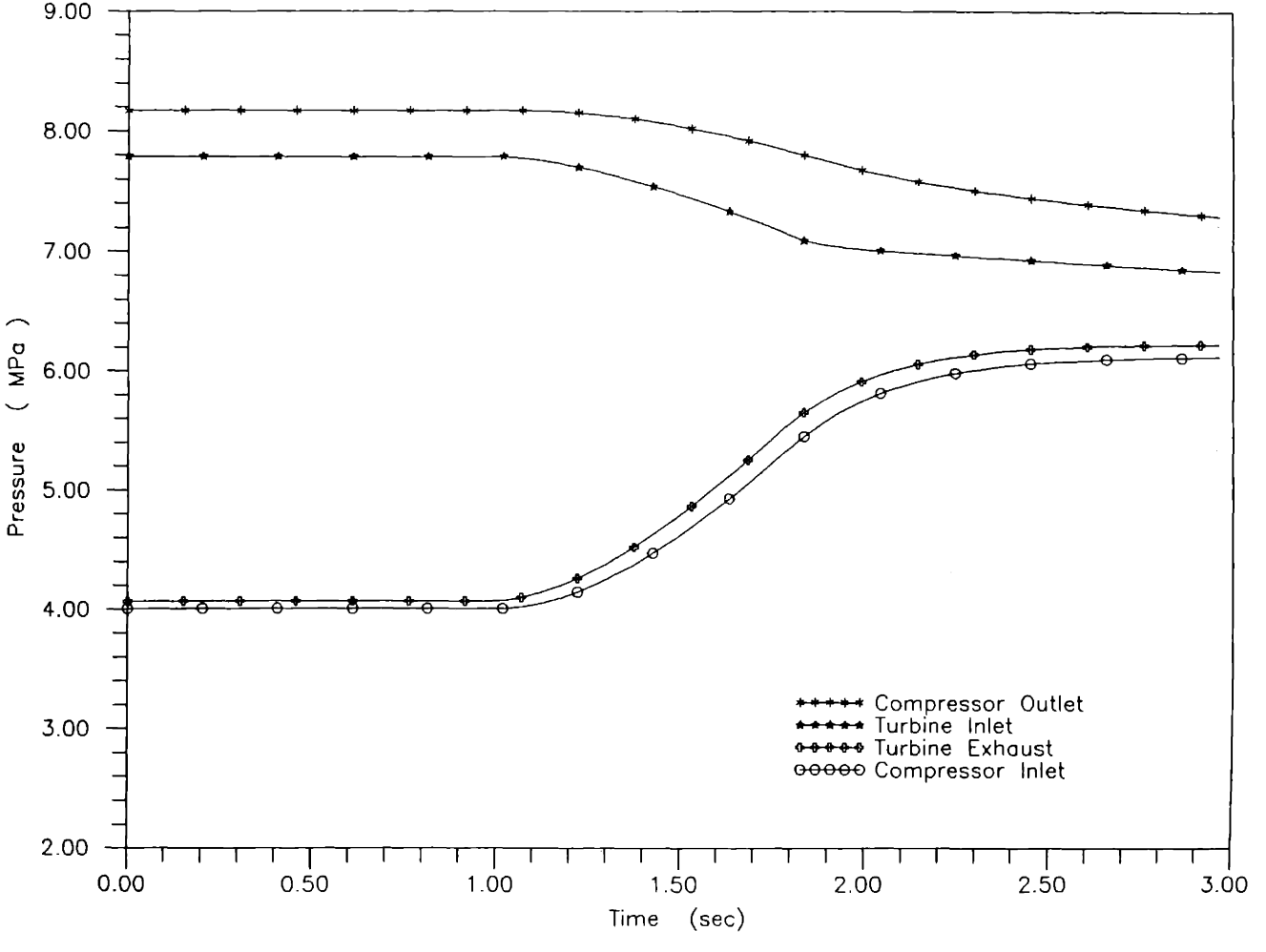

Figure 5.8 (d) Pressure transient responses during shutdown process in case of the shaft break between turbine and generator in the alternate rotor configuration

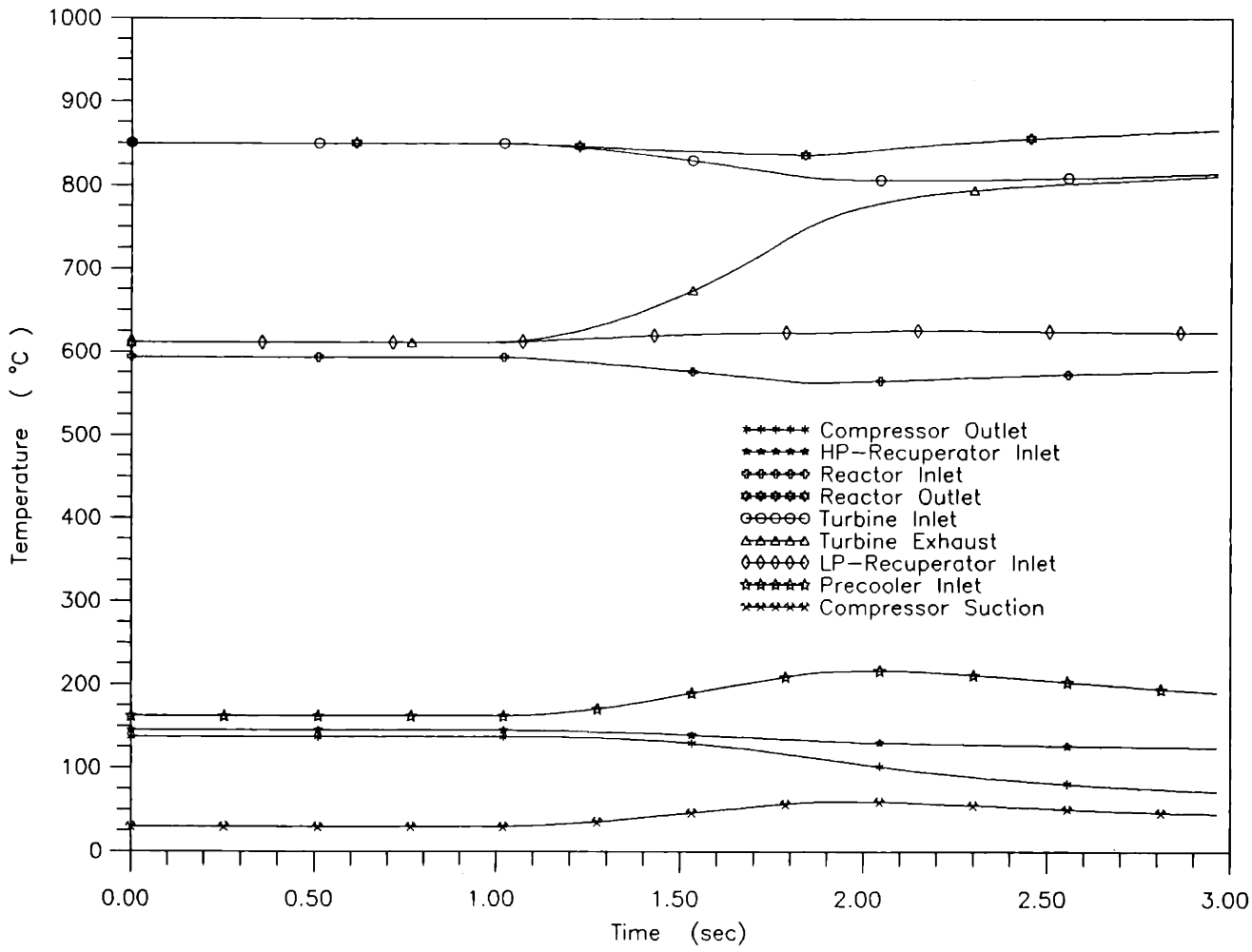

Figure 5.8 (e) Temperature transient responses during shutdown process in case of the shaft break between turbine and generator in the alternate rotor configuration

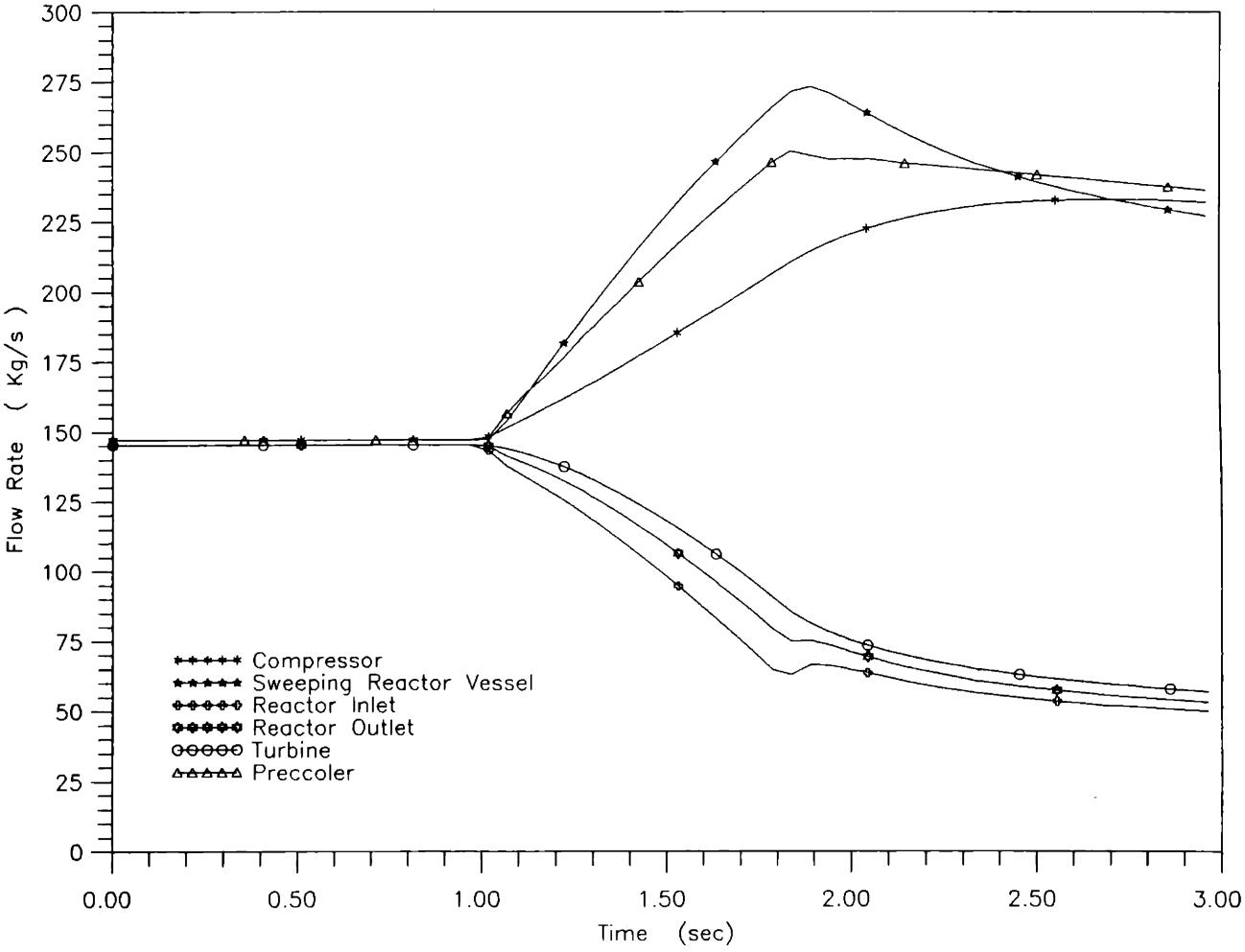

Figure 5.8 (f) **Flow transient responses during shutdown process in case of the shaft break between turbine and generator in the alternate rotor configuration**

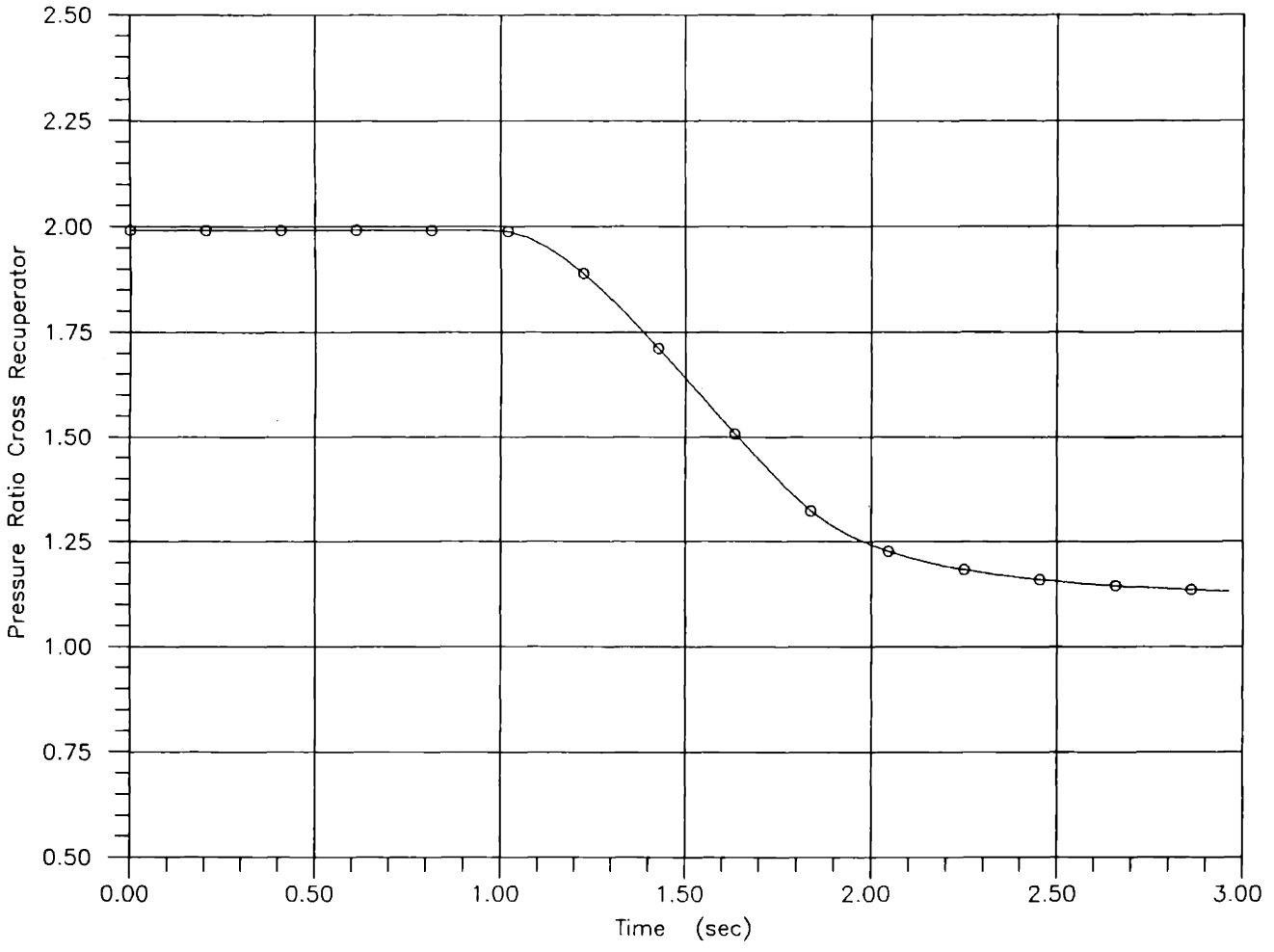

Figure 5.8 (g) **Transient pressure difference across the wall of the recuperator during shutdown process in case of the shaft break between turbine and generator in the alternate rotor configuration**

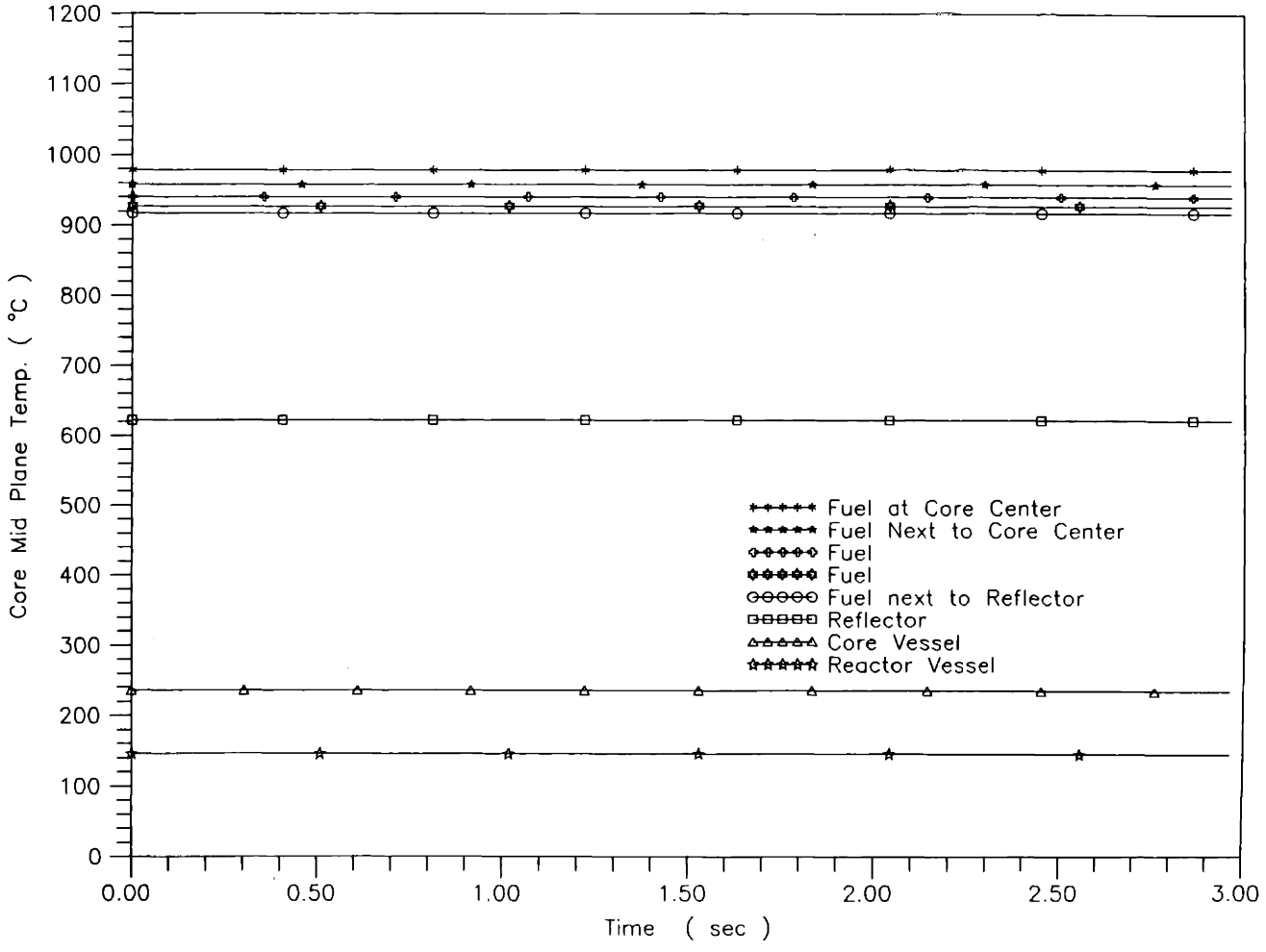

Figure 5.8 (h) Radial temperature transient responses in the core mid plane during shutdown process in case of the shaft break between turbine and generator in alternate rotor configuration

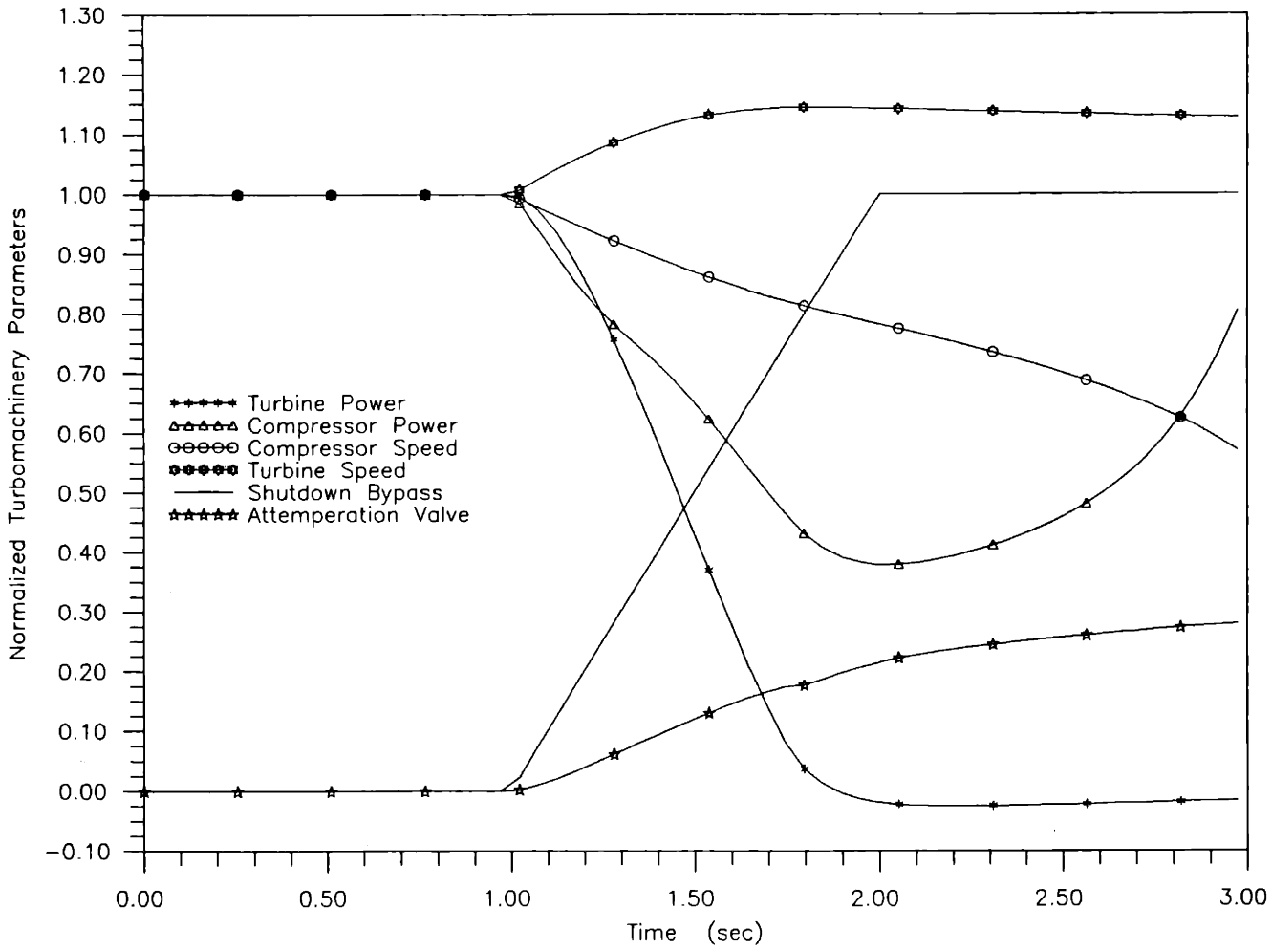

Figure 5.9 (a) Turbomachine parameters in shutdown process in case of the shaft break between turbine and compressor in the alternate rotor configuration

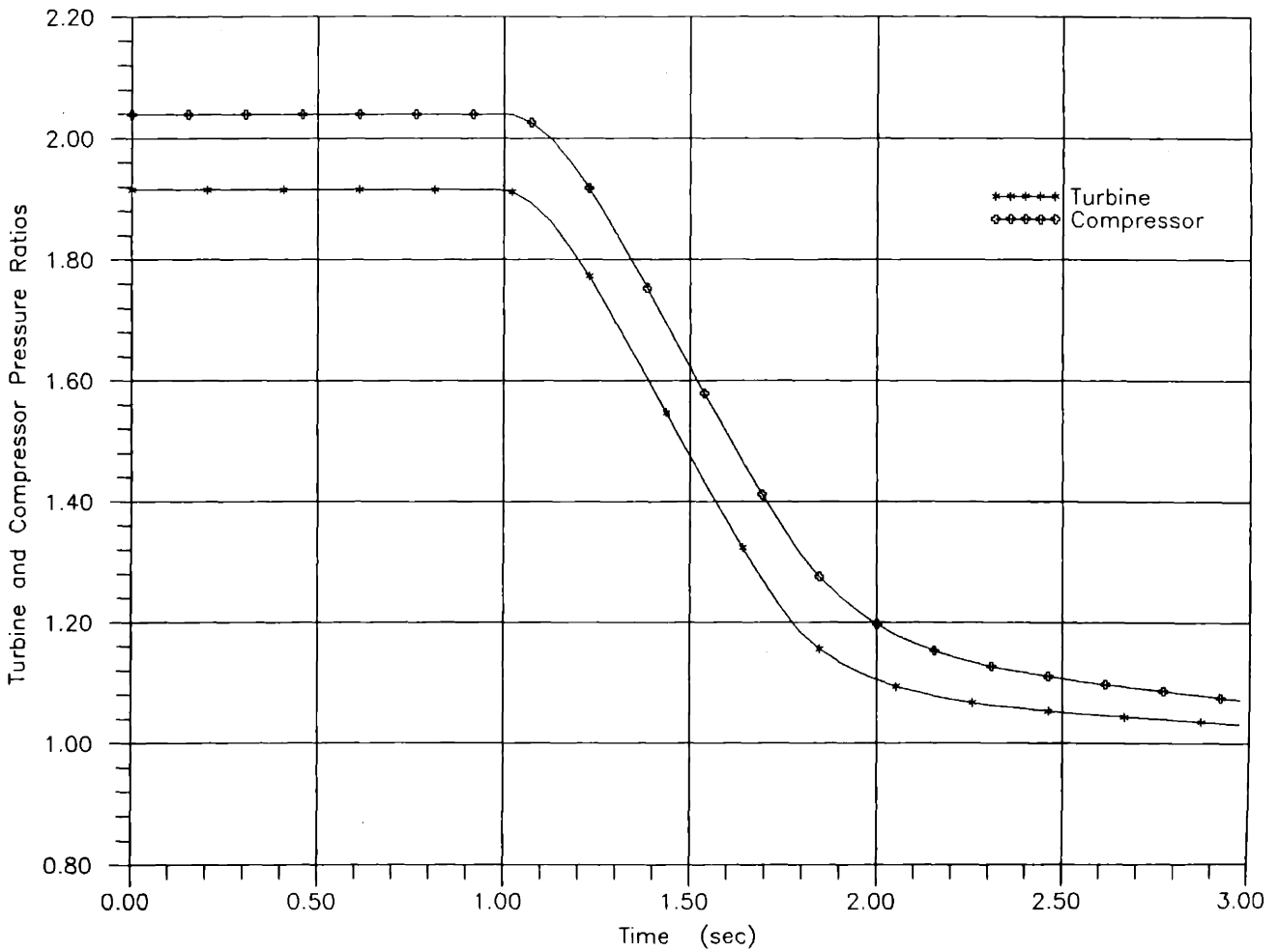

Figure 5.9 (b) Turbine and compressor pressure ratios during shutdown process in case of the shaft break between turbine and compressor in the alternate rotor configuration

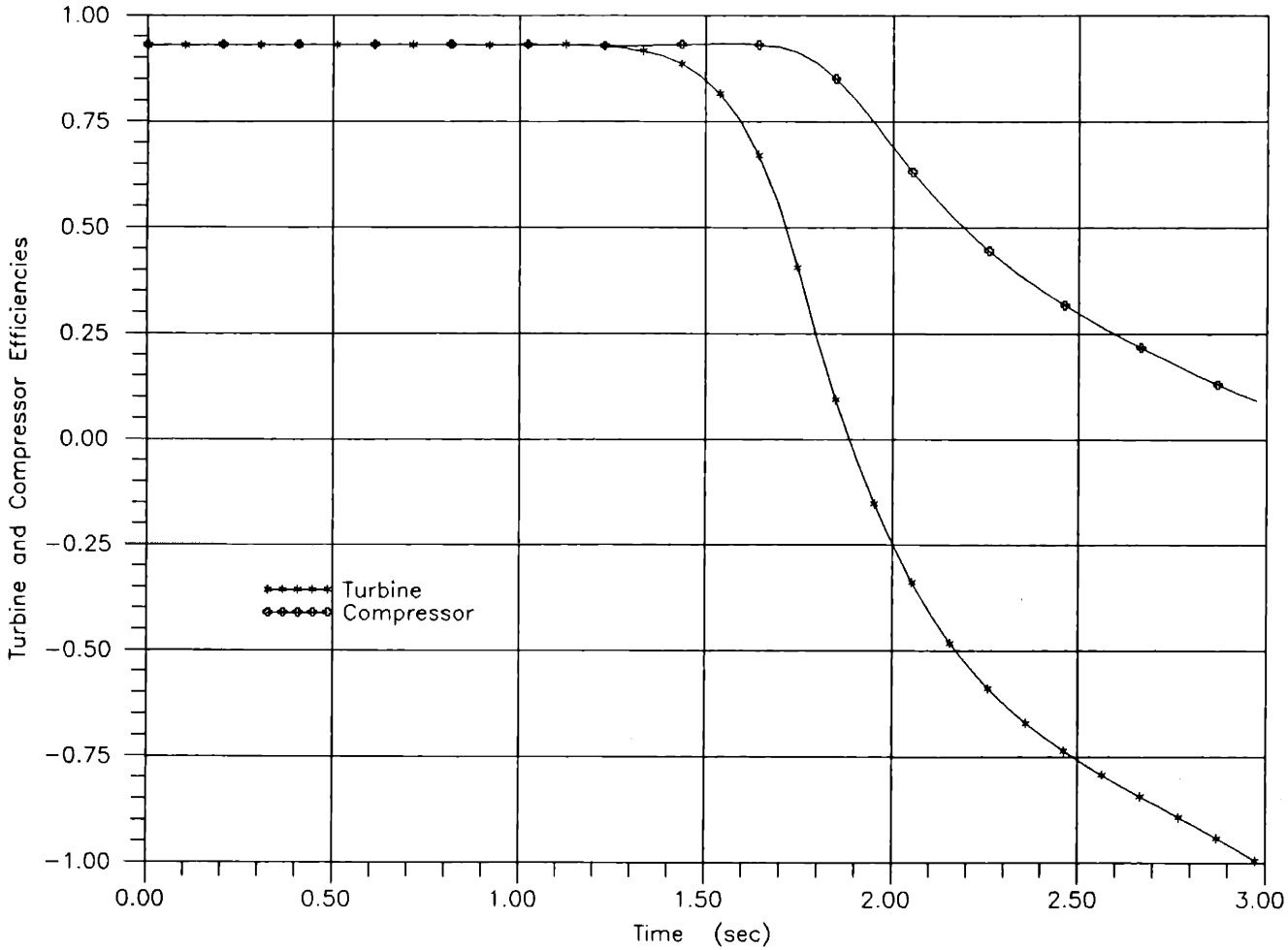

Figure 5.9 (c) Turbine and compressor efficiencies during shutdown process in case of the shaft break between turbine and compressor in alternate rotor configuration

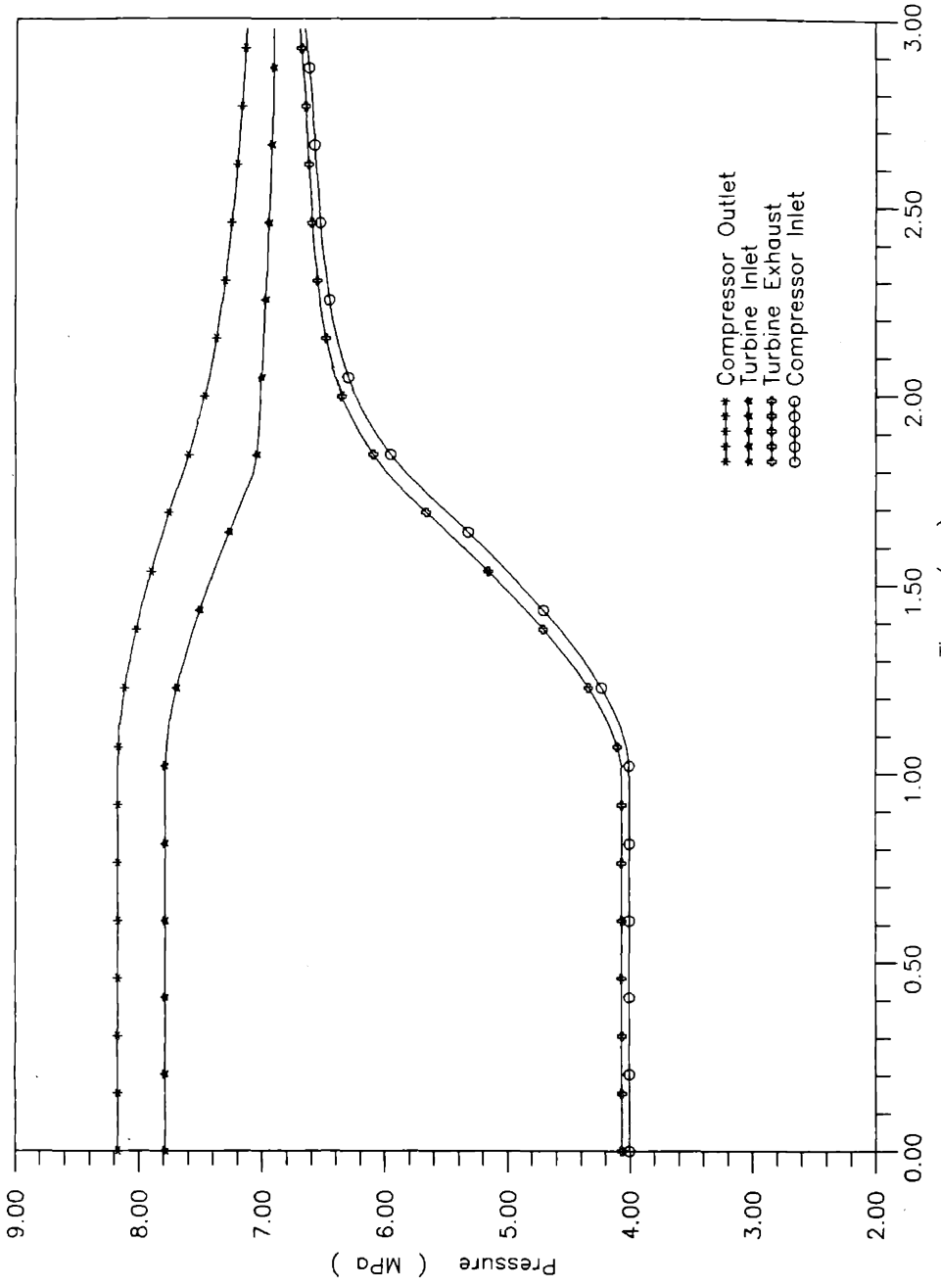

Figure 5.9 (d) Pressure transient responses during shutdown process in case of the shaft break between turbine and compressor in the alternate rotor configuration

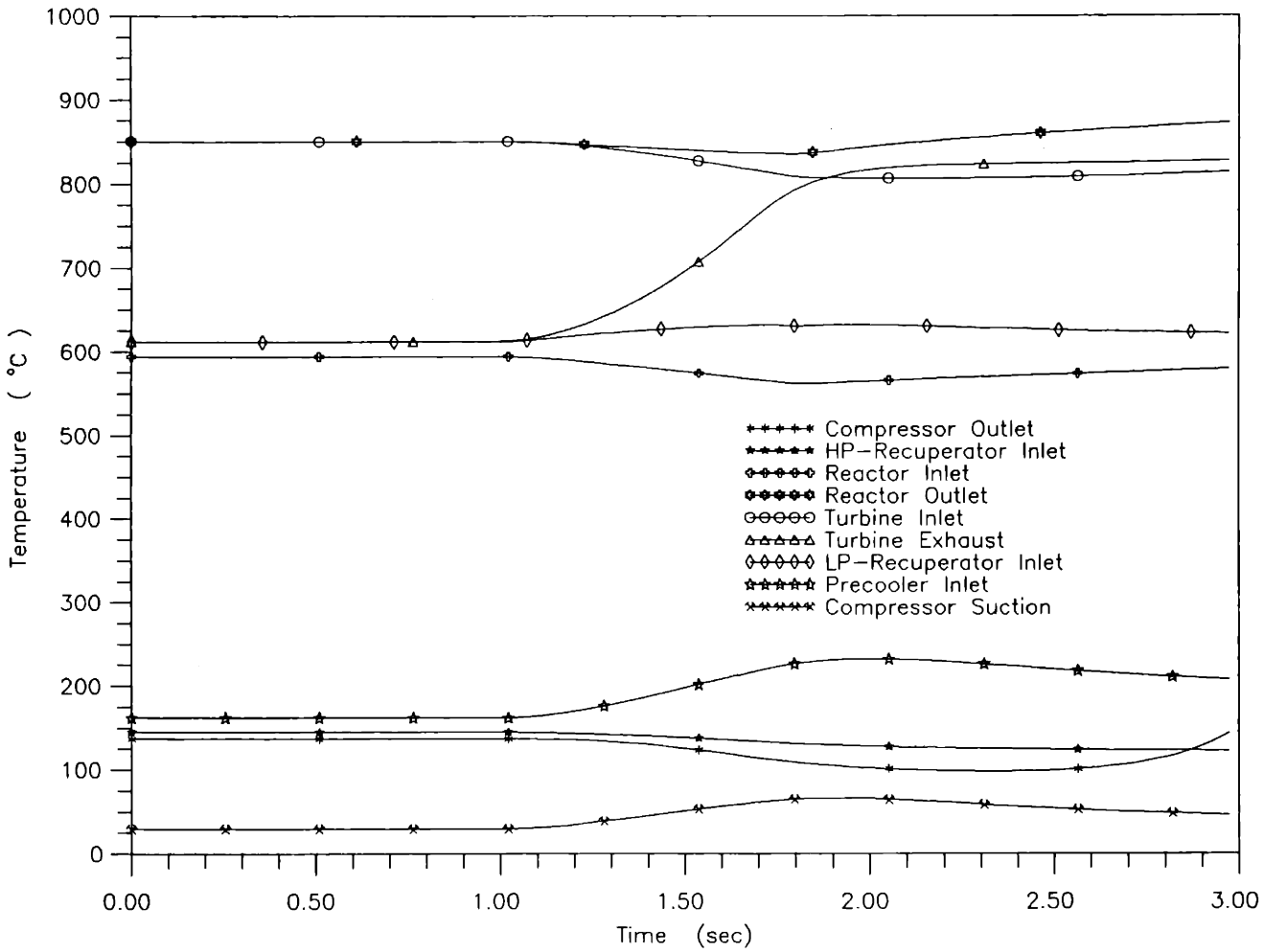

Figure 5.9 (e) Temperature transient responses during shutdown process in case of the shaft break between turbine and compressor in the alternate rotor configuration

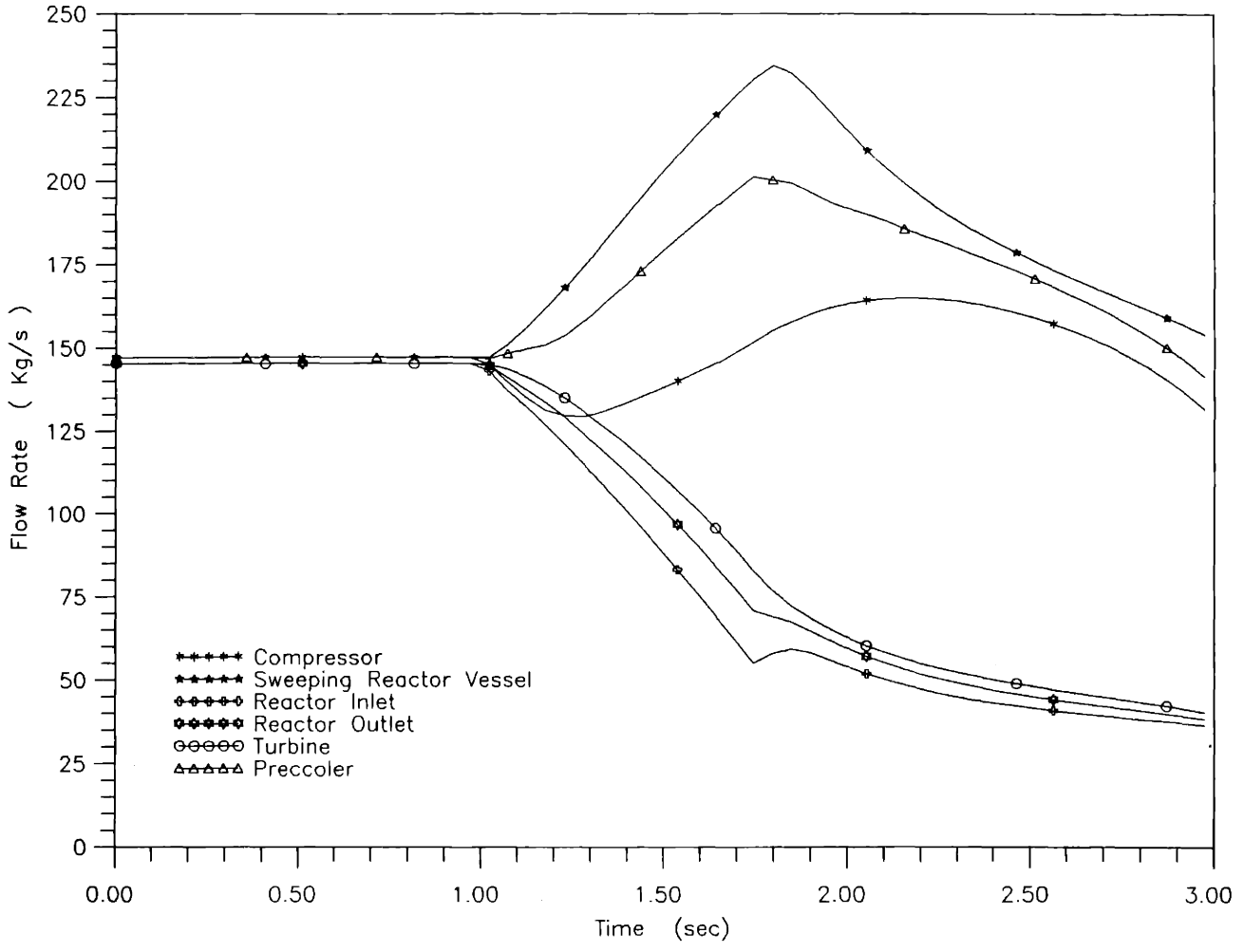

Figure 5.9 (f) **Flow transient responses during shutdown process in case of the shaft break between turbine and compressor in the alternate rotor configuration**

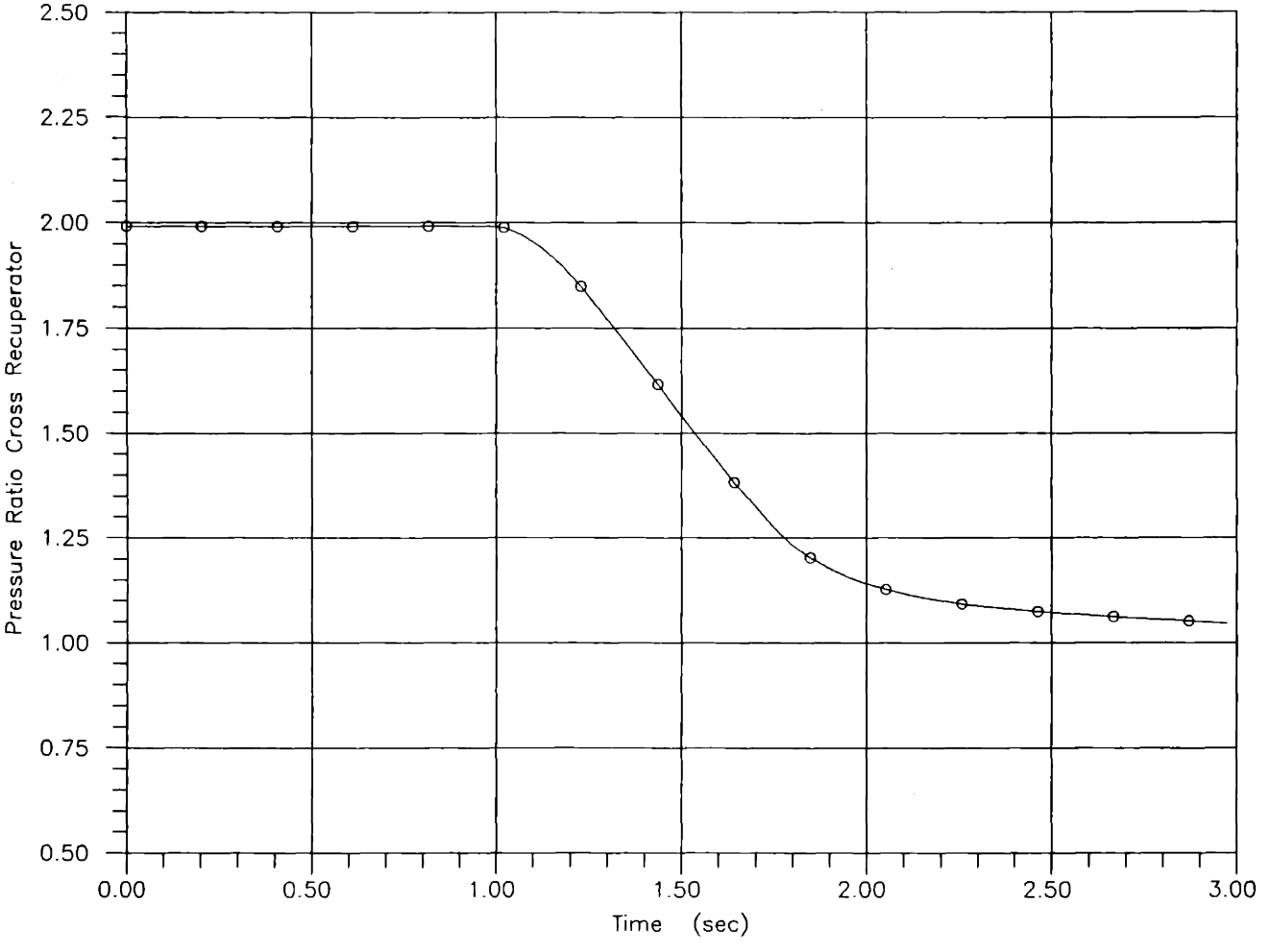

Figure 5.9 (g) Transient pressure difference across the wall of the recuperator during shutdown process in case of the shaft break between turbine and compressor in the alternate rotor configuration

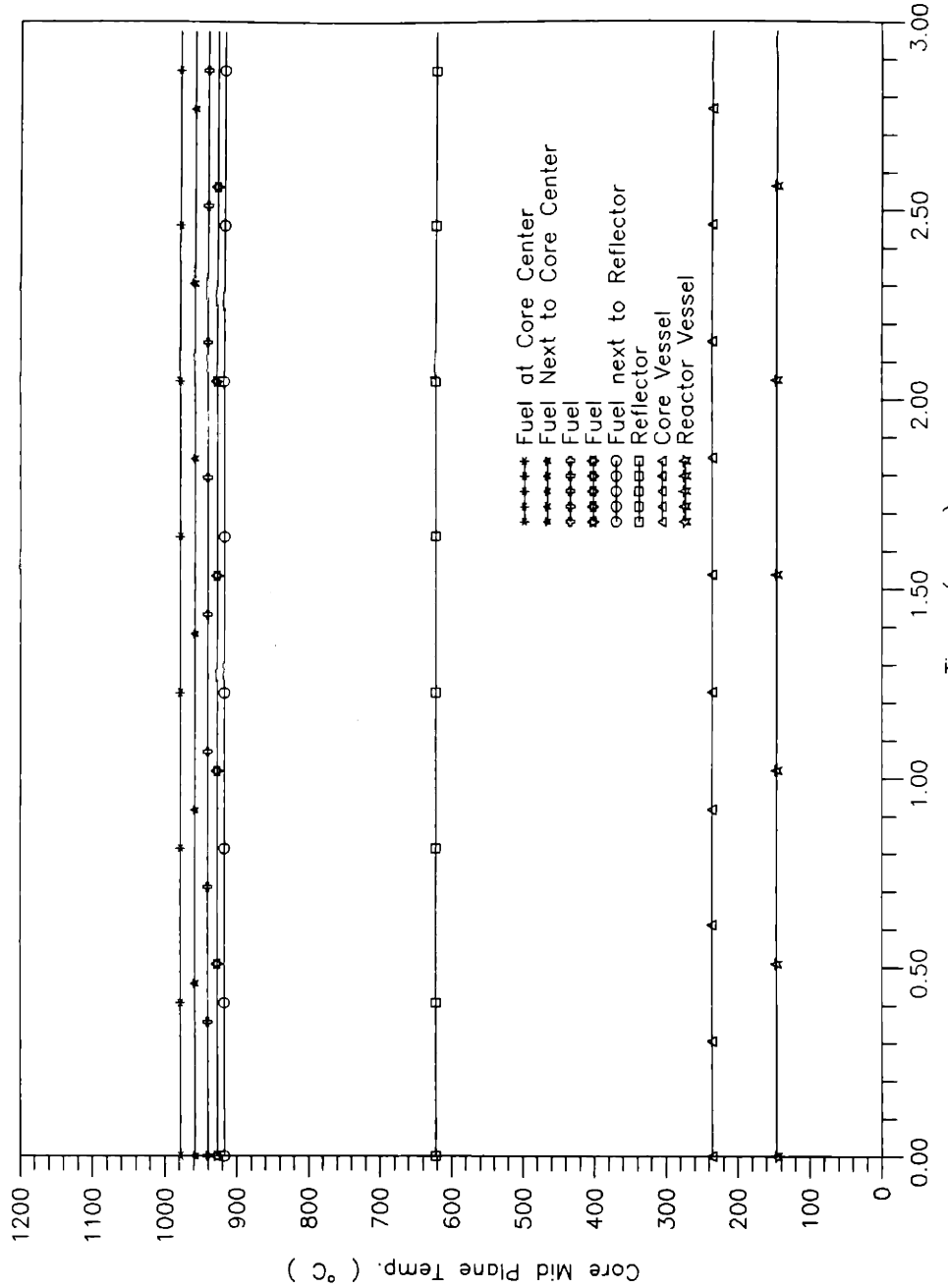

Figure 5.9 (h) Radial temperature transient responses in the core mid plane during shutdown process in case of the shaft break between turbine and compressor in alternate rotor configuration

the core outlet temperature 50°C in excess of nominal. The reactor shutdown is accomplished by the re-insertion of the control rods. Simultaneously, the loop is shutdown to idle state to allow continuous circulation of the helium for decay heat removal.

Figure 5.10 (a) shows the reactor power and reactivity developed for the withdrawal of all control rods with scram. The reactivity shown is the total reactivity contributed by the control rods, temperature feedback, and fission product poisoning. Individual reactivity contributions are shown in Figure 5.10 (b). It can be seen that as the reactor control rods are withdrawn from the core, the reactor power increases rapidly to the maximum 182% of the nominal power. This power increase causes a maximum fuel temperature increase of less than 100°C as shown. The core temperature transient responses are shown in Figure 5.10 (c) for the radial temperature distribution in the core mid plane and Figure 5.10 (d) for the axial temperature distribution.

As the core temperatures decrease considerably, the temperature feedback of reactivity begins to dominate the total reactivity, as shown in Figure 5.10 (b). As the total reactivity becomes positive, the reactor regains criticality. However, the temperature feedback responds as a primary shutdown mechanism to setback the power, and subsequently stabilizes it at a low power level. The reactor criticality only causes a minor fuel temperature increase as shown in Figures 5.10 (c) and (d), largely due to the cooling effect of helium circulation through the core.

Figure 6.7 (e) shows the turbomachinery responses during the loop shutdown. The loop shutdown begins with the PPS to open the bypass valve at t = 70 sec, when the reactor is scrammed. The AC load is disconnected and the turbomachine is controlled at design speed. The turbine and compressor powers experience immediate reduction. The decrease of the turbine pressure ratio, as shown in Figure 5.10 (f), results in the temperature increase of the turbine exhaust flow, as shown in Figure 5.10 (g). To prevent the thermal shock at the

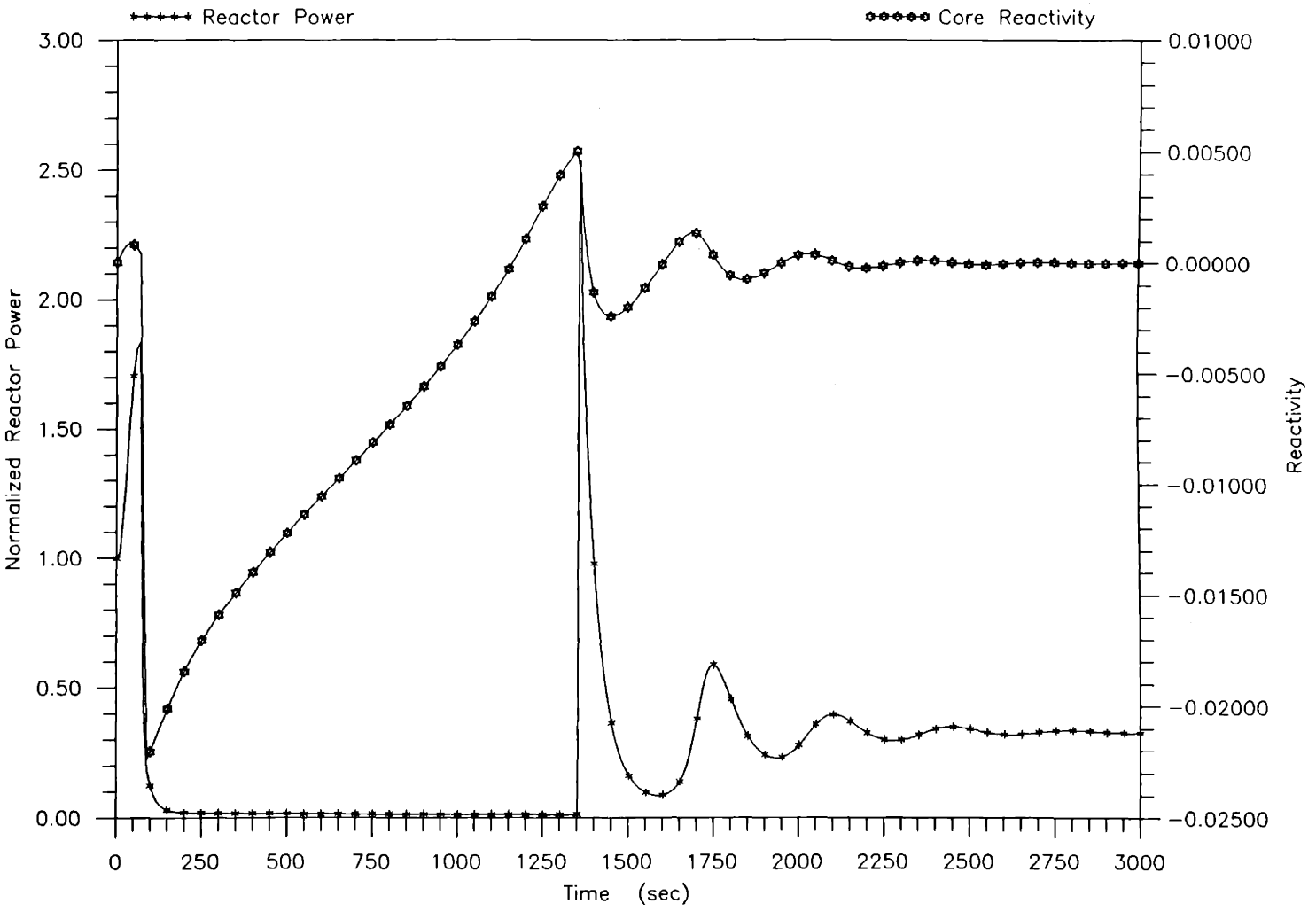

Figure 5.10(a) Reactor shutdown in case of control rod withdrawal at full power

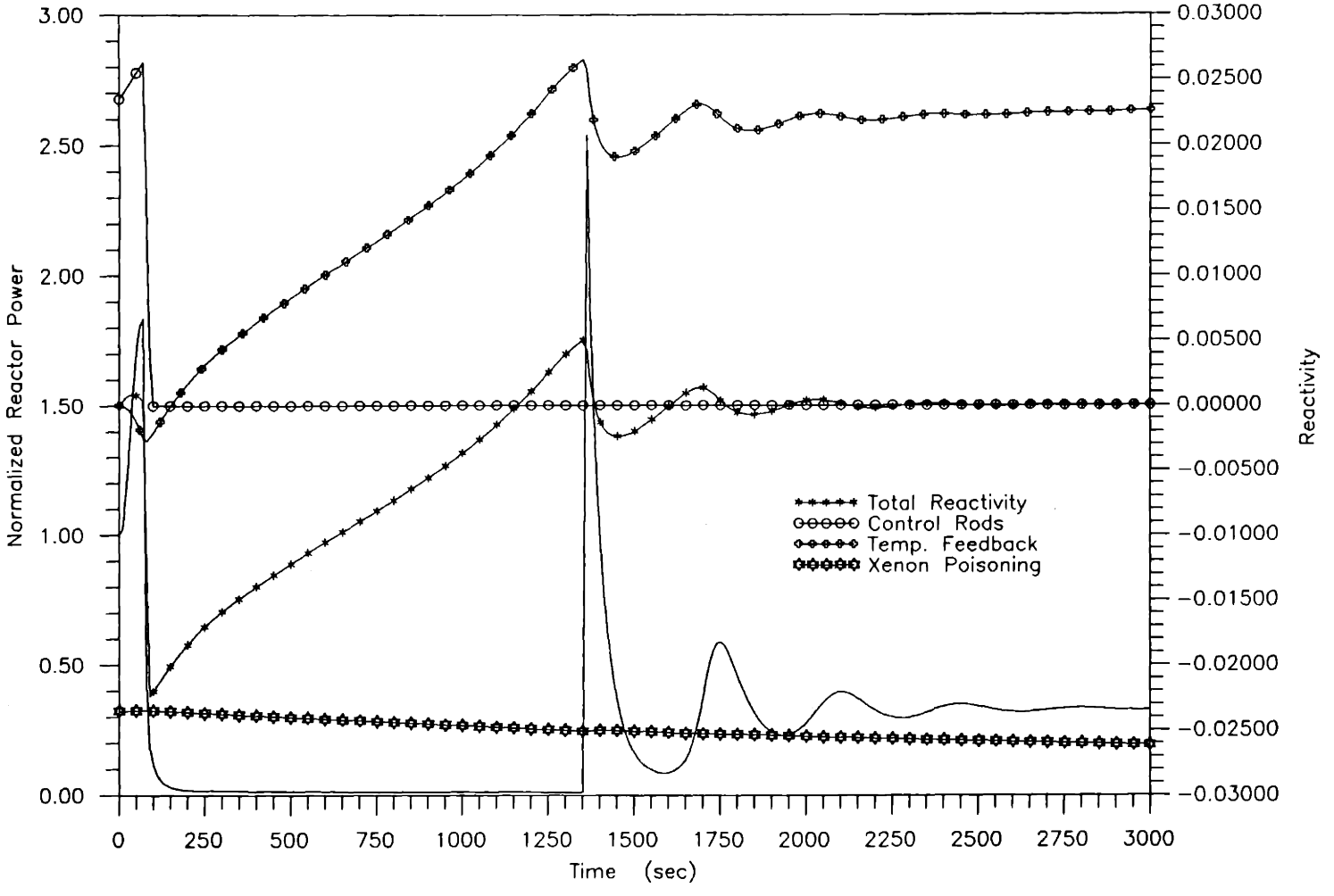

Figure 5.10(b) Reactor shutdown and reactivity contributions in case of control rod withdrawal at full power

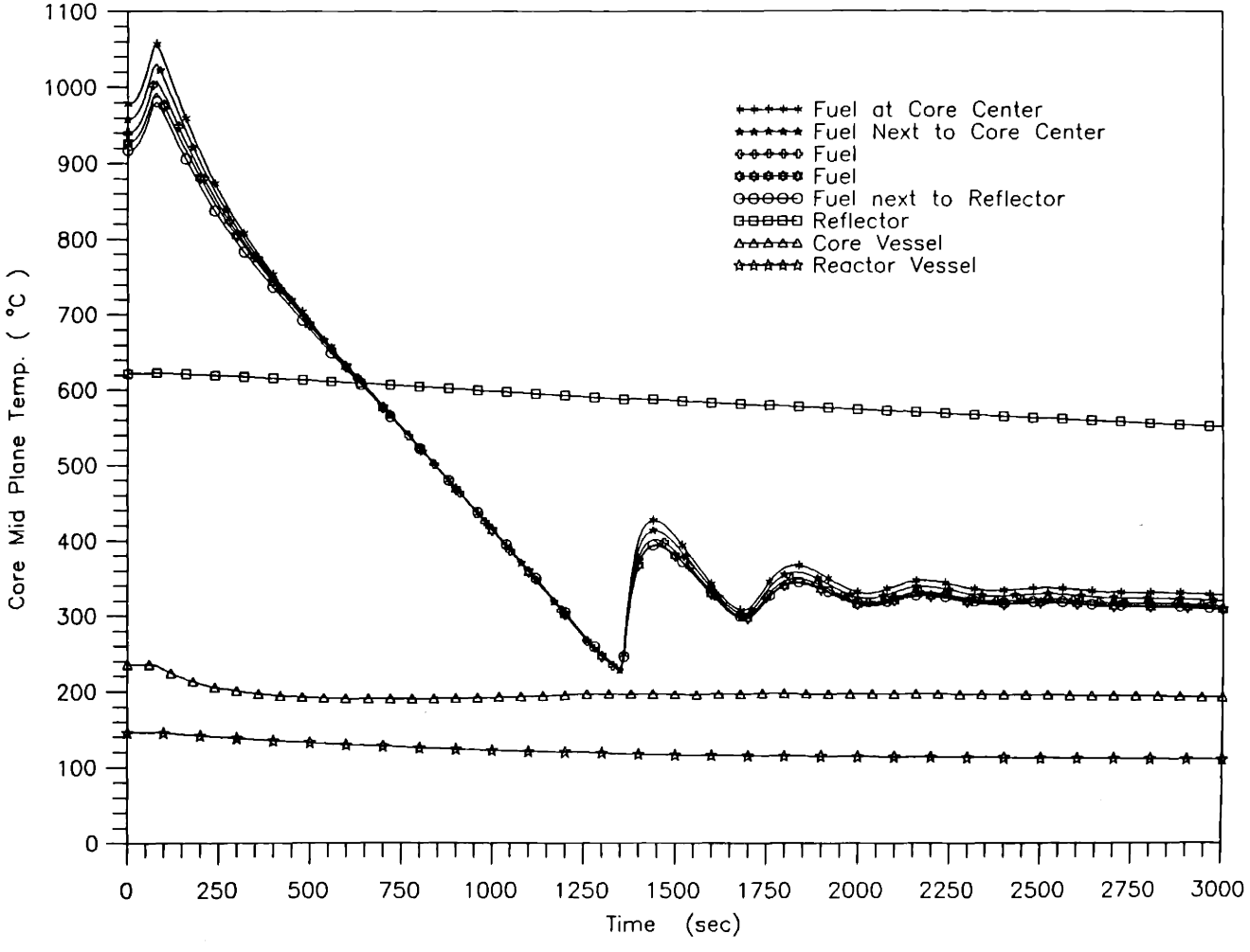

Figure 5.10(c) Radial temperature transient responses in the core mid plane during shutdown process in case of control rod withdrawal at full power

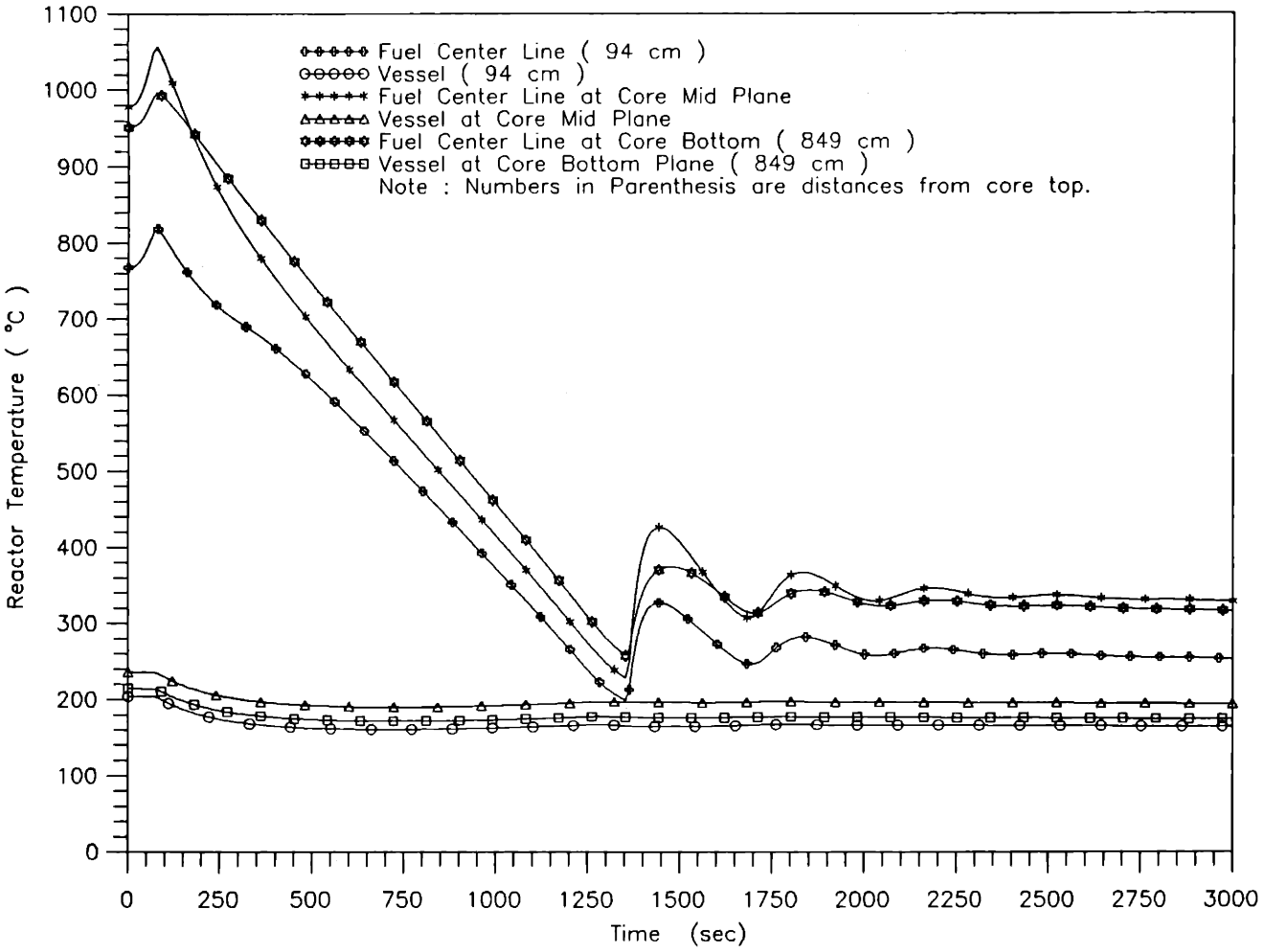

Figure 5.10(d) Reactor axial temperature transient responses during shutdown process in case of control rod withdrawal at full power

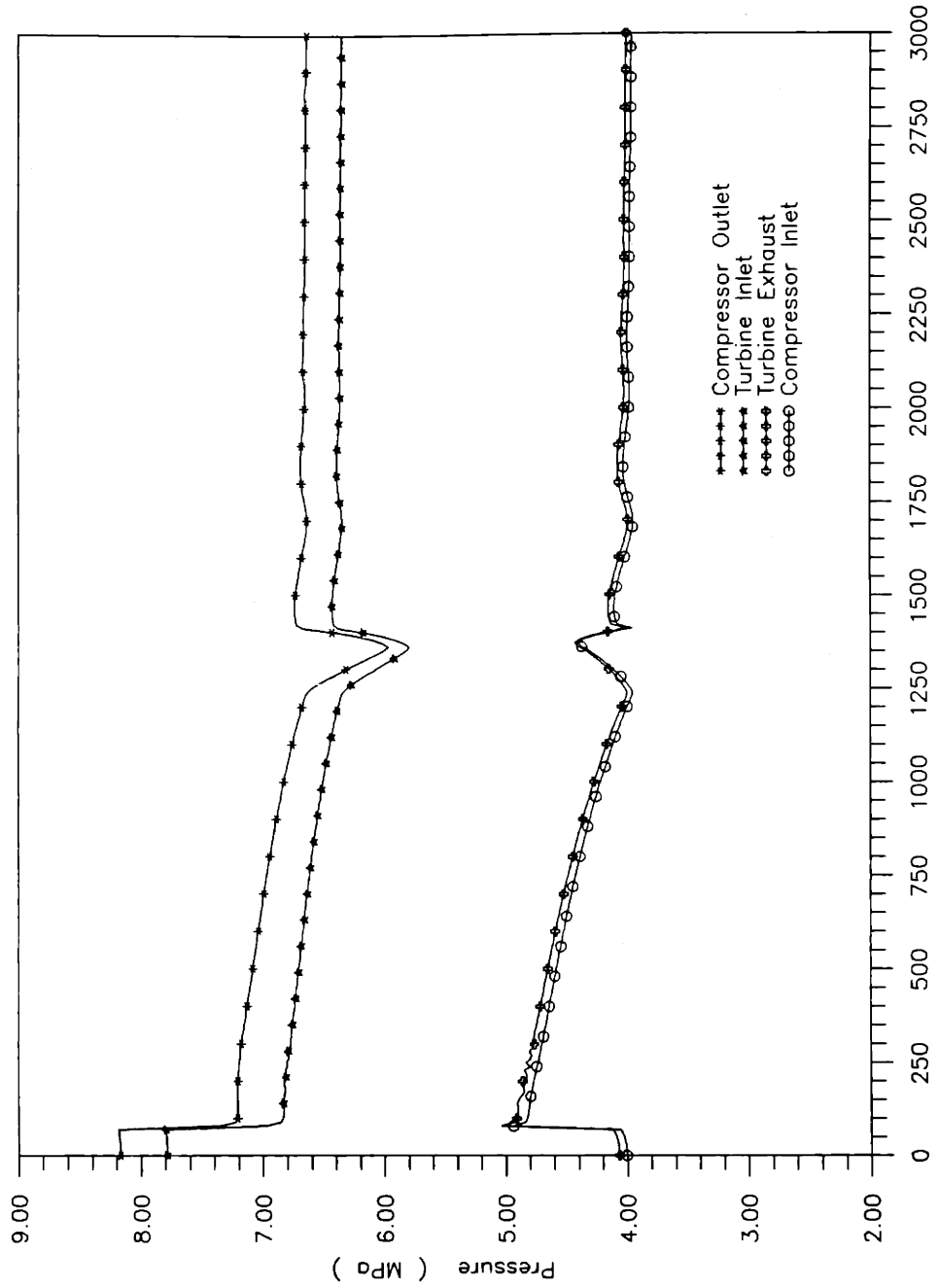

Figure 5.10(f) Pressure transient responses during plant shutdown process in case of control rod withdrawal at full power

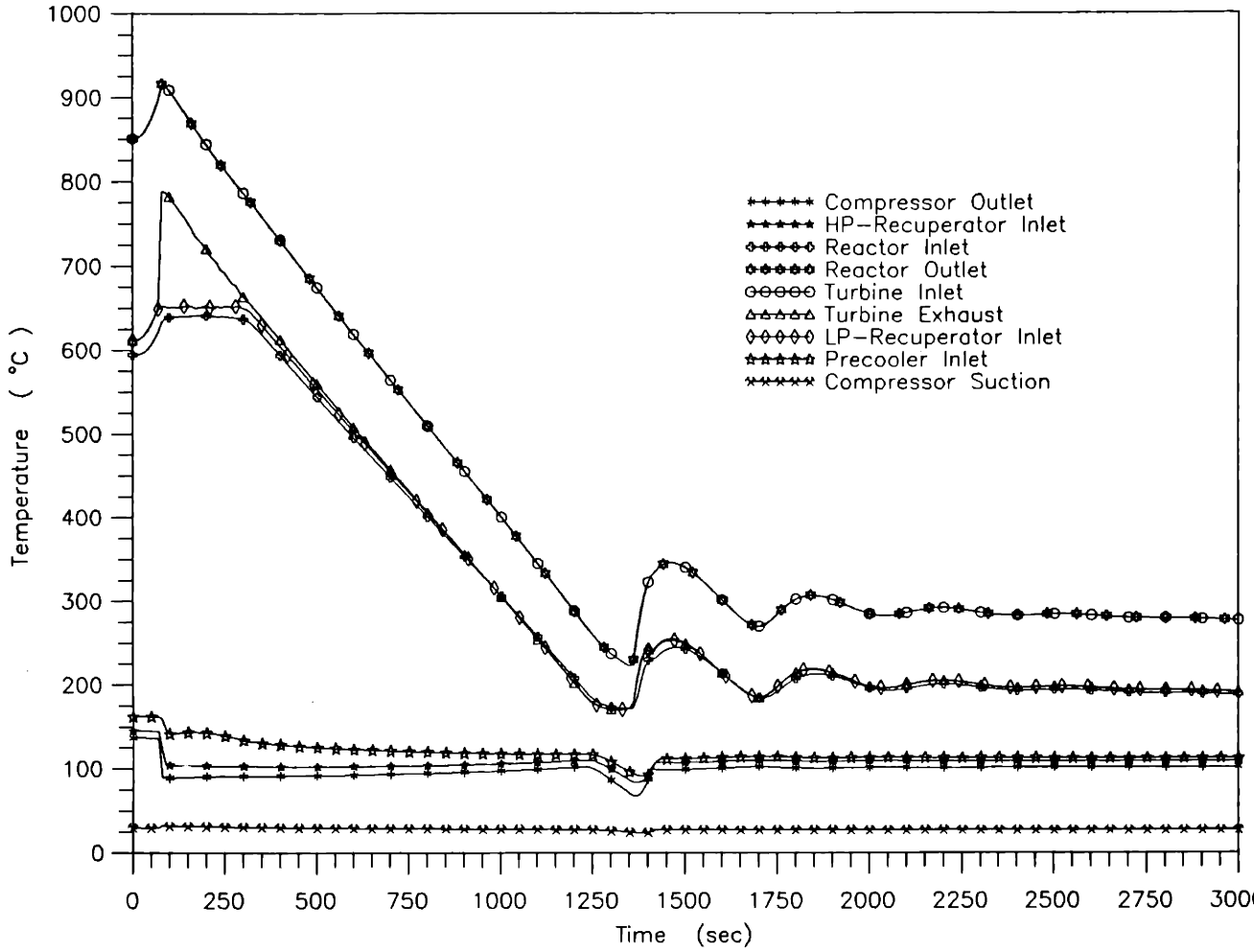

Figure 5.10(g) Temperature transient responses during plant shutdown process in case of control rod withdrawal at full power

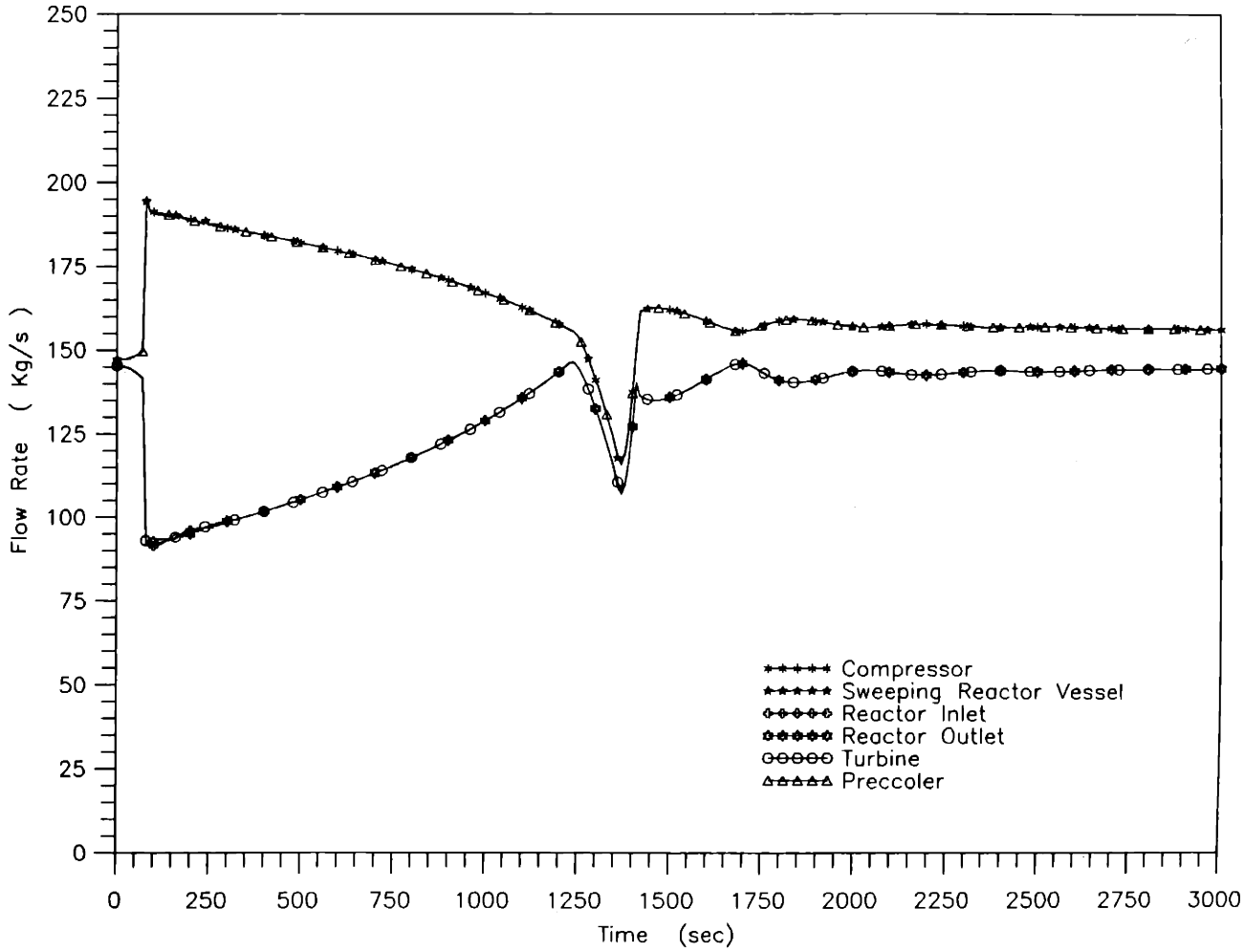

Figure 5.10(h) Flow transient responses during plant shutdown process in case of control rod withdrawal at full power

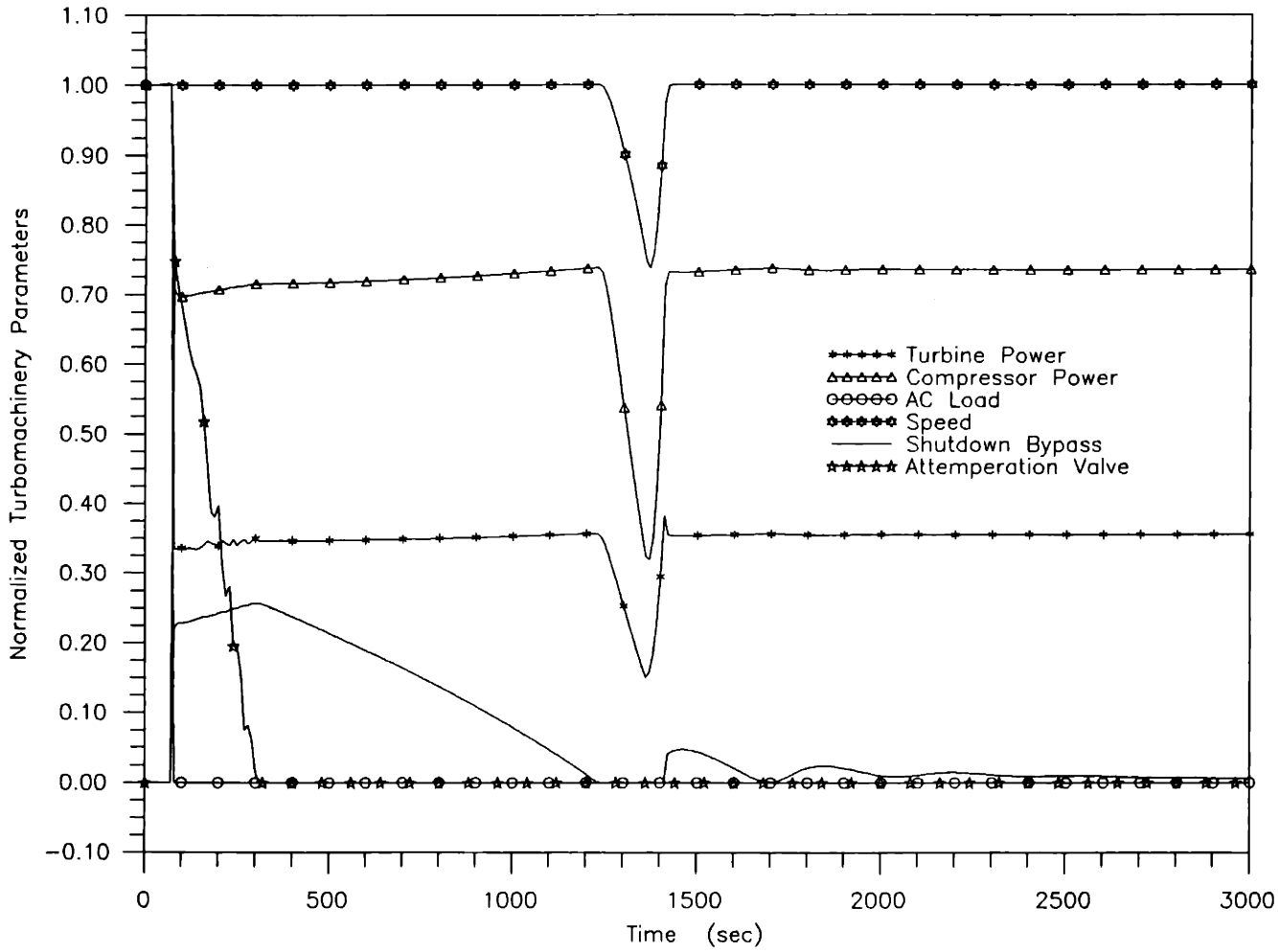

Figure 5.10(e) Turbomachine parameters in shutdown to idle state in case of control rod withdrawal at full power

LP-recuperator, the attemperation valve opens to introduce cold helium from the HP-recuperator inlet to suppress the hot helium discarded by the turbine. As a result, the temperature increase of the LP-recuperator inlet is limited.

As the reactor remains in shutdown condition over long-term period of time, the core temperatures drops substantially, which causes the turbine inlet temperature to decrease. As a result, turbine power also decreases. The bypass valve as shown in Figure 5.10 (e) is gradually closed to compensate for the loss of the turbine power in order to maintain the speed. However, when the valve is completely closed, the turbomachine net power becomes negative, resulting in underspeed of the turbomachine. The turbomachine power increases again when the turbine inlet temperature rises as a result of the reactor criticality. The turbomachine is then controlled again at the design speed by the bypass valve to run at idle.

5.3 Design Basis Accidents

Four design basis accidents have been simulated to analyze the inherent safety features and protection capabilities of the MGR-GT design. Four events are grouped into two pairs, which are (1) inadvertent withdrawal of all control rods with and without reactor scram, and (2) simultaneous system depressurization and withdrawal of all control rods with and without reactor shutdown. The comparison of the simulation results for the first two events can unveil different transient behaviors of the reactor power and temperature when reactor shutdown is and is not available. Simulations for the second pair of the events are intended to evaluate the core heatup transients in the depressurized condition with and without active reactor shutdown. The simultaneous system depressurization and withdrawal of all control rods with no reactor shutdown constitute the worst possible accident related to the MGR-GT design concept.

5.3.1 Inadvertent Withdrawal of All Control Rods with and without Reactor Scram

Inadvertent withdrawal of all control rods causes positive reactivity disturbance in the core. The reactor is automatically scrammed by the PPS on the signal of abnormal excess neutron flux or high reactor outlet temperature. The control rods will subsequently be re-inserted into the core, followed by loop shutdown to idle state to help decay heat removal with continuous helium circulation through the core. The description of the simulation for the control rod withdrawal with reactor scram has been given above.

In the case of control rod withdrawal with the failure of reactor scram, the temperature coefficient of reactivity would be the only shutdown means for reactor power. Figure 5.11 (b) clearly demonstrates the shutdown effect by the temperature reactivity feedback. Initially, the control rods are withdrawn out of the core at the maximum control rod drive speed, resulting in the positive reactivity development. This positive reactivity causes the reactor power to increase. As a result, the core temperatures rise, as shown in Figures 5.11 (b) and (d). However, such temperature increases generate negative reactivity by means of the temperature feedback. As shown in Figure 5.11 (b), the temperature feedback alters the total reactivity in the core from positive to negative. Thus, the reactor power is inherently set back and stabilized after a short period of oscillation.

Because of the reactor power setback, and because the helium is still circulated through the core, no fuel temperature has increased by more than 150°C, and the maximum fuel temperature is limited to less than 1115°C. The maximum temperature increase is only 100°C more than that in the previous accident of the control rod withdrawal accident with reactor scram available. After peak, the fuel temperatures are reduced because of the heat removal by the helium circulation. As the time elapses, the reactor power and fuel temperatures will reach a new steady state.

The simultaneous loop shutdown process is shown in Figure 5.11 (e). It can be seen

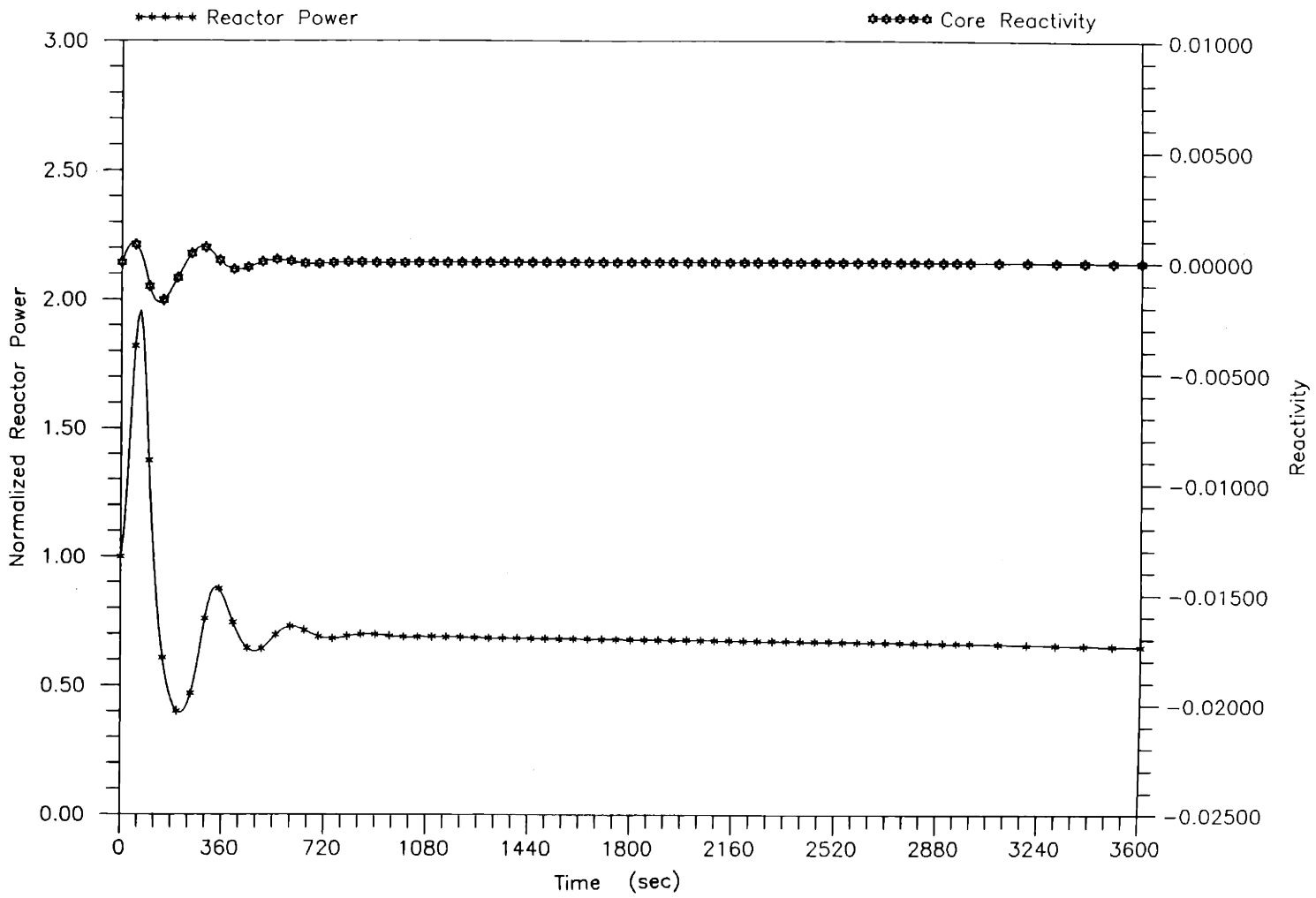

Figure 5.11(a) Reactor power and reactivity transient responses in case of control rod withdrawal and failure of reactor scram

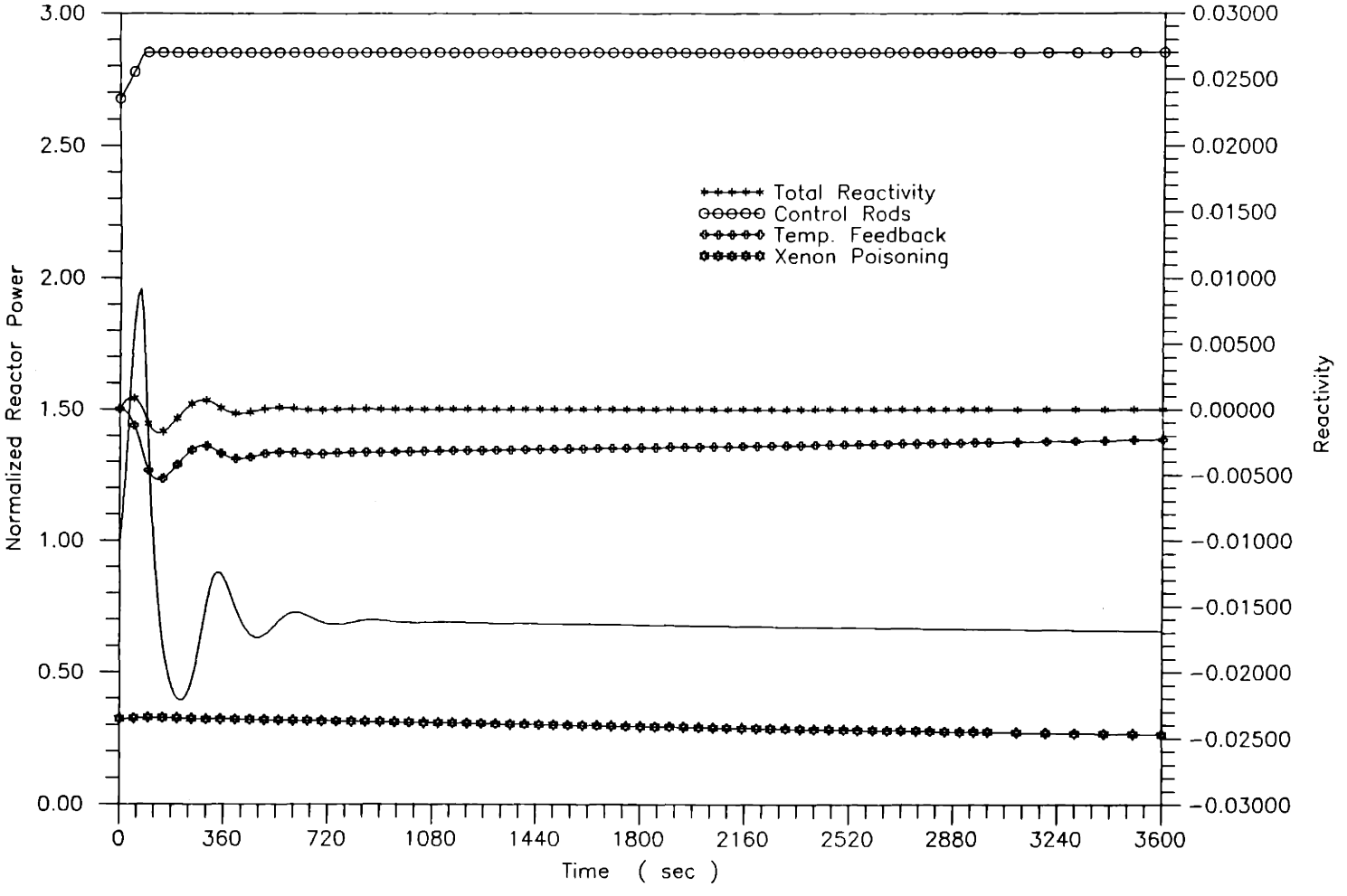

Figure 5.11(b) Reactor power and reactivity contributions in case of control rod withdrawal and failure of reactor scram

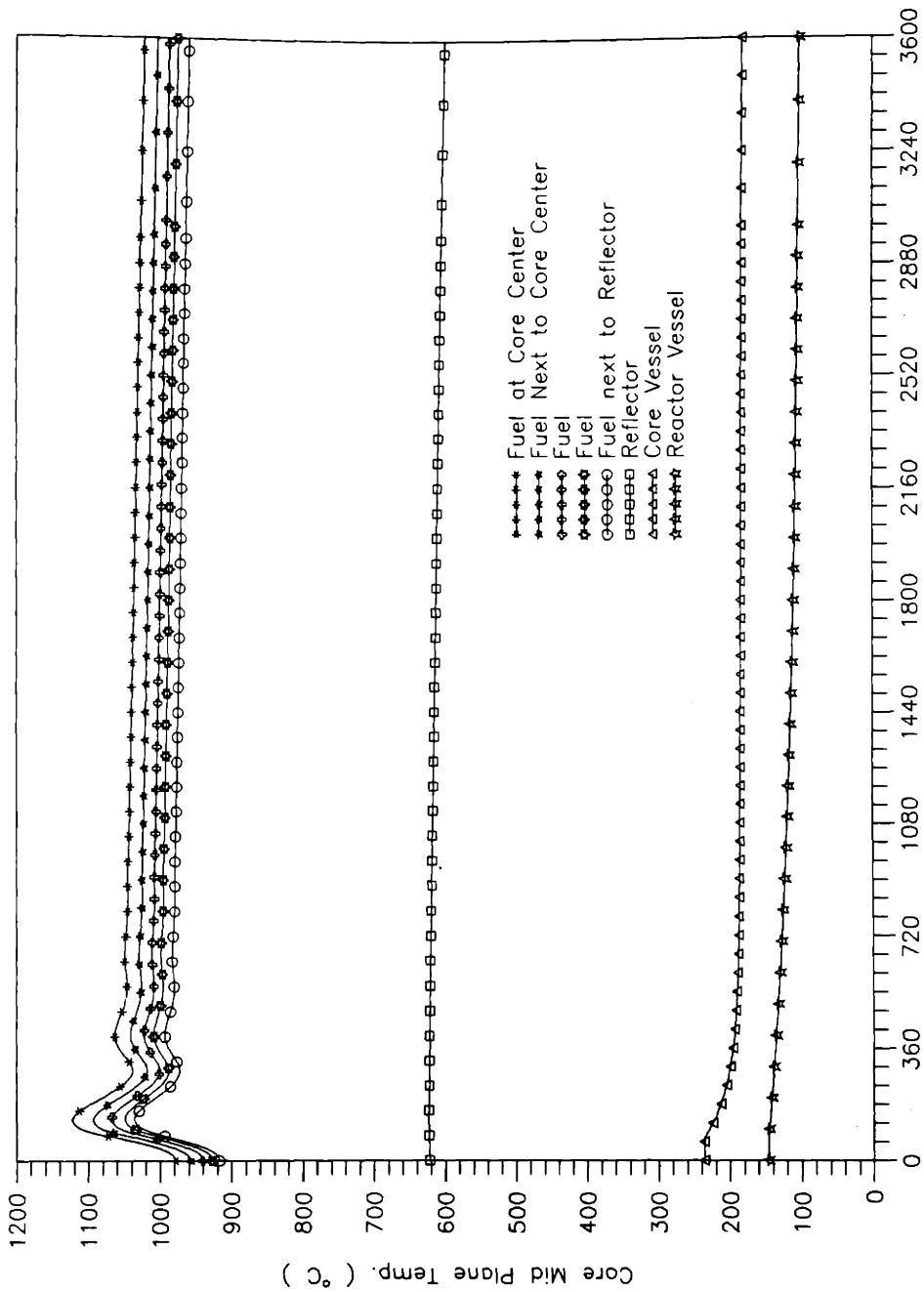

Figure 5.11(c) Radial temperature transient responses in the core mid plane in case of control rod withdrawal and failure of reactor scram

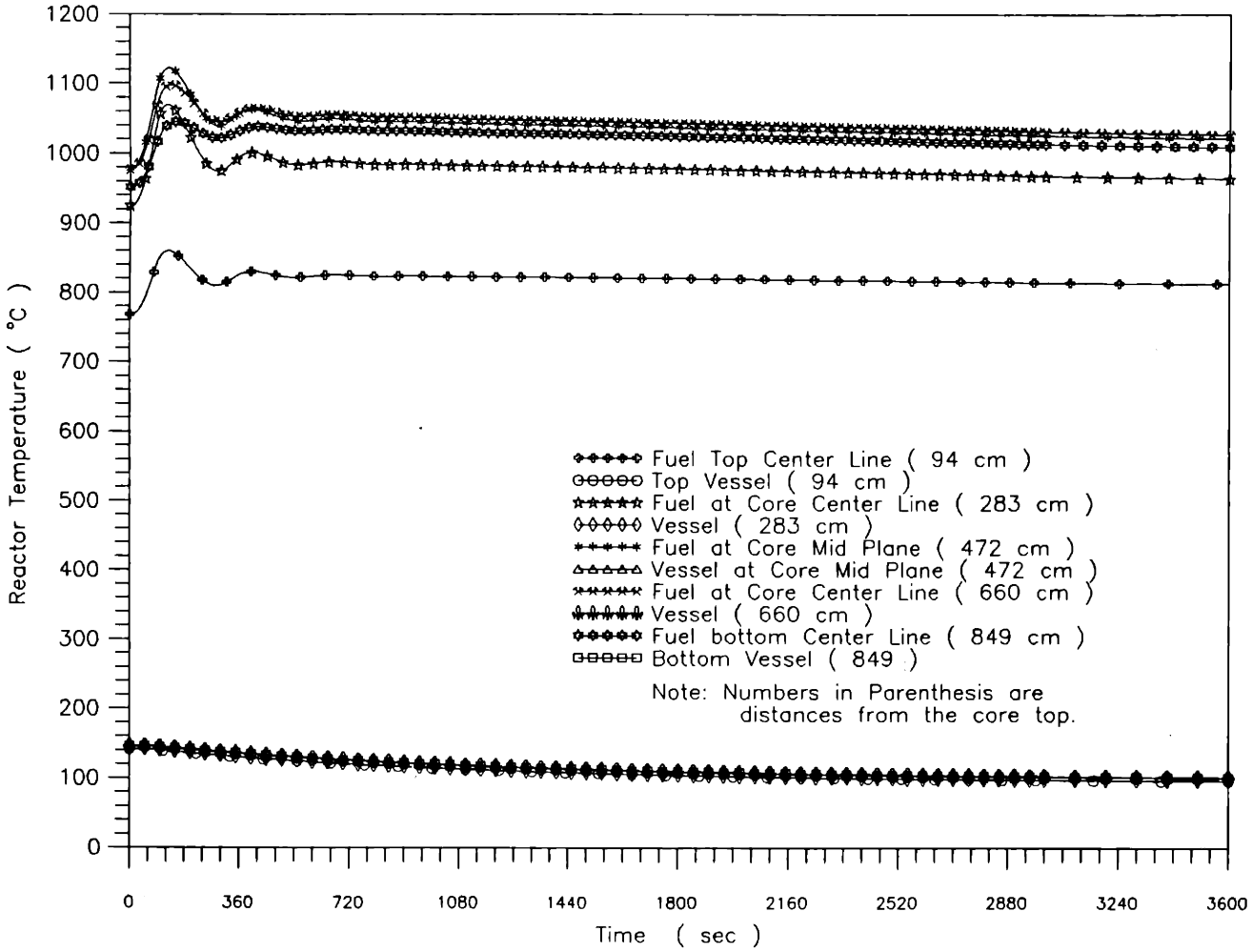

Figure 5.11(d) Reactor axial temperature transient responses in case of control rod withdrawal and failure of reactor scram

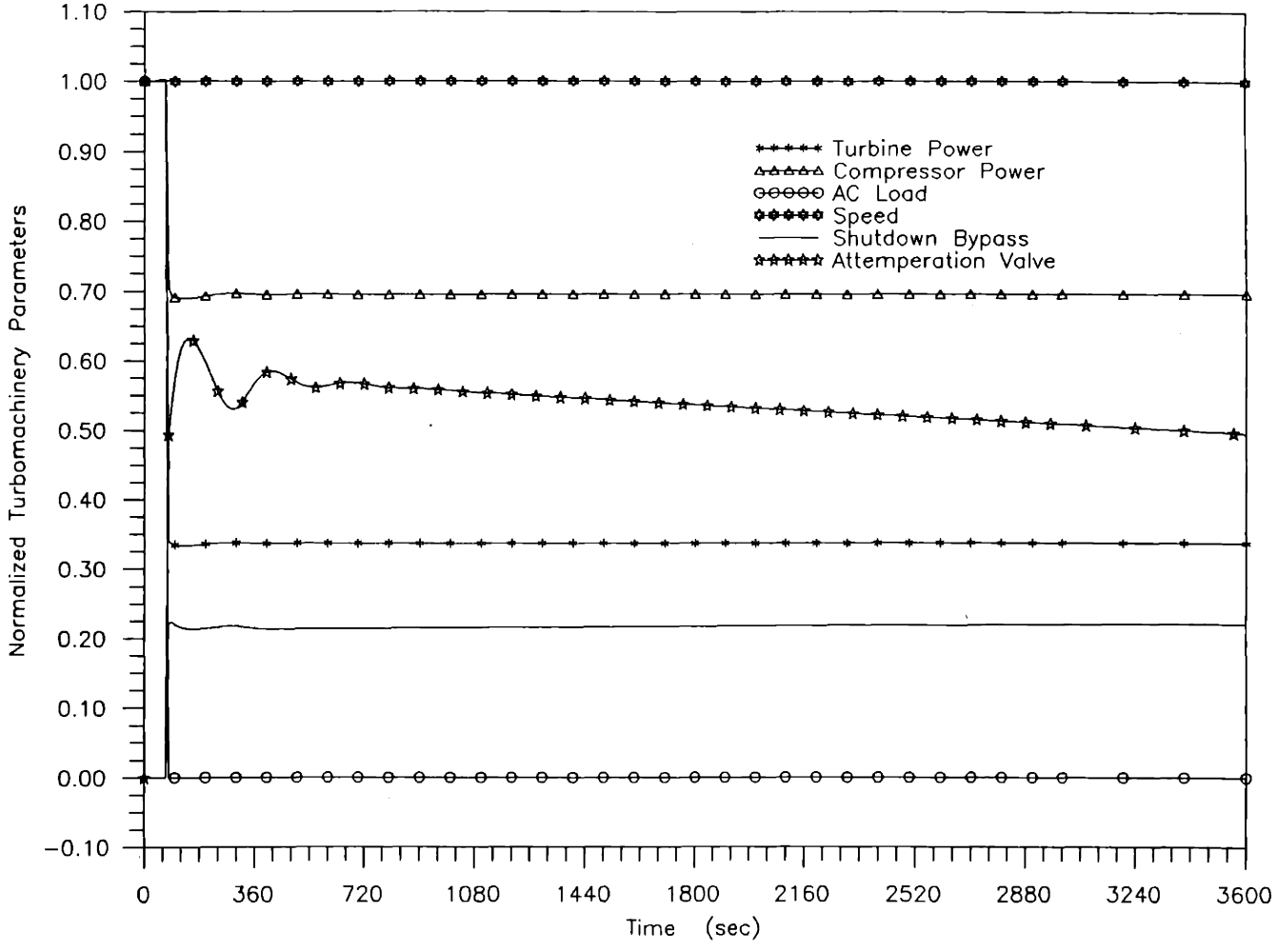

Figure 5.11(e) Turbomachine parameters in loop shutdown to idle state in case of control rod withdrawal and failure of reactor scram

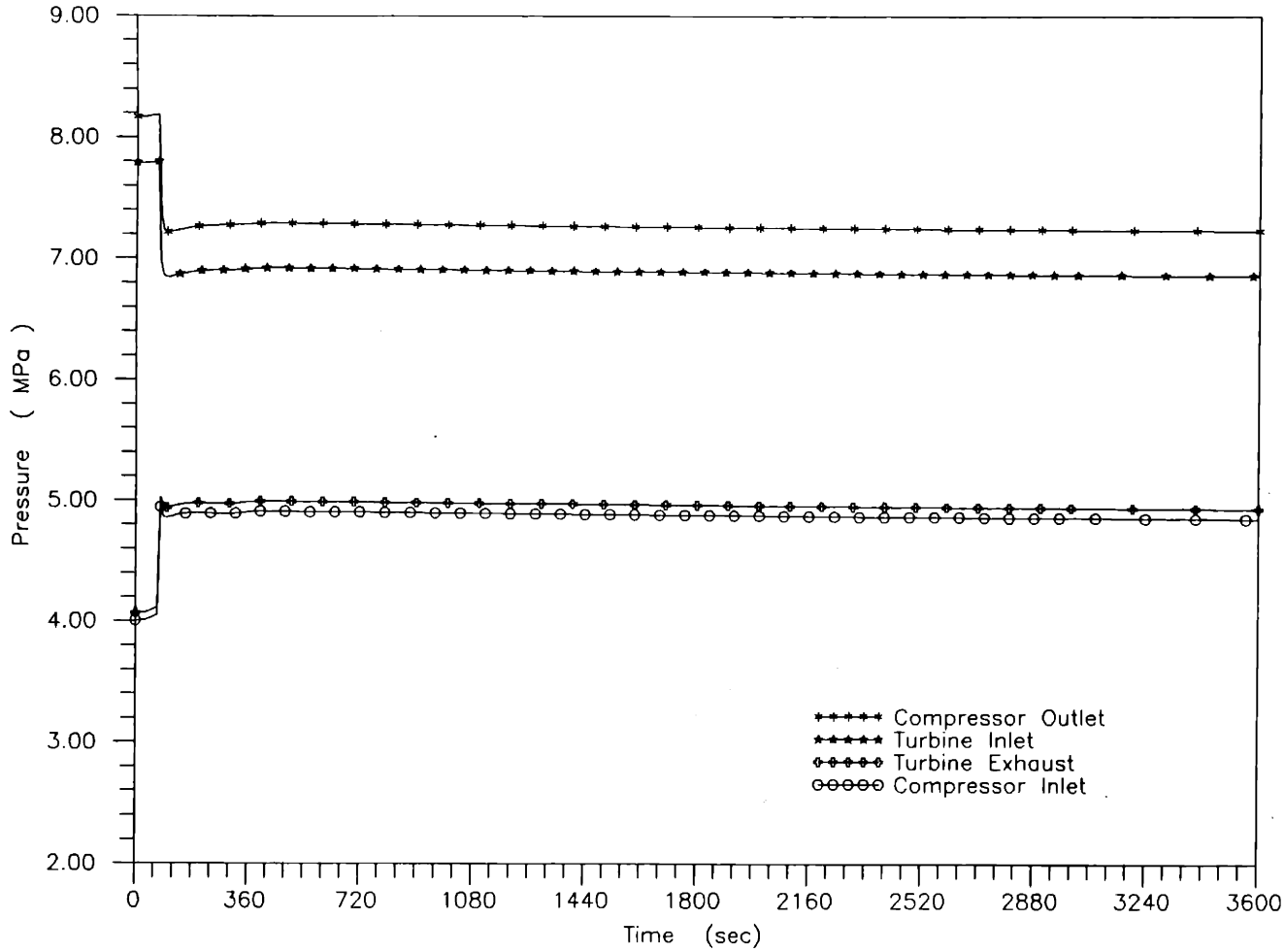

Figure 5.11(f) Pressure transient responses during loop shutdown to idle state in case of control rod withdrawal and failure of reactor scram

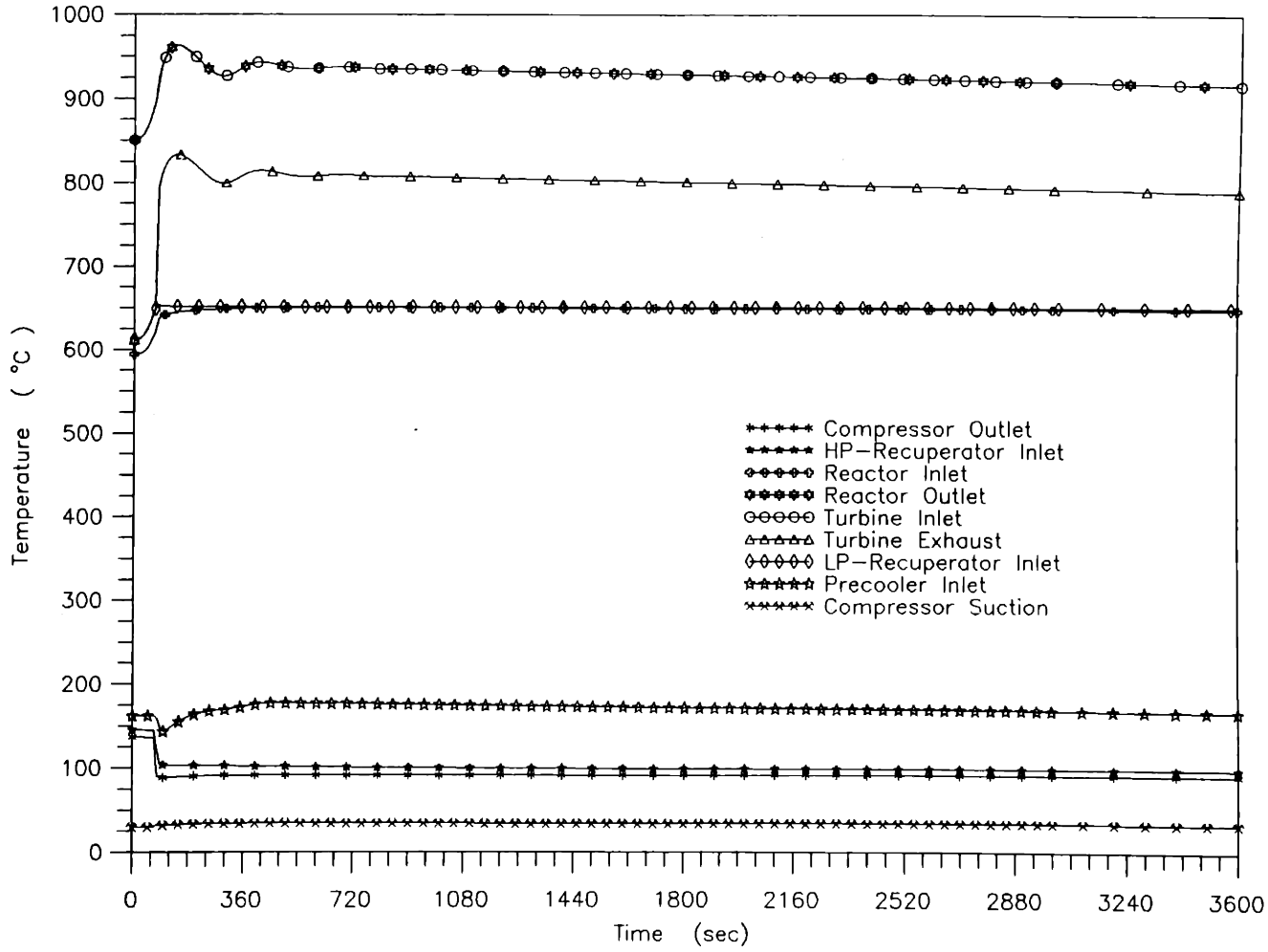

Figure 5.11(g) Temperature transient responses during loop shutdown to idle state in case of control rod withdrawal and failure of reactor scram

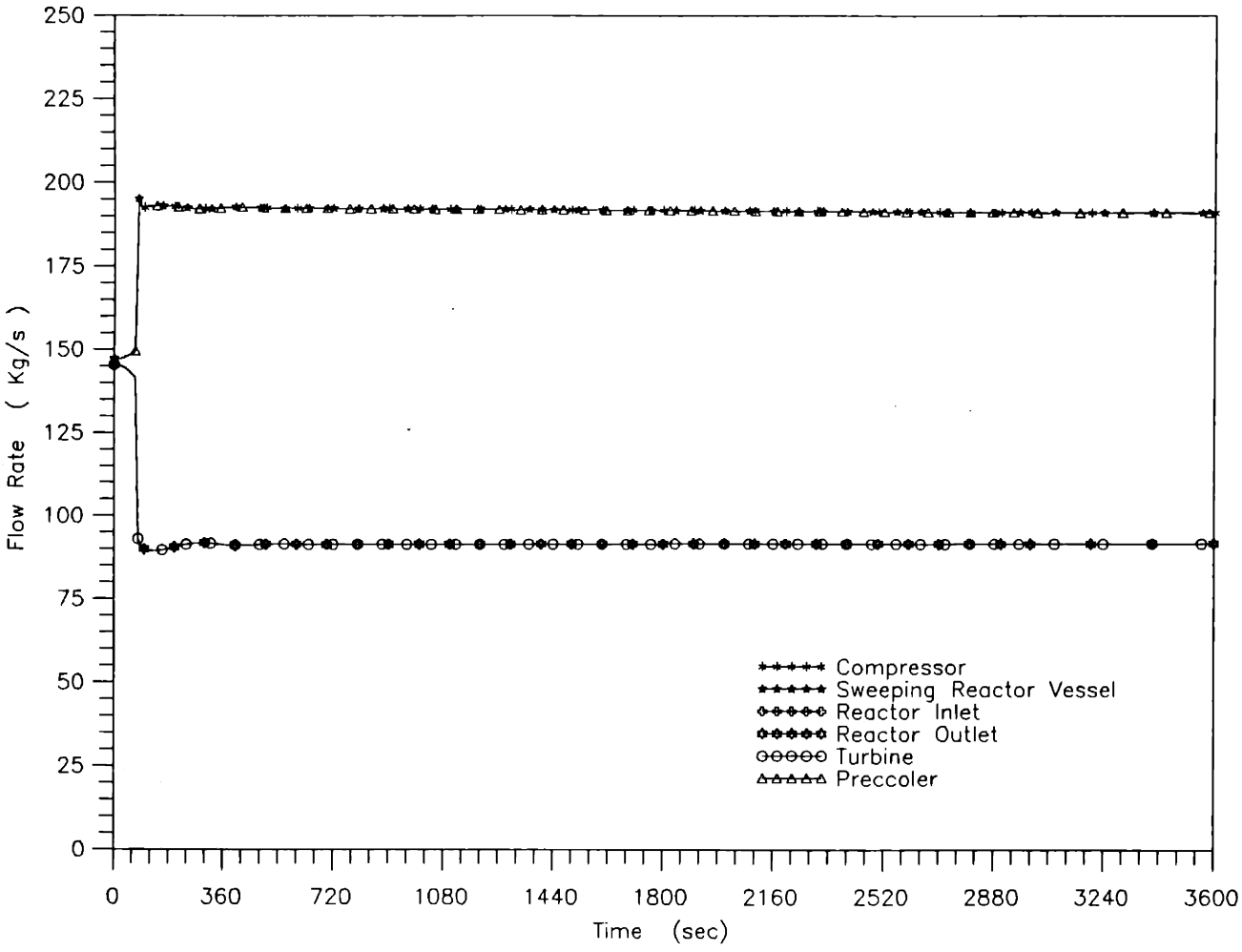

Figure 5.11(h) Flow transient responses during loop shutdown to idle state in case of control rod withdrawal and fialure of reactor scram

that the turbomachine is maintained at the design speed throughout the entire period by the shutdown bypass valve. The turbine and compressor powers are reduced to a new steady state. Because of the substantial reduction of the turbine pressure ratio, as shown in Figure 5.11 (f), the turbine outlet temperature as shown in Figure 5.11 (g) increases considerably. The attemperation bypass valve is maneuvered by the PPS attemperation controller to control the thermal condition on the LP-recuperator inlet. As a result, the LP-recuperator inlet temperature is kept nearly constant during the loop shutdown. The flow transient responses are depicted in Figure 5.11 (h). As can be seen, helium is circulated through the reactor core at approximately 62% of the nominal flow rate to remove the heat from the core and to dissipate it to the water flow of the precooler.

5.3.2 Simultaneous System Depressurization and Control Rod Withdrawal

In case of simultaneous system depressurization and control rod withdrawal, decay heat removal by helium circulation after reactor shutdown would not be available. The natural heat conductance by heat conduction and radiation becomes the only decay heat removal mechanism. It is assumed that the system depressurization follows a pressure boundary break at the upper crossduct, and simultaneously, the control rods are withdrawn from the core at the maximum speed of the control rod drive mechanism, resulting in a total 0.35% worth of the positive reactivity insertion in the core. The reactor is scrammed by the PPS sensor signal indicating abnormal low system pressure. The scram is accomplished with the control rods being re-inserted into the core and the small absorber spheres released in the columns of the side reflector.

Figure 5.12 (b) shows detailed transient responses of the reactor power and reactivity contribution by individual reactivity components. As can be seen, the reactivity of fission product poisoning dominates the transient behavior of the total reactivity during the early

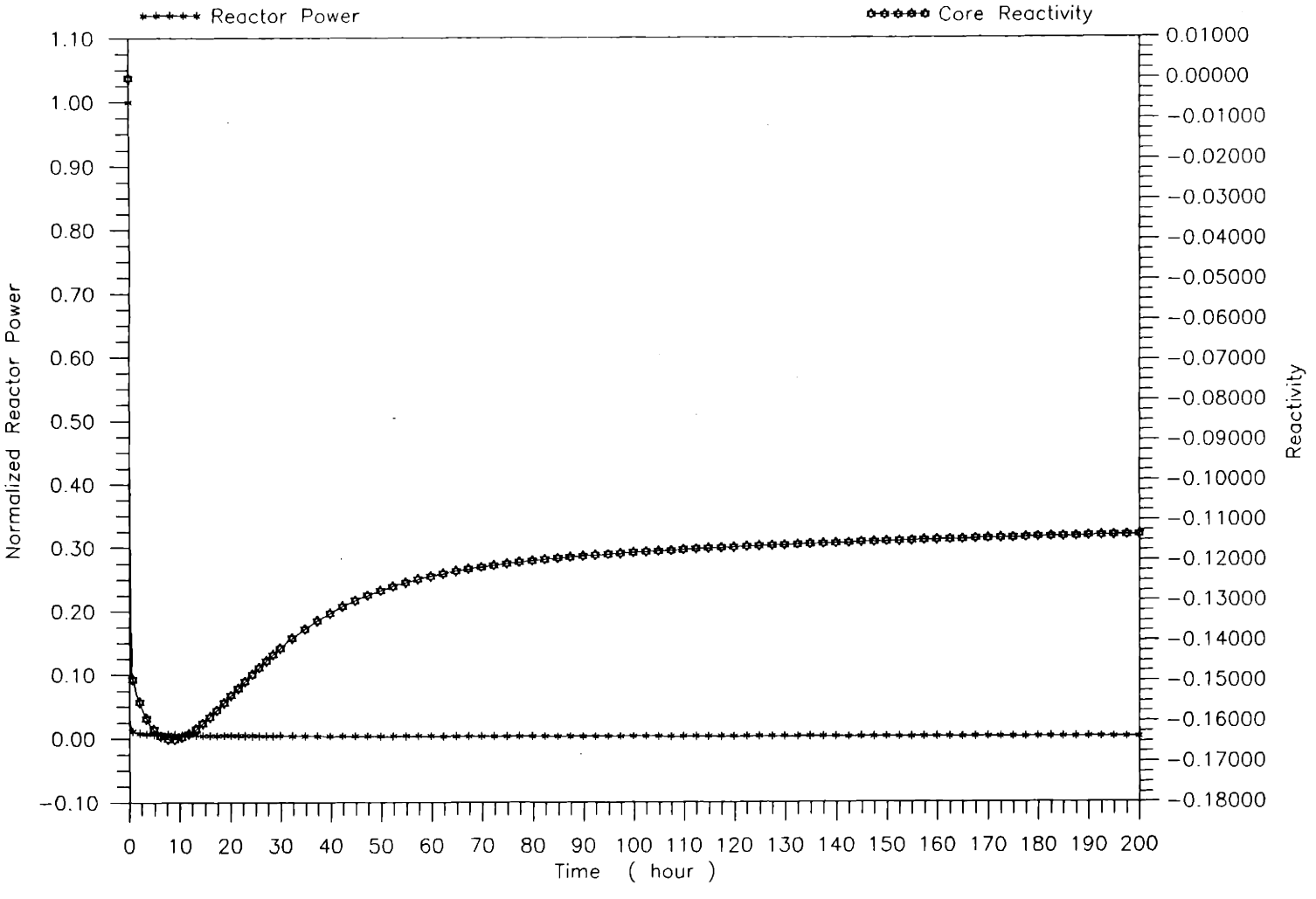

Figure 5.12(a) Reactor power and reactivity transient responses in case of simultaneous system depressurization and control rod withdrawal with subsequent reactor scram

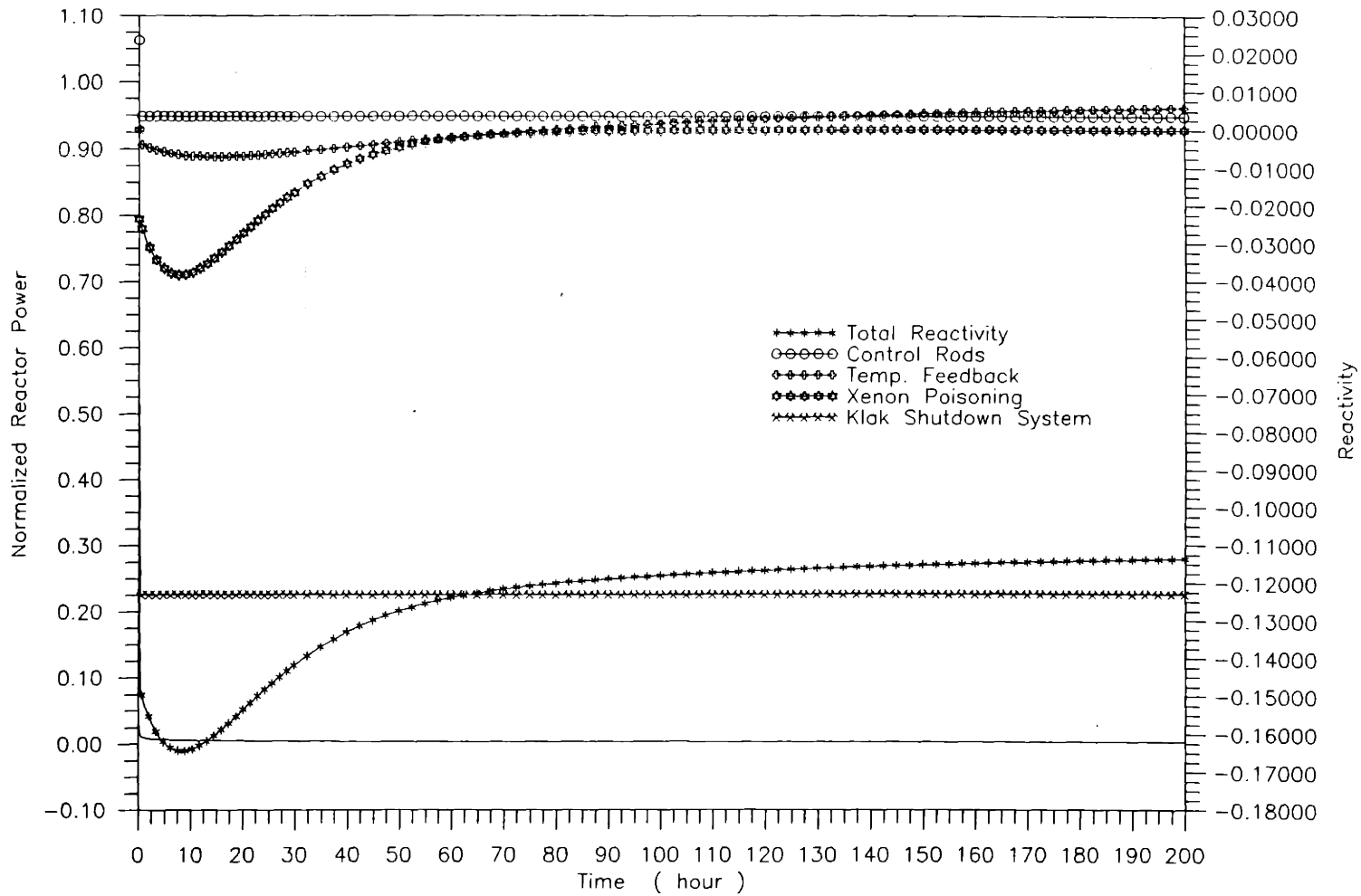

Figure 5.12(b) Reactor power and reactivity contributions in case of simultaneous system depressurization and control rod withdrawal with subsequent reactor scram

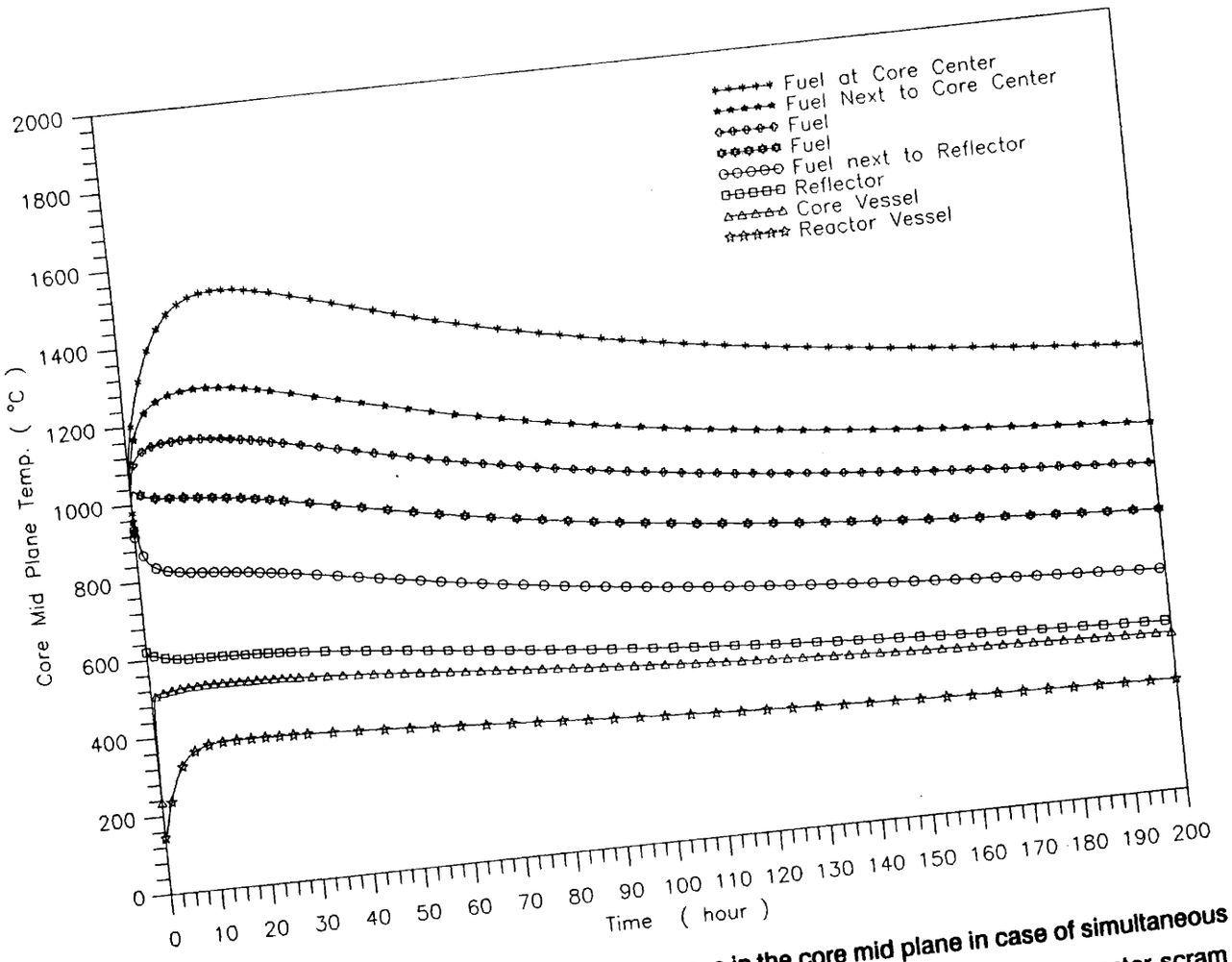

Figure 5.12(c) Radial temperature transient responses in the core mid plane in case of simultaneous system depressurization and control rod withdrawal with subsequent reactor scram

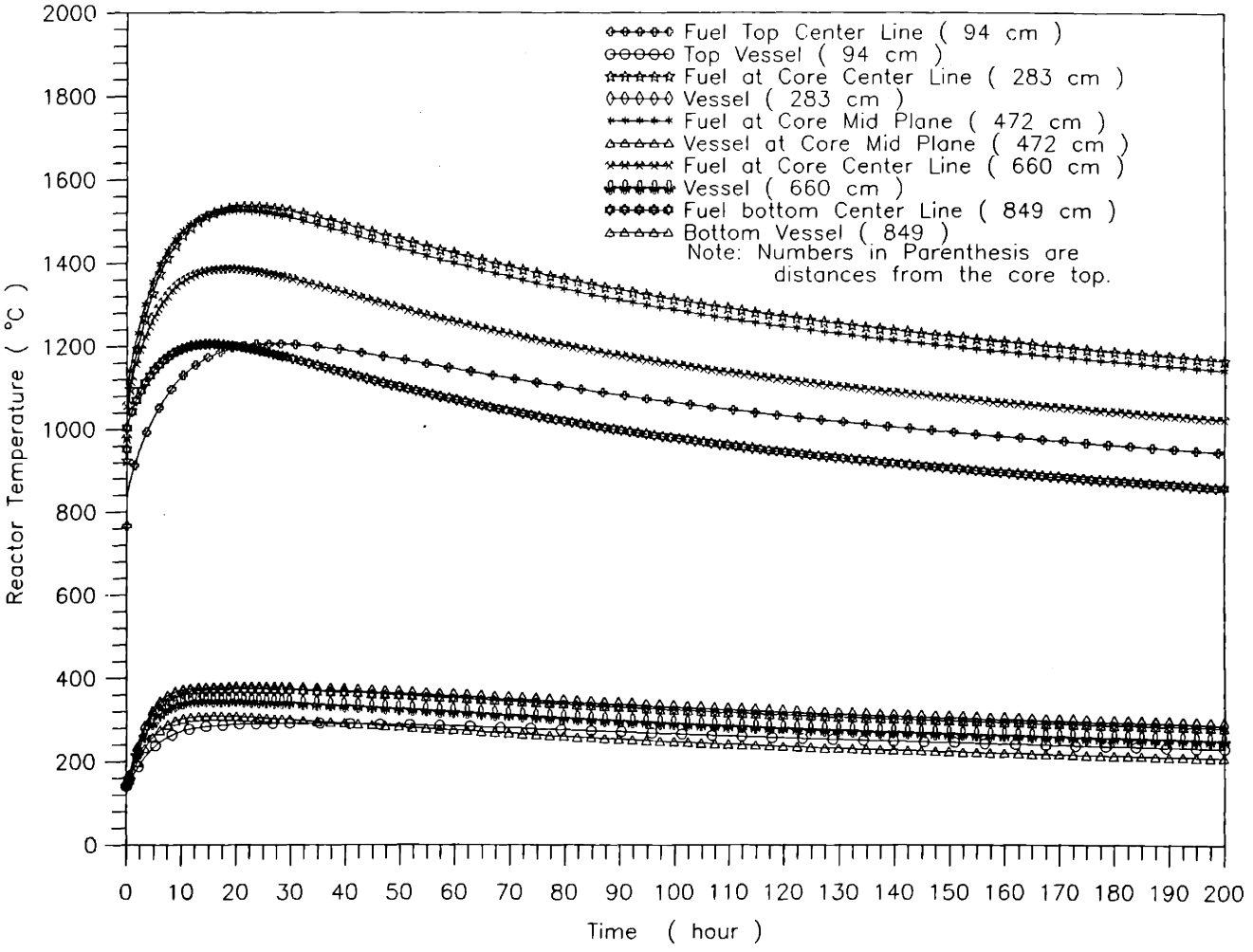

Figure 5.12(d) Reactor axial temperature transient responses in case in case of simultaneous system depressurization and control rod withdrawal with subsequent reactor scram

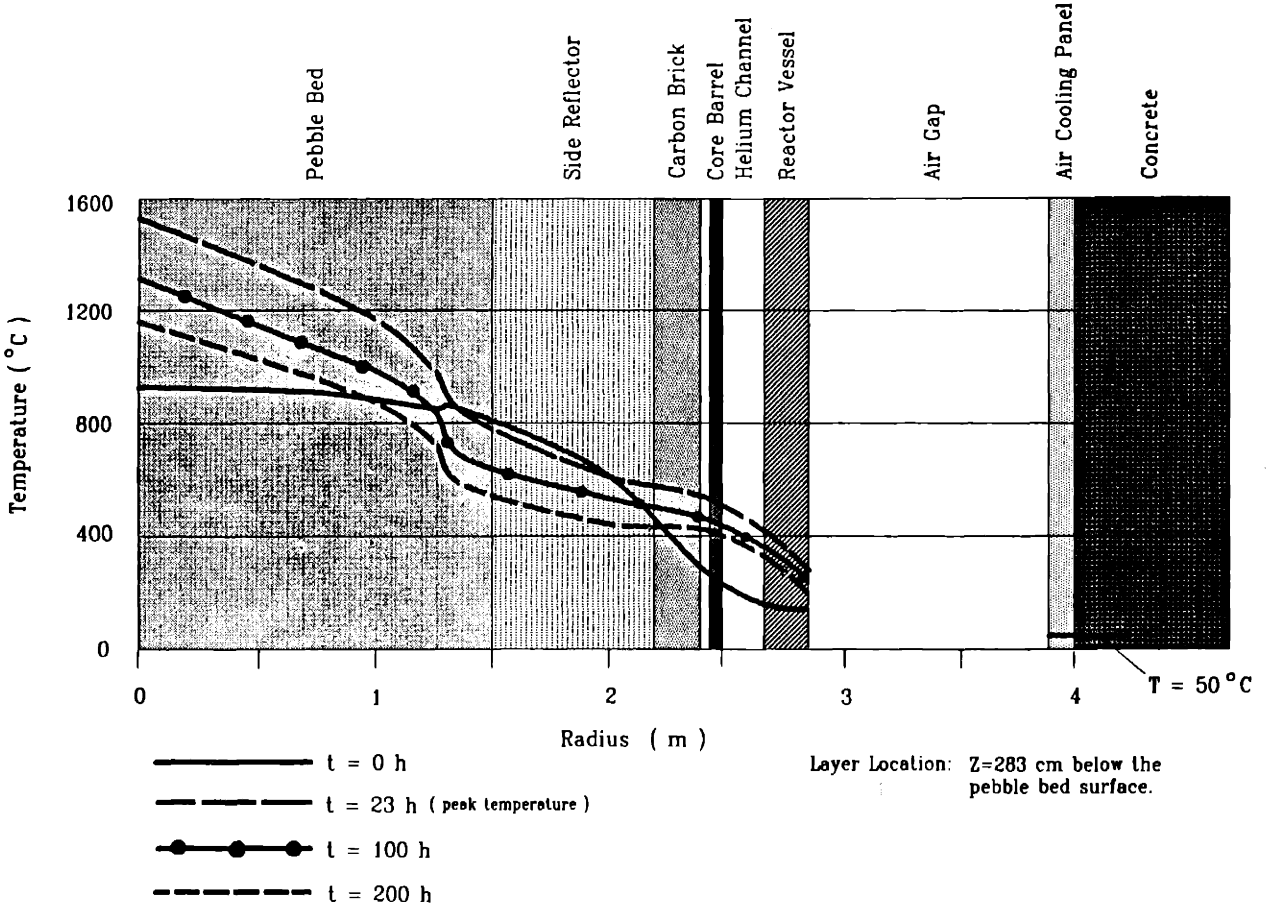

Figure 5.12(e) Reactor radial temperature transient distribution in case of simultaneous system depressurization and control rod withdrawal with subsequent reactor scram

hours of transient. The negative reactivity of fission product poisoning peaks at about 9.5 hours after the initiation of the reactor shutdown and gradually vanishes over 100 hours. The large amount of the reactivity contributed by Klak reactivity shutdown system provides sufficient negative reactivity required for keeping the reactor power subcritical.

Figures 5.12 (c) and (d) show the transient temperature distributions in the radial direction at the core mid plane and axial direction. As can be seen, the maximum temperature is limited to 1550°C, occurring at t = 23 hours at the core centerline 2.82 meters below the top plane of the core. The radial temperature transient distribution at the plane of the maximum core temperature is shown in Figure 5.12 (e). During the entire core heatup period, the maximum reactor vessel temperature reached is 380°C as shown in Figure 5.12 (d) at the same plane as that of the maximum fuel temperature.

The combination of the system depressurization and withdrawal of all control rods with failure of reactor shutdown constitutes the worst possible accident with regard to the safety of reactor in the MGR-GT. Figure 5.13 (b) shows detailed transient responses of the reactor power and reactivity contributions by individual reactivity components. As can be seen, The power and reactivity demonstrate more complicated transient behaviors than those in the foregoing accident. The control rods are withdrawn from the core and remain out afterward. The power increase causes the fuel temperatures to rise as shown in Figures 5.13 (c) and (d). The temperature reactivity feedback responds to shutdown the reactor power as shown in Figure 9.13 (b).

As the time elapses, the reactivity of fission product poisoning starts to dominate the core manipulation of reactivity. The negative reactivity of fission product poisoning peaks at about 9.5 hours after reactor shutdown and gradually vanishes afterward. As a result, the total core reactivity increases. Eventually, the temperature feedback reactivity is suppressed by the positive reactivity due to the vanishing of the fission product poisoning reactivity.

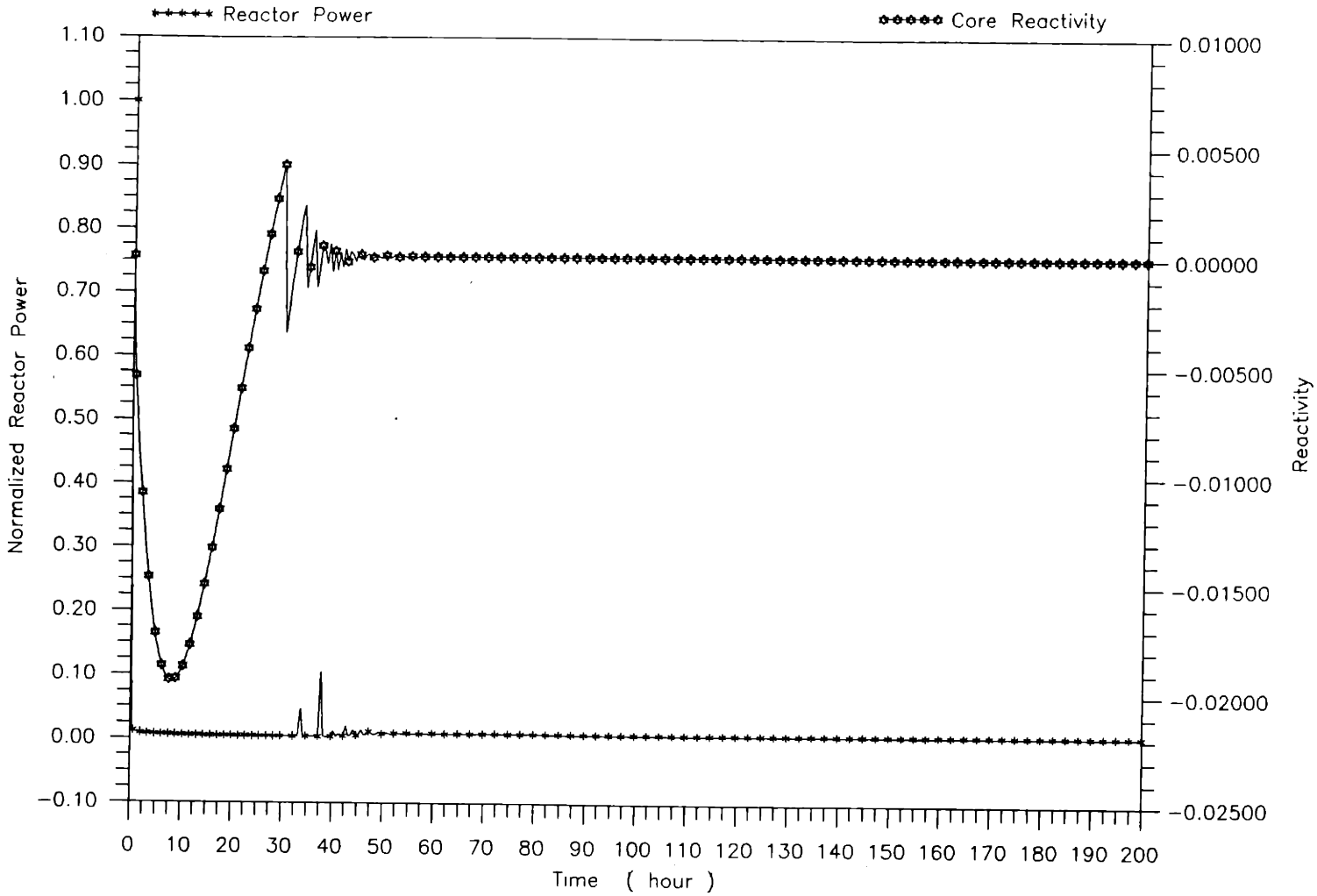

Figure 5.13(a) Reactor power and reactivity transient responses in case of simultaneous system depressurization and control rod withdrawal with failure of control rod re-insertion

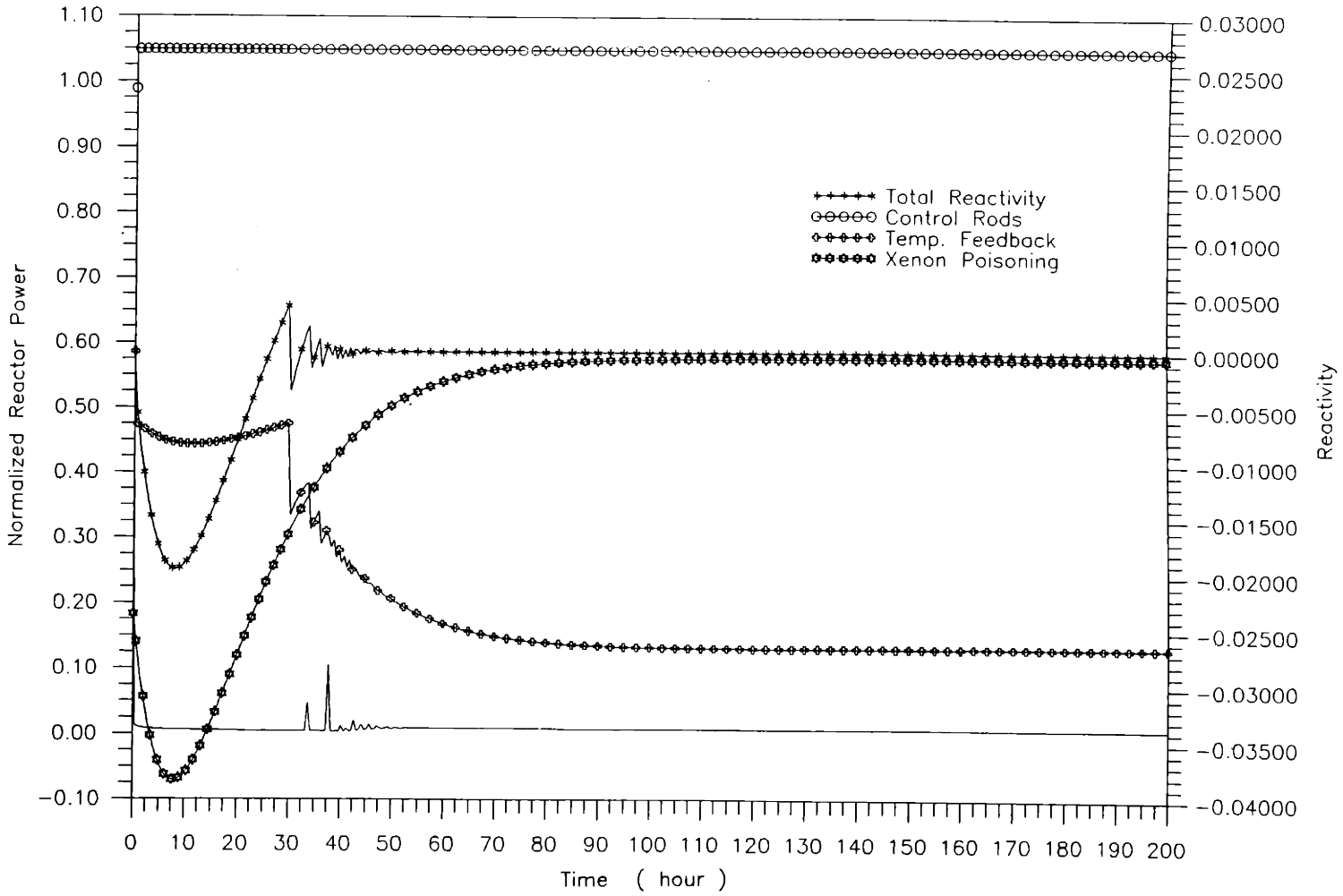

Figure 5.13(b) Reactor power and reactivity contributions in case of simultaneous system depressurization and control rod withdrawal with failure of control rod re-insertion

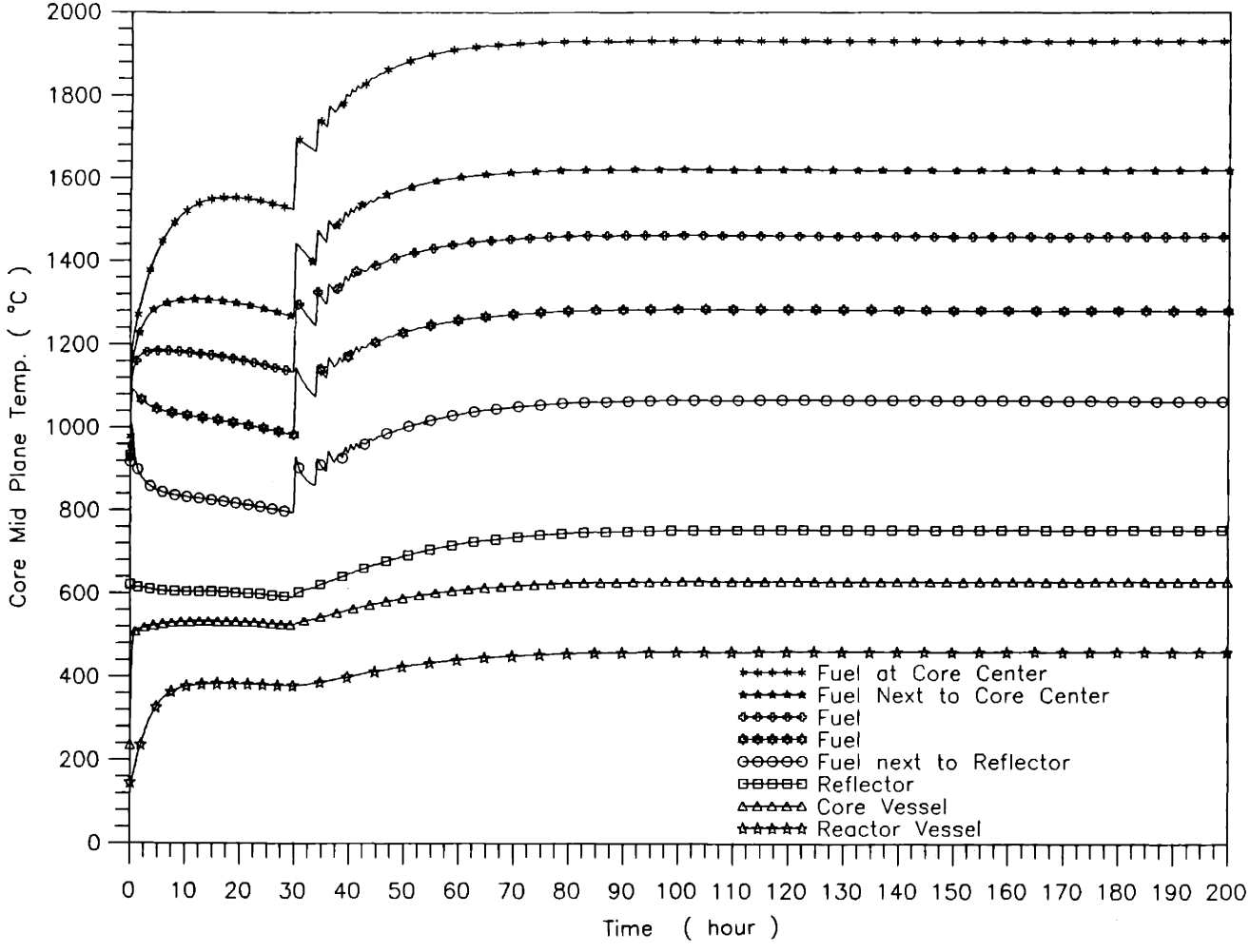

Figure 5.13(c) Radial temperature transient responses in the core mid plane in case of simultaneous system depressurization and control rod withdrawal with failure of control rod re- insertion

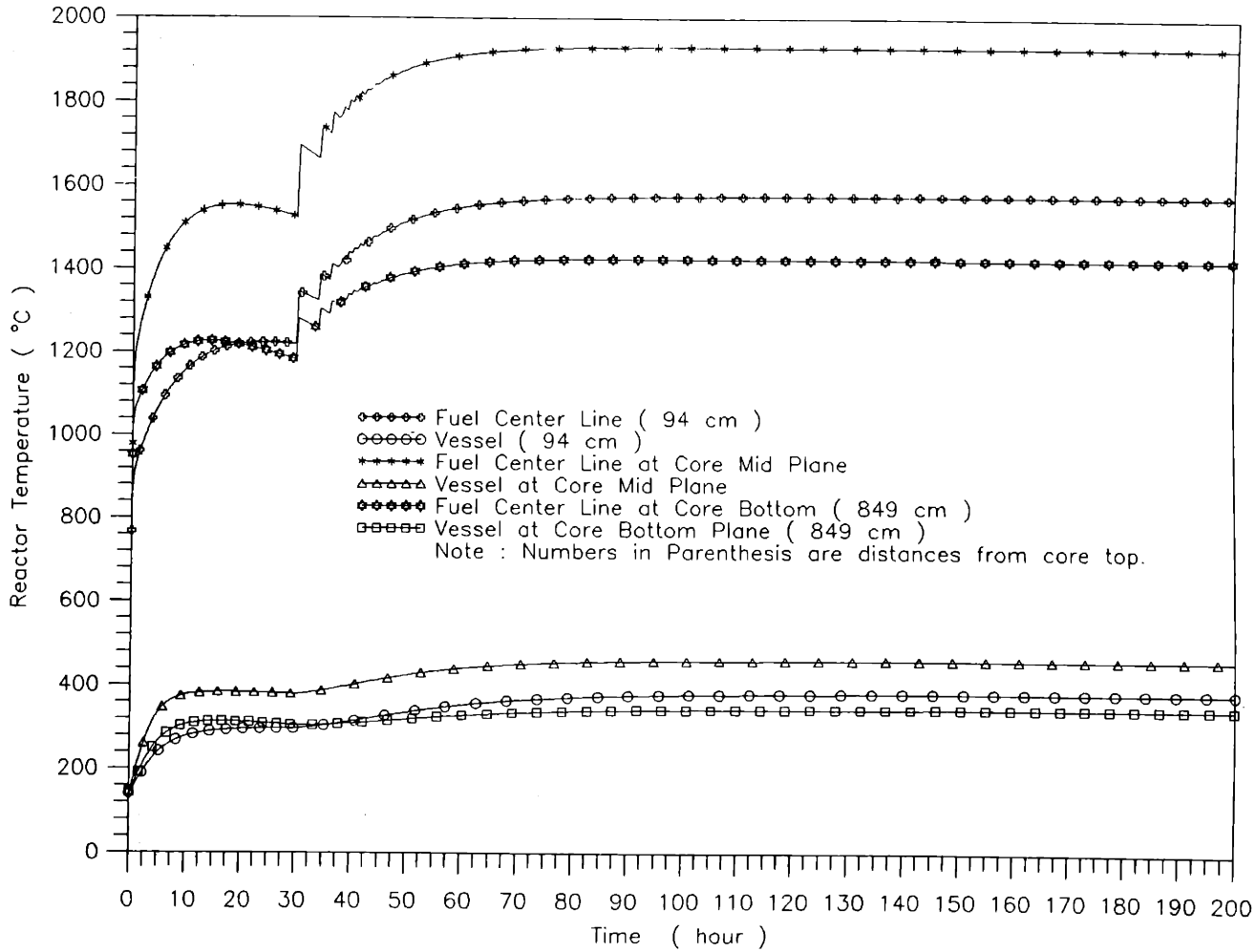

Figure 5.13(d) Reactor axial temperature transient responses in case in case of simultaneous system depressurization and control rod withdrawal with failure of control rod re-insertion

Consequently, the reactor become critical again at t = 33 hours.

The reactor criticality generates the power relatively larger than the decay heat generation. This increased reactor power causes the fuel temperatures to increase, as shown in Figures 5.13 (c) and (d). The temperature coefficient reacts to setback reactor power, and after short period of oscillation, stabilizes the power on a low, steady-state level. On this power level, the total core reactivity is maintained at zero by the temperature coefficient.

The maximum temperature reached in this accident is 1950°C, occurring at the core centerline 2.82 meters below the top plane of the core. However, it should be pointed out that this temperature might not reflect the correct maximum temperature in this accident. This is because that the temperature reactivity feedback does not take the spatial fuel temperature distribution into consideration. When such fact is considered, the hot spots in the core would have much stronger and earlier temperature feedback effect than that of the core average temperature feedback. The peak temperature would therefore be expected to be lower than that predicted based on the average temperature reactivity feedback model. The peak temperature achieved during depressurized criticality is best evaluated by the more detailed neutronic models. The peak predicated by [A1] is only 1620°C. This result also implies that our consideration of temperature feedback is basically conservative.

5.4. Beyond Design Basis Accidents

In case of loss of water flow in the precooler, the temperature of the precooler core will increase substantially as it is assumed that the helium continues to flow through the core of the precooler and no loop shutdown ensues the accident initiation. As a consequence of the precooler heatup, the inlet temperature of the compressor increases, resulting in the increasing power consumption by the compressor. As the net power of the turbomachine becomes negative, the rotor would be decelerated. The inherent precooler overheat

protection is provided as the rotor runs down and the helium is prevented from flowing to the precooler. The results of the simulation for this accident are shown in Figures 5.14 (a) to (h).

As can be seen in Figure 5.14 (a), the speed of the turbomachine drops quickly as the turbine and compressor powers decrease. The deceleration of the rotor reduces the helium flow rate to the precooler, as shown in Figure 5.14 (b). As a result, the increase of the precooler temperatures as shown in Figure 5.14 (c) is limited. Because of loss of heat sink of the precooler water, the plant circuit experiences heatup transient, as shown in Figure 5.14 (d). The helium heatup in the low pressure side of the circuit causes the pressure to increase, as shown in Figure 5.14 (e). Consequently, the cycle pressure ratio is reduced, which is the inherent factor assuring loop shutdown. Figure 5.14 (f) shows the temperature transient in the recuperator, whereas the reactor power and fuel temperature responses are shown in Figures 5.14 (g) and (h).

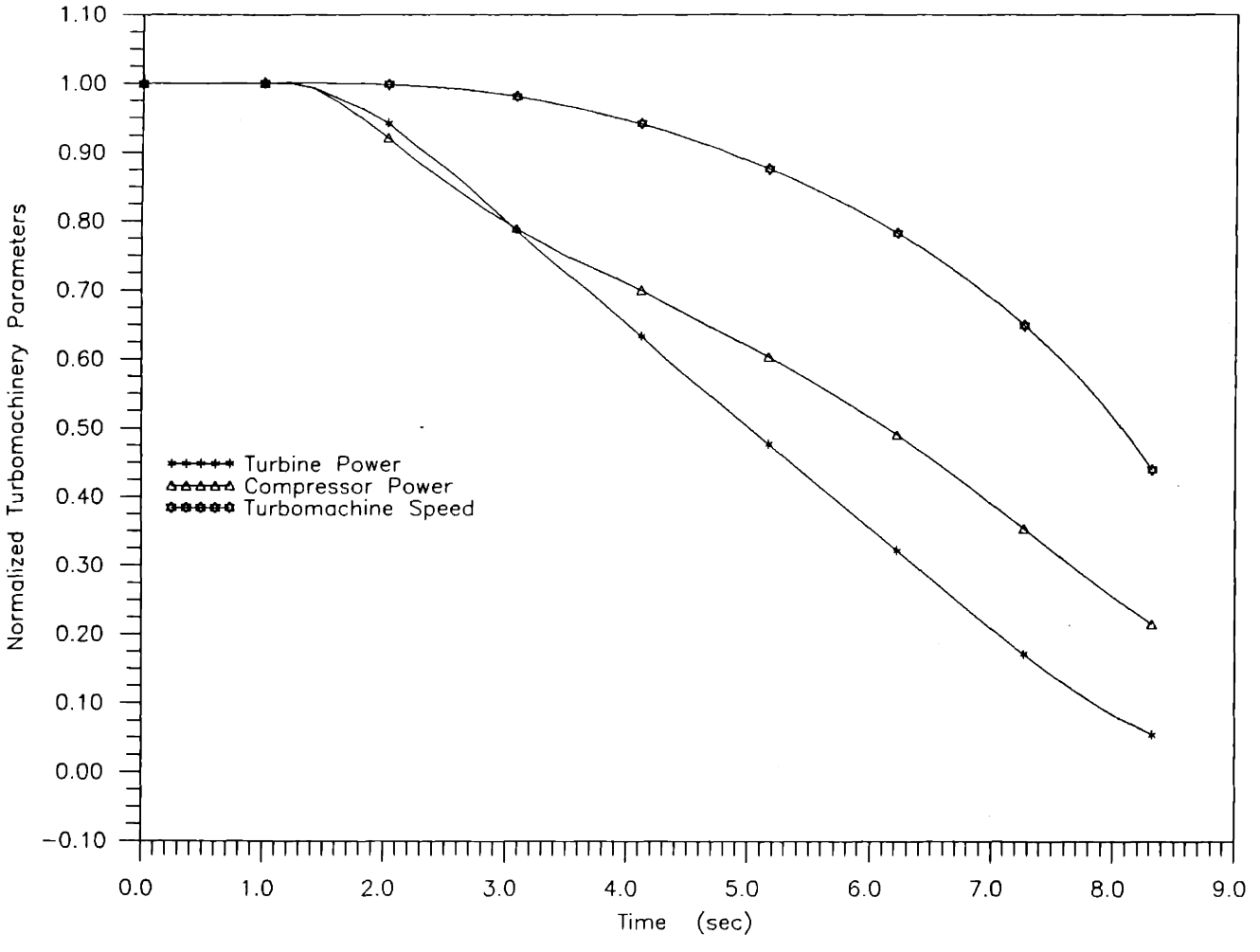

Figure 5.14(a) Turbomachine parameters in case of loss of precooler water flow

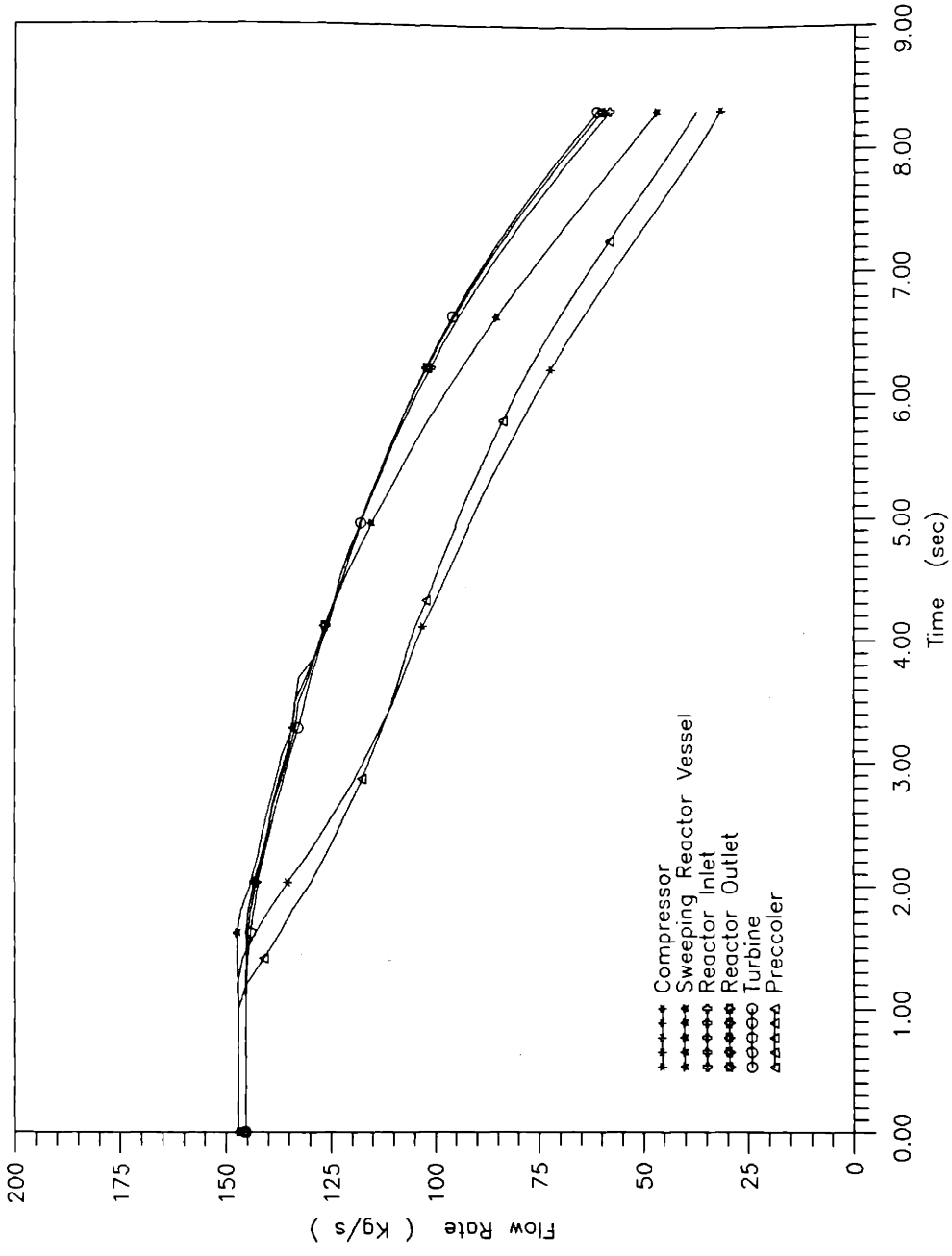

Figure 5.14(b) Flow transient responses in case of loss of precooler water flow

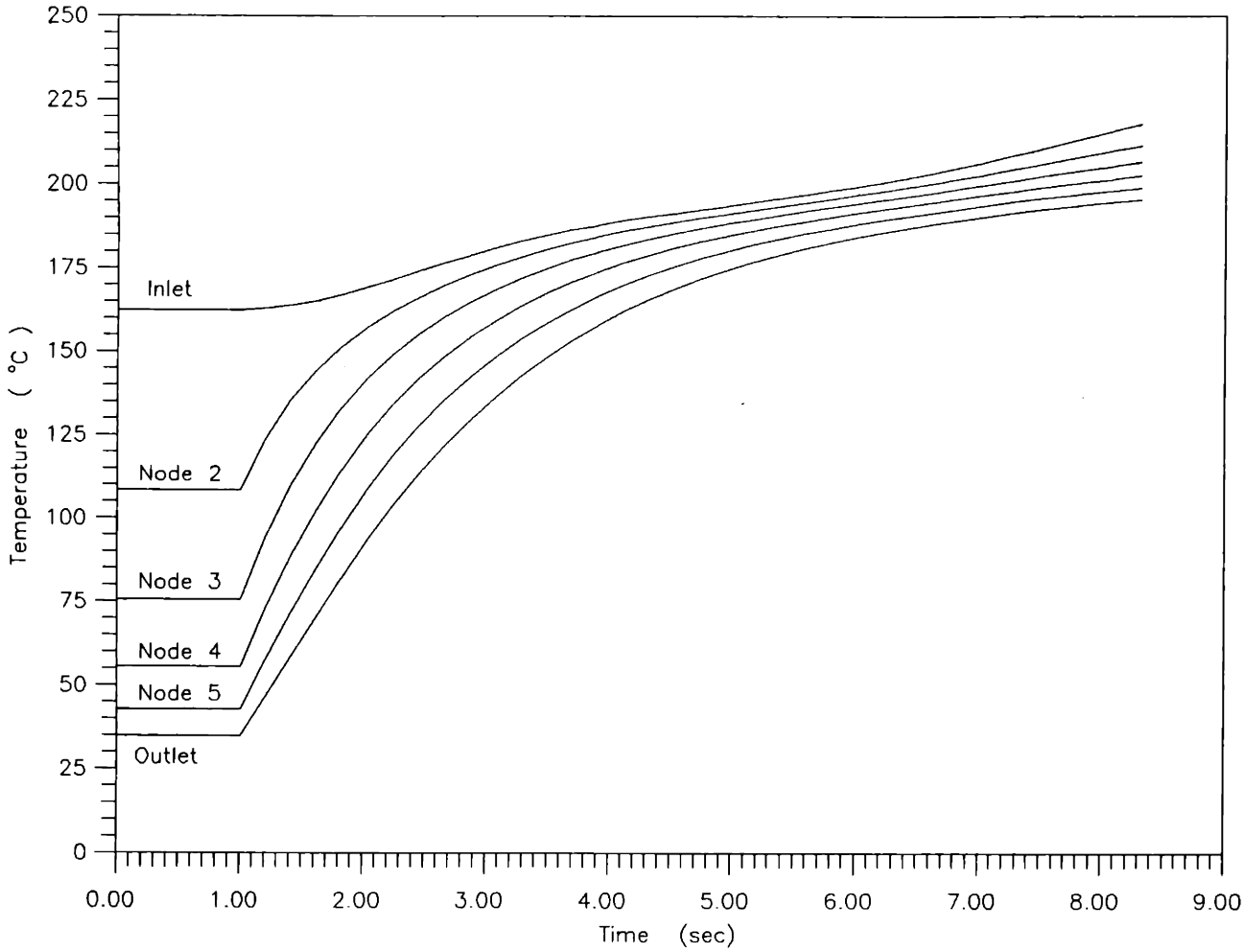

Figure 5.14(c) Precooler temperature transient responses in case of loss of precooler water flow

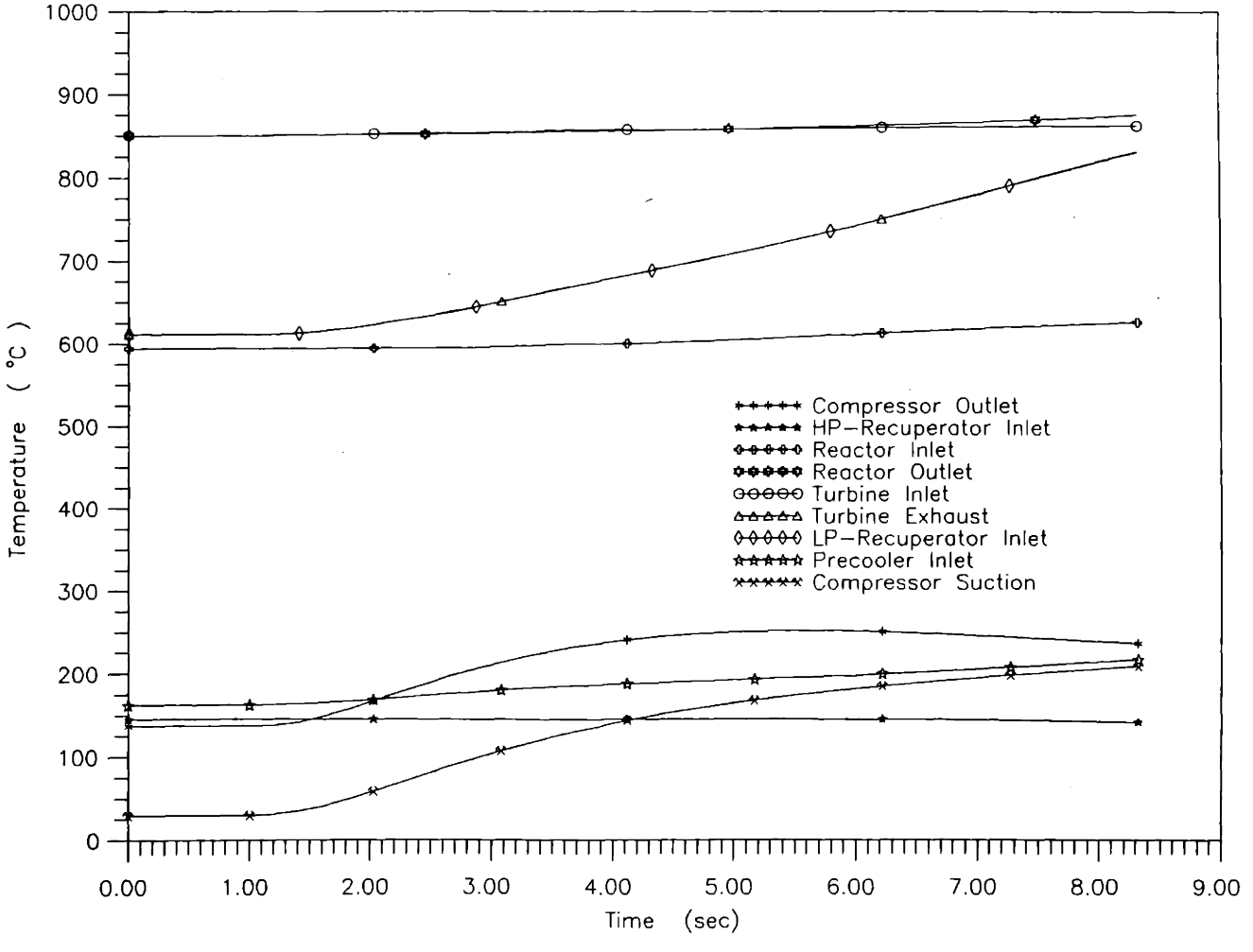

Figure 5.14(d) Temperature transient responses in case of loss of precooler water flow

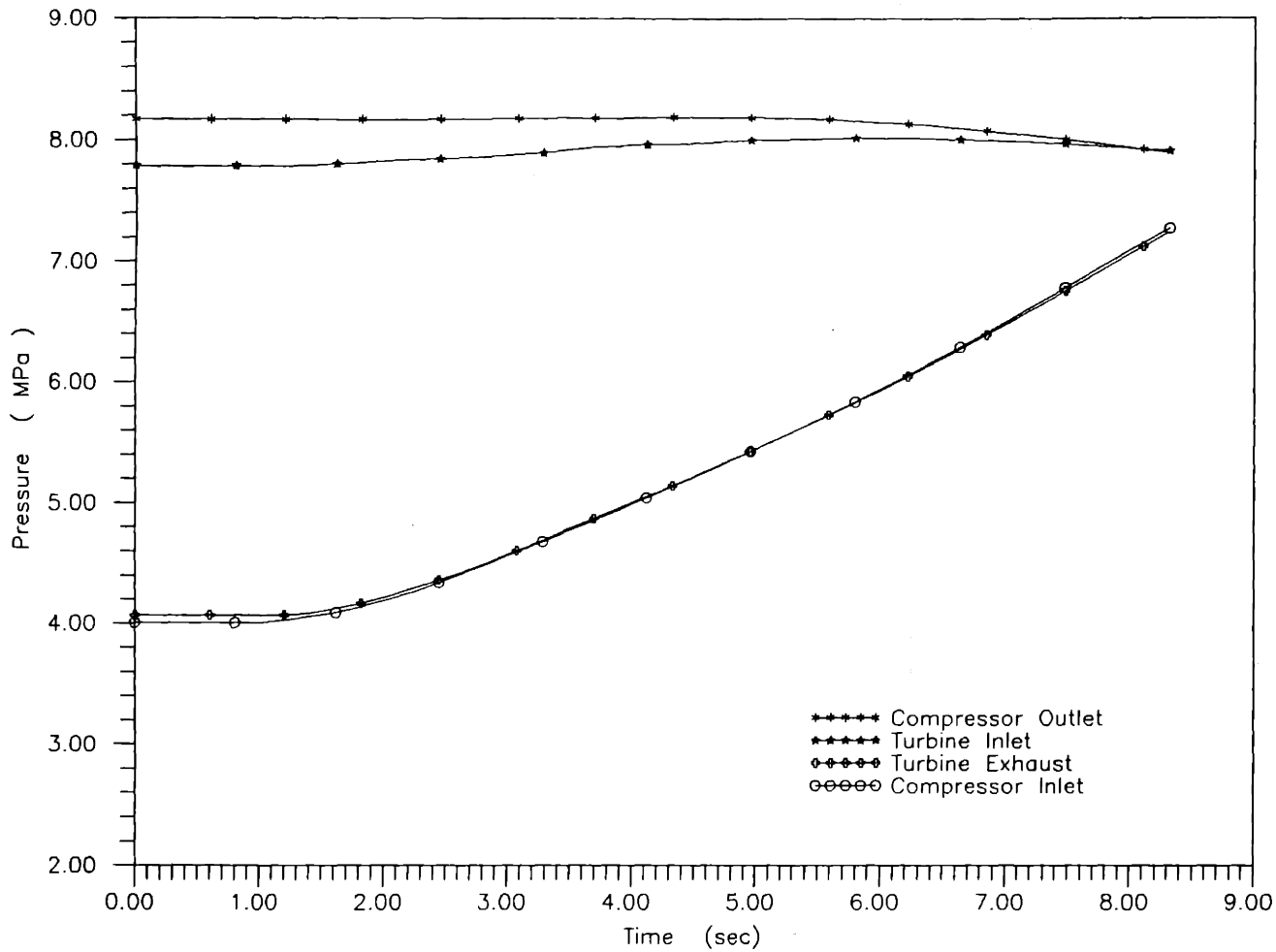

Figure 5.14(e) Pressure transient responses in case of loss of precooler water flow

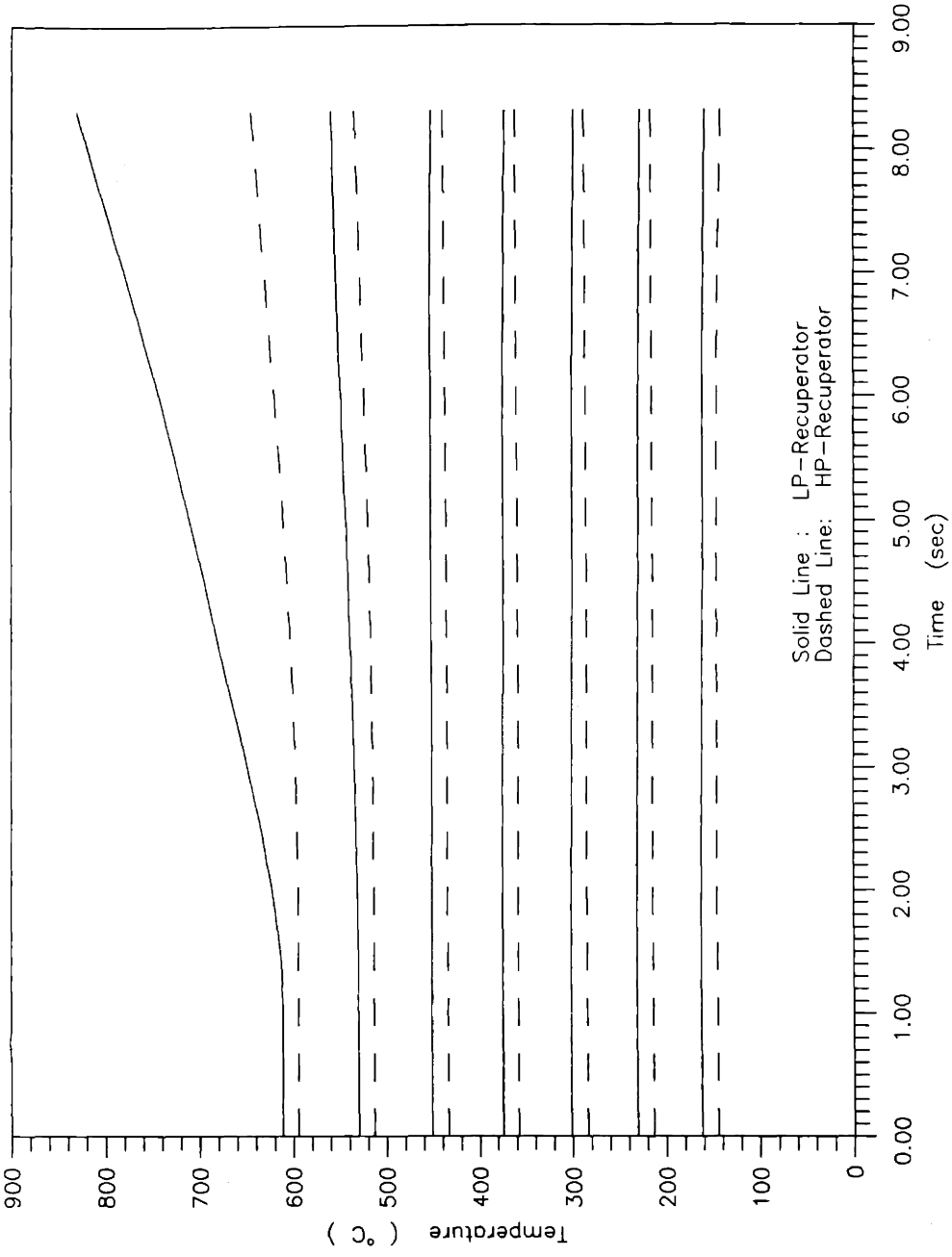

Figure 5.14(f) Recuperator temperature transient responses in case of loss of precooler water flow

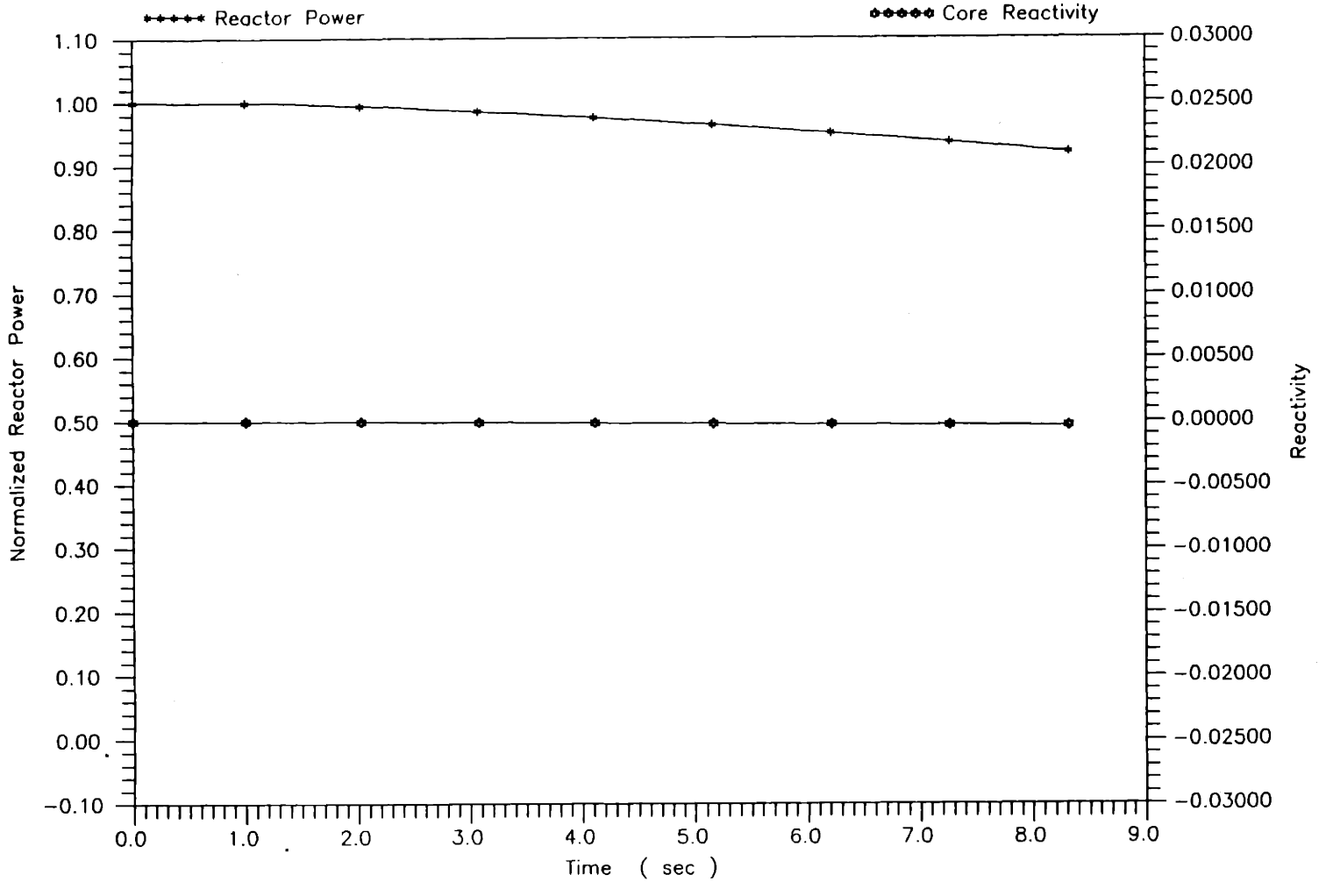

Figure 5.14(g) Reactor power and reactivity transient responses in case of loss of precooler water flow

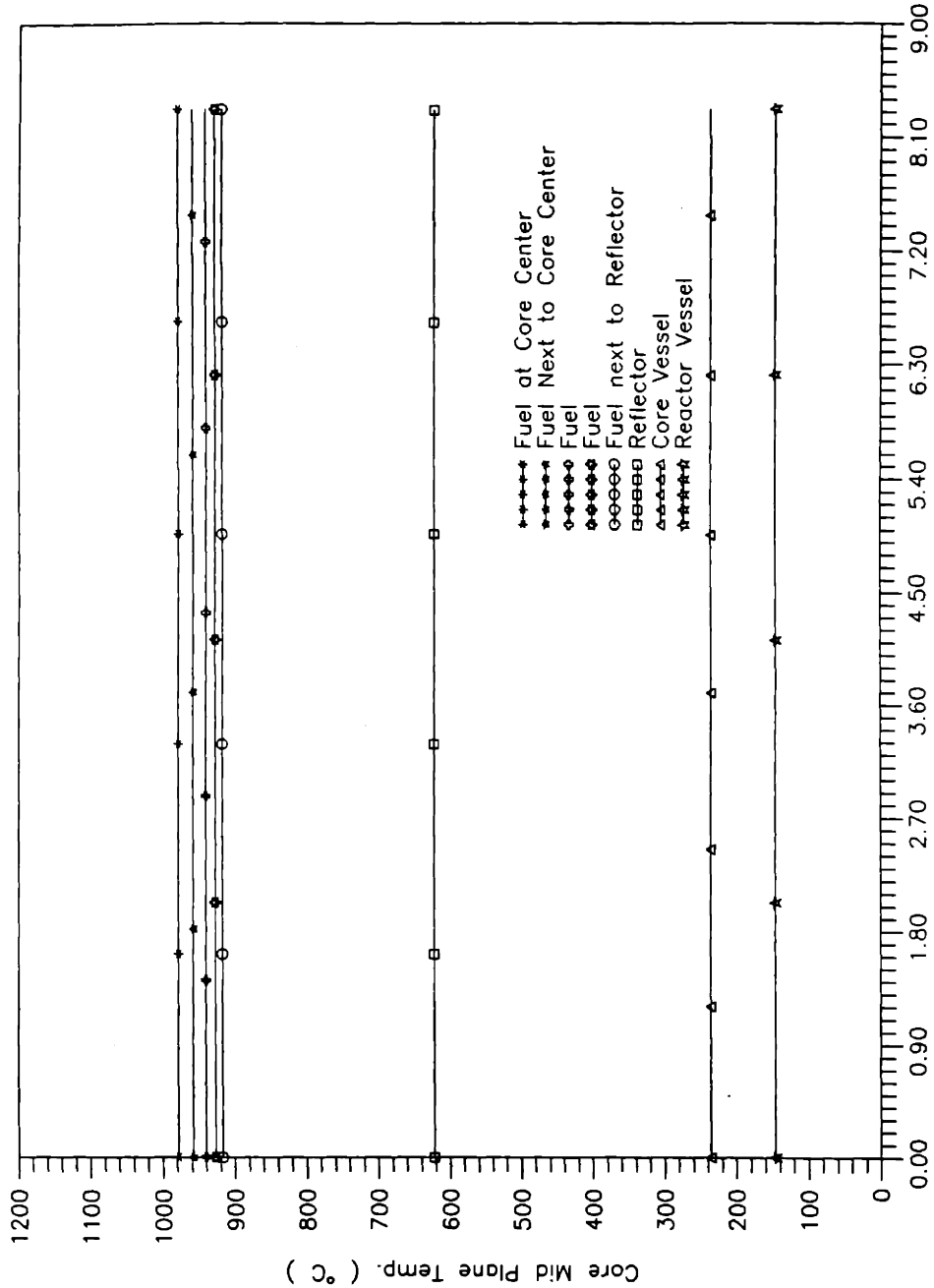

Figure 5.14(h) Radial temperature transient responses in the reactor mid plane in case of loss of precooler water flow

Reference

[A1] "An Assessment of the INTERATOM/KWU Modular HTGR Concept," Gas-Cooled Reactor Associates, Southern California Edison Co., General Electric Co., Combustion Engineering, Inc., Bechtel Group, Inc., September 1985.

Chapter Six

Summary and Recommendation

6.1 Summary of Conclusions

A control system design has been developed which enables automated operation and protection for the MGR-GT power plant. The control is accomplished by means of simultaneous control functions to regulate reactor power, to control electric load and turbomachinery speed, to control the temperature of the helium to the turbine, to prevent thermal overstresses in plant components during transients, and to support scheduled control maneuvers for plant startup and shutdown. In addition, the control system provides emergency protective actions to prevent the plant components from damage and to mitigate the likelihood of bounding safety events in case of severe accidents.

The control system consists of a Plant Regulation System and a Plant Protection System. It is integrated with the reactor reactivity control and shutdown system, the inventory control system, and the bypass control and shutdown system, and is based on unique control approaches regarding the requirements of the regulatory and protective control for nuclear power plants. The control for the plant power output to accommodate changes in electric load demand relies primarily on the helium inventory regulation, enabling high system efficiency over extended load ranges. Limited bypass control is utilized in supporting the inventory control to achieve rapid load following capabilities. The reactor power is controlled with reactivity control rods, based on the strategy of maintaining a constant coolant temperature at the core outlet. Such approach minimizes the occurrence of thermal transients and temperature redistribution in the core during reactor power changes. The control functions were implemented by controllers based on the state-space feedback control

methodology.

It has been shown that the MGR-GT using the proposed control system is a robust controllable power plant. The control system enables ramp power changes up to ±5%/min as well as ±10% step power changes in the operational power range from 100% to 25% of the nominal. In addition, high efficiency is maintained over an extended power range. Figure 6.1 summarizes the MGR-GT power control approach showing cycle efficiencies over the full power range.

The full-scale transient simulation program, GTSim, was developed as the primary tool in optimizing the control system design and performing transient analysis to investigate the plant dynamic characteristics during normal as well as extreme conditions. Solution algorithms built into GTSim enable the simultaneous solution of a large, stiff system of nonlinear equations, representing the dynamic behavior of the overall power plant. The high structural modularity and flexibility of the code permit independent maintenance and upgrade of code subsystem modules and should require minimum changes in the code as the physical design of the plant evolves. This program, with the capabilities of simulating a broad range of transient events including far off-normal behavior, is expected to play a significant role in the future design study of the MGR-GT.

A wide spectrum of transients has been simulated for the MGR-GT, including operational events and accidents, and "design" and "beyond-design-basis" accidents. The simulations were carried out to evaluate the controllability as well as the safety and protection features of the MGR-GT.

6.2 Recommendation for Future Study

The following areas are recommended as issues to be developed in the future modeling and control study for the MGR-GT:

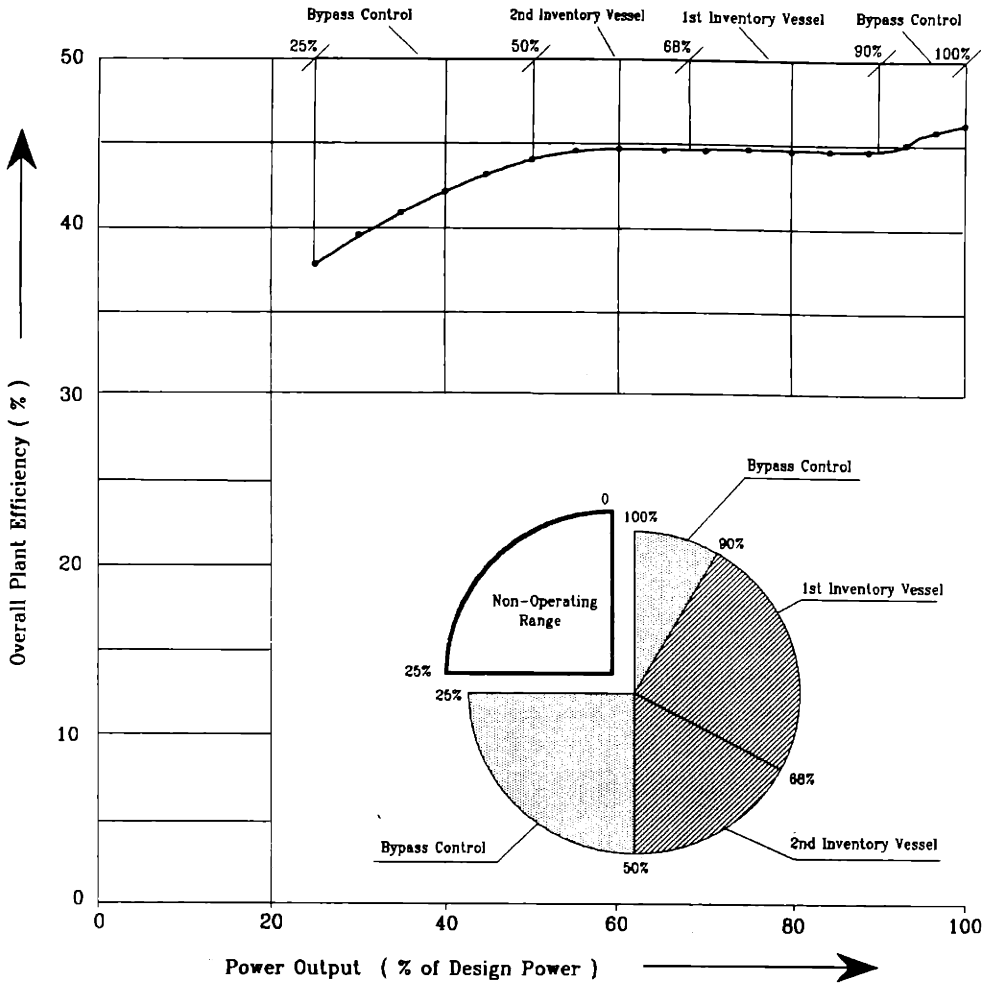

Figure 6.1 The MGR–GT power control approach and efficiency

(1) Currently, the core neutronics is approximated by the point reactor kinetics model whose temperature reactivity feedback mechanism is based on the average core temperature. This model is considered sufficient for reactor power control. Comparisons performed between point and more detailed space-dependent model calculations show that even for the maximum reactivity excursion possible for MGR reactors, there is little discrepancy in the behavior of the total reactor power with time if the shape of neutron flux remains basically unchanged[M1]. However, this model is not valid for predicting the peak temperatures in core heatup transients because the temperature profiles in the core may be altered considerably over a long-term period of core heatup. The distortion in the temperature profiles results in uneven reactivity distributions generated by temperature reactivity coefficient. The negative reactivity feedback is much stronger near the peak temperatures than the average temperature feedback. The simulations performed in this study have shown that the accurate prediction of the local power during re-criticality after the disappearance of the negative reactivity contributed by fission product buildup is essential to the calculation of the maximum peak temperatures. The much stronger negative reactivity feedback near peak temperatures tends to keep the local core areas from criticality, thus the peak temperature. It is recommended that a space-dependent neutron kinetics model be developed and incorporated in the GTSim for plausible simulations of core heatup transients.

(2) The characteristics maps of the turbine and compressor should be extended to cover the extremely low and zero speed operation so that simulations for plant startup from stationary state could be performed. The simulations from stationary state of the plant also require the modification to the heat transfer models in the heat exchanges and reactor core to enable correct predication in the laminar flow region.

(3) In the future, the design of the control system can be extended to determine the redundancy in sensor signal validation and fault tolerant instrumentation necessary to achieve

the desired level of control system availability.

(4) The helium is modeled as a real gas in the development of the thermal hydraulic model. It has been shown that the model enables the prediction of nonlinear dynamic behavior of the helium at high temperature and pressure regions, which an ideal gas model is incapable of simulating. However, this model should be validated with benchmark experimental data in the future.

(5) Both main solution algorithms implemented in GTSim involve vector-matrix manipulation with iteration in solving the large-scale system of equations representing the MGR-GT system model. In addition, the iteration in each step of integration requires multiple evaluations of sub-sets of equations for the individual component or subsystem models. The nature of such solution algorithms suggests great potential for utilizing the advanced computer architectures incorporating vector pipelines, and multiple CPUs sharing centralized memory. Initial efforts have been made in vectorizing and parallelizing the GTSim code on the MIT Cray-2 four CPU supercomputer, which has resulted an average simulation speedup of a factor of 16 over a scalar code, only a factor of 3.4 less than real-time simulation. It is expected that a real-time operation can be achieved with further optimization of the code.

Reference

[M1] Massimo, L.,"Physics of High-Temperature Reactors," Pergamon Press, New York, 1976.